

THÈSE

En vue de l'obtention du

DOCTORAT DE L'UNIVERSITÉ DE TOULOUSE

Délivré par :

Institut National des Sciences Appliquées de Toulouse (INSA de Toulouse)

Cotutelle internationale avec:

Présentée et soutenue par : Vu Hiep DANG

Le lundi 2 december 2013

Titre:

Phases d'initiation et de propagation de la corrosion des armatures du beton arme fissure en environnement carbonique ou salin

École doctorale et discipline ou spécialité :

ED MEGEP: Génie civil

Unité de recherche :

Laboratoire Materiaux et Durabilite des Constructions de Toulouse

Directeur(s) de Thèse : M. Raoul FRANCOIS

Mme. Valerie L'HOSTIS

Rapporteurs:

M. Mark ALEXANDER
M. Dario CORRONELLI

Autre(s) membre(s) du jury:

M. Jean-Paul BALAYSSAC Mme. Delphine NEFF M. Ngoc Anh VU

Auteur: DANG Vu Hiep

Titre: Phases d'initiation et de propagation de la corrosion des armatures du béton armé

fissuré en environnement carbonique ou salin

Thèse de doctorat de l'Institut National des Sciences Appliquées de Toulouse

Spécialité: Génie Civil

Résume:

Cette thèse s'intéresse à l'étude la corrosion des armatures du béton armé à la fois sur les

conditions de son initiation et de sa propagation mais également sur ses conséquences à

long terme sur le fonctionnement en service des ouvrages.

Parce que les fissures sont un paramètre intrinsèque du fonctionnement des ouvrages en

béton armé, une partie de la thèse est consacrée à l'étude de l'initiation de la corrosion et

les conditions de sa propagation.

Le démarrage d'une étude à long terme sur les conditions de l'initiation et de la

propagation de la corrosion en ambiance saline est présenté : il s'agit de la mise en place

de poutres en béton armé de 3 m de longueur conservées en charge, pour des

dimensionnements à l'ELS et à l'ELU, sous cycles d'humidification séchage en brouillard

salin. Le dimensionnement de cette étude prend en compte les effets pervers d'une étude

précédente initiée par Raoul François en 1984 : en effet l'accouplement de deux poutres

par le chevêtre de chargement conduit à une fissuration due à une moment positif pour

une poutre et à un moment négatif pour l'autre et donc à une surface tendue fissurée

horizontale « supérieure » directement exposée au brouillard salin dans un cas et une

surface fissurée horizontale « inférieure » (cas classique) dans l'autre cas. Par ailleurs,

dans un souci de simplification de la mise en place, le moment négatif correspond

également à une position en haut de coffrage des armatures tendues et donc à une

interface de moins bonne qualité en raison du top-bar effect. Les premiers résultats

confirment l'initiation précoce de la corrosion mais montrent que l'influence des fissures

sur la propagation dépend des conditions de leur exposition et de l'enrobage et qu'un

Ī

simple critère d'ouverture limite ne peut pas décrire l'éventuelle propagation de la corrosion.

Une étude a été réalisée sur la carbonatation en présences de fissures et sur ses conséquences sur l'initiation et la propagation de la corrosion. Des échantillons annulaires de mortier renforcé par une armature HA ont été fissurés en utilisant le montage dit « coeur expansif » développé par Gagné et al en 2001. Les résultats ont montrés que quelque soit l'ouverture des fissures mécaniques, il y a une carbonatation des lèvres de la fissure et de l'interface acier-béton. La carbonatation de l'interface acier-béton est vraisemblablement due à l'endommagement mécanique induit par le chargement et le transfert des contraintes de l'acier vers le mortier lors de la création des fissures. Cet endommagement se traduit également par la présence de micro-fissures internes autour de l'armature. Après exposition à des cycles d'humidification séchage, la corrosion se développe tout le long de l'armature mais avec une épaisseur plus importante en sous-face de l'armature ou la qualité de l'interface est moins bonne. Les résultats montrent que les fissures de corrosion induites par le développement de la couche de rouille prennent naissance à partir des micro-fissures dues à l'endommagement mécanique. Ce résultat est cohérent avec le développement des fissures de corrosion observées dans la partie sur l'initiation et la propagation de la corrosion en ambiance saline.

Une autre partie de la thèse est consacrée à l'étude des propriétés mécaniques résiduelles de poutres en béton armé corrodées par 26 à 28 années de conservation majoritairement sous charge de flexion en ambiance saline.

On s'intéresse d'abord au comportement en traction simple des aciers corrodés. Il est très difficile de connaître la contrainte réelle de rupture en traction des aciers corrodés « naturellement » dans le béton contaminé par l'exposition aux chlorures. En effet, la corrosion induite par les chlorures conduit à des piqûres de géométries très diverses qui rendent difficile l'évaluation de la section résiduelle d'acier. Cependant, il apparait que la contrainte effective de plasticité est peu affectée, la contrainte ultime est légèrement augmentée significative d'un écrouissage plus important après corrosion et surtout l'élongation à rupture est drastiquement réduite par la présence des piqures de corrosion.

L'effet de la corrosion des armatures sur le comportement en flexion est ensuite étudié. Pour les poutres étudiées avec un ratio d'armatures tendues de 0.96%, la corrosion se traduit par un changement du mode de rupture, de l'écrasement du béton comprimé après une phase de plastification des aciers à la rupture fragile et brutale des armatures tendues

après corrosion. La diminution de la capacité portante est proportionnelle à la perte de section d'acier dans les sections les plus sollicitées. La perte de ductilité ou diminution de la flèche à rupture des poutres en béton armé est très importante et pourrait remettre ne cause la sécurité dans le fonctionnement des éléments corrodés. Il apparait que le changement de la ductilité d'une poutre en béton armé est corrélé avec le changement de ductilité des aciers due à la corrosion.

L'effet de la corrosion sur la résistance à l'effort tranchant est ensuite étudié. Pour ce faire des éléments courts (poutres épaisses) sont testés en flexion simple. Les résultats montrent que la corrosion peut conduire à des changements de fonctionnement mécanique mais que la résistance vis-à-vis de l'effort tranchant est globalement peu affectée par la corrosion des armatures longitudinales ou des cadres d'effort tranchant. La complexité des phénomènes mis en jeu sur des éléments courts et l'importance des bielles de béton comprimées dans les effets d'arc peuvent expliquer ces résultats. Par ailleurs, la capacité d'ancrage des armatures droites corrodées apparait très largement supérieure à celle attendue compte tenu de la présence des fissures de corrosion et des prévisions issues de la littérature. Le confinement dû à l'appui et le fait que la corrosion naturelle n'affecte pas tout le périmètre des barres d'armatures peuvent expliquer ces résultats surprenants.

Mots Clés : Corrosion, fissures, chlorures, carbonique, armature, perte de section d'acier, capacité résiduelle de charge, contrainte-déformation, allongement à rupture, ductilité, limite d'élasticité.

Thèse soutenue le 02 décembre 2013 à l'INSA de Toulouse devant la commission d'examen composée de :

Mark ALEXANDER	Rapporteur
Dario CORONELLI	Rapporteur
Jean-Paul BALAYSSAC	Examinateur
Raoul FRANÇOIS	Examinateur
Valerie L'HOSTIS	Examinateur
Delphine NEFF	Examinateur
Ngoc Anh VU	Examinateur

Author: DANG Vu Hiep

Title: Initiation and propagation phases of re-bars corrosion in pre-cracked reinforced

concrete exposed to carbonation or chloride environment

PhD thesis at l'Institut National des Sciences Appliquées de Toulouse

Specialty: Civil Engineering

Abstract:

This thesis aims to study the reinforcement corrosion embedded in reinforced concrete

structures on both initiation and propagation of corrosion and its long-term consequences

on the service life of structures.

Because the cracks are an intrinsic parameter of reinforced concrete structures, a part of

the thesis is carried out to study the corrosion initiation and propagation in cracked

concrete.

Firstly, a long-term study on the conditions for the initiation and propagation of corrosion

in saline environment is presented: it is the reinforced concrete beams 3 m long kept in

loading at serviceability load limit state (SLS) and ultimate load limit state (ULS) under

wetting-drying cycles of salt spray. The design of this study takes into account the side

effects of a previous study started in 1984 by Raoul François: indeed, the coupling of two

beams by the loading device leads to flexural cracks due to a positive moment for a beam

and a negative moment for another beam. Thus a horizontal surface of a beam, cracked

"superior", directly exposed to salt spray and a horizontal surface of another beam,

cracked "inferior" (classical case), was hidden. Moreover, for beams with negative

moment, "superior" cracked surface corresponds to a position on top of form (bleeding

surface), thus a lower quality of concrete due to the top-bar effect is expected. The first

results confirm the early initiation of corrosion, but shows that the influence of pre-cracks

on the propagation of corrosion depends on their conditions of exposure and concrete

cover thickness. A simple limit criterion of crack opening cannot describe the corrosion

propagation stage.

A study was conducted in carbon dioxide condition with presence of cracks to examine its

impact on the initiation and propagation of corrosion. Annular mortar samples, reinforced

with HA reinforcement, were cracked using the test set up called "expansive core"

V

developed by Gagné et al. in 2001. The results showed that whatever the mechanical crack opening, the crack edge and the steel-concrete interface were carbonated. Carbonation of the steel-concrete interface is likely to be due to mechanical damage induced by loading and stress transfer from the steel to mortar when creating cracks. This damage is also caused by the presence of internal micro-cracks around the steel bar. Following exposure to wetting-drying cycles, corrosion develops throughout the reinforcement but with a greater thickness of rust layer on the underside of the reinforcement where the quality of the interface is weaker. The results showed that the corrosion cracking induced by the development of rust layer arises from internal micro-cracks due to mechanical damage. This result is consistent with the development of corrosion cracks observed previously in saline environment.

Another part of the thesis is to study the residual mechanical properties of corroded reinforced concrete beams of 26-28 years exposed to a saline environment under bending load. The behavior of single tensile steel corroded extracted from these corroded beams is studied. It is very difficult to know the true stress of tensile steels corroded "naturally" in concrete contaminated by exposure to chlorides. Indeed, the corrosion induced by chlorides leads to create corrosion pits with various geometries that make it difficult to determine accurately the residual steel cross-section. However, it appears that the true yield stress is unaffected, the true ultimate stress is slightly increased by corrosion but the total elongation at failure is drastically reduced by the presence of pitting corrosion. The effect of reinforcement corrosion on flexural behavior is then studied. For RC beams studied with tension reinforcement ratio of 0.96%, the corrosion resulted in a change in failure mode, from concrete crushing in compression after yielding of tensile steel to brittle failure of tension reinforcement. The decrease of the load bearing capacity is proportional to the loss of steel section in the mid-span section. The loss of ductility or decrease in deflection at failure of reinforced concrete beams is very important and could be the limiting factor for the service life of corroded RC structures. It appears that the change in ductility of corroded reinforced concrete beam is correlated with the change in ductility of the steel due to corrosion. The effect of corrosion on the shear behavior is then studied. To make this, the short-shear span beams (deep beams) were tested under three point bending until failure. The results showed that corrosion can lead to changes in mechanical behavior but load bearing capacity of deep beams is generally unaffected by corrosion of longitudinal reinforcement and stirrups. These results can be explained by a

coupled behavior between arch action and beam action leading to change in load transfer mechanism and failure mode. In addition, the capacity of straight end anchorage of corroded reinforcement appears to be very much higher than expected despite the presence of corrosion cracks. Concrete confinement effect due to the end support reaction and the "natural" corrosion condition which do not lead to a homogeneous damage all around perimeter of re-bars may explain these surprising results.

Keywords: Corrosion, cracks, chloride, carbon dioxide, reinforced steel, steel cross-section loss, shear, load bearing capacity, stiffness, stress-strain, ultimate elongation, ductility, yield stress.

Dedication

TO MY BELOVED PARENTS

TO MY BELOVED WIFE & SON

ACKNOWLEDGMENTS

This thesis could be completed by so many helps and supports from my

family, my supervisors and my friends...

To all members in my family for their immense love and support,

they are always in my heart.

▼ To my professor, Mr. Raoul François, and my co-supervisor, Mme.

Valerie L'Hostis, I would like to say "thank you very much" for all

everything and thank for always having believe in me.

▼ To my friends in France, I am very happy to have them always beside

to support me every time and everywhere ... and they are always in

my mind.

The author feels grateful to the engineers, technicians and office staff of

LMDC - Toulouse, of LECBA - CEA Saclay - Paris for their kind helps.

Without their support, the author would not have embarked on this

venture.

Finally, the author would like to express his appreciation to Vietnam

International Education Development (VIED) - Vietnamese Ministry of

Education & Training and CEA Saclay - Paris for providing financial

support to the author during the course of his dissertation.

DANG Vu Hiep

Toulouse, December 2013

ii

TABLE OF CONTENTS

Acknowleagment	-
Table of contents	iii-
Resume	1-
Part I: Mechanical consequences of corrosion on the behavior of RO	elements
Chapter I: Literature review on mechanical behavior studies	26-
I.1. Effect of corrosion on bond between steel bar and concrete and steel bar	
behavior in direct tension	27-
I.1.1. Effect of corrosion on bond between concrete and re-bar	27-
I.1.1.1 Top-Bar effect of RC structures corroded	28-
I.1.1.2. Effect of corrosion on bond between concrete and re-bar	31-
I.1.1.3. Research by G.J. Al-Sulaimani et al	32-
I.1.1.4. Research by Abdullah A.Almusallam et al	35-
I.1.1.5. Research by P.S. Mangat et al	38-
I.1.1.6. Research by Congqi Fang et al	40-
I.1.1.7. Research by Lan Chung et al	42-
I.1.1.8. Research by D. Coronelli et al. and K.Z. Hanjari et al	43-
I.1.2.9. Summary	45-
I.1.2. Effect of corrosion on steel behavior (ductility- yield stress)	49-
I.1.2.1. Research by Abdullah A. Almusallam	50-
I.1.2.2. Research by John Cairns et al	54-
I.1.2.3. Research by C.A. Apostolopoulos et al. and R. Palsson, M. Saeed Mirza	57-
I.1.2.4. Research by Han-Seung Lee et al	58-
I.1.2.5. Research by Castel et al	60-
I.1.2.6. Summary	61-
I.2. Loading-bearing capacity of corroded reinforced concrete beam	-63
I.2.1. Research by Abdullah A. Almusallam et al	65-
I.2.2. Research by J. Rodriguez et al	65-
I.2.3. Research by Pritpal S. Mangat et al	67-
I.2.4. Research by Abul K. Azad et al	68-
I.2.5. Research by Torres-Acosta et al	69-

I.2.6. Research by A. Castel et al	70-
I.2.7. Research by Sanchun Yoon et al	
I.2.8. Research by Y. Balim et al	75-
I.2.9. Research by T. Vidal et al	
I.2.10. Research by Tamer El Maaddawy et al	79-
I.2.11. Research by Ruijin Zhang et al	
I.2.12. Research by Goitseone Malumbela et al	
I.2.13. Summary	
Reference	90-
Chapter II: Experimental results on long-term corroded beams	
II.1. Effect of corrosion of steel on steel properties	
II.2. Effect of corrosion of steel on flexural behavior	112·
II.3. Effect of corrosion of steel on shear behavior	147-
II.4. Effect of corrosion of steel on ductility of RC beam	172-
II.5. Summary	
Part II: Effect of pre-cracks on the corrosion initiation and propag	ation
Part II: Effect of pre-cracks on the corrosion initiation and propage Chapter III: Literature review on corrosion in carbon dioxide and chloride	ation
Chapter III: Literature review on corrosion in carbon dioxide and chloride	
Chapter III: Literature review on corrosion in carbon dioxide and chloride Environment	205-
Chapter III: Literature review on corrosion in carbon dioxide and chloride Environment	205- 206-
Chapter III: Literature review on corrosion in carbon dioxide and chloride Environment	205- 206- 206-
Chapter III: Literature review on corrosion in carbon dioxide and chloride Environment	205- 206- 206- 207-
Chapter III: Literature review on corrosion in carbon dioxide and chloride Environment	205- 206- 207- 208-
Chapter III: Literature review on corrosion in carbon dioxide and chloride Environment	205- 206- 207- 208- 212-
Chapter III: Literature review on corrosion in carbon dioxide and chloride Environment	205- 206- 207- 208- 212-
Chapter III: Literature review on corrosion in carbon dioxide and chloride Environment	205- 206- 207- 208- 212- 212-
Chapter III: Literature review on corrosion in carbon dioxide and chloride Environment	205- 206- 207- 208- 212- 214- 217-
Chapter III: Literature review on corrosion in carbon dioxide and chloride Environment	205- 206- 207- 212- 212- 214- 217-
Chapter III: Literature review on corrosion in carbon dioxide and chloride Environment	205206207212214217220-
Chapter III: Literature review on corrosion in carbon dioxide and chloride Environment III.1. Corrosion in CO ₂ environment and consequences of carbonation on material properties III.1.1. Summary on carbonation process in concrete structures III.1.1.1. Carbonation of Portlandite Ca(OH) ₂ III.1.1.2. Carbonation of calcium silicate hydrates C-S-H III.1.1.3. Carbonation of other constituents of cementitious materials III.1.1.4. Main factors affecting carbonation III.1.5. Profile of carbonation III.1.1.6. Effect of pre-cracks on carbonation propagation III.1.2. Consequence of carbonation on material characteristics III.1.2.1. Change in pH value	205206207208212214217220220-

III.1.2.5. Change in properties of transport of concrete	
III.1.3. Corrosion induced by Carbonation	
III.1.3.1. Corrosion mechanism	
III.1.3.2. Cracking of the concrete cover due to corrosion in	
CO₂ environment	
III.1.3.3. Change in mechanical properties of reinforcement	
III.1.3.4. Effect of pre-cracks on steel corrosion in CO₂ environment	
III.1.3.5. Nature of corrosion products	
Reference	
III.2. Corrosion in chloride environment in presence of crack	
III.2.1. Introduction	
III.2.2. Influence of pre-cracks	
III.2.3. Steel corrosion in presence of cracks in chlorides	
Reference	
Chapter IV: Experimental program in chloride environment	
IV.1. Literature review on the Experimental program on pre-stressed	
RC beams of Rance (Benchmark des poutres de la Rance)	
IV.2. Synthesis of the Experimental program on RC beams at the L.M.D.C	
-Toulouse (Since 1984 to present)	
IV.3. Experimental program conducted during this thesis at the L.M.D.C	
-Toulouse (Since 2010 to present)	
IV.4. Summary	
Reference	
Chapter V: Experimental program in CO ₂ environment	
V.1. Initiation and propagation of steel corrosion in presence of crack	
V.2. Development of corrosion products in relation to pre-cracks	
General conclusion	356-

Résume:

La corrosion des armatures des structures en béton est un énorme problème économique pour le monde entier.

Le béton est sans doute la meilleure protection de l'acier vis-à-vis de la corrosion en raison du pH élevé de sa solution interstitielle présente dans la porosité. Cependant, il existe deux causes principales d'amorçage de la corrosion : la diminution du pH de la solution interstitielle due à la carbonatation (réaction du gaz carbonique avec les hydrates du béton conduisant à la formation d'un acide faible) qui permet la corrosion de l'acier, ou rupture local du film passif recouvrant l'acier en raison de la présence d'un taux minimum d'ions chlore.

L'influence des fissures « fonctionnelles » du béton armé sur la corrosion des armatures est un sujet controversé sur lequel il n'existe pas de consensus au niveau national ou international. La difficulté majeure est sans doute liée à la notion même d'influence : s'agit d'un effet à court terme ou à long terme, est-ce lié au protocole expérimental utilisé (essais accélérés sous champ électrique), à l'environnement agressif choisi (surface fissurée horizontale exposée aux chlorures). L'influence des fissures du béton armé est également un sujet complexe qui fait intervenir la qualité, la résistivité et l'épaisseur du béton d'enrobage, l'orientation des fissures par rapport aux armatures et les phénomènes de cicatrisation des fissures.

La présence de fissures dans les structures en béton est supposée induire au moins trois effets significatifs (Bentur et al., 1997): (1) un accès privilégié aux chlorures et au CO₂ pour dépassiver l'acier en fond de fissure, (2) un accès privilégié à l'oxygène contribuant à accélérer le processus de corrosion (courant cathodique), (3) elles conduisent à une hétérogénéité physique et chimique au niveau de l'acier susceptible de favoriser le processus de corrosion. A noter, que cette vision qu'on pourrait qualifier de « matériau » ne prend pas en compte le comportement du béton situé entre les fissures, en effet après fissuration, le béton entre les fissures est remis en tension par les armatures fonctionnant comme des tirants : ce phénomène qui conduit à rigidifier les structures en béton est appelé effet raidissant du béton tendu (Tension Stiffening Effect), peut conduire à une autre fissuration du béton d'enrobage (cover controlled cracking) préjudiciable à la durabilité car correspondant à

un endommagement plus diffus du béton d'enrobage (Gilbert, 1999) (Castel & François, 2011).

Deux mécanismes de corrosion sont théoriquement possible pour l'acier dans le béton armé.

- (1) une corrosion par macro-cellules (ou corrosion galvanique) (macro-cell corrosion) dans laquelle l'acier en fond de fissure dépassivé est une zone anodique et l'acier situé entre les fissures, encore passivé, est une zone cathodique de consommation de l'oxygène. La qualité et l'épaisseur du béton d'enrobage interviennent ainsi pour limiter l'accès de l'oxygène dans la zone cathodique.
- (2) une corrosion par micro-cellules ou par piqûres (micro-cell corrosion, pitting corrosion) dans laquelle les zones anodiques et cathodiques sont côtes à côtes. Ce cas devrait correspondre à une dépassivation plus généralisée de l'acier même si ce n'est pas exclu que ce type de corrosion apparaisse en fond de fissure sous réserve que l'oxygène puisse accéder par la fissure. La répartition des piqûres est alors en relation avec des hétérogénéités de l'acier ou de l'interface acier béton (présence de vides).

A noter que ces deux types de corrosion en présence de chlorures peuvent donner lieu à des pertes de masse localisées que l'on peut appeler communément piqûres de corrosion. En conséquence la confusion est souvent possible entre les deux types de corrosion, d'autant plus que la corrosion par courant galvanique sera localisée alors que la corrosion par piqûres intrinsèquement localisée peut conduire une corrosion dite généralisée par rapport à une vision macroscopique (Zhang et al., 2009). A noter également que les deux types de corrosion peuvent être simultanés.

Une fois que la phase de propagation de la corrosion est active, les détériorations de la structure sont caractérisées par un éclatement du béton d'enrobage, résultant du caractère expansif des produits de corrosion, et s'accompagnent d'une réduction de la section des aciers ainsi que d'une perte d'adhérence acier-béton. Comparativement, la corrosion due aux chlorures est plus dangereuse que celle due à la carbonatation à cause de son développement rapide et le risque de rupture soudaine pour le cas des environnements sévères. Les principaux facteurs environnementaux mis en cause sont les chlorures provenant de l'eau de mer ou de l'air marin et l'utilisation de sels fondants pour le déverglaçage des routes.

La corrosion conduit à la détérioration du comportement mécanique des structures, qui est fonction de leur état de corrosion. La majeure partie des études consacrées à la durée de vie considère que le critère de fin de service correspond au démarrage de la phase de propagation de la corrosion. Pourtant, cet instant ne signifie pas que la performance de la structure est mise en cause. Les recherches menées au LMDC montrent que la phase de propagation de la corrosion peutreprésenter une part importante de la durée de vie des ouvrages en béton armé. Ne considérer que la phase d'initiation semble représenter donc une démarche trop conservative. Ainsi, pouvoir prédire l'évolution du comportement mécanique des structures en béton armé au cours de leur vieillissement est un objectif d'importance majeure pour les maîtres d'ouvrage afin de prévoir éventuellement des réparations, le renforcement de la structure, un programme de maintenance ou, au contraire, la destruction et le remplacement de l'ouvrage.

Les objectifs de la thèse sont:

- Etudier le processus d'initiation et de propagation de la corrosion en présence d'une préfissuration d'origine mécanique en ambiance saline ou carbonique.
- Caractériser expérimentalement des effets de la corrosion sur les propriétés mécaniques des structures en béton armé exposées en atmosphère saline.

L'étude de l'initiation et de la propagation de la corrosion en ambiance carbonique est basée sur l'utilisation de petit échantillons de mortier armé fissurés par le dispositif dit du « cœur expansif » mis au point par Gagné et al., 2001.

L'étude de l'initiation et de la propagation de la corrosion en ambiance saline est basée sur la réalisation d'un nouveau programme de poutres en béton armé conservée en charge (et donc fissurées) en ambiance saline. Ce programme a l'ambition de compléter celui mis en place par R. François en 1984 en utilisant les mêmes compositions et géométries mais en modifiant les conditions d'expositions.

L'étude de la phase de propagation de la corrosion et de ses conséquences sur le fonctionnement mécanique en service ou à rupture, est basée sur l'analyse du vieillissement d'éléments en béton armé, et plus particulièrement sur l'analyse exhaustive de deux poutres corrodées notée A2CL1 et A2CL2. Ces poutres font parties d'un ensemble d'éléments de trois mètres longueur, conservés depuis 27 ans enambiance saline et sous différentes intensités de chargement en flexion trois points. Il s'agit donc de conditions de vieillissement très proches de celles des structures réelles. Cette partie expérimentale est la suite d'un

programme de vieillissement du béton armé démarré en 1984 à Toulouse, évoqué ci-dessus, et dont le support en était la thèse de doctorat de Raoul François. Il a bénéficié d'un financement de l'AFREM (Association Française de Recherche et d'Etudes sur les Matériaux) et de l'AFB (Association Française du Béton) qui ont depuis fusionnées pour donner naissance à l'AFGC (Association Française du Génie Civil). L'objectif initial de l'étude était de comprendre les relations existantes entre la fissuration de service (structurale) du béton armé et la corrosion des armatures. En effet, les règlements de calcul (de l'époque) limitaient l'ouverture des fissures structurales afin d'obtenir une durée de vie suffisante en environnement agressif sans que ces mesures s'appuient sur des bases expérimentales suffisamment pertinentes. L'objectif de l'étude était donc clairement d'apporter des données supplémentaires pour pouvoir proposer une modification des règlements le cas échéant.

Les résultats (R. François) ont montrés que si effectivement, on constate une corrosion précoce (quelques semaines) en fond de fissures structurales, celle-ci stoppe rapidement et n'évolue pratiquement plus. Le niveau de corrosion obtenu en fond de fissure n'est donc pas significatif et doit être négligé pour une prédiction de la durée de vie à long terme. Les restrictions que l'on peut apporter à cette affirmation sont l'ouverture des fissures ne dépassait pas 0,5 mm et le fait que la sollicitation est statique (pas de mouvement d'ouverture et refermeture de fissures pouvant gêner la cicatrisation).

Cependant, on a constaté également que la phase de propagation de la corrosion a débuté presque en même temps pour les poutres de type B à faible enrobage (1 cm) que pour les poutres A à fort enrobage (4cm) avec dans ce dernier cas des fissures de corrosion démarrant à l'intersection entre fissures de flexion et armatures tendues. C'est donc pourquoi un nouveau programme expérimental a été mis en œuvre dans le cadre de cette thèse en « inversant » la disposition des nouvelles poutres B et nouvelles poutres A, pour mieux comprendre le rôle des conditions d'expositions.

Le choix de restitution des résultats obtenus dans cette thèse est de proposer outre une analyse bibliographique sur la propagation de la corrosion et ses conséquences mécaniques, une succession de chapitre basée sur des articles publiés ou en relecture.

Le premier chapitre correspond à une bibliographie sur les conséquences de la corrosion des armatures sur le comportement mécaniques des structures en béton armé. On discute des résultats concernant la modification des propriétés mécaniques des armatures en acier en

traction en terme de contrainte de plastification, contrainte de traction à rupture et allongement maximal à rupture. On fait également le bilan des études sur la modification de l'adhérence acier-béton liée à la corrosion des armatures. Puis la modification du comportement global : réponse en flexion et réponse vis-à-vis de l'effort tranchant sont ensuite présentés. Les différentes méthodes utilisées pour mesurer le taux de corrosion sont également discutées. Les différentes techniques pour induire la corrosion : accélération sous champ électrique, conditions naturelles, sont également présentées et discutées.

Le second chapitre concerne les résultats expérimentaux obtenus à partir des essais de mécaniques réalisés sur 2 poutres issues du programme expérimental mis en place en 1984 par R. François. Ceprésente l'étude de l'évolution du faciès de corrosion des armatures et ses conséquences sur le comportement mécanique en service du béton armé. Le travail expérimental est consacrée à l'étude exhaustive de deux poutres, notées A2CL1 et A2CL2 âgées de 27 ans et soumises à l'effet couplé du chargement et de la corrosion en atmosphère saline, avec en particulier l'évaluation de la fissuration de la corrosion, la distribution de la corrosion mesurée par les pertes de section le long des armatures ainsi que l'évolution du comportement mécanique à rupture. Une étude mécanique du comportement en traction des aciers corrodés est également menée.

Dans la première partie du chapitre 2, l'impact de la corrosion sur les propriétés mécaniques de l'acier a été étudié. Après avoir testé les poutres jusqu'à la rupture, les barres d'acier corrodées ont été récupérées de la poutre corrodée A2CL2 et non corrodée A2T. Comme le nombre d'échantillons de barres corrodées était limité, les données obtenues dans une autre thèse de doctorat (Inamullah Khan, 2012) sur une autre poutre corrodé A2CL3ont été également utilisées pour avoir suffisamment de résultats. Les barres d'armature ont été nettoyées en utilisant une solution de Clark ANSI / ASTM G1-72 afin d'éliminer tous les produits de corrosion. Le degré de corrosion des armatures a été évalué en mesurant la perte de diamètre à l'aide d'un pied à coulisse après le retrait complet des produits de corrosion. Il est très difficile de mesurer la perte précise du diamètre de cette manière à cause de la forme de la surface de l'armature corrodée qui est très tortueuses et varie considérablement suivant la longueur de la barre. Par conséquent, la perte de poids de la barre d'acier a également été utilisée pour calculer la perte de diamètre (mesurée sur des segments de barres de quelques mm de longueur).

Les barres d'acier ont été testées en traction en utilisant une machine de capacité 250 kN. Deux LVDT ont été utilisés pour mesurer l'allongement des barres d'acier. La longueur de base pour la mesure de l'allongement était de 200 mm pour chaque barre d'acier. Les résultats obtenus sont utilisées pour tracer les diagrammes de contrainte-déformation pour chaque échantillon testé. En utilisant des diagrammes contrainte-déformation, la limite élastique, la résistance à la rupture et l'allongement des barres d'acier ont été comparées pour les barres corrodées et non corrodées.

Les contraintes nominales ont été calculées en utilisant le diamètre nominal de la barre d'acier. Les contraintes réelles ont été calculées de deux manières différentes. La première méthode utilise le diamètre réduit mesuré avec le pied à coulisse. Pour éviter la difficulté de mesureavec un pied à coulisse dans le cas de piqures qui ne réduisent pas le diamètre de façon uniforme, une deuxième méthode basée sur la perte de masse de la barre d'acier corrodé, a été utilisée. Voici ci-après quelques conclusions tirées des résultats expérimentaux. La limite d'élasticité nominale de barres diminue avec le degré de corrosion des armatures en relation avec le fait que la corrosion réduit la section transversale. Toutefois, lorsque la section transversale réduite a été utilisée à la place de section nominale, il a été remarqué que la limite d'élasticité vraie de toutes les barres corrodées et non corrodées avaient la même valeur. On peut dire que la corrosion ne modifie pas la limite élastique des barres d'acier. La contrainte à la rupture nominalediminue avec le degré de corrosion des armatures en relation avec le fait que la corrosion réduit la section transversale. Cependant, la contrainte vraie à rupture des aciers corrodés augmente par rapport aux témoins. Pour toutes les barres non corrodées, le rapport entre la vraie contrainte à la rupture et la vraie limite d'élasticité est d'environ 1,13 qui qui signifie que les barres d'acier utilisées en renforcement dans les poutres en béton armé sont classées dans la classe B selon l'Eurocode 2. Dans le cas des barres corrodées, ce rapport est de 1,26. Par conséquent, les barres corrodées seraient classées dans la classe C, ce qui nécessiterait un plus grand allongement à la rupture par rapport aux prescriptions de la classe B.

Les barres corrodées n'ont pas montré le plateau plastique au-delà de la limite élastique et de plus le phénomène d'écrouissage est plus marqué avec une augmentation de la contrainte à rupture. Cependant l'allongement à rupture est considérablement réduit pour toutes les armatures corrodées. C'est potentiellement le problème le plus important lié à la corrosion,

en effet presque toutes les barres d'acier corrodées ont une déformation à la rupture en dessous de la valeur minimale (0,05) requise par l'Eurocode 2 pour les aciers de classe B. Ce point peut compromettre la requalification des structures corrodées.

En revanche, pour tous les échantillons corrodés, on obtient une valeur moyenne d'environ 200 GPa pour le module d'élasticité qui correspond au module élastique de l'acier non corrodé.

La deuxième partie du chapitre 2 présente les résultats expérimentaux en flexion de la poutre A2CL1 fortement corrodée pour évaluer sa performance résiduelle à long terme. La poutre corrodée A2CL1 et une poutre non corrodée A2T du même âge ont été testés sous flexion trois points jusqu'à la rupture.

La carte de fissuration de la poutre corrodée A2CL1 après 27 ans d'exposition en ambiancé saline a été élaboré. En plus des fissures transversales de flexion, qui ont résulté de la flexiontrois points initiale, qui sont localiséesdans la partie centrale de la traction de la poutre, beaucoup de fissures de corrosion ont également été observées le long des armatures tendues. On peut noter une différence importante avec une poutre issue du même programme, la poutre A2CL3 testée par Khan et al en 2012, qui est une corrosion importante des armatures « comprimées » pour la poutre A2Cl1 alors qu'en dépit d'un enrobage identique, les armatures « comprimées » de la poutre A2CL3 n'étaient pas affectées par la corrosion.

Les cartes de corrosion ont également été élaborés, qui montrent l'étendue de la corrosion sur les barres longitudinales tendues FS (barre antérieure) et BS (barre postérieure). Les cartes sont tracées dans deux directions: l'orientation vers le bas pour le côté de l'acier directement exposé aux fissures et à solution saline et la direction vers le haut dans laquelle la face d'acier a une couverture de béton beaucoup plus épaisse. Il est constaté que l'attaque de corrosion n'est pas uniforme. Beaucoup de piqûres de corrosion ont été observés de façon hétérogène sur les barres de traction et la perte maximale de section des armatures tendues atteint 50% au niveau des piqûres de corrosion les plus importantes. Les armatures « comprimées » présentent également une corrosion très développée et non uniforme avec des pertes locales de sections atteignant presque 50% de la section initiale.

Après avoir testé les poutres en flexion, les barres d'acier ont été récupérées. La perte de diamètre de ces barres d'acier corrodées a été mesurée avec un pied à coulisse après le retrait complet des produits de corrosion (en utilisant une solution de Clark ANSI / ASTM G1-72).

Pour les armatures de traction, la réduction de section maximale a eu lieu sur la barrepostérieure BT, près de la mi-portée qui correspond au de point de défaillance au cours de l'essai de flexion de la poutre. Une réduction de section moyenne d'environ 26% sur les deux barres tendues a été mesurée à l'emplacement de la rupture car l'armature antérieure FT présente une corrosion faible en face de la section de rupture de la barre BT.

Un test de résistance à la traction a été réalisé à la fois sur des barres d'acier corrodées et non corrodées pour caractériser le comportement en traction. Les courbes contrainte-déformation ont été tracéespour les barres d'acier. Il a été observé que la corrosion a un impact beaucoup plus important sur la ductilité que sur la résistance. Ce point pourra être crucial pour la requalification des structures, car l'acier corrodé ne possède plus la ductilité minimale imposée par les codes de dimensionnement tel que l'Eurocode 2.

Au cours des essais de flexion, il a été observé que la corrosion avait largement réduit la flèche maximale à rupture de la poutre et modifié le type de rupture passant de l'écrasement du béton comprimé pour le témoin à la rupture fragile des aciers tendus pour la poutre corrodée. Cela implique que la corrosion affecte non seulement la résistance des poutres, mais aussi induit une fragilité dans leur comportement. Par conséquent, les grandes déformations, qui se produisent dans lesstructures en béton-armé en flexion avant la rupture, ne se produiront pas dans le cas d'un renforcement très corrodé, éliminant ainsi l'avertissement le plus souhaitable avant la défaillance de la structure. Une diminution de 47% de la flèche ultime de la poutre corrodée a été enregistrée par rapport à la poutre témoin, ce qui indique clairement que la corrosion affecte directement le comportement ductile des poutres en béton armé et peut changer le mode de défaillance des poutres en béton. Le modèle de Castel et al a été utilisé pour prendre en compte la perte de ductilité des aciers tendus. Dans ce modèle, la diminution de la ductilité est liée à la perte maximale de section d'acier. Il a été noté que les résultats obtenues à partir des essais de traction sur les barres d'acier de la poutre A2CL3 et A2CL1, ont vérifiés le modèle proposé par Castel et al.

La charge ultime de la poutre corrodée a également été réduite par rapport à la poutre témoin. Une réduction de 26% de la capacité de charge de la poutre corrodé a ainsi été observée. La diminution de la capacité de charge de la poutre corrodée est principalement due à la réduction de section d'acier en raison des piqûres de corrosion sur les barres principales de traction.

Il a été conclu que le comportement mécanique d'une poutre corrodée diffère de son comportement avant la corrosion de trois façons principales: une diminution de la capacité portante caractérisé par un changement dans le mode de défaillance du béton, une réduction de la flèche maximale à rupture liée au comportement fragile de l'acier corrodé, et une diminution de la rigidité globale due à la corrosion des barres et la perte d'adhérence acierbéton. Ce dernier point n'étant pas le plus important et pouvant varier en fonction de la fissuration transversale.

La troisième partie du chapitre 2 présente l'étude expérimentale et analytique de trois poutres courtes très corrodées, critiques vis-à-vis ducisaillement, pour évaluer le comportement au cisaillement des poutres endommagées par la corrosion à long terme. Ces trois poutres sont extraites des poutres A2CL1 et A2CL2 qui ont été coupées en poutres critiques au cisaillement avec une portée entre appuis de 1400, 1210 et 750 mm chacune. Des poutres témoins de même portée sont également testées en flexion 3 points.

Les cartes de fissuration ont été établies et les largeurs de fissures ont été mesurées en utilisant une loupe binoculaire avec une précision de 0,02 mm. Beaucoup de fissures de corrosion ont été observées le long des armatures tendues. Pour la poutre A2CL1-A, la largeur maximale enregistrée pour les fissures de corrosion est de 1,8 mm sur la face avant et de 0,42 mm sur la face arrière. Pour la poutre A2CL2-B, la taille maximale de la fissure sur la face avant est de 0,5 mm à mi-portéetandis que la taille maximale de la fissure sur la face arrière est de 1,54 mmà proximité du support. Pour la poutre A2CL2-A, la taille maximale des fissures est 0,9 mm près de l'appui.

Les cartes de corrosion des poutres corrodées A2CL1-A, A2CL2-A et A2CL2-B ont été établies. Les cartes ont été tracées dans deux directions: la direction vers le bas, ce qui était du côté de l'acier directement exposés aux fissures et à la pulvérisation de brouillard salin, et vers le haut, dans lequel l'acier regarde le cœur de la poutre. On peut constaterque l'attaque de corrosion n'a pas été uniforme. Beaucoup de piqûres de corrosion ont été observés sur les barres de traction et la perte maximale de section des armatures dues aux piqûres de corrosion était de 45% pour la poutre A2CL1-A alors quelle atteint 30% pour les poutres A2CL2-B et A2CL2-A. Les barres longitudinales et les étriers étaient sévèrement corrodés et la perte de masse est plus grande dans les zones où les fissures de corrosion sont plus larges. Il convient également de noter que les armatures compriméesdes poutres A2CL2-A et

A2CL2-B ne faiblement corrodées en dépit du fait qu'elles avaient le même enrobage de béton que les armatures tendues. Pour la poutre A2CL1-A qui présentait une forte corrosion des armatures comprimées, la corrosion des étriers est beaucoup plus développée dans la partie tendue des poutres, dans les régions directement en contact avec armatures en traction. Tous les étriers sont corrodés dans la zone tendue, même ceux qui sont à proximité des supports et qui ne se trouvaient pas en regard d'une fissure en flexion.

Dans cette étude, les poutres ont une portée en cisaillement a = 700 mm, 605mm et 375 m, une profondeur effective d = 224 mm et donc un rapport a / d qui vaut 3,125 ; 2,7 et 1,67 qui correspond à des portées courte en cisaillement et même une poutre-voile pour A2CL2-A. Pour la poutre A2CL1-A avec la portée la plus longue, on constate une rupture en cisaillement pour la poutre témoin alors que la poutre corrodée montre une rupture en flexion. La corrosion conduit a un changement dans le mode de rupture et se traduit par une ductilité plus importante en dépit d'une fragilité plus importante des armatures corrodées. Le comportement des poutres témoin et A2CL2-B sont peu différent avec une rupture fragile due au glissement des armatures tendues pour la poutre témoins et par une rupture du béton sur appui pour la poutre corrodée en raison des fissures de corrosion transversales et longitudinales conduisant au détachement d'un morceau de la poutre. Pour la poutre A2CL2-A la plus courte, la rupture est de type cisaillement à la fois pour la poutre témoin et pour la poutre corrodée avec cependant une flèche à rupture ici encore plus importante pour la poutre corrodée. La capacité d'ancrage des armatures tendues joue un rôle important avec de façon surprenante un meilleur ancrage dans le cas des poutres corrodées.

Le ratio a/d est un paramètre très important pour la capacité portante des poutres avec deux tendances distinctes dans le comportement entre poutres courtes et poutres élancées et un changement de comportement aux alentours d'un rapport a/d égal à 3.

Les glissements des armatures tendues au niveau des appuis ont été mesurés pour toutes les poutres corrodées A2CL1-A, A2CL2-B et A2CL2-A et pour les trois poutres témoinscorrespondantes. Le glissement est mesuré en plaçant un LVDT à chaque extrémité de chaque barre d'armature afin d'enregistrer son déplacement horizontal. Les glissements enregistréssont plus élevés pour les poutres témoins que pour les poutres corrodées. Ce résultat est très surprenant étant donné que le développement important à la corrosion est censé réduire l'adhérence et donc l'ancrage droit des barres, d'autant plus que des larges

fissures longitudinales étaient présentes autour de l'armature. Une tentative explication pourrait être que des vides d'air, formés en raison de l'effet du ressuage et du tassements du béton frais en dessous des barres d'acier, ont été remplis avec des produits de corrosion dans le cas de poutres corrodées alors que ces vides sont restés dans le cas des poutres témoins en raison de l'absence de corrosion. Ces produits de corrosion augmententla résistance au glissement de l'armature en acier. Par ailleurs, la présence des fissures de corrosion au niveau du support augmente la pression du béton sur les armatures lors du chargement et augmente ainsi le confinement (Cairns et al., 2008).

En raison du changement de comportement mécanique des poutres voiles corrodées, il sera très difficile de prévoir la charge de rupture en fonction du degré de corrosion. En effet, il ne semble pas y avoir de corrélation entre l'intensité de l'endommagement dû à la corrosion et le changement de capacité portante. Ces résultats vont dans le même sens que ceux obtenus par Khan et al sur des poutres naturellement corrodées et ceux de Azam et Soudki, 2012 sur des poutres corrodées sous champ électrique.

La quatrième partie du chapitre 2 concerne l'étude du changement de ductilité des poutres élancées en fonction du niveau de corrosion des armatures tendues. Les résultats disponibles dans la littérature montrent une ductilité qui peut augmenter ou diminuer en fonction du niveau de corrosion qui peut s'expliquer par 3 raisons principales :

- La méthode de corrosion : en effet une corrosion sous champ électrique conduit à une corrosion différente de la corrosion naturelle, plus uniforme avec une modification limitée de la ductilité des barres d'acier corrodée et donc un comportement en flexion d'une poutre en béton armé peut différent de celui d'une poutre saine
- Le type de rupture : on ne peut comparer la ductilité d'une poutre corrodée et d'une poutre témoin que si le mode de rupture est identique. En effet, les ruptures par cisaillement en particulier sont toujours fragiles et non comparables avec celle obtenues en flexion après un palier plastique des armatures tendues
- Le facteur de ductilité classiquement employé : en effet, celui-ci est basé sur le rapport entre la flèche à rupture et la flèche au palier plastique. Mais la corrosion des armatures diminuent les deux termes : flèche au palier plastique puisque la section d'acier est plus faible ; flèche à rupture parce que la section d'acier est plus faible et parce ce que l'acier corrodé est moins ductile en traction. On a donc un paramètre dont le numérateur et le

dénominateur diminue en même temps : le résultat peut donc aller dans le sens de l'accroissement ou de la diminution d'autant plus que la flèche au palier plastique est un terme petit.

A partir des résultats de la littérature, nous proposons de définir un nouvel index de ductilité basé sur le rapport de la flèche à rupture d'un élément corrodé par rapport à sa flèche avant corrosion. Ce paramètre se rapproche ainsi de celui utilisé pour définir la ductilité de l'acier en traction en fonction du niveau de corrosion : rapport de la déformation ultime de l'acier corrodé sur la déformation ultime de l'acier sain. Nous commençons par définir un nouveau

modèle de ductilité de l'acier corrodé en traction $d_f = \frac{\mathcal{E}_{ucorr}}{\mathcal{E}_u}$

$$d_f = e^{-0.05.C\%}$$
 (C < 15%)

$$d_f = 0.5$$
 (C $\geq 15\%$)

qui est légèrement différent de celui proposé par Castel et al, car la perte de ductilité maximale est de 50% au lieu des 20% du modèle de Castel et al.

A partir d'un modèle de comportement non linéaire du béton armé en flexion mis au point par Vu et al., 2010 nous avons calculé la flèche à rupture des poutres en béton armé de type A en fonction du degré de corrosion en se basant sur soit une rupture du béton comprimé pour une déformation conventionnelle de 3.5 e-3 soit une rupture des aciers tendus pour une valeur basée sur le nouveau modèle de ductilité proposé. Le résultat présenté figure 1 montre qu'à partir d'environ 10% de corrosion, le mode de rupture de la poutre passe d'une rupture du béton comprimé à une rupture fragile des aciers tendus et que les résultats expérimentaux sont bien représentés par le calcul de la ductilité des poutres en béton armé.

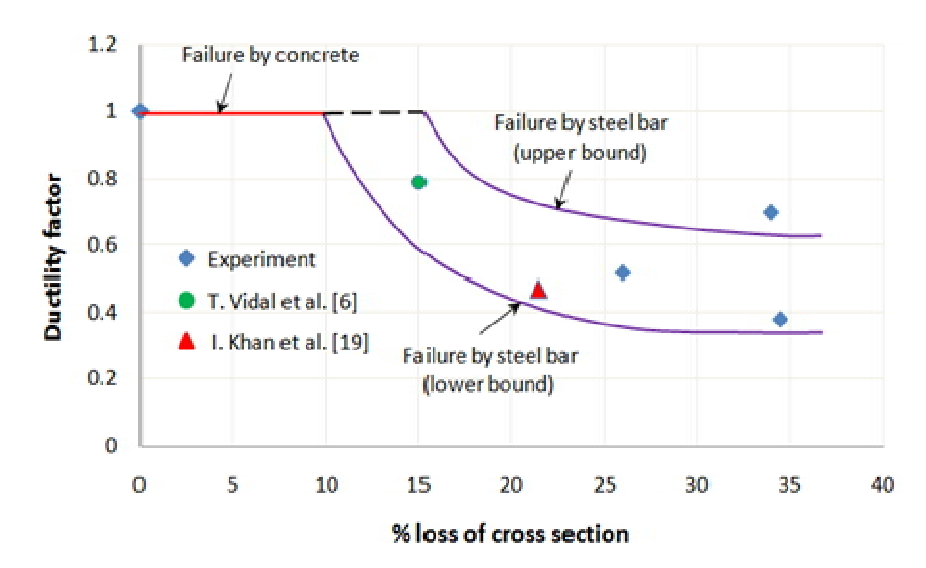


Figure 1 : comparaison entre la ductilité calculée des poutres de type A et les résultats expérimentaux

La perte de ductilité des poutres en flexion avec la corrosion apparait comme un facteur critique pour une requalification « réglementaire » du comportement.

La première partie du chapitre 3 est une revue bibliographique de la corrosion des armatures du béton armé en environnement carbonique. La pénétration du gaz carbonique dans le béton armé conduit a une baisse du pH et a une dépassivation des armatures qui conduit à une corrosion généralisée le long des armatures différentes de celle obtenue en présence de chlorures. La nature des produits de corrosion a souvent été étudiée sur des ouvrages très anciens et à long terme la couche de corrosion est constituée de Goethite α -FeOOH du coté métal et de lépidocrocite γ -FeOOH du coté extérieur.

La seconde partie du chapitre 3 est une revue bibliographique de l'influence de la fissuration d'origine mécanique sur la corrosion des armatures.

Le phénomène de corrosion des armatures est toujours décrit en deux phases : initiation et propagation. La phase d'initiation correspond à la période avant amorçage de la corrosion et la phase de propagation à la période ou la corrosion est active et se développe.

a) Initiation de la corrosion en fond de fissure

La corrosion des armatures est toujours initiée en fond de fissure en quelques semaines à la fois en présence de chlorures ou de carbonatation.

En effet, même si on trouve dans la littérature traitant des relations entre propriétés de transfert et fissuration qu'il y avait une restriction de la pénétration des chlorures ou du gaz carbonique en dessous d'un certain seuil d'ouverture de l'ordre de 10-50 micro-m, cette restriction concerne le renouvellement des chlorures et du CO₂ mais pas leur capacité à pénétrer dans les fissures même très fines pour atteindre l'armature et se propager ensuite sur la zone endommagée de l'interface acier-béton. Dans le cas de l'exposition aux chlorures, la pénétration des chlorures dans les fissures est retardée pour une ouverture de fissure inférieure à l'ouverture critique au sens mécanique, qui correspond à la fin de l'existence d'un phénomène d'interaction entre les lèvres de la fissure. Néanmoins, en dépit de ce délai, le mécanisme de corrosion est toujours le même. La corrosion s'initie en fond de fissure parce que le seuil critique de concentration en chlorures est atteint. Il y a un développement de la corrosion sur quelques mm le long de l'acier en raison de l'endommagement mécanique de la liaison acier béton qui est générée par la création de la fissure, car les chlorures peuvent diffuser dans cette zone endommagée. Alors en fonction des conditions environnementales, la corrosion peut s'arrêter ou se propager conduisant ainsi à la création de fissures de **corrosion** en raison de la pression exercée par les oxydes sur le béton d'enrobage.

Toutes les études disponibles dans la littérature confirment une initiation précoce de la corrosion en présence de fissures. (Beeby, 1978) (Bentur et al, 1997) (Li, 2000), (Jacobsen et al, 1998) (Yoon et al, 2000) (Kondratova et al., 2003) (François and Maso, 1988) (Arya and Ofori-Darko, 1996) (Schieβl and Raupach, 1997) (Okada and Miyagawa, 1980) (Ohno et al., 1996) (Susuki et al., 1990) (François et al., 1999) (François et al., 2006) (Gautefall et al.,1983) (Berke et al.,1993) (Lorentz et al., 1995) (Ramm et al., 1998) (Wang et al., 2000) (Mohammed et al., 2001) (Katawaki, 1997) (Makita et al., 1980) (Tottori et al., 1999) (François et al., 1998) (Arya et al., 1996) (Abahneh and Sheban, 2011) (François et al., 2012) (Arya and Wood, 1995) (Bentur et al., 1997) (Neville, 2002) (Pettersson and Jorgensen, 1996) (Scott and Alexander, 2007) (Suzuki et al., 1990) (Otieno et al., 2010).

b) Propagation de la corrosion en fond de fissure

Le démarrage de la corrosion s'initie toujours en fond de fissure mais la poursuite du phénomène de corrosion en lien avec les fissures (phase de propagation) est toujours en débat. A noter que la notion de poursuite ou d'arrêt de la corrosion est liée à la cinétique de corrosion, « l'arrêt » de la corrosion correspondant à une cinétique très faible. Le fait qu'il y

ait débat prouve que les deux types de résultats : poursuite de la corrosion dans la zone fissurée ou absence de poursuite de la corrosion dans la phase fissurée ont été trouvés par différents chercheurs. Les conditions d'obtention de ces résultats sont donc de nature à modifier la conclusion dans un sens ou dans l'autre. La littérature est donc partagée en deux classes de résultats :

- La fissuration et en particulier l'ouverture des fissures accélère la propagation de la corrosion), (Pettersson and Jorgensen, 1996) (Scott and Alexander, 2007) (Suzuki et al., 1990) (Otieno et al., 2010)
- La fissuration et en particulier l'ouverture de fissures n'a pas d'effet sur la phase de propagation de la corrosion, (Arya and Wood, 1995) (Bentur et al., 1997) (Beeby 1978) (François et al., 1999) (François et al. 2006) (Schieβl and Raupach, 1997)

A noter que la majeure partie des études sur ce sujet correspond à un environnement salin et que ces études ont été menées dans des conditions accélérées avec un courant imposé et pour des périodes courtes de quelques semaines a quelques mois.

On doit distinguer également le type d'environnement : saturé en permanence (structure immergée) ou bien avec des conditions variables (structure aérienne). Les conditions immergées n'étant pas dangereuses en raison du manque d'oxygène limitant les réactions cathodiques.

Le point de vue développé par François et al., 1994 a été schématisé sous forme d'un modèle phénoménologique qui est présenté figure 2 en comparaison avec le modèle de Tuutti, 1980 qui est celui consensuellement admis pour le béton armé non fissuré.

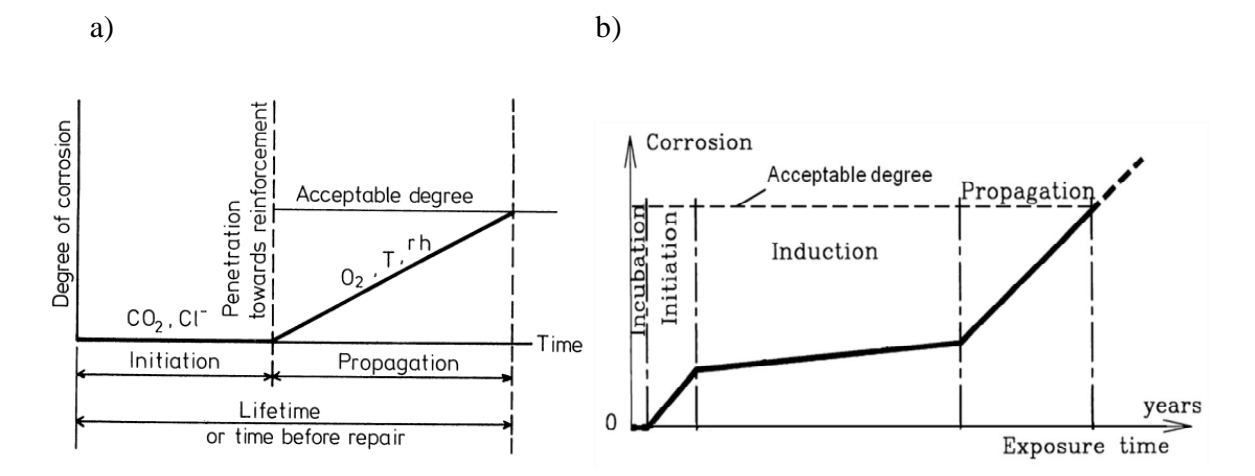


Fig.2:.Comparaison entre le processus de corrosion du béton armé non fissure, modèle phénoménologique de Tuutti (a) et le processus de corrosion du béton fissuré, modèle phénoménologique de François et al (b)

Le chapitre 4 présente dans une première partie les résultats obtenus à long terme en corrosion naturelle dans le cadre du benchmark des poutres de la Rance. En effet, les essais de corrosion basé sur de la corrosion naturelle sont extrêmement rare en raison du temps nécessaire pour obtenir une corrosion suffisante. Une synthèse du programme mis en place à Toulouse par R. François est ensuite présentée. Puis le nouveau programme expérimental à long terme mis en place dans le cadre de cette thèse est présenté. Ce programme reprend le mode et type de chargement ainsi que le type d'exposition par cycles au brouillard salin mais modifie le sens de coulage ainsi que la position dans l'enceinte à brouillard salin des poutres en béton armé. Les nouvelles poutres A sont coulées avec des armatures tendues en bas du coffrage et une exposition telle que la zone tendue soit la face inférieure par rapport à la pulvérisation du brouillard salin. Les nouvelles poutres B sont coulées avec les armatures tendues en haut du coffrage (et présente donc un défaut de mise en place du béton lié au ressuage dénommé en anglais par le terme « top bar effect ») et avec une exposition de la zone tendue en face supérieure par rapport à la pulvérisation du brouillard salin (voir figure 3)

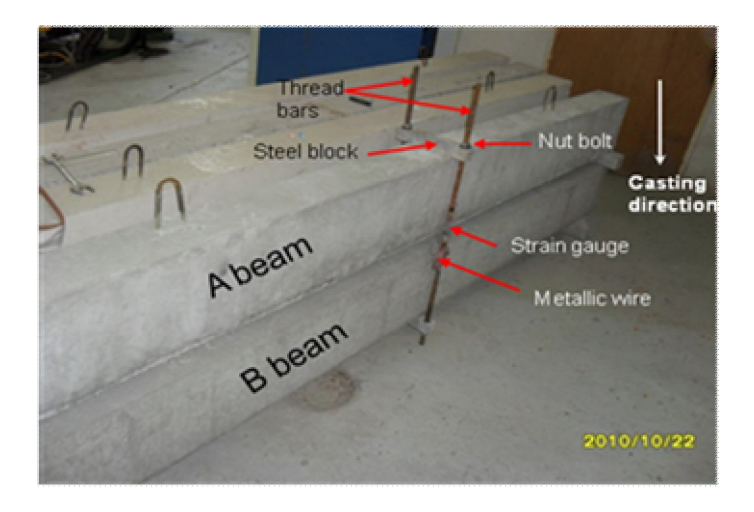


Figure 3 : conditions d'exposition des nouvelles poutres A et B mise en œuvre dans cette thèse

Les chlorures sont donc amenés à s'accumuler sur les surfaces supérieures des poutres qui correspondent à la face comprimée pour les nouvelles poutres A et à la face tendue pour les nouvelles poutres B. A noter que la face supérieure des nouvelles poutres B est protégée de la pulvérisation des chlorures par la présence au dessus de la poutre A (figure 4)

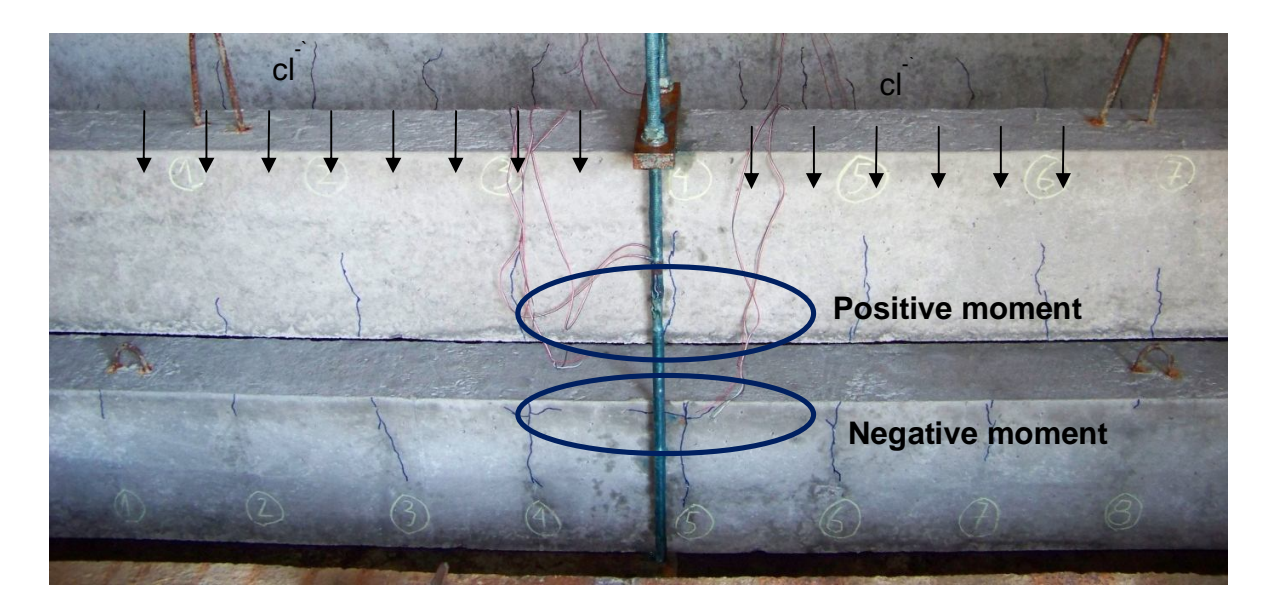


Figure 4: exposition aux chlorures des poutres A et B

Ce chapitre traite ensuite des premiers résultats obtenus à court terme (2 ans) sur le nouveau programme expérimental. Ceux-ci confirment l'initiation précoce de la corrosion en fond de fissure et ensuite la présence d'une phase dormante comme prévue par le modèle de François

et al., 2012 avec la reprise de la corrosion lorsque les chlorures atteignent les armatures à travers l'enrobage. Ce qui prend environ 1 an pour la zone tendue des nouvelles poutres B en raison des conditions d'exposition et ce qui n'est pas encore le cas pour les armatures tendues des nouvelles poutres A.

Le chapitre 5 traite de la carbonatation et de la corrosion en résultant dans des échantillons de mortier pré-fissuré. L'objectif de cette étude expérimentale est d'étudier les conditions de développement de la corrosion en fond de fissure. La démarche générale utilise un dispositif expérimental appelé le « cœur expansif » qui permet de générer des fissures d'origine mécanique d'ouverture contrôlée. Une large gamme d'ouverture de fissure a été étudiée : de 0 à environ 600 μ m pour couvrir le champ d'application concerné par les structures en béton armé avec les « petites » fissures inférieure à 40 μ m, qui se situent sous la valeur du seuil critique de fissuration, qui correspond à l'existence d'une interaction mécanique entre les lèvres des fissures et pour laquelle une restriction de l'accès des agents agressifs existe. Les fissures intermédiaires 40 μ m – 300 μ m qui correspond au domaine d'application des restrictions environnementales des règlements de calculs et des fissures plus large au-dessus de 300 μ m pour élargir le champ d'application et l'étude de la réponse en corrosion en fond de fissure.

Les échantillons utilisés dans ce programme expérimental sont constitués de mortier en forme d'anneau circulaire de 50 mm de hauteur, 150 mm de diamètre externe et 50 mm de diamètre interne. Desbarres d'acier HA (Haute Adhérence) de diamètre de 8 mm ont été utilisées comme renfort dans des échantillons. La barre en acier HA de forme circulaire avec un diamètre de 100 mm est maintenue à centre du moule.

Les échantillons ont d'abord été soumis à une carbonatation accélérée dans une ambiance à 50% de gaz carbonique et une humidité de 55% après séchage dans une étuve à 50°C pour une partie des éprouvettes ou sans séchage pour voir uniquement l'effet des fissures. Les résultats montrent qu'il y a toujours carbonatation des lèvres des fissures et que la carbonatation se propage tout le long de l'interface acier-béton à partir de l'intersection de l'armature annuaire avec les fissures transversales. Cette carbonatation de l'interface apparait très superficielle pour les faibles durées d'exposition en ambiance carbonique et laisse supposer une repassivation possible des armatures après un amorçage de la corrosion. Cependant ce résultat laisse aussi penser que la faible dimension des échantillons conduit à

un endommagement total de l'interface acier-béton après fissuration (ce qui correspond au cover controlled cracking initialement montré par Goto, 1971) qui serait alors différent de celui observé sur des poutres en béton armé : limité à la dizaine de premiers mm à partir de la fissure et ensuite généré à partir de la longueur de transfert comme montré par Castel et François, 2011.

Les échantillons fissurés et carbonatés sont ensuite mis en corrosion naturelle par une succession d'immersion dans l'eau et de séchage dans l'ambiance du laboratoire. Les résultats montre que la corrosion se développe à partir des fissures d'origine mécanique et conduit à la création de fissures de corrosion qui sont initiées à partir des micro-fissures d'origine mécanique présentent à l'interface acier-béton en raison du chargement mécanique et de la création des fissures do'rigine mécanique (le cover controlled cracking) comme le montre les figures 5 et 6.

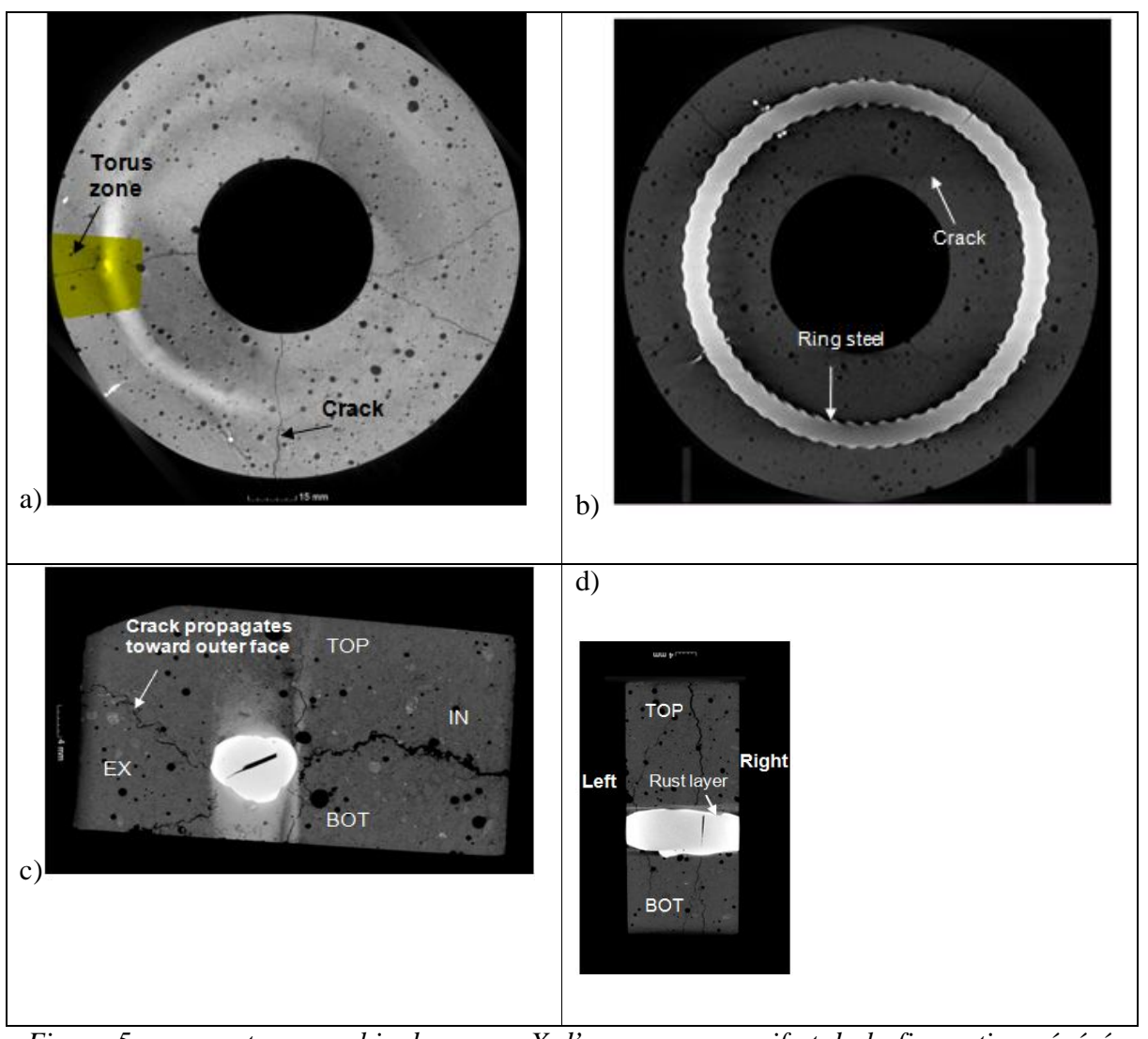


Figure 5 : vue en tomographie de rayons X d'un cœur expansif et de la fissuration générée par le chargement mécanique et par le développement de la corrosion

La figure 6 montre aussi que la corrosion due à la carbonatation est présente tout le long du périmètre de l'armature, ce qui est différent de la corrosion initiée par les chlorures, mais que cependant l'épaisseur de la couche de produits de corrosion n'est pas constante le long du périmètre. En particulier, l'épaisseur de la couche de rouille est plus importante sur la partie inférieure (par rapport au sens de coulage) de l'armature, ce qui correspond à la zone plus poreuse de mortier en raison du phénomène de ressuage et tassement du béton frais, et ce qui confirme l'influence de la qualité de l'interface sur le phénomène de corrosion. Le développement de la couche de rouille se traduit par une présence de Goethite à proximité de

l'armature et la présence de ferrihydrite au contact du mortier. Les analyses au microscope électronique montrent aussi qu'il y a une diffusion des produis de corrosion vers le mortier, créant ce qu'on appelle le milieu transformé mais aussi inversement une diffusion des ions calcium et de la calcite de la matrice cimentaire vers la couche de produits de corrosion.

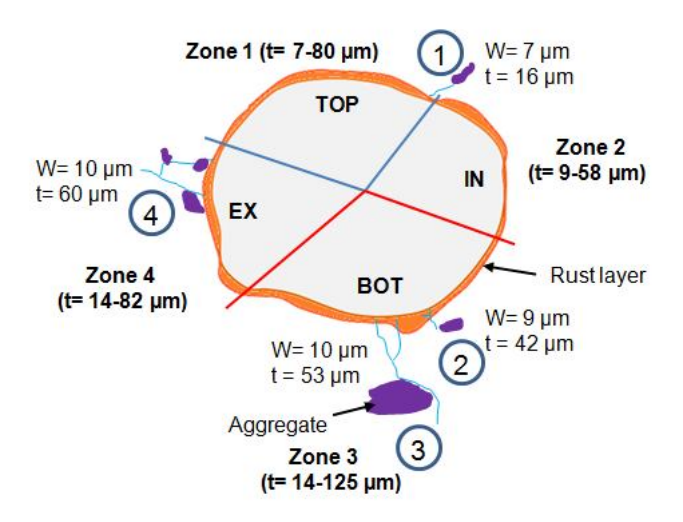


Figure 6 : vue de la section d'une armature avec le développement typique de la couche de produits de corrosion tout autour du périmètre et le développement des micro-fissures d'origine mécanique en fissures de corrosion due à la pression des produits de corrosion.

En conclusion, les résultats expérimentaux obtenus sur les éprouvettes armées annulaires sollicitées en traction par une pression interne jusqu'à obtenir des fissures d'ouvertures différentes comprises entre 0 µm et 600 µm permettent de préciser le processus de corrosion en présences de fissures d'origine mécanique.

- quelque soit l'ouverture de la fissure, le gaz carbonique atteint rapidement l'armature au niveau de son intersection avec la fissure et conduit à une carbonatation tout le long de l'interface. En présence d'humidité, il s'en suit un démarrage de la corrosion avec une propagation de long de l'interface acier béton sur toute la longueur de l'armature dans la zone qui est endommagée par la création de la fissure et la reprise des efforts de traction du béton vers l'acier.
- Le développement des oxydes dans la zone d'interface acier-béton autour conduit à la génération de contraintes de traction supplémentaires dans le mortier qui est déjà sollicité par la pression interne appliquée par le cœur expansif et donc logiquement au développement des

micro-fissures mécaniques (cover controlled cracking) en fissures de corrosion qui apparaissent alors à la surface extérieure de l'échantillon (initiées au niveau de la fissure mécanique) ou les contraintes de traction mécaniques sont les plus fortes. La quantité d'oxydes nécessaires pour fissurer l'échantillon est très faible (quelques dizaines de micro-m d'épaisseur suffisent).

En conclusion, cette thèse a confirmé la complexité du phénomène de corrosion des armatures, ainsi que la complexité de ses conséquences sur le comportement mécanique des structures.

Ainsi l'influence de la pré-fissuration sur l'initiation de la corrosion a été clairement confirmée mais la propagation de la corrosion est clairement dépendante de l'enrobage, des conditions d'exposition et de l'endommagement mécanique de l'interface acier-béton.

La corrosion modifie la loi de comportement de l'acier en traction, avec une augmentation du coefficient d'écrouissage qui modifie le ratio entre la contrainte ultime et la contrainte élastique de l'acier. Mais plus important encore, la corrosion réduit l'allongement maximal à rupture ce qui conduit à une rupture prématurée et fragile de l'acier et donc de l'élément en béton armé. Les caractéristiques résiduelles de l'acier apparaissent ainsi ne plus respecter les prescriptions des codes de calcul tels que l'Eurocode 2 et posent clairement le problème de la requalification des structures corrodées.

Le comportement vis-à-vis de la résistance en flexion confirme que la perte de section d'armatures est le paramètre essentiel qui contrôle le changement de capacité vis-à-vis du palier plastique ou de la charge ultime. La prise en compte du changement de ductilité des aciers tendus en raison de la corrosion peut aussi permettre de prédire la flèche maximale à rupture.

Le comportement vis à vis de l'effort tranchant déjà complexe dans le cas des structures saines, apparait au moins aussi complexe en présence de corrosion. Les méthodes classiques de dimensionnement apparaissent largement insuffisantes pour prévoir le comportement de la structure saine et encore plus éloignée en présence de corrosion. Les calculs basés sur un treillis bielle de compression-tirant semblent beaucoup plus réalistes. Cependant, un travail important sur la modélisation reste à faire.

GENERAL INTRODUCTION

Reinforced concrete (RC) is a very versatile, useful and widely used composite building material consisting of concrete and embedded reinforcement. Concrete, in an un-cracked condition, provides an effective cover to protect reinforcement from corrosion. The high alkalinity of concrete pore solution places reinforcing steel in a thermodynamically passive corrosion region where corrosion rates are practically negligible. Additionally, concrete provides a dense covering material over reinforcement, which delays the ingress of various aggressive substances such as chloride ions, carbon dioxide, moisture, oxygen induced reinforcement corrosion. Reinforcement is typically provided by high bond reinforcing steel bar to produce controlled cracking in tensile zone of RC members because of the lack of resistance of concrete in tension but this reinforcement is vulnerable due to chloride attack or carbon dioxide contamination of concrete.

Cracking of concrete and reinforced concrete may occur due to service loads and various physical and chemical processes. In particular, mechanical load-induced cracking is unavoidable in RC. The existing of crack can enable rapid ingress of aggressive substances and an accelerated depassivation of reinforcing steel leading to corrosion initiation. Nevertheless the conditions of propagation of corrosion after this initiation at crack tip, is still in debate. In particular, the micro-cracks at the interface between two materials generated by loading can develop to be larger cracks when steel bar corrodes or favor the propagation of corrosion. Another important point concerning the propagation of corrosion in cracked concrete is the location of cracked tensioned concrete surface in regard with chloride attack: in particular, horizontal upper surface appears to be the worse conditions.

Reinforcement corrosion causes a loss of the bar diameter which can affects adversely the mechanical properties of steel bar in terms of its ultimate strength, yield strength and ductility. Moreover, when reinforcement corrodes, the corrosion products occupy a much larger volume than original steel, and eventually exert a large force on the concrete surrounding it to cause cracks. If corrosion cracks propagate to surface of structures, the concrete cover could be spalled off. In addition, corrosion of the reinforcing steel causes changes in the environment at the steel-concrete interface, and both layer of the corrosion

products and de-confinement due to opening of corrosion cracks cause loss of bonding at the steel-concrete interface. The bond strength between reinforcement and concrete diminishes progressively as corrosion of reinforcement processes. This affects importantly the load response and deflection of RC. The mechanical performance of corroded RC beams has been studied by many authors since the 1970s and this research has contributed significantly to the increase in knowledge of the behaviour of corroded RC structures. Almost all investigations show that corrosion can reduce both the deflection and ultimate strength of RC members and these reductions can lead to premature failure of beams. It is very important to have the reliable information on both the load bearing capacity and the serviceability of corroded RC beams to promote the validation of future mechanical models and reduced uncertainties due to numerical simulations. But most studies available are based on accelerating the corrosion by applying an anodic current to rebar which correlation with real on-site corrosion is very limited. Moreover, very limited studies dealing with the behaviour of naturally corroded structures can be found at this moment. The major highlight of this thesis is the use of naturally long-term corroded RC members kept under sustained loading in chloride environment. Another important aspect of the research work presented is the study of the shear capacity in relation with both longitudinal (tension) and transversal (stirrups) reinforcement corrosion.

The main objectives of this thesis are:

- 1, to study the mechanical behavior of naturally long-term corroded RC beams in both flexure and shear aspect including modes of failure and deflection, ductility.
- 2, to examine the behavior of corroded reinforcement and to compare it with non-corroded reinforcement in terms of ultimate stress, yielding stress, strain and ductility, elastic modulus.
- 3, to study the corrosion initiation and propagation of pre-cracked RC elements in chloride and carbon dioxide conditions.

This study is experimental investigations on "naturally" corroded RC beams and on carbonated ring-shaped mortar samples reinforced with deformed steels. Based on experimental results, several findings are drawn. The following is a brief description of the contents of each chapter in the thesis:

<u>Chapter I:</u> This chapter covers literature review on the bond behavior between corroded reinforcement and concrete, mechanical properties (stress, ductility) of corroded reinforcement inside concrete and load-carrying capacity of corroded RC beams. The technique for measuring corrosion degree, effect of corrosion type: natural or accelerated corrosion on the structural damage are also discussed.

<u>Chapter II:</u> This chapter describes the experimental program conducted at the LMDC - Toulouse to test two long term corroded RC beams and two control RC beams at the same age of 27 years. The flexural and shear behavior of the tested beams are discussed. The modes of failure and ductility of beams are also described.

<u>Chapter III:</u> The available literature review on steel corrosion in carbon dioxide and chloride is reviewed. The change in concrete or mortar characteristics is highlighted. The influence of pre-cracks on the ability of carbon dioxide to diffuse along a crack and then carbonation along the steel-concrete interface is mentioned. Furthermore, the evolution of corrosion products under natural environment or carbon dioxide in the laboratory is presented.

<u>Chapter IV:</u> This chapter presents the experimental program on RC beams built during the thesis. It includes twelve RC beams, coupling each other under loading during corrosion process. A visible observation on corrosion cracking and chloride profile on two beams are described and first results are discussed.

<u>Chapter V:</u> The experimental results in carbon dioxide environment, tested on ring shaped mortar specimens, are presented. The initiation and propagation corrosion as well as the formation of rust layers in presence of pre-cracks are discussed.

Finally, the general conclusions are introduced.

The chapter II and chapter V consist of several research papers, which are either already published in an international journal or in the process of publication. In order to keep in their original format in this thesis, there are repetitions of some sections, e.g. experimental context, exposure conditions, material properties etc.

References: All the references used in chapter I and IV are given at the end of each chapter. For chapter III, since it covers two different sources of corrosion: the corrosion in carbon dioxide and the corrosion in chloride, the references are listed at the end of each part.

Part I:

Mechanical consequences of corrosion on the behavior of RC elements

Chapter I:

LITERATURE REVIEW ON MECHANICAL BEHAVIOR STUDIES

GENERAL

This chapter reviews the effect of corrosion on the concrete-steel interface bond stress, on mechanical properties of steel embedded in concrete and on mechanical behaviour of RC beams from previous works. Firstly, the impact of corrosion on bond stress between concrete and rebars is presented. The test procedures and results are discussed. The part describing the behaviour of corroded steel bars is highlighted. It is important to understand that the corrosion influences the shape of cross-section of rebar, the shape of stress-strain diagram as well as the stress and total elongation. Finally, the flexural behaviour of corroded RC beams is analyzed in two cases: corrosion in the absence of load and corrosion under a sustained load. The load-carrying capacity along with failure mode of corroded RC beams is considered. This chapter gives a clear idea needed for studying the RC beams that corroded "naturally" in chloride environment in the long-term.

I.1. EFFECT OF CORROSION ON BOND BETWEEN STEEL BAR AND CONCRETE AND STEEL BAR BEHAVIOR IN DIRECT TENSION

The behavior of a Reinforced Concrete (RC) member is considerably influenced by the bond stress between the concrete and reinforcing steel, yield strength as well as ductility of steel bar. This section presents some results on the effect of corrosion on bond and steel bar behavior in tension based on previous studies.

I.1.1. Effect of corrosion on bond between concrete and re-bar

Because initial bond depends on geometrical characteristics of RC cross-section, it is important to remind these main aspects to have a better understanding on change of bond due to corrosion. The main geometrical effect of RC cross-section on bond is the "top-bar effect".

I.1.1.1. Top-Bar effect of RC structures corroded

One of the most important issues of RC structures is the loss of steel-concrete bond when casting the deep concrete members having the horizontal reinforcement bars perpendicular to the casting direction. This phenomenon is called the top-bar effect because the horizontal reinforcements located near the top-casting surface are the most affected. It can state that the reduction of bond strength is a function of concrete depth under steel bars. Explaining for this phenomenon, A. Castel et al. [1], Masayuki Hoshino [2], Geoffrey B.Welch and Bruce J.F.Patten [4] interpreted that there are two reasons herein: first, the settlement of fresh concrete leads to the formation of voids under fixed horizontal bars, which reduces the bond strength; secondly, the bleeding water tends to stay on the lower steel-concrete interface, thus increasing the size of voids at these locations when this trapped water evaporates. Subsequently, the local quality of the bond between the two materials is significantly deteriorated.

In design codes such as ACI 318-08 or EC2-2002, the top-bar effect is taken into account by applying a location factor ψ_t or a coefficient related to the quality of the bond condition and the position of the bar during concreting η_1 . Accordingly, ACI 318-08 requires the location of the horizontal reinforcement such that more than 12in. (30cm) of fresh concrete is cast below, the development length need to increase by 30%; EC2-2002 [25] requires the reduction of the ultimate bond stress up to 30% of the design value of the ultimate bond stress where the deep section is more than 25 cm. Many publications [3, 4, 6-10] reported on the effect of debonding at steel-concrete interface with respect to bar-placement in concrete and corrosion of embedded steel bars.

Tayfun A. Soylev and R. François [7-9] conducted a series of experiments on the relationship between corrosion of reinforcement and presence of voids at steel-concrete interface. The authors made five panel elements from a plywood formwork with 200 cm high and cross section of 20 x 20 cm. Each panel has 13 horizontal re-bars with the centre to centre spacing of 15 cm. Smooth round steel bars (Φ =10 mm) were used. After curing for 28 days at 100% RH, each panel was cut into 13 prismatic specimens with a steel bar at the centre of each prism as shown in Fig. I-1.

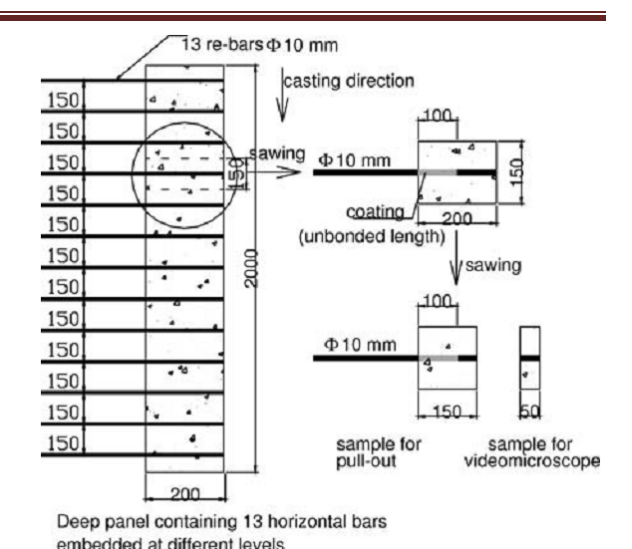


Fig. I-1. Specimen details for testing [7]

Next, each prismatic specimen was sawed into two parts of 15 and 5 cm, which were subjected to pulling-out test and video microscope examination, respectively. The sample concrete used to assess corrosion were subjected to wetting-drying cycles. In each cycle, the samples were put under the NaCl solution of 35 g/l for one week, and then kept in laboratory conditions for 4 weeks. After 11 cycles, the samples were broken out and measured corroded surface area. From this study, researchers pointed out two important results: first, the correlation between the height of concrete members and ultimate bond strength (τ_{max}) at steel-concrete interface; secondly, the effect of debonding at steel-concrete interface on steel bar corrosion. The ultimate bond stress reduces as a function of the concrete depth below the horizontal bar. This means that the number of voids and size of ones at the bottom part of the bar increase along the height of members. Consequently, the corrosion rate of steel increases along the concrete section height. These results showed clearly that the role of voids (defects) at interface between steel and concrete has a significant effect on the ability of corrosion initiation of embedded steel reinforcement.

Tarek Uddin Mohammed et al. [10-12] studied the reinforced concrete specimens that were accelerated the corrosion in the laboratory and others that were exposed to tidal environment for long period. The samples in the laboratory had the dimension of 12 x 23 x 28 cm. The steel cage is composed of one stirrup and four main steel bars. The stirrup was made of six steel elements: two vertical elements were parallel with the casting direction and four horizontal elements were perpendicular to the casting direction. All of the steel elements are

glued by epoxy and isolated electrically inside the concrete. The detail of samples is shown in Fig. I-2.

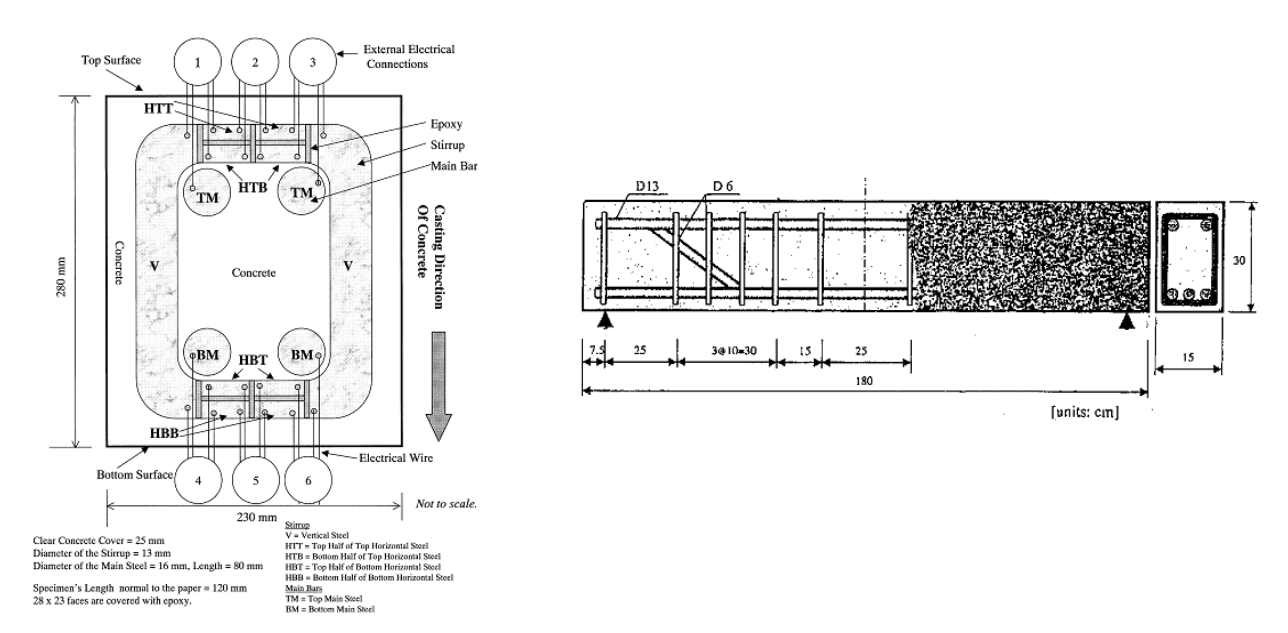


Fig. I-2. Details of specimens in laboratory (left) [10] and in marine environment (right) [11]

28 day after curing, the specimens were kept in a closed chamber subjected to an automatic wetting (24 h) with spraying 3.5% saltwater and drying (60 h) with temperature of 60°C and 80% RH. The samples in marine environment (for 23 years) compared with samples in the laboratory were 6 uncracked concrete beams, size of 15 x 30 x 180 cm as shown in Fig. I-2. They concluded that gaps under horizontal reinforcement steels perpendicular to the pouring direction of concrete are always existed. The presence of gaps at steel-concrete interface is very important to initiate and propagate corrosion of steel in concrete.

Fig. I-3 presents qualitatively the development of corrosion around a steel bar embedded in concrete according to casting direction concrete. It could be noticed that the lower half of reinforcement may be more serious corroded with respect to upper half as remarked by T.A. Soylev and R.François [9]. The air voids, formed below the steel bars, were filled up with corrosion products. However, the upper surface of steel is the nearest to concrete cover that allow the ingress of more chloride ions. The oxides developing on this would disperse the

surrounding concrete. Then, the corrosion cracks were generated by expanding volume of rust. The formation of corrosion cracks could offer the poor confinement between concrete and reinforcement, which reduces the bond stress. Nevertheless, the appearance of rust products could also offer resistance to slipping of steel reinforcement and so increasing the bond strength. A heterogeneous corrosion type around rebar perimeter may still be assure the perfect bond between two materials.

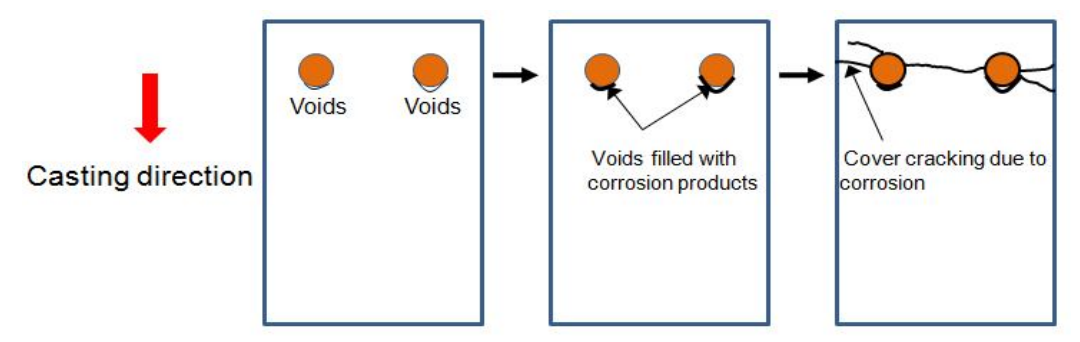


Fig. I-3. Impact of location around perimeter of steel bar on its corrosion process

I.1.1.2. Effect of corrosion on bond between concrete and re-bar

Bond between reinforcement and concrete is vital to ensure the general performance of two materials. When the external load applies to a reinforced concrete member, there is a transfer of force between concrete and rebar in order to withstanding both compression and tension forces. This transfer of force produces bond stresses. The bond between steel bar and concrete is influenced by several parameters, such as concrete cover depth, concrete strength, stirrups, lateral pressure, shape of rebar and the yielding and spacing of reinforcement bars [13].

As the steel bar is corroded, the increase of volume of the corrosion products results in a "bursting" pressure on the surface of the bar and the surrounding concrete, which induces longitudinal splitting cracks in the samples. The higher the corrosion levels the wider the crack widths. At high corrosion level, this leads to the breakdown of bond and friction at the steel-concrete interface. However, at low corrosion level, corrosion products will improve the bond at the steel-concrete interface due to increased diameter of a corroded rebar forming from products of rust. Corrosion may display localized pitting and loss of the height of the

ribs over the bar length, thereby making weak the rib-concrete mechanical interlocking force transfer mechanism.

Fig. I-4 [13] shows the influence of corrosion on bond strength and load carrying capacity of RC members.

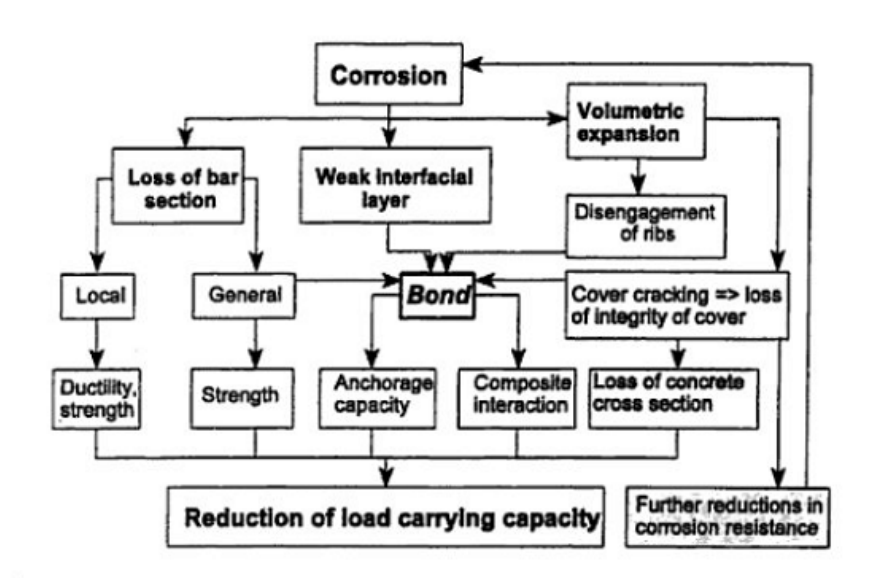


Fig. I-4. Effect of corrosion on residual load carrying capacity [13]

Several literatures [14-18] related to this problem will be discussed below.

I.1.1.3. Research by G.J.Al-Sulaimani et al. (1990) [14]

An extensive experimental program was conducted by G.J.Al-Sulaimani et al. [14] in which four test series were carried out on various specimens with different composition of the concrete matrix. The first two series were the cubic samples of size 15x15x15 cm containing centrally embedded bars to test pullout. The final series were the RC beams of dimensions $15 \times 15 \times 100$ and $15 \times 15 \times 300$ cm with an embedment length of 144 mm and 300 mm, respectively to study corrosion-bond behavior for beams.

To speed up the corrosion process, a constant current density of 2 mA/cm² was impressed on embedded steel in pullout or beam samples. The bond-corrosion relationship was recorded at four stages of corrosion: non-corrosion, corrosion corresponding to pre-cracking,

cracking, and post-cracking. Plot of bond stress against free-end slip in pullout test for 10 mm bars corresponding to four corrosion stages is shown in Fig I-5. The best bond stress was exhibited by the samples having the loss of bar weight of 0.87%. The bond strength value at corrosion level of 0.87% is about 1.5 times as high as that of 0% (no corrosion). Likewise, there is an increase in the bond strength at pre-cracking corrosion level of 1.5% in comparison with this at corrosion level of 0%. This can be explained because of increased surface roughness of bars with the growth of rust products that tend to enhance the holding capacity of the bar. Another way to express the relation between bond stress and corrosion level for pullout tests are shown in Fig. I-6.

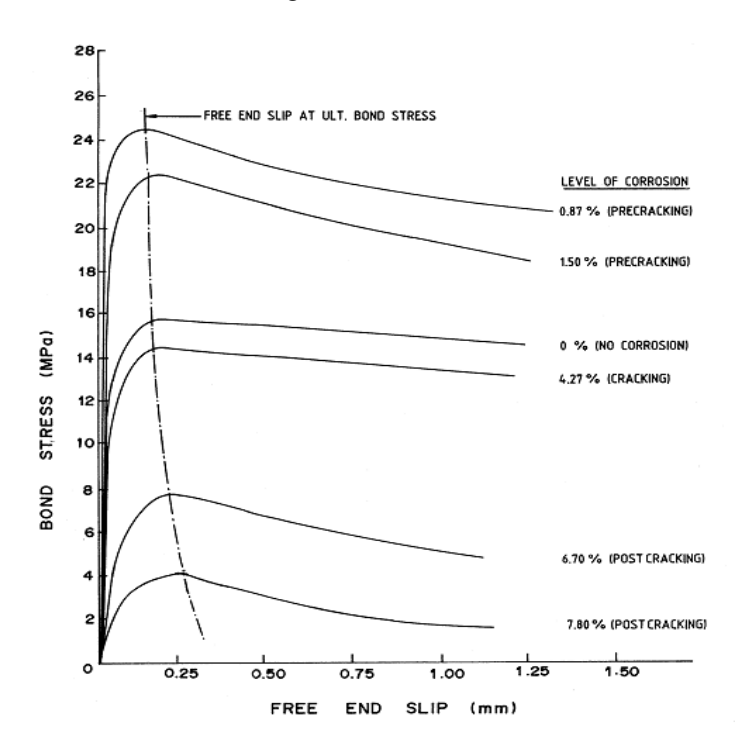


Fig. I-5. Bond stress-free end slip relation for different levels of corrosion, 10 mm bar (cubic samples) [14]

Fog. I.6 shows that the bond strength grows with the growth of percentage of corrosion up to around 1% of mass loss of steel. At higher corrosion levels, the bond stress drop markedly until it can be negligible at mass loss of steel of about 8.5%, 7.5%, 6.5% post-cracking corrosion for 10, 14, 20 mm bars, respectively.

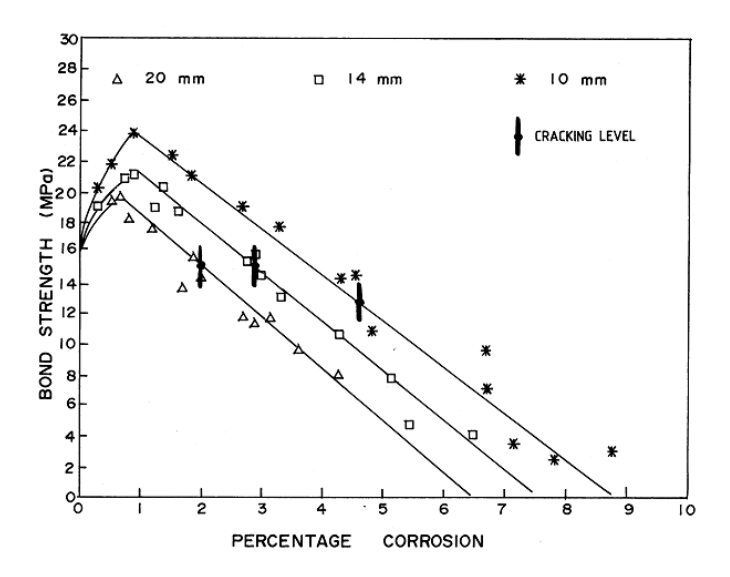


Fig. I-6. Bond stress versus level of corrosion, (cubic samples) [14]

For beam tests such as series of samples 15 x 15 x 100 cm, a similar trend is also observed in Fig. I-7. From Fig. I.7, it is seen that the bond stress increases 1.34 times versus un-corroded sample as corrosion level increases up to 0.5% and then decreasing as corrosion level increases over 0.5% even when beam samples were not enough development length (144 mm long compared to 300 mm long upon request from ACI 318-83). Interestingly, up to 5% corrosion level, the pullout test generated the bond stress equalizing to 0% corrosion level. The researchers also shown that in beams with adequate extending length, the bond value for various degrees of corrosion was lower than that in beams with insufficient development length for similar corrosion rate. A possible explanation is that the bond stress at the steel-concrete interface, in this case, transmitted on a shorter embedded length.

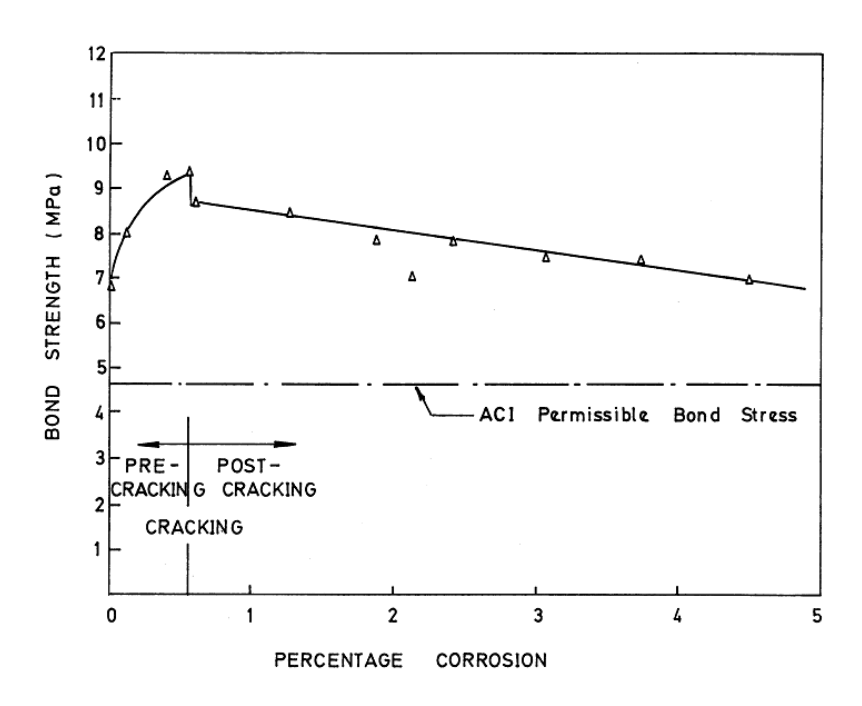


Fig. I-7. Bond stress-level of corrosion relation, (beam samples 15x15x100 cm) [14]

Increasing the bar diameter implied the higher bursting forces resulting from the corrosion process cause cracking of the concrete, whereas the thickness and quality of concrete cover over the reinforcement characterize the resistance to the splitting corrosion forces. Thus, cover thickness/bar diameter C/d_b ratio is a significant corrosion protection parameter. In this work, they found that about 4% rebar mass loss due to corrosion was needed to initiate cracking for a diameter C/d_b ratio of 7, meanwhile only 1% mass loss was found to be sufficient to crack the concrete cover with a C/d_b ratio of 3. These results clearly point to the need for careful detailing of C/d_b ratio for protection against corrosion in structural concrete.

I.1.1.4. Research by Abdullah A.Almusallam et al. (1996) [15]

In their work "Effect of reinforcement corrosion on bond strength", they studied the effect of reinforcement corrosion on the ultimate bond strength and slip at the steel-concrete interface, together with effect of size and shape of rib on ultimate bond strength in corroded RC members. The cantilever specimens of size 152x254x279 mm with a 12 mm diameter deformed bar were selected. The steel frame was constituted by two compression steels of

254 mm long and four U-shaped stirrups. The compressive strength of concrete at 28-day was 30 MPa. The cross section and reinforcement details of test specimens are shown in Fig. I-8.

To accelerate reinforcement corrosion, the samples were partially immersed in water but the steel bar was totally above the water level; simultaneously a constant high current of 0.4 A (10.4 mA/cm²) was applied to the reinforcement surface. The correlation between ultimate bond strength and corrosion level are graphically illustrated in Fig. I-9. The results of their study demonstrated that prior to corrosion cracking stage the ultimate bond stress increases up to 17% as the degree of corrosion increases from 0% to 4%. This phenomenon occurs similarly to G.J.Al-Sulaimani's test [14]. Notwithstanding, the corrosion level at which the best bond strength could reach is dissimilar, 1% for G.J.Al-Sulaimani's test and 4% for A.Almusallam's test. This is due to the difference in diameter bar, C/d_b ratio, and dimension of sample. Nevertheless, the bond stress falls sharply by around 71% in cracking stage (levels of corrosion ranging between 4% and 6%). This is attributed to a decrease in radical pressure of surrounding concrete to reinforcement steel due to cracking concrete cover. The bond still remains due to the friction between rust layer and concrete along with the effective ribs of bars. Fig. I-10 presents the relationship between ultimate bond strength and rib profile corresponding to various corrosion levels.

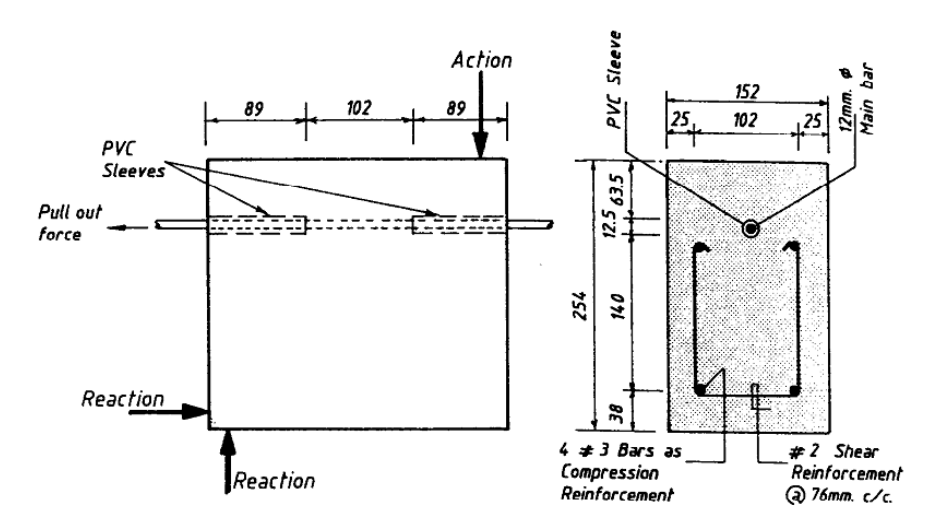


Fig. I-8. Specimen detail for testing [15]

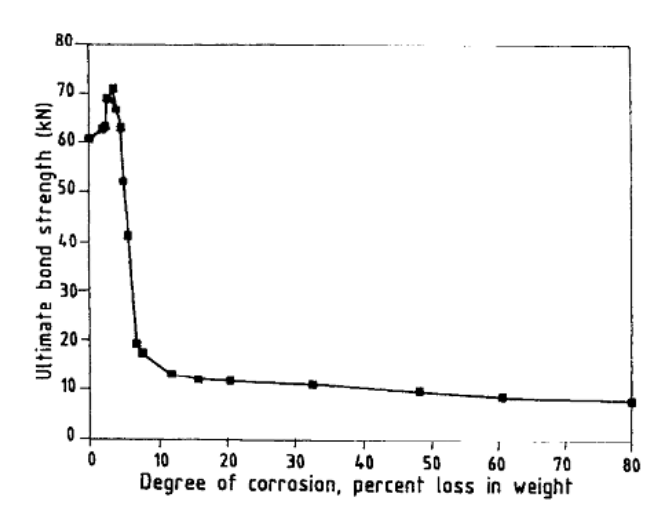


Fig. I-9. Ultimate bond strength at different degrees of corrosion [15]

In theory, a reduction in rib profile will decrease the ultimate bond strength due to the decrease in the mechanical interlocking of concrete around the bar [60]. Yet from Fig. I-10, it was observed that as the height of ribs diminished up to 26%, corresponding to 4% of corrosion degree, the ultimate bond strength increased by about 17%.

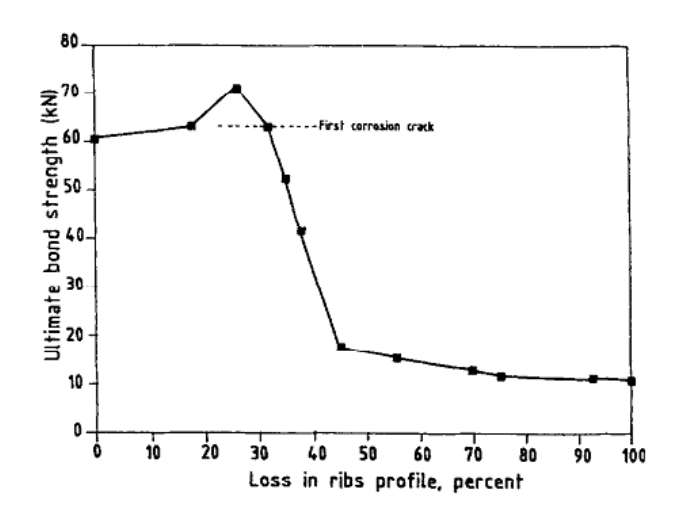


Fig. I-10. Influence of loss of rib profile on ultimate bond strength [15]

The reason for this is that at beginning of corrosion stages, the increase in both the roughness of bars and the confinement of the bar with the concrete dominated the reduction in geometry and size of ribs leading to the increase in bond strength in this stage. At higher corrosion levels, due to the formation of new cracks and a significant degradation in rib profile, the bond capacity dropped remarkably and the working of deformed bars was more and more similar to the plain bar. Finally, if loss rate of rib profile beyond around 45%, it can be seemed that the interlocking action at steel-concrete interface is nearly negligible. They also recorded no significant change in the bond strength from 45% to 100% rib degradation.

I.1.1.5. Research by P.S.Mangat et al. (1999) [16]

A study on the bond of steel with concrete was conducted by P.S.Mangat and M.S.Elgarf. Differing with Abdullah A.Almusallam's experiments, they carried out the test on RC beams of dimensions 100x150x910 mm. Each beam composed of two half length of 430 mm, interconnected at the bottom by two deformed steel bars, each of 10 mm diameter and 1100 mm in length as shown in Fig. I-11. At the top of the middle of each beam, two steel hinges with high toughness were attached to a 3mm thick steel plate by the bolts in order to allow for rotation of two concrete blocks. The concrete composition with 1% NaCl by weight of cement was made. The compressive strength of the concrete after 28 days was 45 MPa.

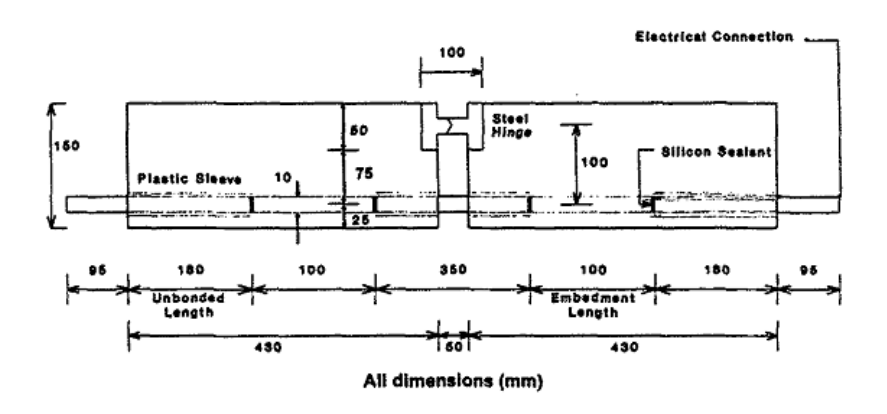


Fig. I-11. Details of beams for testing [16]

15 days after casting, the samples were subjected to accelerated galvanic corrosion systems and immersed in a 3.5% NaCl solution. A direct current of intensity of 0.8 and 2.4 mA/cm² was applied to the surface of rebar with the duration ranging from 14.4 hrs to 80 hrs. At the age of 28 days after casting, the beams were tested under four-point bending to verify the relationship between external load and free-end slip at various corrosion degrees (Fig. I-12). They suggested that at corrosion degrees from 0% to 0.4%, no free-end slip occurred at steel-surrounding concrete interface until the bond was breakdown completely corresponding to the appearance of longitudinal cracks of 0.05 mm wide. Moreover, the maximum load carried by beams increases up to 25% with an increase in level of corrosion of up to 0.4%. For the beams with higher corrosion of 0.4%, there are three behavior stages of load-slip relationship. The first stage conforms to a very small slip at very low loads. The second stage corresponds to increasing slightly in free-end slip of rebar as the load rises up to the maximum load. The third stage agrees with increasing the slip soon after reaching the peak of the load. These were also observed by [14, 15].

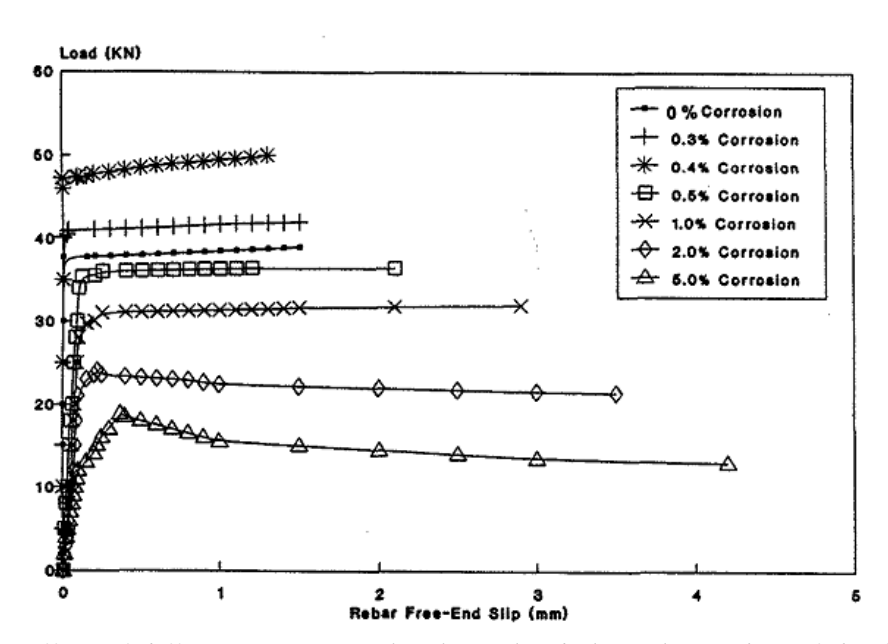


Fig. I-12. Effect of different corrosion levels on load-slip relationship of the flexural tests [16]

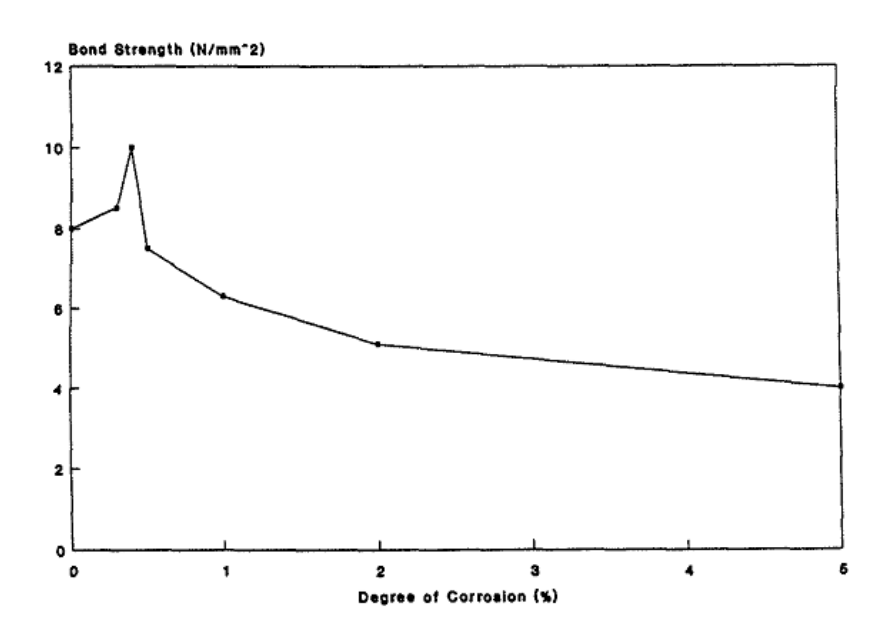


Fig. I-13. Effect of different corrosion levels on bond strength [16]

Fig I-13 shows the effect of degree of corrosion on the bond strength of beams. The best bond strength obtains from 0.4% corrosion degree of reinforcing steel. With $C/d_b=2$, this result is coincided with G.J.Al-Sulaimani et al.'s result [14] for sample beams ($C/d_b=2.4$) (Fig.I-6). Above 0.4% degree of corrosion, the bond plunges with higher degree of corrosion. Unlike G.J.Al-Sulaimani et al.'s data [14] (Fig.I-6), at a corrosion level of 5%, the bond strength is reduced by over 50% the capacity bond of uncorroded beams. This reduction is due to the fact that longitudinal cracking widths are more than 0.2 mm wide, which result in a loss of confinement of the concrete-steel interface.

I.1.1.6. Research by Congqi Fang et al. (2004) [17]

In this work, forty specimens of size 140x140x180 mm were tested to evaluate the effect of corrosion on bond and bond-slip behavior. They were reinforced with a 20 mm diameter smooth or deformed reinforcement at central cross section. Two groups with and without stirrups were used to evaluate the influence of confinement of the steel bar on the ultimate bond strength and free-end slip for various degrees of corrosion under pullout loads. The average compressive strength of the concrete after 28 days was 52.1 MPa. To aid

reinforcement corrosion, the samples were then soaked in a 5% NaCl solution for 3 days. Thereafter, a direct current (40 mA/cm²) was impressed on the steel bar, as the specimens were under saltwater in a plastic tank. The corrosion time and time of initiation crack for each sample were recorded. The results clearly highlight that for deformed bars without stirrups, bond strength decreased with the increase in corrosion degree. The authors also agreed that when the corrosion degree was very low, bond strength increased as the corrosion degree increased. Nevertheless, they did not reveal how much the critical corrosion degree value in which the bond strength increases in comparison with non-corroded samples. Meanwhile, for deformed bars with stirrups, corrosion level had no substantial effect on the bond strength even when corrosion level was up to 6% (by mass loss) (Fig. I-14). This almost contrasts to Abdullah A.Almusallam's outcomes [15]. The same thing was happened with round bars with stirrups at a corrosion degree of 5.2%. These imply that effect of steel bar profile and stirrups on bond strength in corroded steel is quite powerful, particularly for deformed bars.

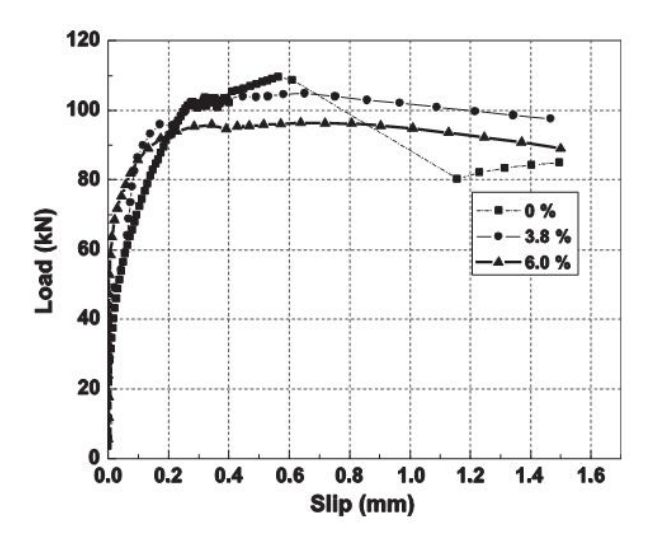


Fig. I-14. Effect of different corrosion levels on slip for deformed steel bar with stirrups [17]

Stirrups seem to have an important effect because of the control of the longitudinal cracking due to corrosion: indeed theses corrosion cracks are perpendicular to the stirrups.

I.1.1.7. Research by Lan Chung et al. (2004) [18]

The programme involved testing seventy RC slab specimens of dimensions 90 x 500 x 1100 mm. Each slab was reinforced with five 10 mm diameter steel bars in tension with 25 mm concrete cover to the tensile face spaced at 100 mm centre to centre along the length of slab shown in Fig. I-15. Three middle bars were arranged with different lengths to simulate different development length for them. All samples were divided into three groups: Group I, Group II, Group III. Each group had the various development lengths of steels I and II and various corrosion levels. The main aim of this study is to examine the effect of corrosion levels on bond strength and development length in the one-way flexural members. The 28 day compressive strength of concrete was 18.8 MPa. To facilitate rapid corrosion, the accelerating admixture was added at a rate of 3% by weight of cement and a high water-cement ratio of 0.547 was used. One day after casting, the slabs were demolded and instantly kept in 3% salt solution. After sinking at least three days in saltwater, a direct current induced corrosion along the bar was applied. The magnitude of corrosion was measured using percentage mass loss.

The RC slabs were tested under four-point bending with a constant moment region of 100mm in middle after being subjected to accelerated corrosion. From this study, it was concluded by the authors that 2% corrosion level is the critical corrosion level effecting bond strength, that is to say the bond stress tends to increase as the corrosion level increases up to 2%. Following 2% of corrosion degree, due to the reduction of rib height and loss of cross-section, the bond stress rapidly decreases (see Fig. I-16). For slabs designing insufficient development length, the failure pattern is pullout when the bond stress reaches maximum bond strength. For slabs designing sufficient development length, the pullout is likely to occur as the corrosion rate is greater than 2% because of debonding at concrete-steel interface. At this time, crack width and deformation of slabs increase fast.

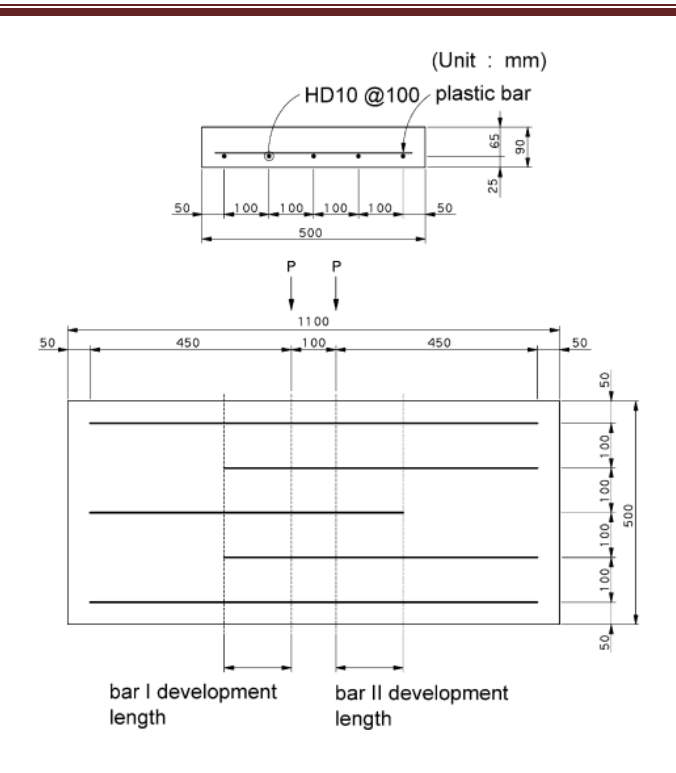


Fig. I-15. Details of slab specimens [18]

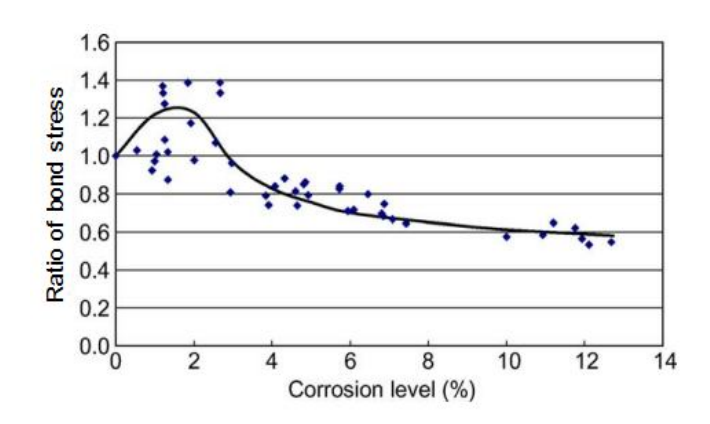


Fig. I-16. Ratio of bond stress vs. corrosion level. [18]

I.1.1.8. Research by D.Coronelli et al. [69] and K.Z. Hanjari et al. (2010) [70]

A study on anchorage capacity of a corroded reinforcement was conducted by D.Coronelli et al. [69] and K.Z. Hanjari et al. [70]. Twenty two beam-end specimens were cast using a concrete grade of C30/37. The specimens were reinforced with the main

longitudinal reinforcement of 20 mm diameter and the transverse reinforcement of 8 mm. The main rebars were embedded in the concrete over a 210 mm length. Two sample types were examined, with and without stirrups. The sample geometry and arrangement of steel bars are displayed in Fig. I-17. The average cubic strength of concrete curing 28 days at 20°C and 50% RH was 37.5 MPa without chlorides and 34.3MPa in the mix with 3% chlorides.

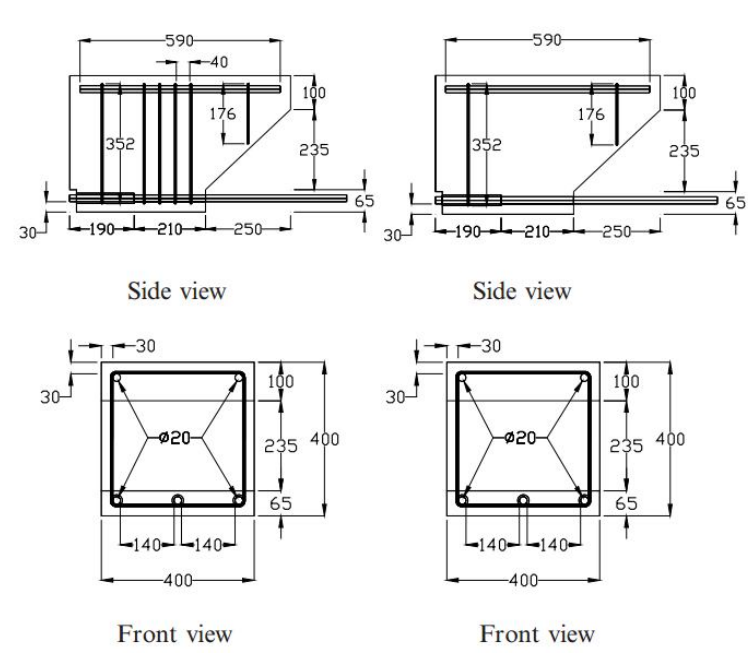


Fig. I-17. Details of beam ends for pull-out test, with stirrups-type A (left) and without stirrups-type B (right) [69]

The beam-ends were subjected to the accelerated corrosion by impressing a direct current of 1.43 A/m² (0.143 mA/cm²) to reinforcement during 7 months. For samples with stirrups (type A), the stirrups were isolated using electrical tape to avoid corroding. The goal is to show the influence of stirrups on anchorage capacity in the pull-out test. Table I-1 presents the anchorage capacity (bond stress) slip at the maximum anchored force. The experimental results clearly indicated the important effect of stirrups on bond stress at concrete-rebars interface. In case of reference specimens, the 15% loss of bond stress observed in samples without stirrups compared with samples with stirrups.

Table I-1. Comparison of bond strength and slip of reinforcement for two sample types

Specimen	Tested bar	Corrosion condition	τ _{max} (Mpa)	Slip at τ_{max} (mm)	
Type A with stirrups	Corner	Reference	5.05	0.36	
	Comer	Corroded	5.52	0.13	
	Middle	Reference	8.11	0.17	
		Corroded	6.44	0.09	
Type B	Corner	Reference	4.34	0.08	
	Comei	Corroded	2.64	0.02	
	Middle	Reference	7.05	0.13	
	whate	Corroded	6.08	0.06	

This reduction was even greater (up to around 50%) when the level of corrosion of main steel bars was 8.5% (by weight loss). Interestingly, with stirrups-reinforced specimens at low amount of corrosion (0.73%), a slight increase (9%) in bond resistance was noted. However, this beneficial effect will be lost at higher corrosion levels. The authors also showed that the position of main bar had a significant influence on the bond strength. These findings were recorded in an earlier research by D.Coronelli [71].

I.1.1.9. Summary

A number of studies into the variation in bond strength as corrosion progresses have been undertaken by using various test methods and exposure conditions. In general, there are two experimental categories namely pullout tests and flexural tests, which were widely used by many researchers in the past. The specimen conditioning in the majority of tests was nearly similar. They used the same techniques to accelerate the corrosion process in order to shorten the corrosion time. Some authors preferred to mix concrete with chlorides ranging from 1% [16] to 5% [17] by weight of cement then curing samples in ponds with NaCl solution with concentration of 3% [18] to 5% [17] parallel with it a constant current was applied to the rebar. While others made their specimens without mixing chlorides into concrete mixture but then the samples were wholly or partially immersed in water subsequently applying a constant current density of 2mA/cm² [14] to 0.4A/cm² [15]. These

corrosion methods lead to the difference in bond behavior of corroded samples as mentioned earlier.

In addition, the selection of type of specimens for bond test is very important as it significantly influences the bond characteristics. For pullout specimens, the presence of stirrups increases the confinement of steel bars in concrete; therefore, perhaps the corrosion rate slightly affects the bond stress between concrete and reinforcing steel [17, 70]. Although the pullout test [14, 15, 17, 69, 70] is easier way to test the bond strength of bars in a laboratory, it still exists some disadvantages as follows:

- ➤ In this test, the concrete is in compression at the loaded end while the steel is in tension. This is quite different from RC beam or slab specimens in which the concrete around the tensile reinforcement is in tension. The bond behavior is not as actual as in the concrete beams.
- At the loaded end, the concrete is in local compression; thus, it not only increases the bond strength but also eliminates the transverse tension cracking. The results of bond stress are not precise for structural design purposes. The steel bars sustain the external force prior to the concrete. It is fully inverse to RC beams of in-service structures in which the concrete carries initiatively.

Another way to test the bond stress of steel reinforcement corroded in concrete is beam tests [16, 18]. This test really expresses the bond stress in the actual flexural members. Therefore, the results of bond stress are truly more reliable. Nonetheless, it has several drawbacks:

- At the supports of the beam, due to the reaction restraint that results in the increase in confinement of concrete to steel bars the bond stress may therefore, increase at these locations.
- > The test specimen configuration is relatively complicated. It requires a preparation carefully.

A number of outcomes from published data have been recorded. It can be summarized that there is a general trend of changes in bond behavior as corrosion develops as graphed in Fig. I-18 [21] for both smooth bars and ribbed bars in concrete.

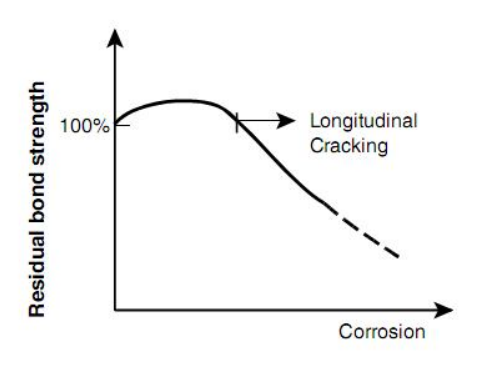


Fig. I-18. Typical relationship between the residual bond strength and corrosion levels [21]

At a small corrosion level, it seems that bond strength extends to a new value before the slip at concrete-steel interface enhance rapidly. In other words, reductions of bond strength take place sharply after appearing the longitudinal cracks on surface of structures [21]. Stirrups or confinement due to support would play an important role by controlling the opening of corrosion cracks and then risk of spalling. At this state, the loss of bond strength may very magnify. For instance, G.J.Al-Sulaimani et al. [14] recorded bond strength losses exceeding 62% at a level of corrosion of 5% and bond resistance becomes negligible as corrosion level reaches to 7.5%. While, Lamya Amleh and Saeed Mirza [22] suggested that with 5% weight loss due to corrosion, there is only around 18% loss of bond strength.

Variations in the loss of bond reported by different researchers are also due to the fact that the most of authors used reinforcing steel of different diameters in their tests as well as their specimen geometries were different (see Table I-2). More importantly, the concrete cover thickness-to bar diameter ratio (C/d_b) along with the water to cement ratio is found to be most significant parameters in evaluating the residual bond strength [14, 23, 24].

CHAPTER I: Literature review on mechanical behavior studies

Table I-2. Test procedures and experimental results on bond strength of corroded specimens from some previous studies

Authors	-	orrosion echnique			Compressive					
		NaCl	Currrent/ Potential	d _b	C/d _b	strength	Stirrups	Sample test		Bond capacity
G.J.Al- Sulaimani et al.	1990	2 mA/cm2	10- ribbed	7	30	not given	pullout		increased until 1% corrosion degree	
		2 m	2 IIIA/CIII2	12- ribbed	2.4	40	yes		beam	increased until 0.5% corrosion degree
Abdullah A.Almusallam et al.	1996		10.4 mA/cm2	12- ribbed	5.5	30	yes	pullout		increased until 4% corrosion degree
P.S.Mangat et al.	1999	1% by cem ent wt.	0.8-2.4 mA/cm2	10- ribbed	2	45	not		beam	increased until 0.4% corrosion degree
Congqi Fang et al.	2004		40 mA/cm2	20- ribbed	3	52.1	yes	pullout		not affected until 6% corrosion degree
Lan Chung et al.	2004	3% by cem ent wt.	27V	10- ribbed	2.5	18.8			slab- one way	increased until 2% corrosion degree
D.Coronelli, K.Z. Hanjari	2010	0.143 mA/cm2	20- ribbed	1.5	37.5	yes	pullout		increased for corner bar; decreased for middle bar	
			0.143 mA/cm2	20- ribbed	1.5	37.5	not	pullout		decreased for both corner bar and middle bar

It should be borne in mind that the flexural stiffness of RC beams corroded is also related to bond properties at concrete-steel bar interface. This was already mentioned by A.Castel et al. [34], T.Vidal et al. [39].

Evidently, many researchers had attempted to point out the relation between the bond capacity and corrosion rate of steel bars. However, it appears very difficult to relate precisely between them. Even so, with such results, they would help engineers to understand the changes in bond behavior of reinforcement induced by corrosion.

A study on bond stresses at the ends of beam (i.e. the anchorage capacity) in naturally corroded RC beams under flexural test would help to clarify the impact of steel corrosion on the bond strength between reinforcing steel and concrete. This will be mentioned in chapter II, section II.3.

I.1.2. Effect of corrosion on steel behavior (ductility- yielding)

The corrosion affects not only the bond resistance but also the mechanical properties of steel such as yield strength, ductility. These two characteristics are important for performance of RC elements. The stress at the yield point, referred as the yield strength, is very important property of steel reinforcement. Reinforcement is generally characterized by its yield strength. Typical stress-strain curves for hot rolled steel are shown in Fig.I-19 [25]. The curves exhibit an initial elastic portion, a yield plateau, a strain hardening range in which stress again increases with strain, and finally a range in which the stress drops off until fracture occurs. Ductility refers to the ability of the structure or its components to provide resistance in the inelastic domain of response. It includes the ability to sustain large deformations and a capacity to absorb energy. For hot rolled steel, the ductility of rebar is defined as the ratio of ultimate deformation at collapse to deformation at yielding and given by:

$$\mu = \frac{\varepsilon_u}{\varepsilon_y} \tag{I.1}$$

Eurocode 2 [25] defined ductility by the ratio of tensile strength to the yield stress,

$$\left(\frac{f_t}{f_y}\right)_t$$
 and the elongation at maximum force, ε_{uk} . The minimum value of $\left(\frac{f_t}{f_y}\right)_t$ and ε_{uk} is

1.05 and 2.5%, respectively in Eurocode 2. The letter k refers to characteristic value, i.e. at least 95% tests must be satisfied the required values.

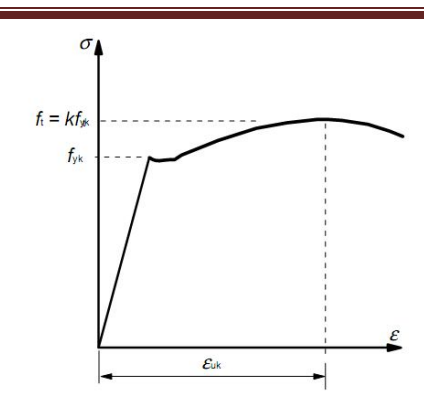


Fig. I-19. Typical stress- strain curves for hot rolled steel [25]

Regarding to methods of tension test, to be able to compare the experimental results, ASTM- A370 [72] recommended the gage length equalizes to four times the diameter of steel reinforcement and total length of sample is at least five times larger than steel diameter. Of course, the gage length (base length) also depends on the machine and testing equipments in the laboratory. Here, it is underlined that the variations in gage length would lead to the variations in ultimate strain of samples, which may not be representative of the material. Another point needs to show that with corroded steel bars, the presence of pitting attack on the surface would make the load from grips transmits eccentrically with the axis of the specimen at the beginning and during the test, but also pitting attack would lead to a variation in the location of the center of gravity of the residual cross-section along the bar inducing local bending moment. This certainly results in the deviation in load-elongation or stress- strain diagram. The requirement of minimum strain at fracture or minimum elongation is very essential for the safety of the structure and in order to ensure that the steel is ductile enough to undergo larger deformation before fracture.

In this section, the mechanical properties of reinforcing steel induced by corrosion are discussed from previously various experimental works. Two mechanical parameters need to define: firstly, nominal stresses (yielding or ultimate) are calculated based on nominal steel bar area; secondly, effective stresses or true stresses (yielding or ultimate) are calculated based on residual corroded steel bar area.

I.1.2.1. Research by Abdullah A.Almusallam (2001) [27]

A study on the effect of degree of corrosion of steel bars on their mechanical properties was performed by Abdullah A.Almusallam [27]. He used 6 and 12mm diameter ribbed

reinforcing steels that were embedded in concrete specimens. After casting, the concrete samples were cured for 28 days. For accelerated corrosion, direct current of 2 mA/cm² was impressed on the bar embedded by using an integrated system incorporating a small rectifier with a built-in ammeter to monitor the current and a potentiometer to control the current intensity. The specimens were partially immersed in 5% NaCl solution in a glass fiber tank so that the reinforcement was totally above water resulting in the formation of products due to reinforcement corrosion. After the desired level of reinforcement corrosion was obtained, the steel bars were extracted from concrete specimens by splitting them along the line of the steel bars. The degree of corrosion was measured as the gravimetric loss in the weight of the reinforcing bars. The steel bars were afterwards tested in tension to assess their mechanical behaviors such as elongation limits, limits of yield stress. The results indicated that when the corrosion degree increased, the corresponding elongation of rebar prior to break decreased. Figure I-20 shows a plot between the load and the elongation of steel bars with various degree of corrosion.

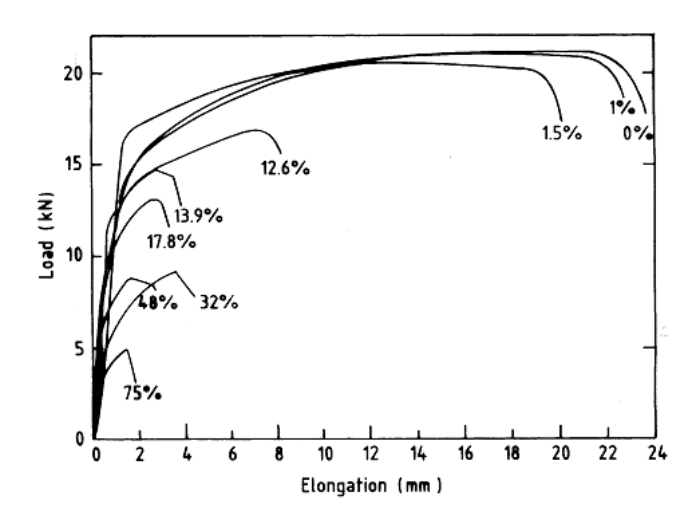


Fig. I-20. Load versus elongation for 6mm diameter of rebar [27]

It can be seen that non-corroded bars (0% corrosion) had a larger ultimate strain than corroded-bars even when corrosion level was only 1% rebar mass loss. For instance, the total elongation of steel bars at 1% corrosion is around 2.8 times (280%) more than that of steel bars at 12.6%. This means that the yield plateau of non-corroded bars was longer than that of

corroded-bars. In other words, the corrosion of reinforcement decreased its ductility. Reinforcing steel bars with 12.6% or more reinforcement corrosion indicate a brittle behavior. The rebar was abruptly fractured with a small elongation, affecting the safe performance of the structure. The bar shape and bar size are also affected by increasing corrosion. The author found that for a rebar mass loss over 40%, there was a change in configuration of reinforcing steel bars. Some locations on rebar surface became slimmer that results in the reduction of cross-section area of bars locally, referred to as pitting attack. When these steel bars suffered from tensile test, the stress would be concentrated at slim sections. Thereby, steel bars would be easily cracking or more brittle behavior. In addition, he concluded that the actual load carried by bars dropped with increasing level of reinforcement corrosion. However, the true ultimate strength of bars was nearly constant because of a drop in the cross-section of the bars. Figure I-21 shows a relationship between the true ultimate strength of 6mm diameter steel bars and mass loss due to corrosion.

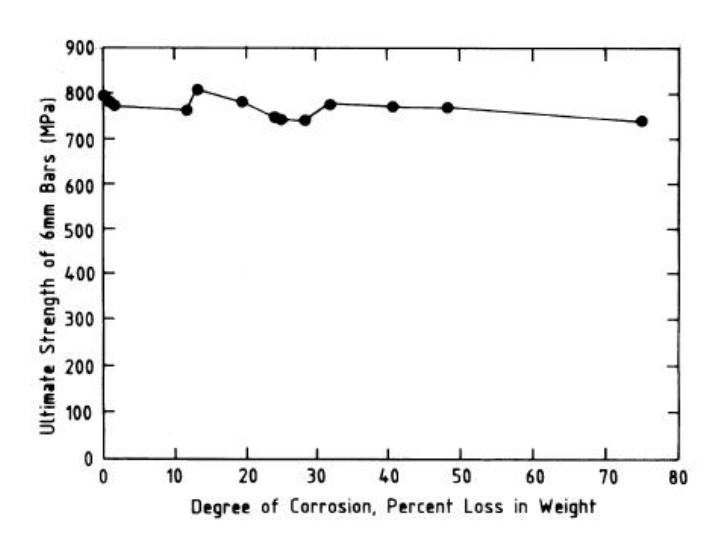


Fig. I-21. True ultimate strength versus the degree of corrosion in 6mm diameter of bars [27]

The true ultimate strength of the reference bars and rebars corroded to 75% was 796 and 740.8 MPa, respectively. Similarly, for 12mm diameter steel bars, the variation of the true ultimate strength at different corrosion levels was slight and fluctuated surrounding the value of roughly 800 MPa as shown in Fig. I-22.

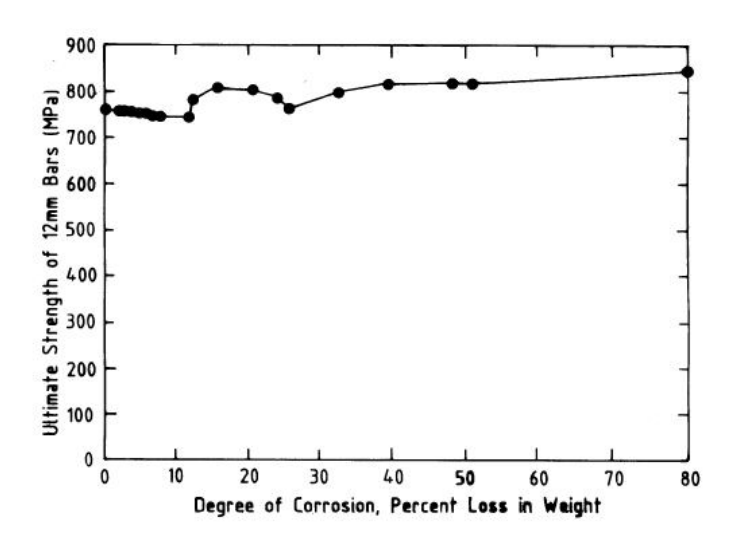


Fig. I-22. True ultimate strength vs. the degree of corrosion in 12mm diameter of bars [27]

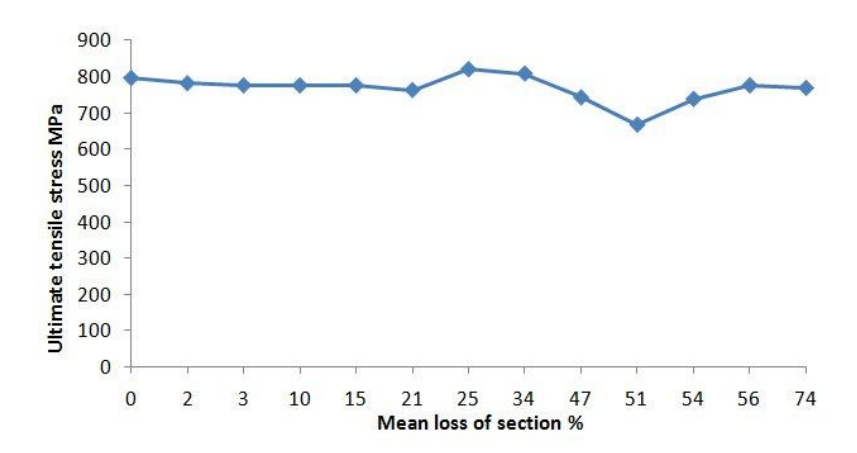


Fig. I-23. Effect of mean loss of section on true UTS in 6mm diameter of bars [27]

Figure I-23 reviewed from the data in [27] shown the relationship between the true ultimate tensile stress (UTS) and percentage of average section loss. In general, there was a low reduction trend in UTS as the mean section loss increased. About 21% mean loss of section due to corrosion leaded to 4.1% loss of the UTS, while 74% mean loss of section caused 3.4% loss of the UTS.

I.1.2.2. Research by John Cairns et al. (2005) [28]

In their study "Mechanical Properties of Corrosion-Damaged Reinforcement", they monitored the changes in mechanical properties of reinforcement as result of corrosion process through physical and mechanical tests with simulated and real corrosion damage. Firstly, they modeled the type of pitting corrosion by partially removing section of bar using a multifluted, hemispherical and mill with a cylindrical shank on 12, 16, 20, 24 mm diameter deformed bars as plotted in Fig I-21. The 5, 10, 20, 30, 40, 50% of cross-section loss rates were created on the bar section. The sound and damaged steel bars were then subjected to tensile testing. They found that in case of increasing the section loss, the ductility of steel bars reduced markedly. For example, for 12mm diameter-reinforcing bars, 5% loss of section due to pitting attack caused up to 40% loss of ductility, whilst 50% loss of section due to pitting attack resulted in around 80% reduction of ductility (Fig. I-25). Moreover, there was a linear reduction of ultimate load as the section loss develops. The yield stress at between 20% and 50% loss of section rate was more difficult to point out due to the much shorter longitudinal strain, making the bars become more brittle.

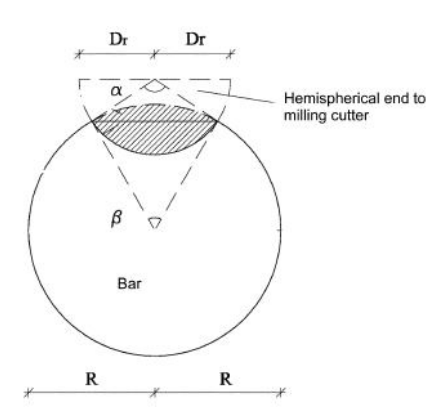


Fig I-24. Schematic of machined defect geometry [28]

The second series of test were conducted on 25 bars that were cast in the corners of cubic beam end-type bond specimens. To promote corrosion process, specimens were submitted to cycles of 1 day wetting with 3% salt solution and 6 days drying at a relatively humidity of about 70%. During the no-spray part of the conditioning cycle, a direct current density of

0.01 and 0.05mA/cm² was impressed to reduce the necessary timescale. Residual cross sections of samples were determined by weighting bars, and then loss of the cross section and average corrosion penetration were calculated.

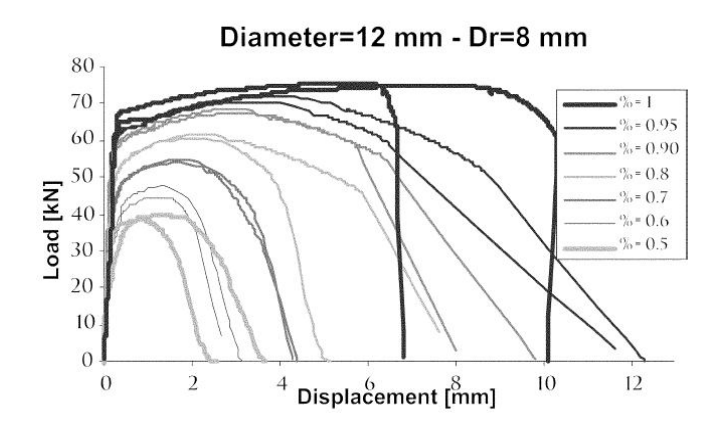


Fig. I-25. Effect of artificial pitting on total elongation of 12mm diameterbars with 8mm radius machined defects of various depths [28]

Their results showed that the decrease in ultimate elongation is always greater than the decrease in ultimate load at the same section loss degree (Fig. I-26a and Fig. I-26b).

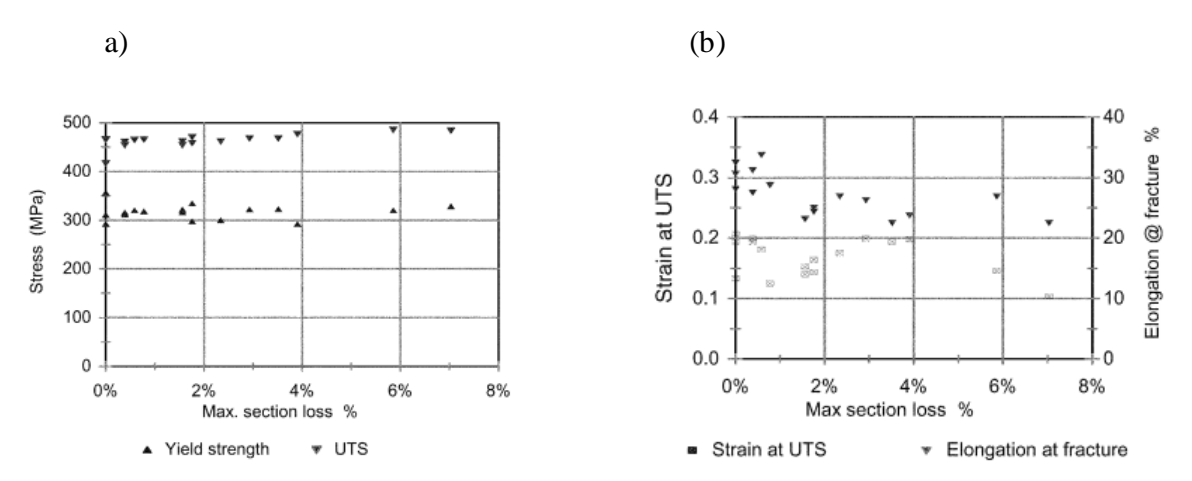


Fig. I-26. (a) Tensile strength versus loss of section; (b) Ductility versus loss of section [28]

From data on stress vs. maximum section loss of reinforcing steel bars corroded, it indicated that there was no loss in true yield strength whilst there was a slight increase in true ultimate tensile strength with further max. section loss (Fig. I-26a). Only about 5.7% increase in ultimate tensile strength (UTS) at 7% maximum rebar section loss was noted. The data on strain at UTS vs. maximum section loss of reinforcing steel bars corroded indicated that a 7% maximum rebar section loss resulted in about 28% loss of its elongation. Obviously, the reduction in ductility is more noticeable than the reduction in strength. They suggested that the nominal UTS f_u and yield stress f_y sharply reduced with higher average section loss as plotted Fig. I-27.

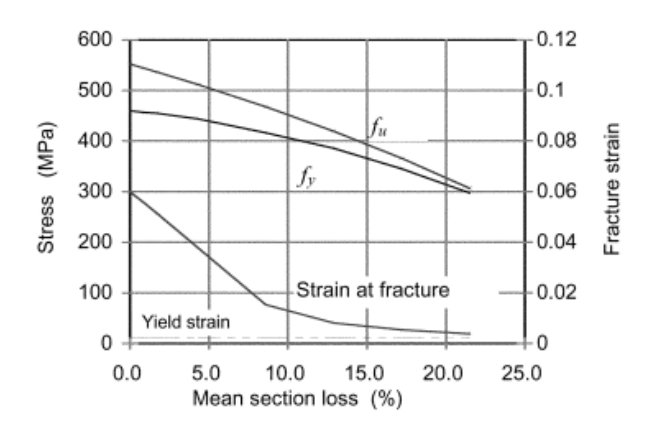


Fig. I-27. Impact of mean section loss on residual stress [28]

In addition, they proposed the percentage average section loss- nominal mechanical properties equations that express as follows:

$$f_v = (1.0 - \alpha_v. Q_{corr}) f_{vo}$$
 (I.2)

$$f_u = (1.0 - \alpha_u. Q_{corr}) f_{uo}$$
 (I.3)

$$\varepsilon_{\rm u} = (1.0 - \alpha_1. \, Q_{\rm corr}) \, \varepsilon_{\rm o}$$
 (I.4)

Where f_y , f_u , and ϵ_u are yield strength, ultimate strength and elongation corresponding to ultimate strength after time t, based on the original cross section, respectively; f_{yo} , f_{uo} , and ϵ_o are yield strength, ultimate tensile strength, and elongation of the noncorroded bar, respectively; Qcorr is average section loss, expressed as a percentage of original cross section; and α_y , α_u , and α_l are empirical coefficients.

I.1.2.3. Research by C.A.Apostolopoulos et al. (2008) [30] and R. Palsson, M.Saeed Mirza [32]

C.A.Apostolopoulos et al. [30] tested seven specimens from reinforcement bars embedded in real structures and exposed in natural corrosion, coastal area of Athens, Greece for 40 years. The reinforcement used in these buildings was BSt 420 of DIN 488-1 and the nominal diameter of the tested specimens was 10 mm. From the bars, specimens of 250 mm length, 150 mm gauge length were cut and then the tensile tests were performed. The amount of corrosion was measured as the gravimetric loss in the weight after washing reinforcing bars. Fig. I-28a plotted both nominal yield and ultimate stress versus mass loss. It can state that the nominal ultimate stress reduces significantly while the nominal yield stress does not almost affect as degree of corrosion increases, which is dissimilar to John Cairns et al.'s results [28]. The true yield and ultimate stress at different corrosion level are given in Fig. I-28b. In general, the corrosion has a little effect on these parameters, slightly decreasing trend in true ultimate stress and slightly increasing trend in true yield stress.

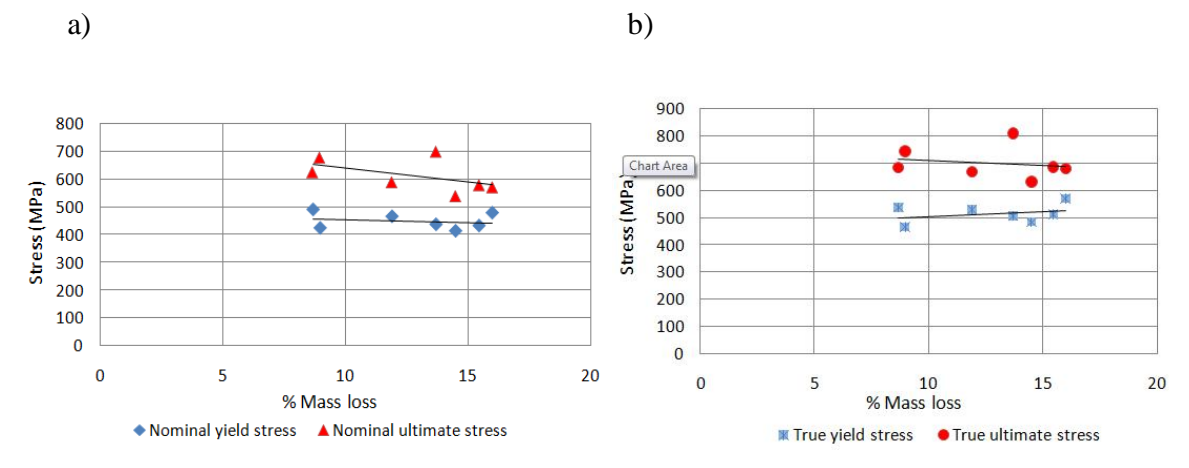


Fig. I-28. Influence of loss of mass due to steel corrosion on stress (data from [30])

Figure I-29a presented the reduction of elongation with loss of cross-section area of steel bars that derived from experimental values by C.A.Apostolopoulos et al. [30]. This trend line seems to be relatively consistent with the data of Ragnar Palsson and M.Saeed Mirza [32] as given in Fig. I-29b.

Ragnar Palsson and M.Saeed Mirza [32] collected samples of steel reinforcing bars corroded by chloride and carbon dioxide from Dickson Bridge in Montreal, Canada. The nominal diameter was 16mm. The diameter of corroded reinforcing bars was measured over the gage length of 25 mm by a vernier caliper and the cross-sectional areas computed simultaneously. Their mechanical responses were tested in tension to failure. The results revealed that both the nominal yield stress and ultimate tensile stress are not affected as the loss of cross-section increases.

These experimental results from steel bars embedded in real structural concrete are useful to assess the actual change of mechanical properties.

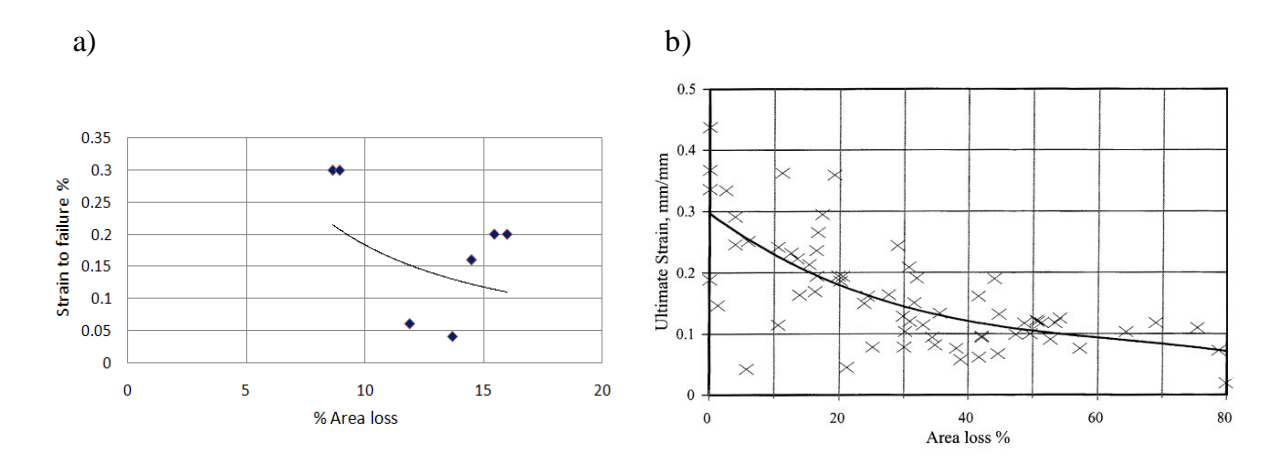


Fig. 1-29. Influence of cross-section loss on elongation: (a) for mean area loss [30]; (b) for area loss that compares between smallest area of corroded bars and area of uncorroded bars [32]

I.1.2.4. Research by Han-Seung Lee et al. (2009) [33]

A study on the relationship between the degree of steel bar corrosion and the mechanical properties of reinforcing steel was performed by Han Seung Lee et al. [33] In their experimental programs, two corrosion methods were used. In the first technique, they applied a constant current to steel bars embedded in concrete samples when the samples were soaked in 3% NaCl solution. This technique tends to lead to uniformed corrosion like carbonation-induced corrosion in concrete. In the second technique, the wetting-drying

cycles at a high temperature in environmental chlorides were adapted. Accordingly, this method tends to lead to local or pitting corrosion. The RC concrete specimens, reinforced with steel bars of 10 or 13 mm diameter, mixed 6 kg ion chlorides/m³ of the concrete mix were subjected to cycles with 5 days wetting (RH is equal to 98%) and 2 days drying (RH is equal to 50%) at temperature of 60°C. The amount of corrosion was expressed as percentage of difference between the weights before and after washing corroded reinforcements. Based on the experimental results, the authors found that the mechanical properties of reinforcing steels corroded by chlorides adding in concrete are lower than those of reinforcing steels corroded by a constant current, even if the percentage of mass loss is the same. This was attributed to the influence of pitting in chloride corrosion that causes the local stress. Figure I-30 demonstrated their point of view. Similar to John Cairns et al. [28], they confirmed that as the corrosion became more severe, the nominal yield point, nominal ultimate tensile point as well as the elongation declined dramatically.

Han-Seung Lee et al. [33] pointed out that there was very high relationship between the reinforcement corrosion degree and mechanical properties of steel bars. Equations for mechanical properties of reinforcement corroded were established as a function of corrosion percentage.

$$\sigma_{\rm cy} = (1.0 - \alpha. \, \Delta_{\rm w}/100). \, \sigma_{\rm sy}$$
 (I.5)

$$\sigma_{\rm ct} = (1.0 - \beta . \Delta_{\rm w}/100). \sigma_{\rm st}$$
 (I.6)

$$E_{cs} = (1.0 - \gamma . \Delta_w/100). E_{ss}$$
 (I.7)

$$\delta_{\rm c} = (1.0 - \delta . \Delta_{\rm w}/100). \delta_{\rm s}$$
 (I.8)

Here, σ_{cy} , σ_{ct} , E_{cs} , and δ_c are nominal yield point, nominal ultimate tensile strength point, elastic modulus and elongation of corroded reinforcement, respectively; σ_{sy} , σ_{st} , E_{ss} , and δ_s are yield point, ultimate tensile strength point, elastic modulus and elongation of sound reinforcement; α , β , γ , and δ are experimental constants or reduction factors; Δ_w is corrosion percentage, expressed as a percentage of mass loss. Comparing with John Cairns's equations [28], it can be seen that a good agreement between two studies was reachable.

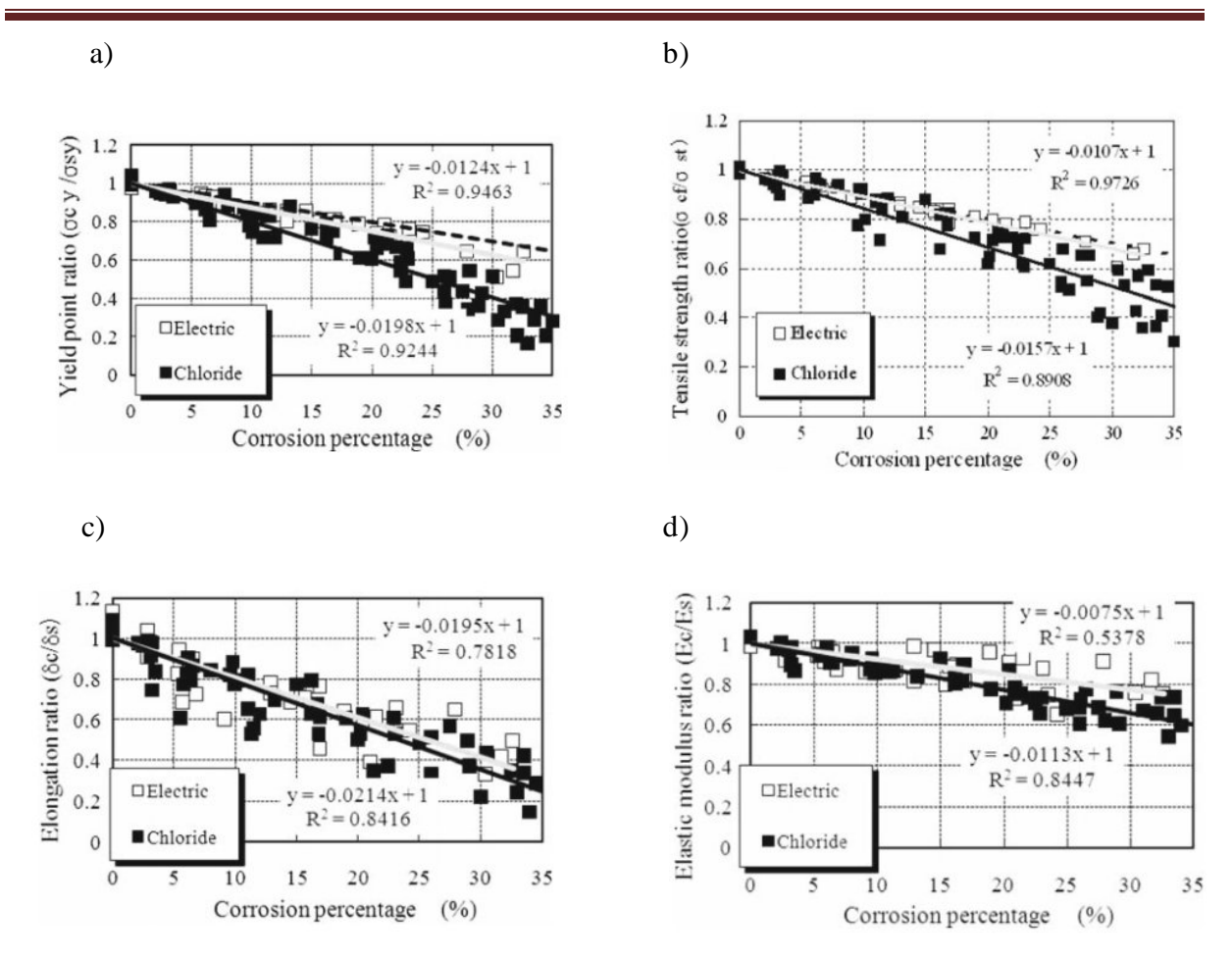


Fig. I-30. Relationship between corrosion percentage Δ_w and (a) Yield point ratio; (b) Tensile strength ratio; (c) Elongation ratio; (d) Elastic modulus ratio [33]

I.1.2.5. Research by Castel et al. (2000) [35]

Castel et al. [35] have proposed a model to predict the loss of ductility versus the maximum loss of steel cross section. This model is based on the experimental results of steel bars, the pitting corrosion attack was simulating by creating local notches on the steel surface. The trend of the model is an exponential function which could represent the relationship between ultimate strain of corroded reinforcement bar and degree of corrosion (C%) (Fig. I-31):

$$\varepsilon_{stu} = \varepsilon_{stu}^{i} e^{-0.1C\%}$$
 if C% $\leq 15\%$ (I.9)

$$\varepsilon_{\text{stu}} = 0.2 \varepsilon_{\text{stu}}^{i}$$
 if C% > 15%

Where, ϵ_{stu} : ultimate strain for corroded rebar

 $\varepsilon_{\text{stu}}^{1}$: ultimate strain for non-corroded rebar

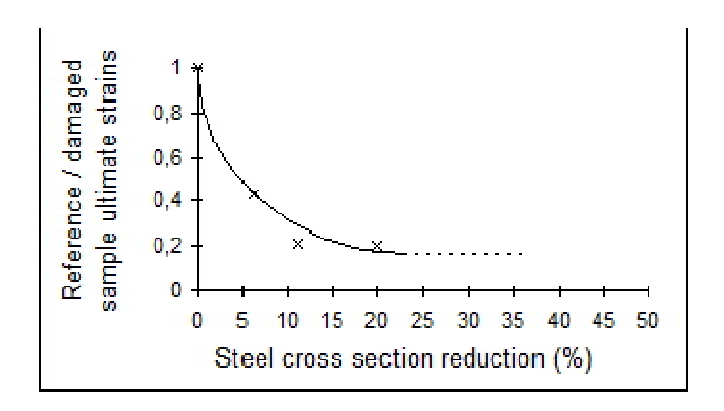


Fig. I-31. Evolution of reinforcement strain versus steel cross section reduction from [35]

It should be noted that Castel et al. [35] tested the reinforcement steel of 12mm diameter. Similarly, Cairns et al. [28] reported the effects of simulated pitting damage on residual bar ductility. The corrosion damage on re-bars of 12 mm diameter was also simulated by machined defects.

I.1.2.6. Summary

The present section has considered the impact of reinforcement corrosion on its mechanical behavior. The researchers shown that the corrosion influences not only the rebar shape, decreasing its cross-section diameter, degrading its ribs but also the stress- strain relationship. From previously results, it can be conclude that the corrosion has a disadvantageous effect on the behavior of the bars, particularly elongation or ductility. In general, the literatures reported that the nominal yield stress and nominal ultimate tensile stress are affected by the corrosion but the effect level is less than that of the total elongation.

Only two published literatures [30, 32] studied several mechanical properties of naturally corroded reinforcement. Accordingly, the true yield and ultimate strength are generally not

affected by corrosion because of the weak corrosion level. Nevertheless, a point that is under question is the fact that the nominal yield and ultimate stresses increase or decrease. Furthermore, the other mechanical properties such as elastic modulus, strain hardening modulus are not indentified in [30, 32]. Only Han-Seung Lee et al.'s work [33] mentioned the reduction in elastic modulus but their work carried out in artificial corrosion condition, which does not exactly present the corrosion concept [67]. All the reports consented the dramatic decrease in ductility of corroded steel bars. C.A.Apostolopoulos et al. [30] tested on rebars of 10 mm diameter pointed out the 15% loss of area lead to a 65% loss in ultimate elongation. Ragnar Palsson and M.Saeed Mirza [32] tested on rebars of 16 mm diameter indicated that a loss-sectional area of around 25% corresponded to a 39% loss in mean ultimate strain. It is expected that the diameter of steel bars would influence the ultimate strain or ultimate elongation. In addition, the gage length also could cause the various outcomes in the literature.

Another aspect, which needs to discuss, is that the technique uses to measure the corrosion level. The researchers preferred to evaluate the corrosion level through the loss of mass. In fact, this method offers the accurately global loss of cross-sectional area along rebar length. Thus, it is the average loss measurement rather than local loss measurement. Yet, the fracture locations in tensile test of corroded reinforcement are usually at pitting attack, at which the cross-section is commonly smallest. Because of this reason, the obtained results from previous studies may be conservative. Using the vernier caliper to determine the reduction in cross-section could induce the large scatter with experimental results. This is because the shape of localized corrosion (pitting attack) cross sections varied from roughly elliptic to quadrilateral that is difficult to determinate the real section area. Therefore, it should be paid attention to measurements of residual cross-section.

With type of pitting corrosion that causes the notch effect on the surface of reinforcement, the steel bar has a localized deformation in the tensile test. Thus, the corroded steel bars can be fractured suddenly even when the strain is much smaller [28].

However, the majority of outcomes available show that the tests were performed under accelerated corrosion conditions by using an impressed current, thereby, the quantitative results from these studies should be needed more thoughtful examination prior to applying to in-service structures. No research work has recorded in detail the property parameters of

naturally corroded steel bars such as true yield stress, true ultimate stress, elastic modules, hardening modulus. This is necessary to model or analyzes the behavior of RC member corroded in chloride environment. Further discussion on this is in chapter II, section II.1.

I.2. LOADING-BEARING CAPACITY OF CORRODED REINFORCED CONCRETE BEAM

Numerous studies on the flexural capacity of RC beam corroded were reported by different researchers in the past [34-58]. It is necessary to summarize the list of published works related to this issue (Table I-3). From Table I-3, it can be seen that almost of the corroded experimental programs used the artificial corrosion technique by applying a constant current to the reinforcement surface and the bars served as the anode. Only a few experiments used the climate accelerated technique that is the nearest natural corrosion by spraying NaCl solution with cyclic wetting drying. Similarly, the majority of tests was imposed the load after a complete corrosion process. In other words, the samples were corroded in the absence of a sustained load, which is rarely occurred in the actual structures. In sub-section from I.2.1 to I.2.5, the structural response of RC beams corroded in the absence of loading is briefly discussed then the mechanical response of corroded beams under an imposed load is mentioned.

CHAPTER I: Literature review on mechanical behavior studies

Table I-3. Summary of tests on residual capacity of corroded RC beams

Investigators	Year	Specimen size	Types of corrosion		Note
A. A. Almusallam et al.	1996	Slabs one-way: b=305mm; l=771mm; t=63.5mm		Impressed current	corrosion prior to loading
J.Rodriguez et al.	1997	Beams: b=150mm; h=200mm; l=2300mm or l=2050mm		Impressed current	corrosion prior to loading
P.S. Mangat et al.	1999	Beams: b=100mm; h=150mm; l=910mm		Impressed current	corrosion prior to loading
A.Castel et al	2000	Beams: b=150mm; h=280mm; I=3000mm	Spraying salt solution		Simultaneous corrosion and load
S. Yoon et al.	2000	Beams: b=100mm; h=150mm; l=1170mm		In salt solution then impressed current	Simultaneous corrosion and load
Y.Balim et al.	2003	Beams: b=100mm; h=160mm; l=1500mm		Carbonation and then impressed current	Simultaneous corrosion and load
T.Vidal et al.	2003	Beams: b=150mm; h=280mm; l=3000mm	Spraying salt solution		Simultaneous corrosion and load
R.Capozucca et al.	2003	Beams: b=100mm; d=126mm; l=2450mm		Impressed current	corrosion prior to loading
T. El Maaddawy et al.	2005	Beams: b=152mm; h=254mm; l=3200		Impressed current	Simultaneous corrosion and load
Yingang Du et al.	2007	Beams: b=150mm; h=200mm; l=2100mm		Impressed current	corrosion prior to loading
L. Chung	2007	Slabs one-way: b=500mm; l=1200mm; t=90mm		Impressed current	corrosion prior to loading
Torres-Acosta et al.	2007	Beams: b=100mm; h-150mm; l=1500mm		Adding NaCl in concrete mixing then impressed current	Corrosion prior to loading
A.K.Azad et al.	2007	Beams: b=150mm; h=150mm; l=1100mm		Impressed current	corrosion prior to loading
R. Zhang et al.	2009	Beams: b=150mm; h=280mm; l=3000mm	Spraying salt solution		Simultaneous corrosion and load
G.Malumbela et al.	2009	Beams: b=153mm; h=254mm; l=3000mm		Impressed current	Simultaneous corrosion and load
A. Ababneh et al.	2010	Beams: b=115mm; h=150mm, I=280mm	In salt solution		Loading prior to corrosion
I. Khan et al.	2011	Beams: b=150mm; h=280mm; l=3000mm	Spraying salt solution		Simultaneous corrosion and load

I.2.1. Research by Abdullah A. Almusallam et al. (1996) [56]

Abdullah A. Almusallam et al. [56] investigated the influence of the reinforcement corrosion on the flexural strength, ductility and deformation of RC concrete slabs. The steel bars were corroded by impressing a constant current of 2A (15 mA/cm²) and partially immersing in a 5% NaCl solution. The slabs tested had dimensions as seen in Table I-3 and were reinforced with steel bar of 6 mm diameter and center-to-center spacing of 57 mm along longer side of slabs. The slabs were tested in flexure using a simply supported system with a total span of 610 mm. A uniformly distributed load was applied to the slabs. They concluded that a sharp reduction in the ultimate flexural strength of slabs with an up to 29% corrosion level of reinforcement (mass loss of steel bars). The decrease in the ultimate flexural strength of slabs with 5% reinforcement corrosion was 25%, while at 25% reinforcement corrosion, the ultimate flexural strength of slabs declined 60%. Slabs with corroded reinforcement exhibited considerably reduced ductility as the corrosion degree increased. With 1.5% bar corrosion, the ductility of slabs reduced by around 28%. It can be explained by the loss of the cross-section of bars and the decrease in bond strength with surrounding concrete.

I.2.2. Research by J. Rodriguez et al. (1997) [57]

J. Rodriguez et al. [57] carried out experiment on 31 beams with sizes of 150 x 200 x 2300 mm and 200 x 150 x 2050 mm. To take into account the interaction between corrosion and loading, they varied the level of corrosion and detailing of reinforcement. Corrosion was promoted by adding 3% CaCl₂ by cement weight to concrete mix. Then, in order to get the required corrosion level, a current of about 100 mA/cm² was applied to the reinforcement for 100 to 200 days. Beams were simply supported and two symmetric loads were applied at a distance of 800 mm from each support. The study indicated that corrosion increased deflections and crack widths at the service load, at the same time, decreased strength at the ultimate load, and caused an increase in both the spacing and width of transverse cracking due to bond deterioration. It was also observed that corrosion could change the type of failure experienced by RC beams with usual reinforcement ratios at the maximum load. In this case, uncorroded beams failed mostly by bending and corroded beams failed mostly by

shear. Figure I-32 shown the types of failures that were observed by the authors as testing corroded beams at the ultimate load.

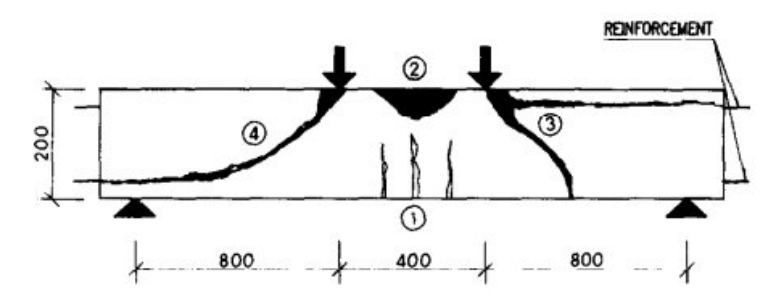


Fig. I-32. Types of failure of beams with corroded reinforcement [57]

Accordingly, there were four types of failure in beams as described below.

Type 1: Failure by bending that occurred in both corroded and uncorroded beams with a low tensile reinforcement ratio (0.52%).

Type 2: Failure by bending that produced in beams with uncorroded tensile reinforcement of a high ratio (1.51%) and most corroded beams with a high ratio of shear reinforcement (spacing 85 mm).

Type 3: Failure by shear that occurred in nearly all beams having a high ratio of corroded tensile bars (1.51%) and large stirrup spacing (spacing 170 mm).

Type 4: Failure by shear combined with anchorage failure of tensile bars that found in corroded and un-corroded beams with curtailed tensile reinforcement (only 50% of their tensile reinforcement anchored outside the support zone).

More importantly, the authors concluded that by using the reduced sections of steel and concrete with conventional RC models such as standard methods of EC2 [25], residual values of the ultimate moment and shear force can be predicted for RC members damaged by high level of corrosion. However, this method of calculating the strength of damaged members had the drawback because it was not possible to consider the loss of bond between concrete and steel bar within the span.

I.2.3. Research by Pritpal S. Mangat et al. (1999) [52]

Pritpal S. Mangat et al. [52] conducted a testing program on 111 under-reinforced concrete beams in order to study their residual flexural capacity after being subjected to various levels of corrosion. Nine groups of beams were cast, having dimensions of 100 x 150 x 910 mm. Total 111 RC beams submerged in 3.5% NaCl solution were corroded by two external power supply sources at four different rates of either 1, 2, 3, or 4 mA/cm². The beams were tested under 4 point-bending to evaluate the load-deflection curves and ultimate flexural strength. The reduction in reinforcing bar diameter was defined as the degree of reinforcement corrosion. The degree of corrosion induced in the reinforcement had a marked effect on displacement of beams. Similarly, the level of corrosion was also found to have an effect on the flexural load capacity. When corrosion level was less than 2.5%, it had little influence on deflection of beams. Meanwhile, if corrosion was more than 3.5%, the residual load capacity of corroded beams was significantly affected.

The researchers proposed a regression equation from the data available that related between the level of corrosion and residual flexural strength, as seen in Equation I.10.

$$B\% = \left\{ 1 - \sin^2 \psi \left(\frac{2RT}{D} \% \right) \right\} 100 \tag{I.10}$$

Here, R is the material loss per year (cm/year); T is the elapsed time in years after corrosion initiation (years); D is reinforcing bar diameter (mm); ψ is a coefficient depending on corrosion current density.

Eq. (I.10) is implied that it can be used to create nomograms for ascertaining the residual flexural strength of beams with corroded reinforcement.

It was also determined that corrosion has a significant effect on the deflection and capacity of RC beams and the reduction in steel cross-sectional area. They indicated that the reduction of the flexural capacity is mainly attributed to the reduced steel-concrete bond strength rather than the reduction in reinforcing bar cross section. The typical mode of failure under four-point bending test of beams with corroded reinforcement was presented as seen in Figure I-33. At 60 to 70% of ultimate load, horizontal splitting of concrete took place along the tensile reinforcing steel interface probably favored by the absence of stirrups. At

90% of ultimate load, vertical cracks appeared at mid-span of beams, typical failure mode of flexural elements if the anchorage at the beam ends was still maintained. It is different from the type of failure on J. Rodriguez et al.'s corroded beams [57]. A possible explanation is because the tensile bars were fully anchored in the form of U-shaped hooks at the beam-ends. Thus, the final failure of the beams did not take place until anchorage at the beam ends was no longer maintained. Moreover, the difference in size of beams as well as ratio of shear span to effective depth of cross section likely affect the failure mode.

The effect of the curing time prior to the initiation of corrosion was also investigated in this study. A number of beams were pre-cured for various periods of 16 days, 28 days, 6 months, and 1 year and then corroded to 5% corrosion. The residual strengths for all of these beams were nearly 70% of the control beams. This finding allowed concluding that the curing period before corrosion (up to 1 year) seem to have no effect on residual flexural strength of the corroded beams.

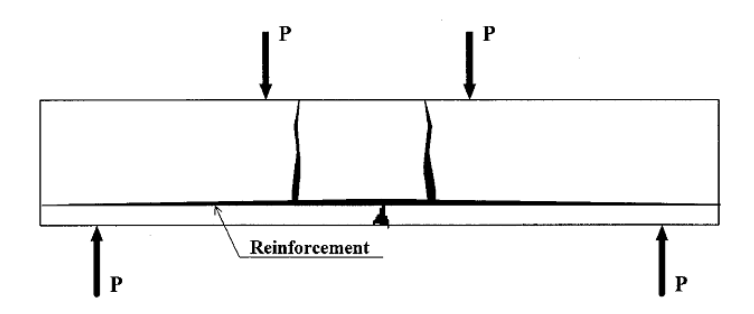


Fig. I-33. Types of typical failure of beams with corroded reinforcement [52]

I.2.4. Research by Abul K.Azad et al. (2007) [49]

Abul K.Azad et al. [49] carried out the experiments that predict the relationship between the reinforcement corrosion and load-carrying capacity of RC beams. For this purpose, 56 beams of size 150 x 150 x 1100 mm, reinforced with two 10 mm or two 12 mm bottom bars and two 8 mm top bars, were corroded by adding 2% NaCl by weight of cement to mixture then immersing partially them in 5% NaCl and applying a current of 2 mA/cm² and 3 mA/cm². The period of corrosion T was 4, 6, and 8 days. Four beam groups were used with different concrete covers, reinforcing steel diameters. All the beam samples were tested in a

four-point bending test. They suggested that the value of $(I_{corr} \, x \, T)$ was the most significant factor affecting the residual flexural strength of a corroded beam. When of $(I_{corr} \, x \, T)$ increased, both flexural strength and serviceability were impaired heavily. A corroded beam showed a larger deflection than an uncorroded one because of the reduction of flexural stiffness due to corrosion that increased with increasing of $(I_{corr} \, x \, T)$.

From the experimental data in this study, the authors proposed a predictive model for the estimation of the residual flexural strength of corroded beams. This model had taken into account not only the loss of cross-sectional bars but also the loss of bond strength at concrete-steel interface through the factor β . A two-step approach is suggested as follows:

- \clubsuit The remaining moment capacity $M_{th,c}$ is calculated by using the reduced cross-sectional area of tensile steel with conventional RC models.
- \clubsuit The value of $M_{th,c}$ is then multiplied by a correction factor β to obtain the predicted residual strength of beams M_{res}

$$M_{res} = \beta M_{th,c}$$
 (I.11)

$$\beta = \frac{14.7}{D(I_{cor}T)^{0.15}} \le 1.0 \tag{I.12}$$

Where, D is the diameter of the rebar (mm); I_{corr} is the corrosion current density (mA/cm²); and T is the duration of corrosion (days).

The mode of failure of all beams was the flexural-shear type failure.

I.2.5. Research by Torres-Acosta et al. (2007) [75]

Torres-Acosta et al. [75] cast 12 RC beams with dimensions of 100 x 150 x 1500 mm. The rebars of 10 mm in diameter were corroded by adding 3% NaCl (by weight of cement) during concrete mixing. 50 days after casting, a current density of 80 μA/cm² was applied for 40, 80 or 200 days. The beams were subsequently tested in flexure under three-point loading. They have found that in case of uniform corrosion, 10% average loss of diameter of the tensile bars results in a decrease of as much as 30 and 40 % in the flexure load capacity. However, in case of highly localized corrosion (deep pits), 10% average loss of diameter of the tensile bars can decrease as much as 60% % in the flexure load capacity. Moreover, the RC beams with a high pit depth provided a different load-deflection curve in compared with

beams with low pit depth or without deep pits, since these beams fractured completely at location where the deep pits appeared. These results give a hint that the pit depth is a important parameter to predict remaining load capacity of corroded beams.

I.2.6. Research by A.Castel et al. (2000) [34, 35]

A.Castel et al. [34, 35] conducted long-term and extensive experimental research to determine the global mechanical behaviour of RC beams with corroded reinforcement in their service and ultimate states. Total 36 RC beams of dimensions 150 x 280 x 3000 mm cast with two different section types A and B placed in a chloride environment under sustained loading. At the same time, 36 additional RC beams were used as control beams and stored in laboratory conditions. The beams were load in a three-point bending by coupling a type A beam with a type B beam. Two loading levels were applied: level 1 ($M_{ser1} = 13.5 \text{ kNm}$) corresponded to maximum loading of type A beams for durability in an aggressive environment (serviceability limit-state requirements in an aggressive environment) and to maximum loading of type B elements for resistance (ultimate load limit state in a non-aggressive environment). The beams stored under sustained level 1 loading were called A1 and B1. The level 2 ($M_{ser2} = 21.2 \text{ kNm}$), the type A beam corresponded to maximum loading

for resistance (ultimate load limit state in a non-aggressive environment), while type B beam corresponded to 80 % of the failure load and was equal to twice the design service loading in an aggressive environment according to French standards. The beams stored under sustained level 2 loading were called A2 and B2. The details of reinforcement steel of A beam and B beam are shown in Figure I-34a. The experimental system and conservation of beam are shown in Figure I-34b.

The aggressive environment is a salt fog (35 g/l of NaCl corresponding to the salt concentration of sea water) generated through the use of four sprays located in each upper corner of a confined room (Fig. I-34b). After 6 years of storage, the beams were submitted to wetting–drying cycles in order to accelerate the corrosion process:

0 to 6 years: continuous spraying under laboratory conditions ($T^{\circ} \approx 20^{\circ}C$),

6 to 9 years: cycles spraying under laboratory conditions ($T^{\circ} \approx 20^{\circ}C$), one week of spraying and one week of drying,

9 years to 13 years: cycles spraying, one week of spraying and one week of drying, however the confined room was transferred outside, so the beams were exposed to the temperature of the south-west of France climate, ranging from 5.1 to 21.3°C average value per month.

In the first part, four beams in which two corroded beams of type B beam and two control beams of type B beam with dimensions of $150 \times 280 \times 3000$ mm were studied. These beams were naturally corroded in a salt fog environment for 14 years in an attempt to emulate actual field conditions. They were then subjected to three-point loading to determine their ultimate strength. The average degree of corrosion reported was 10% in tensile zone; the reduction in flexural strength was 20% and a reduction in ductility was about 70% when testing beams until fracture as shown in Fig. I-35.

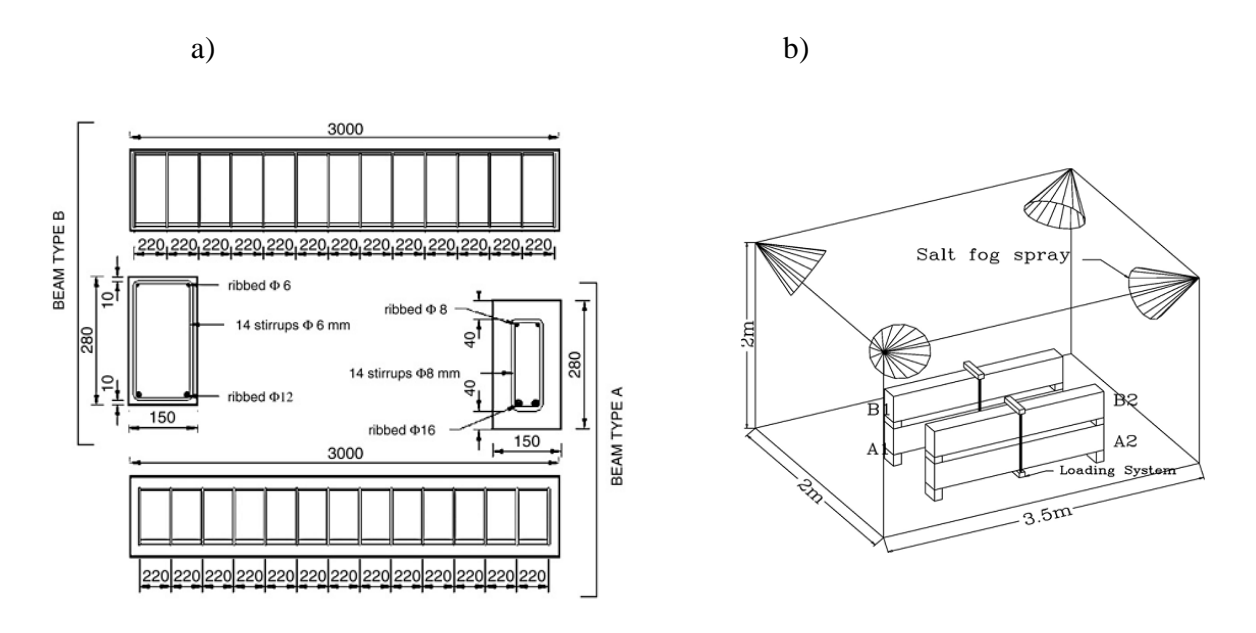


Fig. I-34. (a) Detail of reinforcement steel of A beam and B beam (b) Experimental system and exposure condition of beams

The researchers gave some assumptions to be able to explain the behaviour of beams with reinforcement steel corrosion. They include the concrete cracks in compressive zone, the reduction of steel cross-sectional area in tensile zone, and the local loss of bond stress at interfacial steel-concrete. The authors demonstrated that concrete cracks resulting from compressive reinforcement corrosion have an insignificant effect on the global behaviour of RC beams in service. They also proposed that the decrease in stiffness was due to the reduction of both the steel cross-sectional area and bond strength. This was attributed to the fact that the maximum cross-section loss of tensile steel near the mid-span of the beam was 20%, which can result in a stiffness decrease of 15%. However, the total stiffness loss of the corroded beams tested was about 35%. Thus, there was a 20% difference in loss that had not found the cause, which the researchers suspected to be the result of bond deterioration.

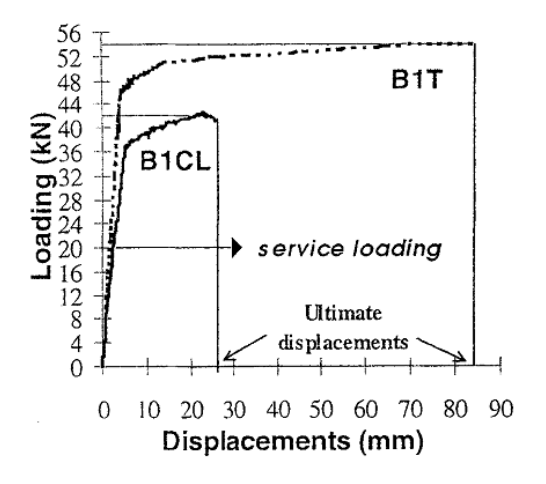


Fig. I-35. The relationship between loading and displacement of beams at mid-span [34]

Moreover, the reduction in remaining ultimate strength was found to equalize to the loss of maximum steel cross-section (20%). Thereby, A.Castel et al. concluded that the reduction in steel-concrete bond had an insignificant effect on the ultimate behaviour and thus the residual capacity can be determined by taking into account the reduction of steel cross-sectional area alone.

In the second part, the authors focused to further understanding the separate and coupled effects of bond stress and decrease in steel cross-sectional area. Two control beams with similar dimensions and type to those in the first part of this study were used to facilitate this second part. Bond stress loss was simulated by removing the concrete cover and exposing

the tensile reinforcing bar on a variable length, while a corrosion-pitting attack was simulated by using a grindstone to create local notches on the tensile steel surface. Based on the available data, the researchers illustrated that pitting corrosion located between flexural cracks has little influence on the global behavior of RC beams when bond strength was not modified. Conversely, when both bond strength and steel cross-section were reduced, the global behavior of RC beams was greatly affected. If the bond strength was reduced but the steel cross-sectional area was not modified, the evolution of the deflection in the mid-span was also increased. A significant increase in the deflection in the mid-span was observed when both loss of bond strength and loss of cross-section were occurred. This was attributed to the increase in steel stress at the crack locations, due to the reduction of both steel cross-sectional area and in tensile concrete contribution.

Finally, they concluded that corrosion of RC beams is always a coupling phenomenon between steel cross-section loss and reduction of bond strength. Predicting the residual carrying capacity or non-fragile behaviour must consider both effects.

I.2.7. Research by Sanchun Yoon et al. (2000) [36]

Sanchun Yoon et al. [36] tested 10 RC beams of dimensions 100 x 150 x 1170 mm, reinforced with a single 19 mm diameter in tensile zone. Two groups of beams were defined. In the first group, beams were tested while under a sustained load; in the second group, other beams were preloaded then unloaded for test corrosion. The reinforcement was corroded by exposing the beams to cycles of 4 days wetting with 3% NaCl solution and 3 days drying in the air, and then impressing electric potential of 27 volts. Details of specimen names and their loading levels are listed in Table I-4 below.

The results showed that beams that were previously loaded to high loads have shorter corrosion initiation periods. Similar results were observed on beams under sustained loads. In addition, sustained loading had a more significant effect on the reinforcement corrosion rate than did previous loading and the rate of corrosion was increased with higher load levels for both types of loading. These findings can be explained that after unloading, several microcracks in the concrete would be smaller and no longer discontinuous, so inhibiting the ingress of chloride ions. In contrast, at higher loading levels or sustained loading during corrosion process, crack widths are wider and continuous, thus facilitating the ingress of

chloride ions into deeper concrete. The beam displacement was recorded daily by LVDTs placed on a reference frame.

After 50 days of testing, an external current was applied to two beams under sustained loading. As a result, deflections of these beams were significantly increased. More particularly, after around 65 days, a much more increase in deflections was observed. This implied that the level of corrosion together with loading levels had a seriously influence on serviceability of RC beams corroded.

Cassimons	Flexural loading, % of ultimate load*	Ponding, Stage I	External current, Stage II
Specimens	ultilliate load	Foliding, Stage 1	External current, Stage II
AP00	0% load	No	No
AS45	45% sustained load	No	No
AS75	75% sustained load	No	No
NP45	45% previous load	NaCl	~ 50 days after ponding
NP75	75% previous load	NaCl	~ 50 days after ponding
NS45	45% sustained load	NaCl	~ 50 days after ponding
, NS75	75% sustained load	NaCl	~ 50 days after ponding
, NS00	0% load	NaCl	After moist curing
NS20	20% sustained load	NaCl	After moist curing
NS60	60% sustained load	NaCl	After moist curing

Table I-4. Summary of beam specimens in the study

The remaining flexural capacity of RC beams was plotted in Fig I-36.

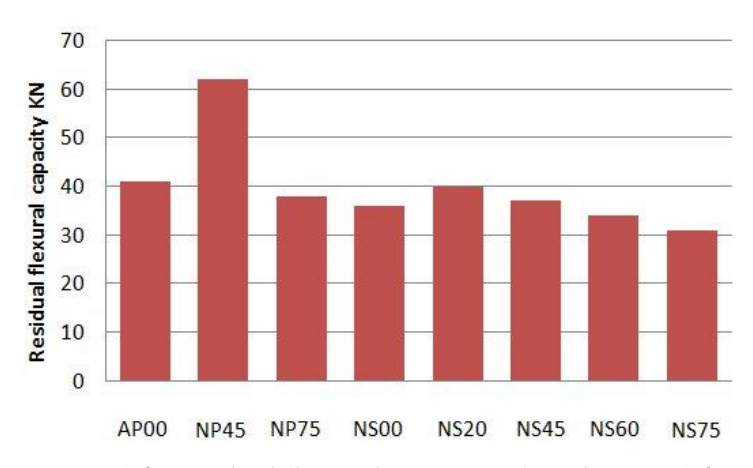


Fig I-36. Residual flexural capacity of RC beams [36]

It is clear that the remaining capacity of the beams subjected to sustained loading was much lower than that of the beam subjected to preloading with the same load level. The residual capacity of the beams applied to 75% of the failure load was lower than that of the beams subjected to 45% for both of the group. However, there was a surprise herein is that corroded beam NP45 was found to be significantly stronger capacity than the uncorroded beam AP00. The author in this study did not explain this result. In order to further understand the effect of corrosion on remaining flexural loading, Figure I-37 shown the relation between the mass loss of steel bar and residual loading capacity of beams.

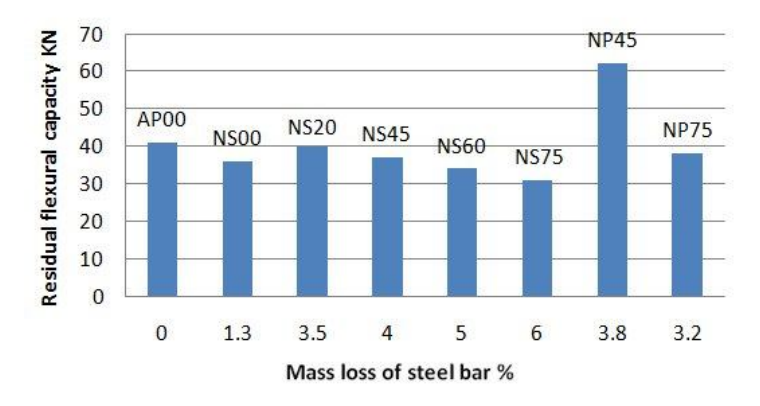


Fig I-37. Residual flexural capacity against loss of bar mass [36]

The mode of failure of each beam depends mostly on the value of load and corrosion degree. The tests indicated that failure type changed from a shear failure of concrete to a pullout of the reinforcing bar due to deterioration of bond stress when the degree of corrosion and load increased gradually. Note that, these beams were designed with only one longitudinal steel bar, without the stirrups. Thus, the behavior as well as failure modes in their work were not representative of in service structures.

I.2.8. Research by Y. Balim et al. (2003) [37]

In their experiments, 12 beams of dimensions 100 x 160 x 1500 mm were cast, reinforced with a single 16mm diameter steel bar in tension and two 8 mm diameter steel bar in compression. The shear reinforcement was 8 mm diameter steel bars which were

placed at 60 mm centre to centre spacing and was limited to the shear span of beams. Corrosion process was initiated through carbonation and was accomplished by placing the beams in a CO_2 filled pressure chamber for six weeks (that was kept at 80 kPa) and then placing the beams in 3% NaCl solution with a current density of about 0.4 mA/cm². The samples were simultaneously corroded and loaded to either 23% or 34% of the ultimate load (P_u) for 30 and 35 days. The degree of corrosion calculated using Faraday's Law.

Figure I-38 expressed the relation between the deflection ratio and corrosion rate for each series beams. The deflection ratio was defined as the average defection of the corrosion beams to the control beams ratio. It can be seen that even at low level of corrosion, the deflection of all beams was increased sharply as a result of combining effects of load and corrosion. The ratio of deflection grown up quickly until degree of corrosion of approximately 0.6%, after which increased deflection was slower and more stable up to around 6% corrosion degree.

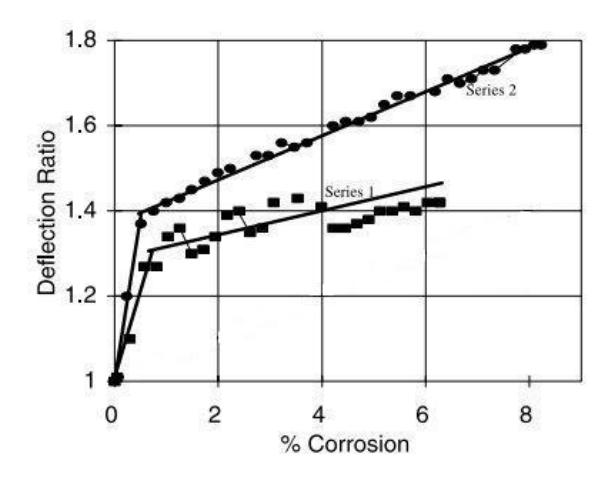


Fig. I-38. Effect of corrosion on deflection ratio of RC beams.

Series 1: correspond to 0.23P_u; Series 2: correspond to 0.34P_u [27]

The authors reported that beams that were corroded under a load of 23% exhibited an increase in deflections of 27% within three days of accelerated steel corrosion. For beams under a sustained load of 34%, the increase in deflections after three days of accelerated steel

corrosion was 50%. This implies that after 3 days of accelerated corrosion, the mass loss of reinforcing steel can be reached up to 0.6%. The researchers attributed this initial increase in deflection to early crack formation on the underside of the beam. Obviously, the effect of simultaneous load and corrosion is very different from the effect of corrosion in absence of load even at very low level of corrosion.

I.2.9. Research by T. Vidal et al. (2003) [39-41]

Similarly to A. Castel's experimental program that tested the beams corroded for longterm duration, T. Vidal et al. [39-41] used two corroded beam of 17 years old among 36 beams as mentioned in section I.2.5. Both of them were tested until failure. The result after 17 years in environmental chloride shown that the maximum weight loss of the tensile steel bar in the central part of a A1CL beam was around 15%, causing maximum reduction of stiffness of up to 40%. However, in theory, if the average mass loss of two tensile bars is 15%, the average stiffness loss of beam is only 11%. So, the reduction in steel weight cannot explain to 40% loss of bending stiffness. The researchers assumed that in addition to reduction of cross-sectional area of reinforcing steel, the deterioration of the concrete-steel bond strength in tensile zone due to corrosion is an important factor that explains the loss of bending stiffness of the corroded beam. At failure, the load bearing capacity of corroded beam was reduced by 13% in comparison to the control beam. This value is relatively closed to the maximum mass loss of two tensile bars. This also implies that the degradation of bond strength at concrete-steel interface seems to have no effect on the load bearing capacity. It is also found that the ductility of A1CL beam after 17 years was reduced by around 22% (Fig. I-39).

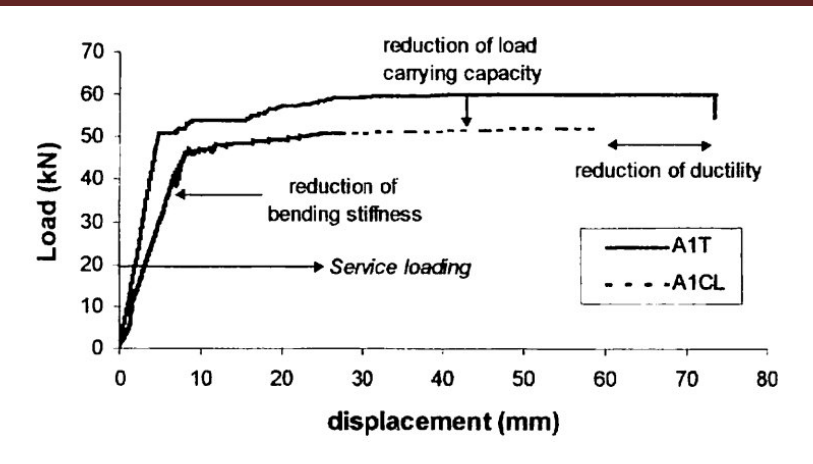


Fig. I-39. Mechanical behavior of corroded beam A1CL and control beam A1T [40]

The test of B2CL2 was presented in another reference [39]. They found a maximum mass loss of tensile steel of 22% to correspond to loss in bending stiffness of around 20% after 14 years whilst a maximum mass loss of tensile steel of 41% corresponded to loss in bending stiffness of about 40% after 17 years. So, there was an important loss in bending stiffness between 14 and 17 years. A clear explanation for this finding is that from 14 to 17 years, the global corrosion propagation of the tensile reinforcing steel was developed therefore causing the dramatic loss of steel cross-section and breakdown of the concrete-steel bond stress in this stage.

In addition, they found that the crack concrete cover in the compressive zone due to corrosion of the steel bars has little influence on the structural behavior under service loading but leading to a decrease in load-carrying capacity and a reduction in ductility of beams.

The failure mode of corroded beam was different from the control beam. The control beam collapsed by failure of the compressive concrete whereas the corroded beam collapsed by yielding and failure of the tensile reinforcement. The reason for this is because there are reduction in cross-sectional area and ductility of steel bars due to corrosion, resulting in the concentration stress at the pitting position that increases tensile stress of steel bars to yield and ultimate strength early.

I.2.10. Research by Tamer El Maaddawy et al. (2005) [38]

A research study was performed by Tamer El Maaddawy et al. [38] in order to investigate the combined effect of corrosion and sustained loads on the structural behavior of corroded RC beams. Nine beams with size of 152 x 254 x 3200 mm were tested for corrosion periods of 50, 110, 210, 310 days. These beams were reinforced with two 15 mm diameter deformed bars in tension and two 8mm diameter round bars in compression. The shear reinforcement was 8 diameter round steel bars spaced at 80 mm centre-to-centre in the shear span and 333 mm centre-to-centre in the constant moment region. 4 out of 8 beams were simultaneously corroded and loaded to approximately 60% of yielding moment of a control beam while the other four beams were corroded in absence of a sustained load. The reinforcing bar was corroded by adding 2.25% chloride ions by weight of cement to the concrete mixture used to cast the middle 1400 mm of the sample to a height of 100 mm from the tensile face of the beams as seen in Fig. I-40. To initiate corrosion in test specimens, a current density of 215 mA (0.143 mA/cm²) was used.

They found that for beams corroded with load, corrosion cracks were observed after 53h while for beams corroded in the absence of a sustained load, cracks were observed after 95h. They attributed the different time of crack initiation to the presence of load during the corrosion development. If the beams were corroded with a sustained load, the flexural cracks facilitated the ingress of chloride ions and oxygen into the concrete, thus increasing the rate of corrosion.

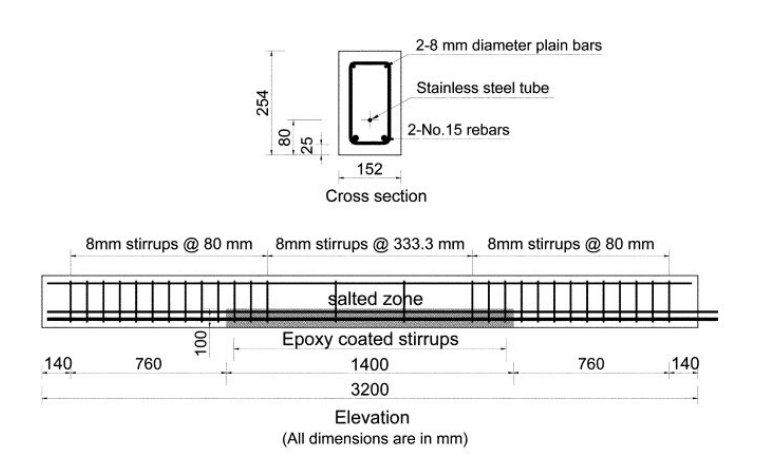


Fig. I-40. Lay-out of test beams [38]

Furthermore, at steel-concrete interface, the presence of microcracks due to loading damaged the bond stress between concrete and steel bar and thus accelerated the appearance of the first visible corrosion crack. The authors drawn the cracking maps for all beams corroded at the end of each corrosion phase. Accordingly, the maximum corrosion crack widths of beams corroded under loading were always larger than those of beams corroded without loading. In addition, for the corroded beams with loading, two longitudinal corrosion cracks at the tensile face and near each corroding bar were observed. On the side face of beams, some corrosion cracks discontinued were also drawn but the number of them in beams corroded in presence of a sustained load was more than that in beams corroded in absence of a sustained load. These findings implied that the effect of loading on the appearance, width and quantities of cracks are very important.

The mass losses of steel in beams corroded under load were larger than corresponding losses of steel in beams corroded in the absence of a sustained load by around 9% for the first two phases of corrosion. This is again due to the flexural cracks in beams corroded under load that increased the penetration of oxygen and chloride ions into concrete at the first two corrosion phases. Therefore, this went up the steel mass loss during the first two corrosion phases.

The mechanical response of total beams corroded was plotted in Fig. I-41.

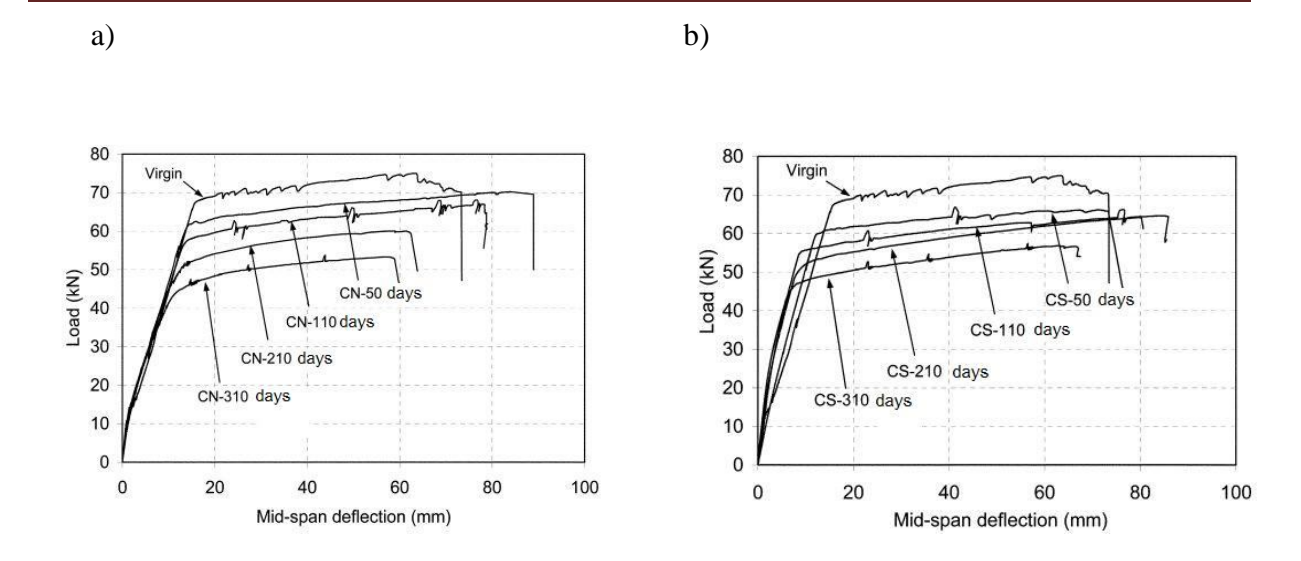


Fig. I-41. Loading-deflection relationship for (a) beams corroded without load; (b) beams corroded under load [38]

It can be seen that in general, the load-carrying capacity of beams corroded under a sustained load was slightly lower than that of beams corroded without a sustained load at the same degree of corrosion and when the amount of corrosion increased, the residual load capacity decreased. They pointed that at levels of corrosion below about 15% steel mass loss such as CN-50 beam (8.9%), CN-110 beam (14.2%), and CS-50 beam (9.7%), the ductility of beams increased compared with the control beam. These results are converse with the tested results from A. Castel et al. [34, 35], T. Vidal et al. [39-41]. The researchers explained that the initial increase in ductility of corroded beams could be ascribed to the decrease in the cross-sectional area of the tensile steel reinforcement caused by corrosion. At higher levels of steel mass loss, due to the formation of pitting corrosion, which caused the reduction in the elongation of steel and stress concentration, the ductility of the corroded beams declined.

I.2.11. Research by Ruijin Zhang et al. (2009) [42-44]

Similarly to A. Castel [34, 35] and T. Vidal [39-41], this research came from a long period of experimental program dedicated to the study of a natural corrosion performed on RC beams under loading in an aggressive environment. Ruijin Zhang et al. [42-44] studied two

long term corroded beams called B1CL1 and B2CL1 after 14 years and 23 years, respectively. Both beams were tested up to failure in order to determine the evolution of corrosion pattern of reinforcing steel and its effect on serviceability limit state (SLS). The tested results shown that the corrosion patterns observed were different relative to time, mechanical effects, bar location and corrosion crack width. The bending cracks had no important influence on the long term corrosion process because the healing progress of cracks resulted from the expansive rust products that fill the gaps of cracks and prevent the oxygen and chloride ions to reinforcing bar. The compressive steel bars of beams were affected by the "top-bar" effect, so forming the gaps between the concrete and the bottom face of the horizontal steel. These gaps were distributed almost all along the reinforcing steel, leading to formation of corrosion cells. This explained why the corrosion developed uniformly along the lower half part of bars in the compressive zone. The crack width induced by corrosion played an important role in the corrosion pattern. For small corrosion crack widths, the pitting corrosion is the main corrosion pattern. In this stage, the corrosion cracks are very small, narrow and distributed separately. For wide corrosion crack widths, the general corrosion grows and becomes predominant. In this stage, the corrosion cracks are interconnected and wider along the rebars. In this study, the critical corrosion crack width, which leads to the change in corrosion pattern, was suggested in range between 0.5 mm and 1.5 mm.

The remaining load-bearing capacity of corroded beams compared to control beam is shown in Fig. I-42. The maximum cross-section reduction on the tensile reinforcement bars of B2CL1 beam was 36.3% after 23 years resulted in the decrease in ultimate capacity by 40% and the decrease in bending stiffness by up to 90%. After a period of 14 years, B1CL1 beam indicated the loss in ultimate loading of around 20% and loss in bending stiffness of about 15% when the maximum cross-section reduction of 19% reached on the tensile reinforcement bars.

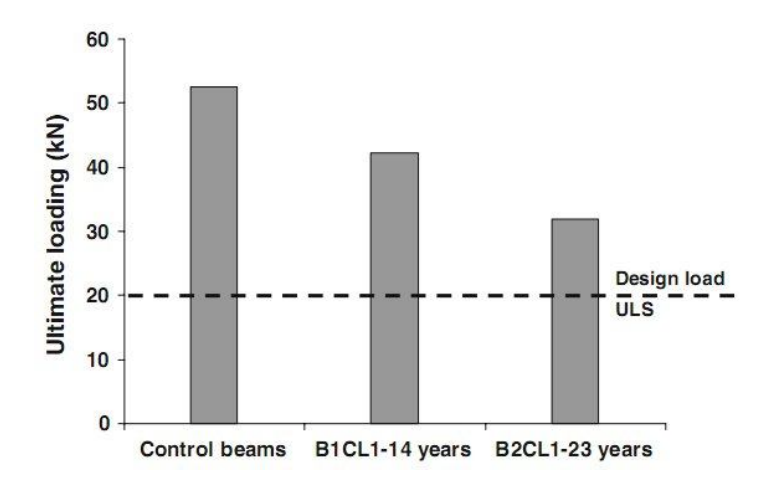


Fig. I-42. Comparison between the residual ultimate load of corroded beams and control beam [44]

It is clear that the residual ultimate capacity of corroded beams is proportional to the tensile steel cross-section reduction during the corrosion process. Whereas, the reduction rate of beam bending stiffness is higher than the reduction rate of steel cross-section. This implies that in addition to the steel cross-section reduction due to corrosion, the debonding between concrete and steel affects significantly the deflection of the corroded beams.

From the experimental outcomes reported, they proposed Serviceability Limit State (SLS) criteria for RC structures in a chloride environment. These criteria included a modelling of the pitting corrosion attacks, the ultimate capacity and the serviceability versus time for both initiation and propagation phases of a corrosion process.

I.2.12. Research by Goitseone Malumbela et al. (2010) [45-48]

Goitseone Malumbela et al. [45-48] tested 20 RC beams with dimensions of 153 x 254 x 3000 mm, corroded under five various levels of sustained loads: 0%, 1% (low deflections), 8% (high deflections but no flexural cracks) and 12% and 16% (high deflections and flexural cracks) of the ultimate load-carrying capacity of a non-corroded beam. The objective of this study is to define more clearly the structural performance of RC beams corroded while suffered from different level service loads. Each beam was reinforced with three 12 mm

diameter steel bars in tension and two 8 mm diameter steel bars in compression. The closed stirrups of 8mm diameter were placed at 100 mm spacing within 1000 mm away from each end of a beam. Accelerated steel corrosion was limited to the tensile steel bars over a length of 700 mm that corresponded to the middle section of the beams. The tensile surface of the mid-span of each beam plunged into a pond that filled with a 5% NaCl solution. Two stages of corrosion process were used: the first one the accelerated corrosion by impressing an anodic current density of 150 mA and then by natural steel corrosion. The accelerated corrosion process consisted of a ponding cycle of four days wetting and two days drying under natural air. However, for beams 4-7, four days drying cycles were used instead. The total wetting time in each beam was limited to 40 days.

They concluded that the moment of inertia (stiffness) of beams with an applied load of 8% of the ultimate load that had no flexural cracks was nearly equal to the moment of inertia of beams had flexural cracks due to applying load of 12% of the ultimate load after 50 days of corrosion. This is because in corroded beams under loading, concrete in tensile zone has little effect on the stiffness of the beam even with the beams without transverse cracks due to loading. For the non-corroded beams while testing under load, the deflections were remained constant with the time of corrosion, whereas, the deflections of corroded beams under load were increased continuously with the degree of corrosion. Because the corrosion process only took place at the middle of beams, the maximum mass loss of reinforcing bars occurred on the centre bar and close to the centre of corrosion zone. Moreover, the authors found that the levels of the sustained load during the corrosion process did not have a significant effect on the maximum mass loss of steel. For example, reference [48] shown that the beam 4 with around 23% maximum loss of mass of bar only sustained load at the level of 1% meanwhile the beam 7 that carried a 8% of ultimate load underwent the maximum corrosion level of around 11%. Probably, the current density was a principle factor affecting significantly the mass loss of steel rather than the loads. From the average mass loss of beam 4 and beam 7, it could be concluded that the loss of steel mass in beams with four days drying cycles were larger than that in beams with two days drying cycles. The reason is that with two days drying the concrete cover not yet completely dried, so leading to larger volumetric product of rust in the pore system, which impeded the corrosion agents such as oxygen, chloride ions to reach the steel bars. The relationship between ultimate flexural moment of beams and the maximum mass loss of steel were established as seen in Fig. I-43.

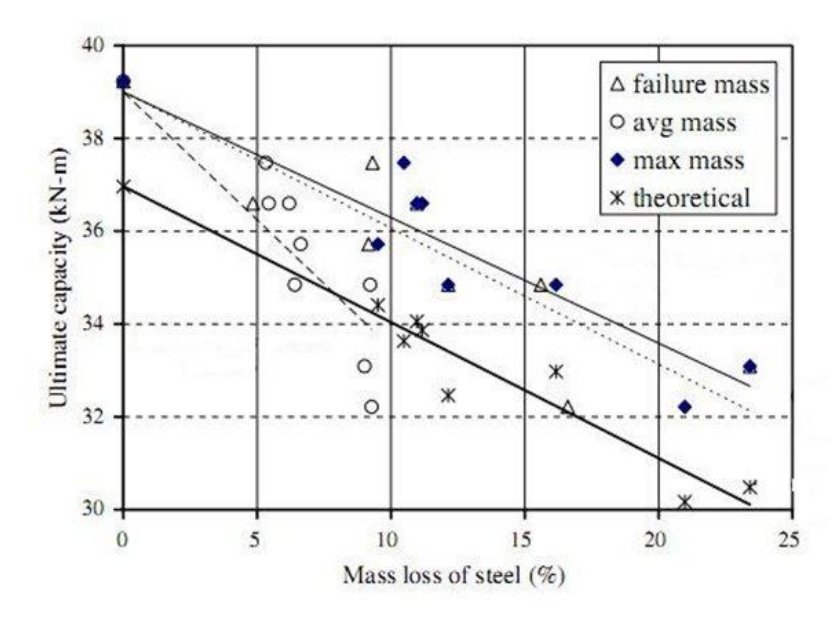


Fig. I-43. Moment-carrying capacity as a linear function of the maximum mass loss of steel [48]

Trends can be observed in each plot that the ultimate moment capacity of beams reduced linearly with an increase in both maximum mass losses of steel and average mass losses of steel. However, if compared to the average mass loss of steel, the maximum mass loss of steel had a better relation with the theoretical moment ultimate capacity. Based on various experimental results of corroded beams, they shown that for 1% maximum mass loss of steel, there was a corresponding 0.7% loss in the residual ultimate moment of RC beams.

I.2.13. Summary

From the experimental results of the authors above, several important conclusions are made:

1. Effect of applying load on corrosion process

The presence of corrosion under applying a load influenced the time to the first corrosion crack. For beams that were corroded in the presence of a sustained load, the corrosion

process was initiated much earlier than in beams corroded in the absence of a sustained load or previous loading. This means that the time to the first visible corrosion crack is diminished. The higher loading levels, the earlier corrosion initiation [36, 38]. The reason is because the number of cracks, crack widths, and microcracks enhances then connecting flow paths at the higher level load, promoting water, oxygen, chloride ions into the surface of reinforcing steel. The widening rate of corrosion crack widths of beams corroded under load is larger that of beams corroded without load at the early time of corrosion. Over a long-term corrosion, this rate is reduced due to an accumulation of corrosion products around the steel bars, which prevented the diffusion of corrosion agents from the surface of steel bars. Furthermore, according to [59-61], when RC beams subjected to a mechanical load and simultaneously affected by a corrosion process of the reinforcement bars, the damage to paste-aggregate interface occurred and resulted in an increase of porosity in this area. Thus, the aggressive ions more quickly reach to the surface of reinforcing bars and spread along their length. This is not possible to obtain in RC beams that were corroded in the absence of a load.

The presence of corrosion influenced the flexural capacity and the ductility of the beams for both the corrosion with loading and the corrosion without loading. However, with the beams corroded in combination with the load, the residual load-carrying capacity was lower than the unloaded beams at the same corrosion degree. The reduced remaining strength resulted from the loss of cross-sectional area of steel and damage of bond at the steel-concrete interface due to expansive corrosion products. Residual load-bearing capacity of corroded RC beams was found to linearly decrease with an increase in the mass loss of steel, in particular, the maximum mass loss of tensile steel. For specimens that were corroded under load over a long term corrosion, the corrosion process significantly reduced the bending stiffness (up to 90%) [44] and ductility (up to 70%) [34].

2. Effect of steel corrosion on ductility loss of RC beams

The literature reported that under service load level, the deflection of corroded specimen increases in comparison to control specimen. The main reasons to cause this are due to the loss of cross section area of steel bar and degradation of concrete-steel bond strength. The reduction in flexural stiffness along with cross-section loss leads to the change in mode of failure at ultimate load. Therefore, the ultimate deflection of corroded RC members could

increase or decrease depending mostly on corrosion level and amount of reinforced steel. A conventional ductility ratio (classical ductility ratio), which is defined as a ratio deflection (Δ) at failure to the corresponding deflection at yield, hardly uses to evaluate the ductility in the case of steel corrosion. This will be discussed more in chapter II, section II.4.

3. Effect of corrosion type: natural or accelerated corrosion on the structural damage The majority of tests have been conducted under accelerated conditions by using an impressed current to the embedded reinforcing steel. This technique is used so that tests can be completed within a reasonably fast time because the process of natural steel corrosion is very slow such that the times needing to cause a considered corrosion are in the order of tens of years. The factor that affects mostly the test results is the impressed current density level. Based on calculating the current density of Goitseone Malumbela [67], it is seen that a variation in the level of impressed current density I_{corr} between $3 \mu \text{ A/cm}^2$ [62] and $10400 \,\mu\,\text{A/cm}^2$ [15] was investigated. Alonso et al. [62] and J.A.Gonzalez et al. [66] reported that for in-service structures that corroded naturally under the contamination environment, the level of corrosion ranged normally from $1 \mu \,\text{A/cm}^2$ to $3 \,\mu \,\text{A/cm}^2$ and seldom values of the order of 10 μ A/cm². In a study on prediction of corrosion rate in RC members, M. B. Otieno et al. [73, 74] accelerated the corrosion tests by subjecting the samples to a cycle of 3-day wetting (5% NaCl) and 4-day drying in laboratory air (t^o = 16-24° C, RH= 60-75%) for up to 100 weeks. This corrosion process is clearly closest to the natural corrosion. They measured the corrosion rate using the coulostatic LPR technique. An average corrosion rate of around 1 µA/cm² was depicted in cracked samples due to loading. In case of uncracked samples, the average corrosion rate was just 0.1 µA/cm². Therefore, a maximum artificial current density of 10400 μ A/cm² is about 3500 times higher than the natural current density (assuming $3 \mu \text{ A/cm}^2$). That is to say the level of corrosion caused by a current density of 3μ A/cm² over a period of one year can be obtained within two hours when a current density of $10400 \,\mu$ A/cm² is applied. P.S. Mangat and M.S.Elgar [52] found that at the same corrosion degree, under higher current density, the deflection of RC beams is greater when comparing to corrosion under lower current density. Figure I-44 exhibits the

resulted from some literatures.

comparison between accelerated corrosion rates with natural corrosion rate of $3 \mu \text{ A/cm}^2$

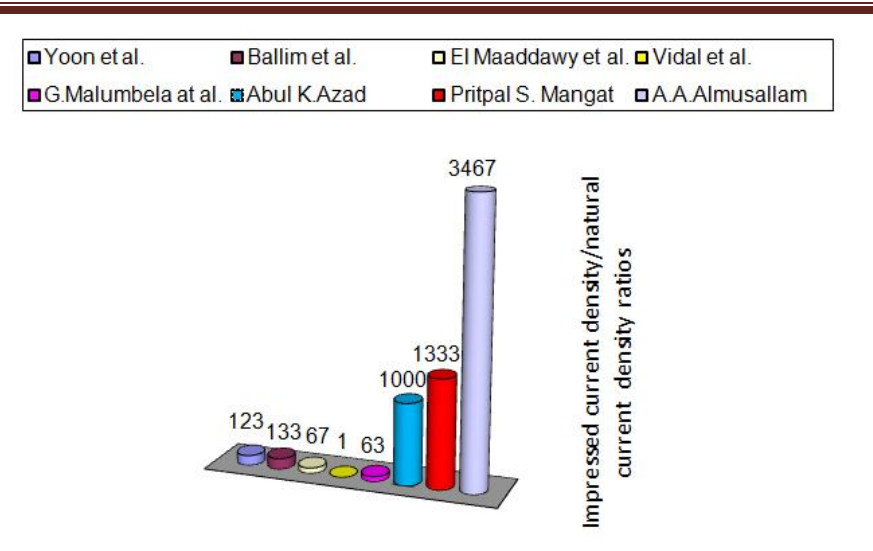


Fig. I-44.The impressed current density-natural current density ratio from various authors [67]

A fast corrosion rate lead to insufficient oxidation thus the rust products presents different compositions and colors at the initiation stage [65]. Indeed, the reddish-brown products are often found in the real structures where steel corrosion is natural, meanwhile in accelerated corrosion tests, corrosion rust products are often greenish-black in color and larger in the term of volume. This indicates that there are different volume densities in the products. A wider corrosion crack is expected by using accelerated steel corrosion. Tamer El Maaddawy et al. [63] evaluated the concrete side strain behavior, the crack width, and the mass loss due to accelerated corrosion by the current density levels between 100 and 500 μ A/cm². This study found that the strains measured for samples applied to 350 and 500 μ A/cm² current densities were significantly higher than those measured for samples applied to 100 and $200 \,\mu$ A/cm² at the same time. The current density level had no effect on the corrosion crack patterns irrespective of high degree of corrosion of steel bars. On the contrary, the impressed current density level had a significant effect on the maximum crack widths due to expansion of corrosion products. The crack width rose with an increase of impressed current density at the same degree of corrosion. They concluded that an impressed current density below $200 \,\mu$ A/cm² does not change the structural behavior of corrosion affected RC specimens that would be observed under natural steel corrosion.

With such as rapid corrosion rate, the corroded characteristics of steel bar surface, the mechanical behavior of corroded bar, and the load-bearing capacity must be affected. Yingshu Yuan et al. [64] concluded that the surface of the steel bar under an artificial corrosion showed nearly uniform corrosion around the whole surface of steel bar while under natural corrosion, the corrosion distributed locally at the lower half of the steel bar surface. In the case of natural corrosion, the location and intensity of the corrosion are perfectly random. Furthermore, the chemical compositions of corrosion products formed in a natural, chloride contaminated environment and those produced using the impressed current method could be different because of the time intervals of the corrosion process as well as the lack of chlorides. This affects the spatial distribution of corrosion products, leading to influence on steel-concrete bond that would result in the deferent structural behavior. This point of view was strongly supported by A. Poursaee and C.M. Hansson [68]. They suggested that "if the goal is to assess a 100 year service life, spending a minimum of a few weeks or months on evaluation should be considered reasonable and necessary. Accelerating the corrosion by applying an anodic current to rebar should be avoided unless the goal is to assess circumstances in which this happens in practice, such as stray current corrosion" [68]. Moreover, impressed current might also impeached the repassivation phenomena in cracked RC elements due to healing or self-healing of cracks which could occurred in natural process corrosion.

In general, the effect of impressing an anodic current to the embedded steel to accelerate corrosion process is still in dispute. Thus, the research works on concrete structures corroded naturally or closest to nature condition is necessary to in-depth understand the real behavior as well as proposing recommendations for in-field structure.

References

- **1. A. Castel, T. Vidal, K.Viriyametanont, and R. François**., 2006, "Effect of Reinforcing Bar Orientation and Location on Bond with Self-Consolidating Concrete", ACI Structural Journal, pp. 559-567.
- **2. M. Hoshino**., 1989, "Relationship between bleeding, coarse aggregate, and specimen height of concrete", ACI Materials Journal, V. 86, No. 2.
- **3.** M. Reza Esfahani, M. Lachemi, M. Reza Kianoush., 2008, "Top-bar effect of steel bars in self- consolidating concrete (SCC)", Cement & Concrete Composites 30, pp. 52–60.
- **4. Geoffrey B.Welch, Bruce J.F.Patten**., 1965, "Bond strength of reinforcement affected by concrete sedimentation", Journal of American concrete institute.
- **5. Arthur P.Clark**., 1949, "Bond of concrete reinforcing bars", Journal of American concrete institute.
- **6. Rex C. Donahey, David Darwin.**, 1985, "Bond of top-cast bars in bridge decks", ACI Stru ctural Journal, pp. 55-66.
- **7. T. A. Soylev, R.François**., 2006, "Effect of bar-placement conditions on steel-concrete bond", Materials and Structures 39:211–220.
- **8. T. A. Soylev, R.François**., 2003, "Quality of steel-concrete interface and corrosion of reinforcing steel", Cement and Concrete Research 33: 1407–1415.
- **9. T. A. Soylev, R.François**., 2005, "Corrosion of reinforcement in relation to presence of defects at the interface between steel and concrete", Journal of Materials in Civil Engineering, Vol. 17, No. 4.
- **10. T. U. Mohammed, N. Otsuki, H. Hamada, and T. Yamaji.**, 2002, "Chloride-induced corrosion of steel bars in concrete with presence of gap at steel-concrete interface", ACI Materials Journal, V. 99, No. 2.
- **11. T.U. Mohammed, N. Otsuki, and M. Hisada**., 1999, "Corrosion of Steel Bars with Respect to Orientation in Concrete", ACI Materials Journal, V. 96, No. 2.

- **12. T. U. Mohammed, N. Otsuki, H. Hamada, and T. Yamaji**., 2002, "Chloride-indue corrosion of steel bars in concrete with presence of gap at steel-concrete interface", ACI Materials Journal.
- **13. CEB-FIB.**, 2000, "Bond of reinforcement in concrete: State-of-art report", 434 pages, ISBN 978-2-88394-050-5.
- **14. G. J. Al-Sulaimani, M. Khleemullah, I. A. Basunbul, and Rasheeduzzafar.**, 1990, "Influence of corrosion and cracking on bond behavior and strength of reinforced concrete members", ACI Structural Journal, pp. 220-231.
- **15.** A. A. Almusallam, A. S. Al-Gahtani, A. Aziz and Rasheeduzzafar., 1996, "Effect of reinforcement corrosion on bond strength", Construction and Building Materials, Vol.10, No.2, pp.123-129.
- **16. P. S. Mangat, M. S. Elgarf.**, 1999, "Bond characteristics of corroding reinforcement in concrete beams", Materials and Structures, Vol. 32, pp 89-97.
- **17. C. Fang, K. Lundgrenb, L. Chena, C. Zhua**., 2004, "Corrosion influence on bond in reinforced concrete", Cement and Concrete Research 34: 2159–2167.
- **18.** L. Chung, S.Ho Cho, J.Ho Jay Kim, S.Tae Yi., 2004 "Correction factor suggestion for ACI development length provisions based on flexural testing of RC slabs with various levels of corroded reinforcing bars", Engineering Structures 26: 1013–1026.
- **19. K. Bhargava**, **A.K. Ghosh**, **Y. Mori**, **S. Ramanujama**., 2007," Corrosion-induced bond strength degradation in reinforced concrete—Analytical and empirical models", Nuclear Engineering and Design 237: 1140–1157.
- **20.** Leroy A.Lutz, Peter Gergely., 1967, "Mechanical of bond and slip of deformed bars in concrete", ACI Journal.
- **21. J. Cairns, Y.Du, D.Law**., 2007, "Influence of corrosion on the friction characteristics of the steel/concrete interface", Construction and Building Materials 21: 190–197.
- **22. L.Amleh, S. Mirza**., 1999, "Corrosion influence on bond between steel and concrete", ACI Structural Journal, V. 96, No. 3, pp.415-423.
- **23. X. Fu and D. D. L. Chung**., 1997, "Improving the bond strength between steel rebar and concrete by increasing the water/cement ratio", Cement and Concrete Research. Vol. 27. No. 12. pp. 1805-1809.

- **24. R. Ravindrarajah, K. Ong.**, 1987, "Corrosion of steel in concrete in relation to bar diameter and cover thickness", ACI journal, SP 100-84, pp. 1667-1677.
- **25. EUROPEAN STANDARD prEN 1992-1-1, 2002 Eurocode 2**: Design of concrete structures Part 1: General rules and rules for buildings.
- **26. Commit euro-international du beton**., 1991, "CEB-FIB model code 1990", 437 pages, ISBN 07177 1696 4.
- **27. A. A. Almusallam**., 2001, "Effect of degree of corrosion on the properties of reinforcing steel bars", Construction and Building Materials 15: 361-368.
- **28.** J. Cairns, G.A Plizzari, Y. Du, D. W Law, C. Franzoni., 2005, "Mechanical Properties of Corrosion-Damaged Reinforcement", ACI Materials Journal, V.102, No.4, pp.256-264.
- **29. C. A. Apostolopoulos, V. G. Papadakis**., 2007, "Mechanical behavior of reinforcement stirrups BSt 500_s at corrosive environment", Journal of Materials Engineering and Performance, Volume 16(2), pp.236-241.
- **30.** C. A. Apostolopoulos, V. G. Papadakis., 2008, "Consequence of steel corrosion on the ductility properties of reinforcement bar", Construction and Building Materials 22: 2316–2324.
- **31.** C. A. Apostolopoulos and D. Michalopoulos., 2007, "The impact of corrosion on the mechanical behavior of steel undergoing plastic deformation", Materials and Corrosion, 58, No. 1, pp.5-12.
- **32. R. Palsson and M. Saeed Mirza**., 2002, "Mechanical response of corroded steel reinforcement of abandoned concrete bridge", ACI Materials Journal, V.99, No.2, pp.157-162.
- **33. H. Seung Lee, Y. Sang Cho.**, 2009, "Evaluation of the mechanical properties of steel reinforcement embedded in concrete specimen as a function of the degree of reinforcement corrosion", Int J Fract 157:81–88 DOI: 10.1007/s10704-009-9334-7.
- **34. A. Castel, R. Francois, G. Arliguie**., 2000, "Mechanical behaviour of corroded reinforced concrete beams Part 1: Experimental study of corroded beams", Materials and Structures/Materiaux et Constructions, Vol. 33, pp 539-544.
- **35. A. Castel, R. Francois, G. Arliguie**., 2000, "Mechanical behaviour of corroded reinforced concrete beams Part 2: Bond and notch effects", Materials and Structures/Materiaux et Constructions, Vol. 33, pp 545-551.

- **36. S. Yoon, K. Wang, W. Jason Weiss, and Surendra P. Shah.**, 2000, "Interaction between Loading, Corrosion, and Serviceability of Reinforced Concrete", CI Materials Journal, V. 97, No.6.
- **37. Y. Balim, J. C. Reid.**, 2003, "Reinforcement corrosion and the deflection of RC beamsan experimental critique of current test methods", Cement & Concrete Composites 25: 625–632.
- **38. T.El Maaddawy, K. Soudki, and T. Topper**., 2005, "Long-term performance of corrosion-damaged reinforced concrete beams", ACI Structural Journal, V. 102, No. 5.
- **39. T. Vidal, A. Castel, R. Francois.**, 2007, "Corrosion process and structural performance of a 17 year old reinforced concrete beam stored in chloride environment", Cement and Concrete Research 37: 1551–1561.
- **40. T. Vidal, A. Castel, R. Francois**., 2003, "Physical, chemical and mechanical analysis of a reinforced concrete beam corroded in chloride environment", ACI journal, SP 212-5, pp.59-76.
- **41. T. Vidal, A. Castel, R. Francois**., 2004, "Analyzing crack width to predict corrosion in reinforced concrete", Cement and Concrete Research 34: 165–174.
- **42. R. Zhang, A. Castel, R. Francois**., 2010, "Concrete cover cracking with reinforcement corrosion of RC beam during chloride-induced corrosion process", Cement and Concrete Research 40: 415–425.
- **43. R. Zhang, A. Castel, R. Francois**., 2009, "The corrosion pattern of reinforcement and its influence on serviceability of reinforced concrete members in chloride environment", Cement and Concrete Research 39: 1077–1086.
- **44. R. Zhang, A. Castel, R. Francois**., 2009, "Serviceability limit state criteria based on steel-concrete bond loss corroded reinforced concrete in chloride environment", Materials and Structures 42: 1407–1421.
- **45. G. Malumbela, P. Moyo, M. Alexander**., 2009, "Behavior of RC beams corroded under sustained service loads", Construction and Building Materials 23: 3346–3351.
- **46. G. Malumbela, P. Moyo, M. Alexander**., 2010, "Influence of corrosion crack patterns on the rate of crack widening of RC beams", Construction and Building Materials 25: 2540–2553.

- **47. G. Malumbela, P. Moyo, M. Alexander**., 2009, "Structural behaviour of beams under simultaneous load and steel corrosion", Concrete Repair, Rehabilitation and Retrofitting II Taylor & Francis Group, London, ISBN 978-0-415-46850-3.
- **48. G. Malumbela, P. Moyo, M. Alexander**., 2010, "Variation of steel loss and its effect on the ultimate flexural capacity of RC beams corroded and repaired under load", Construction and Building Materials 24: 1051–1059.
- **49. A. K.Azad, S. Ahmad, Syed A.Azher**., 2007, "Residual strength of corrosion-damaged reinforced concrete beams", ACI Materials Journal, V. 104, No. 1.
- **50. A. Ababneh, M. Sheban**., 2010, "Impact of mechanical loading on the corrosion of steel reinforcement in concrete structures", Materials and Structures DOI 10.1617/s11527-010-9688-3.
- **51.** I. Khan, R. Francois, A. Castel., 2011, "Mechanical behaviour of long-term corroded reinforced concrete beam", Modelling of Corroding Concrete Structure, RILEM workshop, Madrid, Spain.
- **52. P. S. Mangat and M. S. Elgar.**, 1999, "Flexural Strength of Concrete Beams with Corroding Reinforcement", ACI Structural Journal, V. 96, No. 1.
- **53.** Y. Du, L. A. Clark, and A. H. C. Chan., 2007, "Impact of Reinforcement Corrosion on Ductile Behavior of Reinforced Concrete Beams", ACI Structural Journal, V. 104, No. 3.
- **54. R. Capozucca, M. Nilde Cerri.**, 2003, "Influence of reinforcement corrosion-in the compressive zone -on the behaviour of RC beams", Engineering Structures 25 (2003) 1575–1583.
- **55. J. Jeppsson and S. Thelandersson**., 2003, "Behavior of Reinforced Concrete Beams with Loss of Bond at Longitudinal Reinforcement", Journal of Structural Engineering © ASCE.
- **56. A. A. Almusallam, A. S. Al.Gahtani, A. Rauf Aziz, F.H. Dakhil, and Rasheeduzzafa**., 1996, "Effect of reinforcement corrosion on flexural behaviour of concrete slabs", Journal of Materials in Civil Engineering.
- **57. J. Rodriguez, L. M. Ortega, J. Casal.**, 1997, "Load carrying capacity of concrete structures with corroded reinforcement", Construction and Building Materials, Vol. II, No. 4. pp. 239-248.

- **58. L.Chung, H. Najm, P. Balaguru**., 2008, "Flexural behavior of concrete slabs with corroded bars", Cement & Concrete Composites 30: 184–193.
- **59. A. Castel, R. Francois, G. Arliguie**., 1999, "Effect of loading on carbonation penetration in reinforced concrete elements", Cement and Concrete Research 29: 561–565.
- **60. R. Francois, J. C.Maso.**, 1988, "Effect of damage in reinforced concrete on carbonation or chloride penetration", Cement and Concrete Research, Vol. 18, pp. 961-970.
- **61. R. François, G. Arliguie**., 1991, "Reinforced concrete: correlation between cracking and corrosion", ACI journal, SP 126-65, pp.1221-1238.
- **62. C. Alonso, C. Andrade, J. Rodriguez**, J. M. Diez., 1998," Factors controlling cracking of concrete affected by reinforcement corrosion", Materials and Structures, Vol. 31, pp 435-441.
- **63. T.A. El Maaddawy, K. A. Soudki**., 2003, "Effectiveness of impressed current technique to simulate corrosion of steel reinforcement in concrete", Journal of Materials in Civil Engineering, Vol. 15, No. 1.
- **64.** Y. Yuan, Y. Ji, and S. P. Shah., 2007, "Comparison of two accelerated corrosion techniques for concrete structures", ACI Structural Journal, V. 104, No. 3.
- **65. S. Care, A. Raharinairo**., 2007, "Influence of impressed current on the initiation of damage in reinforced mortar due to corrosion of embedded steel", Cement and Concrete Research 37: 1598–1612.
- **66. J. A. Gonzalez, C. Andrade, C. Alonso, S. Feliu**., 1995, "Comparison of rates of general corrosion and maximum pitting penetration on concrete embedded steel reinforcement", Cement and Concrete Research, Vol. 25, No. 2. pp. 257-264.
- **67. G. Malumbela.**, 2010, "Measurable parameters for performance of corroded and repaired RC beams under load", Thesis of Doctor of Philosophy, University of Cape Town.
- **68. A. Poursaee, C.M. Hansson**., 2009, "Potential pitfalls in assessing chloride-induced corrosion of steel in concrete", Cement and Concrete Research 39: 391–400.
- **69. D. Coronelli, K. Zandi Hanjari, K. Lundgren and E. Rossi**., 2010, "Severely Corroded Reinforced Concrete with Cover Cracking: Part 1. Crack initiation and Propagation", Modeling of corroding concrete structures, RILEM workshop, Madrid, Spain.

- **70. K. Zandi Hanjari, D. Coronelli and K. Lundgren**., 2010, "Severely Corroded Reinforced Concrete with Cover Cracking: Part 2. Anchorage Capacity", Modeling of corroding concrete structures, RILEM workshop, Madrid, Spain.
- **71. D. Coronelli.**, (2002), "Corrsion cracking and bond strength modeling for corroded bars in reinforced concrete", ACI Structural Journal, V. 99, No. 3.
- **72. ASTM-A 370-97a**, 1997, "Standard Test Methods and Definitions for Mechanical Testing of Steel Products", American Society for Testing and Materials.
- **73. M.B. Otieno, M.G. Alexander and H.D. Beushausen**., 2010, "Corrosion in cracked and uncracked concrete-influence of crack width, concrete quality and crack reopening", Magazine of Concrete Research, 61, No. 6, 393-404.
- **74. M. Otieno, H. Beushausen and M. Alexander**., 2012, "Prediction of corrosion rate in reinforced concrete structures a critical review and preliminary results", Materials and Corrosion, 63, No. 9, 777-790.
- **75. A. A. Torres-Acosta, S. Navarro-Gutierrez, J. Terán-Guillén**., 2007, "Residual flexure capacity of corroded reinforced concrete beams", Eng Struct, 29(6):1145-52.

Chapter II:

EXPERIMENTAL RESULTS ON LONG-TERM CORRODED BEAMS

GENERAL

The experimental program was undertaken to study the mechanical behaviour of corroded RC beams as well as mechanical properties of corroded steel bars, which extracted from these RC beams. The modes of failure and the ultimate carrying capacity of the beams were also investigated. The ductility of beams in term of defection at midspan was examined. The test specimens consisted of two corroded beams and two control beams of 27 years. This chapter presents details of experimental results on these beams:

- The change in steel properties due to corrosion
- The change in loading capacity for slender beams
- The more complex behaviour of corroded shear critical beams
- The change in ductility for slender beams

II.1. EFFECT OF CORROSION OF STEEL ON STEEL PROPERTIES

Article:

Raoul Francois, Inamullah Khan, Vu Hiep Dang, Impact of corrosion on mechanical properties of steel embedded in 27-year-old corroded reinforced concrete beams, Materials and Structures, 2012.

DOI 10.1617/s11527-012-9941-z.

Abstract. This paper deals with the impact of corrosion on the mechanical properties of steel in reinforced concrete. Steel bars were extracted from two 27-year-old corroded reinforced concrete beams that had been exposed to a chloride environment. Bars with different degrees of corrosion and with different corrosion pit depths were tested in tension. A comparison was made between nominal and true stress for corroded and control steel specimens. It was noted that the degree of corrosion strongly affected the mechanical properties of the steel, particularly the ultimate stress and strain.

Interestingly, the true yield strength of all the corroded steel bars remained almost constant while their true ultimate strength was considerably increased.

A reduction of the ultimate elongation appeared to be the major effect of corrosion and affected the compliance with standards.

Keywords. Corrosion, reinforced steel, stress strain curves, ultimate elongation, ductility, yield stress.

1. Introduction

Corrosion is one the biggest threats currently faced by the reinforced concrete industry. Corrosion products exert a pressure that easily surpasses the very limited tensile strength of concrete and thus leads to cracking and spalling of the concrete cover. In addition, corrosion of the reinforcing steel bars weakens the bond between steel and concrete and hence can reduce the service life of the structure [1, 2].

Many researchers have investigated the impact of corrosion on the mechanical properties of steel and most of these studies deal with accelerated corrosion induced by impressed current applied to the surface of the reinforcement embedded in the concrete. This is very different from natural corrosion [16]. M. Maslehuddin et al. [3] performed tests on steel bars exposed to the atmosphere for 16 months and found that rusting did not affect the ultimate and yield strength of the bars. Abdullah A. Almusallam [4] tested 6-mm and 12-mm steel bars embedded in concrete and subjected to accelerated corrosion. Using the actual cross- sectional area, a marginal decrease was found in the ultimate tensile strength of the steel bars as the degree of reinforcement corrosion increased but the total elongation of the bars decreased with the increasing degrees of corrosion. C.A. Apostolopoulos and V.G. Papadakis [5] studied the tensile behavior of reinforcing steel bars of Class BSt 420, a type of steel that is no longer produced. Apparent and effective stresses were calculated on the basis of the initial non-corroded cross-section of the steel bars and the true cross-section of corroded steel bars respectively. According to these

results, effective yield stress remained almost constant with increasing corrosion while apparent yield stress and effective and apparent ultimate stress decreased as the corrosion rate increased. A significant loss of ductility was also observed. Han-Seung Lee and Young-Sang Cho [6] observed a decrease in nominal yield point and nominal elastic modulus as the degree of reinforcement corrosion increased. J. Cairns et al. [7] investigated the effect of local pitting due to corrosion on steel bars. Corrosion pits were simulated by removing a section of bar using a multifluted, hemispherical end mill with a cylindrical shank. They found that reduction of the maximum load was proportional to the damaged area while reduction in the force at the yield point was slightly less proportional to the cross-section. Y.G. Du et al. [8] carried out an experimental study on 108 reinforcement samples, among which were 30 steel bars embedded in concrete, which were subjected to artificial corrosion. They concluded that the residual yield stress and the ultimate stress of corroded reinforcement in concrete decreased with an increasing corrosion level.R. Palsson and M.S. Mirza [9] tested the corroded steel reinforcing bars recovered from an abandoned bridge. They divided the samples into four groups according to the level of corrosion. They reported that both average nominal yield and ultimate stresses were almost the same for all the groups but a slight increase in yield stress was noted in the case of pitted specimens. A drastic decrease in ductility with increasing degrees of corrosion was also reported. Reinforced concrete bars become corroded by two mechanisms: the ingress of chloride ions into the concrete and carbonation of the concrete. The effects of chloride ion ingress are more marked than those of carbonation. Weiping Zhang et al. [10] investigated the effect of corrosion on the rebars obtained from RC beams of a carbonated inland building over 30 years old. A noticeable fall in both yield and ultimate strengths was recorded. The research works discussed above are summarized in the table 1 below keeping in view the parameters studied in the present work.

Table 1. Summary of previous research work

Authors	Testing specimen	Corrosion condition	Nominal Yield strength	Nominal Ultimate strength	True Yield strength	True Ultimate strength	Ductility	Elastic Modulus
Maslehuddin et al.	Bare bars	Atmospheric corrosion/Rustin g	Not affected	Not affected	Not stated	Not stated	Not stated	Not stated

CHAPTER II: Experimental results on long-term corroded beams

Almusallam et al.	Bars in concrete	Accelerated	Not stated	Decreased	Not stated	Marginally decreased	Decreased	Not stated
Palsson and Mirza	Bars in concrete	Service/ chloride	Not affected	Not affected	Not stated	Not stated	Decreased	Not stated
Apostolopoulos and Papadakis	Bars in concrete	Accelerated	Not affected	Decreased	Decreased	Decreased	Decreased	Not stated
Lee and Cho	Bars in concrete	Accelerated	Decreased	Not stated	Not stated	Not stated	Decreased	Decreased
Cairns et al.	Bars in concrete	Artificial/ Local pitting	Not stated	Not stated	Not affected	Increased	Decreased	Not stated
Du et al.	Bare bars /Bars in concrete	Accelerated	Decreased	Decreased	Decreased	Decreased	Decreased	Not stated
Weiping Zhang et al.	Bars in concrete	Carbonation	Not stated	Not stated	Decreased	Decreased	Decreased	Not stated

^{*}Nominal stresses are calculated based on nominal steel area

*True stresses are calculated based on residual corroded

area

Clearly, a better understanding of the effects of corrosion on the mechanical properties of reinforcement is needed, particularly concerning natural corrosion processes, because they are very important for modeling the mechanical behavior of corroded RC members. Moreover, it can be seen that there is still a lack of data on the influence of corrosion on nominal and true stress in the pre-yield and post-yield behavior of steel bars.

In the present work, corroded and non-corroded steel bars were extracted from 27-years-old concrete beams exposed to a chloride environment under a sustained loading. The bars were subjected to tensile tests and the influence of corrosion on their pre-yield and post-yield behavior of steel bars was studied.

2. Experimental Context

A long-term experimental program was started in 1984 at the Laboratoire Matériaux et Durabilité des Constructions (L.M.D.C.) at INSA-Toulouse (France). A set of 36 reinforced concrete beams of similar dimensions (300×28×15 cm) as supplied by industry, cast with two different section types, A and B, were stored in a chloride environment under sustained loading. At the same time, another set of 36 reinforced concrete beams of the same composition were cast but stored under normal laboratory conditions (non-aggressive environment) to serve as control beams. At different stages,

experiments were carried out to collect data such as the cracking map, chloride content, and mechanical behavior under service load [11, 12]. Some of the beams were tested until failure to evaluate their ultimate capacity and inspect the distribution of rebar corrosion. In this paper, steel specimens were collected from two corroded and two control A beams to study the effect of corrosion on the mechanical properties of the steel.

2.1 Reinforced Concrete Specimens

The beams were divided into two groups, type A and type B beams, which had different reinforcements, but the same ordinary reinforcing steel (yield strength=500MPa) was used. Beams A had the maximum 40-mm concrete cover and beams B had the minimum 10-mm cover (Fig. 1). The composition of the concrete is given in Table 2. Water content was adjusted to obtain a slump of 7 cm. The average compressive strength and elastic modulus obtained on cylindrical specimens (110×220 mm) were 45 MPa and 32 GPa at 28 days. Only steel bars extracted from the tensile zone of beams A were tested here.

Table 2. Concrete composition (kg/m³)

Mix component		
Rolled gravel (silica + limestone)	5/15 mm	1220 kg
Sand	0/5 mm	820 kg
Portland Cement: OPC HP (high perform)		400 kg
Water		200 kg

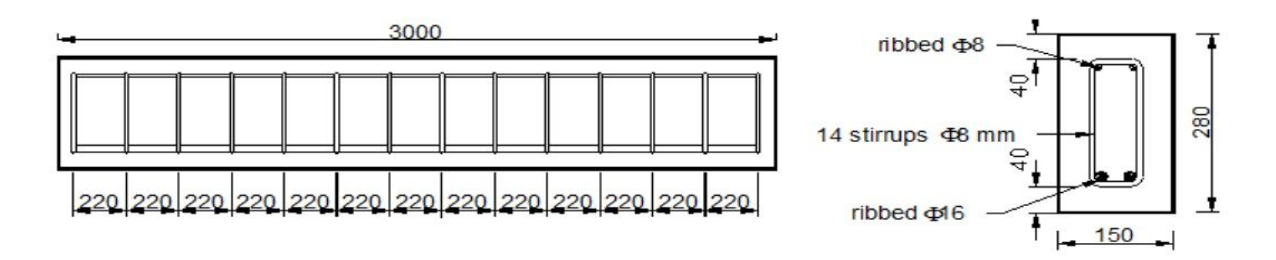


Figure 1. Layout of reinforced concrete beam type A

2.2 Beams exposure environment

The beams were kept in an aggressive chloride environment. The aggressive environment was a salt fog (35g/l of NaCl, corresponding to the salt concentration of seawater) generated by four sprays located at each of the upper corners of a confined

room (Fig. 2). After 6 years of storage, the beams were subjected to wetting-drying cycles in order to accelerate the corrosion process:

- 0 to 6 years: continuous spraying under laboratory conditions ($T^{\circ}\approx 20^{\circ}C$),
- 6 to 9 years: spraying cycles under laboratory conditions (T°≈20°C), one week of spraying and one week of drying.
- 9 to 19 years: spraying cycles, one week of spraying and one week of drying. However, the confined room was transferred outside so the beams were exposed to the temperatures reigning in the south-west of France climate ranging from −5°C to 35°C.
- 19 to 27 years: cycles were stopped and the beams were unloaded; the beams were subjected to the temperature of the south-west of France and corroded naturally.

The control beams had the same concrete composition and reinforcement lay-out but was stored in a laboratory room at 50% of R.H. and 20°C.

2.3 Loading of Beams

The beams were loaded in three-point flexure by coupling a type A beam with a type B. According to French standards, the level 1 loading (M_{ser1} = 13.5 kN m) corresponded to maximum loading of type A beam for durability in an aggressive environment (serviceability limit-state requirements in an aggressive environment) and to maximum loading of type B element for resistance (ultimate load limit state in a non-aggressive environment). The beams stored under sustained level 1 loading were called A1 and B1. The level 2 loading value for the type B beam (M_{ser2} =21.2kN m) corresponded to 80% of the failure load and was equal to twice the design service loading in an aggressive environment according to French standards. For the type A beam presented in this paper, it corresponded to maximum loading for resistance (ultimate load limit state in a non-aggressive environment). The beams stored under sustained level 2 loading were called A2 and B2. For all of these beams, the upper surface corresponded to the bleeding surface.

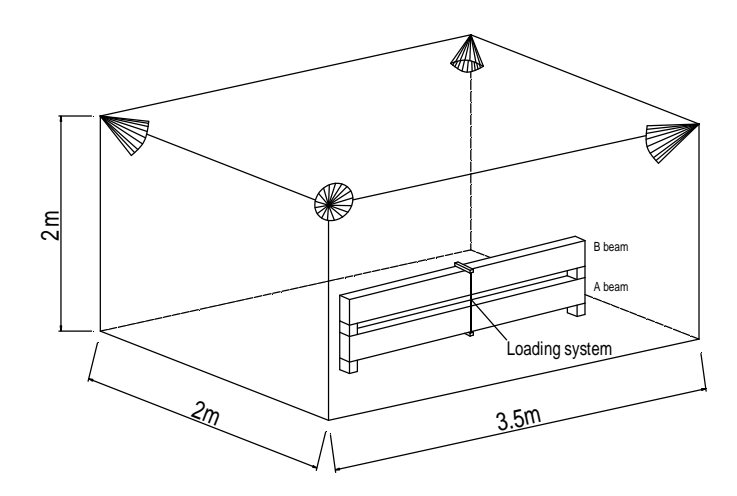


Figure 2. Loading system and environment of beams

3. Experimental Program

3.1 Test Specimens

Two sets of beams were selected, each set containing one corroded and one control beam of the same age (27 years old). The beams were chosen to have different corrosion crack widths in order to have different losses of rebar cross-section [13, 14]. Each longitudinal bar extracted from the beam was cut into several pieces of average length 450 mm. Details of the specimens are given in table 3. For corroded beams A2CL1 and A2CL3, A2 indicates the beam type, suffix "CL" indicates that beams were exposed to chloride environment while the last digit indicates the beam number. Whereas the two control beams were simply named as A1T and A2T. Steel bars recovered from both front side FS and back side BS of beams were cut into several parts and are named accordingly, e.g. FS Part 1 indicates that steel bar specimen is taken from front side bar FS of the beam.

Table 3. Experimental specimens

	Beams	Nominal diameter of main reinforcement	Concrete cover	Specimen Number
Set I	A2CL3	16 mm	40 mm	FS Part 1
				FS Part 2
				BS Part 1
				BS Part 2
	A2T			Control 1
				Control 2
Set II	A2CL1	16 mm	40 mm	FS Part 3
				FS Part 4
				BS Part 3
				BS Part 4
				BS Part 5
	A1T			Control 3

3.2 Measurement of loss of diameter of corroded steel

After cutting, the rebars were cleaned using Clark's solution ANSI/ASTM G1-72 in order to remove all the corrosion products. The degree of reinforcement corrosion was assessed by measuring the diameter loss with the help of a vernier caliper after complete removal of the corrosion products. It was very difficult to measure the precise diameter loss in this way since the surface shape of the corroded reinforcement varied substantially. Therefore, the weight loss of the steel bar was also used to calculate the diameter loss. The steel bars with pitting attack were cut to lengths of 1-2 cm depending on the length of pit corrosion. The piece was then weighed to an accuracy of 0.001g and its mass loss was determined. The following equation was used to measure the percentage diameter loss from the mass loss.

$$\%d = 100 \left[1 - \sqrt{1 - \frac{\Delta M}{M_0}} \right]$$

Where: ΔM is the mass loss and M_0 is the mass of the sound steel.

Determining the real cross-section at the failure location of the steel bar was very difficult due to the complex shape of the corrosion damage (see figure 9). The smallest diameter measured with the vernier caliper gave a conservative value of the residual cross-section and could induce a large scatter in the results which may not have been representative since the residual cross-section varied widely around the disk: scatter could be of the order of 20%. The loss of mass of steel for a length of 10-20 mm cut from the bar around the failure location gave an average loss of cross section but the results were affected by scatter due to the fact that the corrosion shape was not constant along the cut length and that irreversible strain induced by yielding before failure affected the real value of the length of the bar section when determining the average residual diameter from weight measurement. Nevertheless, because corroded bar underwent brittle failure, the necking process was reduced and then the effect on modifying the length of steel section was limited. Tentatively, scatter could be taken as approximately 10%.

3.3 Uniaxial tension tests of reinforcement

After assessing the weight loss, the steel bars with pitting attack within the initial length were tested in tension to evaluate their mechanical properties. They were tested using a machine of 250 kN capacity. Two LVDTs were used to measure the bar elongation. The base length of each steel bar was 200 mm. The load and elongation data were recorded using a computerized data acquisition system at pre-determined load intervals up to failure of the specimen. The data obtained were utilized to plot stress-strain diagrams for each of the specimen tested. Using the stress-strain diagrams, yield strength, ultimate strength and the elongation of the steel bars were compared.

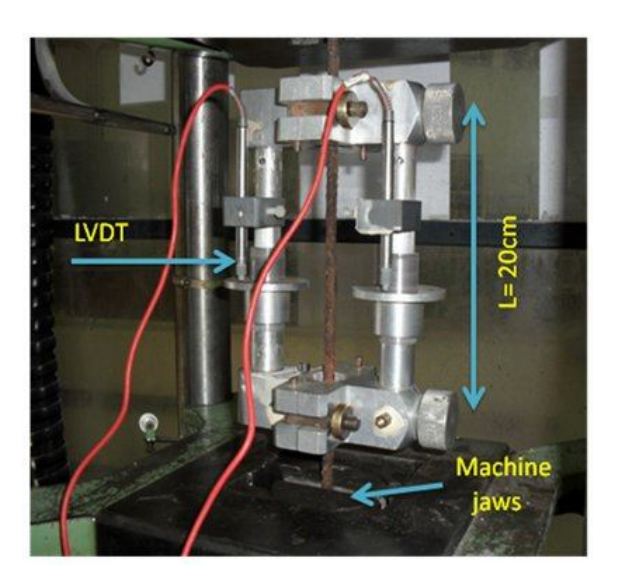
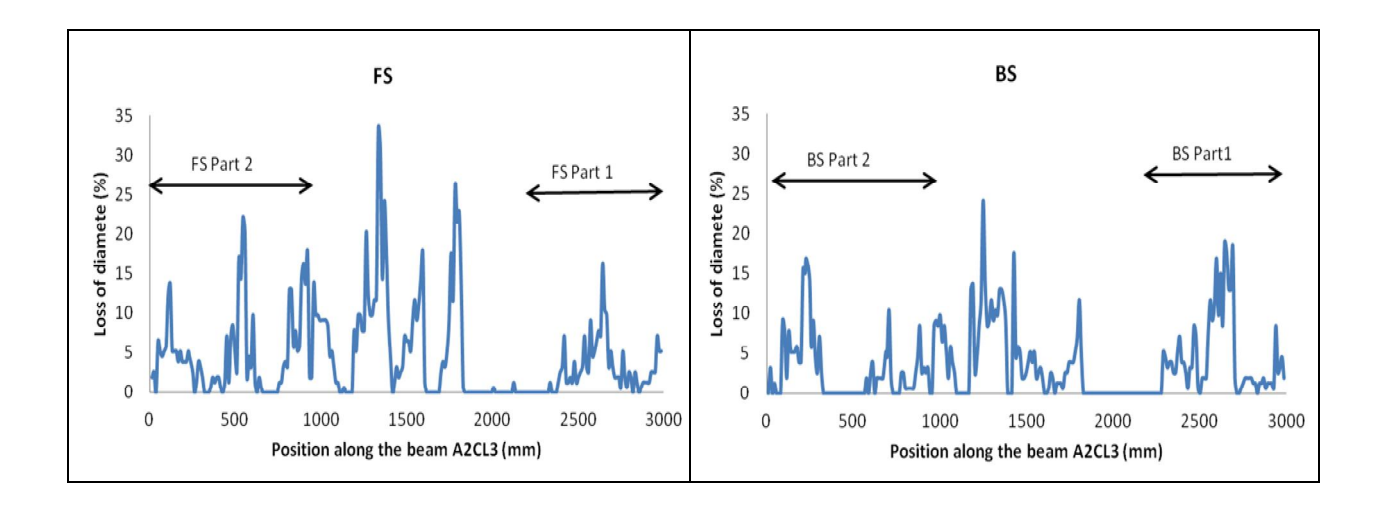


Figure 3. Typical arrangement for tensile test on steel bar

4. Experimental results

4.1 Loss of diameter for rebars.

The loss of diameter of the steel reinforcement is presented in this section. Figure 4 shows the diameter loss for beams A2CL3 and A2CL1. FS and BS indicate Front Side and Back Side main longitudinal bars of the beam.



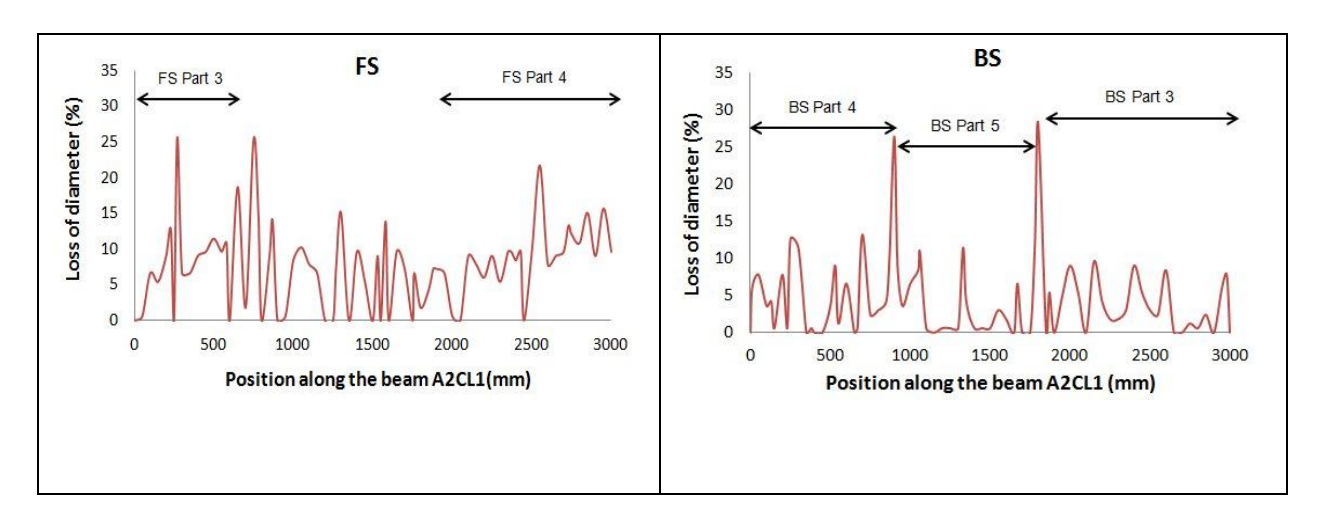


Figure 4. Loss of diameter of reinforcement along the length of beam for FS and BS tensile bars in beams A2CL3 and A2CL1 (part (i) refers to pieces of bar tested in tension)

4.2 Mechanical behavior of steel bar

4.2.1 Effect of corrosion on residual strength of steel bar

Table 4 shows the nominal and true stresses of corroded and control bars. Three types of stress values are presented. Nominal stresses were calculated using the nominal diameter of the steel bar for both corroded and non-corroded steel bar. True stresses were calculated in two different ways. The first used the reduced diameter measured with the vernier caliper. To avoid the difficulty of measuring the precise diameter with a vernier caliper, the second method used to measure the diameter loss was calculated from the mass loss of the corroded steel bar. True stresses calculated on the basis of this diameter loss are also presented in the table 4. In addition, true stresses for control bars were calculated on the basis of the real diameter (between ribs) of the bar measured by vernier caliper. For control bar 1 and control bar 2, the true diameter measured with the vernier caliper was 15.3 mm and for control bar 3 it was measured as 15.7 mm. If there is no plateau between the elastic and the plastic behavior of steel, then the yield strength can be calculated as the stress at which the specimen reaches a strain of 0.2%.

Table 4. Nominal and true stresses

Φ (mm)	% Diam. Loss (measured by vernier caliper)	%Diam. Loss (measured from mass loss)	Specimen	f _y (MPa)	$f_{yd(MPa)}$	$f_{ym(MPa)}$	$f_{t(MPa)}$	$f_{td(MPa)}$	$f_{tm(MPa)}$
16	22	14.7	FS Part 1	393	706	590	469	843	704
16	15.6	10.9	FS Part 2	495	708	686	522	801	723
16	17	10.8	BS Part 1	440	638	605	570	827	784
16	16.8	13.5	BS Part 2	447	744	635	550	915	803
16	0	0	Control 1	540	616	616	618	705	705
16	0	0	Control 2	540	616	616	605	690	690
16	26.5	26.6	FS Part 3	323	581	601	422	821	786
16	21.7	23.9	FS Part 4	348	494	600	471	781	812
16	11.4	22.4	BS Part 3	373	478	619	467	600	776
16	12.05	19.7	BS Part 4	447	578	684	530	682	820
16	9.0	15.2	BS Part 5	505	605	714	546	665	760
16	0	0	Control 3	567	560	581	624	637	654

 $f_{y=}$ Nominal yield stress $f_{t=}$ Nominal ultimate stress $f_{yd=}$ True yield stress (vernier caliper diam. loss) $f_{td=}$ True ultimate stress (vernier caliper diam. loss) $f_{ym=}$ True yield stress (mass loss) $f_{tm=}$ True ultimate stress (mass loss)

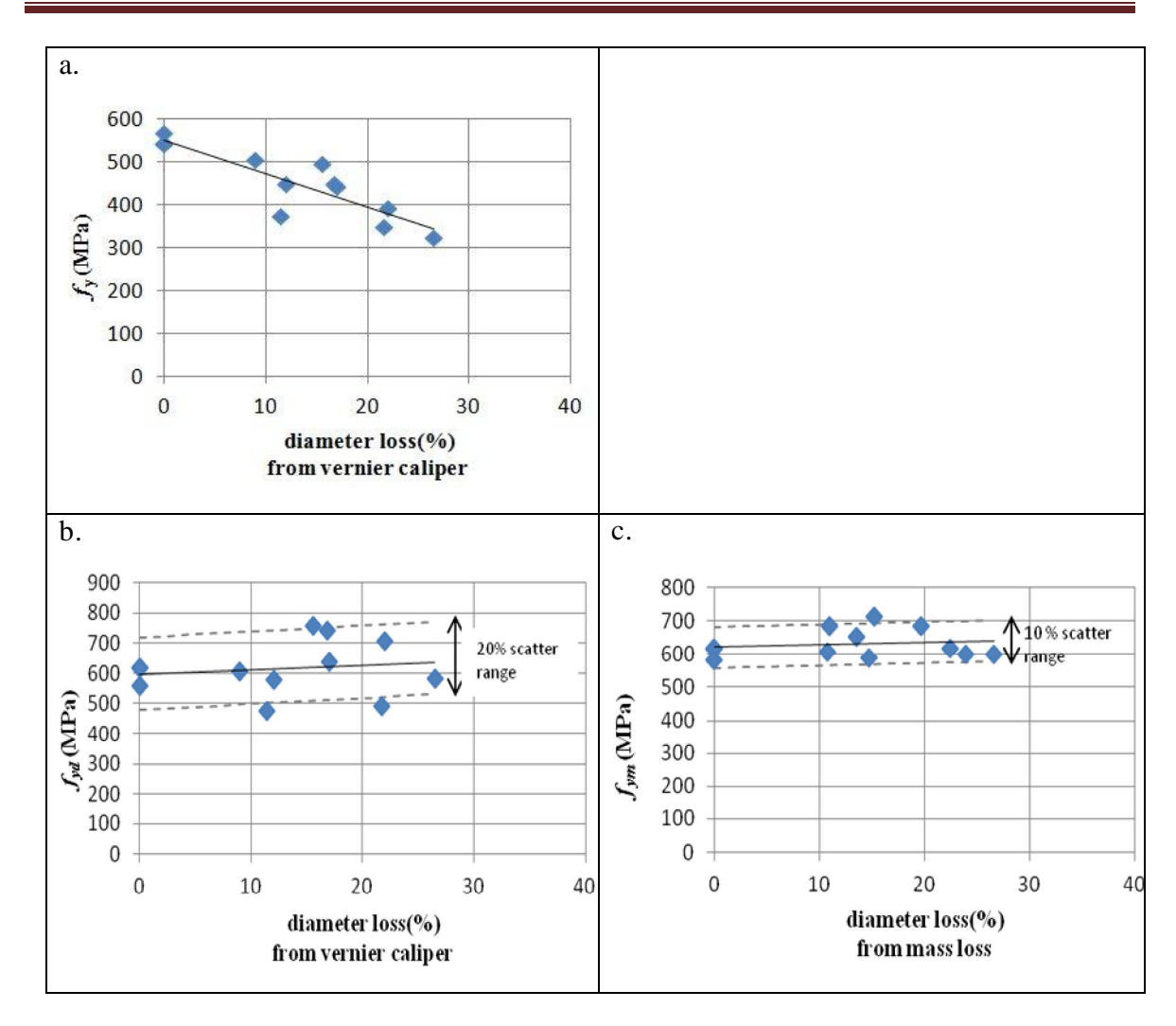


Figure 5. Nominal and true yield stresses in 16 mm diameter steel bar specimens. a)

Nominal yield stress b) True yield stress calculated using reduced diameter measured from vernier calliper c) True yield stress calculated using reduced diameter calculated from mass loss

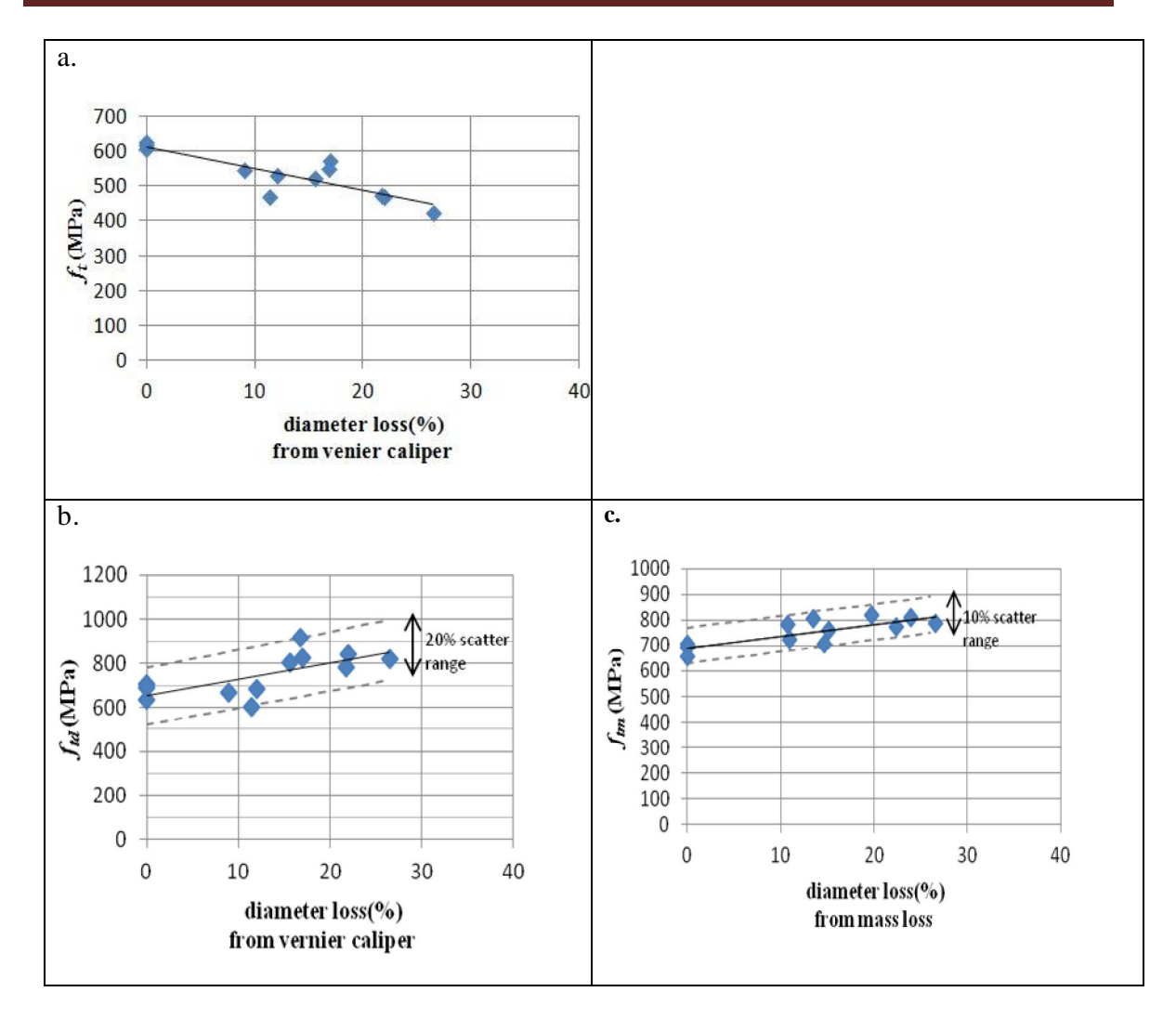


Figure 6. Nominal and true ultimate stresses in 16 mm diameter steel bar specimens. a) Nominal ultimate stress b) True ultimate stress calculated using reduced diameter measured from vernier calliper c) True ultimate stress calculated using reduced diameter calculated from mass loss

Figure 5(a) shows that the nominal yield strength of bars falls with the degree of reinforcement corrosion in relation with the fact that corrosion reduces the cross-section and hence ultimately the nominal yield strength. However, when the reduced cross-sectional area was used instead of the nominal steel cross-section, it was noticed that the true yield strength of all corroded and control bars had the same value. Figure 5(b) and 5(c) represent the true stresses calculated using the reduced cross-section on the basis of diameter loss measured by vernier calliper and diameter loss calculated from the mass

loss. It can be said that corrosion hardly alters the yield behavior of steel bars. These results are in agreement with the results of C.A. Apostolopoulos and V.G. Papadakis [5], who also found that corrosion, had no significant effect on the true yield strength of the steel bars.

Figure 6(a) shows that nominal ultimate strength falls with the degree of reinforcement corrosion in relation with the fact that corrosion reduces the cross-section. Figure 6(b) and 6(c) represent true ultimate stresses and show an increase in ultimate strength with increasing degree of corrosion. Almost all the corroded bars failed at a pit location and the increase in true ultimate strength at the pit can be explained by the fact that the failure path is imposed by the pit and does not correspond to the weakest point of the steel bar as is the case for non-corroded bar. This was explained by Castel et al. [11]. The increase in ultimate strength with the increasing reinforcement corrosion was also observed by Cairns et al. [7].

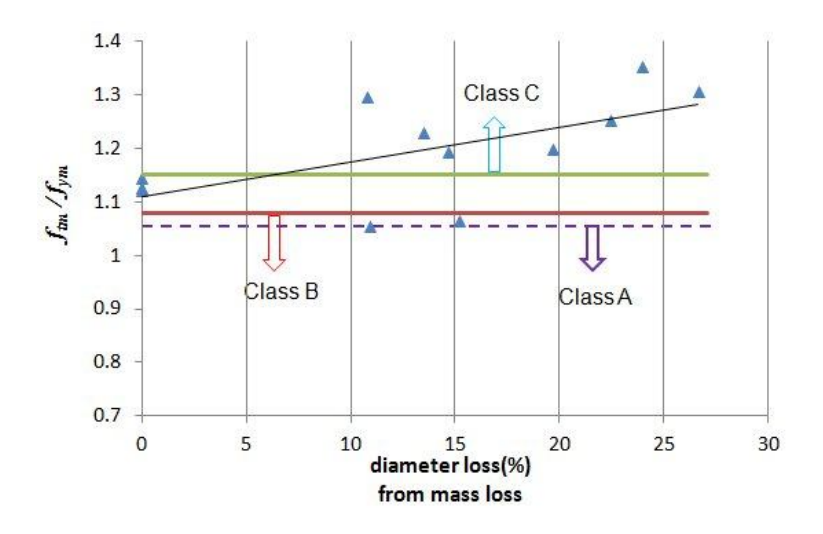


Figure 7. Relationship between f_{tm}/f_{ym} ratios and diameter loss

In Figure 7 the f_{tm}/f_{ym} ratios of the control and corroded specimens are presented. As expected, it was difficult to obtain a curve fitting to these results because of the larger scatter observed. However, there was a tendency for the f_{tm}/f_{ym} ratio to increase as the percentage of diameter loss increased. For all control bars, the ratio of f_{tm}/f_{ym} was about 1.13 which means that steel bars embedded in RC beams are Class B according to EC2

[17] (table 5). In the case of corroded bars, almost all the specimens showed an f_{tm}/f_{ym} ratio of over 1.15. Therefore, the corroded bars would be classified as Class C, which requires a higher ultimate elongation than class B.

Table 5. Properties of	f rainforcament	according to Annex	$C \circ$	of Eurocode 2 [17]
Tuble 5. I roperties of	reinjorcemeni	according to Annex	c_{0}	j Eurocoae 2 [17]

Product		Bars	
Class	A	В	С
Characteristics yield strength f_{yk} (MPa)	400 to 600		
Minimum value of $k = f_x/f_y$	≥1.05	≥1.08	≥1.15
			<1.35
Characteristic strain at maximum force,	≥2.5	≥5	≥7.5
$\mathcal{E}_{uk}\left(\% ight)$			

4.2.2 Effect of corrosion on the ductility of a steel bar

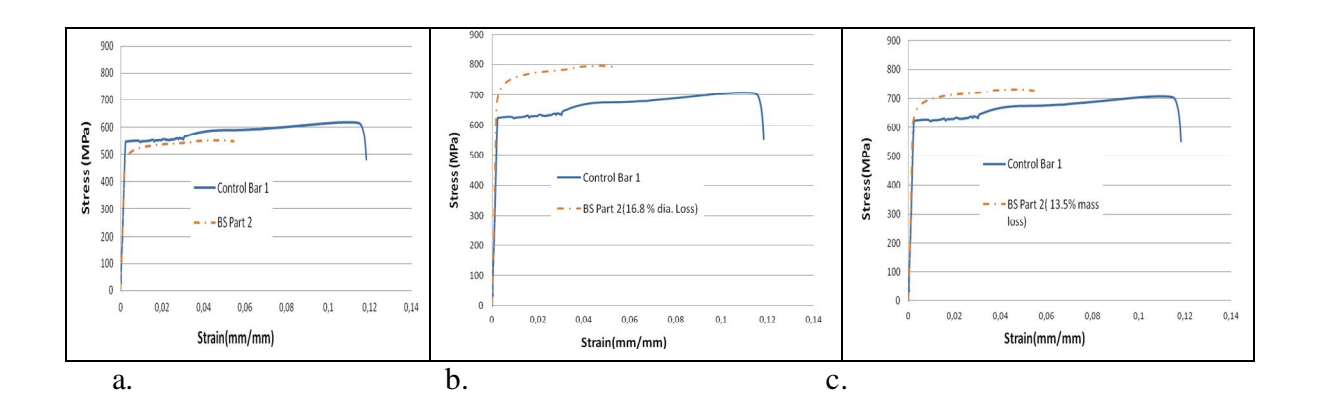


Figure 8. Stress-strain relationship for a corroded and a non-corroded steel bar specimen. Stress evaluated on the basis of nominal diameter (a), true diameter measured with vernier calliper (b) and diameter loss calculated from mass loss (c)

Figure 8 compares the stress-strain curves for a corroded and a non-corroded steel bar specimen. It can be seen that corrosion has much more impact on ductility than on strength, for which the results show a shorter yield plateau and easier occurrence of

unanticipated brittle breakage with no indication of necking at the time of breakage. The reduction of the ultimate failure strain of corroded steel is due to stress concentration at corrosion pits which reduces the ductility reserve.

From figure 8, it can be seen that the corroded bars did not show any yield plateau and it underwent a hardening stage directly after the yield stress. They reached the ultimate strength very much sooner than the non-corroded rebar, reducing the ultimate strain and hence reducing the ductility. This type of behavior was observed for all the corroded rebars. Clearly, corrosion does change the shape of the stress-strain curve. The disappearance of the yield plateau in corroded steel bars may be attributed to the location of corrosion pits and their depth and width, as explained by X. Gang et al. [15]. These authors performed a simulation analysis to study the effect of corrosion on deformed steel bars. From the simulation analysis, they found that the severe effect of corrosion on steel bars occurred when corrosion attacked the base circle of the steel bar. Corrosion did not greatly affect the behavior of steel bars if only the transverse or longitudinal ribs were corroded. According to X. Gang et al, as the corrosion pit width increases the yield plateau gradually shortens until it disappears, with a direct shift from the elastic stage to the hardening stage. Critical values of the corrosion pit width and depth on the base circle of the steel bar are the key factors in the disappearance of the yield plateau. Figure 9 shows the corrosion pits of a few specimens with different pit widths and depths.



Figure 9. Corrosion pits of a few specimens

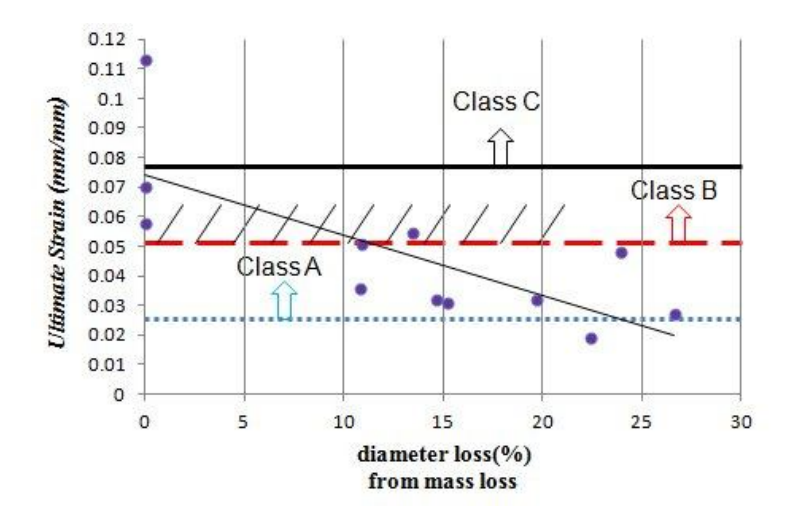


Figure 10. Ultimate strains of 16 mm diameter steel bar specimens

Figure 10 shows the reduction of ultimate strain with increasing corrosion rate. A drastic decrease in ultimate strain with increasing corrosion rate is observed by almost all researchers [3-9]. It is also interesting to see that almost all the corroded steel bars have an ultimate strain below the minimum value (0.05) required by EC2 [17] for Class B. It can be stated that the EC2 corrosion requirements for ductility are no longer achieved and

the corroded structural elements no longer satisfy standard specifications. They cannot be used even if their load capacity is still higher than the ULS load prescription.

4.2.3 Effect of corrosion on Elastic/Young's modulus E_s of steel

The elastic strain modulus or Young's modulus, E_s , was calculated for all the steel bars from the stress strain curves obtained from the experimental tests. The results are presented in Figure 11. The elastic modulus was calculated on the basis of the average loss of mass of each specimen evaluated over the whole test length of the rebar because, unlike the failure behavior, the elastic behavior is not related to maximum pitting but to the sum of the elastic strain all along the rebar. All the samples showed an average value of approximately 200 GPa which is the Elastic modulus of structural steel given in the codes. From this result, it can be concluded that corrosion does not change the elastic modulus of steel bar.

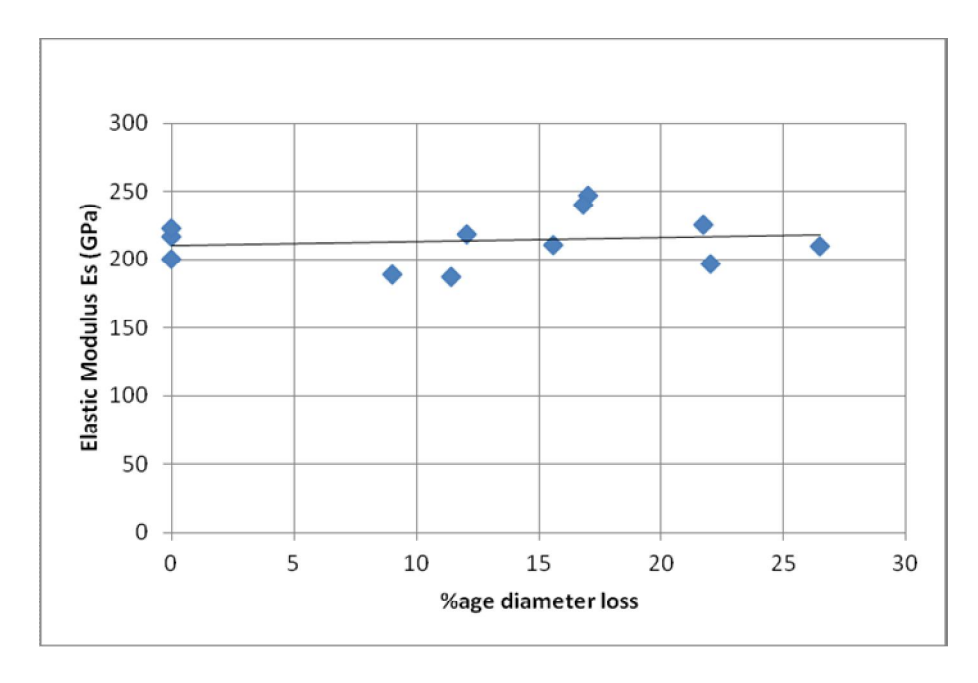


Figure 11. Elastic modulus values (E_s) of steel samples

4.2.4 Effect of corrosion on post-yielding behavior of steel bar

It is important to note the post yielding behavior of corroded reinforced bars. As mentioned earlier, just after the yielding load was reached, the typical stress-strain curves of all steel bars showed no yield plateau and brittle fracture occurred as soon as the stress reached its maximum value, without any indication of necking. More interestingly, the slope of the stress-strain curve of the post-yield response was steeper for almost all corroded samples than for the control samples, as seen in Fig.8. This implies that the strain hardening modulus of corroded bars is higher than that of the control bars after both reach yielding point. Figure 12 shows the values of the strain hardening modulus of steel samples. It can be seen from the graph that the strain hardening modulus, E_p , of the steel samples increased with increasing degree of corrosion. Thus, it is necessary to pay attention to the constitutive law for corroded reinforcement when estimating the mechanical performance of a reinforced concrete member subjected to a corrosive environment.

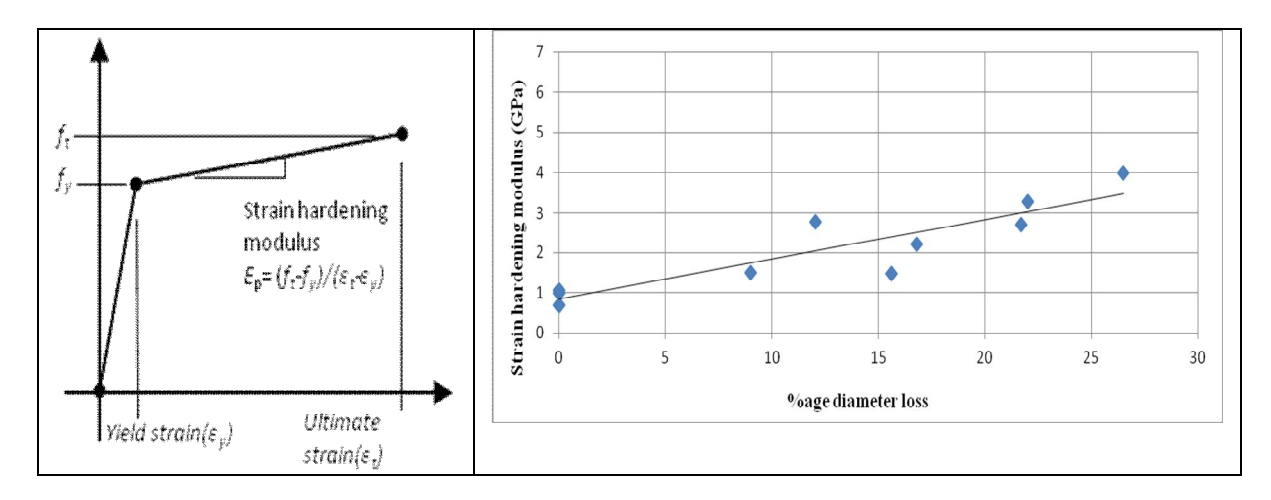


Figure 12. Strain hardening modulus (E_p) values of steel samples

4.3 Reduced steel area at Necking

Another way to demonstrate the loss of ductility is to record the reduced area at necking after steel bar failure. The reduced area was calculated as the difference between the initial cross-section and the final cross-section divided by the initial cross-section. The final cross-section was measured at the failure point of the steel bar. A reduced final cross-section was observed because of necking, although necking was more prominent in the control bars. Figure 13 compares the necking areas of the few control and corroded bars.

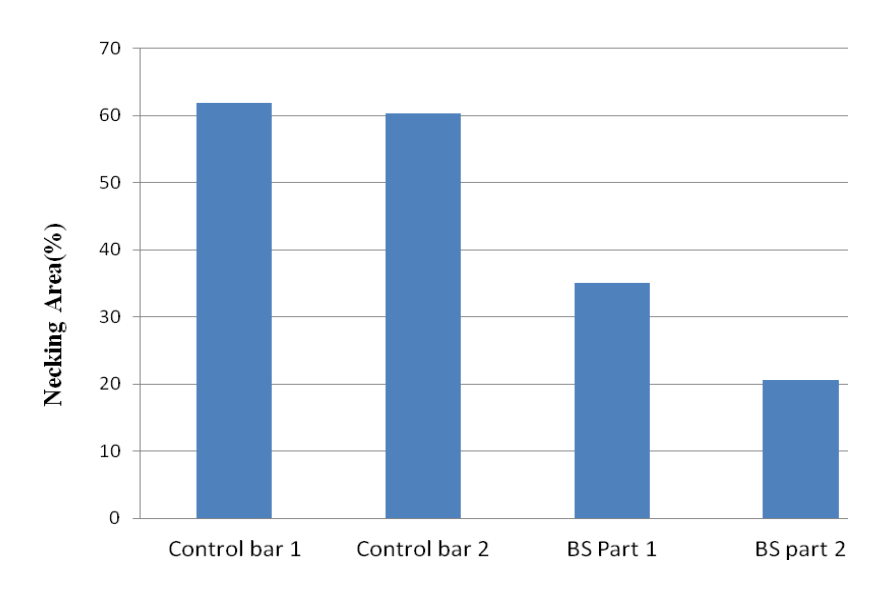


Figure 13. Necking area of control and corroded tensile rebar

4.4 Effect of corrosion on load carrying capacity

It was noted that despite of the reduced cross-section of steel bars, corroded reinforced concrete beams A2CL1 and A2CL3 after 27 years of corrosion were still able to carry the ULS design load. In design calculations, normally yield strength is used thus ignoring any potential enhancement from strain hardening. Moreover, the strain capacity of concrete limits the reinforcement strains and the full ultimate tensile strength of reinforcement is not normally usable in concrete construction as stated by Cairns et al. [7].

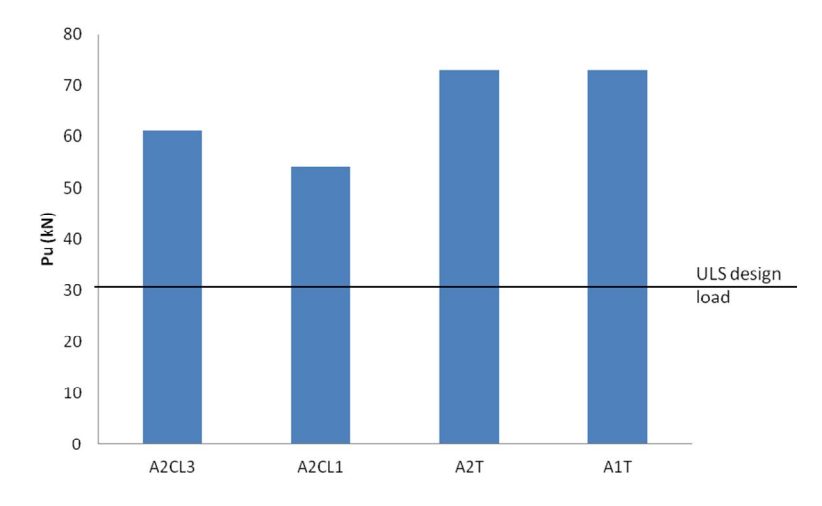


Figure 14. Ultimate load of the beams

5. CONCLUSION

A set of tensile tests was performed on 27-year-old reinforced steel bars corroded by aging inside concrete beams in a chloride environment. The resulting corrosion appeared to be very heterogeneous both along the lengths of the rebars and around the perimeter. The loss of diameter due to corrosion at the location of failure was measured using a vernier caliper and also calculated from the loss of mass of the steel bar at the failure location. The loss of mass gave a better approximation of residual cross-section than the loss of diameter measured with vernier caliper because of the pitting corrosion, the heterogeneity of which reduced the precision of residual cross-section measurement. The average loss of mass along the entire length of the bar was also assessed.

- (1) True yield stress, found by using cross-sectional area calculated from the loss of mass, appears to be constant versus the corrosion level.
- (2) True ultimate stress, calculated using the loss of mass, appears to increase with the level of corrosion, which means that the hardening in post-yielding is greater in presence of corrosion. Corrosion modifies the shape of the stress-strain curve in such a way that the plateau, usually recorded on non-corroded bars, disappears.
- (3) The ratio between ultimate stress and yield stress increases with the increasing corrosion level and could modify the steel class according to standards such as Eurocode 2.
- (4) Ultimate elongation is strongly reduced with increasing corrosion level and has a significant effect on structural reliability since the corroded steel bar no longer respects the ductility prescriptions of standards such as Eurocode 2.
- (5) When the average loss of mass on the whole corroded bar is used in the calculations, the elastic modulus of steel is not influenced by the corrosion level.

The results show that the residual ultimate elongation of a steel bar may be the most important parameter affecting the reliability as far as the structural performance of RC structures damaged by corrosion in chloride environment is concerned.

References

- [1]. Rodriguez J, Ortega L. M and Casal. J, (1994), International Conference on Concrete across borders, Odense, Denmark, Vol.2, pp. 315-326.
- [2]. Rodriguez J, Ortega L.M., Casal J.(1997), Construction and Building Material, Vol.11, No.4, pp. 239-248.
- [3]. Maslehuddin M, Allam I. M, Al-Sulaimani G, Al-Mana A. I. and Abduljauward S. N, (1990), "Effect of rusting of reinforcing steel on its mechanical properties and bond with concrete", ACI Materials Journal, 87, No.5, 496–502.
- [4]. **Abdullah A. Almusallam, (2001)**, "Effect of degree of corrosion on the properties of reinforcing steel bars", Construction and Building Material, Vol.15, Issue 8, pp. 361-368.
- [5]. C.A. Apostolopoulos and V.G. Papadakis, (2008), "Consequences of steel corrosion on the ductility properties of reinforcement bar", Construction and Building Materials, Vol. 22(12), pp. 2316-2324.
- [6]. Han-Seung Lee and Young-Sang Cho, (2009), "Evaluation of the mechanical properties of steel reinforcement embedded in concrete specimen as a function of the degree of reinforcement corrosion", International Journal of Fracture, Volume 157, Numbers 1-2, 81-88.
- [7]. John Cairns, Giovanni A. Plizzari, Yingang Du, David W. Law and Chiara Franzoni, (2005), "Mechanical properties of Corrosion-Damaged Reinforcement", ACI Material Journal, V. 102, No.4, pp. 256-264.
- [8]. Y. G. Du, L. A. Clark and A. H. C. Chan, (2005), "Residual capacity of corroded reinforcing bars", Magazine of Concrete Research, 57, No. 3, pp. 135–147.
- [9]. Palsson R. and Mirza M. S, (2002), "Mechanical response of corroded steel reinforcement of abandoned concrete bridge", ACI Structural Journal, 99, No. 2, pp. 157–162.104.
- [10]. Weiping Zhang, Xiaobin Song, Xianglin Gu, Shibin Li, (2012), "Tensile and fatigue behavior of corroded rebars", Construction and Building Materials 34, V.34, pp. 409–417.

- [11]. Castel A., François R. and Arliguie G, (2000), "Mechanical behavior of corroded Reinforced beam-Part 1: Experimental Study of corroded beams", Materials and Structures, V.33, pp. 539-544.
- [12]. **T. Vidal, A. Castel, R. Francois, (2007)**, "Corrosion process and structural performance of a 17 year old reinforced concrete beam stored in chloride environment", Cement and Concrete Research 37, pp. 1551–1561.
- [13]. **I. Khan, R. François & A. Castel, (2012)**, "Structural Performance of 26 years old corroded reinforced concrete beam", European Journal of Environmental and Civil engineering, Volume 16, Issue 3-4, pg. 440-449.
- [14]. Vu. H. Dang, Raoul François, (2012), "Influence of long-term corrosion in chloride environment on mechanical behaviour of RC beam", Engineering Structures (in review).
- [15]. Xu. Gang, Ai Tiancheng, Wang Qin and Wei Jun, (2010), "Simulation Analysis on Mechanical Properties for Corroded Deformed Steel Bar", Published in proceeding ICDMA'10, Proceedings of 2010 International Conference on Digital Manufacturing & Automation Volume 2.
- [16]. Yingshu Yuan, Yongsheng Ji, and Surendra P. Shah, (2007), "Comparison of two accelerated corrosion techniques for concrete structures", ACI Structural Journal, V. 104, No. 3, pp. 344-347.
- [17]. **BS EN 1992-1-1 Eurocode 2**: Design of concrete structures-Part 1: General rules and rules for buildings, November 2002.

II.2. EFFECT OF CORROSION OF STEEL ON FLEXURAL BEHAVIOR

Article:

Vu Hiep Dang, Raoul François, *Influence of long-term corrosion in chloride* environment on mechanical behaviour of RC beam, Engineering Structures 48 (2013) 558–568.

http://dx.doi.org/10.1016/j.engstruct.2012.09.021

Abstract

The structural performance of a 27-year-old corroded beam was investigated. The cross-sectional area loss, load-carrying capacity, mid-span deflection and force-elongation of some of the corroded reinforcing steel bars were measured. It was found that the mechanical performance after 27 years of heavy corrosion was reduced in terms of both ultimate load and ductility but that ductility would be potentially the biggest problem for the requalification of corroded reinforced concrete members according to the prescriptions of standards. The experimental results revealed a more brittle failure mode of the corroded RC beam in comparison with the ductile failure mode of a control beam of the same age. This was linked to the change in mechanical properties of corroded steel bars in comparison with non-corroded bars.

Keywords: reinforced concrete, corrosion, mechanical behaviour, ductility, brittle failure

1. Introduction

Numerous studies on the mechanical behaviour of RC corroded beams have reported in the past [1-10]. According to these authors, the structural performance of an RC beam is reduced with increasing corrosion level, not only in terms of load-carrying capacity but also in terms of ductility and stiffness [1, 10]. Sanchun Yoon et al. [3] investigated six corroded beams aged under a sustained load to determine the remaining capacity of the beams. They revealed that, as the degree of corrosion of RC beams increased, the loss of

tensile steel mass intensified and the residual load-bearing capacity was reduced. Goitseone Malumbela et al. [5, 6] tested twenty 153 x 254 x 3000 mm RC beams, corroded under five levels of sustained loads. The objective of the study was to define more clearly the structural performance of corroded RC beams subjected to different levels of service load. They found that the deflections of corroded beams under load increased continuously with the degree of corrosion. In addition, they found that levels of load sustained during the corrosion process did not have a significant effect on the maximum mass loss of the steel. Residual load-bearing capacity of corroded RC beams was found to decrease linearly with increasing maximum mass loss of tensile steel. Considering serviceability behaviour, they concluded that the flexural stiffness after the stabilized cracking phase was reached was constant regardless of the increase in corrosion level.

Because the process of natural steel corrosion takes several years to tens of years, the above authors preferred to use an impressed current to artificially increase the corrosion of the embedded reinforcing steel. But Yingshu Yuan et al. [11] showed that, in the case of such artificial corrosion, the corrosion of whole surface of the steel bar was very homogeneous while, under natural corrosion, the corrosion was distributed heterogeneously and mainly on the lower half of the steel bar surface. Because of lack of confidence in the results of accelerated corrosion using impressed current, R.Francois set up an experimental programme in which RC beams were kept in a chloride environment. During a large part of the programme, beams were under sustained loading to study the effect of cracks and load level on the corrosion process. Control beams were also aged under sustained loading so that the residual mechanical properties could be compared at a given age.

In the present paper, the results of experiments on beam A2CL1, one of the remaining 27-year-old concrete beams kept in a chloride environment under a sustained load, are presented and compared to those for a control beam, A2T. The corrosion process of the beam was nearly natural, without any accelerated corrosion using impressed current. The beam was tested until failure. The degree of corrosion and the mechanical properties of the corroded beam, including the load-deflection curve and force-elongation curve of the corroded steel, are analysed. These data would be useful in

the calibration of different types of structural behaviour models using analytical or numerical approaches.

2. Experimental context

A long-term experimental programme was started in 1984 at the Laboratoire Matériaux et Durabilité des Contructions (L.M.D.C) in INSA-Toulouse (France). A batch of 36 RC beams of common dimensions (15 x 28 x 300 cm) as supplied by industry and cast with two different section types, A and B, were stored in a chloride environment under sustained loading. At the same time, another batch of 36 RC beams of the same composition, serving as control beams, were cast but stored under laboratory conditions (non-aggressive environment) in order to provide a comparison at each term of the design process.

Exposure conditions

The beams were kept in a salt fog (35g/l of NaCl corresponding to the salt concentration of sea water) generated by four sprays located in each upper corner of a confined room. After 6 years of storage, the beams were subjected to wetting-drying cycles in order to accelerate the corrosion process:

- 0 to 6 years: continuous spraying under laboratory conditions ($T \approx 20$ oC).
- 6 to 9 years: cycles under laboratory conditions (T≈20°C), one week of spraying and one week of drying.
- 9 to 19 years: cycles of one week of spraying and one week of drying with the confined room transferred outside so that the beams were exposed to the temperatures of south-west France, ranging from -5°C to 35°C.
- 19 to 27 years: cycles were stopped and the beams were unloaded. They were left to corrode naturally at the outdoor temperature of south-west France.

Load levels

The beams were loaded in three-point bending by coupling a type A beam with a type B beam (see figure 1). According to French standards, the level 1 loading (M_{ser1} = 13.5 kNm) corresponded to maximum loading for durability in an aggressive environment for

the type A beam (serviceability limit state (SLS) requirements in an aggressive environment) and to maximum loading for resistance (ultimate load limit state (ULS) in a non-aggressive environment) for the type B beam. The beams stored under sustained level 1 loading were called A1 and B1. Level 2 (M_{ser2}= 21.2 kNm) corresponded to 80% of the failure load and was twice the design service load in an aggressive environment for type B beams. For the type A beam, it corresponded to the maximum service load for resistance (ultimate load limit state-ULS). The beams stored under sustained level 2 loading were called A2 and B2. All the A beams were cast in an inverted position with their tensile steel reinforcement in the top of the form, the compressive steel in the bottom of the form. It should be noted that, according to standards, SLS design corresponds to the load that limits crack width so as to avoid corrosion development in chloride or other aggressive environments. However, experimental results have shown that such a design does not succeed in avoiding corrosion development [16]. At different specific periods, experiments were carried out to collect data such as cracking map, chloride content, and mechanical behaviour under service load [1, 2, 9, 17].

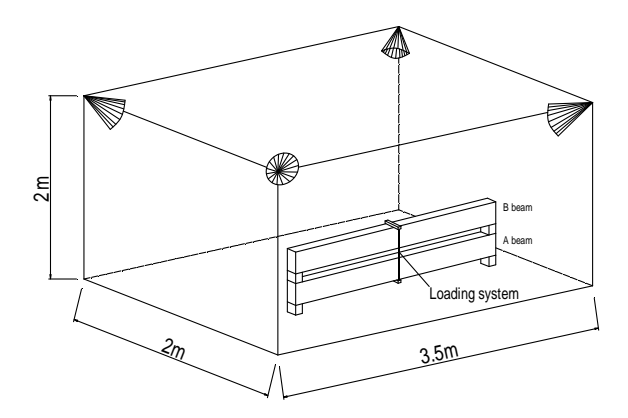


Figure 1. Loading system and conditional exposure of beams in the saline room

Reinforced concrete specimens

The compositions of concrete for each batch are given in Table 1. Water content was adjusted to obtain a slump of around 7 cm. The average compressive strength and elastic modulus obtained on cylindrical specimens (110×220 mm) were 45 MPa and 32 GPa at 28 days. The maximum concrete cover depth provided in type A beams was 40 mm and

ordinary ribbed reinforcing steel (nominal yield strength f_y =500 MPa) was used. The layout of reinforced concrete beam A is showed in Fig. 2

Mix composition		
Rolled gravel (silica+limestone)	5/15 mm	1220
Sand	0/5mm	820
Portland cement: OPC HP (high		
performance)		400
Water		200

Table 1. Proportions of concrete mix (kg/m^3)

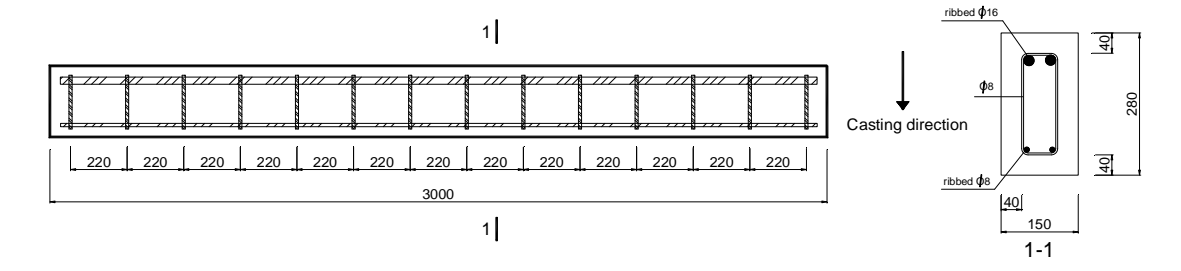


Figure 2. Lay-out of reinforced concrete beam type A (dimensions in mm)

3. Experimental programme

Cracking maps

The crack maps were drawn with the exact locations of flexural transverse cracks and longitudinal corrosion cracking. (The corrosion of longitudinal reinforcement caused only longitudinal cracks.) The flexural crack widths and corrosion crack widths were also measured using a video microscope with an accuracy of 0.01 mm.

Corrosion maps

The corrosion maps of both main bars were drawn in detail after the corroded steel bars had been extracted from the concrete and cleaned in Clark's solution ANSI-ASTM G1-72.

Flexural behaviour

The beam A2CL1 was tested under three point loading to failure to determine its failure load. The mid-span deflection was measured by a numerical sensor with an accuracy of 0.01mm. The load-deflection curve was then plotted.

Ultimate tensile force and strain of main re-bars

Some corroded steel samples were collected from the longitudinal steel reinforcement of beam A2CL1 to test their mechanical properties, especially their loss of ductility. The load-elongation curves were also drawn.

4. Experimental results and discussion

Cracking maps

A2CL1 beam was stored in chloride environment with tension face upward as it can be seen in Fig.1. But for the mechanical flexural test, the beam was loaded with tension face downward which is the normal situation in bending tests. Then cracking maps were plotted in the configuration of test, i.e. the bottom face is tensile face. The cracking maps of corroded beam A2CL1 after 27 years of exposure are presented in Fig.3. The transversal cracks appearing on the tensile zone were generated by the mechanical load. The locations of flexural transversal cracks closely coincided with those of stirrups, approximately 20 cm apart. It should be noted that several transversal cracks propagated through the total depth of the beam because of stirrup corrosion, which increased the stress on the embedding concrete, making the concrete cover crack. Along with flexural cracks, many longitudinal corrosion cracks were observed on the four beam faces. On the front surface, the maximum width of corrosion cracks close to the left and right supports of the beam were 3 mm and 1.4 mm respectively. On the rear surface, the maximum width of corrosion cracks near the central zone was only 0.66mm. This means that the maximum corrosion cracks were distributed randomly along the two sides of the beam; they were independent of the degree of stress in the tensile reinforcement. After 27 years, corrosion cracking developed overwhelmingly along the location of both tensile and compressive re-bars. In particular, the cracks parallel to the tensile re-bars were extensive and mostly interconnected. Nevertheless, the beams previously tested at 17 years and 26 years [9, 16], it was the first A beam that exhibited corrosion cracks along the compressive reinforcement steel. As mentioned above, the tensile surface of the beam exposed to the salt fog plus the damage to the concrete at the interface [18, 19] had led corrosion to develop preferentially in the tensile rebar. On the bottom face, i.e. the tension face, longitudinal corrosion cracks were also observed at the ends of the beam, but were not located in the central part. This indicated that corrosion products were

generated more at the ends of the beam. Thus, combined with maps of corrosion cracks on the front and back surfaces, this information predicted that the corrosion degree of tension steel bars could be larger at the ends of beams than at mid-span.

Corrosion maps

After the concrete cover had been removed, the actual corrosion damage of all reinforcement was observed. Before corrosion maps of all re-bars were drawn, a primary observation of the corrosion on the surface of the tensile steel bar was made. Along the re-bars (Fig.4), the reddish-brown colour of corrosion products was often visible. At some locations, the rusts produced were blackish green in colour. A large amount of pitting corrosion was observed on the face of all steel bars in the tensile zone. Corrosion pits particularly appeared further along the steel face where it was the nearest to the outer surface of the beam. Some bar ribs had been lost over the bar length, thereby decreasing the steel-concrete bond stress in this part of the steel bar.

Fig. 5 shows the distribution of corrosion areas of tension reinforcement steel, measured in two opposite directions on A2CL1 after 27 years of exposure. The first direction was downward on the side of the steel that was directly exposed to cracks. The other was the upward direction where the steel face had much thicker cover. It can be seen that the spread of corrosion on the steel bars was very dissimilar. The pitting corrosion was very heterogeneous and numerous pits were observed on the tensile bars at various positions, viewed in the downward direction, without correlation with initial flexural cracks. Interestingly, the corrosion occurred even in the absence of cracking corrosion. Mostly, the examined face of tensile bars was heavily corroded. As mentioned above, this beam was cast with top-cast tensile bars, thus the "top-bar" effect was due to the settling of concrete below the re-bars. This resulted in the formation of gaps (voids) in the lower half surface of the top-cast bars (Fig.6), so the corrosion rate looking in the upward direction would be theoretically greater than that viewed in the downward direction. Nevertheless, if voids allow corrosion to develop more easily (according to T. A. Söylev et al [20]), the pressure due to oxide formation is delayed [23] and thus corrosion cracks are first generated in the rebar zone without voids, i.e. the part of the upper perimeter of the tensile bars oriented perpendicular to the casting direction of the concrete, see Fig.7.

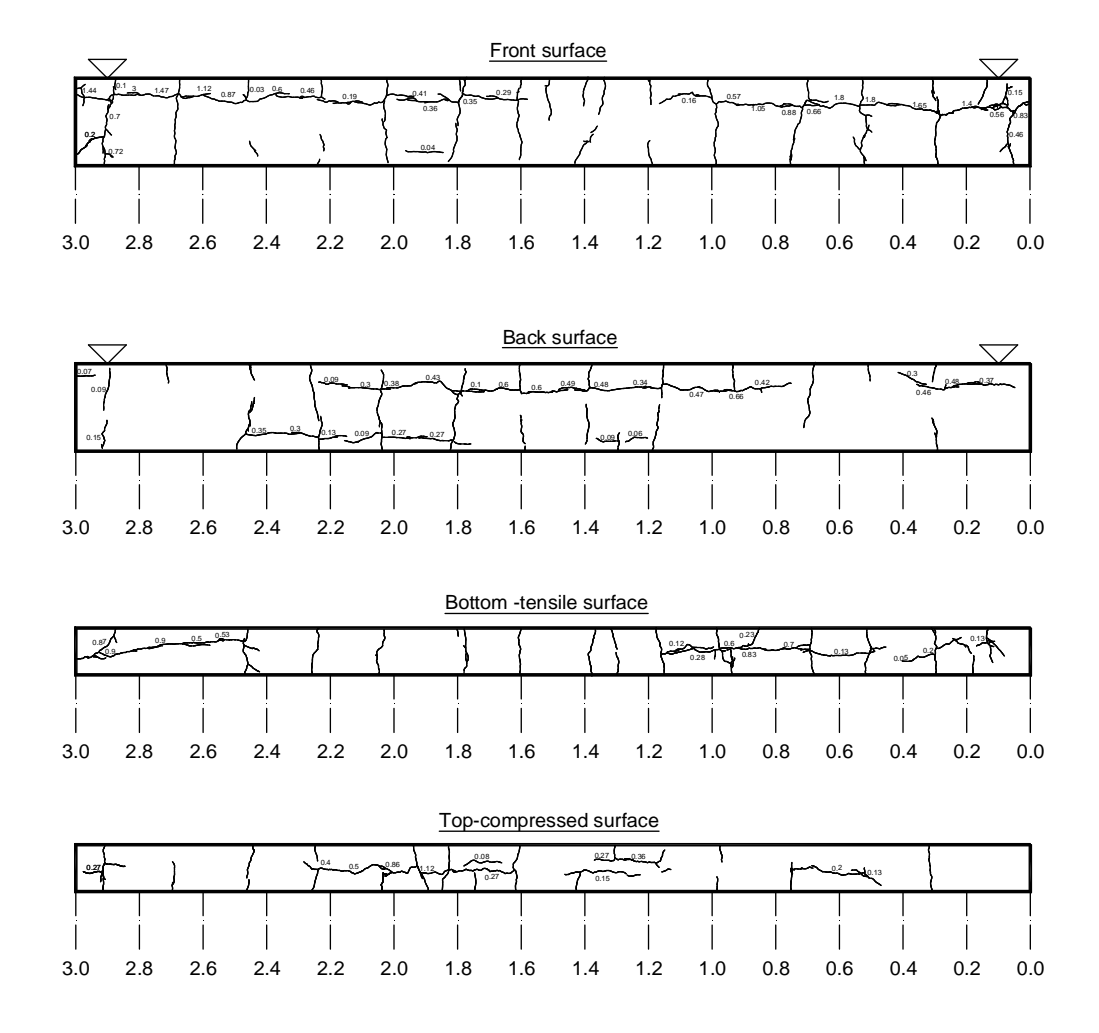


Figure 3. Corrosion cracking map of beam A2CL1 after 27 years of exposure

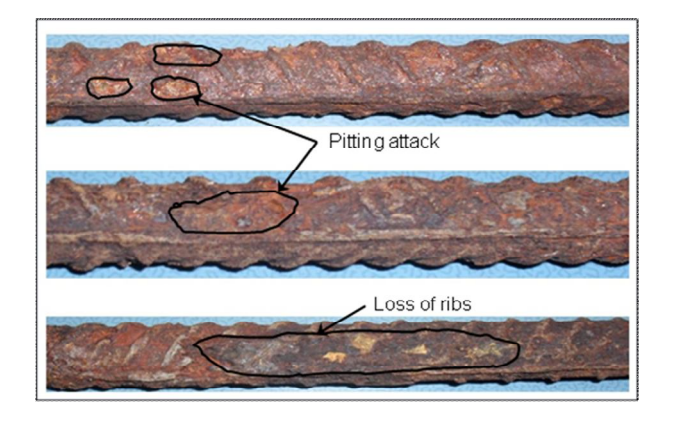


Figure 4. Real corrosion on the tensile steel surface 129

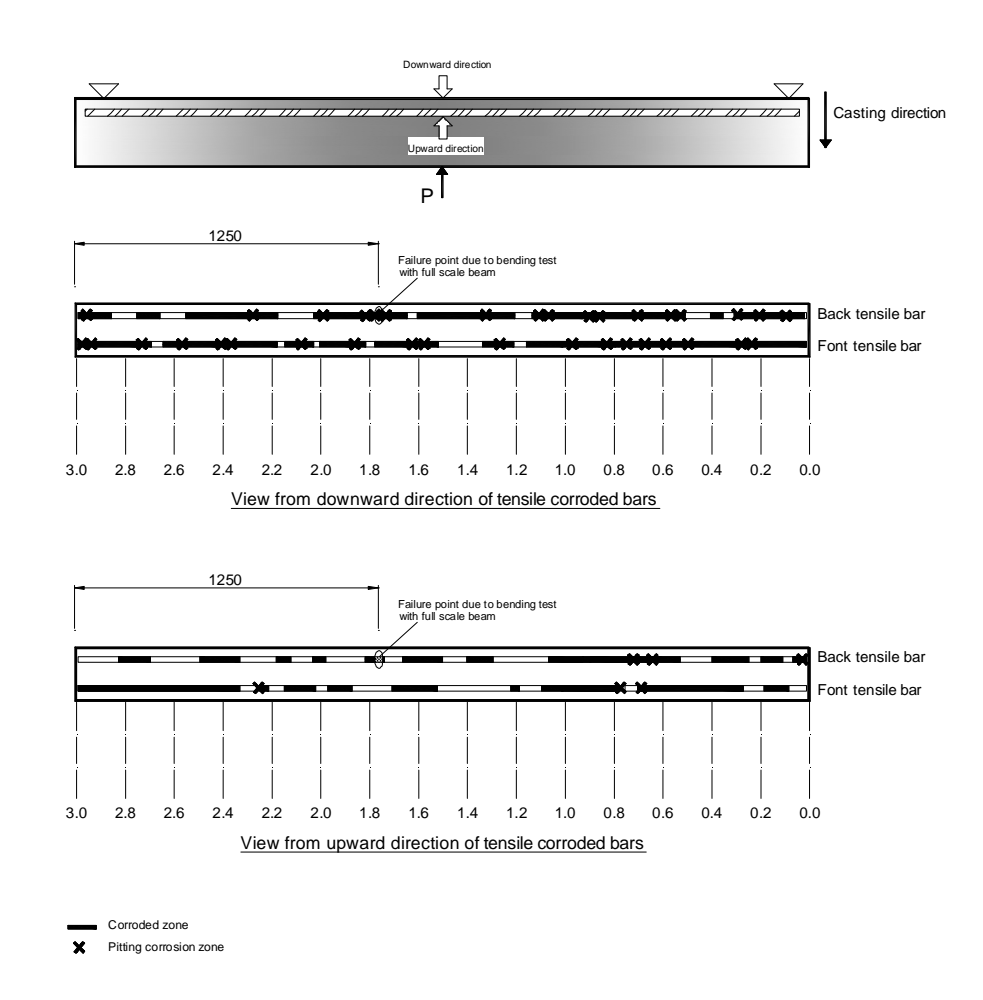


Figure 5. Distribution of corroded locations on beam for tensile re-bars

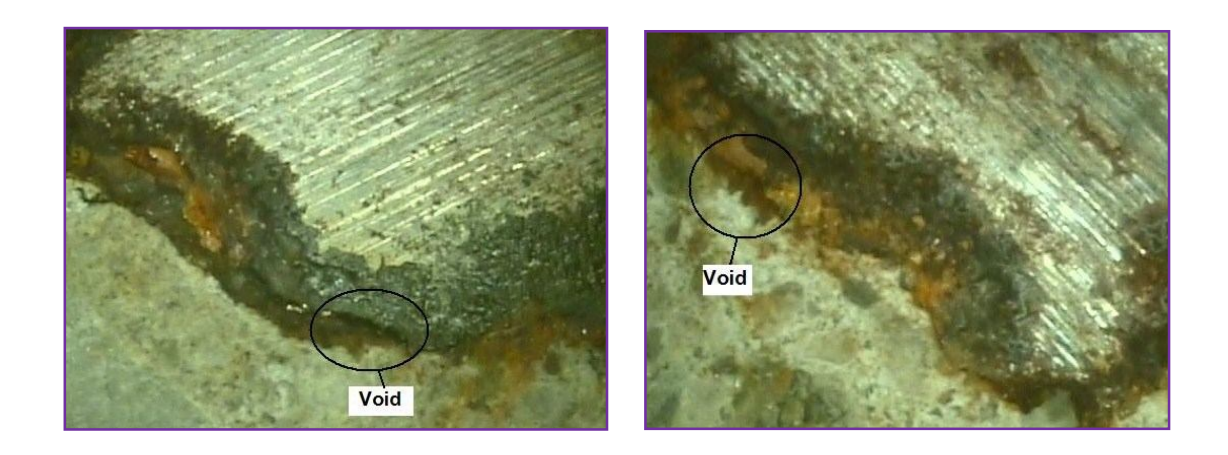


Figure 6. Voids at the steel-concrete interface of tensile bars (top-cast bars)

This could be summarized by the two steps of corrosion propagation proposed by Zhang et al. [17] as follows:

- Localized corrosion (LC): voids formed under the lower part of the steel surface, as shown in Fig.6, and the rust at the steel-concrete interface filled the voids. Consequently, the corrosion cracking would be delayed in the bottom half of the rebar. In contrast, on the upper part of the steel bar, the rust created early radial pressure, leading the concrete cover to crack.
- General corrosion (GC): as the degree of corrosion became more severe, more corrosion products were produced, leading to more widespread corrosion cracking that propagated rapidly. The experimental test showed that the corrosion cracks on the top half of the steel bar extended horizontally to the concrete side surface, Fig 7. This provided a convenient way for the rapid ingress of chloride ion, oxygen, etc. to the reinforcement. This explains why the corrosion rate of the upper half of reinforcing bars, with respect to the concrete casting direction, was greater than that of the lower half.

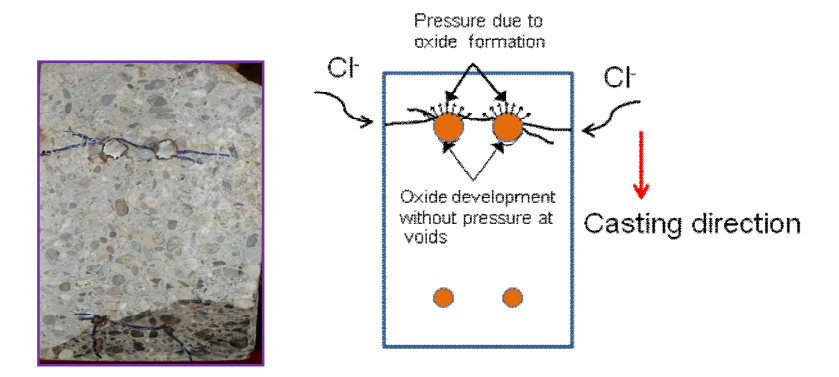


Figure 7. Corrosion cracks between the two tensile bars (internal cracks)

In addition, the fact that the top half part of the steel face was the nearest to the concrete cover, coupled with the effect of increased microcracking with the load in the tensile zone [19] meant that the more aggressive ions reached the surface of the reinforcement bar first and accumulated gradually over time. Therefore, the more aggressive context resulted in more serious corrosion.

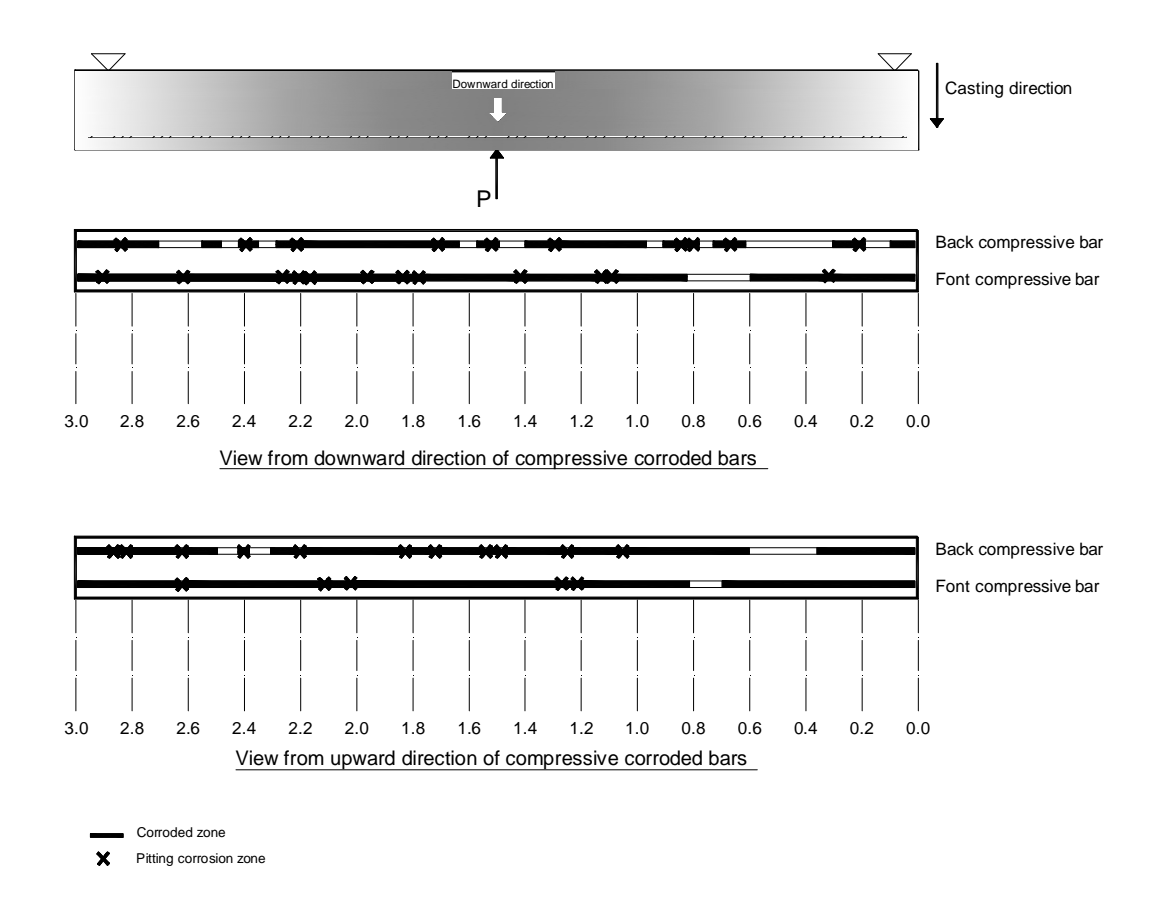


Figure 8. Distribution of corroded locations on beam for compressive re-bars

Fig. 8 presents the corrosion areas on the length of the beam for compressive reinforcement. As for tensile bars, the corrosion level observed on compressive steel bars after 27 years was serious. General corrosion prevailed all along the re-bars but, as mentioned previously, it was the first beam from whole set of A beams that exhibited corrosion cracks along the compressive reinforcement steel. There was no difference in the corrosion degree according to upward or downward direction in this case. Two differences between tensile bars and compressive bars could explain this result. Firstly, upward surface was the bottom face during the exposure to chloride; therefore there is not much chloride accumulation on this surface. Then, there is not a higher chloride increase from upward direction in comparison with lateral surfaces. Secondly, the crack corrosion pattern is different in compressed zone: internal cracks are located at the top half part of the steel face (according to casting direction, see Fig. 7) but they do not correspond to the

upward surface of steel bar. These lead the corrosion rate between upward surface and downward surface of compressed bars is almost similar.

The graphs of steel cross-section loss for both tensile reinforcements are given in Fig.9 and Fig.10. Loss of cross-sectional area was calculated from loss of diameter measured using a vernier calliper. It should be noted that, with this measurement technique, the loss of cross-section could be overestimated because of the change in the surface shape of the steel bar. It is interesting to see that loss of cross-sectional area near the supports seemed greater than that in the mid-span zone, where the moment values are higher. Nevertheless, two big pits were visible in the central area of one tensile bar (BT bar: fig. 9) and one of these serious pits was the cause of the beam failure during the bending test. After 27 years of exposure, the bending moment probably no longer played an important role in the corrosion process. The level of damage in tensile re-bars was different: the average loss of cross section along the front tensile bar (14.2%) was much larger than that along the back tensile bar (8.2%) in spite of a similar stress state and similar aggressive environment. This also means that the behaviour of corroded RC beams should be modelled in 3D instead of 2D as is usually done for RC beams. The difference in corrosion level of tensile bars can be attributed to a variety of causes, such as heterogeneous quality of concrete, crack width, concrete-steel interface, local environmental humidity... and the intrinsically stochastic nature of the corrosion process in the presence of chloride.

The calculated loss of cross-sectional reinforcement along the two steel bars in the compression zone is shown in Figs.11 and 12. Similarly to tension bars, the corrosion evolution of compressive bars was not uniform, even along the same bar. In the case of the back compressive bar, the maximum pit depth, which appeared in the area near the right support, was around 2 mm. The total percentage of steel loss for steel bars in the compression zone (31%) was much larger than that for bars in the tensile zone (22.5%) because of their smaller initial cross-sectional area (8 mm diameter).

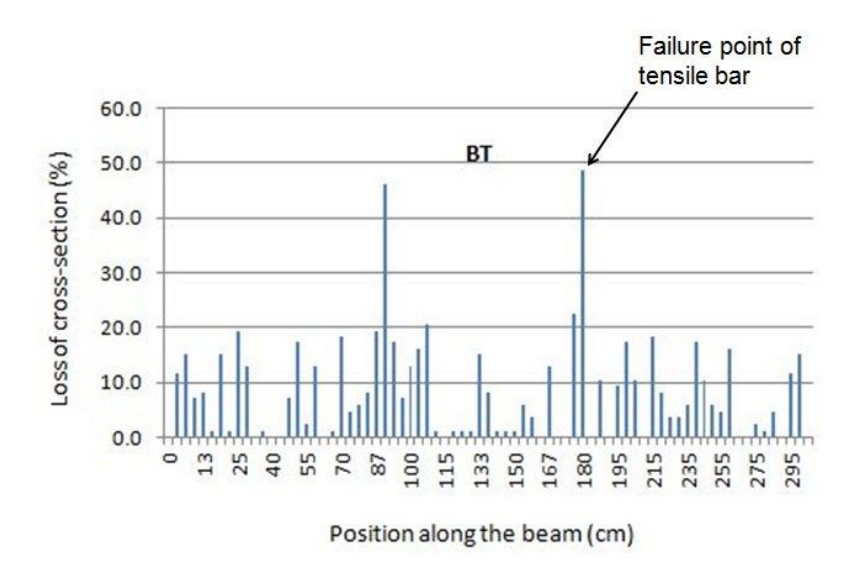


Figure 9. Cross-section loss distribution along the back tensile bar (BT)

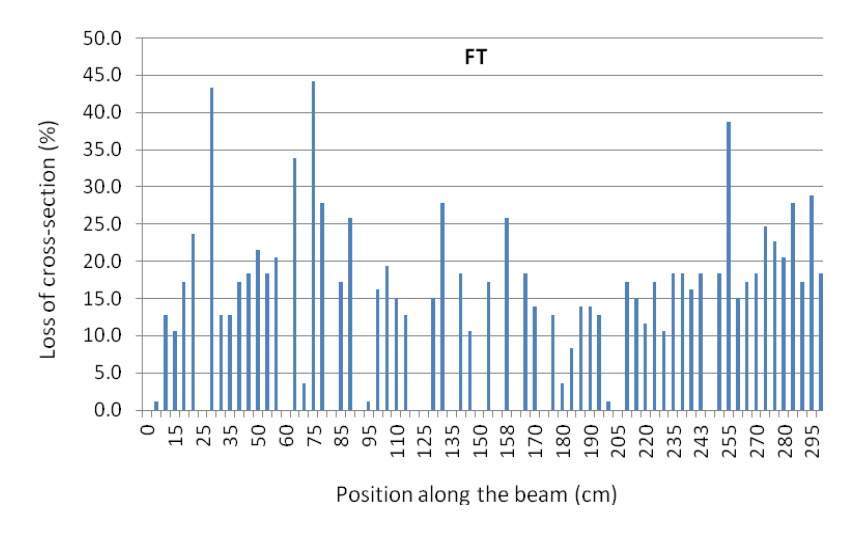


Figure 10. Cross-section loss distribution along the front tensile bar (FT)

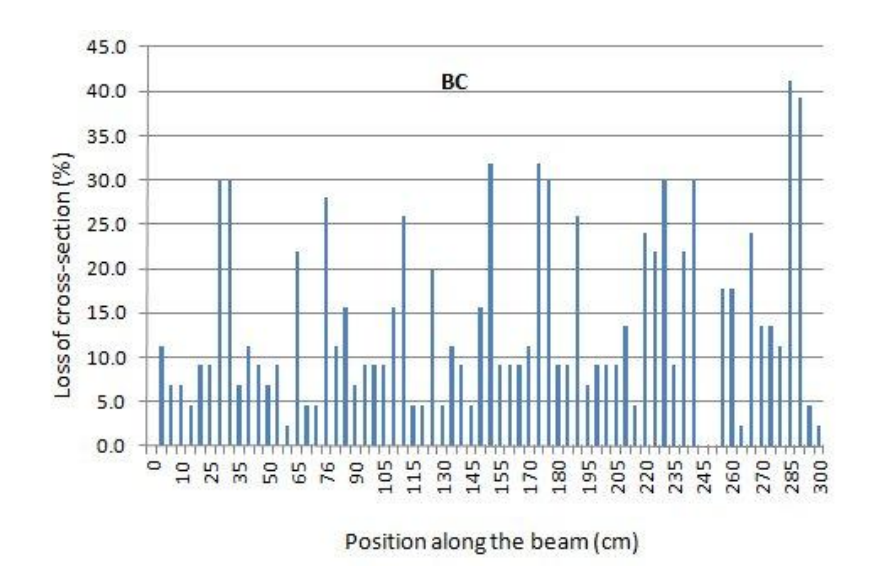


Figure 11. Cross-section loss distribution along the back compressive bar (BC)

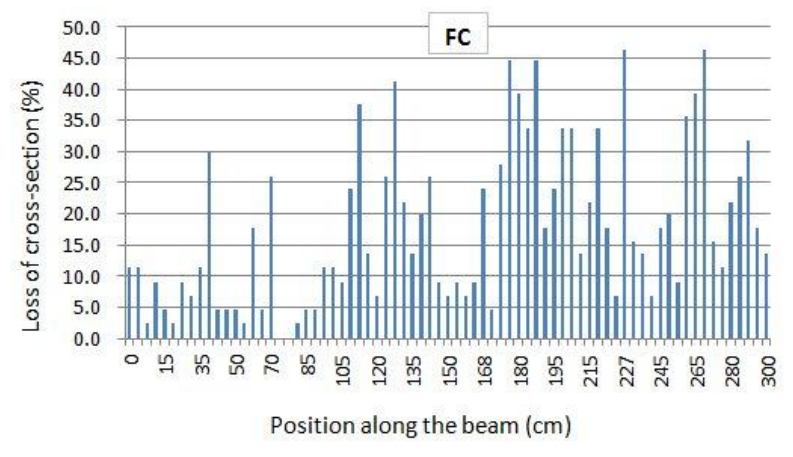


Figure 12. Cross-section loss distribution along the front compressive bar (FC)

Stirrup corrosion

Flexural cracks were located in front of the stirrups in the middle part of span and showed a crack spacing of around 200 mm. This value corresponds to the one predicted by the FIB model code [25] and is in relation to the large concrete cover. After 27 years, new transversal cracks are visible due to stirrup corrosion, especially near the supports. The existing flexural cracks develop to reach the compressive face of beam due to corrosion process as shown in Fig.3. Despite the presence of cracks and the initiation of

corrosion at crack tips after 7 years of storage [21], there was no correlation between the corrosion at 27 years and the initial bending cracking maps. The corrosion map for stirrups is given in Fig.13. The numerals noted adjacent to them indicate the percentage loss of diameter with respect to the original diameter. It is evident that the corrosion of the upper part of all the link bars was more serious than corrosion of the lower part, with many pitting locations such as can be seen on the second, third, twelfth, and fourteenth link bars. Stirrup No.5, with a diameter loss of 55%, lying in the high moment zone, was broken during the flexural test. It is also interesting to observe that the stirrups close to the ends of beam corroded more seriously, leading to transversal corrosion cracks at the two beam ends. This agrees with the observations on the tensile rebar.

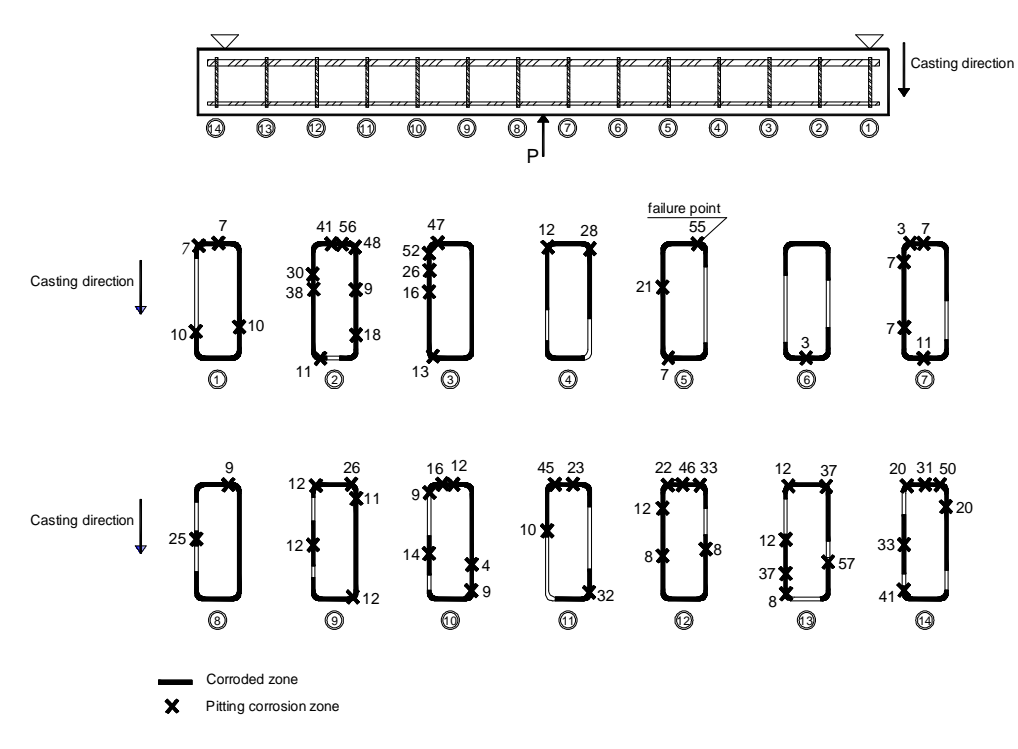


Figure 13. Corrosion distribution on the stirrups

Flexural behaviour

The beam was simply supported and a symmetrical load was applied at a distance of 1400 mm from the supports as shown in Fig.14. A digital sensor placed at the bottom of the beam recorded the displacement at mid-span. The loading speed of 0.3 kN/s was constant during the test.

The results obtained by testing the control beam A2T and the corroded beam A2CL1 are plotted in Fig.15. The yield loading values of A2T and A2CL1 were roughly 66 and 48 kN respectively. The peak loading values were 73 kN for A2T and 54 kN for A2CL1. The reduction in both the yielding and ultimate load in A2CL1 was about 26% in comparison with A2T. However, the ductility of the two beams was quite distinct, with a sharp reduction (47%) for A2CL1. In the usual RC calculation for a cracked crosssection, using the average loss of cross-sectional area of steel bars at the failure point (approximately 26%) and the nominal yield stress of the rebar, the yielding load capacity of A2CL1 is 44.8kN. For A2T, the calculated yielding load capacity is 59.3kN. This implies that the theoretical yielding load for A2CL1 is reduced by about 24% in comparison to A2T. Then the percentage decrease in A2CL1 yielding load for both experiment and calculation coincides with the average maximum reduction in crosssectional area of corroded steels. This result is similar to previous research results (J. Rodriguez et al. [22], Zhang et al. [26]) and confirms that it is possible to predict the residual loading capacity of a corroded RC beam if the average maximum loss of crosssectional area of the tensile bars is known in the zone of highest bending moment.

Fig.3 indicates that corrosion crack widths are not very important at mid-span. The maximum crack width is only 0.66mm. According to existing model which tried to correlate the corrosion crack width to loss of cross-sectional area [30], the loss of cross-section will be limited (around 5.7%). Fig.9 and 10 reveal that average loss of corrosion along BT bar and FT bar is the order of 8.5% and 14.5%, respectively. Moreover, there are some big pits which have several times larger loss of cross section than average loss of cross section. Therefore, the prediction of load capacity of A2CL1 beam from the corrosion cracks would not be reliable enough.

Fig.15 clearly shows that, even though the corrosion state is severe, the working capacity of beam A2CL1 is still in accordance with EC2 [24] in terms of both displacement and load capacity. At the ultimate limit state (ULS) the value of mid-span deflection is only 6.6 mm, which does not exceed span/250. The load capacity is still 80% higher than the design ULS load. Ultimate deflection is strongly decreased but there is no clear ductility limitation for RC members given in current codes. Ductility of RC members is ensured by two parameters: the minimum ultimate elongation of the steel bar and the minimal steel cross-section. It should be noted that the criterion of minimal steel

cross-section is still met by the corroded beam A2CL1 but the steel ductility criterion (ultimate elongation) would be not be sufficient to satisfy the specifications of standards such as Eurocode 2. The tensile tests on steel bars extracted from A2CL1 presented in the next section show a strong decrease of ultimate elongation.

Beam A2CL1 failed suddenly after the peak load because of brittle tensile rupture of the reinforcing steel whereas A2T failed by concrete crushing in the compressive zone. Clearly, the corrosion altered the failure mode of RC beams from failure due to concrete crushing to failure due to rupture of corroded tensile bars. The change in the mechanical response could be explained by the decrease in tensile steel area due to pitting in the highly stressed zone. This concentrated the stress at the pit location, thus limiting the ultimate deformation of the corroded bar. This is discussed further in the next subsection.

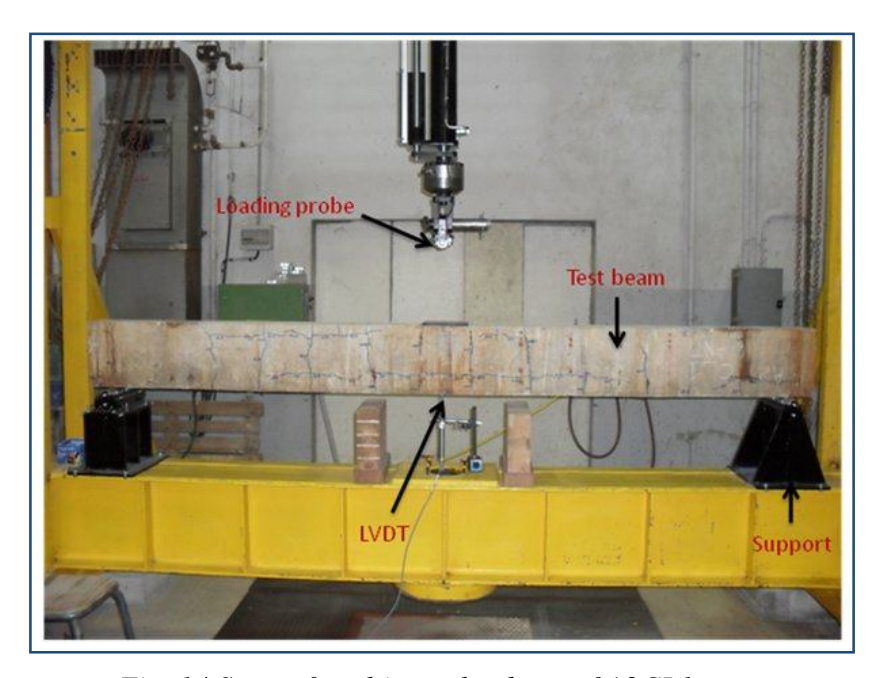


Fig. 14.Set-up for ultimate load test of A2CL1

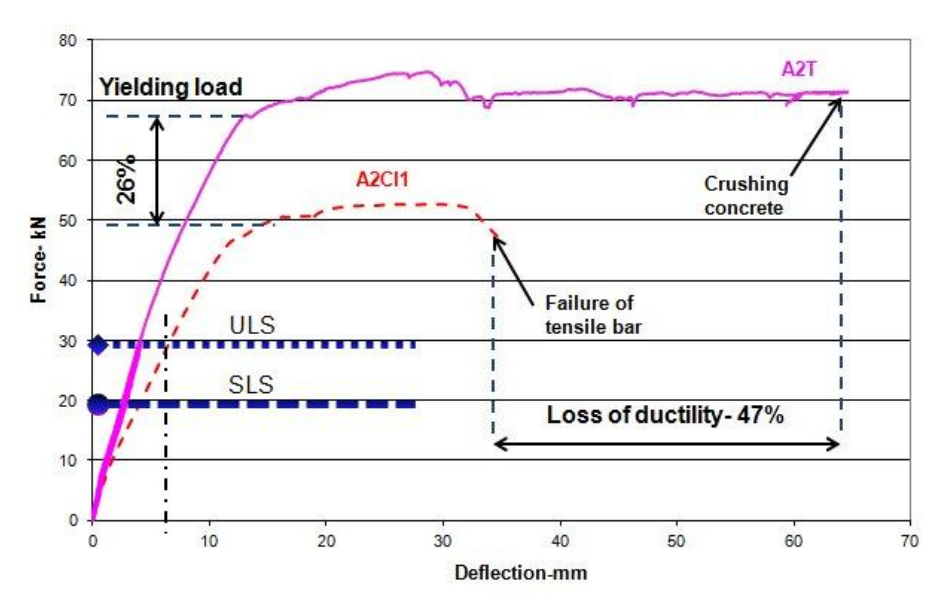


Figure 15. Comparison of load-mid span deflection for A2CL1 and A2T beams
Ultimate tensile force and strain of main re-bars

The mechanical properties of the reinforcing steel, such as ultimate strength and ductility were studied. In order to make a detailed comparison of steel behaviour, steel samples were taken from the control beam and the corroded beam. Figure 16 presents the experimental set-up. The bar specimen was gripped in the machine jaws at each end of the steel reinforcement, so the load was transferred directly to the steel bar until rupture. The mean axial deformation was measured by two LVDTs. The base length of the specimen was 200 mm. Four corroded steel samples showing pitting attack within the initial length were chosen, two in the tensile part and the others in the compressive part of the beam. Table 2 gives the information on loss of average diameter at such pits. Fig.17 plots the force-elongation relationship of the steel samples tested. It is clear that the typical force-elongation curves of all steel bars did not comprise a yield plateau like that recorded with the sound steel bar. The brittle fracture with no indication of necking occurred just when the stress reached its maximum value (Fig.18).

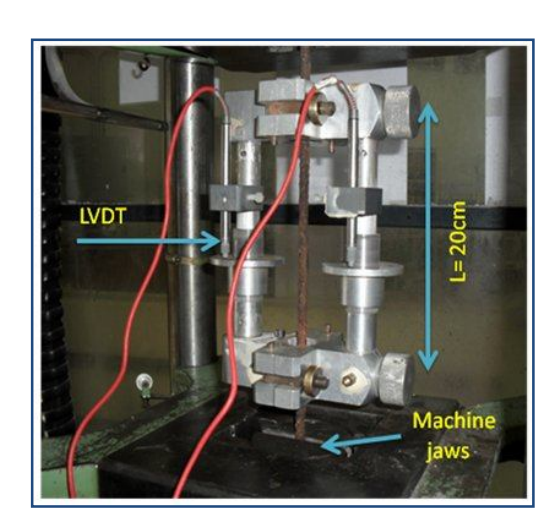


Figure 16. Experimental set-up for tensile test of steel bars

Table 2. The diameter loss at pits within the base length (20 cm)

Location of steel	Diameter- mm	Loss of diameter-%
1-Front	16	26.5
2-Back	16	11.4
2-Back	8	58.1
2-Front	8	32.6

The experiment showed that all corroded steel bars had smaller ultimate elongation. The reason for this was stress concentration at the tips of the corrosion pits, which led to premature yielding of the steel cross-section during loading and thus reduced the plasticity reserve of the steel at pit locations. Moreover, this phenomenon must depend on the shape and depth of pit corrosion that leads to more brittle behaviour.

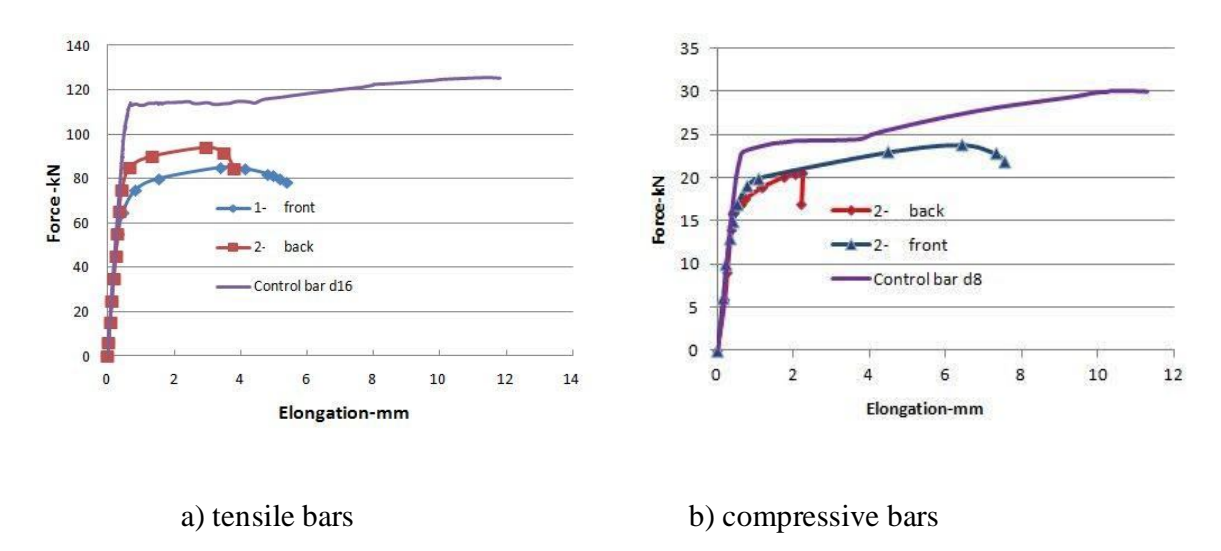


Figure 17. Force-elongation relation of corroded bars

The corroded steel elongation at failure varied greatly, depending mainly on the corrosion intensity and the original reinforcing steel diameter (8 or 16 mm). For tensile bars, table 3 shows that ultimate elongation decreased from 0.058 for non-corroded steel bar to 0.019 and 0.027 for corroded steel bars. So corroded steel bars did not respect the ductility criteria of Eurocode 2 [24] (minimal ultimate elongation = 0.05). To compare the steel bar elongation reached during the bending test of control and corroded beams, the strain at failure was computed using the model of RC members developed by Vu et al. [27]. For the control beam, the concrete compressive strain was 0.035 at beam failure due to concrete crushing, while the tension strain of the steel bar was about 0.0095 which is considerably less than the ultimate elongation of steel. But, for the corroded beam, the steel strain elongation corresponding to beam failure was close to 0.0126, when the concrete strain reached 0.0025. These values are consistent with the failure mode of the control beam but, for corroded beam, the steel elongation strain at failure, 0.0126, was less than the ultimate elongation recorded in tensile tests performed on corroded steel bar. One explanation could be that the failure of A2CL1 beam was due to BT bar failure at a big pit (around 50% loss of cross-section) with a higher loss of cross section than the pits that induced failure in the direct tensile tests of corroded steel bars. The decrease in ultimate elongation with increasing loss of cross-section, then ultimate elongation of steel bars with 50% of loss of cross-section could be limited to 0.0126. Tests performed by François et al. [28] and Cairns et al. [29] support this proposal.

Location of steel	Diameter mm	Elongation mm	Strain mm/mm	Minimal Ultimate strain (EC2)
1-Front	16	5.4	0.027	0,05
2-Back	16	3.8	0.019	0,05
Control	16	11.6	0.058	0,05

Table 3. The ultimate tensile steel bar elongation and strain

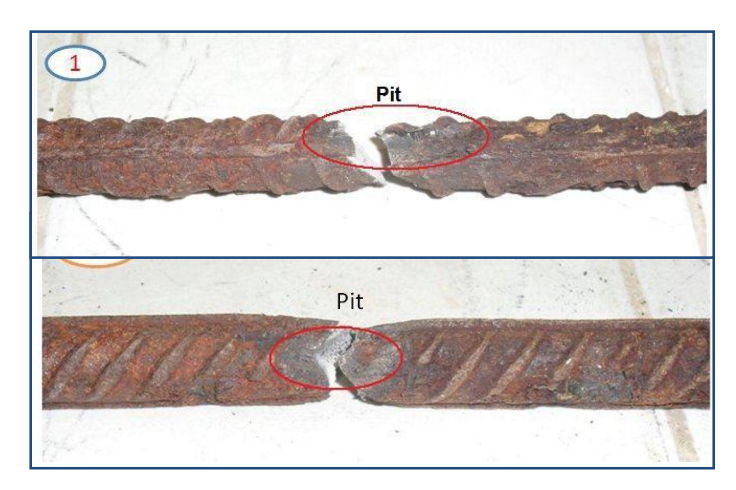


Figure 18. Fracture of several corroded bars at pits in tensile test.

1) 1-front, d=16 mm; 2) 2-back, d=16 mm

5. Conclusions

A 27-year-old corroded beam was tested in bending and compared with a control beam of the same age kept in a non-aggressive environment. Corrosion resulted from natural processes without any impressed current or chloride admixture in the batch during casting. Furthermore, both corroded and control beams were kept under ULS load for a significant time.

Long-term corrosion appeared to be independent of the initial flexural cracking pattern.

The loss of steel cross-section for tensile reinforcement reached 50% of the initial cross-section locally but corrosion appeared to be very heterogeneous in terms of distribution along the perimeter or along the length of re-bars and also from one reinforcing bar to another even if all conditions were strictly identical.

The corrosion led to a change in the failure mode from concrete crushing for control beams to tensile bar failure for corroded beams. The failure of a corroded beam appeared

in the zone of maximal bending moment at the location of a large pit in one of the reinforcing steel bars.

The decrease in both yielding moment and ultimate moment between the control and corroded beams was related to the reduction of steel cross-section at the failure location.

Ultimate deflection of the corroded beam was greatly (50%) reduced in comparison with the control beam. This was because of the reduction of ultimate elongation of the steel bar in tension due to corrosion: the tensile test performed on corroded bars extracted from the beam showed that ultimate elongation of corroded steel did not respect the minimal prescription of design codes such as Eurocode.

Despite the high corrosion level of the A2CL1 beam, the ultimate capacity was still largely above the ULS design load and the deflection at the service load was still well below the maximal value given by current standards. However, the corroded steel bars did not respect the ductility prescription of standards like Eurocode 2, so the A2CL1 beam could not be re-qualified as respecting standards. Thus loss of ultimate elongation of the steel could be the limiting factor for the service life of corroded RC structures.

References

- **1. A.Castel, R.François, G.Arliguie.,** 2000, "Mechanical behaviour of corroded reinforced concrete beams Part 1: Experimental study of corroded beams". Materials and Structures/Materiaux et Constructions, Vol. 33, pp. 539-544.
- **2. A.Castel, R.François, G.Arliguie.,** 2000, "Mechanical behaviour of corroded reinforced concrete beams Part 2: Bond and notch effects", Materials and Structures/Materiaux et Constructions, Vol. 33, pp. 545-551.
- **3. Sanchun Yoon, Kejin Wang, W. Jason Weiss, and Surendra P. Shah.,** 2000, "Interaction between Loading, Corrosion, and Serviceability of Reinforced Concrete", ACI Materials Journal, V. 97, No.6.

- **4. Tamer El Maaddawy, Khaled Soudki, and Timothy Topper.,** 2005, "Long-term performance of corrosion-damaged reinforced concrete beams", ACI Structural Journal, V. 102, No. 5.
- **5. Goitseone Malumbela, Pilate Moyo, Mark Alexander.,** 2009, "Behavior of RC beams corroded under sustained service loads", Construction and Building Materials 23, pp. 3346–3351.
- **6. G.Malumbela, P.Moyo, M.Alexander.,** 2009, "Structural behaviour of beams under simultaneous load and steel corrosion", Concrete Repair, Rehabilitation and Retrofitting II 2009 Taylor & Francis Group, London, ISBN 978-0-415-46850-3.
- **7. Abul K.Azad, Shamsad Ahmad, Syed A.Azher.,** 2007, "Residual strength of corrosion-damaged reinforced concrete beams", ACI Materials Journal, V. 104, No. 1.
- **8. Pritpal S. Mangat and Mahmoud S. Elgar.,** 1999, "Flexural Strength of Concrete Beams with Corroding Reinforcement", ACI Structural Journal, V. 96, No. 1.
- **9. Inamullah Khan, R.Francois, A. Castel.,** 2011, "Mechanical behaviour of long-term corroded reinforced concrete beam", Modelling of Corroding Concrete Structure, RILEM.
- **10. Yingang Du, Leslie A. Clark, and Andrew H. C. Chan.,** 2007, "Impact of Reinforcement Corrosion on Ductile Behavior of Reinforced Concrete Beams", ACI Structural Journal, V. 104, No. 3.
- 11. Yingshu Yuan, Yongsheng Ji, and Surendra P. Shah., 2007, "Comparison of two accelerated corrosion techniques for concrete structures", ACI Structural Journal, V. 104, No. 3.
- 12. John Cairns, Giovanni A Plizzari, Yingang Du, David W Law, Chiara Franzoni., 2005, "Mechanical Properties of Corrosion-Damaged Reinforcement", ACI Materials Journal, V.102, No.4, pp. 256-264.
- **13. C.A.Apostolopoulos, V.G.Papadakis.,** 2007, "Mechanical behavior of reinforcement stirrups BSt 500s at corrosive environment", Journal of Materials Engineering and Performance, Volume 16(2), pp. 236-241.
- **14.** Ragnar Palsson and M.Saeed Mirza., 2002, "Mechanical response of corroded steel reinforcement of abandoned concrete bridge", ACI Materials Journal, V.99, No.2, pp. 157-162.

- **15. Han Seung Lee, Young-Sang Cho.,** 2009, "Evaluation of the mechanical properties of steel reinforcement embedded in concrete specimen as a function of the degree of reinforcement corrosion", Int J Fract 157: 81–88 DOI: 10.1007/s10704-009-9334-7.
- **16. T.Vidal, A.Castel, R.François.,** 2007, "Corrosion process and structural performance of a 17 year old reinforced concrete beam stored in chloride environment", Cement and Concrete Research 37, pp. 1551–1561.
- **17. Ruijin Zhang, A.Castel, R.François.,** 2010, "Concrete cover cracking with reinforcement corrosion of RC beam during chloride-induced corrosion process", Cement and Concrete Research 40, pp. 415–425.
- **18. R.François, J.C.Maso.,** 1988, "Effect of damage in reinforced concrete on carbonation or chloride penetration", Cement and Concrete Research.Vol.18, pp.961–970.
- **19. A.Konin, R.Francois, G.Arliguie.,** 1998, "Analysis of progressive damage to reinforced ordinary and high performance concrete in relation to loading", Materials and Structures/Materiaux et Constructions, Vol.31, pp. 27-35.
- **20. T. A. Söylev and R. François.,** 2005,"Corrosion of reinforcement in relation to presence of defects at the interface between steel and concrete", Journal of materials in civil engineering © ASCE.
- **21. Raoul François and Ginette Arliguie.,** 1998, "Influence of service cracking on reinforcement steel corrosion", Journal of materials in civil engineering.
- **22. J.Rodriguez, L.M.Ortega, J.Casal.,** 1997, "Load carrying capacity of concrete structures with corroded reinforcement", Construction and Building Materials, Vol. II, No. 4. pp. 239-248.
- **23.** Youping Liu and Richard E. Weyers.,1998, "Modeling the Time-to-Corrosion Cracking in Chloride Contaminated Reinforced Concrete Structures", ACI Materials Journal, V. 95, No. 6.
- **24. BS EN 1992-1-1 Eurocode 2:** Design of concrete structures-Part 1: General rules and rules for buildings, November 2002.
- 25. CEB-FIP model code 1990.
- **26. Zhang R., Castel A., François R.,** 2009, "Serviceability Limit State criteria based on steel–concrete bond loss for corroded reinforced concrete in chloride environment", Materials and Structures, Volume 42, Issue 10, Page 1407 1421.

- **27.** N-A.Vu, A. Castel, R. François., 2010, "Response of post-tensioned concrete beams with unbonded tendon including serviceability and ultimate state", Engineering Structures 32, pp. 556-569.
- **28.** François R., Khan I., Dang V-H., 2012, "Impact of corrosion on mechanical properties of steel embedded in 27-year-old corroded reinforced concrete beams", Materials & Structures, submitted.
- **29.** Cairns J., Plizzari G. A, Du Y., Law D.W and Franzoni C., 2005, "Mechanical properties of Corrosion-Damaged Reinforcement", ACI Material Journal, V. 102, No.4, pp. 256-264.
- **30. T.Vidal, A.Castel, R. Francois.,** 2004," Analyzing crack width to predict corrosion in reinforced concrete", Cement and Concrete Research 34, pp. 165–174.

II.3. EFFECT OF CORROSION OF STEEL ON SHEAR BEHAVIOR

Article:

Vu Hiep Dang, Raoul François, Shear behaviour and load capacity of short reinforced concrete beams exposed to Chloride environment, to be submitted.

Abstract: The effect of corrosion of reinforcement on the behaviour of reinforced concrete (RC) deep beams was investigated. Corrosion results of long term (27 years) climate accelerated process in chloride environment which is closed to natural corrosion and lead to a high level of heterogeneous loss of cross-section on both longitudinal reinforcement and transversal reinforcement (stirrups). Control beams of same age kept in non aggressive environment are also tested as a reference. Tension reinforcement did not have a special anchorage since re-bars were straight at edges. For deep beams, the behaviour during bending tests involved a combination of arch action and beam action which could be affected by corrosion in different ways, such anchorage capacity, stirrups corrosion and resulting transversal cracks and loss of cross-section of tension reinforcement.

Nevertheless and despite high corrosion level of steel bars, the ultimate capacity of deep beams is slightly decrease. The change in load transfer mechanism and failure mode could explain these results.

1. Introduction

Corrosion affects the structural performance of reinforced concrete members in many ways such as: sectional area loss of reinforced steel bar, cracking and concrete cover spalling and loss of bond strength between steel bars and surrounding concrete. The localized corrosion (pitting corrosion) of the reinforcing bars results in a local reduction in the cross-sectional area of rebar, leading to a decrease in load carrying capacity and ductility. The generalized corrosion of the reinforcing bars leads to cracking and delaminating of concrete cover, which induces the remarkable disbonding between two

materials. The effect of corrosion on shear strength of RC structures is not as well understood as the flexural strength or bond strength and it needs to be more interpreted.

In a review article on performance of beams corroded under a sustained load, Goitseon Malumbela et al. [15] summarized previous studies carried out to investigate the flexural behaviour of RC beams. Many parameters discussed such as the deflection of structures corroded under load, the correlation between the mass loss and residual strength, the association between the rate of corrosion and rate of corrosion crack opening and the change in stiffness of beams during the corrosion process. Although there are still disagreements on the authors's structural viewpoint, these experimental results brought the further understanding about the effect of reinforcement corrosion on the flexural response of beams in the presence of a sustained load.

Several researchers studied the strength and shear capacity of RC beams with only corroded stirrups [1, 4, 8] or with only complete loss of bond of longitudinal steel bars or corroded longitudinal steel bars [9-11]. While others published the shear strength of RC beams with corroded longitudinal steel and stirrups [2, 3, 12], which represents the actual corrosion in the real structures. Most of these studies have performed investigation on RC beams corroded by applying a current through steel bars embedded in the concrete [1, 2, 12] or both impressing an external current and adding chlorides to concrete mixture [3, 4] instead of a natural corrosion process. Corrosion induced by an impressed current technique tends to lead uniform corrosion, similarly to corrosion induced by carbonation. Moreover, according to [14] the current density very significantly affects the reinforcement-concrete bond strength and the bond strength in turn significantly influences the behaviour of RC members. Y. Yingshu et al. [24] showed that the corrosion induced by impressing current is dissimilar to natural corrosion and could lead to the different consequences on mechanical properties in compared to the in-site corrosion.

To the author's knowledge, there are a few works found in the literature on the influence of corrosion on the shear strength of reinforced concrete beams under the same corrosion condition as natural corrosion. Yan Xi-kang et al. [13] carried out an experimental study of ten very small scale RC beams with the dimension of $100 \times 100 \times 600$ mm. They used artificial sea water, which has the five times higher concentration salt than the

concentration of natural sea water, in order to accelerate corrosion for these beams during 140 days with wetting-drying cycles at a high temperature. The authors observed that most of the beams failure in the shear-compression mode with crushing of top concrete face. They also observed that there is an increase tendency in the load-carrying capacity at larger corrosion rate. It is nevertheless, well known that the shear strength is greatly affected by size of beam, thus such beams probably give limit results. Therefore, it is really required to investigate the mechanism of benefit or loss of shear capacity together with the change in mechanical properties in more detail for corroded RC beams. I. Khan et al. [19] tested two naturally corroded deep beams and one control beam of sizes of 1150 x 280 x 150 mm until failure. These deep beams are 26 years old at the study time. They stated that the corrosion have almost no important effect on the mode of failure. All of three deep beams failed by compressing the strut, which showed that a main incline crack starts from the loading point towards the support. More interestingly, the corrosion did not decrease the anchorage capacity of tensile reinforcement steel. This is attributed to the fact that the corrosion products accumulated and filled up the gap below the steel bars and so increasing the resistance of slip of corroded steel bars.

This study deals with structural performance of some corroded short RC beams kept in salt fog for 27 years with the same concentration as sea water. These corroded RC beams have the shear span length to effective depth ratios (a/d) of 1.67; 2.7; and 3.125 respectively. Experimental results of corroded beams will be compared with results of the corresponding reference beams of the same age to find change in their mechanical properties as well as differences in their behaviour.

2. Experimental program

A program of long-term experiment was started in 1984 at Laboratoire Matériaux et Durabilité des Contructions (L.M.D.C) in INSA-Toulouse (France). Series of 36 RC beams of common dimension (15 x 28 x 300 cm) as supplied by industry cast with two different types A and B were stored in a chloride environment under sustained loading. At the same time, another batch of 36 RC beams of same composition serving as control beams were cast but stored under laboratory conditions (non-aggressive environment) in order to have a comparison. There were two levels of loadings applied on the beam. At

different periods, experiments were carried out to analyzed the data such as: relationship of width of corrosion crack and loss of local steel cross-sectional area, chloride content, stiffness reduction and mechanical behaviour under service load [5-7].

2.1 Exposure conditions

The beams were kept in aggressive chloride environment. The aggressive environment is a salt fog (35g/l of NaCl corresponding to the salt concentration of sea water) generated through the use of four spays located in each upper corner of a confined room. The beams were subjected to wetting-drying cycles in order to accelerate the corrosion process as given in Table 1.

Table 1. Exposure conditions of all RC beams at the L.M.D.C

Duration	Wetting-drying cycles	Temperature-climate	Load?
First 6 years	Continuous spraying	20°C-in the lab	yes
From 6 to 9	1 week-spraying	20°C-in the lab	yes
years	1 week-drying	20 C-III the lab	
From 9 to 19 years	1 week-spraying	from -5° to 35°C-in South-west	yes
	1 week-drying	of France	
From 19 to 26 years	Stopped	from -5° to 35°C-in South-west of France	no
From 26 to 28 years	2 days-spraying	from -5° to 35°C-in South-west	no
	2 weeks-drying	of France	110

Although this was an accelerated version of the real process, the corrosion obtained was much closer to that actually observed in natural conditions, with respect to corrosion distribution, corrosion type and the oxides produced, than those resulting from use of an applied current or a CaCl₂ admixture in concrete.

2.2 Loading conditions

The beams were loaded in three-point flexion by pairing a type A beam with a type B beam (see figure 1). According to French standards at the time of loading, the level 1 loading (M_{ser1} = 13.5 kNm) corresponded to maximum loading versus durability in an aggressive environment for the type A beam (serviceability limit state requirements in an aggressive environment) and to maximum loading versus resistance (ultimate load limit state in non-aggressive environment) for the type B beam. The beams stored under sustained level 1 loading are called A1 and B1. The level 2 (M_{ser2} = 21.2 kNm) corresponded to 80% of the failure load and equal to twice the design service loading in aggressive environment for type B beam. For type A beam, it corresponded to maximum loading versus resistance (ultimate load limit state in non-aggressive environment). The beams stored under sustained level 2 loading are called A2 and B2. All the A beams were cast in an inverted position with their tensile steel reinforcement in the top of the form, the compressive steel in the bottom of the form.

In this paper three corroded short beams, labelled A2CL1-A, A2CL2-A and A2CL2-B, extracted from two beams A2CL1 and A2CL2 corroded in chloride condition of 27 year-old under a sustained load. These short beams then tested in three points bending until failure. Also, the tests on A short control beams with the same span length were conducted.

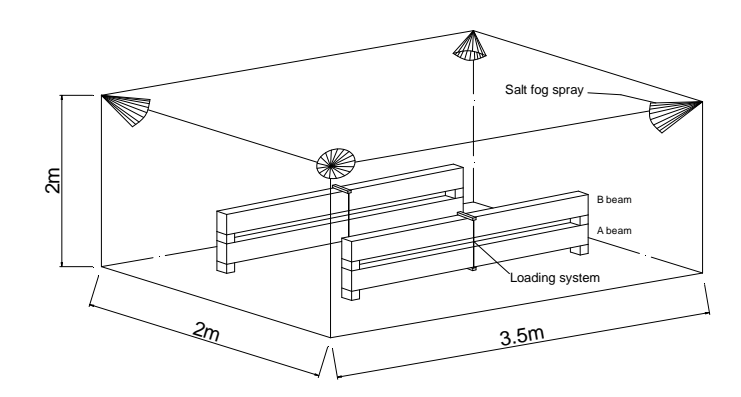


Figure 1. Loading system and conditional exposure of beams in the saline room

2.3 Material properties

The constitutions of concrete for each mixture batch are given in Table 2. Water content was adjusted to obtain a slump of around 7 cm. The average compressive strength and elastic modulus obtained on cylinder specimens (110×220 mm) were 45 MPa and 32 GPa at 28 days. The maximum concrete cover depth provided in type A beams was 40mm to stirrups and ordinary reinforcing steel (yield strength f_y =500 MPa) was used. The reinforcement steel arrangement for reinforced concrete beam A is showed in Fig. 2. It should be noted that the longitudinal steel bars used in all beams were straight without any hook at the ends.

Table 2. Concrete mixture proportions (kg/m³)

Mix composition	Aggregate size	
Rolled gravel (silica+limestone)	5/15 mm	1220
Sand	0/5mm	820
Porland cement: OPC HP (high perform)		400
Water		200

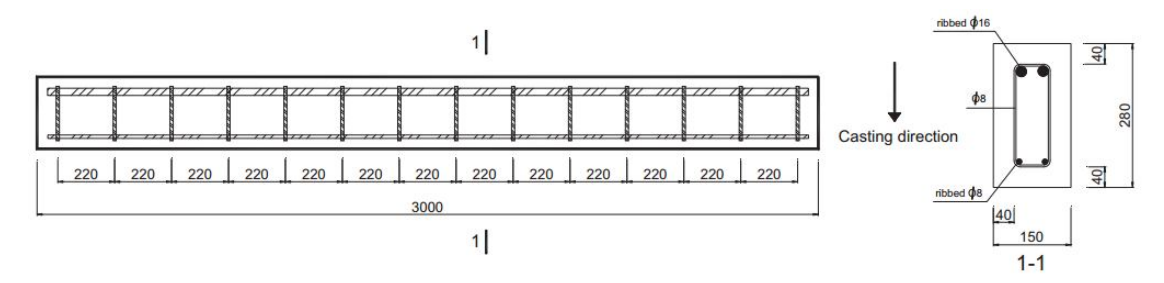


Figure 2. Dimensions and reinforcement details of type A beam (sizes in mm)

3. Experimental details

Test procedure

Beams were loaded under three-bending points with loading speed of 0.2 kN/s until failure. Vertical displacement at mid-span and slip of each of the tensile steel bars at ends of beam were measured by digital sensors during loading as seen in Fig.3. The progress of cracking and the phenomenon of failure were observed visually. An anchorage length of 50 mm was chosen for beams with a/d ratios of 2.7 and 3.125. For beams with a/d ratio of 1.67, the supports are the steel plates of sizes of 150 x 150 mm.

Cracking maps

The crack maps were drawn with exact locations of corrosion cracking. The corrosion of longitudinal reinforcement caused only longitudinal cracks. The corrosion crack widths were also measured by using a portable video microscope with an accuracy of 0.01 mm.

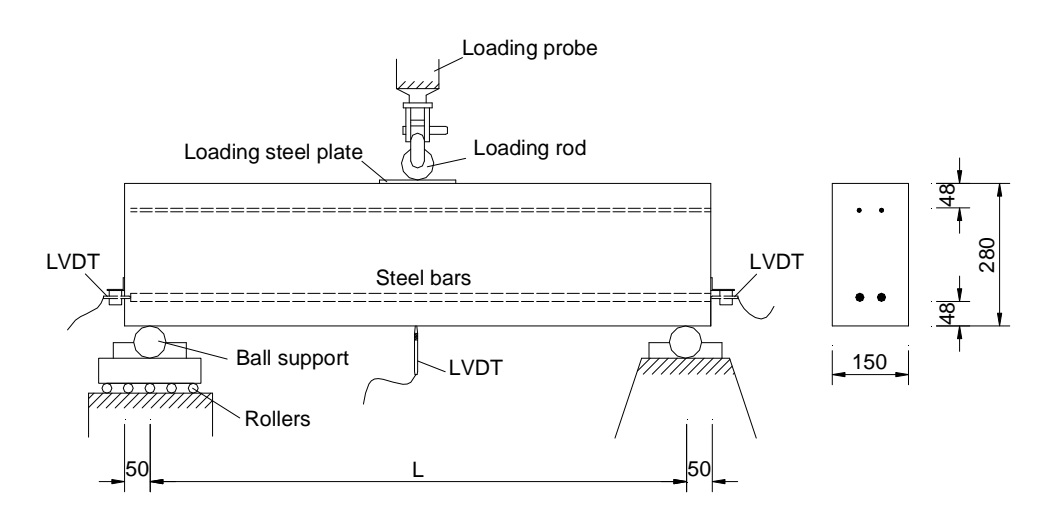


Figure 3. Test setup for ultimate load

Corrosion maps

The corrosion maps of both main steel bars and links were drawn in details after the corroded steel bars were extracted from concrete and made clean by Clark's solution ANSI-ASTM G1-72. The minimum residual diameter of the all longitudinal bars and stirrups were carefully measured by a vernier calliper.

4. Experimental results and discussion

4.1 Cracking maps

The cracking maps of corroded beam A2CL1-A and A2CL2-B after 27 years of exposure in chloride environment are exhibited in Fig.4. It is easy to see that the corrosion cracks of A2CL1-A beam expanded more densely than those of A2CL2-B beam even though they had the same condition of exposure and load level. Indeed, on the face sides and compressive face of A2CL1-A several transversal cracks propagated through its total depth because of stirrup corrosion, which increased the stress on the embedding concrete, making the concrete cover crack. Furthermore, comparing with A2CL2-B the corrosion cracks along the span length of A2CL1-A were existed on the compressive face. The maximum width of corrosion cracks close to the right supports of two beams were 1.4 mm and 1.54 mm respectively. More interesting, the longitudinal corrosion cracks at level of tensile steel bars were mostly interconnected. As mentioned above, the tensile surface of the beam exposed to the salt fog plus the damage to the concrete at the interface [16, 17] had led corrosion to develop preferentially in the tensile rebar. On the tensile face of A2CL2-B, the relatively big longitudinal crack due to corrosion of tension reinforcement steel runs from the right end to left end. These longitudinal corrosion cracks could reduce the steel-concrete confinement, leading the drop of bond stress between two materials. It should be noticed that no corrosion crack was detected in the compressive zone of A2CL2-B beam. Figure 5 presented maps of corrosion crack of A2CL2-A beam at 27 ages. A transversal crack at the right support, where the bending moment is zero, developed its whole depth. This transverse crack location was corresponded to the first location of stirrup of beam. Larger corrosion cracks were found near the beam ends mainly because of the fact that the length of longitudinal reinforcement steels was stopped at only around 10 mm from beam-ends that allow faster chloride ingress through concrete cover.

4.2 Corrosion maps

The distribution of the local steel cross-section reduction along both tensile bars was measured after the mechanical test up to failure. To evaluate the actual corrosion damage, the concrete was completely removed from the reinforcement by using Clark's solution ANSI/ASTM G1-72. The steel cross-section reduction was assessed from the reinforcement diameter loss that measured with the help of a vernier calliper. It should be noted that from this measurement technique, loss of cross-section could be overestimated because of the considerable change in surface shape of steel bar due to corrosion.

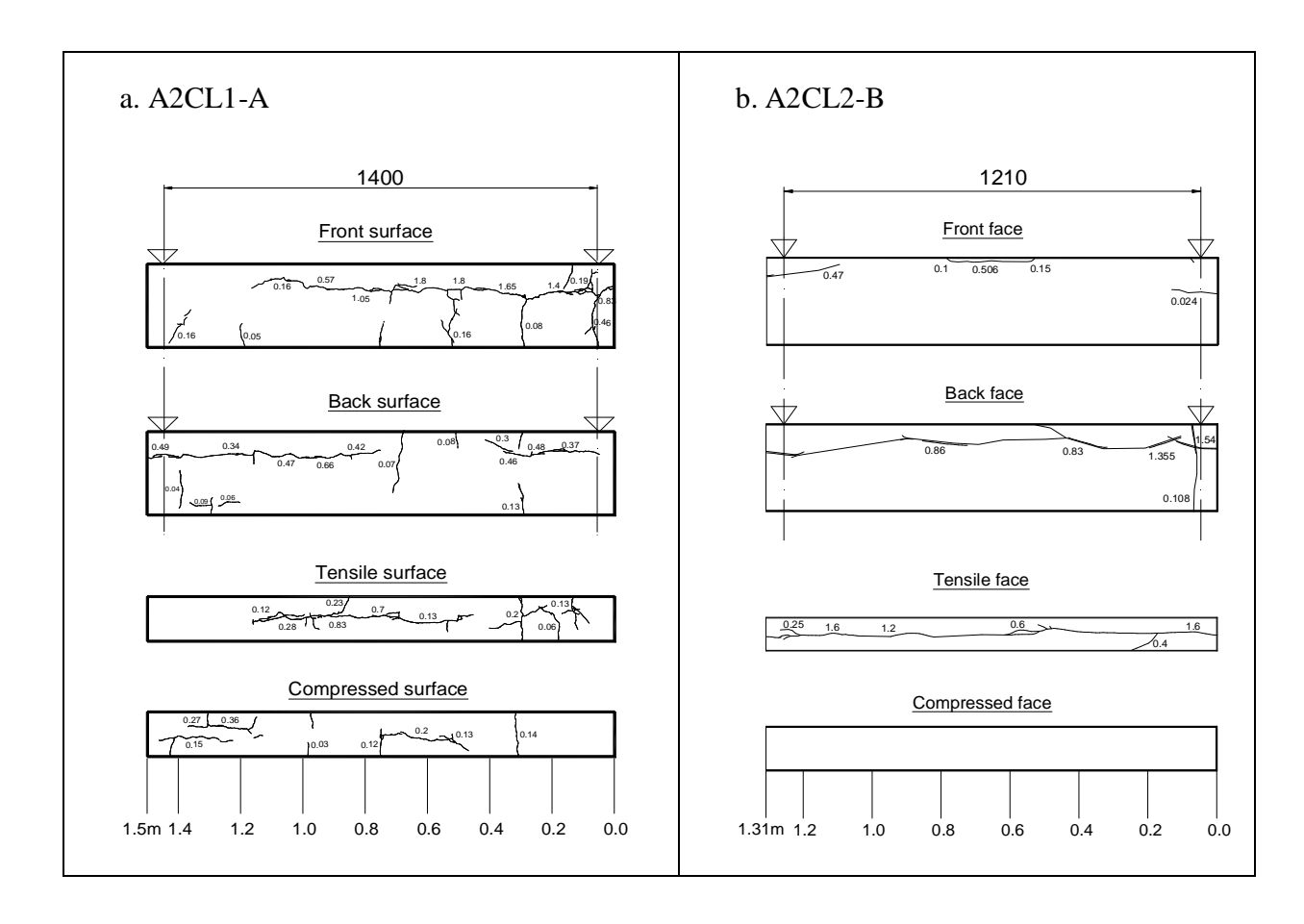


Figure 4. Corrosion crack maps of A2CL1-A and A2CL2-B at 27 years

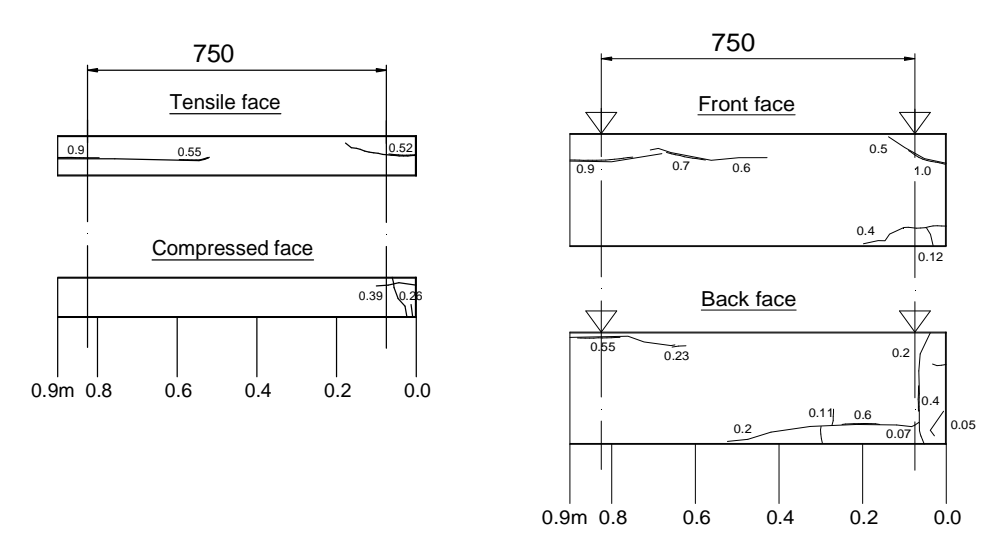


Figure 5. Corrosion cracking maps of beam A2CL2-A after 27 years of storage

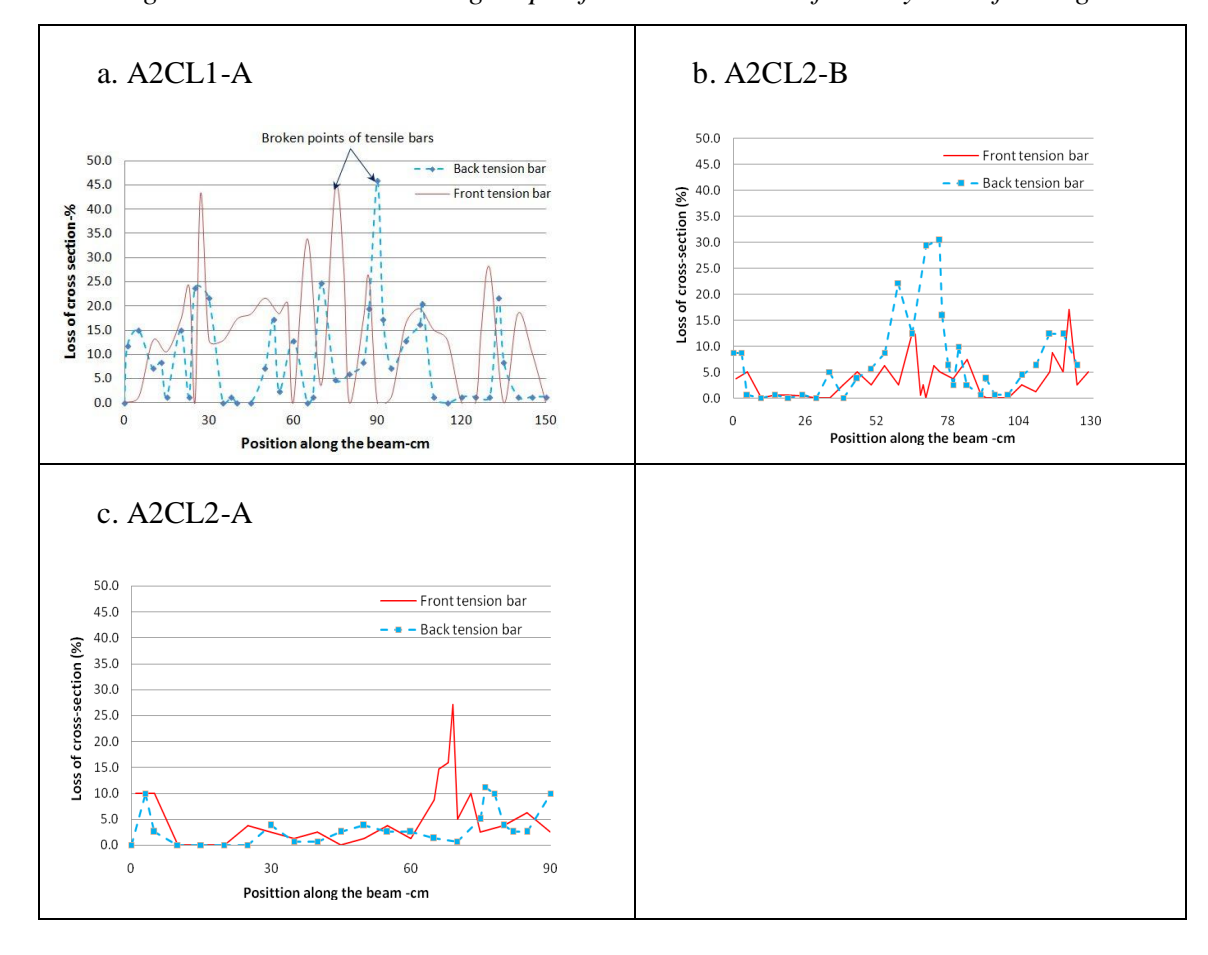
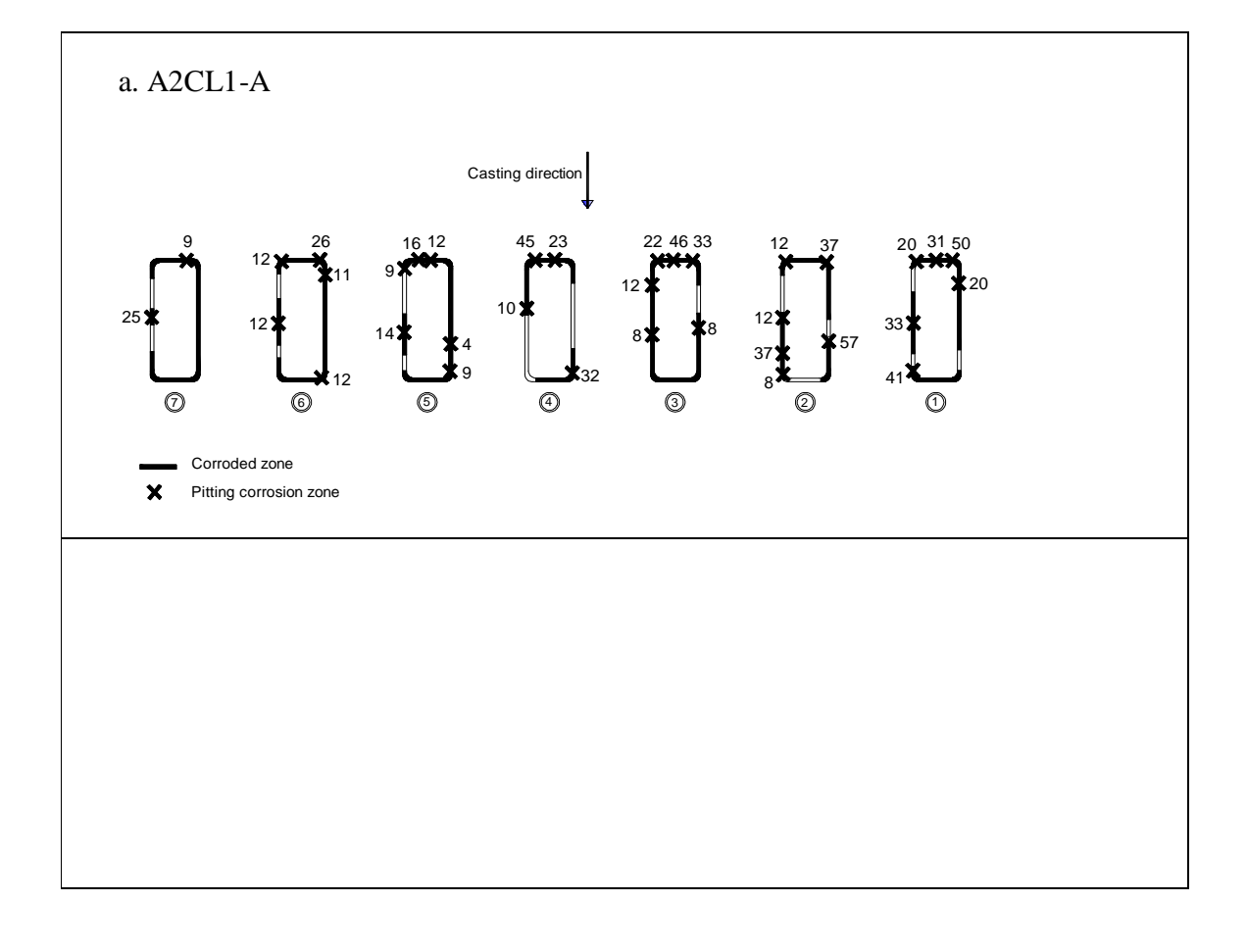


Figure 6. Loss of cross section area along the tensile bars in corroded beams

The calculated loss of cross-sectional reinforcement along steel bars in the tensile zone is shown in Fig.6. It is clearly that the corrosion evolution of tensile reinforcement steels was not uniform, even along the same bar. Numerous pits were observed on the tension reinforcing bars. For A2CL1-A beam, two big pitting attacks were visible in the central zone of both tensile bars, cross-section loss of up to 45%. Interestingly, both of the tensile bars were broken at these serious pits during the flexural test. In case of A2CL2-B, the most severe pits were also distributed in the mid span. In particular, the higher corrosion degree measured on the back tension bar is likely to cause the longitudinal corrosion crack with 1.35mm in width on its back face (see Fig.4b). Similarly, the front tension bar of A2CL2-A beam having much greater level of corrosion at abscissa from 65 cm to 90 cm as plotted in Fig.6c probably induces the longitudinal corrosion crack at the height of steel bars on front face (see Fig.5).



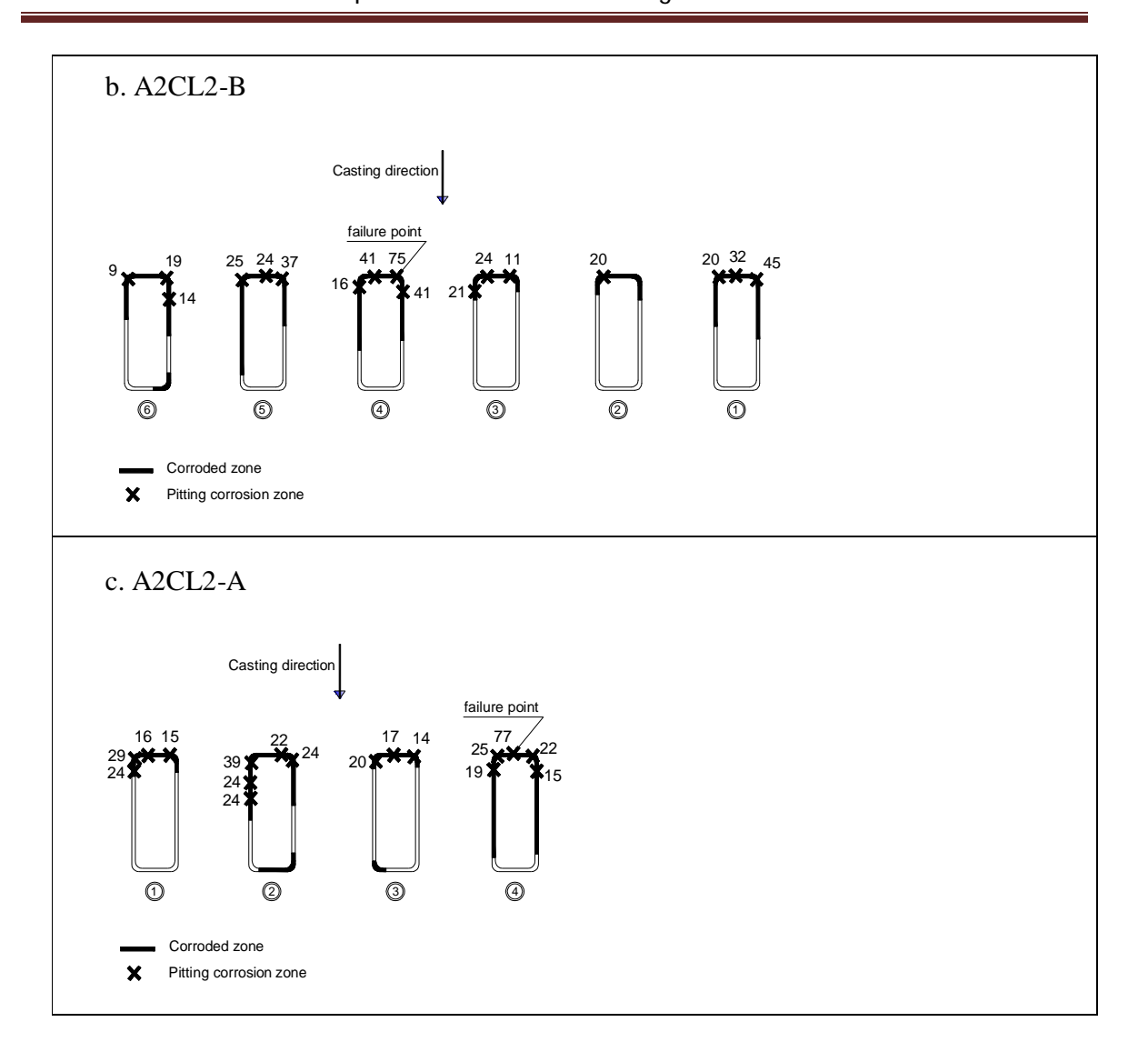


Figure 7. Percentage loss of diameter for stirrups

It must be noted that series A beams were stored in chloride environment with tension face upward (see Fig.1) and A beams were cast with top-cast tensile bars. Therefore, the tensile reinforcing steel and upper parts of link bar in contact with tension re-bars were exposed to chloride spray during storage period. Moreover, the effect of tensioned crack surface and gravimetric access of chloride in cracks led to first corrosion cracks along tension reinforcement, which spread gradually all along beam length. The higher corrosion rate on these zones is due to the higher concentration of chloride. From Fig.7, it is evident that the corrosion state of the upper part of all the stirrups was more serious

than corrosion of the lower part, with many pitting attacks as seen in Fig.8. More importantly, the corrosion of stirrups also developed even those are close to the supports where no flexural cracks exist.



Figure 8. Real corrosion at upper part of stirrups

4.3 Flexural response and strength

To facilitate for analyses and comparisons, the corroded beams A2CL1-A, A2CL2-B and control beams with a shear span to effective depth ratio (a/d) below 4.0 are firstly discussed. According to [29], these four RC specimen beams can be classified as short beams. Flexural load responses of corroded and corresponding control beams were plotted in Fig.9.

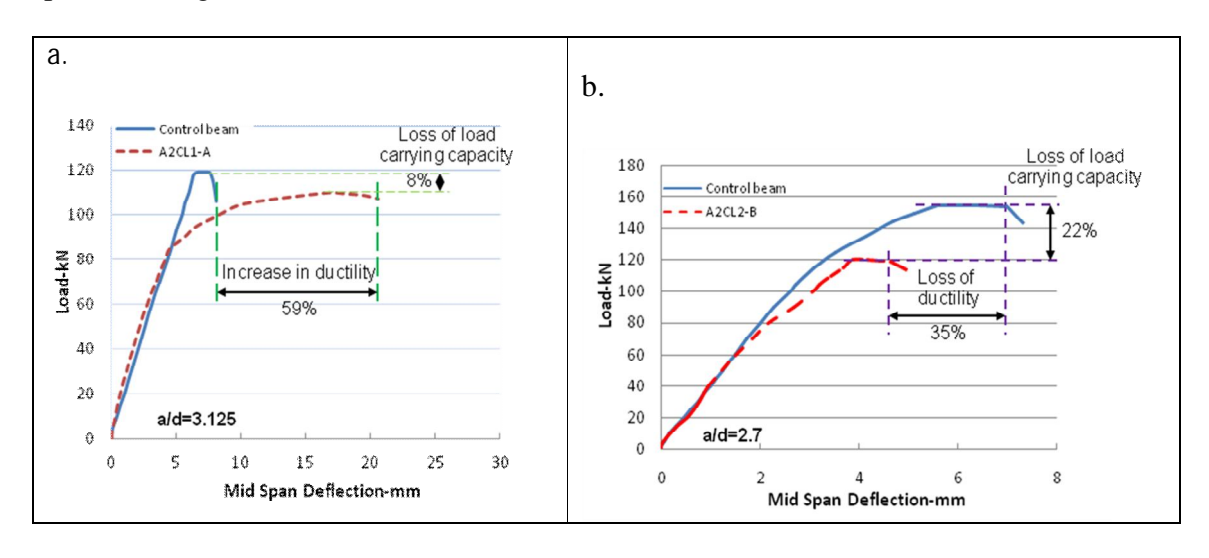


Figure 9. Load-midspan displacement curves at ultimate load

From the load-deflection curves of A2CL1-A and control beam (fig.9a), it can be seen that bearing capacity load of corroded beam A2CL1-A marginally reduces (8%) but its ultimate displacement at collapse is strongly increased by 59%. A possible explanation is that the type of failure of A2CL1-A is failure in bending with breaking of both tensile reinforcement steels (fig.10a), whilst corresponding non-corroded beam fails very abruptly by a critical diagonal crack combined with the rebars slip and crushing of concrete underneath support just after reaching the peak load (fig.10b). In the usual RC calculation for a cracked cross-section, using the nominal yield stress of the control steel bar recorded by R. Francois et al. [25], the calculated yielding load of control beam is 129.42 kN. This value is fairly larger than experimental ultimate load (119.2 kN). This indicates that collapse of control beam and yield of steel bars were not simultaneously occurred. This also explains that why a very short plateau arose on the behaviour curve of non-corroded beam. For this case, corroded beam with high corrosion degree (average of 11.5%) induces a totally different performance, with a conventional shape of load-displacement curve of RC beam.

Beams A2CL2-B and corresponding uncorroded beam exhibited the same loaddeflection behaviour (fig.9b) but final failure modes were very dissimilar (fig.11). Both of them fail suddenly after the peak load, with really small mid-span displacement. The differences in deflection capacity between them are mainly due to the fact that reference beam collapsed by reinforcement slip and shear interaction, meanwhile the collapse of corroded beam occurred by falling off concrete cover at the support. The longitudinal steel corrosion makes shift in failure type. It should be noted that at the beam end, a big transverse corrosion crack with the maximum width of 1.54mm affected importantly the type of failure of A2CL2-B, spalling off concrete in the corner of beam end as seen in Fig.11a. From the figure 9.b, it can be seen that when the load is below 50% of ultimate load of control beam or 38% of ultimate load of corroded beam, their load-deflection curves are almost similar. Nevertheless, when the load increases further, the difference become clear and corroded beam shows a higher deflection than control beam at the same load level. It should be noted that a shear span to effective depth ratio 2.7 is very close to 2.5, which seems the limit between short beams and slender beams [22]. Therefore, for corresponding control beam the hybrid behaviour combined both beam action and arch

action is anticipated. Indeed, figure 11b presents a slip-bending mode of failure with an incline crack staring from loading point towards bottom face and spalling out of concrete cover near the support. If taking into the loss of cross sectional area of A2CL1-A and A2CL2-B at mid span is 31% and 24%, respectively, in table 3, the experimental results are compared with theoretical predictions for yielding strength of RC beams.

Table 3. Experimental results vs. theoretical results

a/d		Experimental values- kN	Theoretical yielding values- kN
	A2CL1-A	89.05-yielding load	91.84
3.125	Control beam	119.2-ultimate load	129.4
	A2CL2-B	120-ultimate load	116.26
2.7	Control beam	155-ultimate load	149.75

A 31% cross section loss of A2CL1-A produces a yielding load of 91.84kN that is well matched with the experimental result (89.05 kN). Table 3 implies that in theory, both A2CL2-B and corresponding control beam will be yielded before failing. Nevertheless, both of them were abruptly broken down, which gives a too small deflection. Thus, they are not able to reach an expectedly superior load-bearing capacity.

Fig.12 exhibited the relationships between the mid-span displacements and load of two RC deep beams (a/h= 1.34) [20], one is corroded beam and other is corresponding uncorroded beam. Although there is no difference in failure mode of two beams (failure of compression strut conjoined with crushing concrete, see Fig.13), the behaviour curves are clearly so different even at a very low load level (around 20 kN). For this case, the corrosion has almost no effect on the failure type of deep beams, which also observed by

several authors [4, 12, 19], but affecting its mechanical properties such as: bending stiffness, ultimate load, ductility. A reduction in the stiffness of corroded beam is more and more significant as the applied force increases. When the compression strut failed with a critical shear crack, the loading capacity of beams dropped suddenly. The shear capacity drops up to 20% compared to control beam but the corroded deep beam shows a more ductile collapse as compared with the control beam. Besides, it can be seen from fig.13 that both of them split at the ends of beam when the ultimate load reached. This is likely ascribed to the poor confinement of the concrete-steel interface since the spacing of stirrups was 22cm for whole beams.

a)





b)





Figure 10. Failure modes of (a) corroded beam A2CL1-A; (b) corresponding control beam

a)





b)





Figure 11. Failure modes of (a) corroded beam A2CL2-B; (b) corresponding control beam

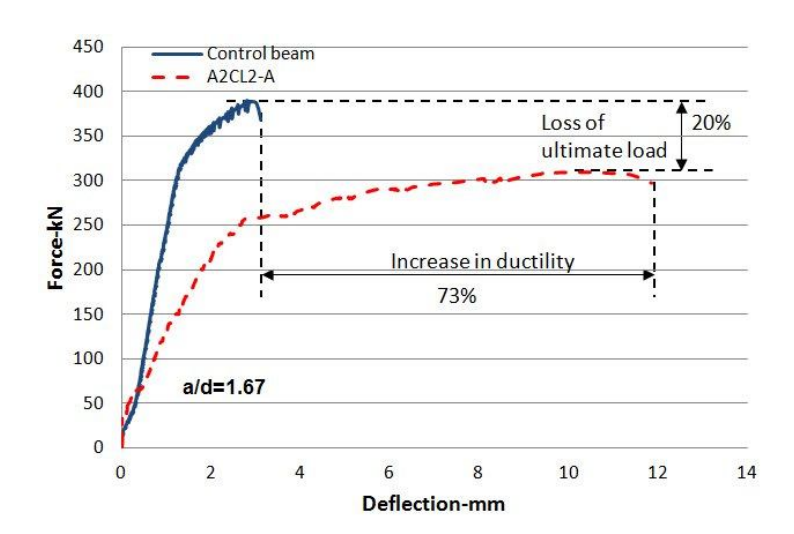


Figure 12. Load-deflection behaviour at ultimate load

Fig.14 displays the load bearing capacity of the control and corroded beams as a function of a/d ratios. Two trend lines are established: the first line corresponds to corroded deep beams and the second one corresponds to corroded slender beams. Obviously, the ultimate strength decreases with increasing the a/d ratios but for deep beams, a more rapid reduction in strength is recorded. This also found by Christopher Higgins et al. [4].

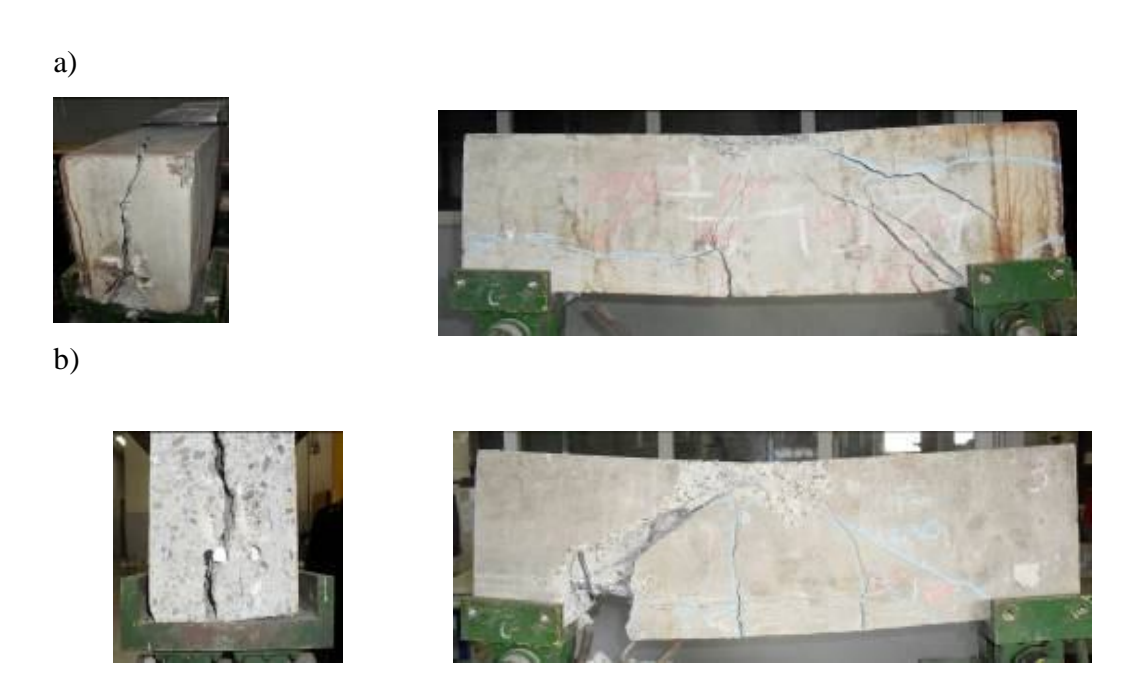


Figure 13. Failure modes of (a) deep corroded beam A2CL2-A; (b) corresponding deep control beam

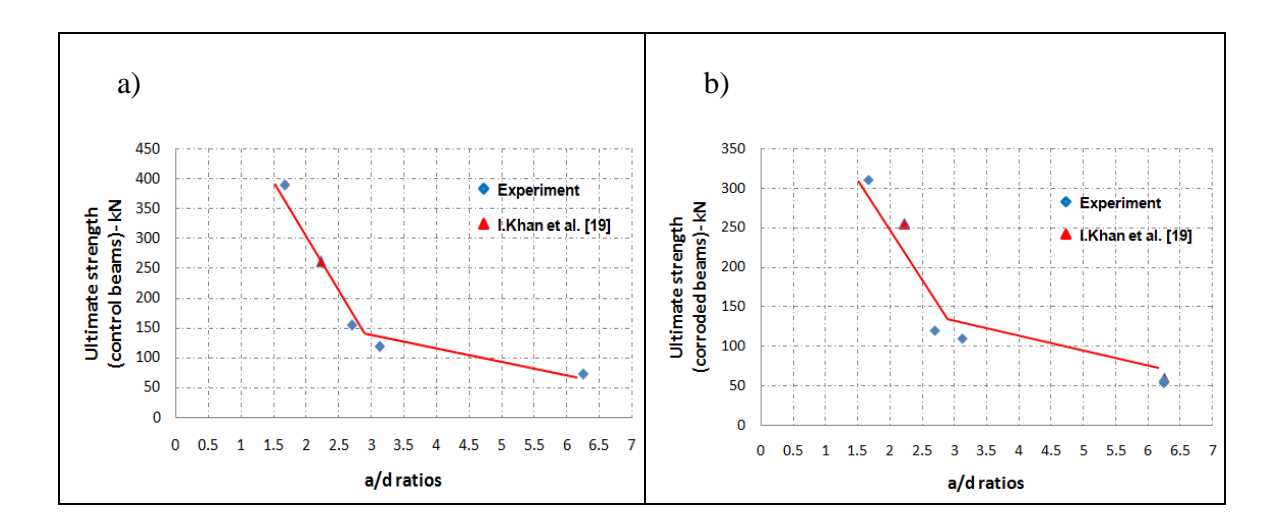


Figure 14. Relationship between Ultimate strength and a/d ratios (a) for control beams; (b) for corroded beams

The tests indicated that the highest corrosion level does not lead to the greatest strength reduction. However, it could be stated that the ultimate load falls as the degree of corrosion increases.

4.4 Anchorage capacity

As mentioned earlier, the free-end slip of all beams was monitored by four LVDTs: LVDT 1 and LVDT 3 measured the horizontal slippage of front bars while LVDT 2 and LVDT 4 measured the horizontal slippage of back bars (Fig. 15).

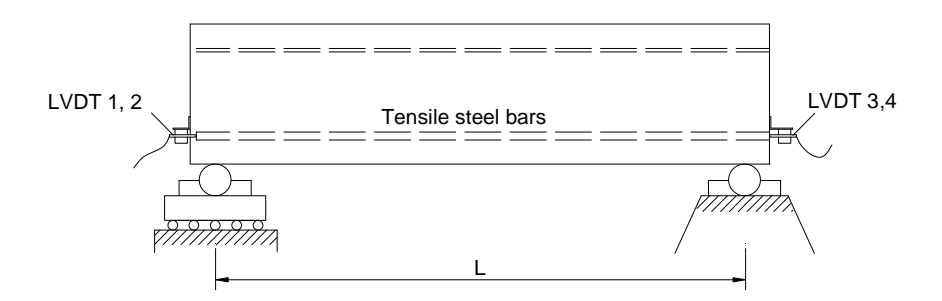


Figure 15. Measurement of free-end slip for tensile steel bars

In case of short beams (a/d < 4), two stages of slipping for control beams can be observed in Fig. 16a, b.

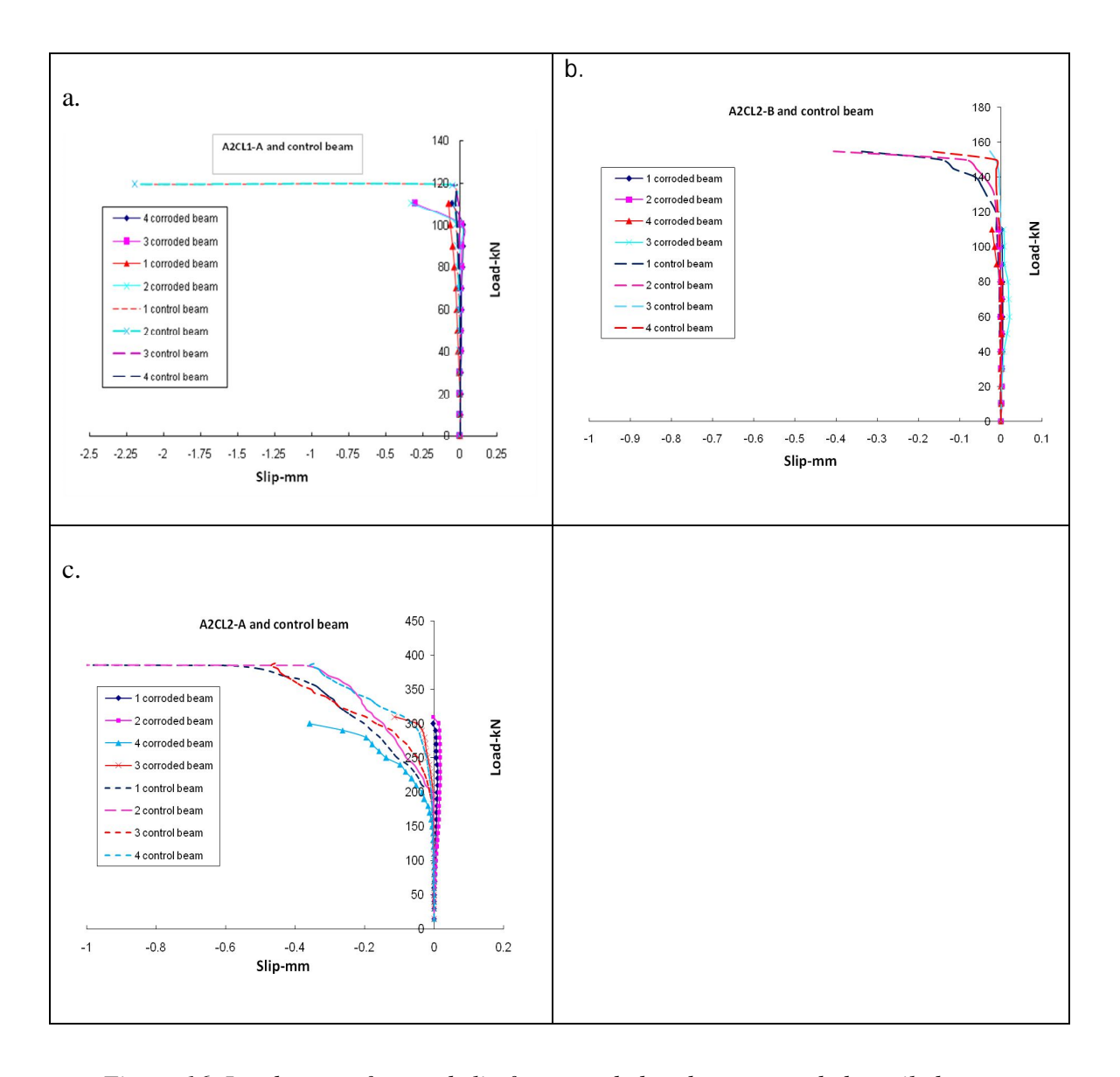


Figure 16. Load versus free-end slip for corroded and non-corroded tensile bars

The first stage, corresponding to before reaching the ultimate load, load-slip curve represents hardly the movement between steel and concrete. The second stage, when the load reached the ultimate load, the slip of tension rebars increased sharply. The situation was quite different from the corroded beams as seen in Fig. 16a, b. The values of slip

recorded on corroded beams were slowly increased until failure of beams. It could state that at the same loading level (below peak load), the resistance of slip of non-corroded steel bars is better than that of corroded steel bars. However, once attaining a maximum load, the more slip measured on non-corroded reinforcement than the corroded reinforcement was found. This demonstrates that the bond stress improves in spite of the corrosion development, in agreement with result studied by I. Khan et al. [19]. Herein, it should be mentioned that the different in mode of failure between corroded and control beams could lead to the different in movement of tensile bars at two ends of each beam.

Concerning deep beams, as exhibited in Fig. 16c, the movement of reinforcement in both beams occurred as the load surpassed 100 kN. For corroded beam, the slip resistance of front bar was greater than that of back bar and slip of front bar was smaller than the slip of both tension bars in control beam. Clearly, there is a variation in bond strength between corroded and control beams prior to the failure of compression strut. Nevertheless, the slip resisted by corroded beam was more than control beam at the ultimate force. This implied that the anchorage capacity of corroded steel bar increases in comparison with non-corroded steel bar. This observation is not the same as K. Z. Hanjari et al.'s observations [26], who conducted the pull-out tests on beam ends corroded by impressing a direct current to surface of steel bars. This result could be explained that because corrosion products formed around steel bars enhance the friction between concrete and steel, the slip resistance of corroded steel increases. Although, the presence of longitudinal corrosion cracks close to support will decrease the concrete confinement, the vertical stress on bar-concrete interface that was generated by a support reaction at the bottom of beam helps to reduce the crack width and prevent the slip of steel bar, as concluded by J. Cairn et al. [27].

5. Conclusion

The effect of corrosion of reinforcement on the behaviour of reinforced concrete (RC) deep beams was investigated. Corrosion results of long term (27 years) climate accelerated process in chloride environment which is closed to natural corrosion and lead to a high level of heterogeneous loss of cross-section on both longitudinal reinforcement and transversal reinforcement (stirrups). Control beams of same age kept in non

aggressive environment are also tested as a reference. Tension reinforcement did not have a special anchorage since re-bars were straight at edges. For deep beams, the behaviour during bending tests involved a combination of arch action and beam action which could be affected by corrosion in different ways.

- Anchorage capacity does not appear to be reduced by corrosion of re-bars even if wide longitudinal cracks exit at the end of corroded beams. The confinement due to the load which re-closed cracks could be an explanation as already mentioned by Cairn et al. [27]
- Stirrups corrosion does not seem to lead to stirrups failure since no premature splitting of the compressive strut were recorded during the tests. Nevertheless, transversal corrosion crack due to stirrups corrosion located on the support location have led to the spalling of beam end and then a premature failure of corroded beam
- For intermediary beams between deep and slender beams, i.e. short beams, the loss of cross-section due to corrosion of tension reinforcement lead to change in failure mode from shear to bending due to reduce bending capacity and then surprisingly to a higher "ductility" since bending failure is less brittle than shear failure despite the fact that the corrosion reduced the ductility of steel bars.

Despite high corrosion level of steel bars with maximum loss reaching 30% of initial cross-section, the ultimate capacity of corroded deep beam is slightly decreased which was also recorded by Khan et al. [19] on naturally corroded beams or Azam and Soudki [28] on accelerated corroded beams. The change in load transfer mechanism and failure mode could explain these results. Prediction of the residual capacity of shear-critical reinforced concrete beams would need to mix and combine different approaches.

References

- **1. C.A. Juarez, B. Guevara, G. Fajardoa, P. Castro-Borges.**, 2011. "Ultimate and nominal shear strength in reinforced concrete beams deteriorated by corrosion", Engineering Structures 33 (2011) 3189–3196.
- **2.Xiao-Hui Wang, Xiang-Hua Gao, Bing Li, Bao-Ru Deng.,** 2011. "Effect of bond and corrosion within partial length on shear behavior and load capacity of RC beam", Construction and Building Materials 25 (2011) 1812–1823.
- **3.J.Rodriguez, L.M.Ortega, J.Casal.,** 1997. "Load carrying capacity of concrete structures with corroded reinforcement", Construction and Building Materials, Vol. II, No. 4. pp. 239-248, 1997.
- **4.Christopher Higgins and William C. Farrow III.,** 2006. "Test of reinforced concrete beams with corrosion-damaged stirrups", ACI Structural Journal/January-February 2006.
- **5.T.Vidal, A.Castel, R. Francois.,** 2004. "Analyzing crack width to predict corrosion in reinforced concrete", Cement and Concrete Research 34 (2004) 165–174.
- **6.R. Zhang, A.Castel, R.Francois.,** 2010. "Concrete cover cracking with reinforcement corrosion of RC beam during chloride-induced corrosion process", Cement and Concrete Research 40 (2010) 415–425.
- **7.T.Vidal, A.Castel, R. Francois.,** 2007." Corrosion process and structural performance of a 17 year old reinforced concrete beam stored in chloride environment", Cement and Concrete Research 37 (2007) 1551–1561.
- **8.Christopher Suffern, Ahmed El-Sayed, and Khaled Soudki.,** 2010. "Shear strength of disturbed regions with corroded stirrups in reinforced concrete beams", Can. J. Civ. Eng. Vol. 37, 2010.
- **9.J.Cairns, and Z. Zhao.,** 1993, "Behaviour of concrete beams with exposed reinforcement", Engrs Structs & Bldgs, 1993, 99, May, 141-154.
- **10. Joakim Jeppsson, and Sven Thelandersson.,** 2003. "Behavior of Reinforced Concrete Beams with Loss of Bond at Longitudinal Reinforcement", Journal of structural engineering, ASCE/October 2003.

- **11. Xin Xue, Hiroshi Seki.,** 2010, "Influence of longitudinal bar corrosion on shear behavior of RC beams", Journal of Advanced Concrete Technology Vol. 8, No. 2, 145-156, June 2010.
- **12. Jin Xia, Wei-liang Jin, Long-yuan Li.,** 2011." Shear performance of reinforced concrete beams with corroded stirrups in chloride environment", Corrosion Science 53 (2011) 1794–1805.
- **13.** Yan Xi-kang, Wang Tie-cheng, Zhang Yu-min., 2004. "Shear strength of reinforced concrete beams under sea water", Transactions of Tianjin University, Vol.10 No.2 Jun. 2004.
- **14. Fédération Internationale du Béton (fib)**. Bond of reinforcement in concrete, state-of-art report. In: International federation for structural concrete, Switzerland; 2000.
- **15.** Goitseon Malumbela, Mark Alexander, Pilate Moyo., 2009. "Steel corrosion on RC structures under sustained service loads- A critical review", Engineering Structures 31 (2009) 2518-2525.
- **16. R.François, J.C.Maso.,** 1988, "Effect of damage in reinforced concrete on carbonation or chloride penetration", Cement and Concrete Research.Vol.18 pp. 961–970, 1988.
- **17. A.Konin, R.Francois, G.Arliguie.,** 1998, "Analysis of progressive damage to reinforced ordinary and high performance concrete in relation to loading", Materials and Structures/Materiaux et Constructions, Vol.31, January-February 1988, pp. 27-35.
- **18. Vu.H. Dang, R. François.,** 2013, "Influence of long-term corrosion in chloride environment on mechanical behaviour of RC beams", Engineering Structures 48 (2013) 558–568.
- **19. I. Khan, R. Francois, A. Caste.,** 2013, "Experimental and analytical study of corroded shear-critical reinforced concrete beams", Materials and Structures, DOI 10.1617/s11527-013-0129-y.
- **20. ACI Committee 318**. Building code requirements for structural concrete (ACI 318-02) and commentary (ACI 318R-02). Farmington Hills (MI): American Concrete Institute; 2002.

- **21. D. Coronelli, P. Gambarova.,** 2004, "Structural assessment of corroded reinforced concrete beams: modeling guidelines", Journal of structural engineering, ASCE/August 2004.
- **22. G. N. J. Kani.**, 1966, "Basic facts concerning shear failure", Journal of the American concrete institute, June 1966.
- 23. Daejoong Kim, Woo Kim, and Richard N.White., 1999, "Arch action in reinforced concrete beams- a rational prediction of shear strength", ACI Structural Journal/July-August 1999.
- **24. Y. Yingshu, J. Yongsheng, Shah Surendra P.,** 2007, "Comparison of two accelerated corrosion techniques for concrete structures". ACI Struct J 2007; 104(3).
- **25. R. Francois, I. Khan, V.H. Dang.,** 2012, "Impact of corrosion on mechanical properties of steel embedded in 27-year-old corroded reinforced concrete beams", Materials and Structures.
- **26. K. Z. Hanjari, D. Coronelli and K. Lundgren**., 2010, "Severely Corroded Reinforced Concrete with Cover Cracking: Part 2. Anchorage Capacity", Modelling of Corroding Concrete Structures, Proceedings of the Joint fib-RILEM Workshop, Madrid, Spain.
- **27. J. Cairns, Y. Du and D. Law.,** 2008, "Structural performance of corrosion-damaged concrete beams", Magazine of Concrete Research, 60, No. 5, 359–370.
- **28. R. Azam, K. Soudki.,** 2012, "Structural performance of shear-critical RC deep beams with corroded longitudinal steel reinforcement", Cement & Concrete Composites 34, pp. 946–957.
- **29. W.W. Kuo, T.J. Cheng, S.J. Hwang.,** 2010, "Force transfer mechanism and shear strength of reinforced concrete beams", Engineering Structures 32, pp.1537-1546.

II.4. EFFECT OF CORROSION OF STEEL ON DUCTILITY OF RC BEAMS

Article:

Vu Hiep Dang, Raoul François, Change in ductility of corroded reinforced concrete beams under chloride environment, Submitted to Cement and Concrete Composites journal.

Abstract:

An experimental study using a three-point bending test on RC beams with dimensions of 150x280x3000 mm, naturally corroded over many years was conducted to evaluate the influence of steel corrosion on structural performance and, in particular, to better understand the change in ultimate deflection in bending and then in ductility. Some previous works by different authors are also discussed. The results show that the conventional ductility factor hardly applies to the assessment of ductile behaviour of corroded beams. A new ductility factor, based on the ratio between ultimate deflection of corroded and non-corroded beams, is proposed. In addition, the relation between ductility factor of corroded beams and cross-section loss in the corroded reinforcing steels was studied on the RC beams tested. The service life of corroded structures appears to be limited by the reduction of ductility in bending behaviour, which is more pronounced on the reduction of load-bearing capacity. This was linked to the change in mechanical properties of corroded steel bars in comparison with non-corroded steel bars.

I. Introduction

Corrosion of the reinforcing steel embedded in concrete is a very serious problem for Reinforced Concrete (RC) structures exposed to a saline environment as the penetration of chloride ions can locally ruin the passive oxide layer existing on the reinforcement surface. Reinforcement corrosion not only reduces the cross-sectional area of the reinforcing steel but may also induce cracking, delamination and/or spalling of the concrete cover, loss of bond strength with surrounding concrete, and deterioration of the anchoring of longitudinal steel bars. All of these factors can act individually or in

combination, leading to greater damage. Corrosion-induced damage may also adversely affect the load bearing behaviour of members during their service life. It is very important to have reliable information on both the load bearing capacity and the serviceability of corroded RC beams. The mechanical performance of corroded RC beams has been studied by many authors since the 1970s and this research has contributed significantly to the increase in knowledge of the behaviour of corroded RC structures. Almost all investigations show that corrosion can reduce both the deflection and ultimate strength of RC members and these reductions can lead to premature failure of beams. In the next section, the works of several researchers will be presented. The ductility and modes of failure of the beam specimens corroded under loading or without loading will be discussed in detail.

II. Previous works on the change in ductility of corroded RC beams

II.1 Change in failure mode for corroded RC members

Ductility is the ability of the structures to sustain large deformations and it is necessary for RC beams to provide an early warning of failure. The type of collapse of concrete members is largely dependent on the amount of steel, and the yield stress and ultimate strain it undergoes in tensile zones, because the tensile strength of concrete is very low. Six failure modes can occur, as follows:

- Shear failure taking place before an RC member reaches its flexural load-bearing capacity.
- Anchorage failure occurring before an RC member reaches its flexural load-bearing capacity.
- Concrete crushing in the compression zone before the tension reinforcement yields. This happens if the tensile force capacity of the steel is high (i.e. high ratio of reinforcement), so the steel does not yield at all.
- Steel and concrete yielding simultaneously. If the tensile force capacity of the steel is moderate, yielding of the steel is accompanied by simultaneous crushing of the concrete.
- Steel yielding first and fracturing prematurely, before the compressive concrete reaches the maximum permissible strain of 0.0035. This situation occurs if the tensile strength of the steel is too low.

-Steel yielding first but still maintaining its strength despite its increasing elongation. If the ultimate tensile strength of the steel is low, steel will be yielded before the strain in the concrete at the top fibre reaches the maximum permissible strain of 0.0035. This is the most desirable type of failure because there is plenty of warning before it occurs. In this case, both the materials reach their ultimate load limit state at the same time.

A failure due to shear is always sudden compared to a failure due to flexure. For RC beams with low span-to-depth ratio or inadequate shear reinforcement, the failure mode can be due to shear.

Many researchers have reported a significant change in the flexural behaviour of corroded specimens, which means that the loading capacity and mode of failure are modified in the presence of steel corrosion. Cairns et al. [10] observed that, for almost all specimens with corroded under-reinforcement, the mode of failure was mainly accompanied by flexure, which meant that the ductility was enhanced. For several corroded specimens with a high reinforcement ratio, failure was imputed to slipping between the reinforcement and the concrete, which could result in lower ductility. Almusallam et al. [11] and Rodriguez et al. [13] indicated that the mode of failure of corroded, under-reinforced flexural members was dependent on the magnitude of the reinforcement corrosion. Failure by sudden longitudinal splitting along the steel bars [11] was recorded and was probably caused by failure of the shear bond between the reinforcing steel and the surrounding concrete. The failure in shear of corroded beams [13] was recorded in most cases, which contrasted with the failure in flexure of the corresponding control beams. According to [13], the two main explanations for this behaviour were the significant reduction in stirrup cross-section and a reduction in the effective depth of the concrete section at the shear span. Clearly, corrosion shifts the failure mode from ductile to brittle. For over-reinforced beams, however, corrosion caused a change from brittle to ductile behaviour [8].

In an important experiment that has been running on corroded beams at LMDC since 1984, various authors [3, 6, 19] have found a change in the bending failure mode of RC beams corroded in a chloride environment, from concrete crushing in the compressive zone of control beams to tensile steel brittle failure at the mid-span of corroded beams. Even though all the beams showed the flexural mode of failure, their ductility varied.

The mechanical properties of the corroded steel bars inside beams affected the failure mode of these beams. In other words, the change in corroded steel ductility had a marked influence on the ductility of the beams. It appears that there is a link between the change in bending failure mode and a loss of ductility of the reinforcement steel taken from corroded beams. The studies mentioned do not indicate what this relation is.

II.2 Evaluating the change in ductility of RC corroded beams

The ductility of RC beams is generally measured by a ratio called the ductility factor (μ) . The ductility factor is determined as the ratio of rotation (θ) , curvature (Φ) or deflection (Δ) at failure to the corresponding property at yield [21], as shown below:

$$\mu = \theta_{u}/\theta_{v}$$
; $\mu = \Phi_{u}/\Phi_{v}$; $\mu = \Delta_{u}/\Delta_{v}$ (1)

The ductility factor is believed to depend on the failure mode. In the present study, the deflection of members will be used as a measure of the ductility factor.

El Maaddawy et al. [5] tested nine RC beams using impressed current to accelerate the corrosion process. One beam was kept as a control beam, 4 beams (group A) were corroded in the absence of loading and 4 beams (group B) were corroded under a sustained load. These beams were under-reinforced ones with 1.24% tension steel. The ductility factors of the control beam and corroded beams are shown in Fig.1a. It can be seen that the ductility of corroded beams is higher than that of the non-corroded beam irrespective of corrosion level. Interestingly, beams corroded with loading proved to be more ductile than beams corroded without loading, even when steel corrosion was increased to 31%. In El Maaddawy's study, it seems that applying load to beams during the corrosion process significantly affects the ductility of the beam rather than the ratio of tensile reinforcement. Fig.1b presents the ductility factor of corroded beams extracted from the results of Cairns et al. [10]. With the tension steel percentage less than the percentage of balanced steel, the ductility of beams was improved as the loss of crosssectional area due to corrosion increased. The authors attributed this to changes in bond stress in the shear span caused by corrosion. However, the rate of ductility increase was different in the two groups. By studying the impact of reinforcement corrosion on the ductile behaviour of RC beams, Du et al. [8], who accelerated the steel corrosion by impressing a direct current on individual sets of bars, concluded that for corroded, overreinforced beams (balanced reinforcement ρ_s =3.1%), ductility improved as the corrosion developed. In contrast, the ductility of corroded under-reinforced concrete beams was slightly impaired as shown in Fig.2a. Torres-Acosta et al. [24], who accelerated corrosion by adding chlorides during casting and impressing an electrical current, tested 10 beams until failure (8 corroded and 2 control beams). The ductility factor resulting from these tests is shown in Figure 2b and does not indicate a clear ductility trend in relation to the degree of corrosion.

It should be noted that the tests mentioned above used different procedures to accelerate the corrosion process, such as mixing the concrete with chloride then applying a current to the steel bar [5] or partially immersing the samples in sodium chloride solution and then a current flowed to reinforcement [8]. Generalized corrosion along the whole steel bar was thus expected to occur in a short time. However, such a corrosion pattern would take tens of years to build up in service structures. If the current density significantly affects structural responses, the accuracy of the ductility factor deduced from the above studies can be called into question.

Figure 3 shows the relationship of ductility factor and level of corrosion in beams corroded over long periods (up to 17 years) [3, 6]. It should be noted that these beams were simultaneously loaded and corroded in a chloride environment that was very different from that of tests accelerated by an impressed current. After tens of years in the corrosive environment, a sharp reduction in the ductility of the beams was recorded. A 20% loss of cross section corresponded to a 75% loss of ductility factor for B1CL1. At a corrosion level of 15%, the ductility factor obtained for beam A1CL1 decreased by 44%. These studies also pointed out that, in the case of A or B beams with ratios of tensile reinforcement of respectively 1.19% and 0.58%, the rupture mode of the corroded beams was by yielding and breaking of the tensile steel in the mid span, whereas the control beam failed by crushing of the compressive concrete following the yielding of the tension steel bars. Thus, the steel corrosion affected the failure mode of RC beams with low levels of reinforcement and influenced both the ductility and the load bearing capacity. More recently, Khan et al. [19] tested a 26-year-old corroded reinforced concrete beam, named beam A2CL3, with the same corrosive environment as in

references [3, 6]. They also showed a significant influence of corrosion on ductility and on the failure mode of the beam. The ductility factor, calculated from the deflection at yielding load, and the failure load, as given in Eq. (1), decreased by around 17%.

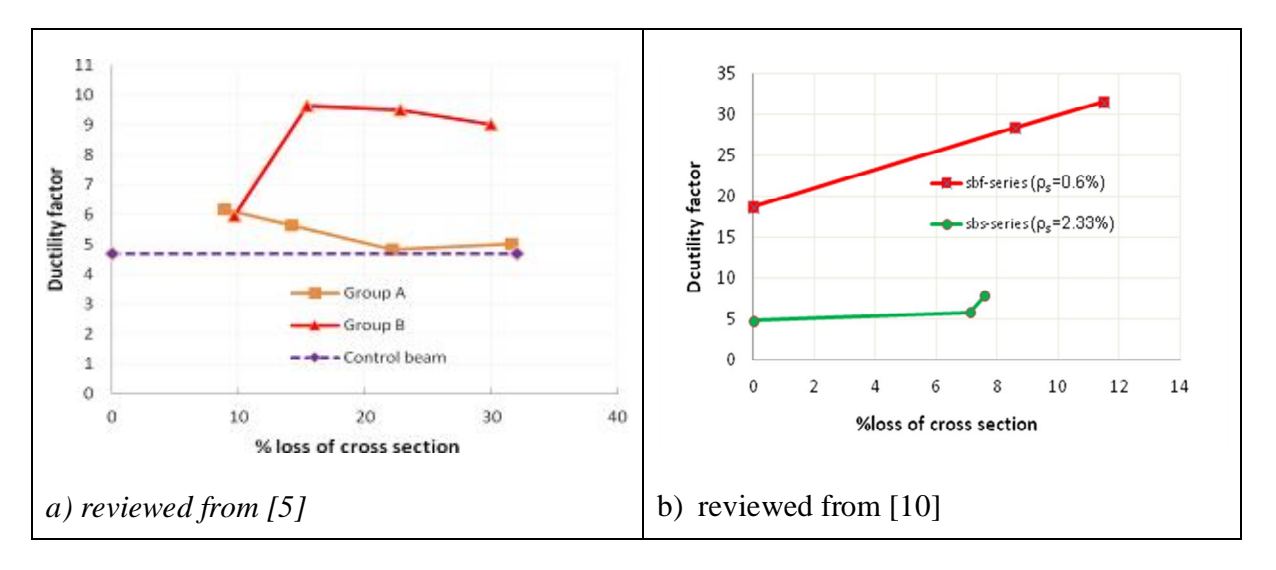


Figure 1. Ductility factor of beam versus corrosion degree of reinforcement (Eq.1)

From the findings discussed above, it can be concluded that ductility can be modified by the damage due to corrosion of the reinforcement. The corrosion of steel modifies its behaviour in terms of ultimate elongation, which is strongly reduced [16], and this can lead to a reduction of the ductility of structural components. To characterize this phenomenon, it would be useful to have an indicator. Of course, there is already an existing ductility factor (Eq. 1) but its classical definition refers to the ratio of ultimate deflection in the post-yielding state to the deflection at the moment of yielding. It appears that this definition is not suitable to characterize the change in ductility due to corrosion, as corrosion leads to both a reduction in the steel cross-section and a reduction in the ultimate elongation of the steel. As a result, the classical expression of ductility index is affected in two opposite ways: firstly, the deflection at the moment of yielding is reduced due to the reduction of the yield load and, secondly, the ultimate deflection in the post-yielding state is also reduced due to the decrease in the ultimate steel elongation.

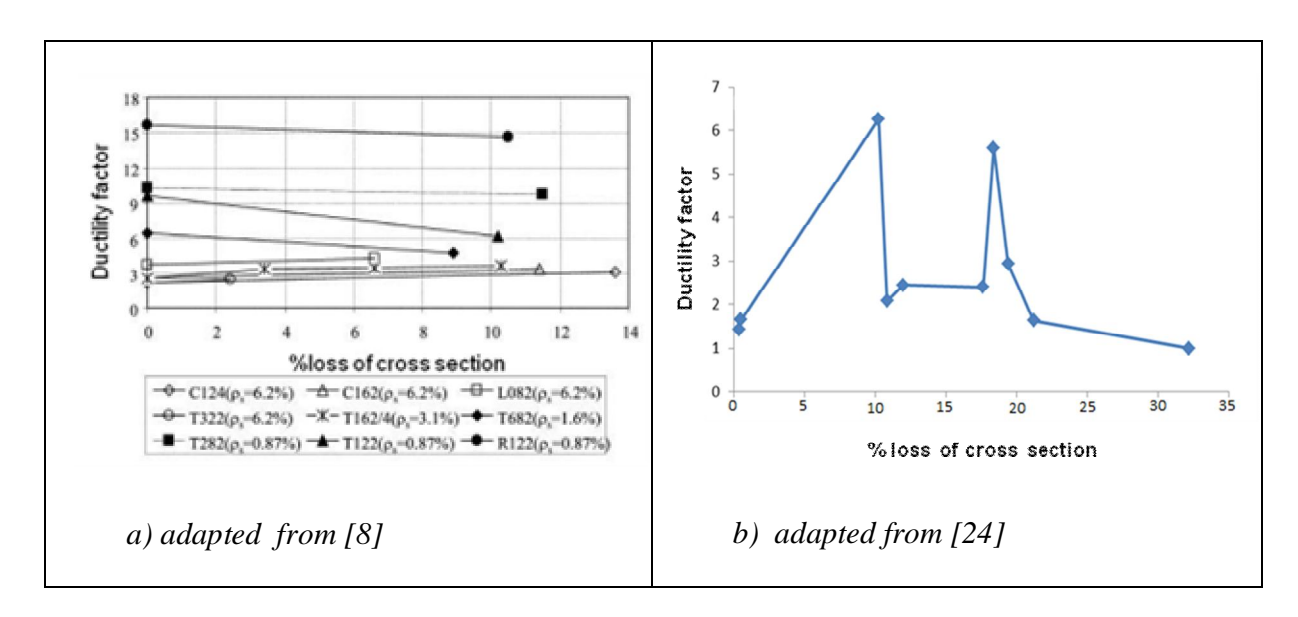


Figure 2. Effect of degree of corrosion on beam ductility factor (Eq.1)

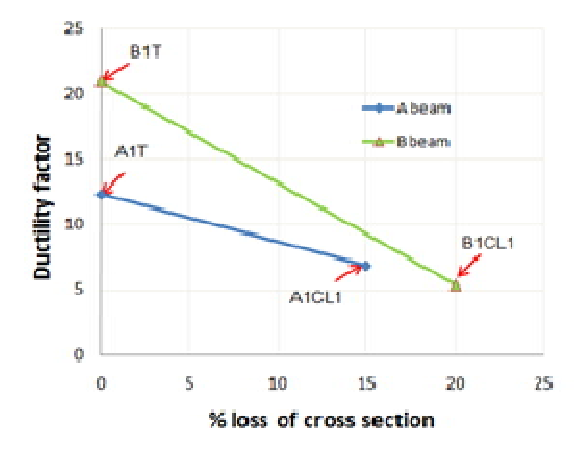


Figure 3. Effect of degree of corrosion on beam ductility factor (Eq.1) reviewed from [3, 6]

Because both numerator and denominator decrease, the ratio calculated from Eq. (1) can decrease or increase for a given intensity of corrosion but without a clear relationship with the reduction of ultimate deflection due to corrosion. Moreover, since the bending stiffness, yielding load level and yielding deflection of corroded members change as compared to non-corroded ones, using Eq.(1) to evaluate ductility capacity is not likely to give accurate results. Thus, we propose a new ductility factor to characterize the

damage due to corrosion, which compares the change in ultimate deflection between the non-corroded state and the corroded state:

$$\mu_{\text{corr}} = \Delta_{\text{u(corroded)}} / \Delta_{\text{u(non-corroded)}}$$
 (2)

The same type of definition is already used to characterize the change in tension behaviour of steel due to corrosion [16, 22] and the change in load-bearing capacity of corroded beams [3].

Using Eq. (2), with regard to the non-corroded beams, the corrosion ductility index is always equal to 1. For corroded beams, the ductility index will change. Data from previous research are re-plotted in Fig.4 according to the new definition of the corrosion ductility index.

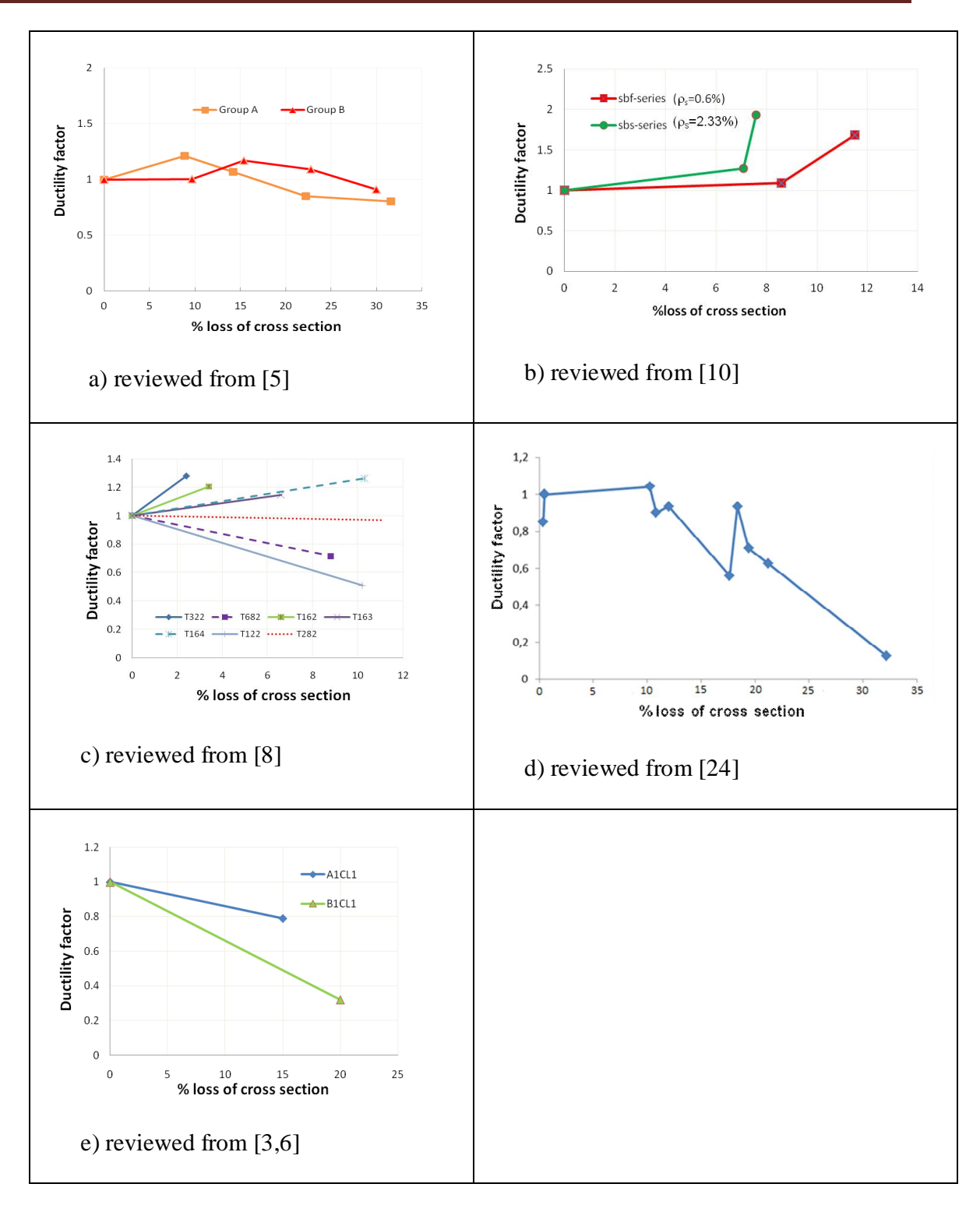


Figure 4. Ductility factor calculated from proposed Eq.(2)

It can be stated that the ductility index shows a decreasing trend in both groups A and B [5] as demonstrated by Figure 4a, which is in contrast to fig.1a. In the cases of sbs and sbf series beams [10], fig. 4b reveals that the ductility of series sbs becomes greater than that of series sbf as the corrosion degree increases. This finding is also in contradiction with fig.1b. There is no change in tendency of the correlation between ductility and corrosion level in Figure 4c and Figure 4e in comparison to Figure 2a and Figure 3, particularly in the results analysed from reference [8]. In other words, the ductility of over-reinforced beams computed as in Eq. (2) still increases regardless of the degree of corrosion. More studies are needed to understand this behaviour better. It should be borne in mind that, to be able to compare the ductility index in the same beam group, the failure mode of all beams in the group must be similar. Unfortunately, the precise mode of failure of corroded beams is not given [5] or is dissimilar [10, 24] or is unclear [8]. It should also be noted that the tests by El Maaddawy et al. [5], Yingang Du et al. [10], Cairns et al. [8], Torres-Acosta et al. [24] were conducted in conditions that artificially corroded the reinforcement and considerably affected the rate of damage as well as structural properties [1, 2]. This technique implies that a generalized corrosion on the whole length of steel bars was expected [25]. Therefore, the corrosion level in Figure 4.a, b, c, d should be the average cross-sectional loss over the whole length of the reinforcing steel. It is also interesting to see that, as the artificial technique was used [5, 8, 10, 24], the corrosion ductility index could be increased or decreased. Hence, the effect of the corrosion of steel on its ductility could be different between artificial corrosion and natural corrosion, and lead to different beam ductility.

In the case of natural chloride-induced corrosion [3, 6], the localized corrosion or pitting corrosion was identified around the centre of the span, which led to the rupture of the corroded tensile steel bar under bending load. Thus, with Figure 4c the corrosion level is the maximum loss of cross section of both tensile bars at the location of the break.

The object of this study was to further analyse the influence of corrosion on the ductility and the mode of failure of RC beams when external loads were applied. Some results of an experimental programme on long-term naturally corroded beams are presented and discussed.

III. Experimental programme

Two 27-year-old corroded beams, called A2CL1 and A2CL2 and one 27-year-old non-corroded beam, named A2T1 were tested in 3-point bending. Results from one 26-year-old corroded beam A2CL3 [19] and one 29-year-old corroded beam A1CL2 are also used for the discussion. The loss of ductility of the corroded beam was measured. Moreover, the tension steel bars taken from the corroded and non-corroded beams used here were tested in direct tension. The ductility loss of the corroded steel bars was also recorded.

III.1 Experimental context

A long-term experimental programme was begun at LMDC in 1984. The aim was to improve the understanding of the steel corrosion process in RC elements and its incidence on structural performance. This large research project consisted of casting a set of 72 RC beams (sizes 3000 x 280 x 150 mm). Half the set, i.e. 36 elements of a size commonly used in the construction industry, were stored in a chloride environment under service load to take the influence of the flexural cracks into account in the corrosion process. At different stages, experimental studies were performed on beams to assess the development of corrosion cracking, to measure the chloride content and to analyse the variation of the mechanical behaviour [3, 6, 12]. The other half set of beams (36) was stored under the same mechanical load but in a non-aggressive environment to be used as control beams with the same long-term effects, like creep and ageing of the concrete. The natural aggressive environment was a salt fog (with a salt concentration of 35 g/l that was similar to seawater) generated using four sprays, located one in each of the upper corners of a confined room. The beams were subjected to wetting-drying cycles in order to accelerate the corrosion process as shown in Table 1.

Although this was an accelerated version of the real process, the corrosion obtained was much closer to that actually observed in natural conditions, with respect to corrosion distribution, corrosion type and the oxides produced, than the corrosion resulting from the use of an applied current or a CaCl₂ admixture in concrete [25]. The beams were divided into two groups, type A and type B beams, which had different reinforcement layouts but used the same ordinary reinforcing steel. Beams A and B had 40 mm and 10 mm, respectively, of concrete cover to the stirrups. According to French standards at the

time of manufacturing [14], 40 mm corresponded to the minimum concrete cover in very aggressive environments (i.e. chloride aggression) and 10 mm corresponded to the minimum concrete cover in a non-aggressive environment. The beams were loaded in three-point flexure by coupling a type A beam with a type B beam. Two loading values were applied:

 M_{ser1} = 13.5 kN m (beams noted A1 and B1) and M_{ser2} = 21.2 kN m (beams noted A2 and B2).

For beams presented in this paper (type A), M_{ser1} corresponded to maximum load when exposed to an aggressive environment. M_{ser2} corresponded to maximum load exposed to a non-aggressive environment.

During the first period of 6 years, the loading level was maintained, in spite of creep of the concrete, by using strain gauges attached to the surface of two thread bars of the loading system. After 6 years, creep effects were smaller and the load was no longer readjusted with time.

Table 1. Exposure conditions of all RC beams at LMDC

Periods	Wetting-drying cycles	Temperature - climate	Loading
First 6 years	Continuous spraying	20°C - in the lab	yes
From 6 to 9 years	1 week of spraying	20°C − in the lab	yes
	1 week of drying		
From 9 to 19	1 week of spraying	climate of south-west France	yes
years		(CSWF), with monthly-average temperatures ranging from 5.1	
	1 week of drying	to 21.3°C (CSWF)	

From 19 to 26 years	Stopped	CSWF	no
From 26 years to present	2 days of spraying	CSWF	no
	2 weeks of drying	C3W1	

III.2 *Material properties*

The composition of the concrete is given in Table 2. Water content was adjusted to obtain a slump of 7 cm. The average compressive strength and elastic modulus obtained on cylindrical specimens (110×220 mm) were 45 MPa and 32 GPa at 28 days. Ordinary ribbed reinforcing steel (nominal yield strength f_y = 500 MPa) was used. The layout of reinforced concrete beam A is shown in Figure 5.

Table 2. Proportion of concrete mix (kg/m^3)

Mix composition	Aggregate size	
Rolled gravel (silica+limestone)	5/15 mm	1220
Sand	0/5mm	820
Portland cement: OPC HP (high perform)		400
Water		200

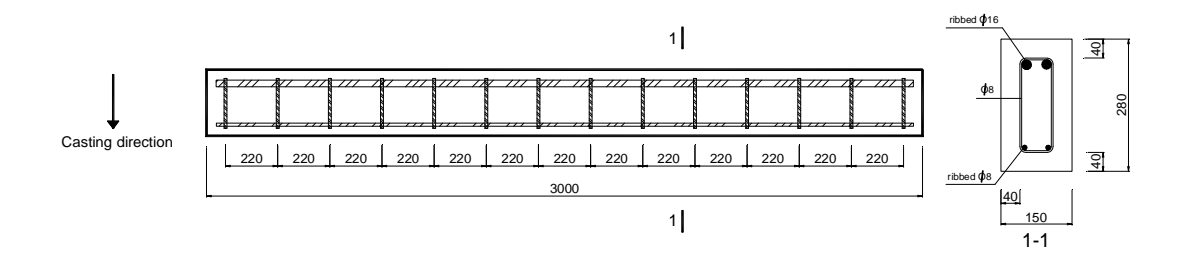


Figure 5. Layout of the reinforcement for type A beams (dimensions are in mm)

III.3 Results and discussion

III.3.1 Cracking map

The cracking maps of corroded beams were drawn with the exact locations of corrosion cracking after 27 years of chloride exposure. The corrosion of longitudinal reinforcement caused mainly longitudinal cracks. The corrosion crack widths were also measured by using a portable video microscope with an accuracy of 0.01 mm.

Figure 6 and Figure 7 show the cracking maps of two beams, A2CL1 and A2CL2, after 27 years of exposure to the saline environment. Only the corrosion crack widths are presented. At the two ends of each beam, transverse cracks due to corrosion close to supports, where the bending moment was zero, can be observed. These transverse crack locations correspond to the locations of stirrups. The corrosion cracking develops overwhelmingly along the location of both tensile re-bars. In particular, the major longitudinal cracks located at the level of the tensile reinforcement are extensive and mostly interconnected. However, a maximum surface crack width of 3 mm was measured at the left end of A2CL1 compared to 2 mm for the widest crack in the middle of beam A2CL2. The maximum corrosion cracks along corroded beams were distributed randomly, independently of the level of the sustained load. According to Ref. [15], when a corrosion crack width reaches approximately 1 mm, spalling of the concrete cover can occur. But visual examinations showed that there was no spalling of the concrete cover. With these large cracks induced by corrosion, the tension reinforcement of beams was highly corroded after 27 years of chloride exposure. In comparison with the corrosion cracks in the compressive zone of A2CL1, beam A2CL2 shows quite a small number of corrosion cracks on the right compression surface. In the case of beam A2CL1,

longitudinal cracks due to corrosion were observed to run along the compressive reinforcement steel. These may imply a high degree of corrosion of the compressive steel bars of A2CL1 versus small corrosion degree of compressive steel bars of A2CL2 is expected. It should be mentioned that all beams tested in this study had the same amount of reinforcement, the same geometry, and the same concrete mixture but they had dissimilar outcomes.

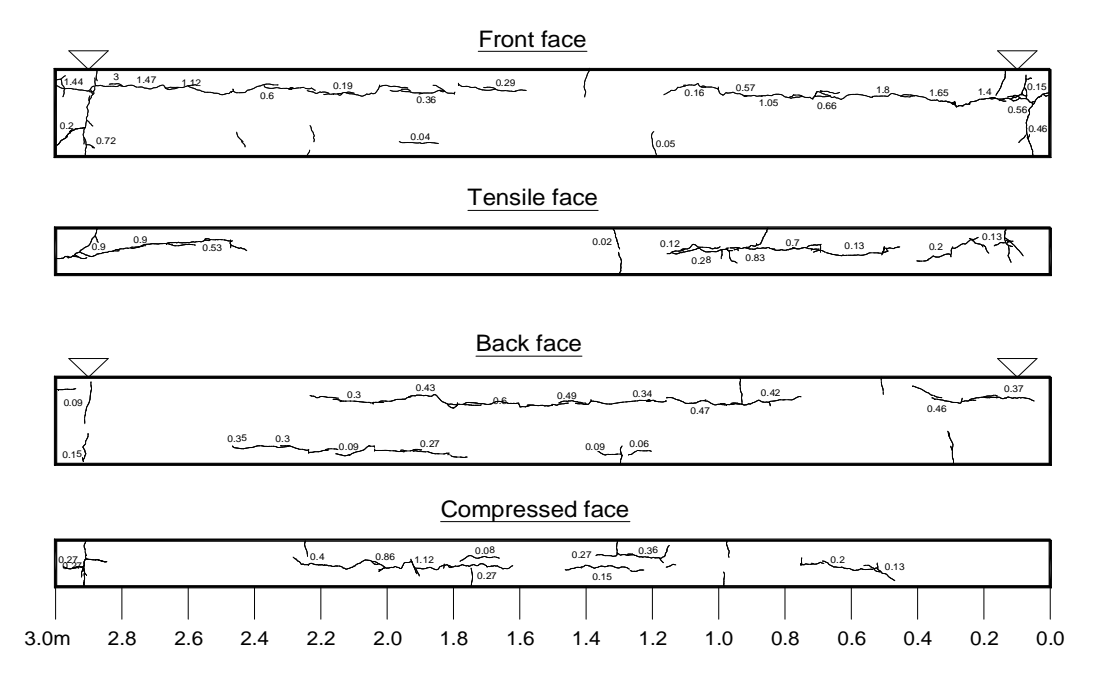


Figure 6. Cracking map of A2CL1 in chloride environment after 27 years (crack widths in mm)

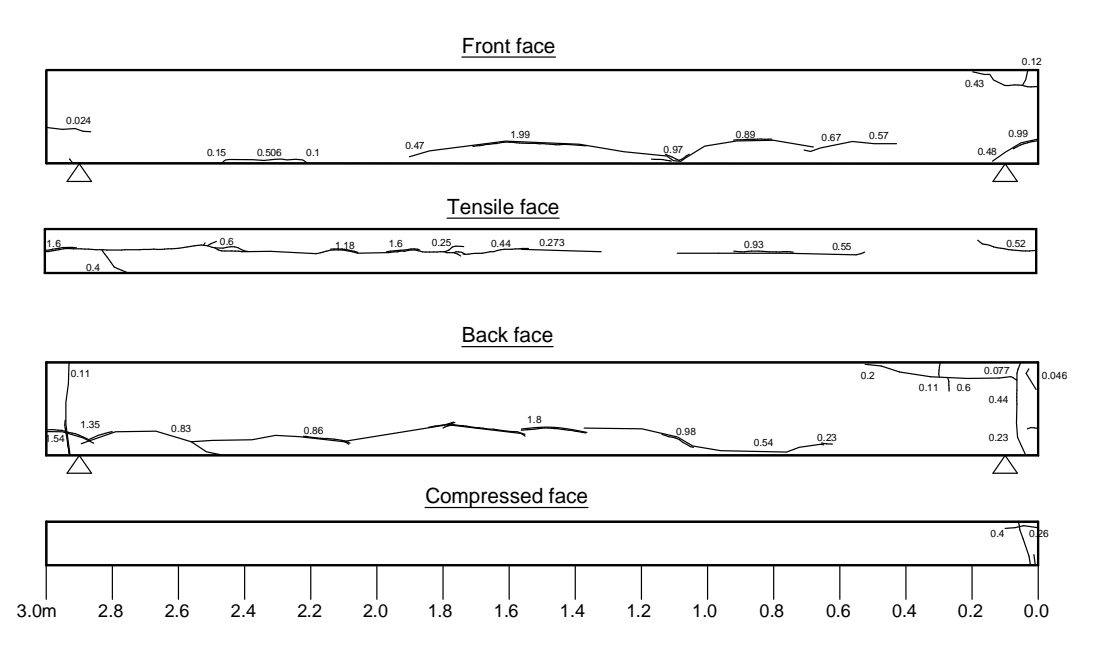


Figure 7. Cracking map of A2CL2 in chloride environment after 27 years (crack widths in mm)

III.3.2 Reinforcement cross-sectional area loss

The distributions of the local steel cross-section reduction along the two tensile bars of the corroded beam were measured after the mechanical test to failure. To evaluate the corrosion damage, the rust was completely removed from the reinforcement using Clark's solution ANSI/ASTM G1-72. The reduction in steel cross-section was assessed from the loss of diameter of the reinforcement, which was measured with a vernier calliper. It should be noted that loss of cross-section could be overestimated with this measurement technique because of the considerable change in the surface shape of the steel bar due to corrosion.

The steel cross-section loss graphs for beams A2CL1 and A2CL2 are presented in Figure 8. The distribution of cross sectional loss in the two beams is very dissimilar. For tension reinforcement steels, the average loss of cross sectional area at the centre of beam A2CL1 seems smaller that near the ends of the beam. In contrast, for beam A2CL2, the loss of cross section at mid-span is much greater than that near the supports. These findings coincide with the cracking width maps as discussed earlier. Nevertheless, the degree of corrosion differs between the beams even when they have sustained the same load level. For example, the average loss of 11.5% in the area of the tensile steel

for A2CL1, measured after 27 years, was much greater than the average loss in area of tensile steel of 6.5% for A2CL2. It is also interesting to observe that big pit locations on the tensile reinforcement of corroded beams were located close to the flexural cracks, which were placed close to stirrup locations. Along the tensile reinforcement, several positions with an intense decrease in cross-sectional area, of up to 48% for the front tension bar of A2CL1 and 38% for the back tension bar of A2CL2, were found. This is directly related to the residual load bearing capacity of corroded beams [3]. Figure 8c, d show a comparison of the magnitude of corrosion between the compressive bars of A2CL1 and those of A2CL2.

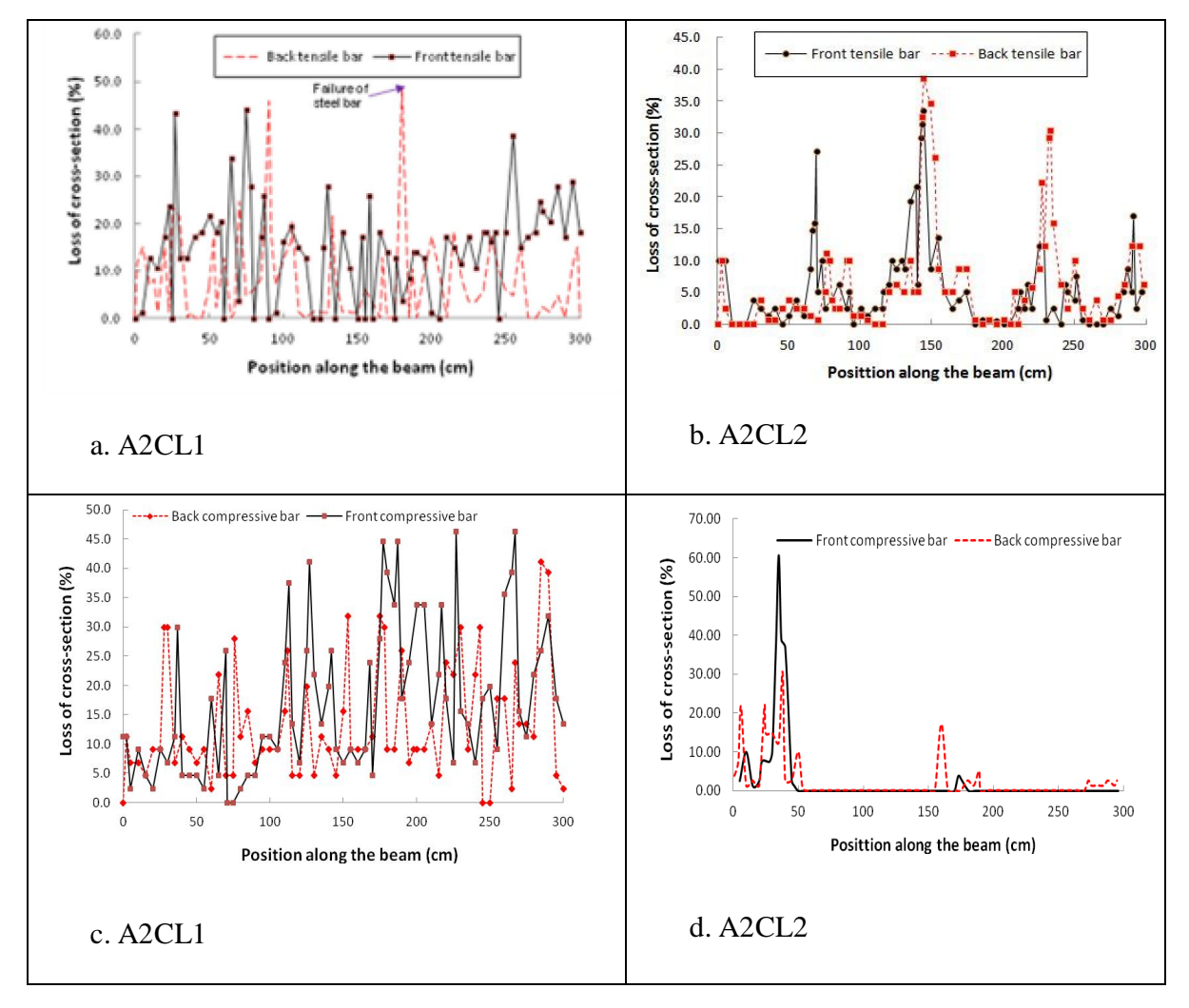


Figure 8. Cross-section loss distribution along the tensile rebars a), b) and compressed rebars c), d) of corroded beams after 27 years

As expected from the observation of cracking maps, after long exposure, the compressed reinforcement corrosion on A2CL2 was much less than the compressed reinforcement corrosion on A2CL1. In fact most of the length of the compressed reinforcement of A2CL2 was not corroded at all.

III.3.3 Loss of ductility of steel bar due to corrosion

The loss of ductility of corroded steel bars extracted from the tested corroded beams [16] and RC beam A2CL2 is shown in Figure 9a. As defined by EC2, the ductility factor $(d_f = \frac{\mathcal{E}_{ucorr}}{\mathcal{E}_u})$ of a steel bar is calculated from the ratio of the ultimate strain of the corroded steel over the ultimate strain of the reference steel. Clearly, the ductility factor shows a decreasing trend as the corrosion degree increases for both corroded beams and corroded steel bars. There is large scatter on the results (Figure 9b) but it seems that an exponential function could represent the relationship between ductility factors (d_f) of corroded reinforcement bar and degree of corrosion (C%).

Equation 3: ductility factor of steel bar in tension

$$d_f = e^{-0.05.C\%} \qquad (C < 15\%)$$

$$d_f = 0.5 \qquad (C > 15\%)$$

The relationship proposed in Equation 3 is quite different from the one proposed by Castel et al. [23] and used by Zhu and François [27]. The difference could be due to the influence of bar diameter and will be discussed later.

The values of d_f depend not only on the maximum loss of cross section but also on the geometry of pit corrosion at the failure location of the steel bar, which explains the large variability of the results (Figure 9b). A given loss of cross-section can correspond to different shapes of the notch induced by corrosion and thus to different stress concentrations and displacement of the centre of gravity in the cross-section, leading to a change in tensile response of the steel bar.

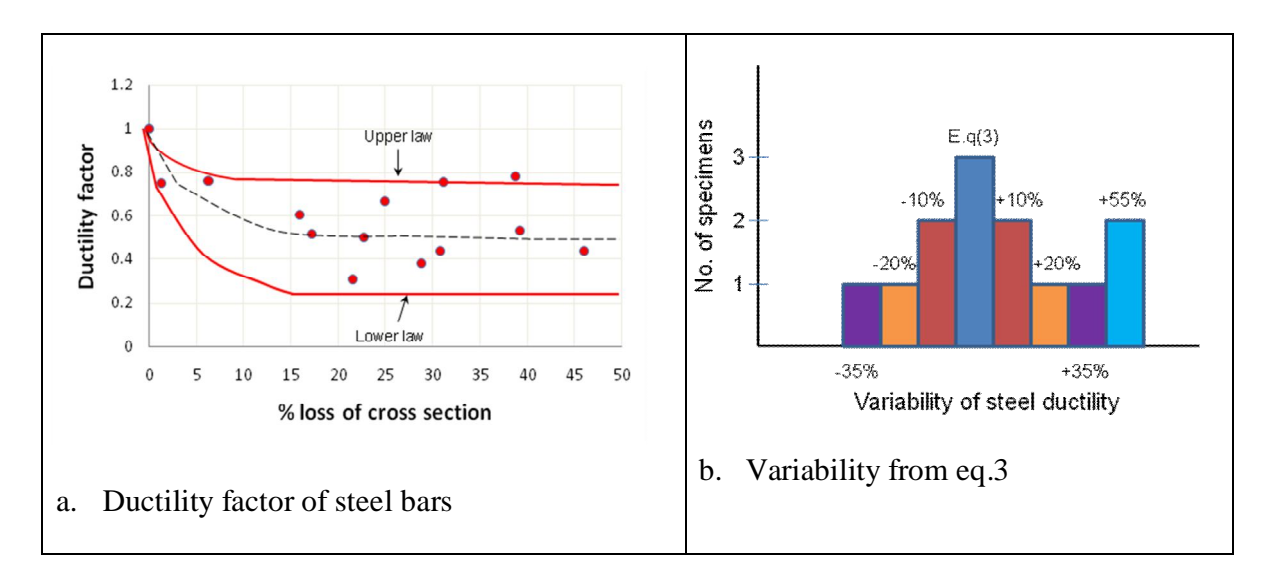


Figure 9. Ductility factor for steel bars versus corrosion: modelling from eq. (3) and variability

Castel et al. [23] have already proposed a model to predict the loss of ductility according to the maximum loss of steel cross-section. This model is based on the experimental results for steel bars, in which the pitting corrosion attack was simulated by creating local notches on the steel surface. The trend of the model is similar to the one proposed in Equation 3 but the asymptotic value of the ductility factor is 0.2 instead of 0.5 (see Equation 4).

Equation 4: ductility factor of steel bar in tension from Castel et al. [23]

$\varepsilon_{\text{stu}} = \varepsilon_{\text{stu}}^{\text{i}} e^{-0.1 \text{C}\%}$	if C%≤ 15%
$\epsilon_{stu} = 0.2 \epsilon^{i}_{stu}$	if C%> 15%

where ϵ_{stu} is the ultimate strain for C% corrosion

It should be noted that Castel et al. [23] tested reinforcement steel of 12 mm diameter. Similarly, Cairns et al. [22] reported the effects of simulated pitting damage on residual bar ductility. The corrosion damage on rebars of 12 mm diameter were also simulated by machined defects. In comparison with series A beams in the present work, a rapid decrease in the ductility of the steel of 12 mm diameter was observed (Figure 10). For Castel's model and the present model, when the degree of corrosion exceeded 15%, the

ductility loss of 12-mm-diameter steel was up to 80% as compared with 50% loss of ductility of 16-mm-diameter steel. On the other hand, when the corrosion level was below 15%, the reduction of ductility of smaller steel bars was significantly higher than that of larger ones at the same corrosion level. The results of the present paper were also compared with those of Zhu and François [27], who conducted the tension test on naturally corroded rebars embedded in an RC beam of 26 years of age but having 12-mm original diameter. Both Cairns et al.'s data and Zhu's data were above Castel's model. Nevertheless, the lowest bound in Cairns et al.'s data and Zhu's data was the same as Castel's model, approximately 0.2. Figure 10 displays the loss in ductility factor as the steel diameter changes. It can be seen that, with bigger diameter rebars, the corrosion level has little effect on loss of ductility but, in the case of smaller diameter rebars, the corrosion level affects the ductility loss more significantly. The explanation could be that the remaining cross-sectional area is too small to withstand greater elongation.

III.3.4 Loss of ductility of RC beams and change in failure modes due to corrosion

The modes of beam failure of are directly related to its deflection capacity and thus to its ductility. The tests revealed that the non-corroded beam A2T1 failed by yielding of the tensile reinforcement, followed by crushing of the concrete under the bearing plate at a peak load of 72 kN. This was the desired type of failure and it indicated the highest deflection capacity of 64 mm. Figure 11 shows the failure modes of four corroded beams: A2CL1, A2CL2, A2CL3 and A1CL2. The difference in degree of steel corrosion is not sufficient to explain the difference of failure types among the beams. In beams A2CL1, A2CL3 and A1CL2, a sudden collapse due to brittle tensile rupture of the reinforcing steel was observed. The failure of the tensile steel took place in a high moment region as shown in Figure 8. This type of behaviour was also recorded by Khan et al. [19].

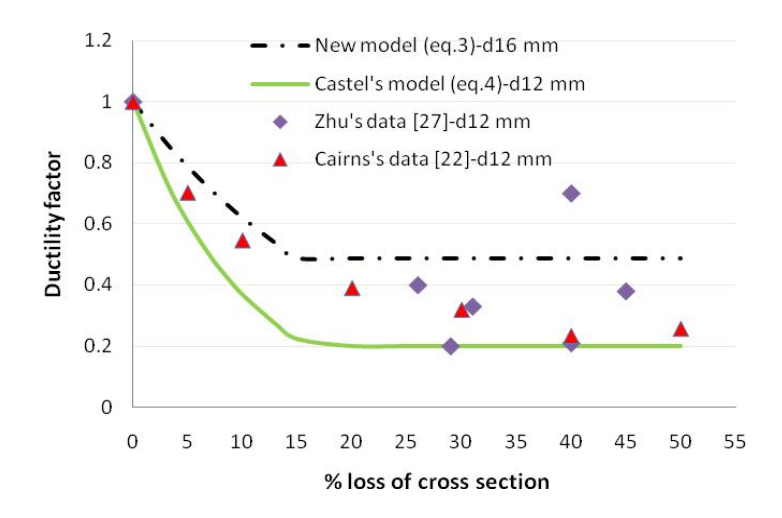


Figure 10. Effect of diameter of steel bar on ductility loss in tension

In the case of A2CL2, the rupture mode was the crushing of the concrete in the compressive zone and delamination of cover concrete at the same time. The cover concrete delaminated through a combination of flexural cracks due to the applied load and longitudinal corrosion cracks, which caused the concrete-steel bond to be lost in this part. However, it was also a brittle failure. The beam with this failure mode showed a moderate displacement capacity, with 44 mm in mid-span deflection. Obviously, the experimental results again confirm that reinforcement corrosion causes the corroded beams to fail in a brittle or less ductile way.



Figure 11. Failure modes for A2CL1 and A2CL2 in bending test

The experimental results computed from the new definition of corrosion ductility index Equation Equation 3) are plotted in Figure 12. It should be kept in mind that the specimen beams in this series had the same amount of reinforcing steel, the same loading level, the same dimensions and quite similar ages of exposure. The ductility factors of beams A2CL1 and A2CL2 were 48% and 31% smaller, respectively, than that of beam A2T1. It is surprising to see that A2CL2, with higher local corrosion at mid-span, shows higher ductility than A2CL1. A2CL3 and A1CL2 show a reduction in ductility of 54% and 62% respectively despite very different local losses of cross-section at the failure location, respectively 21.5% and 34.5%.

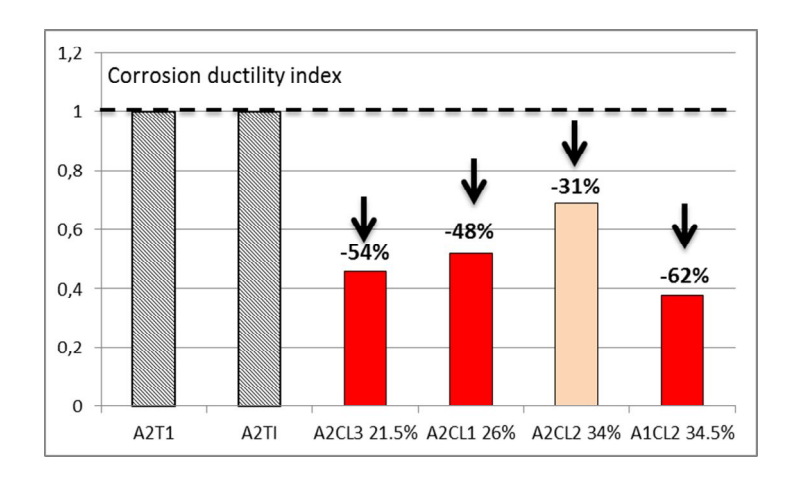


Figure 12. Variation of corrosion ductility index of beams after 27 years

In their study, Torres-Acosta et al. [24] found that three beams showed severe localized corrosion with deep pits. The reinforcement of three specimens, B04, B05 and B10, failed at the cross-section where deep pits appeared during the bending load. This behaviour corresponds to that of the corroded beams A presented in this paper. However, Figure 13 shows that the corrosion ductility index of beams with greater localized corrosion does not necessary correspond to a weaker corrosion ductility index, even though the smallest index corresponds to the deepest corrosion pit.

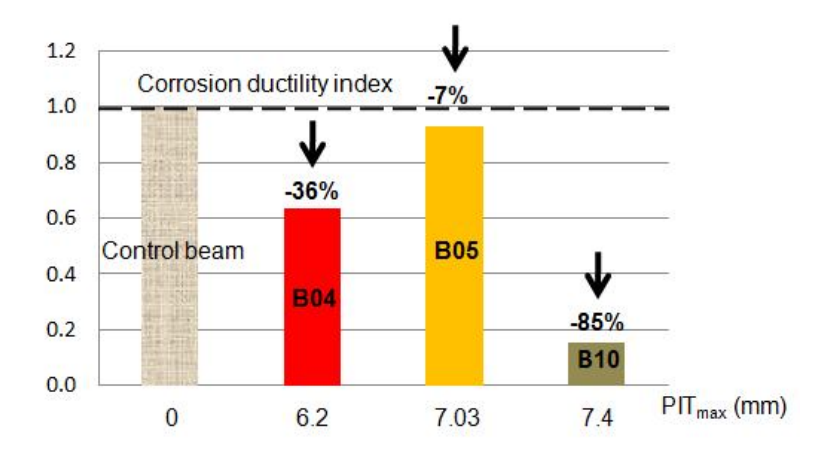


Figure 13. Variation of corrosion ductility index, from [24]: B04, B05 and B10 are beams with deep corrosion pits

The difference between the present results and those from Torres-Acosta et al. [24] may be due to the difference in the corrosion process between climate accelerated (close to natural) corrosion and corrosion accelerated by impressed current.

Figure 14 indicates the reduction of ductility factor for series A corroded beams in relation with the loss of cross-section at the failure location (i.e. mid span of the corroded beams). The evolution of ductility factor was calculated from the non-linear behaviour of RC beams until failure, as described by Vu et al. [26], which allows the ultimate deflection of the beams to be calculated as a function of the ultimate strain of the concrete and the ultimate strain of the tensile bars. An ultimate strain of 3.5E⁻³ for concrete was used to calculate the ultimate deflection that could be reached in the case of concrete crushing. An ultimate strain in tension of 50E⁻³ was used for non-corroded steel bars since it corresponded to the characteristic value of steel bars of Class B proposed by Eurocode 2 [18], and direct tension tests done on steel bars have shown that steel belongs to class B [16]. Thus, in cases of corrosion, the ultimate strain was reduced according to the model proposed in this paper (Equation 3) and using large scatter corresponding to the upper and lower curves shown in Figure 9.

The modelling of the ductility factor of RC beams shows that, with a loss of cross section of around 10%, the ultimate deflection in both of cases of failure (concrete crushing and corroded tension bar failure) was similar, around 58 mm, which is almost the same as the displacement of the control beam. This finding demonstrates that, below 10% of loss of cross-section due to corrosion, the failure mode is concrete crushing. So there is no change of ductility factor below 10% of loss of cross-section of steel reinforcement. Beyond 10%, the beam ductility decreases in relation to the decrease of corroded steel ductility. Experimental results show relatively good agreement with the interval of prediction.

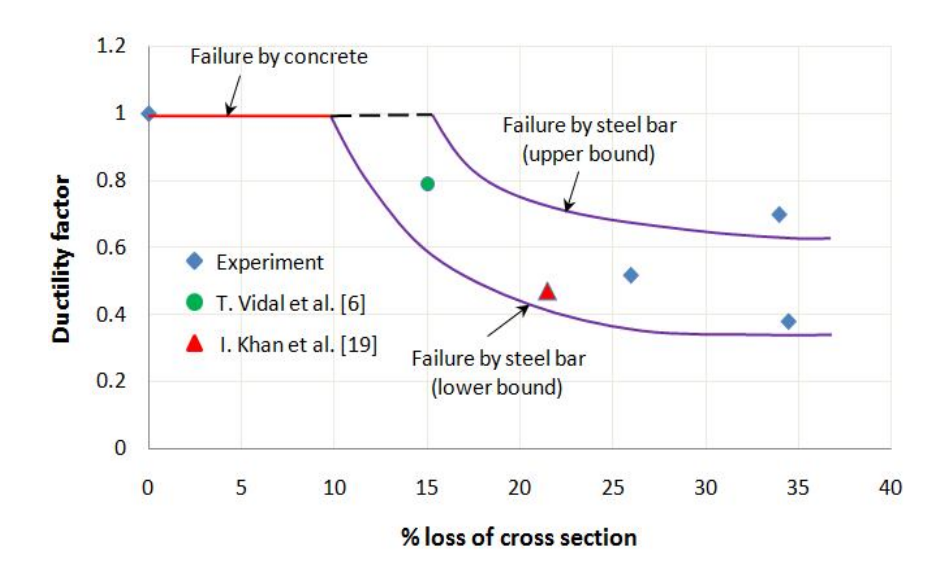


Figure 14. Ductility factor vs. degree of corrosion for RC beams

The ductility of A2CL1, A2CL3, A1CL2 and a previous A beam A1CL1 tested by Vidal et al. [6] agree well with the interval of prediction between the upper and lower boundaries of the proposed model (see Figure 14). For A2CL2, which exhibits a different failure mode, the experimental dot is slightly outside the interval of the model.

At the moment, there is no direct bending ductility requirement for RC elements, nor for corroded concrete elements, in the various standards. Sufficient ductility is ensured by both a minimum content of tension steel bars and a minimum ductility of steel (ductility factor d_f) [18]. Results presented in this paper show that corrosion affects both parameters, reducing steel cross section and reducing steel ductility. The resulting bending ductility of reinforced concrete members could then decrease so drastically as to become unacceptable in terms of safety.

More studies are needed to understand the potential benefit of using large rebar diameters to reduce the loss of ductility of steel bars. This is a critical point for the residual service life of corroded RC structures.

III.3.5 Flexural capacity

The beams were simply supported and a load was applied at a distance at mid-span. A digital sensor placed at the bottom of the beam recorded the displacement at mid-span. The loading speed, of 0.3 kN/s, was constant during the test.

The load-deflection correlation obtained by testing control beams A2T1, A2TI and corroded beams A2CL1, A2CL2, A2CL3 and A1CL2 are plotted in Fig.15. The substantial reduction in both the yielding and ultimate moment for corroded beams is indicated in comparison with control beams. Beam A2CL2 showed a 37% loss of yielding moment but only a 26% reduction in peak moment with a reduction of 34% of cross-section at mid-span. A 26% decrease was recorded in both the yielding and ultimate load in beam A2CL1, corresponding to 26% loss of cross-section at the failure point. A2CL3 exhibited a decrease of 28% in the yielding moment but 18% in load bearing capacity with a reduction of 21.5% of the steel cross-section at the failure point [19]. Beam A1CL2 exhibited 37% of reduction in yielding capacity but only 26% in ultimate capacity, corresponding to a reduction of cross-section at the failure location of 34.5%. Table 3 summarizes the loss of ultimate capacity, yielding capacity and ultimate deflection corresponding to 1% of loss of cross-section for each of the corroded beams.

Table 3. Relative decrease in yielding capacity, ultimate capacity and ultimate deflection for a 1% loss of cross-section between corroded beams and control beams

Beam	Relative cross- section loss (%)	Relative loss of yielding capacity (%)	Relative loss of ultimate capacity (%)	Relative loss of ductility (or ultimate deflection) (%)
A2CL3	1	1.3	0.8	1.7
A2CL2	1	1.1	0.8	1
A2CL1	1	1.2	1.1	1.4
A1CL2	1	1.1	0.8	1.7

Classical RC calculations lead to a 1% loss of both ultimate and yielding capacity for a 1% loss of cross-section with constant yielding and ultimate stresses for steel bars in

relation with the corrosion damage. Table 3 shows that experimental relative loss of yielding capacity was slightly higher than 1 while experimental loss of ultimate capacity was slightly lower than 1. These results are quite similar to the conclusions of El Maaddawy et al. [5], Zhang et al. [12], Malumbela et al. [17] and Torres-Acosta et al. [24], who found that the beam yielding strength was almost proportional to the average reduction in tensile steel cross-section due to corrosion at the centre of the beam, and that ultimate capacity was less impacted, with a ratio of only 1 to 0.7 according to Malumbela et al. [17] and Torres-Acosta et al. [24]. This implies that the reduction in the beam yielding strength was almost proportional to the average reduction in tensile steel cross-section due to corrosion at the centre of the beam, as pointed out by El Maaddawy et al. [5], Zhang et al. [12], Malumbela et al. [17], and Torres-Acosta et al. [24]. For ultimate deflection capacity, 1% loss of cross-section corresponded to 1.4% - 1.7% loss of ultimate deflection for beams that failed by corroded tension bar rupture and 1% for A2CL2, which showed a different failure mode. Thus, the ductility of a beam decreased more rapidly than its ultimate load capacity in this study. Interestingly, even though the corrosion state was serious, the working capacity of corroded beams was still higher than the ULS design load in accordance with EC2 [18] as illustrated in Figure 15.

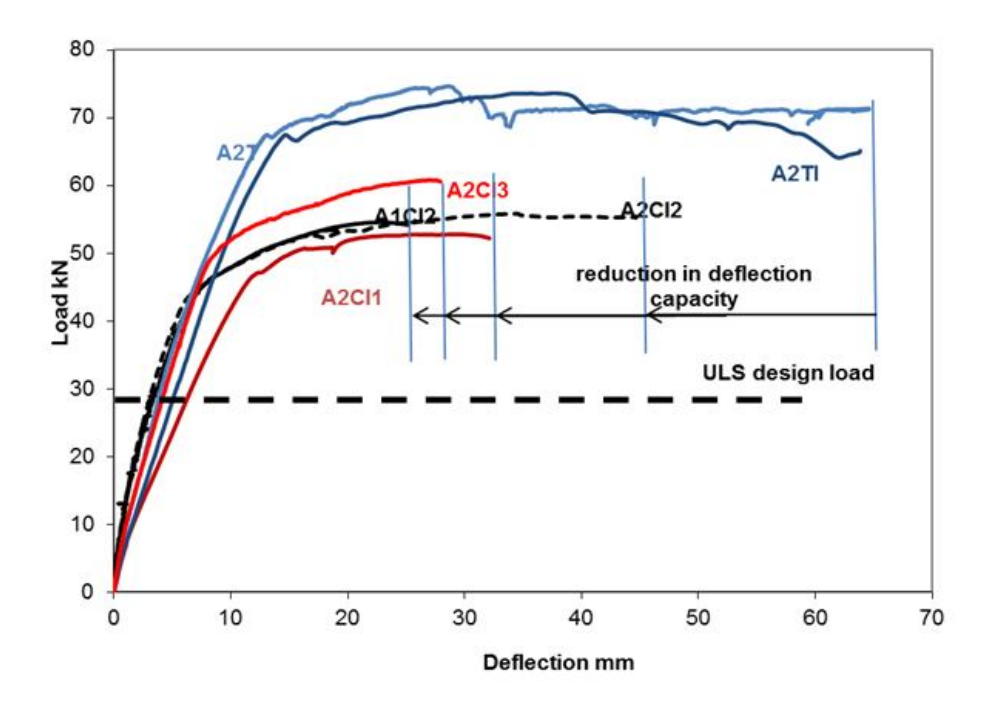


Figure 15. Evolution of load-deflection curves according to the damage due to reinforcement corrosion

III. Conclusion

The change in ductility of RC members due to corrosion of their reinforcement was studied and compared to the change of ductility, also due to corrosion, of steel bars in direct tension test. A new ductility factor is proposed to characterize the change in ductility due to corrosion in RC beams. It is the ratio of ultimate deflection for a given corrosion level over the ultimate deflection of a control beam. This factor corresponds to the definition of ductility for steel bar proposed in the standards: i.e. the ratio between ultimate elongation for a given corrosion level over the ultimate elongation of non-corroded steel bar.

The experimental results used were obtained after a long-term corrosion process in climate accelerated conditions (mostly wetting and drying cycles of salt fog) under sustained loading during a long period of exposure that was representative of actual onsite conditions.

The results show that, for RC elements, corrosion of the reinforcement leads to a change of failure mode from concrete crushing to brittle tensile bar failure due to the decrease of

tension bar ultimate elongation induced by corrosion. The intensity of corrosion damage leading to the change in failure mode should depend on the geometry of the cross-section and the percentage of reinforcement. Beyond this critical level, the ductility of the RC beams parallels the decrease of ductility of the steel bar in tension. More studies are needed to understand the potential benefit of using large bar diameter to reduce this loss of ductility.

Results show that the relative decrease in ductility (or ultimate deflection) corresponding to a given loss of cross section due to corrosion in the most stressed zone is higher than the relative decrease in both yielding and ultimate capacity. As a result, the decrease in ductility of RC beams due to corrosion should be the critical point for the safety and residual service life of corroded structures.

References

- C.Alonso, C.Andrade, J.Rodriguez, J.M. Diez., 1998," Factors controlling cracking of concrete affected by reinforcement corrosion", Materials and Structures, Vol. 31, pp 435-441.
- 2. Pritpal S. Mangat and Mahmoud S. Elgar., 1999, "Flexural Strength of Concrete Beams with Corroding Reinforcement", ACI Structural Journal, V. 96, No. 1.
- **3. A.Castel, R.Francois, G.Arliguie**., 2000, "Mechanical behaviour of corroded reinforced concrete beams Part 1: Experimental study of corroded beams", Materials and Structures/Materiaux et Constructions, Vol. 33, p 539-544.
- **4. A.Castel, R.Francois, G.Arliguie.**, 2000, "Mechanical behaviour of corroded reinforced concrete beams Part 2: Bond and notch effects", Materials and Structures/Materiaux et Constructions, Vol. 33, pp 545-551.
- **5.** Tamer El Maaddawy, Khaled Soudki, and Timothy Topper., 2005, "Long-term performance of corrosion-damaged reinforced concrete beams", ACI Structural Journal, V. 102, No. 5.

- **6. T.Vidal, A.Castel, R. Francois**., 2003, "Physical, chemical and mechanical analysis of a reinforced concrete beam corroded in chloride environment", ACI journal, SP 212-5, pp. 59-76.
- **7. T.Vidal, A.Castel, R. Francois**., 2007, "Corrosion process and structural performance of a 17 year old reinforced concrete beam stored in chloride environment", Cement and Concrete Research 37, pp. 1551–1561.
- **8.** Yingang Du, Leslie A. Clark, and Andrew H.C. Chan., 2007, "Impact of Reinforcement Corrosion on Ductile Behavior of Reinforced Concrete Beams", ACI Structural Journal, V. 104, No. 3.
- **9. Goitseone Malumbela, Pilate Moyo, Mark Alexander**., 2009, "Behavior of RC beams corroded under sustained service loads", Construction and Building Materials 23, pp. 3346–3351.
- **10. J. Cairns, Y. Du and D. Law**., 2008, "Structural performance of corrosion-damaged concrete beams", Magazine of Concrete Research, 60, No. 5, pp. 359 –370.
- 11. Abdullah A. Almusallam, Ahmad S. Al.Gahtani, Abdur Rauf Aziz, Fahd H. Dakhil, and Rasheeduzzafa., 1996, "Effect of reinforcement corrosion on flexural behavior of concrete slabs", Journal of materials in civil engineering.
- **12. R. Zhang, A. Castel, R. Francois**., 2009, "Serviceability limit state criteria based on steel- concrete bond loss for corroded reinforced concrete in chloride environment", Materials and Structures, 42:1407–1421.
- **13. J Rodriguez, L M Ortega, J Casal.**, 1997, "Load carrying capacity of concrete structures with corroded reinforcement", Construction and Building Materials, Vol. II, No. 4. pp. 239-248.
- **14. BAEL** (1983) French Regulations for Reinforced Concrete Structures.
- **15.** The European Union-Brite EuRam III, DuraCrete final technical report, "Probabilistic performance based on durability design of concrete structures", May 2000.
- **16. François R., Khan I., V.H. Dang**., 2012, "Impact of corrosion on mechanical properties of steel embedded in 27-year-old corroded reinforced concrete beams", Volume 46, Issue 6, pp. 899-910, Materials & Structures.

- **17. Goitseone Malumbela, Pilate Moyo, Mark Alexander.**, 2010, "Variation of steel loss and its effect on the ultimate flexural capacity of RC beams corroded and repaired under load", Construction and Building Materials 24, pp. 1051–1059.
- **18. BS EN 1992-1-1 Eurocode 2**: Design of concrete structures-Part 1: General rules and rules for buildings, November 2002.
- **19. Inamullah Khan, R.Francois, A. Castel.**, 2012, "Structural performance of 26 years old corroded concrete beam", European journal of environment and civil engineering, Volume 16, Issue 3-4, pp. 440-449.
- **20. Yingang Du, Martin Cullen, Cankang Li.**, 2012, "Structural effects of simutaneous loading and reinforcement corrosion on performance of concrete beams", Construction and Building Materials.
- **21. Bungale S. Taranath**., 2010, "Reinforced concrete design of tall buildings", by Taylor and Francis Group.
- 22. John Cairns, Giovanni A. Plizzari, Yingang Du, David W. Law, and Chiara Franzoni, 2005, "Mechanical properties of corrosion-damaged reinforcement", ACI Materials Journal, V. 102, No. 4.
- **23. Arnaud Castel**, 2000, "Couplage mecanique et corrosion dans les elements de beton arme", Thèse de Doctorat de l'Université Paul Sabatier.
- **24.** Torres-Acosta A.A, Navarro-Gutierrez S, Teran-Guillen J, (2007), "Residual flexure capacity of corroded reinforced concrete beams", Engineering Structures, 29, pp. 1145-1152.
- **25. Yingshu Yuan, Yongsheng Ji, and Surendra P. Shah**, (2007), "Comparison of Two Accelerated Corrosion Techniques for Concrete Structures", ACI Structural Journal, V. 104, No. 3.
- **26. N.A. Vu, A. Castel, R. François**, (2010), "Response of post-tensioned concrete beams with unbonded tendons including serviceability and ultimate state", Engineering Structures 32, pp. 556-569.
- **27. Wenjun Zhu and Raoul François**, (2013), "Effect of corrosion pattern on the ductility of tensile reinforcement extracted from a 26-year-old corroded beam", Advances in Concrete Construction, Vol. 1, No. 2, pp. 121-136.

II.5. SUMMARY

This chapter discussed various experimental results on the long-term corroded RC beams. The effect of corrosion steel on mechanical performance for both slender and shear beams was studied. The changes in mechanical properties of corroded reinforcement steel were assessed.

From experimental work on corroded RC slender beams, the results revealed that longterm corrosion seems to be independent of the initial bending cracks. The reduction in yielding load of corroded beams was proportional to the maximum reduction of tensile steel-cross section at the mid-span. However, the loss of ductility or ultimate deflection at a given corrosion level in the most stresses zone was greater than the relative loss in both yielding and ultimate load. This was because of the significant reduction of ultimate elongation and slight increase in true ultimate stresses of corroded steel bars extracted from the corroded beams. Interestingly, the corrosion of tensile steel bars led to a change of failure pattern from concrete crushing to brittle tensile bar failure and corrosion of compressive steel bars did not appear to affect the failure mode of corroded slender beams. Based on the experimental data and model developed by N.A. Vu et al. (2010), it is possible to predict the failure mode of corroded slender beams: below 10 % of loss of cross-sectional area, the failure mode would be the concrete crushing in compressive zone; beyond 10%, the failure mode would be failure of steel bars in tensile zone. The results also emphasized that the decrease in ductility or ultimate defection of RC beams due to corrosion should be the critical point for their safety and residual service life.

For corroded RC shear beams, obviously the corrosion of steel had an important impact on the failure mode of short beams but little effect on failure mode of deep beams. In case of short beams, the transversal corrosion crack near the support played an important role on the failure mode and then the reduction in ductility. The tests shown that there was a change in failure mode from shear (control beam) to bending (corroded beam), leading to the increase in ductility. In case of deep beams, the pictures at the end of failure appeared that non-corroded beam and corroded beam both had the same failure mode but the ultimate deflection as well as the shape of force-deflection curves was very different. This is not really logical. This is probably explained by the fact that the behavior of corroded deep beam during test combined a tied arch action with beam action which could affect the failure mode in different ways. Most importantly, the

anchorage capacity of corroded steel bars was enhanced even if the wide longitudinal cracks due to corrosion appeared close to a support. The friction due to corrosion products and transverse pressure due to the reaction of the support when applying load to beam which reduces the corrosion crack width could be an explanation. A prediction of the residual capacity of shear of corroded deep beams should be taken into account these. Clearly, the behavior of shear beam which corroded "naturally" under chloride environment is complex. More research on this is necessary.

Part II:

Effect of pre-cracks on the corrosion initiation and propagation

Chapter III:

LITERATURE REVIEW ON CORROSION IN CO₂ AND CHLORIDE ENVIRONMENTS

GENERAL

In this chapter, the corrosion of steel embedded in concrete structures in carbon dioxide and chloride environments will be mentioned. The impact of pre-cracks on the carbonation propagation or on corrosion initiation and propagation in chloride are discussed. The changes in physical and mechanical properties of concrete due to carbonation are also considered. Furthermore, a discussion on the formation and compositions of rust layer in the atmospheric environment is presented.

III.1. CORROSION IN CO₂ ENVIRONMENT AND CONSEQUENCES OF CARBONATION ON MATERIAL PROPERTIES

III.1.1. Summary on carbonation process in concrete structures

In the air, carbon dioxide CO₂ is found everywhere. As concrete is a porous material, CO₂ may easily penetrate via the pores to the inside of concrete. The carbon dioxide from the gaseous environment would be dissolved in the pore solution system of the cement matrix and reacted with certain compounds of the concrete to form calcium carbonate. Once the carbonation process reaches to the reinforcement, the pH of pore solution will be fallen down below 9. If the carbonation front penetrates sufficiently deeply into the concrete to intersect with the interface of concrete reinforcement, protection is lost and corrosion of steel will initiate. Under penetration of carbon dioxide, the general corrosion on the surface of steel takes place after a lot of years.

To analyze the carbonation of concrete, it is necessary to determine the constituents of hydration of Portland cement that are vulnerable when the carbon dioxide diffuses inside the concrete. These compositions include:

- The portlandite $Ca(OH)_2$, which forms the alkalinity of concrete, permits the passivation of steel bar embedded in concrete.

- The calcium silicate hydrates (C-S-H) with very high specific surface can trap a significant portion of the carbonate ions. In addition, these compounds provide the importantly mechanical strength of concrete and their possible degradation can affect the durability of concrete.
- The chloroaluminates and sulfoaluminates of calcium can absorb potentially the chloride ions and sulphate ions. In this case, the durability of concrete should be considered based secondary mechanisms such as pitting corrosion of reinforcement and the swelling ettringite.

III.1.1.1. Carbonation of Portlandite Ca(OH)2

A portion of CO₂ dissolves in solution according to the reactions (III. 1), (III. 2) and (III. 3), leading to a decrease in the concentration of OH⁻ ion in the pore solution, which reduces the pH. To remain the alkaline medium inside concrete, the portlandite is dissolved according to the reaction:

$$Ca(OH)_2 \Leftrightarrow Ca^{2+} + 2OH^-$$
 (III.1)

The calcium ions then react with the carbonate ions to form calcium carbonate CaCO₃ as equation (III.2)

$$Ca^{2+} + CO_3^{2-} \Leftrightarrow CaCO_3$$
 (III.2)

To simplify the reaction mechanism of carbonation, the $Ca(OH)_2$ is synthesized by the heterogeneous chemical reaction below:

$$CO_2 + Ca(OH)_2 \Leftrightarrow CaCO_3 + H_2O$$
 (III.3)

The fact is that the Eq. (III.3) only indicates simply mechanism of carbonation, all the intermediate steps are hidden. It is noted that the carbonation of Portlandite arises with total water contained in structures.

The isomorphic calcium carbonate exists simultaneously in three compounds: aragonite, vaterite and calcite in crushed samples of hydrated cement paste as detected by Z. Sauman

[3]. The calcite is the most stable form under normal conditions of temperature and pressure during accelerated carbonation tests and is main kind of calcium carbonate formed by carbonation.

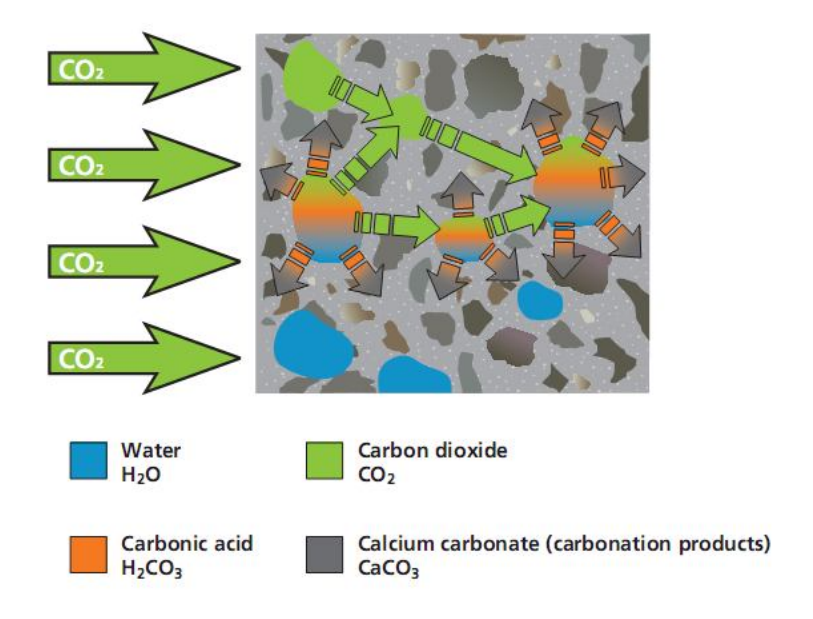


Fig. III-1. Example for reaction between CO₂ and pore water in concrete

III.1.1.2. Carbonation of calcium silicate hydrates C-S-H

The C-S-H formed by the hydration of tricalcium silicate (C_3S) or β -dicalcium silicate (β - C_2S), which together constitute about 75% of a Portland cement by weight [78], controls mostly the concrete strength. The carbonation of C-S-H makes the increase of calcium carbonate, appearance of hydrated silica material [1, 4, 8] (called an amorphous silica gel) and possible free water. More importantly, they can establish a buffer on the pH of pore solution lower than that of portlandite. Therefore, their inclusion in the mechanism of carbonation is not necessary if they do the notable change in pH. However, the changes induced in the microstructure of cement paste are important.

The chemical reaction to synthesize the C-S-H (CaO.SiO₂.nH₂O) with carbon dioxide can be written:

$$H_2CO_3 + CaO.SiO_2.nH_2O \Leftrightarrow CaCO_3 + SiO_2.nH_2O + H_2O$$
 (III.4)

The carbonation of portlandite and calcium silicate hydrates is simultaneous but for portlandite this process has the faster kinetics. Many tests of carbonation on hydrated cement paste show that Ca(OH)₂ and C-S-H are covered with a layer of calcium carbonate, which reduces the degradation of these hydrates. A.M. Dunster [1], who observed the mechanism of carbonation of C-S-H on ground samples of hydrated cement paste exposed to atmospheric carbon dioxide, revealed that at a low relative humidity (65%), the portlandite was still presented after 80 days (Fig. III-2) and the carbonation progress of the reaction was sensitive to the grain size. He concluded the carbonation for calcium silicate hydrate (C-S-H) proceeds via high molecular weight intermediates to give an amorphous hydrous silica material.

G. W. Grooves et al. [2] studied the microstructure of hardened pastes of C₃S and a C₃S/silica fume blend in pure CO₂ at a relative humidity of 72.6% suggested that the structure of C-S-H was maintained despite their decalcification or loss of calcium. This could be explained by the conservation of mechanical properties of paste carbonated. The authors [2] proposed that the carbonation process of C-S-H under typical condition was divided into 3 stages: a) carbonation of outer product C-S-H and the reaction will occurs rapidly at front where the CO₂ concentration is reduced to zero, the inner product C-S-H and C-H crystal react more slowly behind the front; b) continued carbonation of inner zone of C-S-H behind the reaction front giving a zone of partly carbonated C-S-H; c) continued carbonation of C-H crystal at regions of their surface in contact with solution-filled pores.

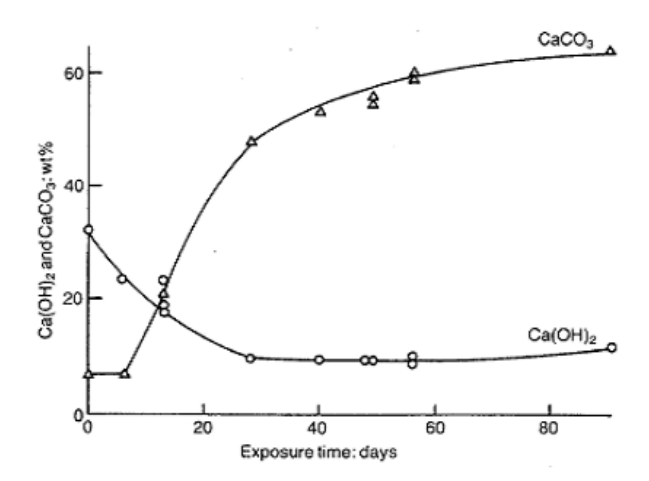


Fig. III-2. Change in quantity of porlandite and calcium carbonate with the exposure time in air ($t=20C^{\circ}$, RH=60%) [1]

In the long term, the dissolution of C-S-H and Ca(OH)₂ is completed, that is to say the ultimate state of degradation corresponds to a mineral accumulation of calcium carbonate and silica gel.

Concerning with the variety in C-S-H phase due to carbonation, Glasser F.P and Matschei T [79] indicated the influence of carbonation on the change of mineral phases of saturated cement paste at 25°C and atmospheric PCO₂ as plotted in Fig. III-3. They pointed out that the mineral components, especially C-S-H, depend on the degree of carbonation and hydration of cement paste.

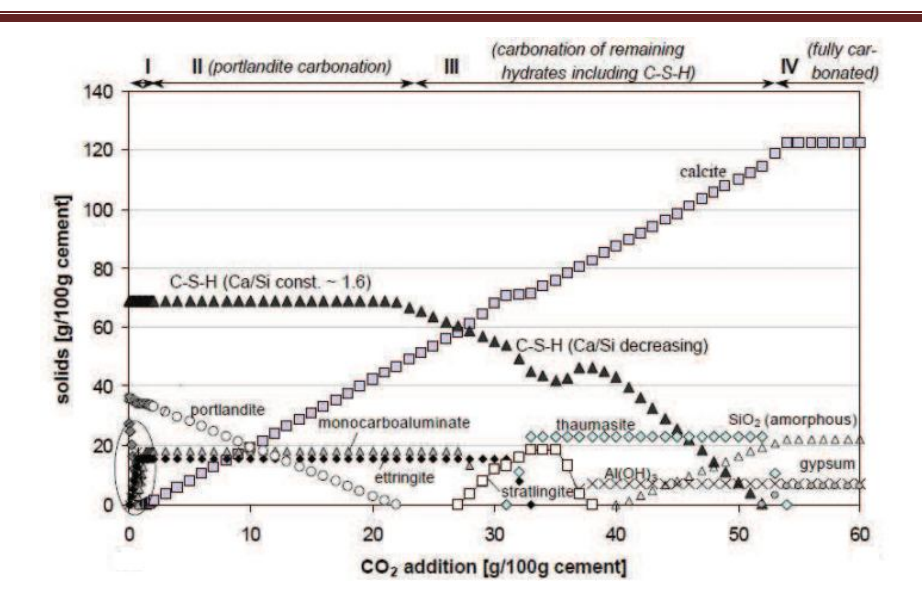


Fig. III-3. Change in mineral phases as function of carbonation degree [79]

Four distinguished zones are evidently identified:

-Zone 1: close to non-carbonated zone, characterized by lower monosulfoaluminates, the presence of ettringite, formation of hémicarboaluminates and then the formation of monocarboaluminates. The pH is in the range of 12.5 at 25 $^{\circ}$ C, which is in agreement with the buffering capacity of portlandite.

-Zone 2: transformation zone of portlandite and the presence of calcite. The portlandite still remains, therefore this zone has maintained a pH at 12.5.

-Zone 3: transformation zone of C-S-H in the absence of portlandite, the increase in calcite content and carbonation front of ettringite. The medium is buffered by the C-S-H, pH decreases with the C/S ratio from 12.5 to 9.9.

-Zone 4: completely carbonated zone, the presence of the maximum threshold calcite and gypsum. Neither the portlandite, nor the C-S-H are present, pH is below 8. A reduction in pH of the pore solution will increase the decalcification of C-S-H gel and therefore increasing the susceptibility of steel reinforcement to corrosion.

The nature of different isomorphous calcium carbonate depends mainly on the relative humidity at which the hydration occurs [72]. The vaterite is formed preferentially at low relative humidity (65%) when a very thin film of water covers the surface of hydrates [3]. Meanwhile, the aragonite is rarely observed [1]. This isomorphous could be an intermediate reaction in the transformation of vaterite into calcite [3]. Finally, the calcite is identified as the relative humidity is high and / or for the carbonation of long period [3].

III.1.1.3. Carbonation of other constituents of cementitious materials

The calcium trisulfoaluminate (ettringite) AFt and calcium monosulfoaluminate AFm have the complex crystal structures, column-shaped for ettringite and sheet-shaped for monosulfoaluminate [9]. For both structures, the sulphate anions located between the layers, are highly mobile and can be substituted by other anions (OH, Cl, CO₃²⁻). The product of carbonation of ettringite and calcium monosulfoaluminate is highly soluble in water and highly reactive [10, 11]. These hydrates (hydrated calcium aluminates) are found in small quantities in cementitious materials with the common sulphate contents and moderate aluminate contents.

III.1.1.4. Main factors affecting carbonation

The spread of the carbonation process through the concrete mainly depends on two factors: the porosity of concrete and the moisture content of atmosphere.

The porosity of concrete: for the carbonation to spread, fresh carbon dioxide from surface of concrete must supply continuously to interior concrete. Low porosity and permeability will decrease the ingress of carbon dioxide from atmosphere, thus delaying the development of carbonation. The porosity and permeability depend on the pore system and the pore size in concrete. Each of different pore size has a different porosity and therefore contributing differently to the overall permeability of the concrete. The pores that give most to the permeability of the concrete are the capillary pores. The capillary porosity is in turn dependent on the w/c ratio. Many studies have been conducted to determine the influence of the w/c on the rate of carbonation. M. Vénuat and J. Alexandre [14] showed that the spread of carbonation in concrete cement CEM I is facilitated when the w/c increases. Similarly, C.

L. Page [15] found that the lower w/c ratio will reduce substantially the permeability of concrete. By decreasing the w/c ratio, the penetration of carbonation will slow down as shown in Fig. III-4. The lower water-cement ratio, the lower CO₂ contents in the concrete and vice versa.

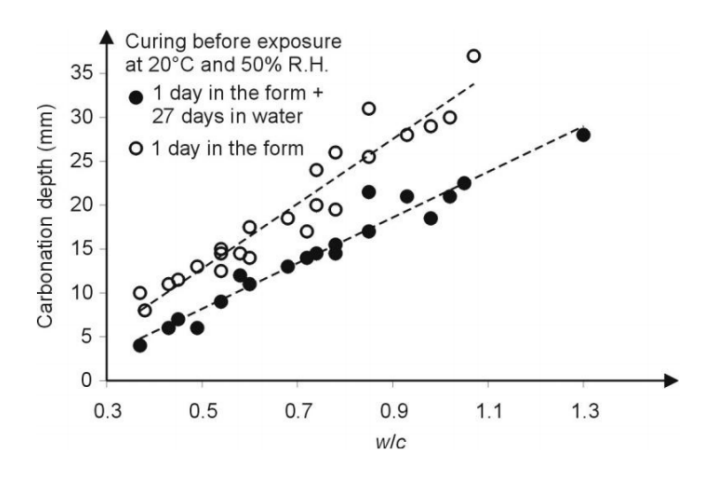


Fig. III-4. Influence of the w/c ratio on the carbonation depth at 20° C and 50% RH [15]

The moisture content of atmosphere: It is noted that both oxygen and water are needed for the carbonation process to continue. The carbonation will not be taken place if the concrete exposures to a dry environment having a relative humidity (RH%) less than 40%. Similarly, there is no carbonation in concrete fully immersed in water, except in the case, the water can entrain air. The humidity of concrete is also a very important parameter. The rate of carbonation is highest at a relative humidity between 50% and 70% [13, 77]. The diffusion of CO_2 within concrete is very slow when RH is lower or higher than that range. Particularly, when the RH in pore system overcomes 90% CO_2 is not able to enter the pore and when the RH is lower than 40% CO_2 cannot dissolve in the water. This means that if the concrete is completely dry, the carbonation reactions are impeded, and if the concrete is completely saturated, the diffusion of CO_2 is inhibited. The correlation of RH- carbonation rate is shown in Fig. III-5.

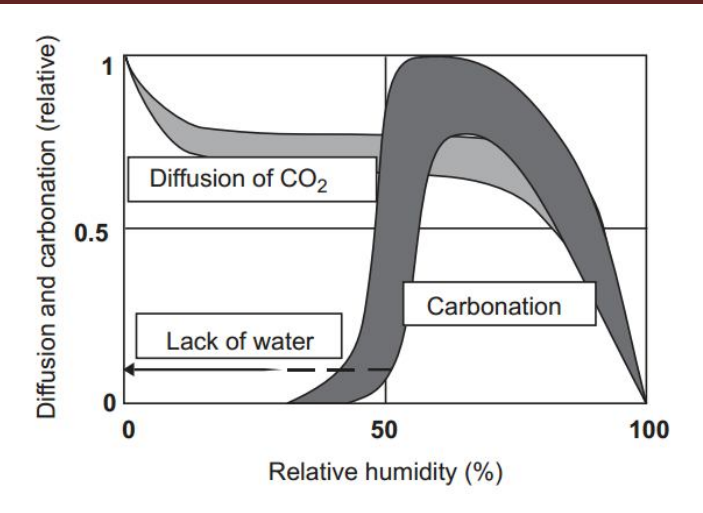


Fig. III-5. Influence of the RH on the carbonation rate [16]

Besides two factors mentioned above, the rate of carbonation is also influenced by the ambient concentration of CO₂. According to Adam Neville [13] in his book "Concrete Neville's Insights and Issues", the CO₂ contents in the air are around 0.03% by volume, whereas in an unventilated laboratory, the content may rise above 0.1%; in cities, it is 0.3% but may rise to 1%. Generally, the higher the amount of CO₂ in the gas phase, the higher is the rate of carbonation. A study on carbonation of concrete incorporating various constituents in both long- and short-term tests, D. W. S. Ho and R. K. Lewis [17] concluded that with accelerated tests carried out in the laboratory, one week of exposure to an atmosphere containing 4% CO₂ will cause the same penetration of carbonation as a year of exposure to a normal atmosphere. T. K. H. Al-Kadhimi et al. [18] studied the carbonation of concrete under a high pressure (1500kPa, 100% pure atmosphere of CO₂) to compare the accelerated carbonation method with natural carbonation. They stated that the microstructure was no different from that produced in concrete by carbonation under natural exposure.

III.1.1.5. Profile of carbonation

Assuming that the profile of carbon dioxide is linear over the thickness carbonated, under steady conditions, the depth of carbonation can be predicted by the following simplified equation:

$$D=K\sqrt{t}$$
 (III.5)

In this equation, D is the thickness of the carbonation layer (mm);

K is a carbonation coefficient (mm/ \sqrt{y}), depending on a lot of factors related to the characteristics of the concrete such as the ratio w/c, the type of cement and environmental conditions as the concentration of carbon dioxide, relative humidity...

t is time of exposure (y).

The equation (III.5) shows that the depth of carbonation is proportional to the root of carbonation time. Fig. III-6 gives a schematic representation of carbonation depth as a function of exposure time.

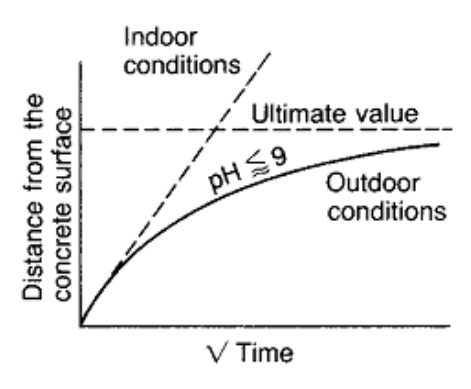


Fig. III-6. Increase of the carbonation depth with time [19]

The most common experimental technique to identify the depth of carbonation is the phenolphthalein test that identifies a change in pH of the pore solution on fresh concrete surface. The non-carbonated concrete zone is purple colour while the carbonated concrete zone does not change colour. The pH value of carbonated zone determined by spraying phenolphthalein indicator is approximately 9. However, in reality the propagation of carbonation is more complex than the results this method proposes. L.J. Parrott [20] investigated the corrosion of steel bar embedded in carbonated concrete for 0.5, 1.5 and 4 years. He concluded that the corrosion of steel in concrete occurred before the carbonation

depth measured by using a phenolphthalein indicator reached the surface of steel. The author suggested that the reason behind it is the presence of partially carbonation zone, in agreement with T. Fukushima et al.'s experimental results [21].

Cheng-Feng Chang and Jing-Wen Chen [22] defined three zones accordingly, fully carbonated zone, partially carbonated zone and non-carbonated zone as shown in Fig. III-7.

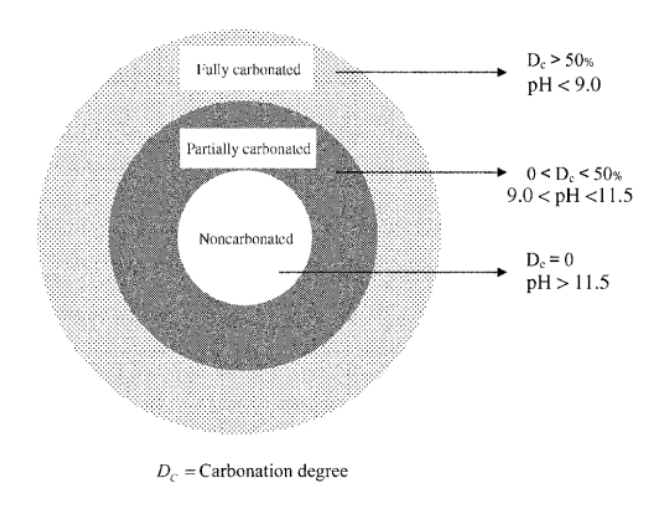


Fig. III-7. Three zones of carbonation characteristic on concrete surface [22]

Y.F. Houst, F.H. Wittmann [6] also described three distinguished zones of carbonation after a sufficiently long period of time: a) the first zone close to the surface exposed to air is fully carbonated or rather its carbonate content is constant; b) the second zone is a transition zone, often called carbonation front, can be observed, where the degree of carbonation decreases gradually to zero and c) the third zone is not carbonated at all. These observations are in agreement with results of Glasser. F.P and Matschei. T [79].

The pH value in the partial carbonation area or transition zone increases with the depth into the concrete ranging from 9.0 to 11.5. Non-carbonated concrete has an alkaline pH of above 11.5, whereas the completely carbonated concrete is more neutral with a pH value of below 9.0. Therefore, to analyze precisely the carbonation front, it is necessary to carry out the tests TGA, TDA, XRD [5, 21, 22].

III.1.1.6. Effect of pre-cracks on carbonation propagation

The carbonation in cracked concrete is a major factor that accelerates the corrosion of steel. For the durability of concrete, it is necessary to control the cracks formed during the service life of a structure. According to P. A. M. Basher et al. [29] cracks can easily occur on the surface of concrete due to the heat of hydration reactions, withdrawal and inadequate curing of concrete. During the hydration process of early-aged concrete, external aggressive agents such as chlorides and CO₂ penetrate through cracks and can lead to the deterioration of reinforced concrete. The cracks also have a considerable influence on the transport properties of cementitious materials. Consequently, they also accelerate the transport of aggressive agents through the concrete and the degradation processes of concrete are faster [30]. These authors suggested that the diffusivity of cracked materials could be increased by a factor ranging from 2 to 10. Ha-Won Song et al. [31] considered the characteristics of diffusivity on the carbonation in cylindrical concrete specimens made with three different w/c ratios (45%, 55%, and 65%) with different crack widths. The results showed that the diffusion of CO₂ increases with increasing crack opening and the w/c ratio as displayed in Fig. III-8.

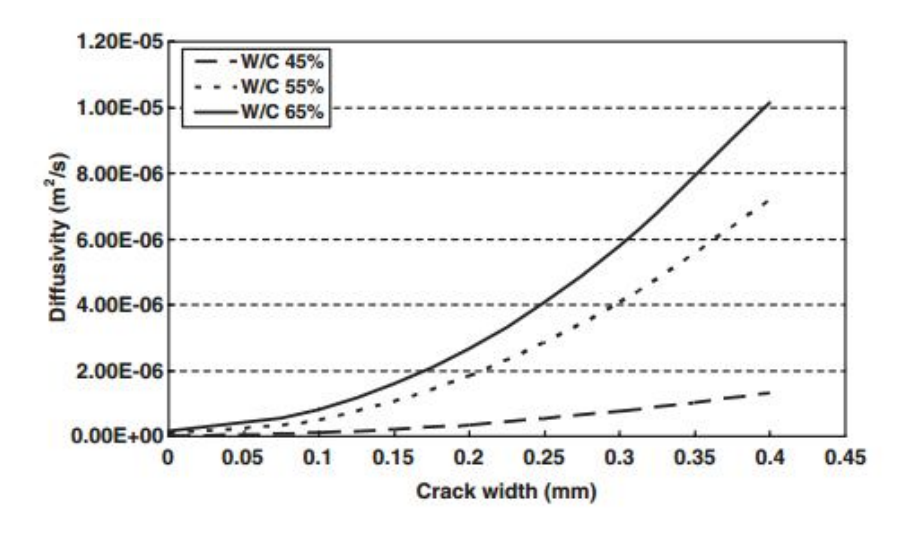


Fig. III-8. Diffusivity of CO₂ vs.crack opening with different w/c ratios [31]

Notwithstanding, they did not indicate the direction of CO₂ diffusion in which diffusivity increases: parallel or perpendicular to crack plane. These authors also showed that the

continuous presence of cracks in cylindrical concrete specimens leads to remarkably change their transport coefficient. Their results also revealed that the influence of the crack is more important for dense materials. Indeed, continuous cracks promote the penetration of ions and contribute to accelerate the dissolution of the solid phase. Therefore, the behavior of cementitious materials is changed.

Recently, S. Alahmad et al. [32] carried out the tests on ring-shaped mortar samples in order to study the effect of crack opening on the ability of carbon dioxide to diffuse along a crack. The samples were mechanically cracked then subjected to carbonation at a temperature of 23° C, relative humidity of 65% and a CO_2 concentration of 50%. After 65 test days, they suggested that there was no diffusion perpendicular to crack plane in crack openings of less than 9 μ m and the perpendicular-to-crack carbonation depths are almost the same as the surface carbonation depth for crack widths of 60 μ m or wider (see Fig. III-9). The results showed that interlocking phenomena in cracks is the main factor limiting the diffusion of carbon dioxide in fine cracks. In the case of the samples with embedded steel ring, interestingly there was always a carbonation of the interface between steel and concrete.

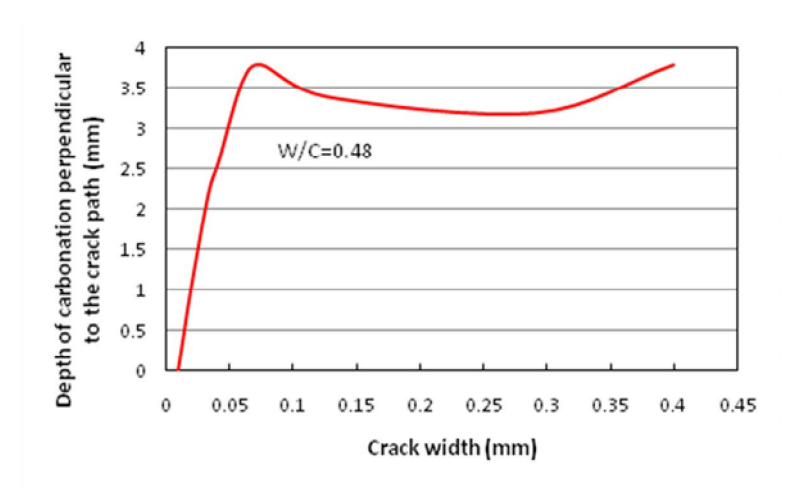


Fig. III-9. Carbonation depth vs. crack width [32]

R. Francois and J.C. Maso [24] studied the influence of mechanical loading on carbonation and chloride penetration of RC beams. These RC beams, sustained in three-point bending load, were kept in an aggressive environment. Eight beams were stored, in loading state, in a

confined enclosure with CO_2 (50%) and air (50%) mixture at RH between 40% and 70% for 24 or 40 weeks. The results showed that the damage to the aggregate-cement paste interface, in the tension zone, leads to increase the penetration of aggressive agents. Carbonation depth was more important in the tensile zone than in the compressed one or at the end of beam zone as displayed in Fig. III-10. The diffusion of CO_2 was always preferential in crack path and along the steel-concrete interface.

A. Castel et al. [33] also studied the effect of the penetration of CO₂ on two 13-year-old RC beams, loading and cracking in the atmosphere. Their results showed that increase in depth of carbonation is correlated with the level of stress of steel in the tensile zone. A higher tensile stress led a greater carbonation front.

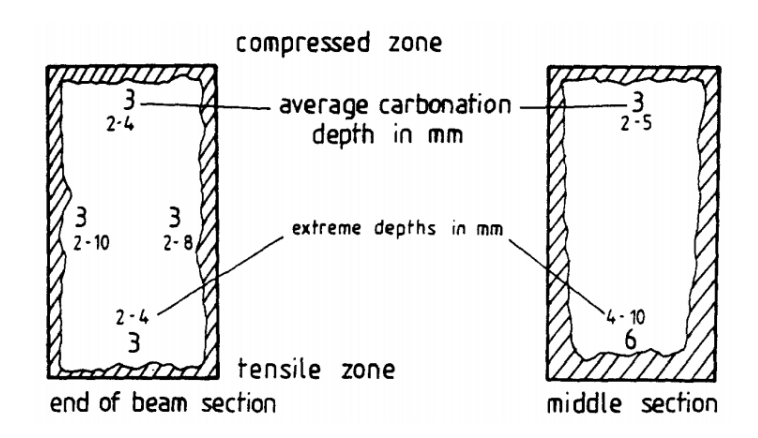


Fig. III-10. Carbonation depth at two beam sections after 40 weeks in CO₂ [24]

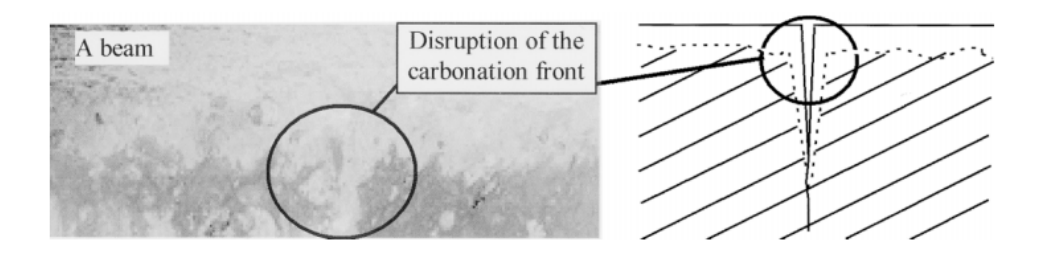


Fig. III-11. Carbonation depth close to flexural crack [33]

The crack openings significantly affect the ability of carbon dioxide to diffuse along the crack path for crack width over 30-50 µm (critical mechanical opening). Below this threshold, there is also penetration along the crack path but a restriction in diffusion perpendicular to crack plane. That means that renewing of CO₂ in tiny cracks is strongly reduced. The phenomenon of formation of the cracks due to corrosion and the effect of rust on healing when the samples corrode in carbon dioxide then subject to cyclic wetting-drying, however, have not been investigated. Furthermore, the lack of data on observing the corrosion at interface between concrete and steel bar in CO₂ of pre-cracked specimens has been noted. The question is the fact that with different crack types of laboratory test-mechanical cracks and different regime of specimens- how is the corrosion state at steel-concrete interface. Further discussion on this is in chapter V, section V.1.

III.1.2. Consequence of carbonation on material characteristics

III.1.2.1. Change in pH value

It is well-known that carbonation leads to the variation in pH level. This process is durable over time when all of the calcium ions from carbohydrates are consumed; the deficiency of hydroxyl ions is not compensated. The level of pH is affected by the pressure of carbon dioxide and other possible aggressive pollutants. In order to indicate the state of iron for different potential- pH values, the Pourbaix diagram [80] is given in Fig. III-12. The pH values in Pourbaix diagrams are those of solution in immediate contact with the metal surface. If potentials and pH value are in "corrosion zone", ferrous ion (Fe²⁺) is the stable substance. This indicates that iron can corrode under these conditions. If the potential and pH are in immunity zone, the iron is thermodynamically immunity from corrosion and no corrosion occurs. If the potential and pH are placed in the passivation zone, oxide will form on surface and iron has undergone passivation state. The change of pH in medium was discussed in §III.1.1.2 & §III.1.1.5.

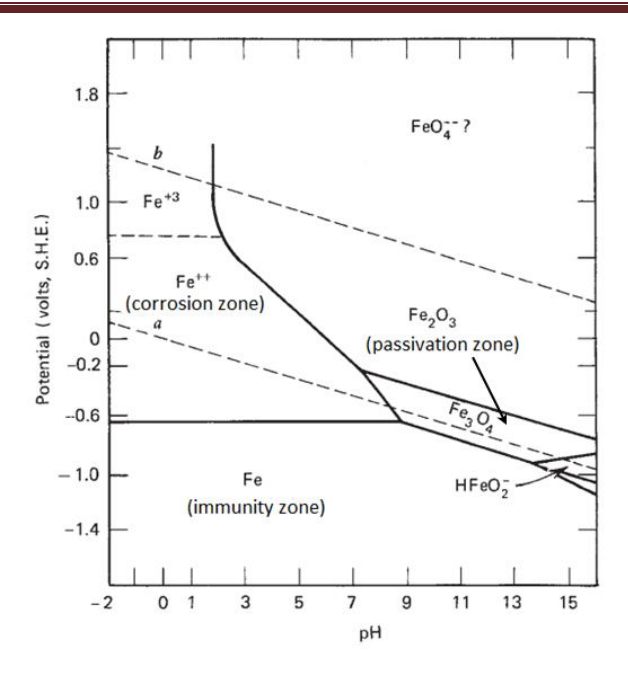


Fig. III-12. Simplified Pourbaix diagram for the iron – water system at 25°C [80]

III.1.2.2. Change in microstructure of materials

The carbonation does change the porosity, reorganisation of microstructure of concrete. That means that it leads to an increase in the volume of the solid phase. The values of the mole volume of portlandite and those of three crystalline forms of calcium carbonate CaCO₃ are compared in table III-1 [34].

Table III-1. Molar volume of calcite, vaterite and aragonite and porlandite [34]

Crystals	Mole volume(cm ³ .mol ⁻¹)	
Ca(OH) ₂ Portlandite	33	
CaCO ₃ Calcite	35	
CaCO ₃ Vatérite	38	
CaCO ₃ Aragonite	34	

Carbonation of Ca(OH)₂ into CaCO₃ causes an increase of volume, depending on the crystal form, which is 6% for calcite, 15% for vaterite and 3% for aragonite. The increase in the molar volumes of calcium carbonate with respect to that of calcium hydroxide

(portlandite) can explain the decrease of the pore volume of the concrete after carbonation. S.E. Pihlajavaara [35] also shown that the total porosity of the carbonated cement paste is essentially smaller than the total porosity of non-carbonated cement paste. Li Ying-Up and Wu Qiu-Dong [77] tested the Portland cement mortar samples storing in the CO₂ chamber of 20%, t=20°C, RH=52% for 90 days. The results showed that carbonation caused a change of pore structure. The total porosity of samples always decreases after carbonation as given in Fig. III-13. Interestingly, with the radius of pores over 10³ Å the pore volume before and after carbonation was almost similar. The author explained that in pores with radius over 10³ Å, CaO was less affected than that in pores below 10³ Å. As a result, as carbonation happens, there was almost no change in properties of these pores. Recently, Hyvert. N [36] and Sam Alahmad [37] also indicated that there was a relatively reduction of pore of carbonated concrete. This decrease depends on the cement type and age of carbonation at the same w/c ratio as given in tables III-2 and III-3.

The results denote that the decrease in porosity due to carbonation is related to not only the carbonation of portlandite but also that of other hydrates such as C-S-H. It indicates that the carbonation improves the permeability of concrete due to the decreases of surface porosity after carbonation and has a lower chloride ion penetration [42]. On the other hand, B. Johannesson and P. Utgenannt [43] recorded the volume expansion during the chemical reactions of carbonation, caused the microcracks at interfaces between the aggregates and bulk of material.

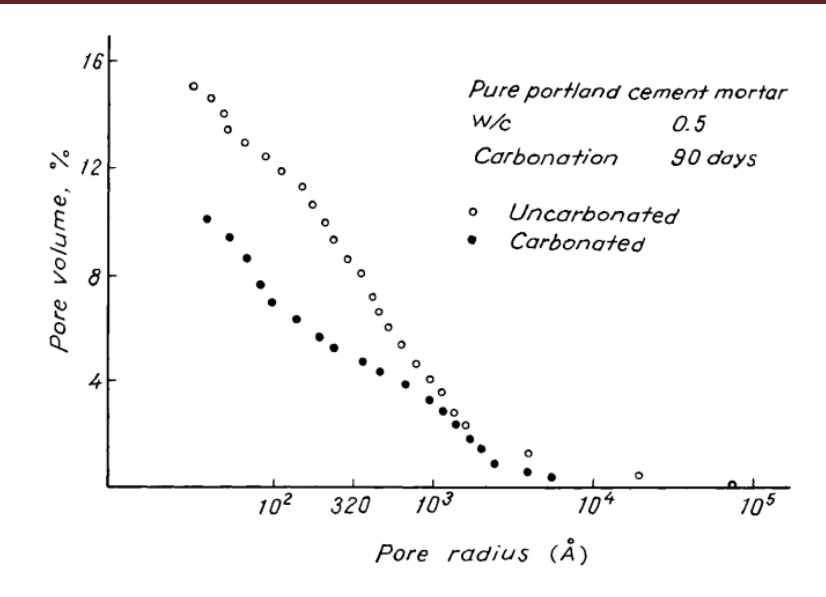


Fig. III-13. Integral curves of pore size distribution [77]

Table III-2. Total porosities measured on mortars with w/c = 0.5 [36]

	CEM I	CEM II	CEM III
Non-carbonated mortar	14.4%	13.9%	12.3%
Carbonated mortar for 296 days in natural atmosphere	12.9%	12.2%	11.3%
Carbonated mortar for 157 days in CO₂ of 50%	8.8%	10.8%	8.3%

Table III-3. Total porosities measured on mortars with w/c = 0.48, CO_2 of 50% at 65 days [37]

	Porosity before carbonation	Porosity after carbonation
Superior zone	18.8%	16.7%
Interior zone	15.4%	13.6%
Extrados face	17.8%	15.8%
Intrados face	17.9%	15.9%
Medium value	17.6%	15.5%

III.1.2.3. Change in mechanical properties of concrete

The decrease in porosity thanks to carbonation causes an increase in strength and elastic modules of concrete. Some of previous works demonstrated these findings. For example, V. Mohan Malhotra et al. [38] tested the compressive strength of high strength concrete at ages up to 10 years, the modulus of elasticity after 2, 4, and 10 years of exposure shown that there is a increasing tendency in compressive strength and modulus of elasticity. In fact, because of high strength concrete, we can expect that carbonation thickness is small, producing a little effect on strength. To better understand changes in the mechanical properties of concrete under various degrees of carbonation, Cheng-Feng Chang and Jing-Wen Chen [22] accelerated carbonation process in a sealed chamber with 20% carbon dioxide at a temperature of 23°C and 70% RH for 48 weeks. They found that compressive strength of carbonated concrete increased by 54.8% as the degree of carbonation reached 100%. Similarly, the carbonation effect had increased the modulus of elasticity by 17.1%. But, the test shown that the shape of stress-strain relationship of carbonated concrete modified as the carbonation level grew. The increase of strength due to the carbonation and the observed brittle failure of carbonated concrete were recorded by Jan Jerga [39] and Rigo da Silva CA et al. [40] too.

III.1.2.4. Change in moisture content capacity of concrete

Carbonation locally induces an accumulation of moisture in the pores due to the release of water from the carbonation of portlandite and C-S-H according to the reactions already mentioned. S. E. Pihlajavaara [35] measured experimentally the evaporable water content on carbonated cement paste after 105°C drying and concluded that there is an increase in evaporation of water from 7 to 17% with w/c ratio of 0.5. Björn Johannesson and Peter Utgenannt [43] tested the Portland cement mortar samples in a climate chamber with a 65% RH, t= 20°C and carbon dioxide content of 1% by volume for 4 months. They found that the noncarbonated mortar adsorbed more water at low relative humidity and less at high relative humidity than well-carbonated mortar. This means that the well-carbonated samples kept significantly less water than the noncarbonated samples. Y. F. Houst [76] concluded that the water adsorption isotherms of carbonated cement pastes are clearly lower than that observed on non-carbonated cement pastes with the same w/c.

More importantly, the amount of water vapor from dissolution of CO₂ can participate in the composition of pore solution and contribute to the transport of aggressive agents.

III.1.2.5. Change in transport properties of concrete

Transport properties affect the durability of concrete because they control the supply of aggressive species, such as carbon dioxide, water and oxygen. The variation of the microstructure associated with carbonation affects the transport properties of cementitious materials. Accordingly, the gas and water permeability, effective diffusion coefficients for ions and gases are altered.

In the literature there are very few results concerning the influence of carbonation on permeability. Peter A. Claisse et al. [44] investigated the effect of carbonation on the permeability and pore structure of concrete. After 140 days of exposure to 5 % concentration of CO₂, carbonation leads to a significant reduction in the permeability because the pore volume and the volume of capillary pores also reduce significantly. This reduction is greatest in poor quality concrete. The carbonation effect decreases the transport coefficients of oxygen and chloride as shown in [36, 44]. Meanwhile, V.T. Ngala and C.L. Page [45]

observed both oxygen diffusion coefficient and chloride diffusion coefficient increase after several weeks exposing to CO₂. Thus, it is complicated to predict the influence of carbonation on effective diffusion coefficient of ions.

III.1.3. Corrosion induced by Carbonation

III.1.3.1. Corrosion mechanism

C. Andrade et al. [81] performed the measurement of corrosion rate of steel concrete exposed to natural weathering with seasonal variations. The authors pointed out that rebar corrosion mechanisms in carbonated concrete can be similar to atmospheric corrosion ones. The atmospheric corrosion mechanism must consider the wetting-drying cycles. In 1987 M. Stratmann et al. [83] proposed a corrosion mechanism in the atmosphere, which can be divided into three stages:

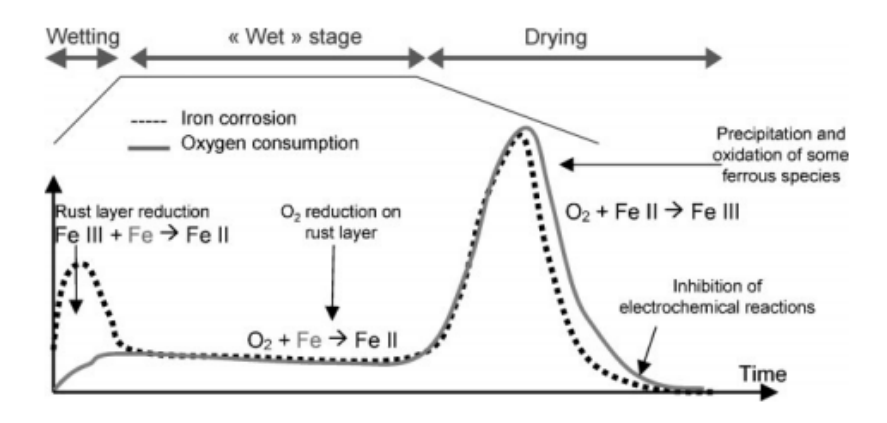


Fig. III-14. Schematic representation of the wetting-drying cycle defining atmospheric corrosion mechanism [82]

Stage 1: wetting of the dry surface

During this stage the cathodic O_2 reduction reaction is very slow compared to the anodic iron dissolution. The rate of the metal dissolution is high, but the amount of dissolved iron is restricted to the amount of reducible FeOOH in the rust-layer. A

corrosion cell starts where the anodic dissolution of iron is balanced by the cathodic reduction of Fe (III) in the rust layer:

$$Fe \rightarrow Fe^{2+} + 2e^{-}$$

$$2\text{FeOOH} + 2\text{H}^+ + 2\text{e}^- \rightarrow 2\text{Fe. OH. OH}$$

Stage 2: wet surface

Once the reducible FeOOH has been used up, the O₂ reduction reaction becomes the cathodic reaction:

$$Fe \rightarrow Fe^{2+} + 2e^{-}$$

$$0.5O_2 + H_2O + 2e^- \rightarrow 2OH^-$$

The metal dissolution rate is determined by the diffusion-limited current density of the O_2 reduction reaction on the pore surfaces. Because the pores in the rust layer are filled with electrolyte, the corrosion rate is quite slow during stage 2, as the diffusion rate is lower in the electrolyte than in the gas phase.

Stage 3: drying out of the surface

During drying-out, the rate of the diffusion limited O_2 reduction reaction is extremely fast due to thinning of the electrolyte film on the inner surface of the rust layer. Accordingly, the corrosion rate is very high, O_2 reduction again being the cathodic reaction. In addition to this, O_2 can reoxidise the reduced Fe²⁺ formed in stage 1.

$$Fe \rightarrow Fe^{2+} + 2e^{-}$$

$$0.5O_2 + H_2O + 2e^- \rightarrow 2OH^-$$

2Fe. OH. OH +
$$0.5O_2 \rightarrow 2FeOOH + H_2O$$

As a consequence of the high corrosion rate stage 3 seems to dominate the metal loss during the whole wet-dry cycle. In the third stage, the reduced layer of γ -FeOOH

(lepidocrocite) and the other ferrous species are reoxidised by oxygen, leading to the formation of α -FeOOH (goethite) and the regeneration of lepidocrocite. The electrolyte film is used up, stopping the corrosion process completely. It is during this final stage that the rust layer composition changes, leading to a different intensity in the corrosion process for the next wet-dry cycle [82].

III.1.3.2. Cracking of the concrete cover due to corrosion in CO₂ environment

As the steel bar is corroded in carbonated concrete, the increase of volume of the corrosion products results in a "bursting" pressure on the surface of the bar and the surrounding concrete, which induces visible cracks in the structures and finally leads to spalling of the concrete above the steel rebars. The higher the corrosion levels result in the wider crack widths.

There have been very few results available on the effect of corrosion on cracking and spalling of the concrete cover in CO₂ condition. Almost all authors simulated the corrosion process induced by CO₂ by impressing a constant current to the embedded reinforcing steel. However, the results published do not reflect the natural characteristics of corrosion [46, 47].

The effect of corrosion on cracking of the concrete cover depends primarily on the diameter of the steel rebars, on the length of the corroding section of the rebar and on the thickness of the concrete cover [48].

L.J. Parrott [49] classified the damage of concrete induced by carbonation as seen table III-4. The corrosion risk due to carbonation of concrete depends on the carbonation depth in relation to the cover.

Table III-4. Classification of carbonation-induced damage [49]

Damage severity	Concrete condition	Reinforcement condition	Carbonation: cover ratio	Further action
Safe	Not cracked	Not corroded	<0.5	None
Mild	Not cracked	Not corroded	>0.5	Estimate time to carbonate cover,
Significant	Minor cracks	Minor corrosion	~1.0	monitor or apply coating Initiate repair, apply coating or monitor
Serious	Cracked, minor spalling	Significant corrosion	>1.0	Full survey and repair
Critical	Cracked, major spalling	Loss of area	>>1.0	Assess residual strength and immediate repair

III.1.3.3. Change in mechanical properties of reinforcement

Carbonation lead to corrosion of reinforcement and its mechanical properties is changed. More recently, Weiping Zhang et al. [41] investigated the effect of corrosion on the reinforcement steel obtained from RC beams of a carbonated inland building over 30 years old. A noticeable fall in both yield and ultimate strengths was recorded. Moreover, a significant degradation in deformability under tensile load was observed.

III.1.3.4. Effect of pre-cracks on steel corrosion in CO₂

Cracks in normal concrete structures are almost unavoidable. There are numerous causes of cracking in concrete such as: shrinkage, settlement, freeze/thaw cycles, creep, design loads, formwork movement, corrosion of reinforcement and so on [19]. If the tensile stress to concrete is exceeded the tensile strength capacity of the concrete, cracking will occur. Cracks most often tend to be tapered or V-shaped due to flexural loads. However, parallel-wall cracks are also common in concrete under direct tension. Once began, cracks create pathways for oxygen, chlorides, carbon dioxide, water into concrete, thus, facilitating the corrosion evolution. In cracked concrete, corrosion will start either in the crack region or in the region

beside the crack. Adapted from Peter Schießl and Michael Raupach [23], two different corrosion mechanisms can take place in the area of a crack in concrete (Fig. III-15):

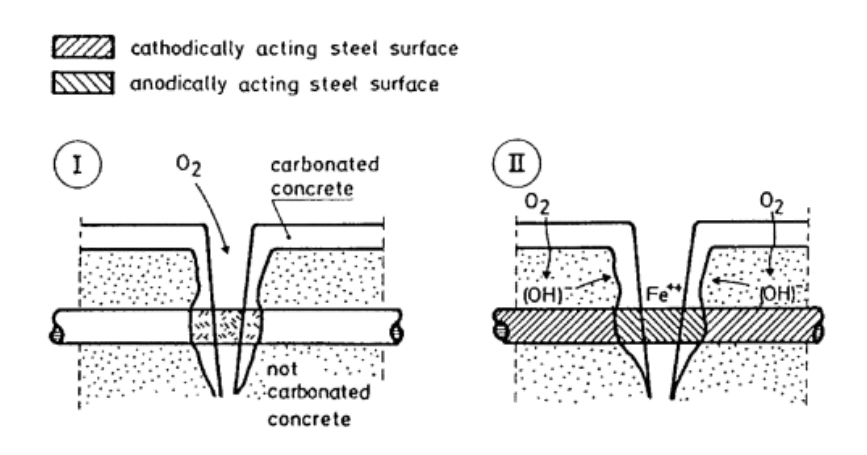


Fig. III-15. Schematic representation of corrosion process [23]

<u>Mechanism I (Microcell corrosion):</u> where both the anode and cathode locate in the zone of the crack. Anodic and cathodic areas are very small and lain close to each other. The oxygen required for the cathodic reactions is supplied via the crack.

<u>Mechanism II (Macrocell corrosion):</u> where the steel bar in the crack zone acts as an anode, and the passive steel surface between the cracks forms the cathode. In this type, the oxygen penetrates mainly through the uncracked zone of concrete. The corroded steel surface area in this case is larger than that in mechanism I. Much higher corrosion rate can be expected.

In extreme case, cracks may affect the structural integrity of the concrete member. Nevertheless, in most instances, cracks do not affect the load-bearing capacity of RC members but may adversely affect its durability by promoting easily aggressive agents to concrete. Factors in relation to cracks that impact on corrosion of RC structures may include: crack width, crack frequency, crack orientation, and crack location [23-28]. However, most of these works related to the reinforcement steel corrosion used a chloride environment. There have been a few researches on the influence of pre-cracks on corrosion of steel in concrete exposed to carbon dioxide. To our knowledge, only one works carried out by Raoul François et al. [24, 27] was dealt with this problem. They studied RC beams with bending

cracks subjected to a confined enclosure of 50% CO₂ [24, 27] for 24 and 40 weeks. To estimate the state of reinforcement corrosion inside beams, an electrical contact welded to steel cage. This contact was linked to the outside by means of a wire. Then, potentials were measured on the surface by means of saturated calomel electrode. The graphs of measured potential were compared with maps of reinforcement corrosion after removing concrete. The results reveal that the corrosion rate in the tension zone is always greater than that observed in the compression zone. The corrosion seems more severe at the intersection between steel bar and crack, but corrosion did not spread along reinforcement from those points.

III.1.3.5. Nature of corrosion products

In this sub-section, we focus discussion on the characterization of steel corrosion embedded in concrete, submitted to the atmospheric environment or to pure carbon dioxide in the laboratory.

III.1.3.5.1. Identification methods of corrosion products

In order to obtain an identification of the oxides or products that are present in rust composition, some methods were popularly used such as X-ray diffraction (XRD), scanning electron microscope (SEM), Mossbauer spectroscopy and Raman spectroscopy. Depending on the applied technology, each of them has the advantages or disadvantages.

Indeed, R. Balasubramaniam et al. [50] showed that XRD is one of the most useful techniques for materials characterization. It is an excellent tool for compound identification when a material has atomic-scale periodicity or crystallinity. For local phase identification, the micro X-ray (μ XRD) diffraction technique can be used to obtain local structural information on scales several hundred μ m thick. However, a biggest lack of XRD is the fact that the presence of amorphous phases cannot be understood by XRD technique. Magnetite, Fe₃O₄ and maghemite, γ -Fe₂O₃ are also very difficult to be able to distinguish by XRD [53]. Further, Desmond C. Cook [51] found that with the quantitative analysis of rust, XRD technique significantly underestimates the goethite fraction in the corrosion products, especially for weathering steel. The author explained that this is due to the presence of the nano-phase oxides whose diffraction lineshapes are very much broadened and are usually

overlooked since they overlap with the sharper peaks due to the larger particles of the same oxide phases also in the coating. Thus, it can state that XRD should be used to identify the general characteristics of rust products and to calculate the fraction of each iron oxide with crystalline large particles greater than about 30nm in length [52].

The scanning electron microscope (SEM) method is the first analytical instrument used for quick observations. It provides both microphotograph and chemical composition of the rust layers. SEM can be used for high-resolution imaging of the surface (up to 1-5nm in size), with a large depth of field, while the best resolution of optical microscope is just about 200nm, which limits significantly the capabilities of application research. The degree of corrosion, surface morphology, particle size and texture can be effectively studied in the SEM. SEM is usually utilized as a complementary analytical technique to determine the characteristic of the corrosion layers.

According to D.C. Cook et al. [52], Mossbauer spectroscopy and Raman spectroscopy are the two most important analytical techniques, which permit complete oxide identification and three-dimensional mapping of the iron oxides as well as measurement of the fraction of each one that form on corroding steels. Mossbauer spectroscopy supplies information about the magnetic field at the nucleus, the valence of the Fe and the type of coordination and order within the ligand shell [53]. No special sample preparation is needed, which ensures that the exact nature of corrosion products is clearly reflected during the investigation [50]. Whilst, the Raman analysis has to performed on a polished metallographic cross-section of samples, which may be affect the structure of its rust layers. Both of them cannot detect metals or alloys. Nevertheless, these techniques can detect all iron species presenting in the sample [73]. D.C. Cook et al. [52] also concluded that Mossbauer and Raman method cannot confirm the presence of chromium in goethite but they can recognize the presence of nano-phase goethite, α-FeOOH with a particle size of less than 15nm. An advantage of Raman analysis over Mossbauer analysis is that because of its high spatial resolution, micro-Raman analysis can identify small fractions of oxides which are too small to be identified by Mossbauer spectroscopy. Beyond the identification and organisation of corrosion products, Raman micro-spectroscopy could provide the quantitative data on the phase proportions which are needed in the establishment of diagnosis indicators [74].

D. L. A. de Faria et al. [54] studied the effect of laser energy source used in the Raman spectroscopy to transform into other compounds in the corrosion products. The results obtained show that increasing laser power causes most of the oxyhydroxides investigated to show the Raman spectrum peaks like the hematite Raman spectrum. Structural transformations of the iron phases due to the laser action were not occurred when the power on the sample is lower than 0.7 mW. The authors indicated that the power threshold depends on the surface morphology and temperature on the sample. 100°C of sample surface is below the temperature required for thermal transformations of iron oxides and oxyhydroxides [55].

Therefore, better understanding of the formation, development and transformation of the iron oxides of steel corrosion can be obtained by correlating the Raman technique and/or the Mossbauer technique with SEM.

III.1.3.5.2. Corrosion products formed on rust layer

The type of corrosion products was primarily dependent on the pH and availability of oxygen. The eight common occurring phases of iron oxides and oxide hydroxides in natural environment or laboratory are given in table III-5. Corrosion products on steel surface include: a) common iron oxides such as magnetite, hematite and maghemite and b) iron oxyhydroxides.

Oxyhydroxides Oxides **Formula Formula** Name Name α -FeOOH Goethite $5Fe_2O_3.9H_2O$ Ferrihydrite β-FeOOH Akaganeite α -Fe₂O₃ Hematite Lepidocrocite γ-FeOOH γ -Fe₂O₃ Maghemite δ-FeOOH Ferrox yhite Magnetite Fe_3O_4

Table III-5. Major forms of iron oxides and oxyhydroxides

Among these compounds, the ferroxyhite and ferrihydrite exist in amorphous form. Hematite, magnetite and maghemite are the most prevalent iron oxides found both in natural form and synthesized form. They are more stable corrosion products as the supply of oxygen increases. One of the characteristics of the iron oxide system is the variety of possible transformations between the different phases. Indeed, it can divide the formation process of corrosion products in the atmospheric condition into four steps as follows [56]:

- The initiation of corrosion can take place after the formation of water droplets on the surface of steel. This step is described as reactions below:

At anode:

$$Fe \rightarrow Fe^{2+} + 2e^{-} \tag{III.6}$$

At cathode:

$$4 e^{-} + O_2 + 2H_2O \rightarrow 4(OH)^{-}$$
 (III.7)

- The formation of corrosion products ferrous hydroxide Fe(OH)₂ in thin film electrolyte:

$$Fe^{2+} + 1/2O_2 + H_2O \rightarrow Fe(OH)_2$$
 (III.8)

Ferrous hydroxide Fe(OH)₂ precipitates from the solution, however, this product is unstable in an oxygenated solution and oxidizes to the ferric form (rust) Fe(OH)₃.

$$4\text{Fe}(\text{OH})_2 + 2\text{H}_2\text{O} + \text{O}_2 \rightarrow 4\text{Fe}(\text{OH})_3$$
 (III.9)

- The formation of FeOOH: access to dissolved oxygen converts ferrous hydroxide to ferric hydroxide according to the following reaction:

$$2\text{Fe}(\text{OH})_2 + 1/2\text{O}_2 \rightarrow 2\text{Fe}(\text{OOH}) + \text{H}_2\text{O}$$
 (III.10)

Fe(OH)₂ oxidizes suddenly forming lepidocrocite (γ -FeOOH) through the intermediate phase (green rust). γ -FeOOH in turn transforms to goethite (α -FeOOH) in the presence of water or low and high values of pH (2–5 and 10–14).

- The formation of γ -Fe₂O₃ and Fe₃O₄: FeOOH is unstable and will transform to Fe₂O₃, Magnetite (Fe₃O₄), and H₂O.

$$2FeOOH \rightarrow Fe_2O_3 + H_2O \qquad (III.11)$$

$$6\text{FeOOH} + 2e^{-} \rightarrow \text{Fe}_3\text{O}_4 + 2\text{H}_2\text{O} + 2\text{OH}^{-}$$

If the corrosion rate is low and the oxidation time is long enough to remove oxygen from crystal and rearrange oxygen, a part of lepidocrocite converts to maghemite (γ -Fe₂O₃). The oxidation product of Fe₃O₄ is either maghemite (γ -Fe₂O₃) or hematite (α -Fe₂O₃) depending on the oxidation temperature and pH. At neutral pH (around 7) or high temperature promotes the formation of the oxide hematite [57, 58]. Fig. III-16 shows the principal components of rust products and their possible phase transformation.

The components of corrosion products with accelerated corrosion tests in laboratories may be different from the natural steel corrosion. When the rate of steel corrosion is high such as accelerated test, the availability of oxygen in concrete (as in non-cracked structures) is not enough to generate the stable corrosion products. It is well-known that the presence of oxygen is a vital factor to govern the composition of rust in structural concrete. Therefore, the samples tested in salt solution or subjected to current density might indicate the soluble, unstable corrosion products as ferrous hydroxide (Fe(OH)₂) and ferric hydroxide (Fe(OH)₃), which constitute a large volume density in products of oxide. Whereas, the specimens found in in-service structures as well as in laboratory where steel corrosion is closest to natural conditions give more stable products thanks to the supply of adequate oxygen.

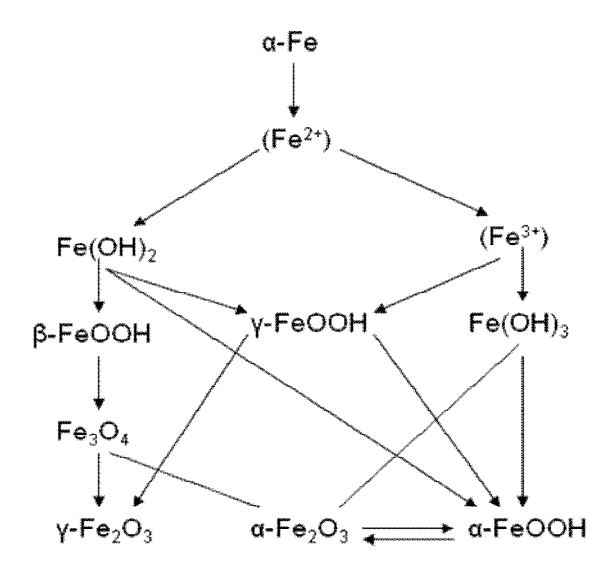


Fig. III-16. A way for formatting crystalline oxides [75]

A lot of researches on characterization of steel corrosion in reinforced concrete structures were carried on. However, most of them have discussed on the components and formation mechanism of rust layers that formed for long period in atmospheric condition. A preliminary summary on works of identification of rust products by authors is given in Table III-6. It is underlined that the works of Amélie Demoulin et al. [59], V. L'Hostis et al. [60] and G.S. Duffó et al. [61] studied on steel samples embedded in concrete or cement paste, while the others examined on bare steel specimens [62-68]. In addition, the chemical compositions of steel used in these studies were different, leading to various structure of the rust layer. The exposure time seems having a little effect on nature of rust constituents. In other words, whatever the exposure time the corrosion products have always the same morphology and are constituted of the same phases. The rust layers always include the iron oxyhydroxides

goethite or lepidocrocite or a mix of two these phases irrespective of steel types and exposure conditions. The rust compositions vary widely as a result of differences in exposure conditions and identification techniques. The literature has reported that there is a change in the proportions of components, structures on rust layers or the appearance or disappearance of intermediate phases.

Indeed, Amélie Demoulin et al. [59] studied the corrosion patterns on samples taken on binder and rebars from two buildings, respectively, aged of 46 and 260 years old in France. They indicated that depending on the location on the reinforcement, the corrosion product distribution is multilayered and has three patterns (see Fig. III-17). Accordingly, type 1 with the average thickness of several tens of micrometers formed two different corrosion layers (external and internal layers). Internal thicker layer is mainly consisted of wüstite and a thinner layer of magnetite and hematite is located at the external zone of the corrosion products.

Table III-6. Typical components of rust on steel for long-term atmospheric corrosion

Authors	Conditional corrosion	Time of exposure	Main composition of rusts	Note	
Amélie Demoulin et al. [59]	Atmosphere	260 years	wüstite, magnetite, goethite, maghemite	steel	
		46 years	wüstite, magnetite, maghemite, goethite, hematite, ferrihydrite,feroxyhyte, lepidocrocite, akaganeite		
V. L'Hostis et al. [60]	Atmosphere	80 years	magnetite, wustite, hematite	embedded in concrete	
		50 years	magnetite/FeO mix, lepidocrocite, goethite, feroxyhite or ferrihydrite		
G.S. Duffó et al. [61]	8		goethite, hematite, magnetite, maghemite, lepidocrocite, akaganeite		
M.Yamashita et al. [62]	Industrial atmosphere	26 years	lepidocrocite, goethite, magnetite	- bare steel	
K.Asami, M.Kikuchi [63]	Coastal— industrialatmosphere	17 years	goethite, akaganeite, lepidocrocite, magnetite, amorphous rust		

CHAPTER III: Literature review on corrosion in carbon dioxide

Sei J. Oh et al. [64]	Rural and Industrial atmosphere	16 years	lepidocrocite, goethite, maghemite, magnetite	
Takayuki Kamimura et al. [65]	Industrial atmosphere	32 years	lepidocrocite, goethite	
		15 years	lepidocrocite, goethite, maghemite	
D. de la Fuente et al.[66]	Industrial atmosphere	13 years	lepidocrocite, goethite, hematite, ferrihydrite,	
	Urban atmosphere	13 years	lepidocrocite, goethite, magnetite/maghemite	
E. Almeida et al. [67]	Rural and urban atmosphere	1-4 years	lepidocrocite, goethite	

Type 2 with the same average thickness of corrosion products as type 1 but the distribution of iron oxides and iron oxyhydroxides alters. A mill scale of several micrometers made of mix of wustite, magnetite and hematite is located at different positions on rust layer: in contact with the metal surface, outermost against the metal surface or in the middle of corrosion layers. Moreover, the appearance of marblings contained mixes of ferrihydrite and maghemite within corrosion products is paid attention to. The researchers concluded it appears that only mixes of ferrihydrite and maghemite (possibly feroxyhyte) in marblings are present in the samples of 46 years. After 260 years, the main phases in these marblings are magnetite and maghemite. Therefore, the possible evolution from ferrihydrite/maghemite to maghemite/magnetite is observed.

Type 3 with the corrosion layer thicknesses of several hundred micrometers contains the abundant marblings. It seems that the mill scale is disappeared in this type. The structure of marblings is also varied from a mix of maghemite and ferrihydrite (without magnetite) to a mix of magnetite and maghemite. The author explained that this progression could be due to wet-dry cycles and specific pH evolution in concrete.

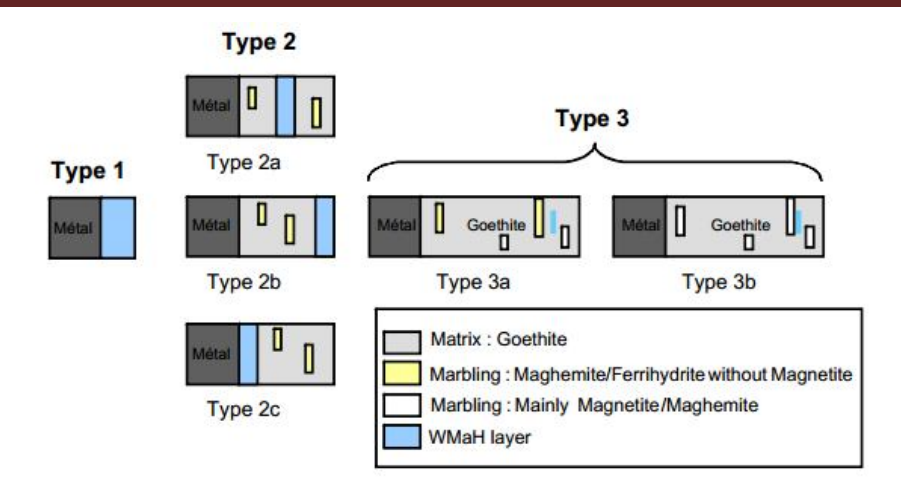
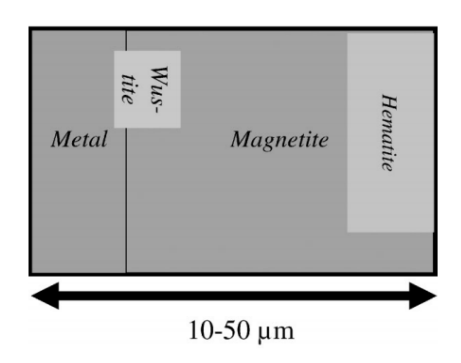


Fig. III-17. Cross section of the rust layers formed on aged buildings [59]

V. L'Hostis et al. [60] analysed rust on ancient reinforcement steel in concrete of two French Historical Monuments aged of 50 and 80 years. The corrosion layers can be divided into two dissimilar types: "initial corrosion layer" (the thickness of 10-50 micrometer) and "thick corrosion layer" (the thickness of 100-300 micrometer). The composition and structures of each of them is presented below in Fig. III-18.

a) Initial layer



b) Thick layer

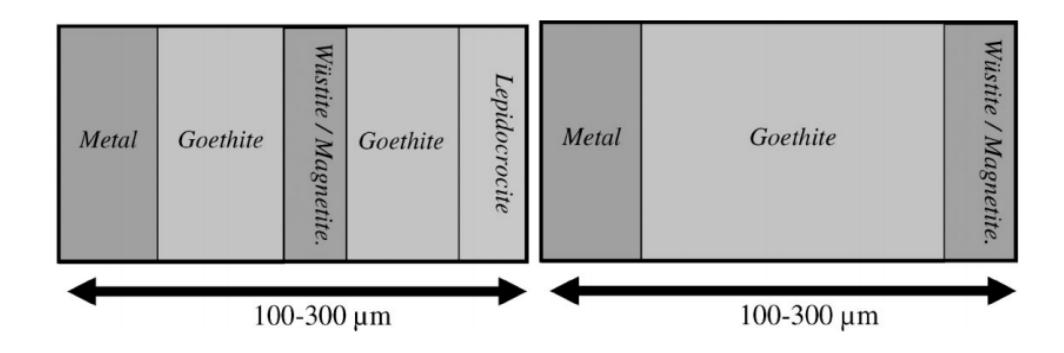


Fig. III-18. The variation of structure on corrosion layers as corrosion scale increases [60]

It is clear that there is a re-distribution in proportion along with quantities of chemical components when compared the "initial layer" with "thick layer". This could be explained that the initial phases (α-Fe₂O₃, Fe₃O₄ and FeO) react during the corrosion processes in presence of the carbon dioxide. This can cause the appearance or disappearance of other phases as hematite, goethite. The presence of goethite on the outer part of the corrosion layer in some cases could be representative of dissolution/reprecipitation phenomena or other mechanisms. The findings of Amélie Demoulin et al. [59] and V. L'Hostis et al. [60] appear to be shown that when thickness of corrosion layer is thin in the order of tens micrometre, magnetite is closest to the steel face-rust interface. After reaching a thickness of several hundred micrometres, the inner zone is mainly composed of goethite-maghemite mix. Interestingly, they detected the presence of wustite (FeO) in the rust constituent.

In fact, it is difficult to identify clearly a type of corrosion products formed on reinforced rebars because of the heterogeneous corrosion level surrounding the steel bars and the presence of defect at interface between concrete and rebars, which may be lead more active corrosion. G.S. Duffó et al. [61] also confirmed this finding. In their study on the characterization of steel rebars embedded in a 70-year old concrete structure, placed in a sulphur-containing environment, they revealed that the rust layers are consisted of laminar layers of different colors, non-uniform distribution round the cross section. The presence of akaganeite in compounds is attributed to the presence of chloride in the cement paste. This is

in agreement with the result's K.Asami and M.Kikuchi [63], who studied rust on mild steel exposed for 17 years in coastal–industrial atmosphere. They found that the proportion of magnetite decreases as the akaganeite concentration increases or Cl⁻ concentration increase.

The difference on structure of rust layers was also reported by several researchers. For instance, K.Asami and M.Kikuchi [63] noted that the rust layer formed on weathering steel for 17 years (bare steel) generally consists of two regions: an inner region, next to the steelrust interface, often consisting primarily of amorphous substance, and an outer region consisting of α-FeOOH, γ-FeOOH and Fe₃O₄. Moreover, α-FeOOH phase amount was distributed homogenously throughout the thickness of this zone (Fig. III-19a). With thicker layers, less Fe₃O₄ appears in outer part of rust, corresponding to more β-FeOOH in the surface of this part. Nevertheless, in a study on ancient iron specimens (bare steel) (100-1600 years in door), Ph. Dillmann et al. [68] showed that there were three distinct rust layers existed on metal substrate. Namely, the inner layer is mainly maked of crystallised phases α-FeOOH and Fe₃O₄; the outer layer is principally composed of γ-FeOOH and the external layer contains the elements coming from the atmosphere such as chlorides, dust (Fig. III-19b). Interestingly, no amorphous phases were clearly identified. A possible explanation is that because of the old age of rust, the amorphous inner layer can transform to a densely packed aggregate of nanoparticles of goethite [62]. The amorphous phase also observed by several authors [65, 67] on steel specimens exposed to the rural, urban and industrial atmosphere from several years to decade. Its location is evidently indicated: placing between the rust layer and the metal surface.

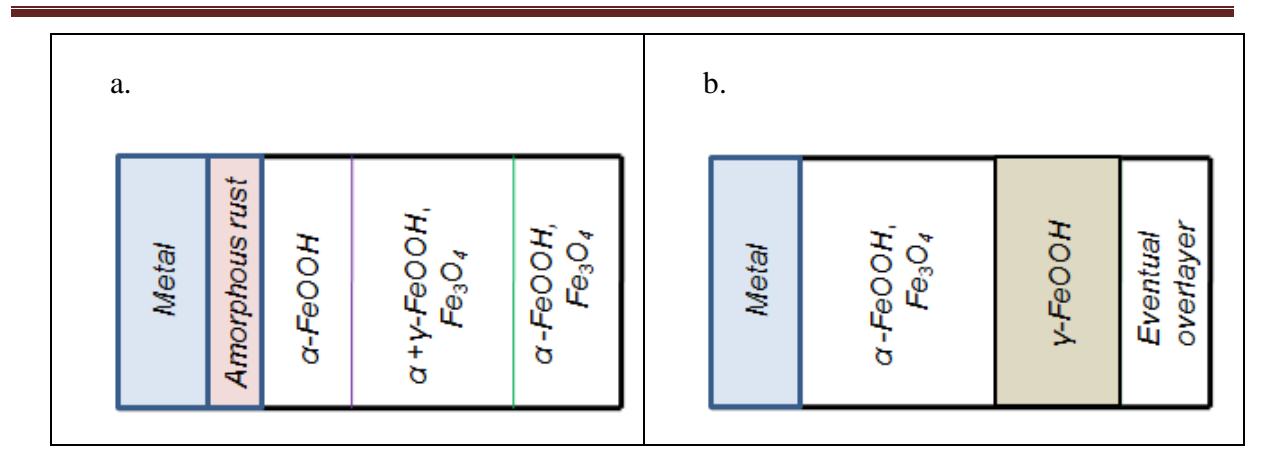


Fig. III-19. The natural distribution of rust layer, according to a) K.Asami and M.Kikuchi [63]; b) Ph. Dillmann et al. [68]

M. Yamashita et al. [62] suggested that γ -FeOOH should exist on top of the α -FeOOH rust layer when the long-term corrosion process is stable as seen in Fig. III-20b. They conclude that the γ -FeOOH, as an initial rust layer, is transformed into a final stable rust layer of α -FeOOH in an atmospheric environment, via amorphous ferric oxyhydroxide (Fig. III-20a). Thus, the final rust layer formed on the weathering steel consists of two layers; one is the outer layer which is mainly comprised of γ -FeOOH and the other corresponds to the inner layer mainly composed of densely packed of α -FeOOH.

From discussions mentioned above, it could be concluded that in the case of long-term corrosion, the goethite phase α -FeOOH always contacts with the metal surface, whilst lepidocrocite γ -FeOOH does not seems in contact with the metal surface.

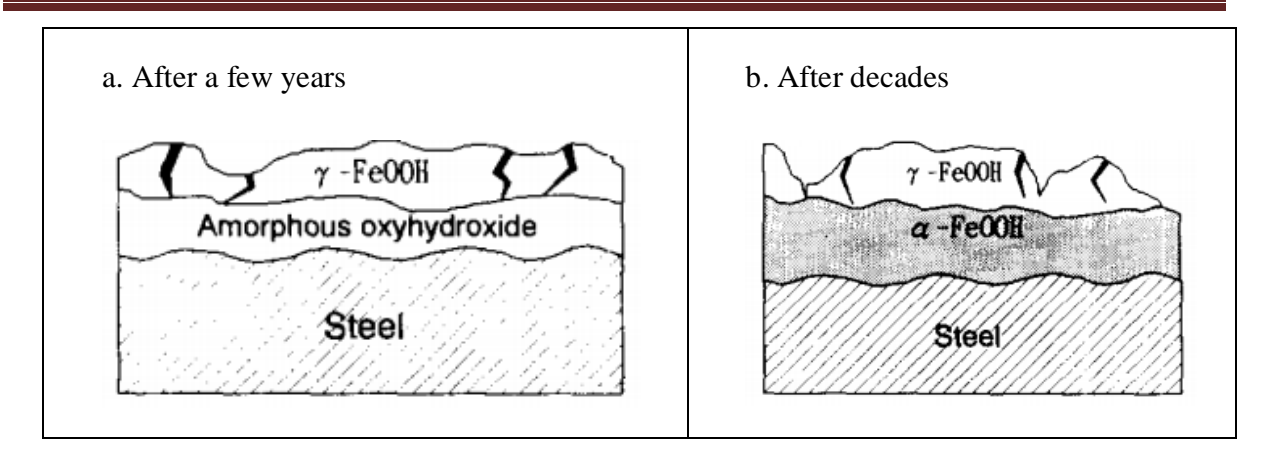


Fig. III-20. Change of rust layer structure on bare steel samples against time of exposure [62]

There are a few studies on the characterization of short-term corrosion of reinforcement steel inside concrete or mortar induced by carbon dioxide in laboratory.

Bruno Huet [70] accelerated the steel corrosion embedded in cement paste by keeping the specimens in CO_2 concentration of 50%, a relative humidity of 60% and a temperature of 20° C. It is noted that these conditions of accelerated carbonation test are very different from those of the natural carbonation which could result in different states of degradation. After 4 months, the author recorded the presence of ferrous hydroxide $Fe(OH)_2$ (green rust) at the metal-oxide interface. The compounds of Fe_3O_4 and α -FeOOH were found in the zone closed to the metal-oxide interface. Finally, α -FeOOH was detected in outer zone of rust thickness. This result is consistent with the growth of oxide layer as given in Fig. III-16.

V. L'hostis et al. [71] investigated the nature of the corrosion products present at the steel-concrete interface on reinforced concrete slabs summited to a climatic chamber with the different temperature and relative humidity for two years (20 and 45°C; 60, 80 and 92% relative humidity and 50% CO_2). The results shown that whatever corrosion conditions, the dominant corrosion products are ferrihydrite and α -FeOOH.

It should be emphasized that the previous works carried on in laboratory in a short span of time do not concern the occurrence of corrosion cracks when the corrosion products expand. Once micro-cracks form around the steel core, they could change locally the environmental

conditions of the concrete. That results in the thicker corrosion layers as well as the variation in their lamellar structure. If remaining the cracks due to corrosion process or pre-cracks due to a certain reason, it could take place the transfer of iron oxides into cement paste and the exchange of minerals in the cement paste into corrosion products. The interest should therefore be to determine if the cracks lead to an activation of the corrosion processes at the cracks- rebars intersection. In other words, how the corrosion cracking and/ or pre-cracks affects the corrosion product development. More discussion on this matter is in Chapter V, section V.2.

References

- 1. **A.M Dunster,** (1989), "An investigation of the carbonation of cement paste using trimethylsilylation", Advances in Cement Research, 2(7): 99-106.
- 2. **G.W. Groves; D. I. Rodway; I. G. Richardson,** (1990), "The carbonation of hardened cement paste", Advances in Cement Research, Volume 3, Issue 11, pages 117 –125.
- 3. **Z. Šauman,** (1971), "Carbonization of porous concrete and its main binding components", Cement and Concrete Research, Volume 1, Issue 6, Pages 645–662.
- 4. **P.A. Slegers, P.G. Rouxhet,** (1976), "Carbonation of the hydration products of tricalcium silicate", Cement and Concrete Reseach 6, pp. 381–386.
- 5. **G. Villain, M. Thiery, G. Platret,** (2007), "Measurement methods of carbonation profiles in concrete: Thermogravimetry, chemical analysis and gammadensimetry", Cement and Concrete Research 37, pp. 1182–1192.
- 6. **Y.F. Houst, F.H. Wittmann,** (2002), "Depth profiles of carbonates forming during natural carbonation", Cement and Concrete Research 32, pp. 1923–1930.

- 7. **V. G. Papadakis, C.G. Vayenas, Michael N. Fardis,** (1991), "Experimental investigation and mathematical modeling of the concrete carbonation problem", Chemical Engineering Science, Volume 46, Issues 5–6, Pages 1333–1338.
- 8. **E. Sakai, K. Kosuge, S. Teramura, and K. Nakagawa,** (1991), "Carbonation of Expansive Concrete and Change of Hydration Products", ACI structural journal, SP 126-53, pp. 989-1000.
- 9. **A. Emanuelson, C. Solberg, C. Evju, S. Hansen**, (2001), "Crystal structures of cementitious compounds. Part 1: Calcium oxide, calcium hydroxide, calcium silicates", ZKG international.
- 10. **Q. Zhou and F. P. Glasser**, (2000) "Kinetics and mechanism of the carbonation of ettringite", Advances in Cement Research, 12(3): 131-136.
- 11. **T. Nshikawa, K. Suzuki, S. Ito, K. Sato and T. Takebe**, (1992), "Decomposition of synthesized ettringite by carbonation" Cement and Concrete Research, 22(1): 6-14.
- 12. L. Bertolini, B. Elsener, P. Pedeferri, R. P. Polder, (2004), "Corrosion of steel in concrete", Wiley-VCH.
- 13. A. Neville, (2006), "Neville's insights and issues", first published, Thomas telford.
- 14. **M. Vénuat et J. Alexandre**, (1968). "De la carbonatation du béton partie II". Revue des Matériaux de construction, (639): 469-481.
- 15. C. L. Page, (1992), "Nature and properties of concrete in relation to reinforcement corrosion", in Corrosion of Steel in Concrete, Aachen.
- 16. **H. Böhni**, (2005), "Corrosion in reinforced concrete structures", First published 2005, Woodhead Publishing Ltd and CRC Press LLC.
- 17. **D. W. S. Ho, R. K. Lewis**, (1987), "Carbonation of concrete and its prediction", Cement and Concrete Research, 17, 489.
- 18. T. K. H. Al-Kadhimi, P. Banfill, S.G. Millard, J. H. Bungey, (1996), "An accelerated carbonation procedure for studies on concrete", Advances in Cement Research, 8(30), 47–59.
- 19. CEB, (1997), "Durable of concrete structures", Thomas Telford.
- 20. **L.J. Parrott**, (1994), "A Study of Carbonation-Induced Corrosion", Magazine of Concrete Research, 46 (3): 23-28.

- 21. **T. Fukushima, Y. Yoshizaki, F. Tomosawa, K. Takahashi**, (1998), "Relationship between neutralization depth and concentration distribution of CaCO₃–Ca(OH)₂ in carbonated concrete", ACI SP–179, pp. 347–363.
- 22. **C. Feng Chang and J. Wen Chen**, (2005), "Strength and Elastic Modulus of Carbonated Concrete", ACI Materials Journal, V. 102, No. 5.
- 23. **P. Schießl and M. Raupach**, (1997), "Laboratory Studies and Calculations on the Influence of Crack Width on Chloride-Induced Corrosion of Steel in Concrete", ACI Materials Journal, V. 94, No. 1.
- 24. **R. Francois, J.C. Maso**, (1988), "Effect of damage in reinforced concrete on carbonation or chloride penetration", Cement and Concrete Research, Vol. 18, pp. 961-970.
- 25. **A.W. Beeby**, (1983), "Cracking, cover, and corrosion of reinforcement", Concrete international, pp.35-40.
- 26. C. Arya, F. K. Ofori-Darko, (1996), "Influence of crack frequency on reinforcement corrosion in concrete", Cement and Concrete Research, Vol. 26, No. 3, pp. 345-353.
- 27. **R. François, G. Arliguie**, (1991), "Reinforced concrete: correlation between cracking and corrosion", ACI journal, SP 126-65, pp.1221-1238.
- 28. **R. François and G. Arliguie**, (1994), "Durability of Loaded Reinforced Concrete in Chloride Environment", ACI journal, SP 145-30, pp. 573-596.
- 29. P. A. M. Basher, S. E. Chidiac et A. E. Long, (1996), "Predictive models for deterioration of concrete structures", Construction and Building Materials, Vol. 10, No.I, pp. 27-37, 1996.
- 30. **B. Gérard and J. Marchand**, (2000), "Influence of cracking on the diffusion properties of cement-based materials- part I: Influence of continuous cracks on the steady regime", Cement and concrete Research 30, pp. 37-43.
- 31. **H. Won Song, S. Jun Kwon, K. Joo Byun et C. Kyu Park**, (2005), "Predicting carbonation in early-aged cracked concrete". Cement and Concrete Research 36, pp. 979–989.
- 32. **S. Alahmad, A. Toumi, J. Verdier, R. Francois**, (2009), "Effect of crack opening on carbon dioxide penetration in cracked mortar samples", Materials and Structures, 42: 559–566.
- 33. **A. Castel, R. Francois, G. Arliguie**, (1999), "Effect of loading on carbonation penetration in reinforced concrete elements", Cement and Concrete Research 29, pp. 561–565.
- 34. **F.Y. Houst and F.H. Wittmann**, (1989) "Retrait de carbonatation", In I.A.B.S.E, 255-260, Lisbonne.

- 35. **S. E. Pihlajavaara**, (1968), "Some results of the effect of carbonation on the porosity and pore size distribution of cement paste", Materials and Structures, 1(6): 521-526.
- 36. **N. Hyvert**, (2009), "Application de l'approche probabiliste à la durabilité des produits préfabriqués en béton", Thèse de l'Université PaulSabatier Toulouse III.
- 37. **S. Alahmad**, (2009), "Traitement des fissurations dans les ouvrages hydrauliques", Thèse de l'Institut National Des Sciences Appliquees de Toulouse.
- 38. V. Mohan Malhotra, Min-Hong Zhang, Paul H. Read, and John Ryell, (2000), "Long-Term Mechanical Properties and Durability Characteristics of High-Strength/High-Performance Concrete Incorporating Supplementary Cementing Materials under Outdoor Exposure Conditions", ACI Materials Journal, V. 97, No. 5.
- 39. **J. Jerga**, (2004), "Physico-mechanical properties of carbonated concrete", Construction and Building Materials 18, pp. 645–652.
- 40. **R. da Silva CA, R. RJP, FS Lameiras, WL Vasconcelos**, (2002), "Carbonation-related microstructural changes in long-term dura-bility concrete", Mater Res; 5(3):287–93.
- 41. **W. Zhang, X. Song, X. Gu, S. Li**, (2012), "Tensile and fatigue behavior of corroded rebars", Construction and Building Materials 34, pp. 409–417.
- 42. N. M. Ihekwaha, B. B. Hope and C. M. Hansson, (1996), "Carbonation and Electrochemical Chloride Extraction from Concrete", Cement and Concrete Research, Vol.26, No. 7, pp. 1095-1107.
- 43. **B. Johannesson, P. Utgenannt**, (2001), "Microstructural changes caused by carbonation of cement mortar", Cement and Concrete Research, Volume 31, Issue 6, Pages 925–931.
- 44. **P. A. Claisse, H. El-Sayad, and I. G. Shaaban**, (1999), "Permeability and Pore Volume of Carbonated Concrete", ACI Materials Journal, V. 96, No. 3.
- 45. **V. T. Ngala and C. L. Page**, (1997), "Effects of carbonation on pore structures and diffusional properties of hydrated cement pastes", Cement and Concrete Research, Vol. 27, No. 7, pp. 995-1007.
- 46. **T. A. El Maaddawy, K. A. Soudki**, (2003), "Effectiveness of impressed current technique to simulate corrosion of steel reinforcement in concrete", Journal of Materials in Civil Engineering, Vol. 15, No. 1.
- 47. Y. Yuan, Y. Ji, and S. P. Shah, (2007), "Comparison of two accelerated corrosion techniques for concrete structures", ACI Structural Journal, V. 104, No. 3.

- 48. **C. Alonso, C. Andrade, J. Rodriguez, J. M. Diez**, (1998)," Factors controlling cracking of concrete affected by reinforcement corrosion", Materials and Structures, Vol. 31, pp 435-441.
- 49. **L. J. Parrott**, (1990), "Damage caused by carbonation of reinforced concrete", Materials and Structures/ Materiaux et Constructions, 23, 230-234.
- 50. **R. Balasubramaniam, A. V. Ramesh Kumar and P. Dillmann**, (2003), "Characterization of rust on ancient Indian iron", Current science, Vol. 85, No. 11.
- 51. **D. C. Cook**, (2005), "Spectroscopic identification of protective and non-protective corrosion coatings on steel structures in marine environments", Corrosion Science 47, pp. 2550–2570.
- 52. **D.C. Cook, S.J. Oh, R. Balasubramanian and M. Yamashita**, (1999), "The role of goethite in the formation of the protective corrosion layer on steels", Hyperfine Interactions 122, pp. 59–70.
- 53. **R.M.** Cornell, U. Schwertmann, (1996), "The Iron Oxides, Structure, Properties, Occurrence and Uses", VCH Verlagsgesellschaft mbH, Weinheim, FRG.
- 54. **D. L. A. de Faria, S. Venancio Silva and M.T. de Oliveira**, (1997), "Raman microspectroscopy of some iron oxides and oxyhydroxides", Journal of Raman Spectroscopy, Vol. 28, 873-878.
- 55. F. R. Pérez, C. A. Barrero, K. García, A. H. Higth Walker, (2010), "Raman Microscopy as a Tool for the Rust Composition Distribution Analysis", Revista Colombiana de Física, Vol. 42, No. 2.
- 56. **X. Kui, D. Chao-fang, L. Xiao-gang, W. Fu-ming**, (2008), "Corrosion products and formation mechanism during initial stage of atmospheric corrosion of carbon steel", Journal of iron and steel research, International, 15(5):42-48.
- 57. **Y. Cudennec, A. Lecerf**, (2006), "The transformation of ferrihydrite into goethite or hematite, revisited", Journal of Solid State Chemistry 179, pp. 716–722.
- 58. **D. L. A. De Faria, S.V. Silva, M. T.d. Oliveira**, (1997), "Raman microspectroscopy of some iron oxides and oxyhydroxides", J. Raman Spectroscopy. Vol.28, 873–878.
- 59. A. Demoulin, C. Trigance, D. Neff, E. Foy, P. Dillmann, V. L'Hostis, (2010)," The evolution of the corrosion of iron in hydraulic binders analysed from 46-and 260-year-old buildings", Corrosion Science 52, pp. 3168–3179.

- 60. V. L'Hostis, D. Neff, L. Bellot-Gurlet, P. Dillmann, (2009), "Characterization of long-term corrosion of rebars embedded in concretes sampled on French historical buildings aged from 50 to 80 years", Materials and Corrosion, 60, No. 2.
- 61. **G. S. Duffó, M. Reinoso, C.P. Ramos, S.B. Farina**, (2012)," Characterization of steel rebars embedded in a 70-year old concrete structure", Cement and Concrete Research 42, pp. 111–117.
- 62. M. Yamashita, H. Miyuki, Y. Matsuda, H. Nagano and T. Misawa, (1994), "The long term growth of the protective rust layer formed on weathering steel by atmospheric corrosion during a quarter of a century", Corrosion Science, Vol. 36, No.2, pp.283-299.
- 63. **K. Asami, M. Kikuchi**, (2003), "In-depth distribution of rust on a plain carbon steel and weathering steels exposed to coastal-industrial atmosphere for 17 years", Corrosion Science 45, pp. 2671–2688.
- 64. S. J. Oh, D.C. Cook, H.E. Townsend, (1999), "Atmospheric corrosion of different steels in marine, rural and industrial environments", Corrosion Science. 41, pp. 1687–1702.
- 65. **T. Kamimura, S. Nasu, T. Tazaki, K. Kuzushita, S. Morimoto**, (2002), "Mossbauer spectroscopic study of rust formed on a weathering steel and a mild steel exposed for a long term in an industrial environment", Materials Transactions, Vol.43, No.4, pp.694 to 703.
- 66. **D. de la Fuente, I. Díaz, J. Simancas, B. Chico, M. Morcillo**, (2011), "Long-term atmospheric corrosion of mild steel", Corrosion Science 53 (2011) 604–617.
- 67. E. Almeida, M. Morcillo, B. Rosales and M. Marrocos, (2000), "Atmospheric corrosion of mild steel: Part I-Rural and urban atmospheres", Materials and Corrosion 51, 859-864.
- 68. **Ph. Dillmann, F. Mazaudier, S. Hærle**, (2004), "Advances in understanding atmospheric corrosion of iron. I. Rust characterisation of ancient ferrous artefacts exposed to indoor atmospheric corrosion", Corrosion Science 46, pp. 1401–1429.
- 69. **I. Suzuki, Y. Hisamatsu and N. Masuko**, (1980), "Nature of Atmospheric Rust on Iron", J. Electrochem. Soc. Volume 127, Issue 10, Pages 2210-2215.
- 70. **B. Huet**, (2005), "Comportement à la corrosion des armatures dans un béton carbonaté. Influence de la chimie de la solution interstitielle et d'une barrière de transport", Thèse de l'INSA de Lyon.

- 71. V. L'Hostis, C. Emptaz, C. Paris, L. Bellot-gurlet, (2012), "Complete characterization of steel corrosion within reinforced concrete slabs in various environments", NUCPERF 2012, Cadarache-France.
- 72. **D. Emeline**, (2010), "Impact de la température sur la carbonatation des matériaux cimentaires-prise en compte des transferts hydriques", Thèse de l'ecole normale supérieure de Cachan.
- 73. **D. Neff, S. Reguer, L. Bellot-Gurlet, P. Dillmann and R. Bertholon**, (2004), "Structural characterization of corrosion products on archaeological iron: an integrated analytical approach to establish corrosion forms", J. Raman Spectroscopy; 35: 739–745.
- 74. L. Bellot-Gurlet, D. Neff, S. Réguer, J. Monnier, M. Saheb and P. Dillmann, (2009), "Raman studies of corrosion layers formed on archaeological irons in various media", Journal of Nano Research, Vol. 8, pp 147-156.
- 75. G. E. Badea, P. Cret, M. Lolea, A. Setel, (2011), "Studies of carbon steel corrosion in atmospheric conditions", ACTA Technica Corviniesis-Bulletin of engineering, Tome IV.
- 76. **Y. F. Houst**, (1996), "The role of moisture in the carbonation of cementitious materials", Internationale Zeitschrift für- Bauinstandsetzen-2. Jahrgang, Heft 1, pp. 49-66.
- 77. **L. Ying-Up and W. Qiu-Dong**, (1987), "The Mechanism of Carbonation of mortars and the dependence of carbonation on pore structure", ACI structural journal, SP 100-98, pp. 1915-1944.
- 78. **J. Chen Jeffrey, J. Thomas Jeffrey, F.W. Taylor. Hal, M. Jennings Hamlin**, (2004), "Solubility and structure of calcium silicate hydrate", Cement and Concrete Research 34, pp. 1499 1519.
- 79. **F. P. Glasser and T. Matschei**, (2007), "Interactions between Portland cement and carbon dioxide", 12th International Congress on the Chemistry of Cements, Montreal.
- 80. **R. Winston Revie, Herbert H. Uhlig**, (2008), "Corrosion and corrosion control, 4th Edition", A John Wiley & Sons, Inc., Publication.
- 81. **C. Andrade, C. Alonso, J. Sarria**, (2002), "Corrosion rate evolution in concrete structures exposed to the atmosphere", Cement & Concrete Composites 24, pp. 55–64.
- 82. M. Morcillo, B. Chico, D. de la Fuente, and J. Simancas, (2012), "Looking Back on Contributions in the Field of Atmospheric Corrosion Offered by the MICAT Ibero-American Testing Network", International Journal of Corrosion, Article ID 824365, 24pages.

83. M. Stratmann, K. Bohnenkamp, and T. Ramchandran, (1987), "The influence of copper upon the atmospheric corrosion of iron," Corrosion Science, vol. 27, no. 9, pp. 905–926.

III.2. CORROSION IN CHLORIDE ENVIRONMENT IN THE PRESENCE OF CRACK

III.2.1. Introduction

Chloride-induced corrosion of steel reinforcement is one of the major threats to durability of RC structures in a marine environment. Many researchers have carried out the tests on concrete structure members to assess the quantification of residual service life. The concrete is undoubtedly the best protection for steel against corrosion due to the high pH of its interstitial solution present in the porosity. However, cracks, which are inevitable in practice, facilitate the transport of chloride ions, moisture and oxygen initiating the steel corrosion faster than in uncracked-concrete. Especially, if the cracks are interconnected, the concrete becomes more permeable and then corrosion progress is much more rapid. The presence of cracks in concrete structures is supposed to lead to at least three significant effects [1]: (1) a privileged access to chlorides and CO₂ to depassivate the steel reinforcement at the bottom of cracks, (2) a privileged access to oxygen contributing to the acceleration of the corrosion process (cathodic current), (3) they lead to a physical and chemical heterogeneousness of steel bar likely to favour the corrosion process.

Theoretically, two corrosion mechanisms can be happend to steel in reinforced concrete:

- (1) macro-cell corrosion (or galvanic corrosion) in which the steel at the bottom of the depassivated crack is an anodic zone and the steel between the cracks, which is steel passivated, is an oxygen consuming cathodic zone. The quality and cover concrete thickness intervene to limit the access of oxygen to the cathodic zone.
- (2) micro-cell corrosion (or pitting corrosion) in which the anodic and cathodic zones are side by side. This case should correspond to a more generalized depassivation of the steel.

Even if it is not to be excluded that this type of corrosion can appear at the bottom of crack on condition that oxygen can enter through the crack. The pitting distribution then has a relationship with the heterogeneousness of the steel bars or the steel bar-concrete interface (presence of voids).

It is to be noted that in the presence of chlorides, both types of corrosion can cause the localized weight loss that can commonly called the pitting corrosion. It also should be remarked that both types of corrosion could occur simultaneously.

The evolution of corrosion of steel embedded in non-cracked concrete can be divided into two phases, the initiation period and the propagation period (Fig.III-21a) [2]. During the initiation period, chloride ions, water and oxygen penetrate through the concrete cover to the steel reinforcement. The initiation period will finish when the aggressive agents in a threshold value reach the level of the steel bars, breaking the passive layer on surface of steel. After that, an active corrosion is taken place (propagation period) at which corrosion products cause concrete cracking and even leading to spalling of concrete cover. In case of cracked concrete structure, Raoul Francois and Ginette Arliguie [3] suggested a model for corrosion process with four periods, the incubation period, the initiation period, the induction period and the propagation period. Because of the presence of cracks, the chloride ions penetrated preferentially through the crack path and reached early the threshold value (about 0.4% per cement mass) at reinforcement steel level, resulting in the initiation phase. After that, corrosion products fill the crack tip and then reduce greatly the corrosion rate: it is the induction phase which duration is influenced by exposure conditions. Development of corrosion products along the steel-concrete interface could lead or not lead to the formation of corrosion cracks. These corrosion cracks are at the beginning very short and very narrow (hairline cracks) but it allows access for aggressive agents, humidity and oxygen to the reinforcement and the corrosion process was spread: it is the propagation phase of corrosion. During propagation phase, the corrosion cracks progressively interconnect and widen along the rebars. The fact is that it is not easy to separate accurately between the end of induction phase and the beginning of propagation phase. Along corroded reinforcement steel, some locations could be in the induction phase but another location could be in the propagation phase. It is the same for initiation phase: some locations of rebars (basically crack tip) are depassivated but other locations are still passivated.

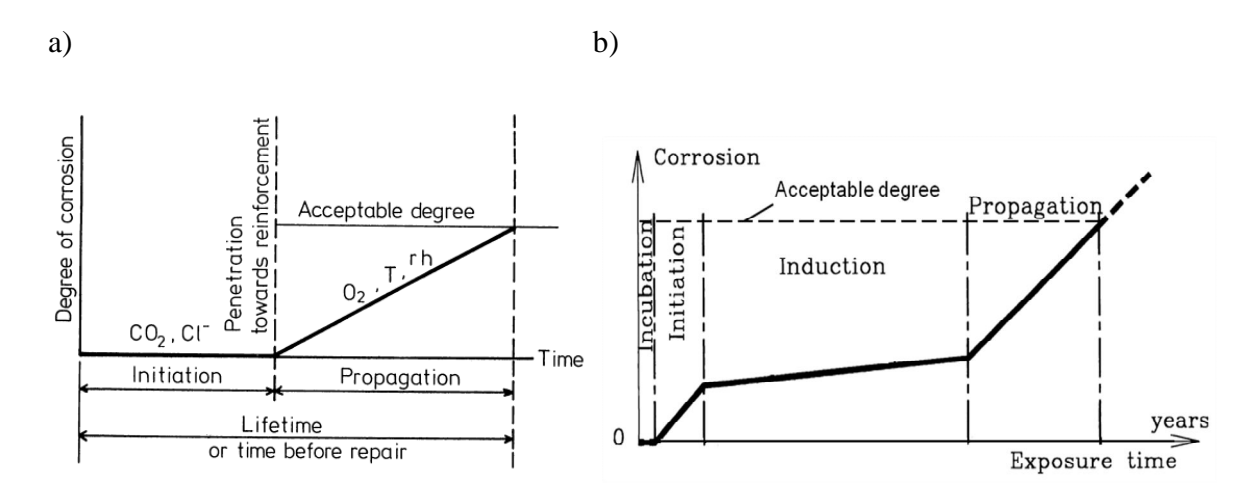


Fig.III-21.Comparison between steel corrosion process of non-cracked concrete (a) [2] and cracked concrete (b) [3]

There are a lot of factors affecting chloride-induced corrosion in cracked concrete structures such as the permeability of concrete cover, water-cement ratio, cement type, interface between steel bar and concrete. Nevertheless, in this part, only effect of pre-cracks on corrosion of steel bars embedded in concrete exposed to saline environment is discussed. The pre-cracks herein are ones in tensile zone due to applying load on structures.

III.2.2. Influence of pre-cracks

III.2.2.1 Influence of pre-cracks on transfer of chloride

In the presence of cracks, the effect of the aggressive environment must be taken into account, either chlorides or carbon dioxide, even if in both cases there is a restriction of the penetration into cracks below a certain opening threshold.

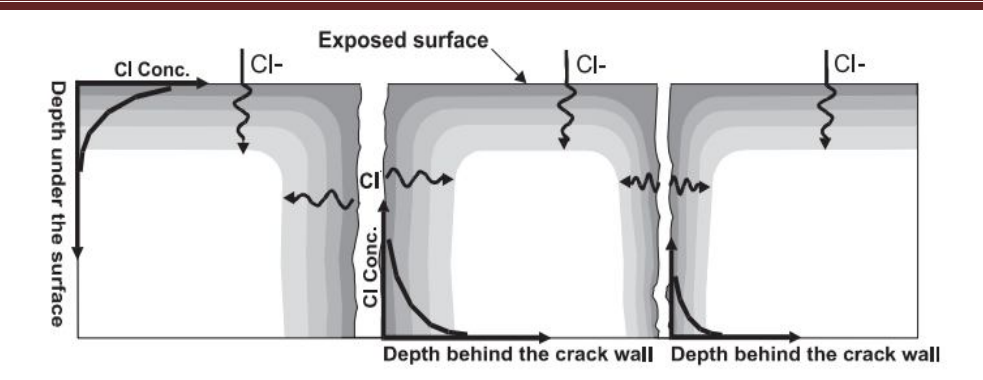


Fig.III-22.Measurement of total chloride profiles from outer surface or from the fracture surfaces [4, 5]

The penetration of chlorides perpendicular to crack plane (Fig.III-22) is delayed in cracks with an opening less than the critical mechanical opening, which corresponds to the end of interaction phenomenon between the edges of the crack. Indeed, M. Ismail et al. [5] measured the chloride penetration profiles on 16 disk-shaped mortar samples, cracked by mechanical load. These mechanical cracks with openings varying from 6 to 325 µm were radial. The total chloride penetration profiles, measured from both the sample surface and perpendicular to crack walls, are shown in Fig.III-23. It could be seen that in case of cracks with crack widths of 55 µm or less, the perpendicular-to-crack profiles are very similar to the base profile of the reference mortar. This finding suggested that the crack opening of 55 µm or less is the threshold value, below which chloride diffusion along the crack path is delayed. The authors studied on mortar samples of 28 days and 2 years old concluded that for crack opening lower than the critical mechanical opening (30 µm), no chloride diffusion take places perpendicular to crack plane, regardless the age at which the crack was induced. It should be noticed that this restriction of the diffusion perpendicular to the crack plane does not correspond to an absence of diffusion in the crack path: it means that diffusion do not lead to the same boundary conditions in crack path as outside. In others words, below the critical mechanical opening, the crack surfaces are still in interaction and then the diffusion in crack path is restricted.

More global studies were made of large sized samples (reinforced concrete beams) that were subjected to bending moment with cracks of a width of up to 0.5 mm by R. Francois and J.C.

Maso [6] or up to 0.25 mm by Y. D. Yan et al [7]. In both studies, the conclusion was that the presence of cracks and tensile stress between the cracks had an effect on the penetration of chloride ions.

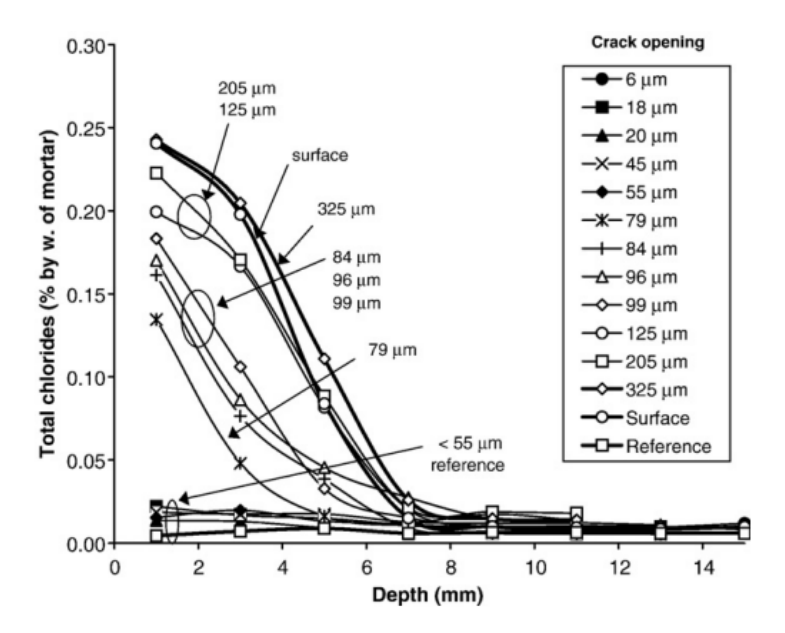


Fig.III-23. Perpendicular-to-crack plane chloride penetration profiles, surface profile and reference profile in samples cracked for ring samples maintained in a saline condition of 14 days [5]

III.2.2.2 Influence of transversal pre-crack width

Probably one of the most debated matters related to the embedded reinforcement corrosion with the presence of cracks is the limitation of surface crack widths, which influences the corrosion process. In order to control the corrosion of steel reinforcement under chloride environment, many researchers have been conducted the relationship between corrosion process and the surface crack width. While it is generally agreed that the laboratory studies indicated the cracked concrete leads to more rapid initiation of corrosion [8-15]. On-field observations [16] also confirmed this point. Therefore, for short-term and low-level of corrosion, the presence of cracks affects the corrosion. However, for medium-or long-term corrosion (propagation period of corrosion), there is still debate about the influence of cracks

on corrosion propagation. On the one hand, some researchers state that the crack width has no influence on corrosion rate.

Beedy. A.W. [10] found in a number of investigations, which were focused on establishing a correlation between crack width and corrosion that there are no reasons to believe in the corrosion rate to be affected by crack width except the larger cracks. He supported his point of view by reviewing the information from many published data. Fig.III-24 is a typical example.

Similarly, R. François and G. Arliguie [9] carried out an experiment program for over 12 years on reinforced concrete beams of 3 m in length, cross-section of 150x280 mm under varied loading states in a chloride environment. The results were monitored at different periods: 3 months, 6 months, 1 year, 5 years, 6 years, 7 years, 11 years and 12 years of exposure. At each of terms, cracking maps were carefully drawn for each beam. After 6 years kept in a confined salt fog, the B2 beam having the width of cracks from 0.05 mm to 0.25 mm was appeared the longitudinal cracks, parallel to secondary re-bar in upper of the beam. Whereas, the A2 beam with larger width of cracks (between 0.05 mm and 0.5 mm) presented no new cracks. From testing results of A and B beams, they concluded that the crack width has no impact on the development of reinforcement corrosion for widths less than 0.5 mm. It is also noted that this value gained from a long term experiment program that used large size of RC beams as in-service structures under both loading and corrosion. In addition, the corrosion process is very close to natural corrosion.

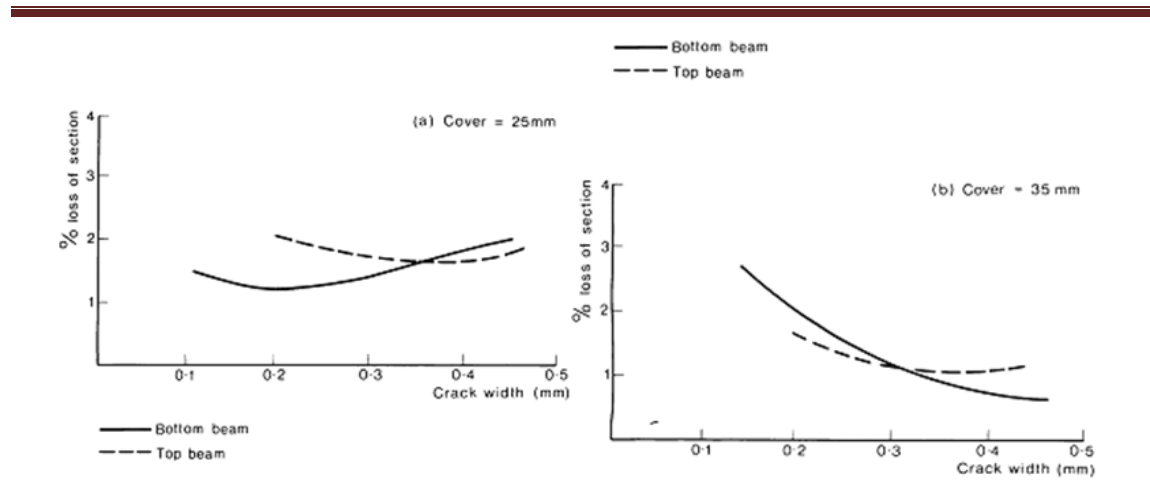


Fig.III-24. Influence of crack width on corrosion in marine environment after 10 years [10]

In a study by Tarek Uddin Mohammed et al [15], the specimens with dimensions of 150 x 150 x 1250 mm and crack widths in ranging 0.1 to 0.4 mm were tested after keeping in a closed saltwater chamber with automatic wetting-drying cycles for 13 weeks. The corroded area of steel bars was recorded at different crack locations on beams. The results shown that the crack widths cannot be correlated to corrosion areas. The presence of a crack irrespective of its width is much more important to cause embedded corrosion of steel bars. Likewise, w/c ratio plays a significant role for onset of corrosion. This was also confirmed by Peter Schießl and Michael Raupach [12]. In their study, a wider crack width lead to increased corrosion of steel bar, but for long term the concrete cover and the concrete composition had a greater impact on corrosion than the surface crack width because the crack width decreased during the time of exposure due to self-sealing phenomenon of crack. No significant correlation between crack width and corrosion rate was found.

On the other hand, some authors maintain that there is an effect of cracks on both initiation and propagation period. N. Otsuki et al. [17] conducted experimentally the influences of bending crack and water-cement ratio (w/c) on the chloride-induced corrosion on main reinforcing bars and stirrups on RC beams of size 150 x 150 x 1250 cm. The specimens were exposed outdoors for 13 weeks. During the exposure period, salt water (NaCl 3.5 wt%) was sprayed at the bottom surface of each specimen everyday. An important effect of flexural

crack and water-cement ratio on corrosion rate was recorded. At intersection between main steel, stirrups and cracks, macrocell corrosion occurred and corrosion rate becomes large in microcell zones.

M.B. Otieno et al. [18] investigated the influence of crack width on corrosion process using 100x100x500 mm long beam specimens with crack widths of 0.4 mm, 0.7 mm and incipient cracks. These beams were then submitted to a weekly cyclic wetting-drying with 5% NaCl solution for around 16 weeks. They concluded that the presence of cracks affects the corrosion development, both initiation and propagation and the corrosion rate increased with increasing surface crack width.

One important point which need to be clarified in the future is the fact that the use of an impressed electric field could force the creation of corrosion cracks and then do not allow the existence of the induction period resulting of cracks healing.

Generally speaking, the corrosion always starts at the bottom of the cracks and the wider cracks will lead to the more rapid initiation corrosion but the propagation of corrosion process linked to the cracks is still under debate.

III.2.2.3 Influence of crack frequency

The diffusion of chloride into cracked concrete depends not only on the surface crack width but also on the number of cracks present along the length of members (crack frequency). In fact, Eurocode 2 [19] gives a relation between the crack width and maximum crack spacing, i.e. the crack width assumed as a function of crack spacing or crack frequency.

A study on the influence of crack frequency on steel bar corrosion in concrete was carried out by C. Arya and F.K. Ofori-Darko [13]. In their work, two series of reinforced concrete beams were selected: A beam has 100 x 135 x 1360 mm long, containing 0,1,4,8,12,16 or 20 parallel cracks, 40 mm deep; B beam has 170 x 150 x 4000 mm long, containing 9 cracks which simulated by nine 10 mm long mild steel segments located along central axis of beams. Beams were accelerated corrosion by spaying 3% NaCl solution for 24 months while B beams were accelerated corrosion by mixing the concrete with 5% NaCl by weight of

cement. From this study, the researchers concluded that the increasing of crack frequency results in an increase of corrosion rate except in the case of 20 cracks where the self-healing process was active in some of the cracks. In other words, the smaller the number of cracks the smaller the amount of corrosion. This work has shown that the crack frequency is more important than the surface crack width to control the steel corrosion. Nevertheless, the procedures of this test indicated that the cracks are smooth, straight and have the same depth along the beam that is not in reality. The process of self-healing could take place at intersecting cracks if loading is constant or unloading does not happen. This also does not occur in practical structures. As a result, the effect of crack frequency observed in this study is far from real.

Crack frequency is also connected to tensile concrete between two consecutives mechanical cracks. In fact, after cracking, the concrete is stiffened by the rebars that operate as tie rods. This phenomenon that leads to the stiffening of concrete structures is called the Tension Stiffening Effect, and can lead to another cracking of covering concrete (cover cracking) that is detrimental to durability because it corresponds to a more diffuse damage to the cover concrete [27, 28]. Indeed, cathodic zone corresponding to steel bar located between cracks could be "feed" by oxygen because of this cover cracking phenomena.

III.2.2.4 Influence of longitudinal crack

The longitudinal cracks, parallel to the reinforcing bars, usually occur in practice in the concrete structures such as continuously reinforced concrete pavements, steel reinforced concrete pipes and parking garage slabs.

Amir Poursaee and Carolyn M. Hansson [20] carried out tests on prismatic concrete samples of size 100 x 100 x 500 mm with crack widths of approximately 0.1 mm parallel (longitudinal cracks) and right angles (transverse cracks) to the re-bar. The goal of this study is to compare the behavior corrosion of steel bar in longitudinally cracked concrete with transversely cracked concrete. Two types of concrete, High Performance Concrete (HPC) and Ordinary Portland Concrete (OPC), were used. The specimens were exposed to a de-icing salt environment for 128 weeks or 124 weeks. They found that, in specimens with 0.1mm

longitudinal crack, there is no significant difference in the corrosion rate between HPC and OPC. This can be explained as the steel bars in concrete is in contact directly with the aggressive environment on very large areas, and therefore the same corrosion level. In contrast, for samples with transverse crack, the steel in HPC exhibits a corrosion rate at least five times lower than that of steel in OPC. The reason is that area of steels taking part in corrosion process for the anodic and cathodic half-cell components was restricted. It was concluded that while the longitudinal cracks have no important effect on corrosion rate irrespective of cement type, the transverse cracks affect significantly corrosion rate for each cement type. Nonetheless, these findings were obtained on beams with one single crack and loading is constant. It is expected that results will be different in case of many cracks under a variable load, which is more close to reality.

III.2.2.5 Influence of crack depth

The effect of crack depth on chloride penetration depth in concrete was shown in Fig.III-25, reviewing from L. Marsavina et al.'s study [21]. The authors made the artificial cracks on concrete cores with a diameter of 100 mm and a height of 50 mm by means of the positioning and removal after approximately 4 h of thin copper sheets inside the specimen. These copper sheets had a thickness of 0.2 mm, 0.3 mm and placed at a depth in the concrete of 5 mm, 10 mm, 15 mm or 20 mm. These specimens afterwards were tested under NT BUILD 492 1999 method.

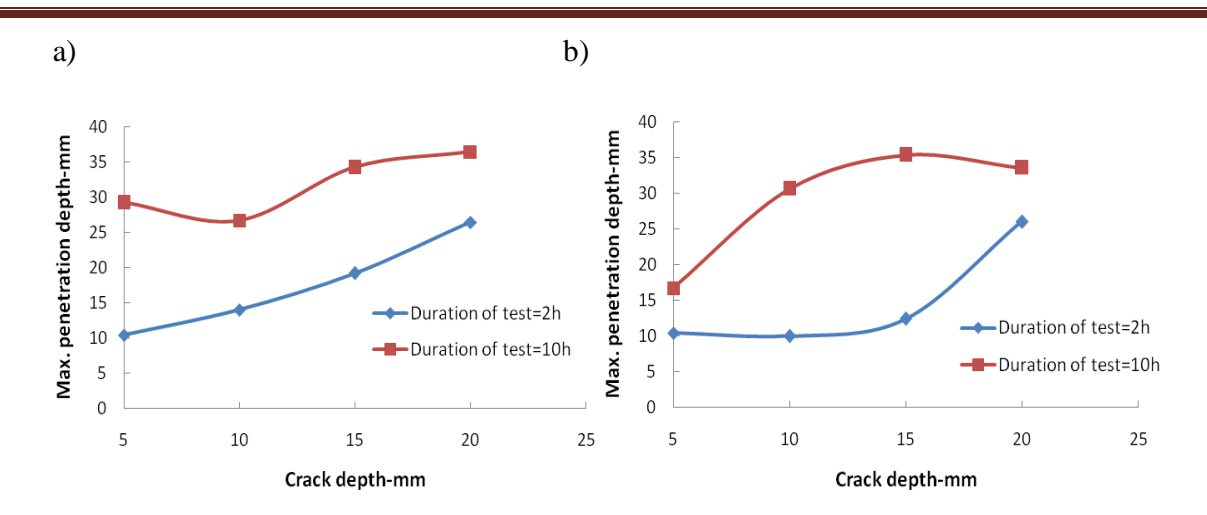


Fig.III-25. Maximum penetration depth for crack width a) 0.2mm; b) 0.3mm [21]

From this figure, it could be seen that if the exposure time is longer (10h), the crack depth is more important than crack width. A higher chloride penetration depth was noted for a higher crack depth. However, it should be emphasized that cracks is artificial ones (notches) with constant width and constant depth. It is very different from the cracks of real concrete structures.

III.2.3. Steel corrosion in presence of cracks in chlorides

III.2.3.1 Corrosion initiation at crack location

In saline environment, the penetration of chlorides into the cracks is delayed for cracks with an opening less than the critical opening (according to rupture mechanics definition), which corresponds to the end of the interaction phenomenon between the edges of crack (see Fig.3). However, despite this delay, the corrosion mechanism is still the same. The corrosion process initiates at the bottom of the crack when the critical chloride concentration level is reached at this location. A very fast initiation of corrosion is observed whatever the opening of the cracks. The transfer limitation of chloride appears in ranging of 40-50 µm, and therefore the standard limitation for crack width is given in some codes as Eurocode 2 [19] cannot prevent the initiation of corrosion. The corrosion then spreads over a few millimeters (10-15 mm) along the rebar from intersecting point with the crack because of the mechanical

damage to the rebar concrete interface, which is generated by the creation of the crack (see Fig.III-26). Thus, depending on environment conditions, the corrosion can stop or spread leading to the formation of corrosion cracks due to the pressure applied on the covering concrete by the corrosion products.





Fig.III-26. Corrosion initiation at the bottom of cracks and along the rebar-concrete interface by the creation of cracks [22]

All studies available in the literature have confirmed an early initiation of corrosion in the presence of cracks [1, 3, 8, 10-16, 23]. This result is logical as the presence of cracks has a significant effect on the penetration of aggressive agents.

III.2.3.2 Propagation of corrosion at crack location

The corrosion always starts at the bottom of cracks, but the propagation of the corrosion linked to the presence of crack (spread phenomenon) is still under debate as discussed earlier in III.2.2. It should be remarked that the propagation or "stop" of corrosion is linked to corrosion kinetics, the "stop" of corrosion corresponding to very low kinetics. The conclusion obtained by the different researchers can change one way or the other depending on the experimental conditions. It should also be borne in mind that the major part of the studies on this subject are carried out in accelerated conditions using an impressed current for short periods of a few weeks or a few months. Indeed, artificial corrosion using impressed current lead to uniform corrosion along the steel bars while the corrosion mainly occurs on the surface of steel that is close to concrete cover under an artificial climate or natural environment [24].

The type of environment needs to take into consideration: permanently saturated (immersed structures), or variable conditions (aboveground structures). Immersed conditions are not being dangerous due to the lack of oxygen, which limits the cathodic reactions. We will focus on aboveground concrete with no saturated limit conditions.

In the case of exposure to chlorides, the research work carried out in an impress electric field and those in climate natural conditions must be separated. Nevertheless, the exposure related to gravity must also be taken into consideration. In fact, the classic crack due to bending moment located in the bottom part of a beam (positive bending moment) do not have the same risk of corrosion as those that arrive in the upper part (negative bending moment). The face of the upper part of a beam is directly exposed to more severe environment during wet periods. The accumulation of chlorides on the upper face is more than this of lower face, leading the chloride content reaches quickly the critical value and the corrosion will propagate earlier. Further discussion on it is in chapter IV, section IV.3.

R. Francois et al. [22] also highlighted the corrosion spread phenomenon form mechanical origin cracks on small mortar samples. This study is based on the original experimental approach using the expansive core, developed by Gagné. R et al. [25], to cause the controlled cracking (in terms of crack width) in a ring of reinforced mortar. The cracks can be assimilated to those obtained on the tie rod rather than on a bending beam. In fact, the orthoradial quasi- uniform stress state leads to almost constant crack widths in the height. Once cracked the ring-shaped mortar samples were subjected to saline solution cycles to accelerate corrosion but without an impressed current. A total of 25 samples were tested. These tests made it possible to obtain a certain number of results relative to the spread of corrosion in the case where the cracked surface is horizontal and exposed to chlorides:

- The corrosion initiates quickly opposite the cracks, even when the cracks have an opening of less than 40 μ m. For the uncracked samples, the visual observation shown neither any visible steel corrosion nor any corrosion crack as shown in Fig.III-27.



Fig.III-27. Uncracked sample kept for 500 days in a wetting-drying in saline environment: no corrosion or no corrosion crack [22]

- The creation of corrosion cracks is preferably in the bottom of crack where the steel-concrete interface was previously damaged due to creation of mechanical cracks.
- Cracking caused by corrosion is quicker if the pre-existing cracks are wider, which can be explained by the easier access for chlorides and oxygen (Fig.III-28).
- The creation of corrosion cracks appears to be time dependant of the loading level and then of the maximal mechanical crack opening.
- In the long term, when the corrosion has spread, the effect of mechanical origin cracks diminishes.

a) b)





Fig.III-28. Spread of corrosion along the rebar-concrete interface (duration 500 days) a) from a 28 μm opening crack; b) from a 280 μm opening crack [22]

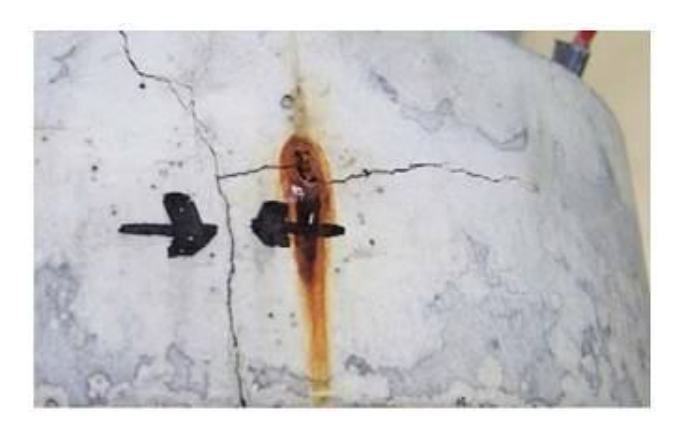


Fig.III-29. Creation of corrosion cracks from the intersection with transverse mechanical crack with reinforcement (duration 800 days) [22]

The propagation of corrosion in pre-cracked RC structures, is linked to the possible repassivation of the rebars at the bottom of crack that can take place after the corrosion has initiated. The variable test conditions in the literature lead to two types of opposing results:

cracking has a significant effect on the spread of corrosion, or on the contrary, has no effect on the spread of corrosion. Research programs which are carried out under an impressed current lead to the first conclusion, i.e. cracks favor propagation of corrosion, while studies which are carried out in natural environment or accelerated climate conditions lead mostly to the second conclusion, i.e. cracks do not correspond to immediate propagation of corrosion: It correspond to the induction phase proposed by François and Arliguie [3]. Nevertheless, It would seem that for natural corrosion (in situ) the case of cracks arriving on a horizontal surface exposed to chlorides is the more favorable for the spread of corrosion by allowing the fast growth of corrosion cracks. However, for this extreme case, the spread of corrosion occurs even for very fine cracks, with an opening of less than 50 µm. The control of cracking within the current maximum crack width proposed by most standards is therefore totally irrelevant. It should be noticed that ACI standard [26] do not limit the crack opening to protect RC structures from corrosion. ACI reminds that the role of cracks in reinforcement corrosion is controversial. ACI quotes the references of Darwin. D. et al. [29], Oesterle. R.G. [30] showed the absence of correlation between crack openings measured at the surface of concrete (in the usual range corresponding to the rebar stress for service loads) and corrosion, to justify the absence of limitation on crack openings. Other ACI's argument is to note that the openings of cracks in concrete structures are highly variable from one structure, or element of structure, to the next. It is therefore pointless to try and control their openings.

References

1. **B.. A, Diamond. S and N. Berke** (1997), "Steel corrosion in concrete, fundamentals and civil engineering practice", E&FN Spon, London, pp. 41-43.

- 2. **K. Tuutti** (1980), "Service life of structures with regard to corrosion of embedded steel", ACI journal, SP 65-13, pp. 223-236.
- 3. **R. Francois, Ginette Arliguie** (1994), "Durability of loaded reinforced concrete in chloride environment", ACI journal, SP 145-30, pp. 573-596.
- 4. **M. Ismail, A. Toumi, R. Francois, R. Gagne** (2004), "Effect of crack opening on the local diffusion of chloride in inert materials", Cement and Concrete Research 34 (2004) 711 716.
- 5. **M. Ismail, A. Toumi, R. Francois, R. Gagne** (2008), "Effect of crack opening on the local diffusion of chloride in cracked mortar samples", Cement and Concrete Research 38 (2008) 1106–1111.
- R. Francois, J. C. Maso, (1988), "Effect of damage in reinforced concrete on carbonation or chloride penetration", Cement and Concrete Research, Vol. 18, pp. 961-970.
- 7. Y. D. Yan, W. L. Jin, J. Chen, (2012), "Experiments of chloride ingression in flexural reinforced concrete beams", Advances in structural engineering Vol. 15 No.2 2012.
- 8. **R. François, J.C. Maso,** (1988), "Effect of damage in reinforced concrete on carbonation or chloride penetration", Cement and Concrete Research, 18, 961–970.
- 9. **R. Francois, G. Arliguie,** (1999), "Effect of microcracking and cracking on the development of corrosion in reinforced concrete members", Magazine of Concrete Research, 51, 143–150.
- 10. **A.W. Beeby,** (1983), "Cracking cover & corrosion of reinforcement", Concrete International 02, pp.35-40.
- 11. **T. Lorentz, C. French,** (1995), "Corrosion of reinforcing steel in concrete: Effects of materials, mix composition, and cracking", ACI Materials Journal, 92,181–190.
- 12. **P. Schießl & M. Raupach,** (1997), "Laboratory studies and calculations on the influence of crack width on chloride-induced corrosion of steel in concrete", ACI Mater Journal, 94, 56–62.
- 13. **A. Arya, F. Ofori-Darko,** (1996), "Influence of crack frequency on reinforcement corrosion in concrete", Cement and Concrete Research, 26, 345–353.

- 14. S. Yoon, K. Wang, W. Weiss & S. Shah, (2000), "Interaction between loading, corrosion, and serviceability of reinforced concrete", ACI Materials Journal, 97, 637–644.
- 15. **T. U. Mohammed, N. Otsuki, M. Hisada, and T. Shibata,** (2001), "Effect of crack width and bar type on corrosion of steel in concrete", Journal of Materials in Civil Engineering, 13, 194–201.
- 16. **M. Makita, Y. Mori & K. Katawaki,** (1980), "Marine corrosion behavior of reinforced concrete exposed at Tokyo Bay", ACI SP-65: Perf of Concrete in Marine, Environment, 271–90.
- 17. N. Otsuki, S. Miyazato, N.B. Diola, and H. Suzuki, (2000), "Influences of Bending Crack and Water-Cement Ratio on Chloride-Induced Corrosion of Main Reinforcing Bars and Stirrups", ACI Materials Journal, V. 97, No. 4, pp. 454-464.
- 18. M. B. Otieno, M.G. Alexander & H.D. Beushausen, (2009), "Corrosion propagation in cracked and uncracked concrete", 2nd International Conference on Concrete Repair, Rehabilitation and Retrofitting, ICCRRR-2, 24-26 November 2008, Cape Town, South Africa, pp. 339–344.
- 19. **BS EN 1992-1-1 Eurocode 2**: design of concrete structures-Part 1: General rules and rules for buildings, November 2002.
- 20. **A. Poursaee, C. M. Hansson,** (2008), "The influence of longitudinal cracks on the corrosion protection afforded reinforcing steel in high performance concrete", Cement and Concrete Research 38, 1098–1105.
- 21. L. Marsavina, K. Audenaert, G. De Schutter, N. Faur, D. Marsavina, (2009), "Experimental and numerical determination of the chloride penetration in cracked concrete" Construction and Building Materials 23, 264–274.
- 22. **R. Francois, I. Khan, N.A. Vu, H. Mercado and A. Castel,** (2012), "Study of the impact of localized cracks on the corrosion mechanism", European journal of environment and civil engineering, DOI:10.1080/19648189.2012.667982.
- 23. **M.B. Otieno, M.G. Alexander, H.D. Beushausen**, (2010), "Corrosion in cracked and uncracked concrete influence of crack width, concrete quality and crack reopening", Magazine of Concrete Research, Volume 62, Issue 6, pages 393 –404.

- 24. **Y. Yuan, Y. Ji, S.P. Shah,** (2007), "Comparison of two accelerated corrosion techniques for concrete structures", ACI Struct J;104(3).
- 25. **R. Gagné, R. François, P. Masse,** (2001), "Chloride penetration testing of cracked mortar samples". In: Banthia N, Sakai K, Gjory OE Concrete under severe conditions, vol 1. University of British Columbia, Vancouver, pp 198–205.
- 26. **ACI 318-05, Building code requirements for structural concrete,** American Concrete Institute, Farmington Hills, Mich.
- 27. A. Castel, R. François, (2011), "Modeling of steel and concrete strains between primary cracks for the prediction of cover controlled cracking in RC beams, Engineering Structures, Vol. 33, Issue 12, pp. 3668-3675.
- 28. **R. I. Gilbert,** (1999), "Flexural Crack Control for Reinforced Concrete Beams and Slabs: An Evaluation of Design Procedures", ACMSM 16, Proceddeings of the 16th Conference on the Mechanics of Structures and Materials, Sydney, Balkema, Rotterdam, pp. 175-180.
- 29. **D. Darwin et al.**, (1985), "Debate: Crack Width, Cover, and Corrosion", Concrete International, V. 7, No 5, American Concrete Institute, Farmington Hills, MI, pp.20-35.
- 30. **R.G. Oesterle,** (1997), "The Role of Concrete Cover in Crack Control Criteria and Corrosion Protection", RD serial No 2054, Portland Cement Association Skokie, IL.

Chapter IV:

EXPERIMENTAL PROGRAM IN CHLORIDE ENVIRONMENT

GENERAL

The purpose of this chapter is to summarize the experimental programs on "natural" corroded RC beams in France. The several important results are underlined. A new test program is built up, including twelve RC beams with the same dimension as the "old beams" cast in 1984 at LMDC. The difference between new RC beams (2010) and old RC beams (1984) is that the cracked-face positions are inverted during the corrosion process. The corrosion process of new RC beams is regularly monitored by video microscopy. The corrosion initiation and propagation of new beams are observed. The effects of cover concrete and top-cracked faces exposed directly to salt water are analyzed.

IV.1. Literature review on the experimental program on pre-stressed RC beams of Rance (Benchmark des poutres de la Rance)

IV.1.1 Presentation of the Benchmark

This French national project is based on a long-term experimental program started 1962 by the "Union Technique Interprofessionnelle des Fédérations Nationales du Bâtiment et des Travaux Publics". Initially 40 prestressed concrete beams were cast and stored in marine environment (Rance dam). In 1976, these beams were moved to the Sainte Anne du Portzic harbour (IFREMER, Brest), in a tidal zone. The objective of this project is to improve the knowledge of the uncertainties due to numerical simulations and measurements: (i) by quantifying the differences between the modeling and the experimental results, (ii) by evaluating the loss of safety margins of reinforced concrete structures exposed to corrosion, (iii) by improving knowledge on the main corrosion parameters influencing the mechanical behavior (reduction of the rebar section and/or reduction of the steel-concrete bond and/or ductility) and (iv) by promoting the validation of some future mechanical models based on the experimental database obtained during this project [1].

The Benchmark is divided into three steps:

CHAPTER IV: Experimental program in chloride environment

- 1) An experimental program has been designed to evaluate the corrosion influence on the mechanical behavior. Two types of mechanical tests have been defined: (i) direct tensile tests (ii) 4-point-bending tests. The results of mechanical tests were kept secret during the numerical simulations even though the distribution of corrosion has been known,
- 2) Various partners have computed the mechanical behavior of the beams under tensile and flexural tests,
- 3) Experimental results and numerical simulations have been compared and analyzed. Conclusions are focused on the pertinence and reliability of the tested mechanical models.

Two types of tests were performed: direct tensile test and bending test. The 4-point bending tests are common experiments in the literature and can simulate quite accurately the behavior of a beam. Meanwhile, few references are available in the literature on the behavior of such structural components in direct tensile test configuration. To give the essential information for a better knowledge of cracking, tensile tests had been performed on several beams. Moreover, some RC beams were selected to test under monotonic and cyclic loadings. Totally, 10 pre-stressed beams were used for assessing the mechanical behavior after 40 years exposure period in marine environment: 4 direct tensile tests, including 2 monotonic tests, 2 cyclic test; and 6 tests in 4-point bending, including 2 monotonic tests, 4 cyclic test [2].

IV.1.2 Materials and layout of RC beams

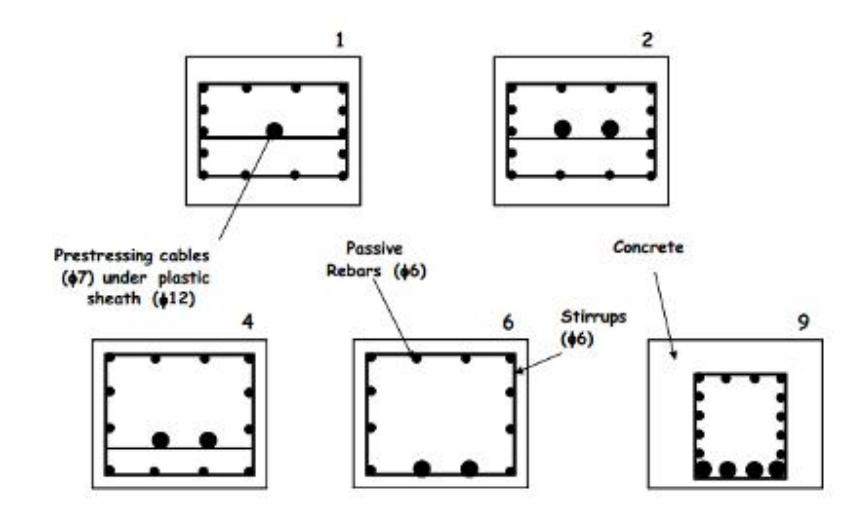
Four concrete types were used as indicated in table IV-1 [1]. Table IV-2 shows the initial porosity (% by volume) and the results of mechanical tests at 28 days [2].

Table IV-1. Composition of concrete mixture [1]

Concrete	Total	Cement	Aggregates grading (kg/m³)			w/c
type	water (l)	(kg/m ³)	Sand 0/5	Gravel 10/25	Gravel 5/15	W/C
1.1	210	300	800	930	320	0.700
1.2	210	400	550	930	290	0.525
2.1	220	300	500	1350	/	0.733
2.2	250	400	450	1350	/	0.625

Table IV-2. Properties of concrete at 28 days [2]

Concrete type	1.1	1.2	2.1	2.2
Porosity (%)	16.4	17	15.3	17.9
Compression strength (MPa)	22.38	29.26	16.5	16.71
Flexure strength (MPa)	2.16	2.28	1.9	1.86



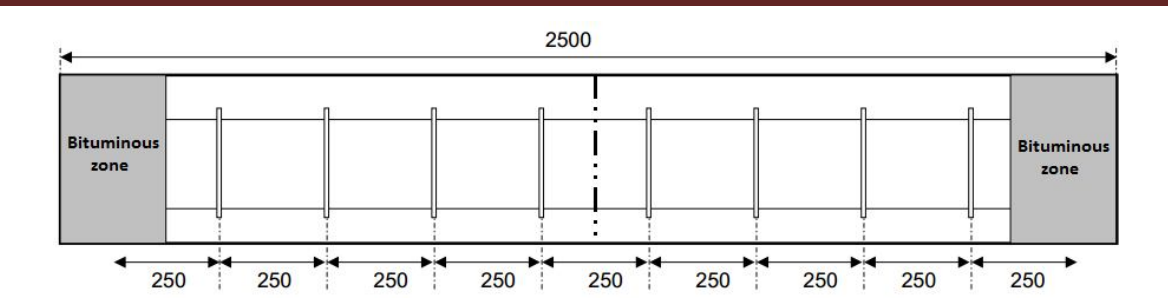


Figure IV-1. Configurations of reinforcement steel for pre-stressed beams [2]

The concrete was pre-stressed with wires,7 mm in diameter, embedded in a plastic sheath, 12 mm in diameter, and anchored at the beam ends. For beams of type 1 and 2, pre-stressed wires were centered along the axis of the beam whereas they were in the lower part of the beam for the beams of type 4, 6 and 9 as indicated on Figure 1.

IV.1.3 Principal results

IV.1.3.1 Mechanical properties of concrete

Table IV-3 summarizes the results of tests on samples of beams after 40 years of exposure in natural marine environment.

Table IV-3. Properties of concrete after 40 years of exposure [2]

	Concrete type			
	1.1	1.2	2.1	2.2
Compression	49.1	68.1	42.9	47.5
strength (MPa)	±6	±4.9	±4.1	±3
Split test (MPa)	5	6.2	5.7	4.8
	±0.6	±1.1	±1	±1.2
Direct tensile test	2.7	3.1	1.8 (1 measurement)	2.7
(MPa)	±0.2	±0.8		±0.4
Elastic modulus	34.7	38.6	30.5	33.1
(GPa)	±2.4	±2.2		±3.4

IV.1.3.2 Mechanical properties of steel bars

Table IV-4 indicates the average values (from three samples) of main characteristics (yield stress, tensile strength and modulus of elasticity) of different steels used in RC beams.

Steel type	Yield stress (Mpa)	Ultimate stress (Mpa)	Young Modulus (Gpa)
Passive steel	309±4	399±17	195±1.5
Prestressing steel	1304±2	1394±21	187±5.4

Table IV-4. Characteristics of two steel types [2]

Figure IV-2 shows the stress-strain curves (the deformation was measured via a strain gauge base 10 mm) for the two types of steel.

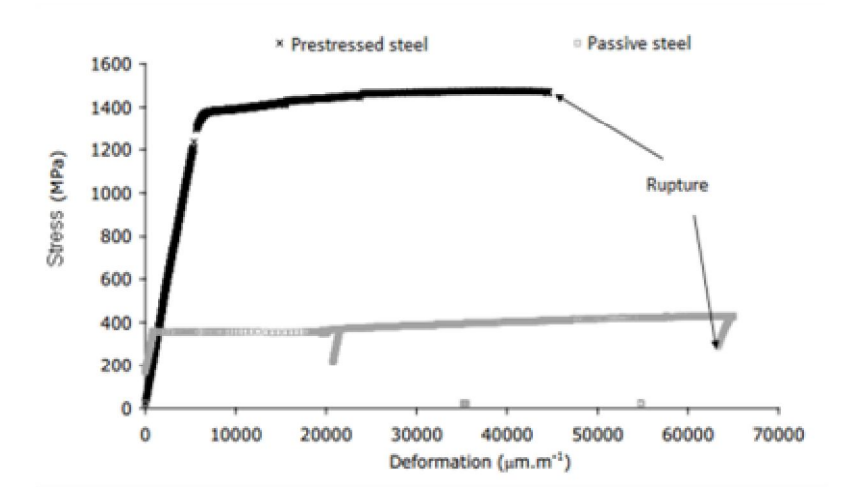


Figure IV-2.Stress-deformation relationship for two steel types [2]

IV.1.3.3 Mechanical behavior of beams

The beams were tested in 4-point bending tests. Bending tests performed on non-centered pre-stressed beams. Two configurations had been conducted: a) in PC configuration (Pre-stressed Concrete), b) in RC configuration (Reinforced Concrete) (Figure IV-3).

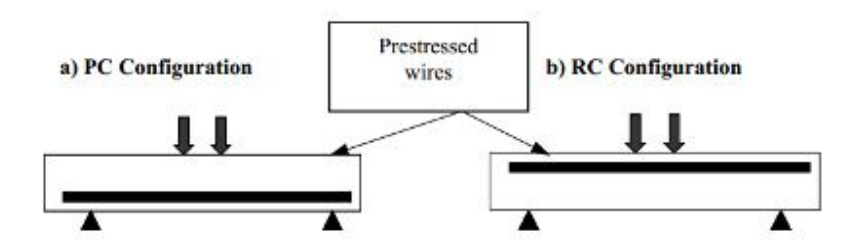


Figure IV-3. Two configurations of the bending test

In the RC configuration, the pre-stressing cables are located in the compressed concrete zone. This approach allows studying the influence of the corrosion of reinforcement bars on the mechanical behavior of the beam (considering that the pre-stress effect is negligible). In the PC configuration, the pre-stressing cables are located in the tensile concrete zone and contribute to the mechanical strength during these tests [2].

The Laboratoire Matériaux et Durabilité des Constructions (L.M.D.C Toulouse) is one of eight partners participated to the numerical simulations. The model that developed by François. R et al. [5] described the mechanical behavior under service and rupture load of pre-stressed concrete elements damaged by corrosion. The model is based on the formulation of a macro-element to be used in FEM analysis, having a length equal to the distance between two consecutive flexural cracks and a cross section equal to the member cross-section. The model allows taking into account the combined effect of the reduction of cross section and the debonding due to corrosion in the mechanical behavior of reinforced concrete members. Moreover, this model considers the tension-stiffening effect by using a transfer length. Table IV-5 provides information related to the macro-element finite (MEF) model used for simulations. The theoretical model approach, the concrete and the steel models and corrosion introduction are listed [1].

Approach	Concrete constitutive law	Steel constitutive law	Concrete- steel bond	Corrosion effect on steel behavior	Model
Local transfer of strain and Strength of materials	Non linear constitutive law	Elastic perfectly plastic diagram	Variable on transfer length	Cross section loss and bond	FE (macro element)

Table IV-5. Information used in MEF

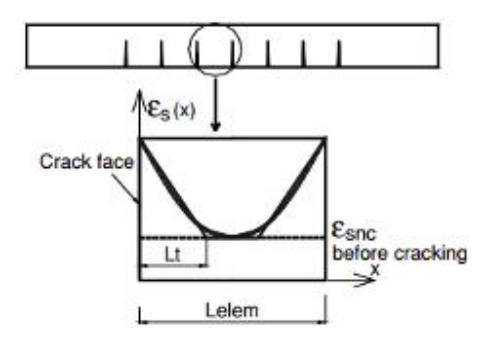


Figure IV-4. Typical tensile reinforcement strain profile between two bending cracks. $\varepsilon_s(x)$ is strain of tensile steel between two cracks and ε_{snc} is strain in the absence of crack [5]

Figure IV-4 describes the typical strain profile in reinforcement located between two flexural cracks on the length of a macro element (L_{elem}). The transfer length L_t is minimum length from crack face to location where the bond stress between the steel and the concrete reaches maximum value. By assuming that strain variation steel and the variation of the height of the neutral axis are linear along the transfer length, the average inertia of the macro-element as well as flexural curvature $\chi(x)$ for a given abscissa of the macro-element is calculated. In case of corroded beams, the new transfer length taking into account corrosion is called L_{tcor} .

$$L_{\text{tcor}} = \left(\frac{L_{t}}{1 - D_{c}}\right) \tag{1}$$

Where, D_c is a scalar bond damage parameter; D_c = 0 there is no damage due to corrosion and L_{tcor} = L_t , D_c = 1 there is total damage of the bond between re-bar and concrete and L_{tcor} = ∞ .

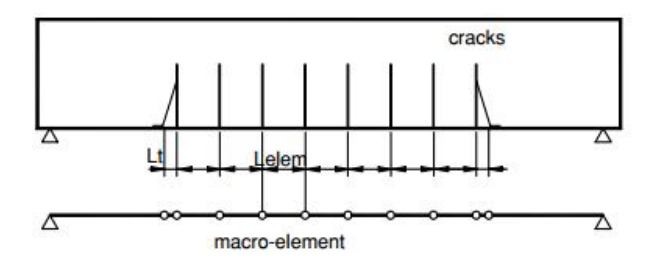


Figure IV-5. Mesh of a reinforced concrete beam using macro elements [5]

In the application of this model, the bond stress is modified via D_c if there is a corrosion crack.

The calculation of the global mechanical behavior of reinforced concrete members is performed by assembling the macro-elements defined between consecutive cracks, plus one L_t length macro-element at each boundary of the cracked zone as shown in figure IV-5.

Concerning to the corroded RC beams of Benchmark under bending test, an example of the comparison between experimental behavior and modeling behavior for RC configuration are present in figure IV-6 [4]. Figure IV-7 presents an example of the load-mid span deflection curve for corroded beams tested in PC configuration. As mentioned above, it is necessary to know the transfer length between steel bar and concrete for each macro element. The transfer length can be determined by testing in tension the prismatic samples as described in [5]. In the absence of measurement, the L_t conventional value of 100 mm is used.

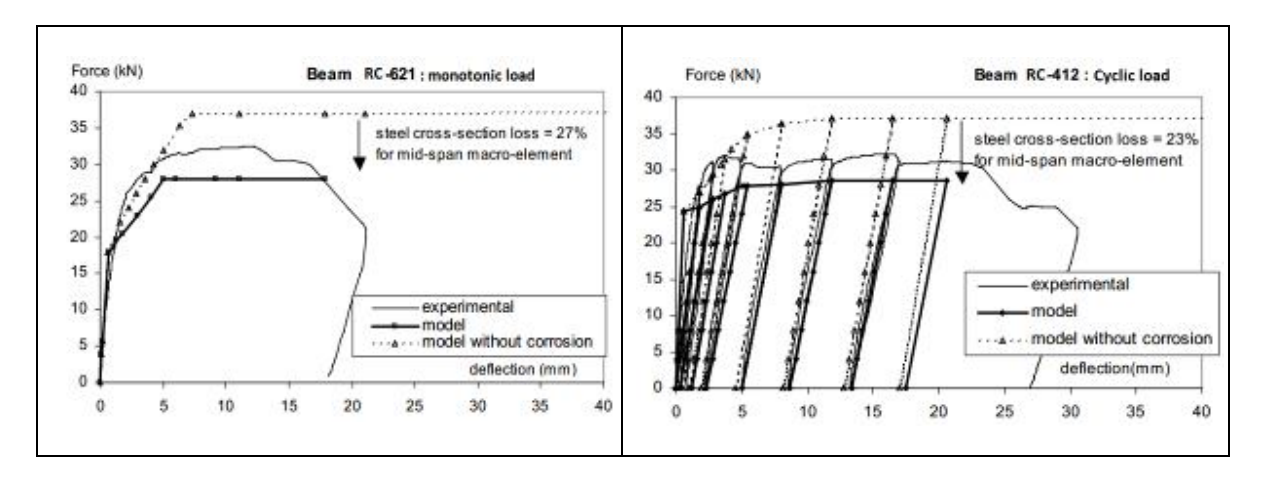


Figure IV-6.Force-Deflection for the 4-points bending test (RC configuration) [4]

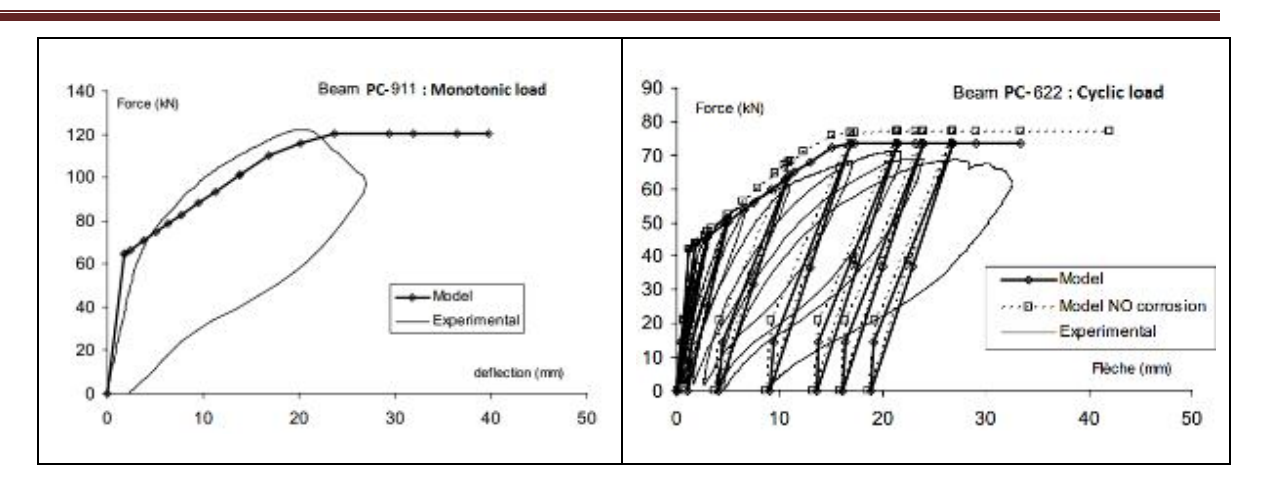


Figure IV-7. Force-Deflection for the 4-points bending test (PC configuration) [4]

The simulations showed the low impact of reinforcement corrosion on the behavior of corroded elements. This low impact is due to the low level of both pitting corrosion and cracking due to corrosion pitting. Thus, much of corrosion reinforcement was not taken into account for the calculation of the debonding. Furthermore, the use of passive rebar with small diameter (d=6mm) is certainly the reason. The numerical simulations are in agreement with experimental results, especially in the cyclic behavior.

IV.1.3.4 Chloride profiles

Ten pre-stressed concrete beams were used to characterize the materials properties and to estimate the aggressive species penetration (chloride profile and carbonation depth). For all tests, the maximum carbonation depth is about 1 mm. Powdered concrete samples were taken for determining "total" and "free" chloride contents and estimating chloride penetration profiles at different locations on the beams according AFPC-AFREM recommendations [7]. Two samples were taken from two locations along the tensile area. The extractions of "total" chlorides were obtained by mixing 5 g concrete powder with saturated nitric acid [6]. Total chloride content is expressed in percent cement mass. A characteristic chloride profile of a concrete structure exposed in tidal marine environment is observed with a maximum value at about 10 mm from the top surface and a slight decrease within bulk structure. Figure IV-8 shows the chloride concentration at the reinforcing bars depth. It can see the measured values (2–4.5% cement mass) exceed the threshold limit (0.5

-1.5%) generally pointed out in literature [7]. Therefore, the active corrosion due to chloride ingress can take place at reinforcing steel surface. The results indicate that the thickness of concrete cover and w/c are important factors determining the ability of chloride and oxygen to access to the rebars surface and developing corrosion process.

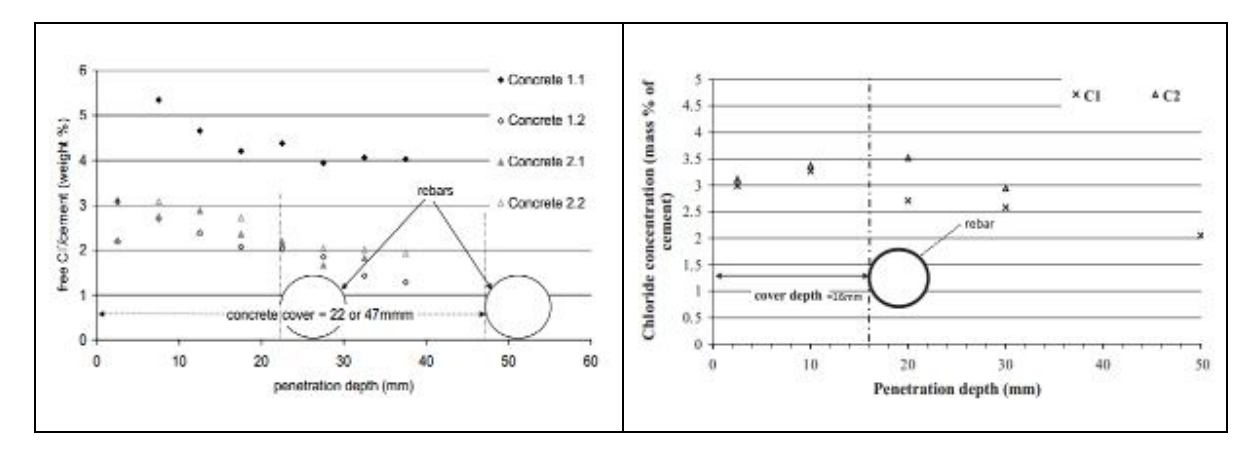


Figure IV-8. Chloride profile at different concrete depths after 40 years of exposure [3, 6]

IV.2. Synthesis of the experimental program on RC beams at the L.M.D.C-Toulouse (since 1984 to present)

IV.2.1 Experimental context

In 1984 in particular, the LMDC began a long-term study of corrosion by François. R [8]. A batch of 36 RC beams of common dimensions (15 x 28 x 300 cm) as supplied by industry and cast with two different section types, A and B, were kept in a chloride environment under sustained loading.

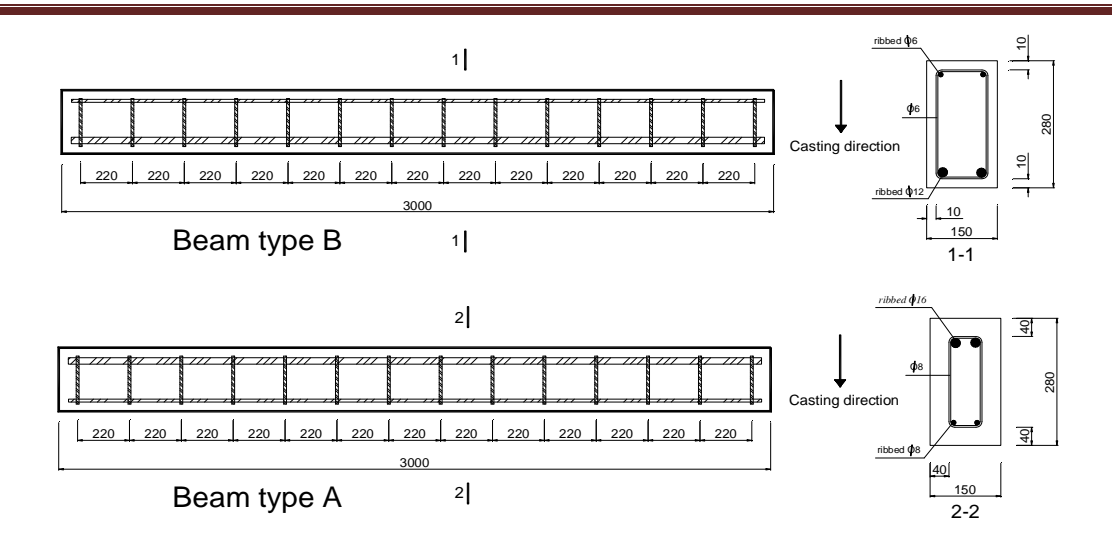


Figure IV-9.Layout of reinforcements for A and B old beams

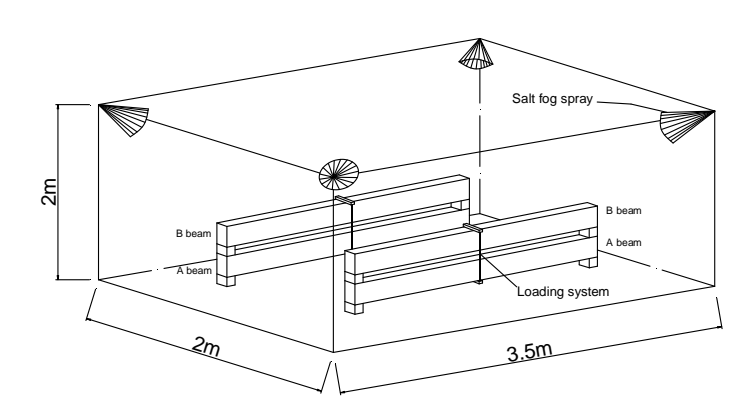


Figure IV-10.Loading system and environmental exposure of old beams

The initial objective of the study was to understand the relationships between service cracking (structural) in reinforced concrete and the corrosion of the rebars. In fact, building codes limit the opening of structural cracks in order to obtain a sufficient service life in an aggressive environment without being based on a sufficiently relevant experimental base (currently only the ACI regulations do not impose a limit to openings for corrosion risks). To assess the relevance of applicable regulations a first type of beam (called A) was therefore designed in relation to the Service Limit State Design (SLS) for highly prejudicial cracking: maximum cover 4 cm (currently this would be 5 cm), limitation of the applicable service load via the maximum stress of tensioned rebars at the bottom of structural cracks (176

MPa), minimum diameter of transverse rebars (8 mm); and a second type of beam (called B) was designed for the least unfavorable Ultimate Limit State (ULS): minimum cover 1 cm (currently this would be 2 cm), minimum transverse rebar diameter 6. All the A beams were cast in an inverted position with their tensile steel reinforcement in the top of the form, the compressive steel in the bottom of the form (Figure IV-9).

Both types of beam were then coupled by using the loading system. For all couples, A beams were underlain B beams during the first 19 years of corrosion process as displayed in Figure IV-10. The aggressive environment was a saline environment with a chloride concentration equivalent to the salt concentration of Atlantic Ocean (35 g/l). The beams were subjected to wetting-drying cycles in order to accelerate the corrosion process as given in Table IV-6.

Wetting-drying **Periods Temperature-climate** Loading cycles Continuous spraying 20°C-in the lab First 6 years yes 1 week-spraying 20°C-in the lab From 6 to 9 years yes 1 week-drying from -5° to 35°C-in South-west of 1 week-spraying From 9 to 19 years yes 1 week-drying France from -5° to 35°C-in South-west of From 19 to 26 Stopped no France years from -5° to 35°C-in South-west of 2 days-spraying From 26 to present no 2 week-drying France

Table IV-6. Environmental exposure of beams

IV.2.2 Principal results

IV.2.2.1 Mechanical behavior of beams

Many publications related to the mechanical performance of corroded beams in this program have been published [9-16]. More discussions are presented in sec. I.2.

IV.2.2.2 Chloride profiles

A. Castel et al. [14] studied experimentally the chloride profile on B1CL beam after 14 years stored in saline condition. Concrete samples were taken using a profile grinder. Samplings were made at 10 cm at least far from concrete cracking (transversal cracks or longitudinal corrosion cracking). Concrete powders were taken in different locations along the tensile reinforcements from an end of beam until the mid-span of beam.

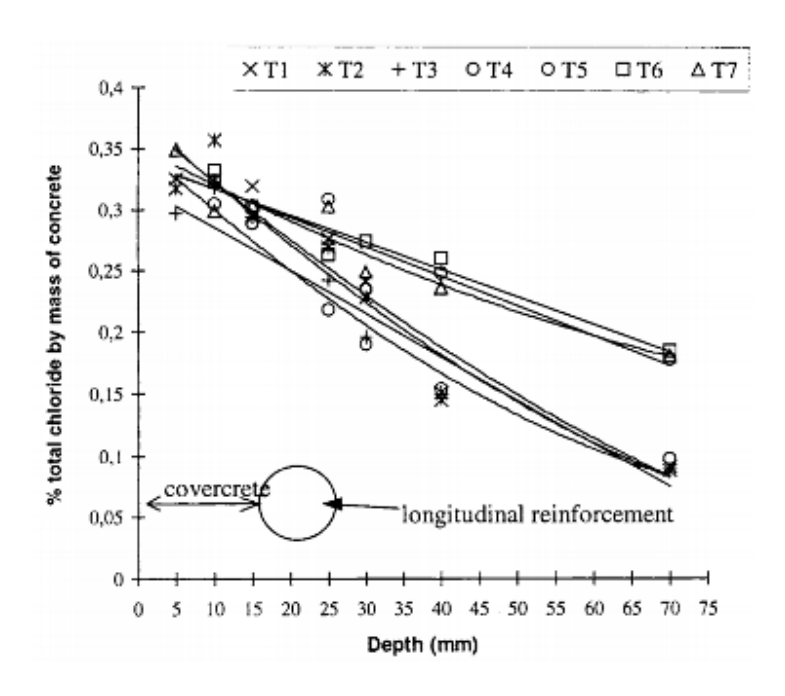


Figure IV-11. Total chloride profiles measured along B1CL beam tensile zone [14]

It can see that the chloride content at 16 mm depth exceeds the 0.05% acceptable value by mass of concrete (0.325% by cement weight). Two families of curves observed on figure IV-11: the first profiles measured on locations T1, T2, T3, T4 at which the bending moment was low and the second family measured on locations T5, T6 and T7 at which the bending moment was high. The total chloride content measured at mid span is more important than that at ends of beam. This means that a strong influence of the mechanical loading on the chloride transfer into concrete must be taken into account when predicting the RC-structure lifetime.

T. Vidal et al. [11] reported the chloride profile through concrete cover against time on B2CL2 beam. At the age of 5 years, drilling was used to collect powder from a circular area

of 10mm diameter, at different depths. At the age of 14 and 17 years, concrete samples were collected using the profile grinder method. Concrete powders were taken in a compressive and a tensile concrete area located in the central part of the beam, at the depth of the reinforcements, i.e. 16mm. Samples were collected from at less 50mm from any concrete crack (corrosion or flexural cracks). Figure IV-12 shows the total chloride content at the level of rebars in the compressive and tensile zone of beam at 5 years, 14 years and 17 years of exposure.

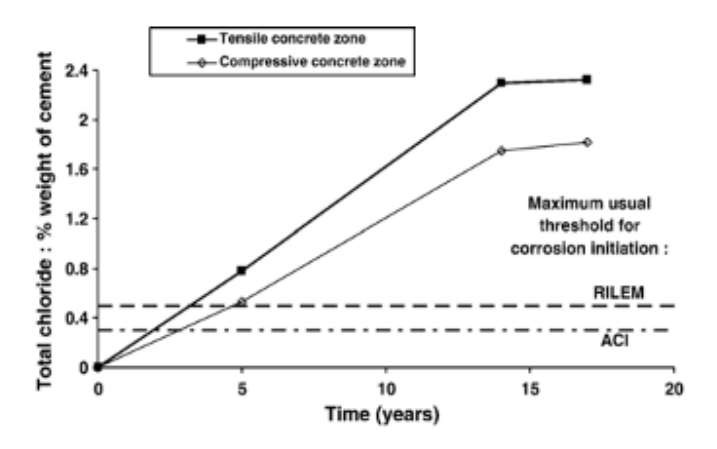


Figure IV-12. Total chloride content at the depth of the reinforcement (16 mm) in the compressive and tensile zone of the corroded beams [11]

After 5years, the chloride content reached and exceeded the RILEM and ACI threshold values, respectively 0.5% and 0.3% by weight of cement, generally used to forecast corrosion initiation in reinforced concrete. The total chloride content seems to increase faster in the tensile zone. This is probably due to a mechanical damage of the tensile concrete, which leads to a significant increase of the chloride diffusion coefficient [14]. Between 14 and 17 years, the total chloride tends to stabilize. In particular, the value seems to reach a maximum chloride threshold that can be contained by the concrete. They suggested that whatever the location, compressive or tensile zones, the concrete is saturated with chloride after 14 years.

IV.2.2.3 Using crack width due to corrosion to predict the reinforcement corrosion

T. Vidal et al. [15] investigated the corrosion crack width on two naturally corroded RC beams over periods of 14years (B1CL1) and 17years (A1CL1). The aim is to find a relationship between the distribution of reinforcement corrosion and the width of cover crack due to corrosion. They proposed a new model to predict the local cross section loss of steel bars from the crack width following two phases of the cracking process: initiation and propagation

✓ Cracking initiation

The local steel cross-section loss ΔA_{s0} that is necessary for cracking initiation can be calculated by Eq.2

$$\Delta A_{s0} = A_s \left[1 - \left[1 - \frac{\alpha}{\phi_0} \left(7.53 + 9.32 \frac{c}{\phi_0} \right) 10^{-3} \right]^2 \right]$$
 (2)

Where ϕ_0 is the bar diameter (mm); α is the pit concentration factor: α = 2 for homogenous corrosion and 4< α <8 for localized corrosion; c is the cover concrete (mm); ΔA_{s0} is the steel cross section loss (mm²); A_s is the sound steel cross section (mm²)

✓ Relation between crack widths and steel cross-section loss

During the propagation phase of corrosion crack, the crack width is proportional to steel cross-section loss. The empirical linear expression predicting crack propagation is given in Eq.3

$$w = K (\Delta A_s - \Delta A_{s0})$$
 (3)

Where w is the crack width (mm); ΔA_s is the steel loss of cross section (mm²); K = 0.0575

T. Vidal et al.'s model predicted well the link between the crack width developments and steel cross-section loss for both crack initiation step and crack propagation step. However, from monitoring on the steel bars of beam B1CL1 after 14 years and A1CL1 after 17 years of exposure, it could conclude that the localized corrosion was still the prominent pattern

along beam except in the central part where generalized corrosion was prominent. Thus, T. Vidal et al.'s model could conveniently use for the first phase of crack propagation due to localized corrosion.

R. Zhang et al. [16] who tested B2CL1 beam after 23years keeping in the chloride environment defined two steps in propagation phase. Indeed, the extensive general corrosion along the tensile reinforcements of B2CL1 beam corresponded to a general corrosion stage defined by authors as a second phase of crack propagation. Therefore, they had chosen the average cross-section loss parameter ΔA_{sm} between two stirrups instead of the local steel cross-section loss parameter ΔA_{s0} to express the prediction of crack propagation under the general corrosion pattern. The empirical equation for predicting the crack width under the general corrosion was as follows:

$$w = 0.1916 \Delta A_{sm} + 0.164 \tag{4}$$

Where w is the crack width (mm), ΔA_{sm} is the average cross-section loss (mm²)

This expression was derived from B2CL1 beam with 16mm of concrete cover to longitudinal reinforcement steels and 12mm steel diameter. R. Zhang et al.'s model did not consider the parameter c/ϕ as well as steel diameter when the new corrosion cracks appear during the second stage of crack propagation.

I.Khan [17] studied on A2CL3 beam at the age of 26years. The corrosion map and distribution of corrosion along tensile bars revealed that this beam was in the second stage of crack propagation. Nevertheless, because of the smaller concrete cover to reinforcement diameter ratio, the corrosion pattern of B2CL1 beam was more generalized than that of A2CL3 beam. If using eq.(4) to calculate the corrosion crack width, for the same average cross-section loss, the crack width is much wider in B2CL1 beam than in A2CL3 beam due to the difference in concrete cover thickness. The larger the concrete cover, the smaller crack width. In order to take into account the effect of c/ϕ and reinforcement diameter, I.Khan has modified the eq.(4) by multiplying ΔA_{sm} by ϕ/c ratio:

$$w = 0.1916 \frac{\phi}{c} \Delta A_{\rm sm} + 0.164 \tag{5}$$

For a given corrosion crack on the surface of concrete element, it is impossible to know whether the reinforcement corrosion embedded is in the "localized corrosion phase" or "general corrosion phase". Thereby, the eq. (3), (4) and (5) should be used together to determine the minimal and the maximal limits of reinforcement corrosion level to assess the change in mechanical behavior of the corroded structure.

IV.3. Experimental program conducted during this thesis at the L.M.D.C-Toulouse (since 2010 to present)

Based on the results and analyses of the side-effects induced by the design of the first experimental program at LMDC presented in previous section (IV.2), a new program was built in 2010. The main change is the location of type A and B beams in the salt fog chamber and also the casting direction for both types of beams according to the location of tension reinforcement. Indeed, opposite to previous program, new B beams are now at the top and A beams are at the bottom of the loading device; and top bar of B beams correspond to tension bar instead of compressive bars and top bar of A beams correspond to compressive bars. The main objective is to understand the effect of top surface corresponding to tension cracked surface on the corrosion development.

IV.3.1 Materials

The quantity of the concrete constituent was given in Table IV-7. A CEM I 52.5R cement (average particle size d_{50} of 14 μ m), river aggregates (0/4 mm fine aggregate (sand), 4/14 mm round coarse aggregate (gravel)) were used to design the concrete mixture in this experimental program. The average compressive strength and elastic modulus obtained cylindrical samples (110x220 mm) were 46 MPa and 33 GPa at age of 28 days in the curing room. The ordinary ribbed reinforcement steel (nominal yield strength f_y = 500 MPa) was used.

Table IV-7. Constituents of concrete mix (kg/m^3)

Mix composition	Aggregate size	
Rolled gravel (silica+limestone)	4/14 mm	1220
Sand	0/4 mm	820
Porland cement: OPC HP (high perform)		400
Water		200

IV.3.2 Details of beam

Similar to RC beams made in 1984 at the L.M.D.C, 12 RC beams with rectangular cross section of 150mm x 280mm dimension and length of 3000mm were cast in the mould as shown in Fig.IV-13. All the steel cages were prepared in the laboratory. Two types of beam: A beam and B beam as displayed in Fig.IV-14:

✓ A beam type (6 samples): each of beams was reinforced with two deformed reinforcements of 16mm diameter in tension zone and two deformed reinforcements of 8mm diameter in compressive zone. The stirrup was 8mm diameter deformed steel bars, 220mm center to center spacing along the whole length of beam. The cover thickness to stirrups was 40mm. Contrary to previous long-term program presented section IV.2, A beams were casted in "classical" way: i.e. tension reinforcement corresponds to bottom reinforcement.





Figure IV-13. Steel cages and mould used for beams

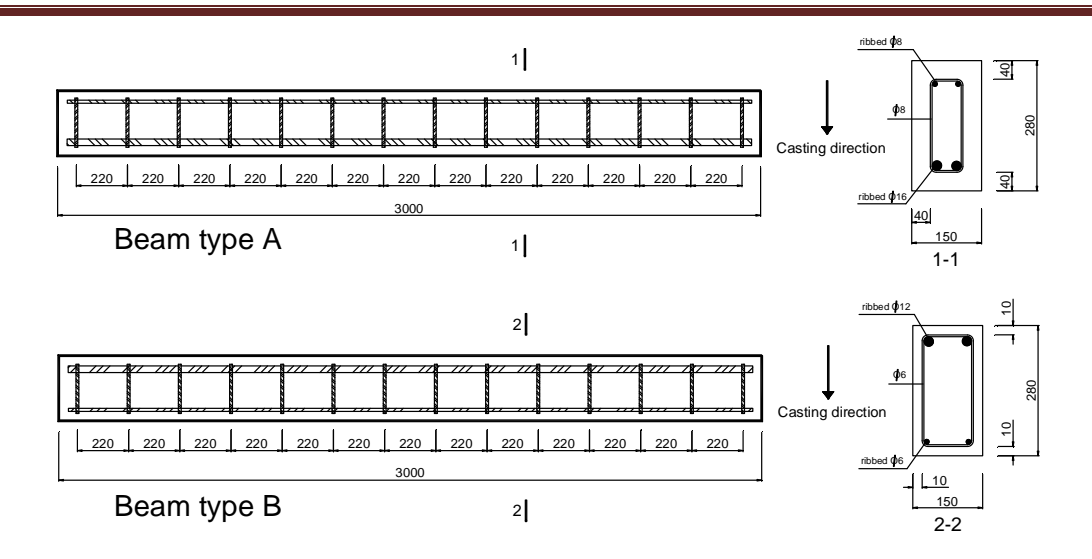


Figure IV-14. Dimensions and reinforcement details of new test beams

✓ B beam type (6 samples): each of the beams was reinforced with two deformed reinforcements of 12mm diameter in tension zone and two deformed reinforcements of 6mm diameter in compressive zone. The stirrup was 6mm diameter deformed steel bars, 220mm center to center spacing along the whole length of beam. The cover thickness to stirrups was 10mm. Contrary to previous long-term program presented section IV.2, B beams were casted in inverted way: i.e. tension reinforcement correspond to top reinforcement

IV.3.3 Casting beams

Firstly, dry mixing of cement, sand and coarse aggregate were mixed for 7 minutes. Then, the water was gradually added, mixing was again carried out for 15 minutes. The water content was adjusted to obtain a slump of nearly 7cm. The concrete was placed in the mould in two layers. To compact the concrete in the mould, the internal vibration method was adopted as seen in Fig.IV-13. After casting, the specimens were placed in the laboratory. It should be noted that all the B beams were cast in an inverted position with their tensile steel reinforcement in the top of the mould, the compressive steel in the bottom of the mould as explained in Fig.IV-14. It is different from B beams cast in 1984 when the tensile steel reinforcement was in the bottom of the mould.

IV.3.4 Applying load and conservation of the beams

Both types of RC beam were coupled using loading system (Fig.IV-15). Two loading levels were applied to the beams:

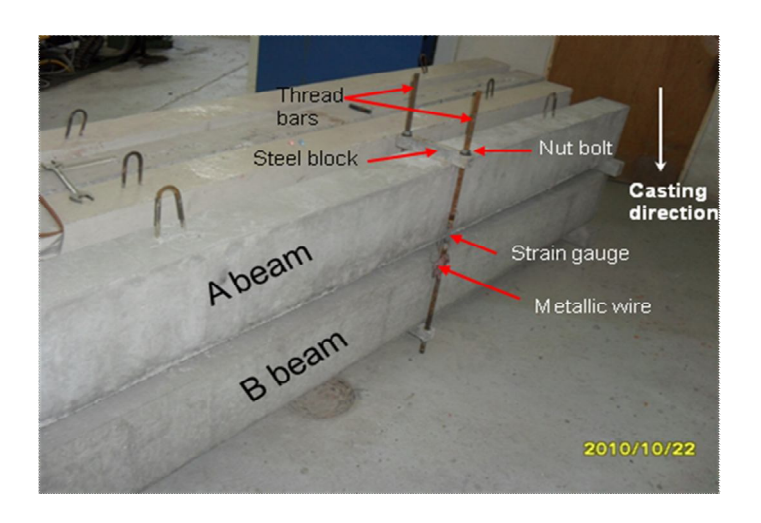


Figure IV-15.Loading system in three-point flexion used for beams

Level 1 loading (P=20kN, M_{ser1}=13.5kNm) corresponded to maximum loading of type A beams for durability in an aggressive environment (serviceability limit-state requirements in an aggressive environment) and to maximum loading of type B elements for resistance (ultimate load limit state in a non-aggressive environment).

Level 2 loading (P=30kN, M_{ser2}=21.2kNm) corresponded to 80% of the failure load and was equal to twice the design service loading of type B in an aggressive environment according to former French standards and to maximum loading of type A elements for resistance (ultimate load limit state in a non-aggressive environment).

The first four weeks of applying the load, loading rates were kept constant by means of an adequate device. After that, the couples were stored outside the laboratory, in a confined room (Fig.IV-17). The beam samples were subjected to the wetting-drying cycles. In each cycle, the salt fog (concentration of 35g/l) was sprayed for two days by six sprays located above and then kept drying for two weeks (temperature ranges from -5 to 35°C, RH ranges from 43 to 97% in the south-west of France).

The maps of flexural cracks due to loading were drawn for all the beams.

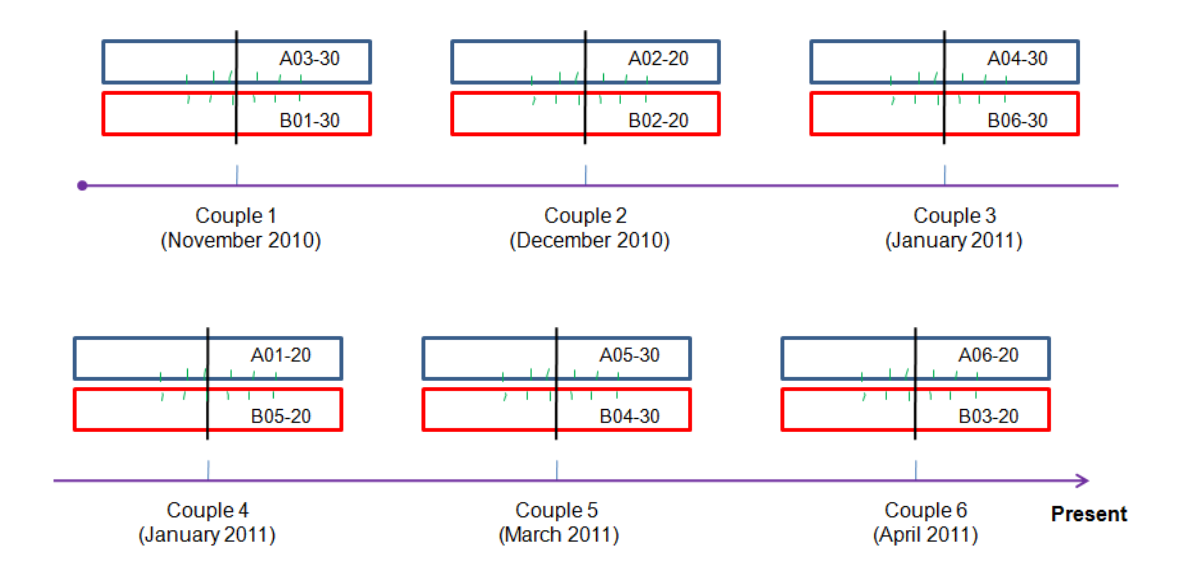
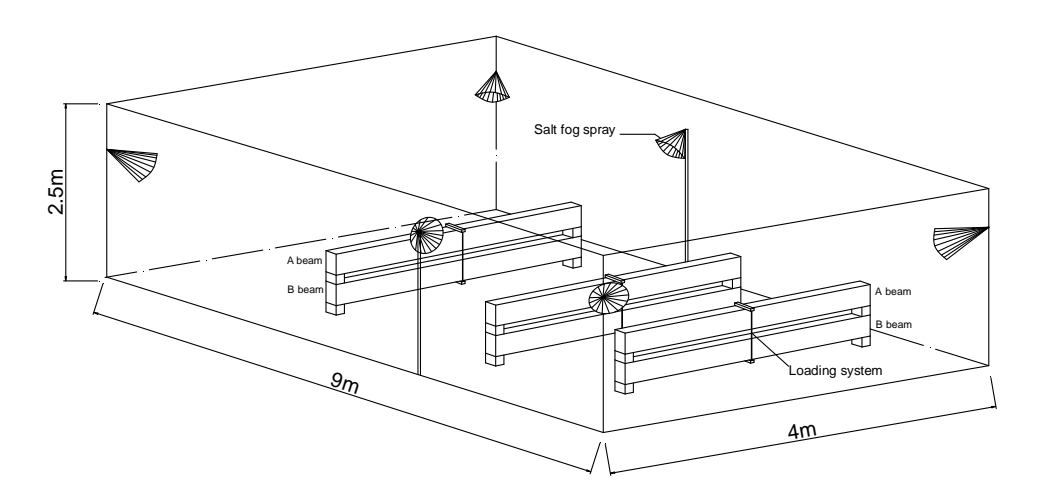


Figure IV-16. Schedule of exposing beams to chloride environment (Note: Each beam designated by number: first number following A, B denotes the beam number, second number following dash denotes the loading value)



CHAPTER IV: Experimental program in chloride environment



Figure IV-17. Exposure conditions of beams

When exposing to chlorides, it should be borne in mind that the gravity must also be considered. In fact, classic cracks due to bending moment located in the bottom part of a beam (positive bending moment) do not have the same risks of corrosion as those that arrive in the upper part (negative bending moment). The cracked upper parts (negative bending moment) are directly exposed to more severe limit conditions during wet periods (accumulation of salt water on the upper surface with increase in chloride content, gravitational filling and then drying of the cracks) (Fig.IV-18). This lead to the chloride content at steel bar depth on negative moment surface reaches quickly the threshold value and the corrosion will spread speedily from the intersection of mechanical cracks with the rebars.

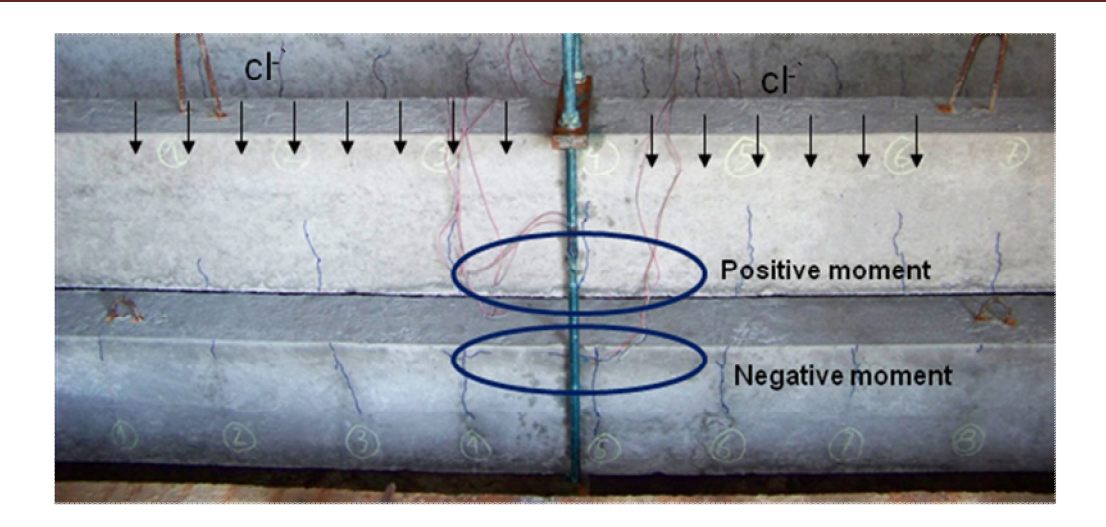


Figure IV-18. Exposure to wetting-drying cycles of saline solution of cracked reinforced concrete beams kept under load with a positive or negative moment: cracked tensile surface on the top or bottom

IV.3.5 Monitoring the corrosion cracking

The visible corrosion crack was regularly inspected by a portable video microscopy with magnification of 175. At present, on all the A beams, no cracks have been observed, which could be detected by the means of video microscopy. The time to first cracking of the cover concrete of B beams is varied between 10 months (B03-couple 6) and 15 months (B05-couple 4). It is very interesting to find that with the same type of beam (B beams), the same load level but the time to cover cracking is dissimilar. This is mainly attributed to the complexity of corrosion under sustained loading.

As an example, we will consider the evolution of corrosion cracks along a lateral side of B03-20. Figure IV-19 presents the formation and spread of corrosion cracks along the longitudinal reinforcement from the intersection of steel and a flexural crack. It can see that on the part close center of beam, the corrosion propagated severely in only 5 months after the appearance of first corrosion cracks (fig.IV-19d). The corrosion crack parallel to tensile reinforcement between two transversal cracks interconnected. At 17 months, the maximum corrosion crack opening was 0.7 mm but not spalling off concrete cover. It should be

remarked that there is a spread of corrosion linked to the presence of bending cracks (and the sustained mechanical cracks) because stirrups closer to the external surface than tensile steel bars do not lead to the creation of corrosion cracks.

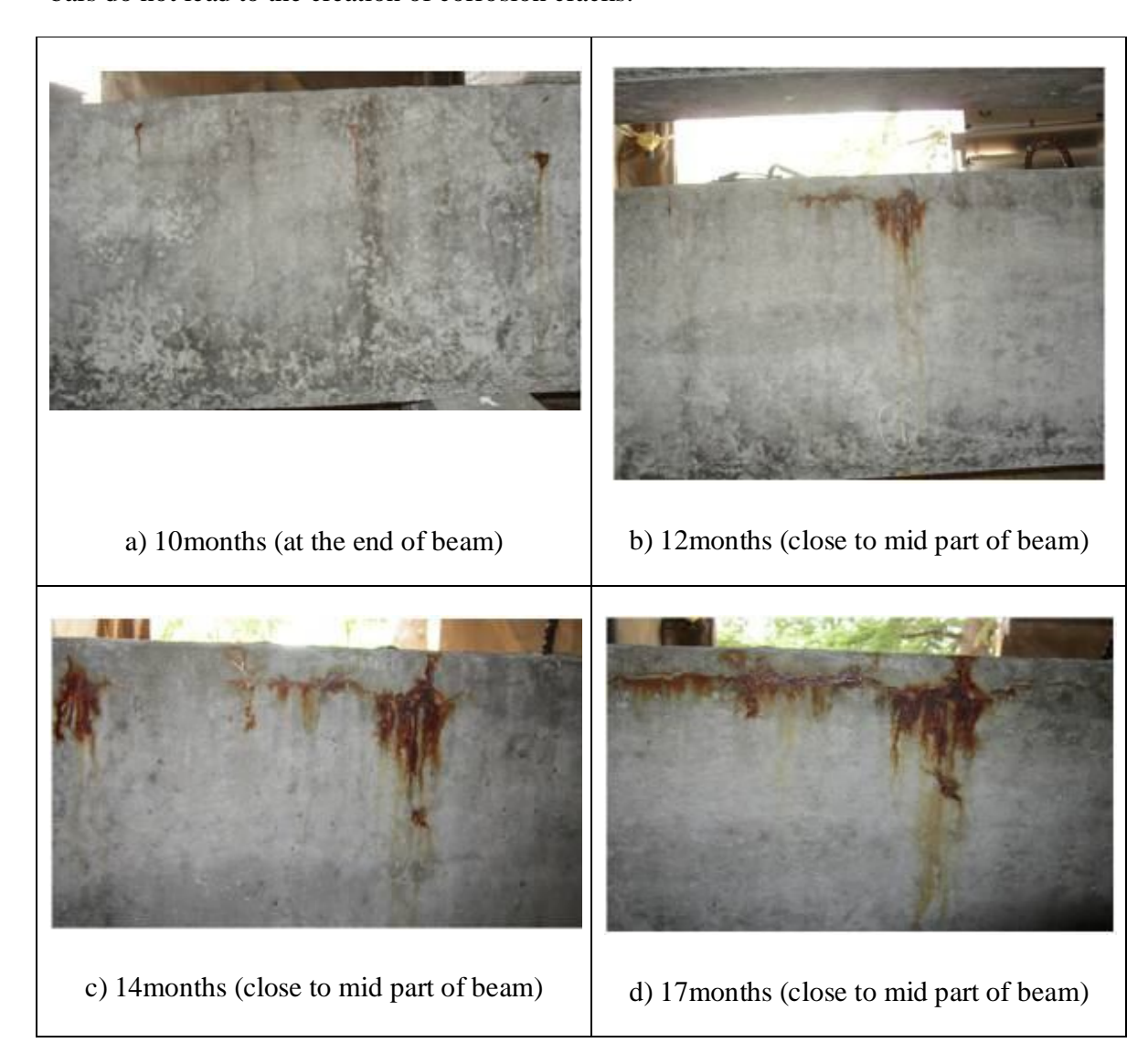


Figure IV-19. Creation of a corrosion crack parallel to tensioned rebars from the intersection of a bending crack and spread of corrosion cracks along tensioned rebars between two bending cracks on B03-20

In order to clarify the development of cracking corrosion, the maps of corrosion crack are shown in figures IV-20 and IV-21. The transversal cracks appearing on the tensile zone were

CHAPTER IV: Experimental program in chloride environment

generated by the mechanical load. On the back surface, the corrosion cracks after 20months run along the level of longitudinal reinforcement were almost extensive.

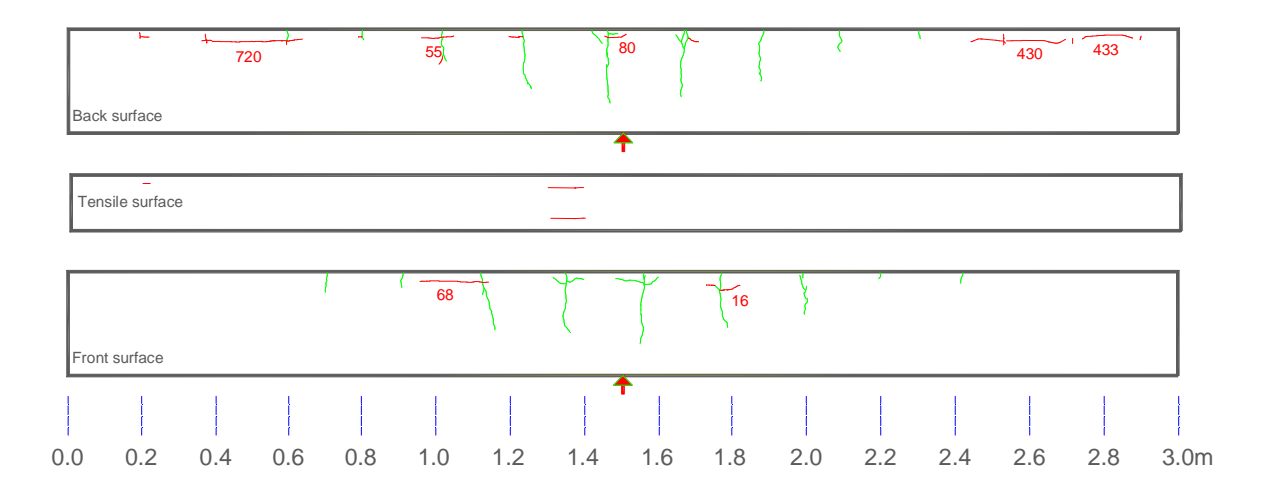


Figure IV-20. Corrosion cracking map of B03-20 after 17 months of exposure (corrosion cracks are red lines, dimension is in micrometer)

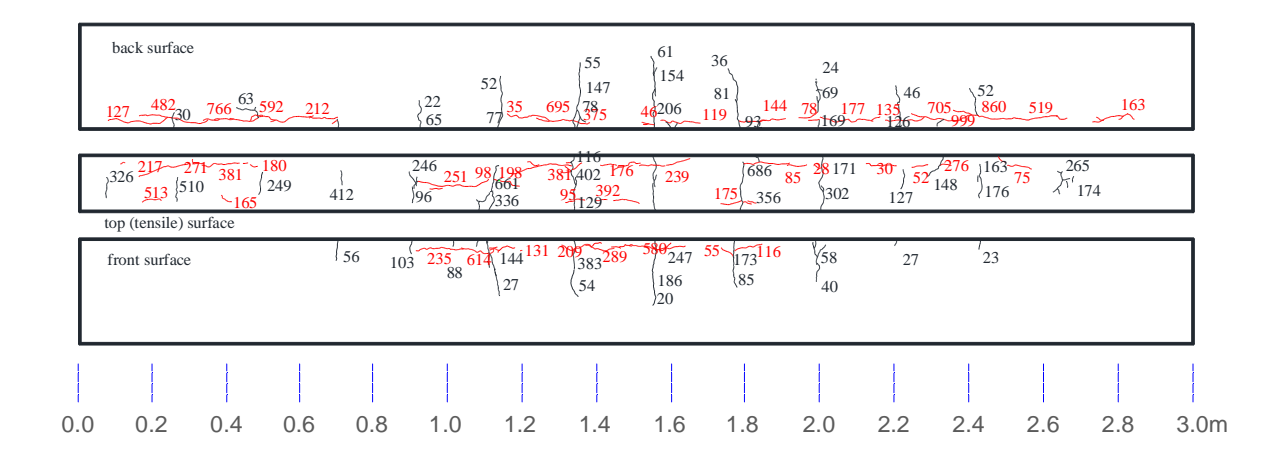


Figure IV-21. Corrosion cracking map of B03-20 after 20 months of exposure (corrosion cracks are red lines, dimension is in micrometer)

From these figures, it can again confirm that the distribution of maximum corrosion cracks is random and independent of the degree of stress in the tensile reinforcement.

IV.3.6 Chloride profiles

At 20 months of exposure in saline room, couple 6 (A06-20 and B03-20) was unloading to study mechanical properties, chemical analyses as well as tomography images. These works were carried out by the help of Mr. Linwen Yu (another PhD student at L.M.D.C). In this part, the first results of chloride content measured on A06-20 and B03-20 are presented.

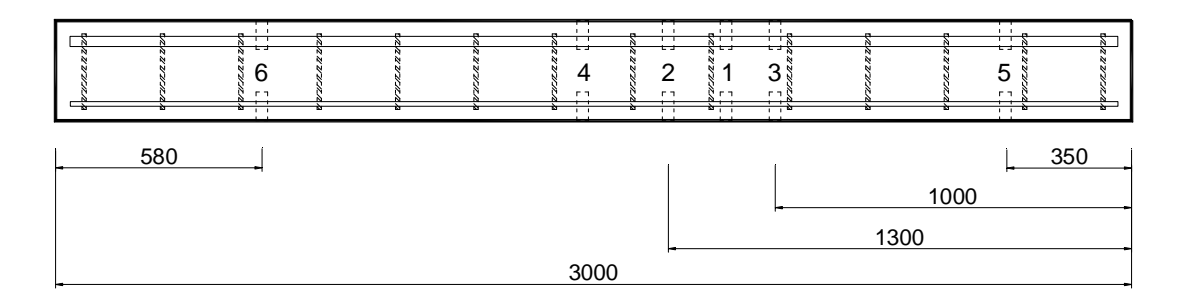


Figure IV-22.locations of drilling specimens for chloride profile test

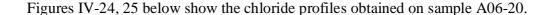




Figure IV-23. Removal of concrete powder for analysis

For each beam, 12 positions away from the cracks were selected to get samples for chloride concentration test, 6 on the tensile surface and 6 on the compressive surface (fig.IV-22). For each location, concrete powders were got by dry drilling with a rotary driller. We carried out

to obtain the samples on a circular area of 30 mm diameter. At each removal, the concrete powder was retrieved by using a brush and spatula. Then, the sampling surface, brush and spatula were cleaned by a jet of compressed air before continuing to the next sampling depth. The powdered concrete samples obtained were used to extract acid-soluble chloride contents. In this study, the total chloride content, based on the weight of cement is determined. Potentiometric titration was used to determine the chloride concentration in the solution. The profile of chloride was plotted up to 46mm in depth (a value of total chloride content is determined at 2, 6, 10, 14, 18, 22, 26, 30, 34, 38, 42 and 46 mm deep).



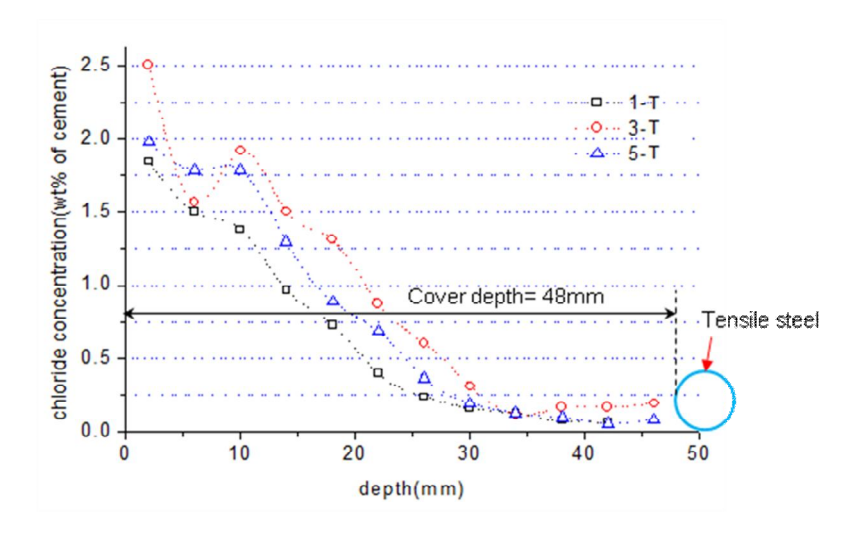


Figure IV-24. Total chloride profile of tensile zone (locations of 1-T, 3-T, 5-T) of A06-20

Results show that for A06-20, the chloride concentration in the tensile zone (bottom surface) is much lower than that in the compressive zone (top surface). This could be explained by the fact that the compressive surface was the upper surface when the beams were under loading, so the gravity effect leads to more accumulation of salt solution on the upper surface. However, in both of cases, the content of chloride at the depth of the rebar has not reached the usually accepted chloride threshold value (0.5% or 0.3% by weight of cement), which is necessary to induce a localized breakdown of passive film and hence initiate the

active corrosion. It could conclude that both compressive and tension reinforcement would not have corroded yet.

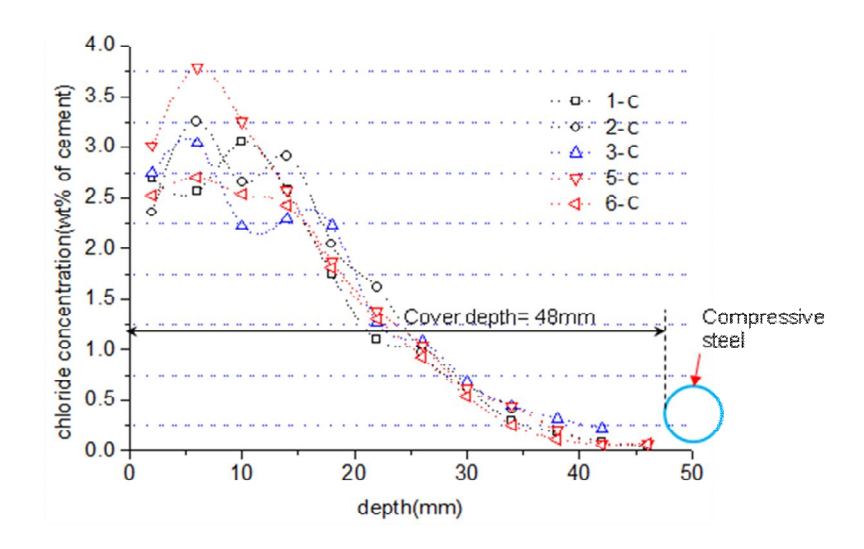


Figure IV-25.Total chloride profile of compressive zone (locations of 1-C, 2-C, 3-C, 5-C, 6-C) of A06-20

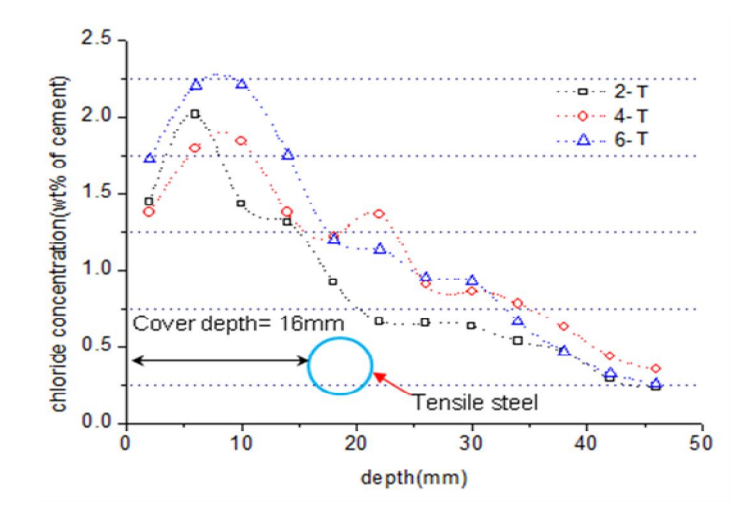


Figure IV-26. Total chloride profile of tensile zone (locations of 2-T, 4-T, 6-T) of B03-20

In case of B03-20, the chloride concentration from top (and tensioned) surface is higher than bottom (and tensioned) surface of A beams but weaker than the chloride concentration recorded from top surface of A beams. This result could be explained by the fact that the

coupling of A and B beams by the loading device lead to the fact that B beams is hidden by A beams from salt solution spray. Nevertheless, after 20 months of exposure, the chloride content near tension reinforcement is higher than the usual chloride threshold initiating corrosion (fig.IV-26). Chloride penetration from bottom (and compressed) surface of B beams is weakly recorded and highly scattered. On some part of the compressive face, the chloride content at 16mm depth is above 0.3% by mass of cement (fig.IV-27) but in some parts is higher than 1%. This indicates that the compressive steel might also be corroded.

It should be emphasized that the location of sprayer was along two ends of beams (see fig.IV-17); therefore, the accumulation chloride content on the part of beam end could be more than the part of mid-beam (as shown in fig.IV-27 below) because of location effect.

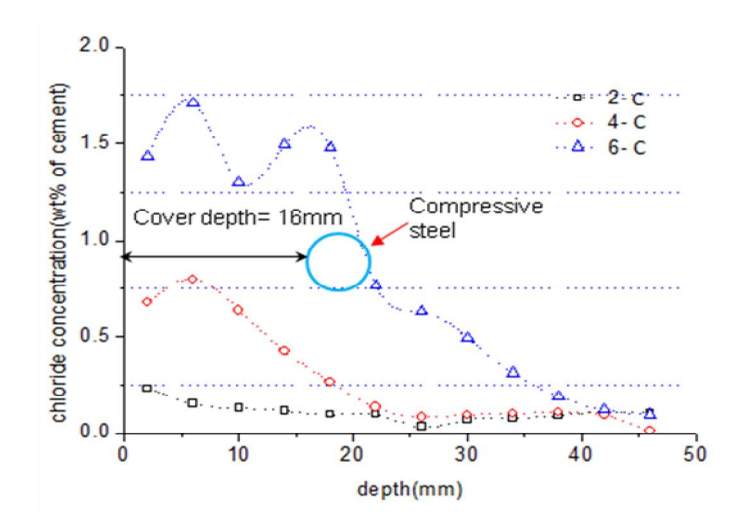


Figure IV-27.Total chloride profile of compressive zone (locations of 2-C, 4-C, 6-C) of B03-20

The measurement of chloride ion profiles perpendicular to crack plane are still carrying out. It is expected that the mechanism of chloride transport through a crack is different from diffusion in a semi-infinite medium [18]. Within this dissertation, we only introduce some first results on beams of A06-20 and B03-20. These works need the additional time to perform. At this moment, further research works related to these RC beams are being conducting. The results would be published in another literature.

IV.4. Summary

We remark the important effect of location of flexural cracks on both chloride concentration and corrosion propagation. Indeed, the non-cracked surface (upward) exposed directly to salt fog could have higher chloride ions than pre-cracked surface (downward), which did not exposed directly to salt fog irrespective of crack openings. Corrosion cracks developed first along tensile reinforcement from the intersection between flexural cracks (on top surface of the beams) and tension rebars. Because the same behavior is not recorded in the case of stirrups which are closer to the concrete surface, it is reasonable to state that damage at steel-concrete interface due to loading favors both corrosion development along the interface and corrosion crack formation as a result of propagation of existing microcracks due to load damage at steel-concrete interface [19].

Moreover, the effect of position along beams should be also considered. This effect could dominate over the influence of loading (tensile stress level of longitudinal reinforcement) at tested sample locations.

References

- 1. **I. Petre-Lazar, O. Poupard & C. Brunet,** (2007), "Inter-comparison of experimental and numerical simulation results on mechanical behaviour of corroded beams", Revue Européenne de Génie Civil, 11:1-2, 9-33, DOI: 10.1080/17747120.2007.9692920.
- 2. **D. Vié & O. Poupard,** (2007), "Bilan des essais sur corps d'épreuve", Revue Européenne de Génie Civil, 11:1-2, 55-95.
- 3. O. Poupard, V. L'Hostis, V. Bouteiller, B. Capra, S. Catinaud, D. Francois, J. Luc Garciaz, S. Laurens, T. Luping, G. Olivier & G. Tache, (2007), "Corrosion

- diagnosis of reinforced concrete beams after 40 years exposure in marine environment by non destructive tools", Revue Européenne de Génie Civil, 11:1-2, 35-54.
- 4. **N. A. Vu, A. Castel & R. François,** (2007), "Modélisation par macro-éléments", Revue Européenne de Génie Civil, 11:1-2, 141-161.
- 5. **R. François, A. Castel, T. Vidal,** (2006), "A finite macro-element for corroded reinforced concrete", Materials & Structures, vol. 39, n° 5, p. 569-582.
- 6. **O. Poupard, V. L'Hostis, S. Catinaud, I. Petre-Lazar**, (2006), "Corrosion damage diagnosis of a reinforced concrete beam after 40 years natural exposure in marine environment", Cement and Concrete Research 36, pp. 504 520.
- 7. **C. M., Andrade C,** (2001), "Round-Robin test on chloride analysis in concrete Part 1 and Part 2", Materials and Structures, vol. 34, p. 532-556.
- 8. **R. François,** (1987), "Béton armé: relation entre fissuration et corrosion", thèse de doctorat, Université Paul Sabatier, Toulouse.
- 9. **A. Castel, R. Francois and G. Arliguie,** (2000), "Mechanical behavior of corroded reinforced concrete beams Part 1: Experimental study of corroded beams", Materials and Structures/Materiaux et Constructions, Vol. 33, pp 539-544.
- 10. **T. Vidal, A. Castel, and R. Francois,** (2003), "Physical, chemical and mechanical analysis of a reinforced concrete beam corroded in chloride environment", CANMET/ACI Sixth International Conference on Durability of Concrete, ACI SP 212-5, V.M. Malhotra Editor, Thessaloniki, pp. 59-76.
- 11. **T. Vidal, A. Castel, R. François**, (2007), "Corrosion process and structural performance of a 17 year old reinforced concrete beam stored in chloride environment", Cement and Concrete Research 37, pp. 1551–1561.
- 12. **R. Zhang, A. Castel, R. Francois,** 2009, "Serviceability limit state criteria based on steel-concrete bond loss corroded reinforced concrete in chloride environment", Materials and Structures 42:1407–1421.
- 13. **I. Khan, R. Francois, A. Castel**, (2012), "Structural performance of 26-year-old corroded reinforced concrete beam", Eur J Environ Civil Eng 16(3-4):440–449.
- 14. A. Castel, O. Francy, R. François, G. Arliguie, (2001), "Chloride Diffusion in Reinforced Concrete Beam under Sustained loading", in: V.M. Malhotra (Ed.), Fifth

- CANMET/ACI International Conference, Recent Advances in Concrete Technology, 2001, pp. 647–662, ACI SP 200, July 29–August 1, Singapore.
- 15. **T. Vidal, A. Castel, R. Francois,** (2004), "Analyzing crack width to predict corrosion in reinforced concrete", Cement and Concrete Research 34, pp. 165 174.
- 16. **R. Zhang, A. Castel, R. François**, (2010), "Concrete cover cracking with reinforcement corrosion of RC beam during chloride-induced corrosion process", Cement and Concrete Research 40, pp. 415–425.
- 17. **I. Khan**, (2012), "Etude expérimentale de la corrosion en béton armé", thèse de Doctorat de l'Université de Toulouse.
- 18. N. Gowripalan, V. Sirivivatnanon, C.C. Lim, (2000), "Chloride diffusivity of concrete cracked in flexure", Cement and Concrete Research 30, pp.725–730.
- 19. **A. Castel, R. François,** (2011), "Modeling of steel and concrete strains between primary cracks for the prediction of cover controlled cracking in RC beams", Engineering Structures, Vol. 33, Issue 12, pp. 3668-3675.

Chapter V:

EXPERIMENTAL PROGRAM IN CO₂ ENVIRONMENT

GENERAL

This chapter provides the full details of test program in carbon dioxide condition and then subjecting to cyclic wetting-drying. The experimental program consisted of two phases:

-The first phase dealt with the effect of mechanical cracks on ingress of CO₂ and the carbonation at steel-mortar interface. It included testing 11 ring-shaped mortar samples that cracked radially by external load. They were kept in a constrained chamber of 50% CO₂ and 65% HR during from 1 week to 23 weeks. Then, corrosion of some of these were accelerated by submitting to wet-dry cycles.

-The second phase involved the study of evolution of corrosion layer under CO₂ and wetdry cycles in the laboratory. It included testing 9 ring-shaped mortar samples that cracked radially by external load and carbonated at crack wall as well as at interface of steel-mortar. These samples were stored in a constrained chamber of 50% CO₂ and 65% HR during period of 15-23 weeks. Then, they accelerated the corrosion process by subjecting to wet-dry cycles until the corrosion cracks on several specimens detected on extrados.

The results of the test will be described and discussed in the following section.

V.1. INIATIATION AND PROPAGATION OF STEEL CORROSION IN PRESENCE OF CRACK

Article:

Vu Hiep Dang, Raoul François, Valérie L'Hostis, Effects of pre-cracks on both initiation and propagation of re-bar corrosion in pure carbon dioxide, EPJ Web of Conferences 56, 06006 (2013).

DOI: 10.1051/epjconf/20135606006

Abstract:

This paper deals with effects of pre-cracks on both initiation and propagation of reinforcement steel corrosion due to carbonation. The ring shaped mortar samples with 8 mm steel bar inside were cracked with different crack widths ranging from 12 micrometers to 600 micrometers and then subjected to carbon dioxide environment for different terms to assess the carbonation profile in cracks and along the interface between steel and concrete, damaged by the internal pressure applied to the ring samples. After carbonation of interface, ring samples were submitted to wetting-drying cycles to study the propagation of corrosion and the effect of corrosion products on healing and then repassivation of steel bar or corrosion cracks development. Results show that irrespective of width of cracks, the carbon dioxide reaches the interface between steel and mortar and propagates along this interface. The samples then subjected to wetting-drying cycles exhibit corrosion development all along the interface, the appearance of oxides does not lead to create corrosion cracks for the duration of the experiments.

1. Introduction

Corrosion evaluation of reinforcing steel embedded in the concrete structures is a very serious problem and it is difficult to determine the corrosion rate because the steel is not visible. The primary cause for the corrosion of reinforced bar is due to the presence of chloride ions and the diffusion of carbon dioxide gas from the atmosphere. Chloride ions locally ruin the passive film provoking localized or pitting corrosion. On the other hand, carbon dioxide reduces the pH of the pore solution, making the passive film destroyed and causing generalized corrosion. The corrosion by carbon dioxide is less studied than by chlorides but may be also dangerous because of failure in the reduced cross section of reinforcement since the mechanical capacity of these sections may be lower than necessary for serviceability and ultimate service life.

There are numerous causes of cracking in concrete such as: shrinkage, settlement, freeze/thaw cycles, creep, design loads, formwork movement, corrosion of reinforcement and so on [1]. The existence of pre-cracks could accelerate the corrosion process by a quicker depassivation of the steel-concrete interface since the cracks create pathways for oxygen, chlorides, carbon dioxide, and water into concrete. There were numerous studies on the chloride diffusion in a crack of concrete members [3-7]. According to them, for long term corrosion the presence of cracks and crack widths has the influence on corrosion propagation [7] but others believe that the crack width has no impact on the development of reinforcement corrosion [3, 5, 6]. One point, which seems critical in the development of the corrosion process in relation to pre-cracks, is the possibility to obtain healing of crack with corrosion products or to obtain the creation of corrosion cracks due to corrosion process at the intersection of crack with the re-bars.

Contrary to chloride environment, the effect of crack openings on the diffusion of carbon dioxide to the steel-concrete interface has not been widely studied. However, S. Alahmad et al. [2] investigated the influence of crack opening on carbon dioxide penetration in cracked ring-shaped mortar samples. They found that crack opening significantly affects the ability of carbon dioxide to diffuse along the crack walls. Moreover, the carbonation of the interface

between steel and mortar always exists regardless of pre-crack widths. The creation of the corrosion cracks and the effect of rust on healing when the samples corrode in carbon dioxide then subject to cyclic wetting-drying, however, have not been studied. The corrosion process at steel–concrete interface of cracked members is whether controlled by the diffusion rate of CO₂ through crack walls.

The aim of this paper is to observe how the carbonation progresses through cracks to reach the steel bar at the interface of mortar-steel bar happens and if crack width is correlated with the damage at interfacial steel-mortar.

2. Experimental methods

2.1. Materials

All the mortar samples were fabricated with a French CPA cement (CEMI 52.5R) having C₃S, C₂S, C₃A and C₄AF contents of 67.8%, 7.1%, 8.6%, and 6.2%, respectively. The standard sand (CEN EN 196-1) was used. All the mortar mixtures were made with a water/cement ratio of 0.48 and a sand/cement ratio of 2.72. Each mortar mixture was made with 1.380 kg of water, 2.875 kg of cement, and 7.830 kg of fine aggregate. Deformed steel bars of 8mm diameter were used as reinforcement in the ring shaped mortar samples. The elastic limit of steel used was 500Mpa. The test samples consist of ring shaped mortar of 50mm height, 150mm external diameter, 50mm internal diameter as shown in Fig.1a. For each sample, a deformed steel bar 8mm of circular shape with 100mm diameter was kept at center of mould by three fixed metal wires. The mould was filled in two steps with a vibration of 30 seconds on a vibrating table at the end of each step. After 24 h, the samples were carefully unmoulded to avoid any cracking and then cured under tap-water until 28 days.

2.2. Preconditioning of the samples

After curing, the all samples were kept in an oven to dry completely at 40°C for 50days. The mass of each sample was weighed at 2 weeks interval by an electric balance with accuracy of 0.001kg. Then the mass was compared each other in order to confirm the absolute drying of samples. The aim of drying the samples is to accelerate the carbonation process.

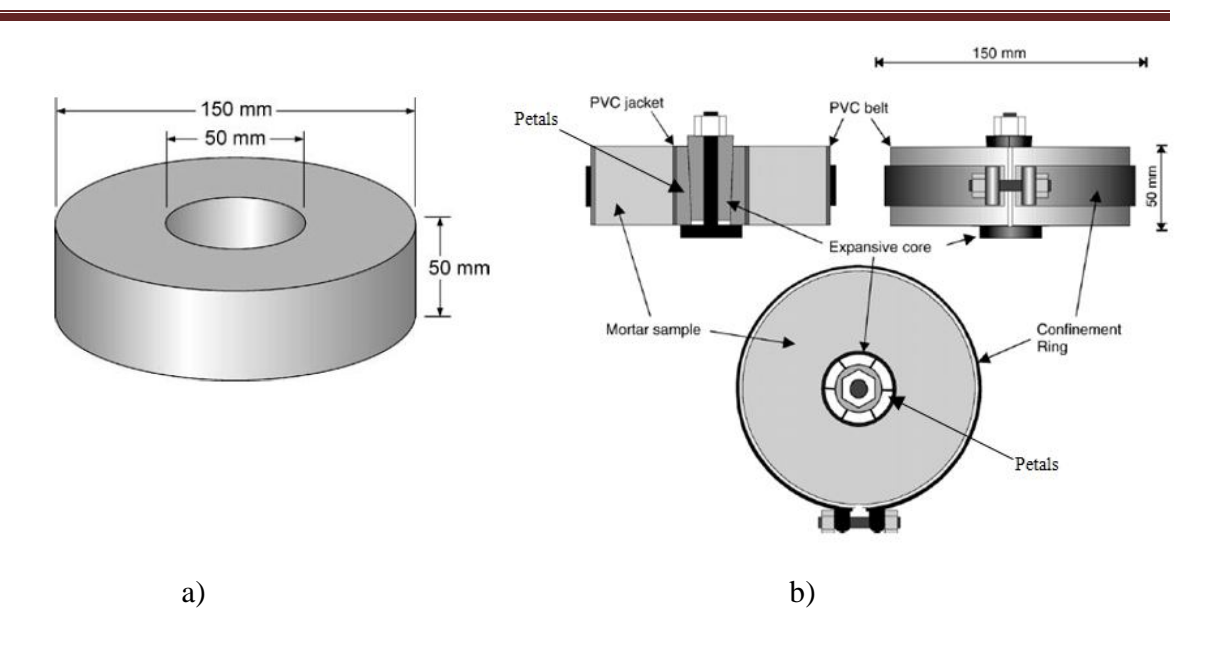


Fig.1. Dimensions of the ring mortar sample (a) ; Apparatus for creating cracks on samples (b)

2.3. Cracking of the mortar samples

Controlled cracking of samples was obtained by the experimental procedure used by Gagne et al. [8] and S. Alahmad et al. [2]. Cracks induced by the expansive core are radial. The number and opening depend on the load applied. Prior to making cracks on the samples, both exterior and interior surfaces were polished by carbon silica powder (number 120) to obtain flat smooth surfaces. The samples were subjected to control the tensile cracking with a mechanical expansive core and an external steel confinement ring (Fig.1b). The expansive core which was inserted into the sample hub consisted of a conical hardened-steel cylinder that slide inside a set of six conical hardened-steel petals. A thin cylindrical PVC jacket held the petals around the conical cylinder. A high-strength steel bolt and nut were used to force the conical cylinder against the petals. This process caused the diameter of the PVC jacket to increase, thus inducing deformation in the internal diameter of the mortar sample. Controlled cracking was achieved by manually adjusting the deformation of the expansive core. During the whole process the sample surfaces were closely monitored and crack widths were detected and measured by a portable video microscope in order to reach the desired crack

widths. It should be noted that there were not longitudinal cracks arisen along exterior perimeter of samples during this stage.

2.4. Exposure conditions

Immediately after the mortar disks had been cracked, they were transferred to a sealed chamber and subjected to carbonation at a temperature of 23°C, a relative humidity of 65% and a CO₂ concentration of around 50%. For each sample group, the exposure time in CO₂ was different that ranges from one week to several months. After keeping in CO₂, the corrosion of some sample groups was studied thanks to wet-dry cycles: one day under tap water-six days in lab atmosphere. With series C samples, the cycles consist of one day wetting under tap water and three days drying in lab air. Table 1 gives the detailed experiment condition for all six groups. At different periods, the samples were chosen to analyze the corrosion pattern.

Table 1. Groups and exposure environment for accelerating corrosion

	Cracking samples								
Name group	M	С	N	S					
Quantity	5	2	7	7					
Exposure in CO2	Yes	Yes	Yes	Yes					
Cyclic wetting- drying	No	Yes	Yes	Yes					

The ring samples taken out of carbonation chamber were broken into two halves: upper (top) half and lower (bottom) half and then carbonation depths measured. For series M samples, the purpose is to study the corrosion progress at the interface of steel-mortar and

along crack path by destructive test. Therefore, the cyclic wet-dry did not carry out for these series. The duration of the accelerated test for each of groups of cracking samples is specifically indicated in table 2. To C samples, only C2 sample was corroded by made cycles of one day wetting under tap water and 3 days drying in the laboratory environment.

3. Experimental results and discussion

3.1. Crack characteristics

The table 2 gives the measured crack openings and the number of cracks on two faces of specimens with help of portable video microscope. The crack opening varies from 12µm to 595µm. The difference between crack opening of the top face and bottom face is quite larger, which ranges from few dozen to several hundred micrometers, depending on the force against PVC jacket.

The carbonation in cracked concrete samples is a major factor that promotes the corrosion of embedded reinforcing steel. Therefore, in terms of the durability of concrete, it is necessary to control cracks formed during the life of a structure. R. Francois and J.C. Maso [11] investigated the influence of sustained load on carbonation or on chloride penetration of RC beams. The results showed that the damage to the aggregate-cement paste interface increases the penetration of aggressive agents in the tension zone. The carbonation depth was always greater than in the tension zone whatever the load levels and time of exposure. They found that there was the diffusion along steel bars from the intersection between crack path and reinforcement. S. Alahmad et al. [2] who tested the disk samples with the same composition of mortar and dimensions as this study concluded that for crack widths below 9 µm, the carbonation did not occur on the face perpendicular to the crack wall. Nevertheless, they found that the interface between steel and mortar was carbonated even if this carbonation did not progress perpendicular to the interface, being superficial for the duration of experiment. From above discussions, it could be predicted that all cracked mortar samples in Table 2 will be at least superficially carbonated through crack path.

3.2. Carbonation and initiation of reinforcement steel corrosion

It is well known that the depassivation of steel bars embedded in concrete can occur for an alkaline pH between 9 and 11[12] or ranging from 8.3 to 12.6 [13], and thus be associated

with a partial carbonation of concrete cover. In order to understand whether carbonation penetration along interface between mortar and steel bar occurs or not, a phenolphthalein pH indicator was used. Each sample was broken into upper half and lower half along its outer perimeter. The phenolphthalein was then sprayed on the fresh mortar surface. The series M were analyzed after 1 to 5 weeks in carbon dioxide. At that time, carbonation process at mortar rebar interface was initiated for M5 sample, which was just exposed to carbon dioxide chamber within one week (see in Fig.2). It can be observed the white-purplish colored region on the interface between reinforcement and mortar of M5 sample. This implies that the carbonation started to spread over interface. It is also different from results obtained on the same samples but exposed to chloride where the corrosion progressed only few millimeters along interface from crack path [10]. We remark that there was a change in color at interface as the phenolphthalein was sprayed. Immediately after the spraying completed, the color did not alter along the interface. Nevertheless, carbonation appears to be very superficial since after few minutes the color changes due to re-increased of pH at steel-mortar interface as shown in Fig.3. A possible explanation is that the pore solution which is still basic (pH=13) goes to fresh surface because of drying of sample exposed to the lab condition.

The M2 specimen subjecting to carbon dioxide for 5 weeks exhibited the almost completed carbonation process along interface since no color change observed on the interface after half an hour. Surprisingly, CO₂ which diffuses into crack path to reach the reinforcement leaded to a total carbonation of interface. This result is different from those obtained on flexural members stored in sustained loading in onsite atmosphere where carbonation appears only few centimeters along interface [11]. In other words, carbonation of interface was stable. Fig. 2c presents the carbonation front at crack face after 5 weeks of exposure. Similarly to M5 specimen, with the presence of pre-crack path the carbonation process occurred partly on the crack face. The depth of carbonation measured on cracked surface was approximately 1.5mm. Therefore, any carbonation along the steel-concrete interface must be due to carbon dioxide gas through cracks. In fact, if the carbon dioxide gas could penetrate through the electrical wire or along three wires, which maintained the ring steel bar, this will not change

CHAPTER V: Experimental program in carbon dioxide environment

the conclusion that interface between steel bars and mortar is fully carbonated since CO_2 can reach the re-bars.

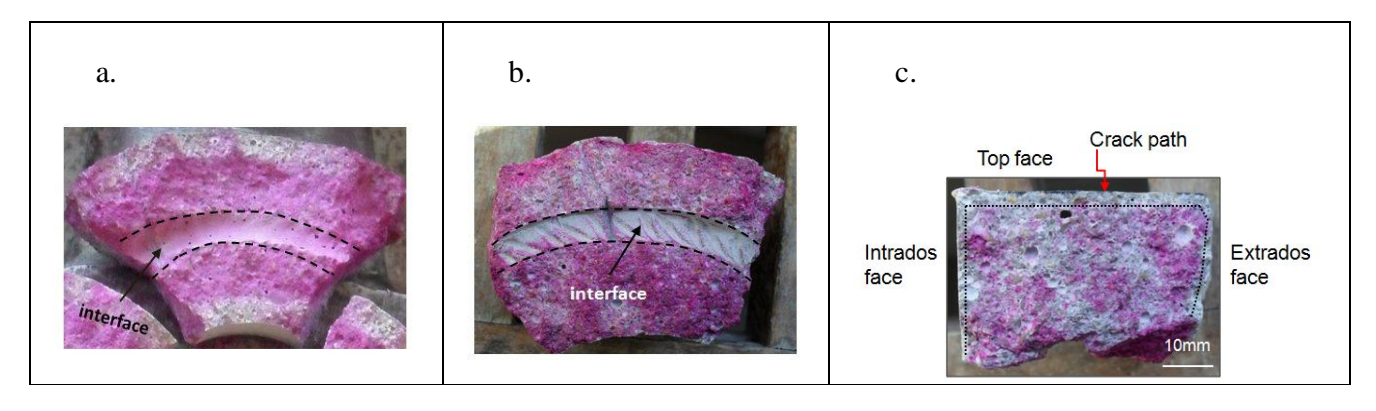


Fig.2. Evolution of carbonation at steel bar-mortar interface: a) M5 sample; b) M2 sample c) Carbonation depth of M2 perpendicular to the crack face

Table 2. Crack widths and exposure environment of tested samples

	No. of cracks										
		1	2	3	4	5	6	7	8	Duration	No. of
Name	Crack width-μm									in CO2	cycles
	Top face	43	72	56	59	-	-	-	ı	3ws	-
M1	Bottom face	22	32	ı	1	-	-	1	1		
	Top face	12	13	-	-	-	-	-	-		
M2	Bottom face	21	38	43	40	34	-	-	-	5ws	-

CHAPTER V: Experimental program in carbon dioxide environment

	Top face	98	99	-	-	-	-	-	-		
М3	Bottom face	50	17	95	43	-	-	-	-	2ws	-
	Top face	65	67	107	-	-	-	-	-		
M4	Bottom face	36	29	27	-	-	-	-	-	4ws	-
	Top face	68	75	60	-	-	-	-	-		
M5	Bottom face	20	33	55	72	-	-	-	-	1ws	-
	Top face	138	34	140	595	141	203	-	-		-
C1	Bottom face	105	153	171	99	289	311	-	-	13ws	
	Top face	230	52	64	-	-	-	-	-		
C2	Bottom face	395	180	161	93	140	394	-	-	23ws	6
	Top face	125	98	86	111	-	-	-	-		
<i>S3</i>	Bottom face	33	22	15	38	-	-	-	-	7ws	-
S6	Top face	81	57	70	-	-	-	-	-	15ws	14

CHAPTER V: Experimental program in carbon dioxide environment

	Bottom face	33	30	141	166	91	50	62	-		
	Top face	300	421	404	366	178	-	-	-		
NI	NI Bottom face	129	83	235	145	233	256	215	73	21ws	38
	Top face	157	274	210	167	259	217	-	-		
N2	Bottom face	240	140	164	132	145	-	-	-	21ws	14

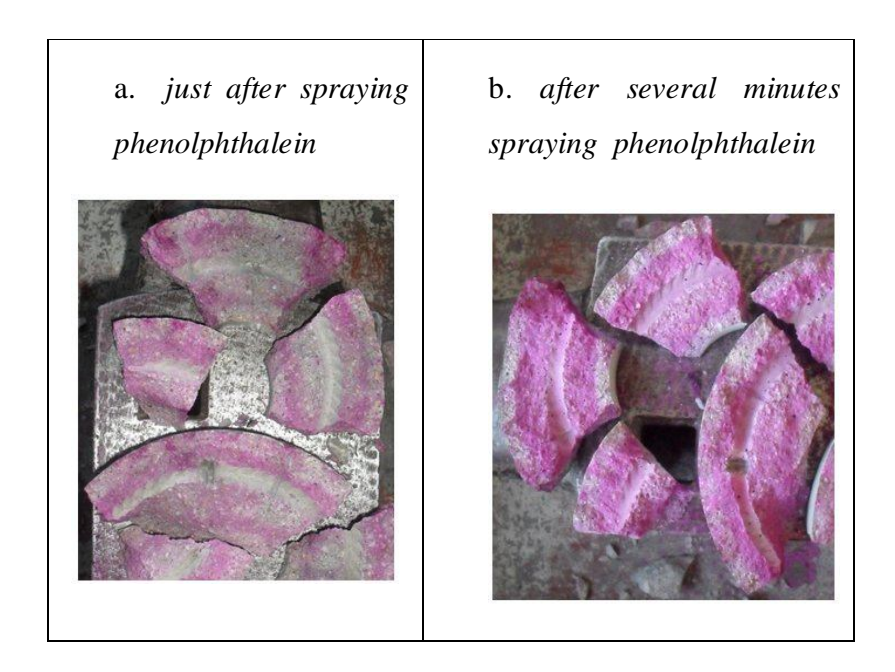


Fig.3. Change in pH at interface of reinforcement-mortar (M5) as spraying phenolphthalein

3.3. Development of reinforcement steel corrosion

The diffusion of carbon dioxide into the interior of a concrete structure depends mainly on two parameters: the existence of cracks and the porosity of concrete. The carbonation process through a crack consists of four steps: diffusion of carbon dioxide into the crack, diffusion of carbon dioxide into the concrete, occurrence of chemical reaction and consumption of hydroxyl ions OH. The initiation of steel bar corrosion in the presence of crack is evidently much faster than it in the absence of crack. The experimental results present that for S3 sample after exposure time of seven weeks to CO₂, the interface and crack face were carbonated and the carbonation front provided by the phenolphthalein test was approximately 10mm. On the steel-concrete interface, some traces of corrosion product were visible. The brown-rust was also more observed on the interface of S6 sample (fig.4b). More rust product also attached to the interface of N1 sample (fig.4d). The samples C2 and N2 with mechanical average crack width of 173µm and 191µm respectively indicated a generalized corrosion along the ring steels. Unlike corrosion pattern caused by chloride ingress, the corrosion pattern of these samples spread over the steel-concrete interface even when the period of time for accelerating corrosion was short term. The appearance of voids between reinforcement and mortar due to "top-cast bar" effect and creation of mechanical cracks which damaged the interface zone could the possible reasons to allow the spreading of carbon dioxide gas along it. For N1 and N2 samples, no corrosion cracks were detected on outer face after 410 days and 240 days respectively of exposure under accelerated conditions. Probably, the pressure results from the formation of oxides and tensile stresses generated by creating of mechanical cracks are still not enough to exceed the tensile strength of the mortar. It should be noted that both of them have the same exposure time to CO2 but the number of cycles of wetting and drying of N1 is more important than that of N2 sample. This major reason explains why the corrosion state of N1 sample is more severe than the corrosion state of N2 sample at steel-mortar interface. We examine further the corrosion propagation of ring reinforcement steel in C2 sample as shown in Fig.5. The mechanical cracks are located on each face of the steel bar. It can be seen that the view from top face of the ring bar exhibited fewer cracks than the view from its bottom face and the distribution of cracks is irregular. On the top face, the portion without cracks revealed no corrosion remaining on this face of the steel bar. On the contrary, the bottom face showed a general corrosion on entire perimeter.

Primarily observing the distribution of corrosion around the steel face, it can see that the corrosion product is irregularly distributed on both bottom face and top face of ring steel. Indeed, as demonstrated in Fig. 6, the thickness of corrosion layer measured by the optical microscopy technique on C2 sample is very different for a given cross section, varying from 0µm to 86µm around the same sample. This implies that there are differences in the carbonation rate along reinforcement steel. The test results also revealed that when the rust layer increases, some cracks parallel to the metal-corrosion product interface appear. As a result, the corrosion protection ability of this layer is poor.

Figures 6 and 7 offer the pictures about metallographic cross sections of C2 and S6 samples that show the rust layer is composed of laminar layers of different colors. The inner part of the rust layer, which is in contact with the steel, is very thin with lighter color. Whereas, the outer part of oxide layer with grey-dark brown in color, close to the cement paste, has the larger thickness. Interestingly, the C2 sample was fully carbonated but partly corroded meanwhile S6 sample was fully corroded but partly carbonated. In this case, the presence of mechanical cracks and time of exposure seem more important than the width of pre-cracks.

4. Conclusion

A preliminary study on corrosion state of reinforcement steel embedded mortar samples in carbon dioxide conditions and then cycles of wetting- drying was carried out. The experimental results showed that in case of mechanically cracked specimens, whatever crack widths allow carbon dioxide to reach the steel-mortar interface. The corrosion starts and then spreading this interface. This also observed by S. Alahmad et al. [2].

The samples then subjected to wetting-drying cycles exhibited corrosion development all along the interface. Nevertheless, the corrosion is not uniform along the perimeter of a given cross-section, which could be link to the casting direction effect. The corrosion rate is generally higher on the bottom of the section than that on the top of the section.

CHAPTER V: Experimental program in carbon dioxide environment



Fig.4. Evolution of corrosion of S3, S6, C2, N1, N2 samples

CHAPTER V: Experimental program in carbon dioxide environment

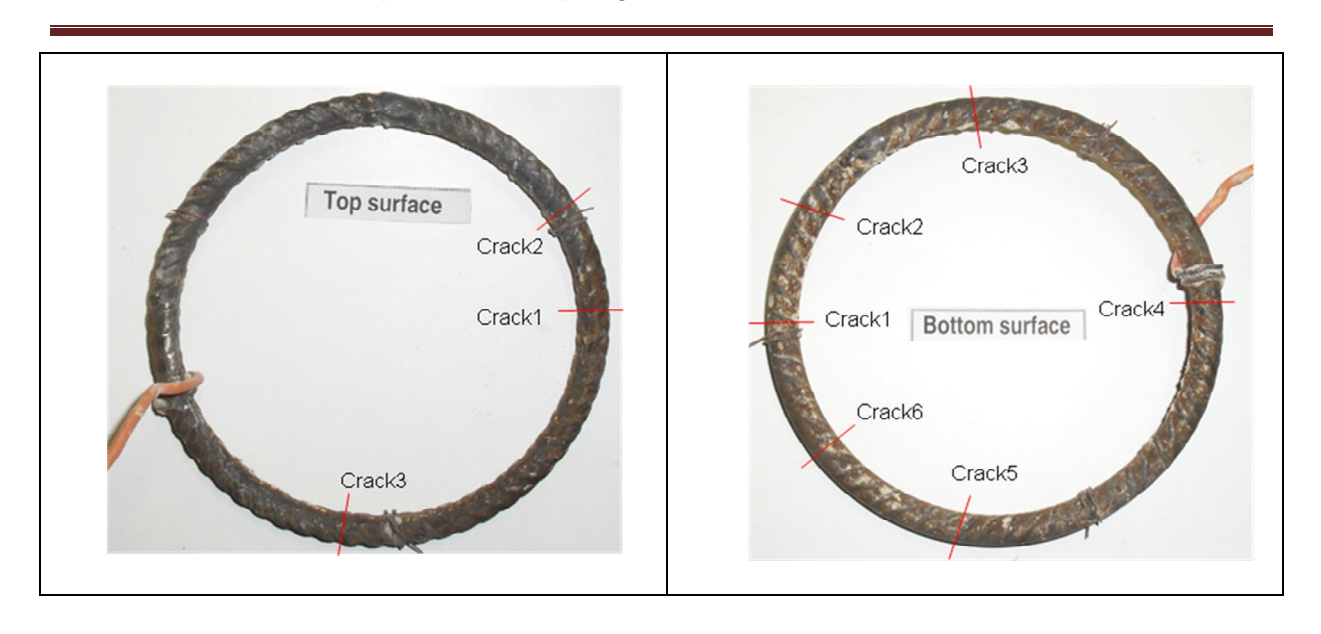


Fig.5. Locating of mechanical cracks and real corrosion on steel bar of C2 sample

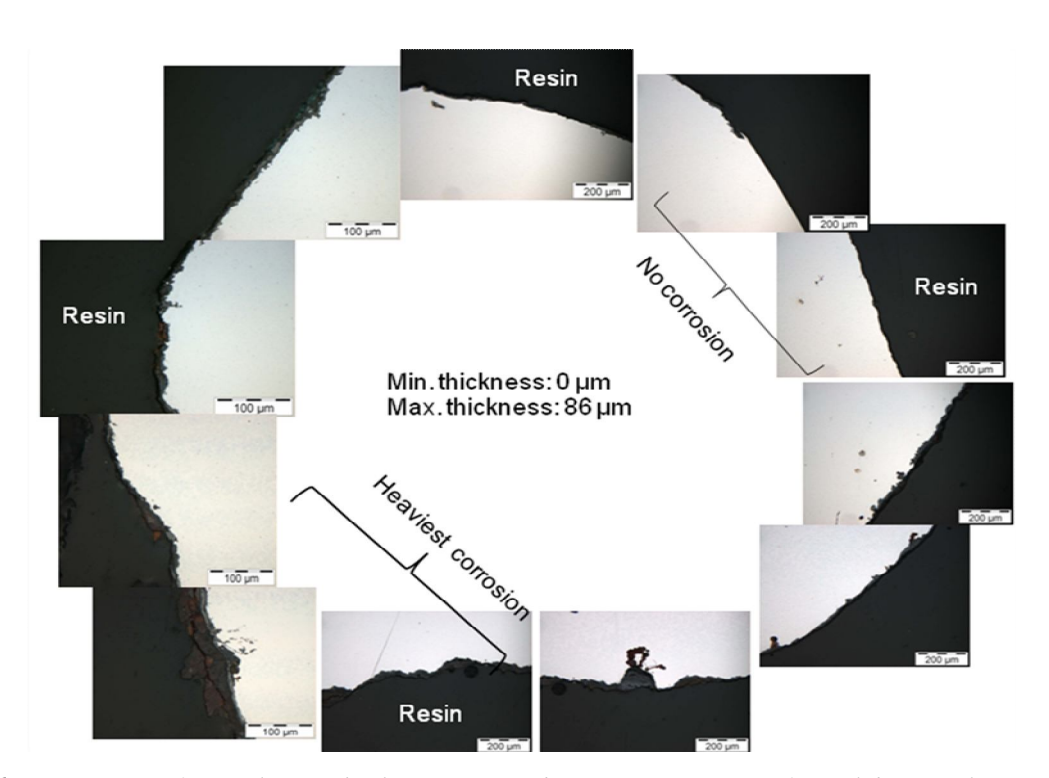


Fig.6. Variation of rust layer thickness around a cross section of steel bar at location of crack3 (top face) for C2 sample

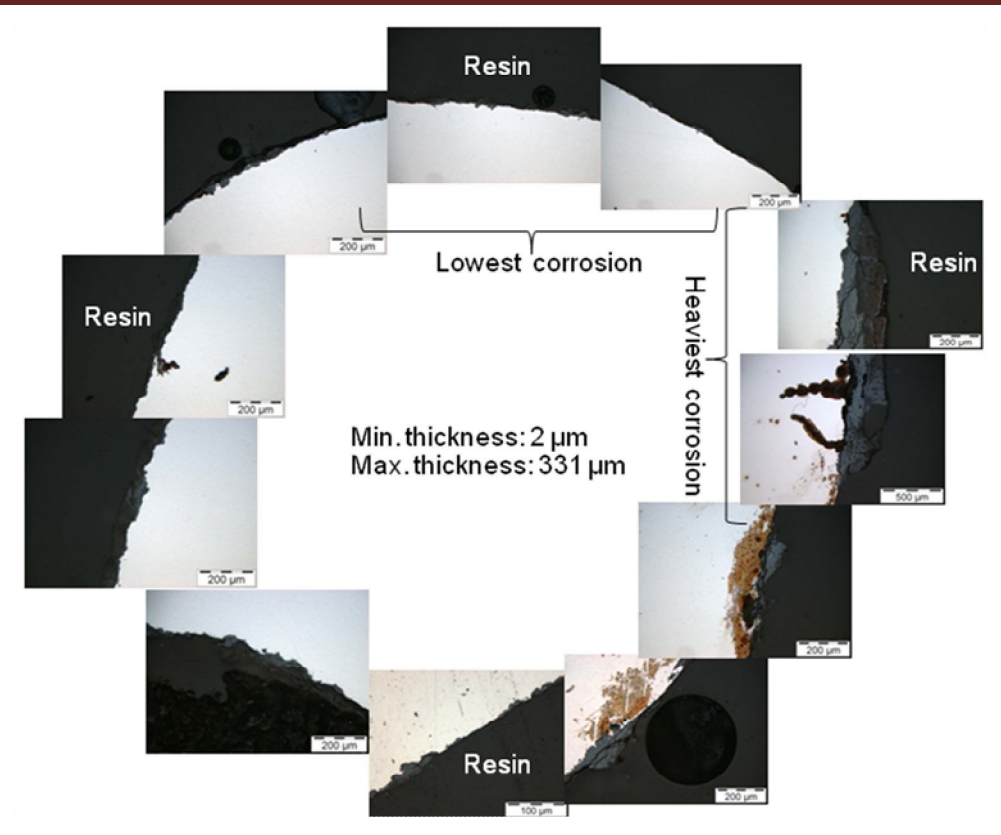


Fig7. Typical cross section of rust layer formed on S6 sample

References

- [1]. CEB., 1997, "Durable of concrete structures", Thomas Telford.
- [2].S. Alahmad, A. Toumi, J. Verdier, R. François, 2009, "Effect of crack opening on carbon dioxide penetration in cracked mortar samples", Materials and Structures, pp.42:559–566.

- [3].Peter Schießl and Michael Raupach, 1997, "Laboratory Studies and Calculations on the Influence of Crack Width on Chloride-Induced Corrosion of Steel in Concrete", ACI Materials Journal, V. 94, No. 1.
- [4]. Tarek Uddin Mohammed, Nobuaki Otsuki, Makoto Hisada, and Tsunenori Shibata, 2001, "Effect of crack width and bar types on corrosion of steel in concrete", Journal of materials in civil engineering.
- [5].A.W.Beeby, 1983, "Cracking, cover, and corrosion of reinforcement", Concrete international, pp. 35-40.
- [6].Raoul François, Ginette Arliguie, 1998, "Influence of service cracking on reinforcement steel corrosion", Journal of materials in civil engineering.
- [7].M.B. Otieno, M.G. Alexander & H.D. Beushausen, 2009, "Corrosion propagation in cracked and uncracked concrete", 2nd International Conference on Concrete Repair, Rehabilitation and Retrofitting, ICCRRR-2, 24-26 November 2008, Cape Town, South Africa, pp. 339-344.
- [8].Gagné.R, François.R, Masse.P, 2001, "Chloride penetration testing of cracked mortar samples". In: Banthia N, Sakai K, Gjory OE, Concrete under severe conditions, vol 1. University of British Columbia, Vancouver, pp 198–205.
- [9]. C.Andrade and C.Alonso, 2004, "Test methods for on-site corrosion rate measurement of steel reinforcement in concrete by means of the polarization resistance mothod", RILEM TC 154-EMC: Electrochemical techniques for measuring metallic corrosion. Materials and structures, Vol. 37, pp. 623-643.
- [10]. Raoul Francois, Inamullah Khan, Ngoc Anh Vu, Hugo Mercado and Arnaud Castel, 2012, "Study of the impact of localized cracks on the corrosion mechanism", European journal of environment and civil engineering, DOI:10.1080/19648189.2012.667982.
- [11]. R.Francois and J.C.Maso, 1988, "Effect of damage in reinforced concrete on carbonation or chloride penetration", Cement and Concrete Research, Vol.18, pp. 961–970.
- [12]. In-Seok Yoon, Oguzhan Copuroglu, Ki-Bong Park, 2007, "Effect of global climatic change on carbonation progress of concrete", Atmospheric Environment 41, pp. 7274–7285.

CHAPTER V: Experimental program in carbon dioxide environment

[13]. L.J.Parrott, 1994, "A Study of Carbonation-Induced Corrosion", Magazine of Concrete Research, 46 (3): 23-28.

V.2. DEVELOPMENT OF CORROSION PRODUCTS IN RELATION TO PRECRACK

Article:

Vu Hiep Dang, Raoul François, Valérie L'Hostis, Dietmar Meinel, Initiation and propagation of Corrosion in pre-cracked carbonated reinforced mortar samples, Submitted to Materials and Structures journal.

Abstract:

This paper deals with the initiation and propagation of corrosion in mortar specimens precracked under mechanical loading and carbonated in climate accelerated conditions (50% CO2-65% HR) for 15 to 23 weeks. Mechanical loading led to transverse macro-cracks and damage at the steel-mortar interface characterized by micro-cracks (cover controlled cracking) which favour the carbonation of crack walls and the interface with the steel bar. Wetting-drying cycles performed after carbonation allow corrosion initiation all along the steel bar because of the carbonated interface and corrosion propagation because of the creation of corrosion cracks which appear to develop from the micro-cracks induced by the mechanical load. Results also show that rust develops all around the perimeter of the carbonated steel bar but that the corrosion layer is thicker in the lower half surface of the reinforcement than that observed in the upper half. Results indicate that the distribution and composition of corrosion products depend on the thickness of the rust layer and that the multilayered structure of rust depends mainly on its thickness.

I. Introduction

Corrosion is one of the primary causes of the limited durability of reinforced concrete members. When internal steel reinforcement corrodes, the corrosion products, which have a greater volume than the original iron, generate internal tensile stress at the steel-concrete interface. As the tensile stress develops, the surrounding concrete cracks and even spalls away if the steel corrosion is serious. Moreover, the micro-cracks caused at the interface between steel and concrete by the tensile stress allow ions to be transported from the concrete surface to the surface of the reinforcement steel. Corrosion thus advances more rapidly.

Cracks are almost unavoidable in normal concrete structures. When pre-cracks exist on the surface of structures, they create pathways for oxygen, chlorides, carbon dioxide and water to travel into the interior of the concrete. As a result, the corrosion process is facilitated. In cracked concrete members, corrosion will start either in a crack zone or in the zone beside a crack [1]. The creation of early corrosion cracks is also a critical point because once corrosion cracking has started, its propagation phase is unlikely to stop. The use of accelerated techniques such as an impressed electrical current almost always leads to the creation of corrosion cracks after corrosion initiation, so it is necessary to work in a natural or artificial-climate-accelerated corrosion environment to be able to understand the effect of precracks on corrosion development. The crack parameters that affect the corrosion of RC members include crack width, crack frequency, crack orientation and crack location [1-6]. Initiation of corrosion is facilitated by pre-cracks but the following step, propagation of corrosion in the pre-cracked zone, is still a subject of debate. According to various authors, corrosion can propagate easily [36, 39] or be blocked by healing or self-healing in pre-cracks [3, 5, 35, 37].

Previous work on the corrosion of RC structures has focused mainly on reinforcing bar corrosion in chloride conditions and few works have studied the progress of corrosion under a carbon dioxide environment in the presence of mechanical cracks. Some studies have used RC beams with dimensions as supplied by industry and subjected them to a 50% CO₂ environment [2, 5] or to the normal atmosphere [7] while they sustained a service load. The research showed that the carbonation front was more marked in the tensile zone of RC beams. The increase in depth of carbonation was correlated with the tensile stress level. The diffusion of CO₂ always followed a crack path and then spread along the steel-concrete interface. Recently, a study has been carried out on the effect of crack opening on the ability of carbon dioxide to diffuse along the crack path [8]. Rather than using RC beams under

loading, the authors used ring-shaped mortar specimens with mechanical cracks. The specimens were placed in a confined chamber with a CO_2 concentration of 50%, relative humidity of 65% and a temperature of $23^{\circ}C$. The results showed that crack opening significantly affected the ability of carbon dioxide to diffuse perpendicularly to the crack walls. But, most importantly, the carbonation of crack walls and of the interface between steel and mortar always occurred regardless of the pre-crack width.

As mentioned above, the studies investigated the impact of cracks on CO₂ penetration into concrete or mortar and there have been no studies on the effect of cracks on the evolution of rust layers in a CO₂ atmosphere with wetting-drying cycles and thus their ability to induce corrosion cracks that lead to the spread of corrosion. Therefore, the aim of this paper is to examine the formation and structure of the corrosion layer in the presence of pre-cracks under accelerated corrosion test conditions in laboratory specimens.

II. Experimental programme

II.1. Test specimens

The test specimens consisted of mortar in a ring shape 50 mm high with an external diameter of 150 mm and an internal diameter of 50 mm as shown in Fig.1a. For each specimen, an 8-mm steel bar shaped into a circle of 100 mm diameter was used as reinforcement and was kept centred in the mould by three fixed metal wires. All the mortar specimens were made with a French CPA cement (CEMI 52.5R) having C₃S, C₂S, C₃A and C₄AF contents of 67.8%, 7.1%, 8.6%, and 6.2%, respectively. Standard sand (CEN EN 196-1) was used. All the mortar mixtures were made with a water/cement ratio of 0.48 and a sand/cement ratio of 2.72. Each mortar mixture was made with 1.380 kg of water, 2.875 kg of cement, and 7.830 kg of fine aggregate. The elastic limit of the steel used was 500 MPa. The mould was filled in two steps with vibration of 30 seconds on a vibrating table at the end of each step. After 24 h, the specimens were carefully demoulded to avoid any cracking and then cured under tap water until they were aged 28 days. The mortar mix was designed to have a mean compressive strength of 60 MPa and the direct tensile strength was 4 MPa at 28 days.

II.2. Preconditioning of the specimens

After curing, all specimens were stored in an oven at 40°C for 50 days to dry completely. Each specimen was weighed at 2 weekly intervals on an electric balance with an accuracy of 0.001kg. Consecutive weights were compared in order to confirm the absolute drying of the specimens. The difference between the last two weight measurements was 1g. The aim of drying the specimens was to accelerate the carbonation process.

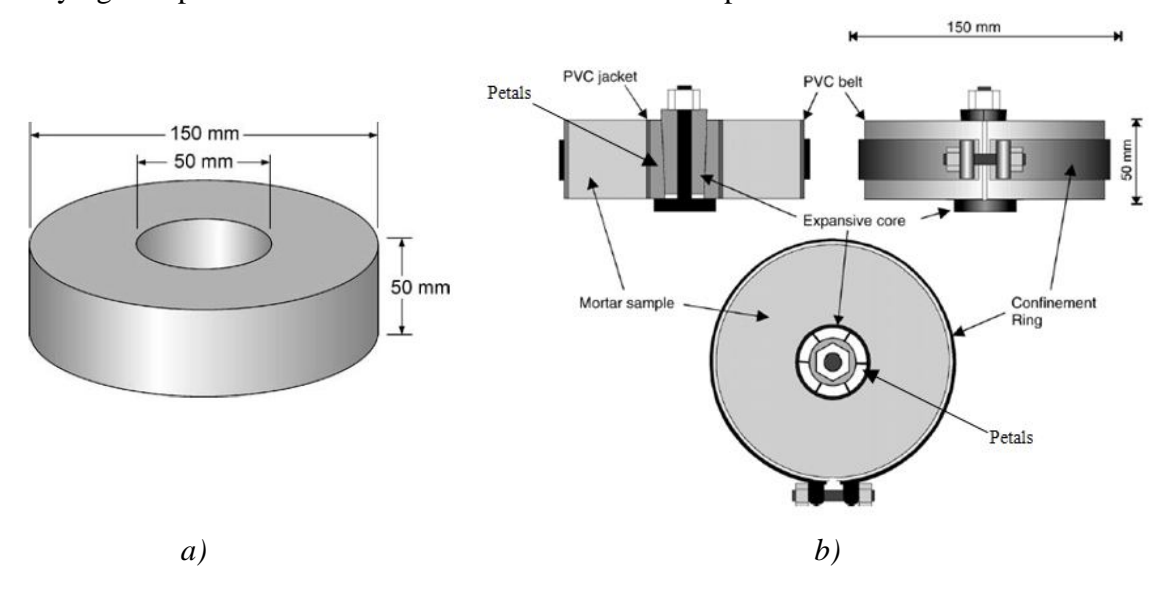


Fig.1. Dimensions of the ring-shaped mortar specimen (a); Apparatus for creating cracks on specimens (b) from Gagné et al. [34]

II.3. Making cracks on the ring-shaped mortar specimens

Controlled cracking of specimens was obtained by the experimental procedure used by Alahmad et al. [8]. The number and opening of cracks depended on the load applied. Before cracks were made on the specimens, both the exterior and interior surfaces were polished with carbon silica powder (number 120) to obtain smooth, flat surfaces. The specimens were subjected to controlled tensile cracking by the use of a mechanical expansive core and an external steel confinement ring (Fig.1b). The expansive core, which was inserted into the specimen hub, consisted of a conical hardened-steel cylinder that slid inside a set of six conical hardened-steel petals. A thin cylindrical PVC jacket held the petals around the conical cylinder. A high-strength steel bolt and nut were used to force the conical cylinder

against the petals. This process caused the diameter of the PVC jacket to increase, thus inducing deformation in the internal diameter of the mortar specimen. Controlled cracking was achieved by manually adjusting the shape of the expansive core. The specimen surfaces were closely monitored throughout the process and crack widths were measured with a portable video microscope in order to reach the desired widths. The process of creating mechanical cracks was carried out in such a way that no longitudinal cracks appeared along the outer perimeter of specimens.

II.4. Accelerated corrosion procedure

It takes many years for reinforcement steel to become moderately or heavily corroded, particularly in an ordinary atmospheric environment. Therefore, it was necessary to use an artificial technique to accelerate the corrosion process in the laboratory. Immediately after the mortar disks had been cracked, they were transferred to a sealed chamber and subjected to carbonation at a temperature of 23°C, a relative humidity of 65% and a CO₂ concentration of around 50%. For each group of specimen, the exposure time in CO₂ varied from one week to several months. At different stages of the work, specimens were taken out of the carbonation chamber so that the experiments could be conducted.

The specimens subjected to CO₂ for 1 to 5 weeks were used to study how the carbonation progressed through cracks to reach the steel bar at the mortar-steel bar interface and whether crack opening was correlated with the damage at the steel-mortar interface, as presented in [9].

After the period in CO_2 , the corrosion of the remaining specimens of each group was continuously studied in wet-dry cycles: one day under tap water followed by six days in the laboratory atmosphere (temperature 20° C, relative humidity 50%). The exposure time is given in Table.1. For these groups, the new cracks generated on the extrados by corrosion were regularly observed with a portable video microscope.

II.5. Specimens analysed

The corrosion products formed at various locations of specimens were characterized by Raman microscopy and scanning electron microscopy (SEM). For each specimen, slices were cut at the locations of mechanical cracks, the locations of both mechanical cracks and visible corrosion cracks on the extrados, and locations without cracks as displayed in Fig.2. The following notations are used for different parts of the specimen:

TOP: the top face of specimen according to casting direction of mortar

BOT: the bottom face of specimen according to casting direction of mortar

EX: the outer lateral face of the specimen (extrados)

IN: the inner lateral face of the specimen (intrados)

All specimens for Raman spectroscopy were mounted in epoxy resin at room temperature. The surface of the section was polished by grinding (SiC, grade 80 to 4000) under ethanol as shown in Fig.3.

X- Ray tomography was used only to view the corroded cross-section of specimen N6.

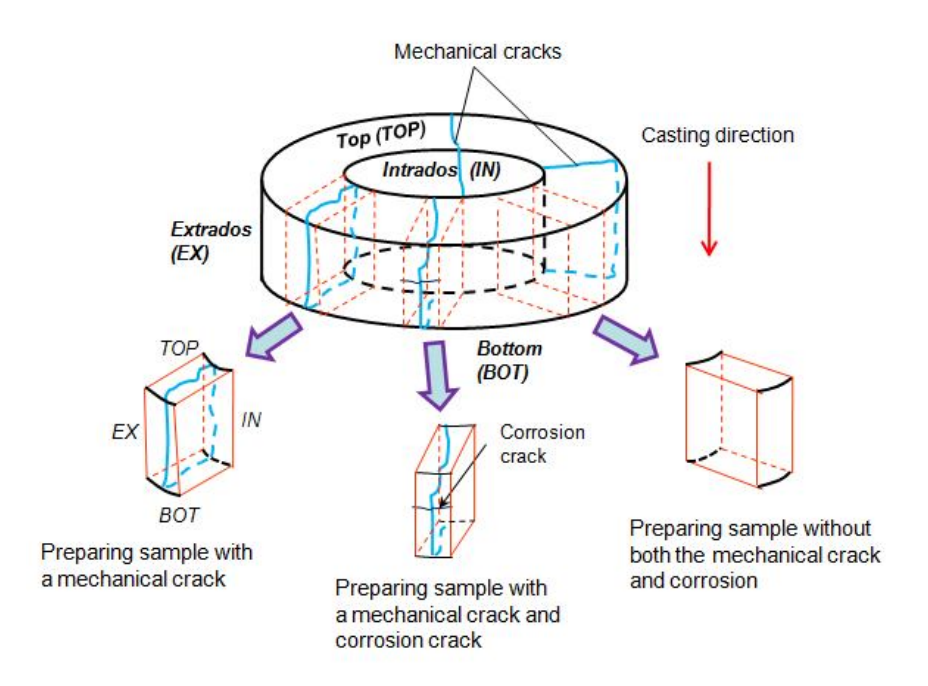


Fig.2. Explanation on specimen preparation for micro-Raman spectroscopy





Fig.3. Sawn slices (above) and polished slice specimen (below)

III. Results and discussion

III.1. Crack characteristics

Table 1 gives the measured surface openings of cracks and the number of cracks on the two faces of the specimens. Cracks induced by the expansive core were radial. Crack opening was between 30 μ m and 395 μ m. The difference between crack opening on the top and bottom faces was quite large, ranging from a few dozen to several hundred micrometres depending on the force against the PVC jacket.

CHAPTER V: Experimental program in carbon dioxide environment

Table 1. Crack widths and exposure conditions of tested specimens

					Number	of cracks	i				
Name		1	2	3	4	5	6	7	8	Duration	No. of cycles
					Crack wi	dth (μm)				in CO ₂	(weeks)
S 1	Top face	97	39	106	65					15ws	73
31	Bottom face	31	21	49	36					15005	13
S5 [*]	Top face	137	59	83						15ws	69
22	Bottom face	86	29	80							
C/	Top face	81	57	70						15ws	14
S6	Bottom face	33	30	141	166	91	50	62			
07	Top face	54	77	69						15ws	77
S7	Bottom face	54	30	78	46	27	46				
N1A	Top face	55	49							- 21ws	77
INTA	Bottom face	74	56	33	92					21005	
N2	Top face	157	274	210	167	259	217			21ws	14
IVZ	Bottom face	240	140	164	132	145				21773	
N5 [*]	Top face	165	32	80	73	119				21ws	69
110	Bottom face	202	171	82	93	60	150				07
N6 [*]	Top face	115	234	235	190	130	116			21ws	16
INO	Bottom face	101	109	52	87					21005	46
C2	Top face	230	52	64						23ws	6
UZ	Bottom face	395	180	161	93	140	394			23005	0

^{*} Specimens showed visible corrosion cracks on the extrados.

Previous results [8, 9] demonstrated that the carbonation process could occur if the crack width was over 9 μ m. Thus, the crack walls of all specimens presented in Table 1 would be carbonated. However, it should be noted that the diffusion of carbon dioxide does not depend only on crack width at the surface. Alahmad et al. [8] also indicated that interlocking plays an important role in limiting the diffusibility of carbon dioxide. In other words, the crack roughness, shape, depth and width at the steel bar surface are important. Further works [8, 9]

concluded that the steel bar-mortar interface was always carbonated even if the crack walls were only partly carbonated. The carbon dioxide gas diffuses through the crack walls to the internal steel bar, then spreads along the interface between steel and mortar. Uniform corrosion is thus expected along the reinforced steel. When the wet-dry cycles were carried out, the progression of corrosion of the steel surface at the location of a crack would be more serious than that at nearby locations away from cracks. This was because more oxygen was available and diffused easily to the steel surface in the cracked zones. It should be noted that crack width has a marked influence on the water permeability of cracked concrete or mortar [12, 13]. The authors suggest that the water permeability of cracked material due to application of a load significantly increases with increasing crack width, in particular for cracks wider than 100 µm [12].

III.2. Visual examinations

First, the visual examinations were performed with the naked eye to detect the new cracks, induced by corrosion, appearing on the external face of ring specimens. Then, further inspections were performed by video microscopy. It was found that the corrosion cracks arose on specimens S5, N5 and N6 as described in Table 2.

Specime n	Number of corrosion cracks	Corrosion crack width (µm)	Corrosion crack length (cm)	Time to first crack (week)*	
S5	1	27	3	54	
N5	1	18	1	48	
N6	2	31 & 20	2.5 & 2.2	48	

Table 2. First corrosion cracks and time of exposure

Fig.4 shows a map of the mechanical cracks and corrosion cracks of specimen N6 after accelerated corrosion of 48 weeks. The observed corrosion cracks were visible on the extrados. Specimen N6, with the widest crack openings and the longer period of carbonation exhibited corrosion cracks earlier. These corrosion cracks were generated from the mechanical transverse crack. The formation of corrosion cracks could result from the residual

^{*} Time to first corrosion crack includes both the time in CO₂ and the wet-dry cycles

tensile stress at the intersection between a mechanical crack and the internal steel bar resulting from the use of the expansive core plus the internal pressure of oxides.

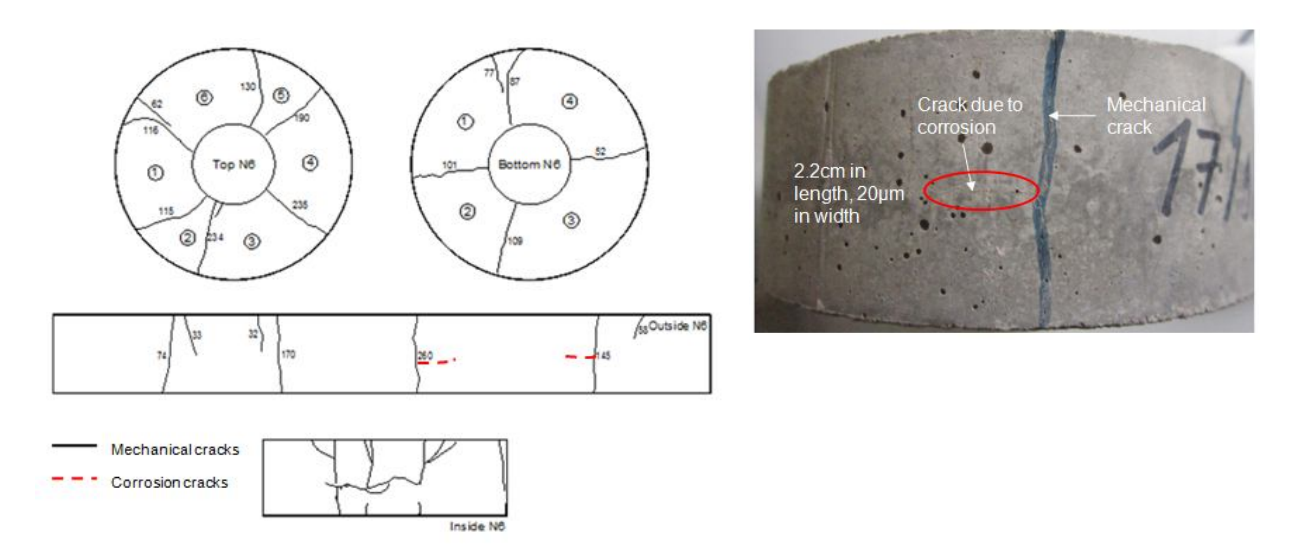


Fig.4. Evolution of corrosion cracks of specimen N6 (all crack widths are in micrometres)

III.3. X- Ray tomography

The internal cracks of specimen N6 as seen by X-ray tomography are presented in Fig.5. The X-ray CT measurements of the concrete torus 17/9/10-Ca N° 6 were made on a 3D CT scanner at BAM (Federal Institute for Materials Research and Testing in Berlin) with a 225 kV micro focus X-ray tube and a flat panel detector with 2k x 2k pixels. The resolution was about 89 µm voxel (volumetric picture element) size for the measurement of the whole specimen and about 20 µm voxel size for the small part that was cut out from the torus. The mechanical pre-cracks induce by the load are clearly visible on fig. 5a and 5b. Micro-cracks are visible on fig. 5c and 5d; they run from the steel-mortar interface to reach, in some cases, the outer surface of the mortar ring specimen and then correspond to the visible cracks on the mortar extrados in fig. 4, which was recorded after 48 weeks of corrosion. Some micro-cracks were still only internal (i.e. not visible on the outer mortar surface) and should correspond to damage induced by the load. When pre-cracks are generated by the load (internal pressure applied to the ring shaped mortar specimen), there is a transfer of force from the mortar to the steel bar, which damages the steel-concrete interface. These micro-

cracks at the steel-concrete interface were first described by Goto [33] and are labelled "cover controlled cracking" in the CEB-FIP model code [38]. These internal micro-cracks are not visible from the outer surface of the mortar but could provide oxygen access to the steel bar during wetting-drying cycles, thus encouraging the development of corrosion. They could also be the origin of corrosion cracks that propagate thanks to the pressure due to rust products. Propagation of existing cracks needs less energy than the creation of new cracks. This could explain why, with the same cover and exposed to the same aggressive environment, corrosion cracks appear more quickly in tensile zones than in compressive zones of reinforced concrete beams, as shown by François et al. [6].

The corrosion products could also be clearly observed around the cross section of the steel bar (Fig.5d). As stated previously, after 48 weeks of climate accelerated corrosion, two corrosion cracks were detected on the outer face of specimen N6.

III.4. Evolution of rust layer thickness

III.4.1.Observed by optical microscope

In order to study how the rust layer evolved, specimens prepared as described in sec.II.5 were examined by optical microscopy. For each rust layer and each width of internal cracks, measurements were made along the perimeter of the steel bar and along the length of cracks from the surface of the steel bar towards the ends of the cracks. The crack width was taken as the average value of all measured points. Specimens N5, S5 and N1A are taken as examples to introduce the distribution of rust layer and crack patterns.

The optical microphotographs of specimen N5, with a mechanical pre-crack but no visible corrosion cracks on the outer surface, are shown in Fig. 6a. It is obvious that the corrosion rate observed in the lower half-surface of the reinforcement steel is greater than that observed in the upper half of the reinforcement steel surface. This could be because of the voids formed in the bottom part of re-bars due to bleeding water and settlement of mortar as recorded by Soylev et al. [10], and Mohammed et al. [11].

Cover controlled cracking led to 3 micro-cracks around the perimeter of the bar. Corrosion products did not penetrate into the crack paths of these 3 micro-cracks and there was no

pitting corrosion anywhere along the steel perimeter. There was also no local increase in thickness of the corrosion layer in front of the 3 internal micro-cracks.

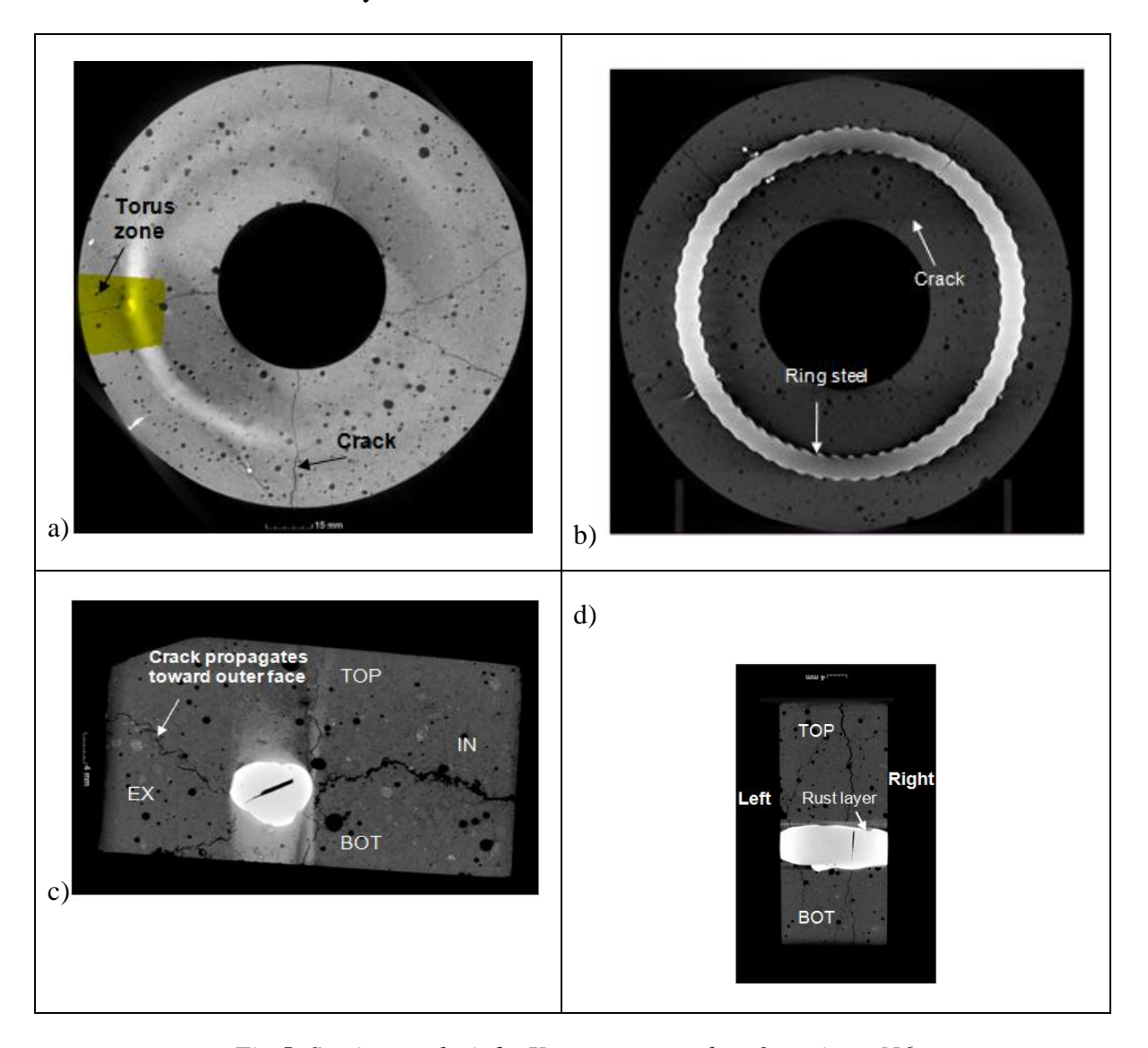
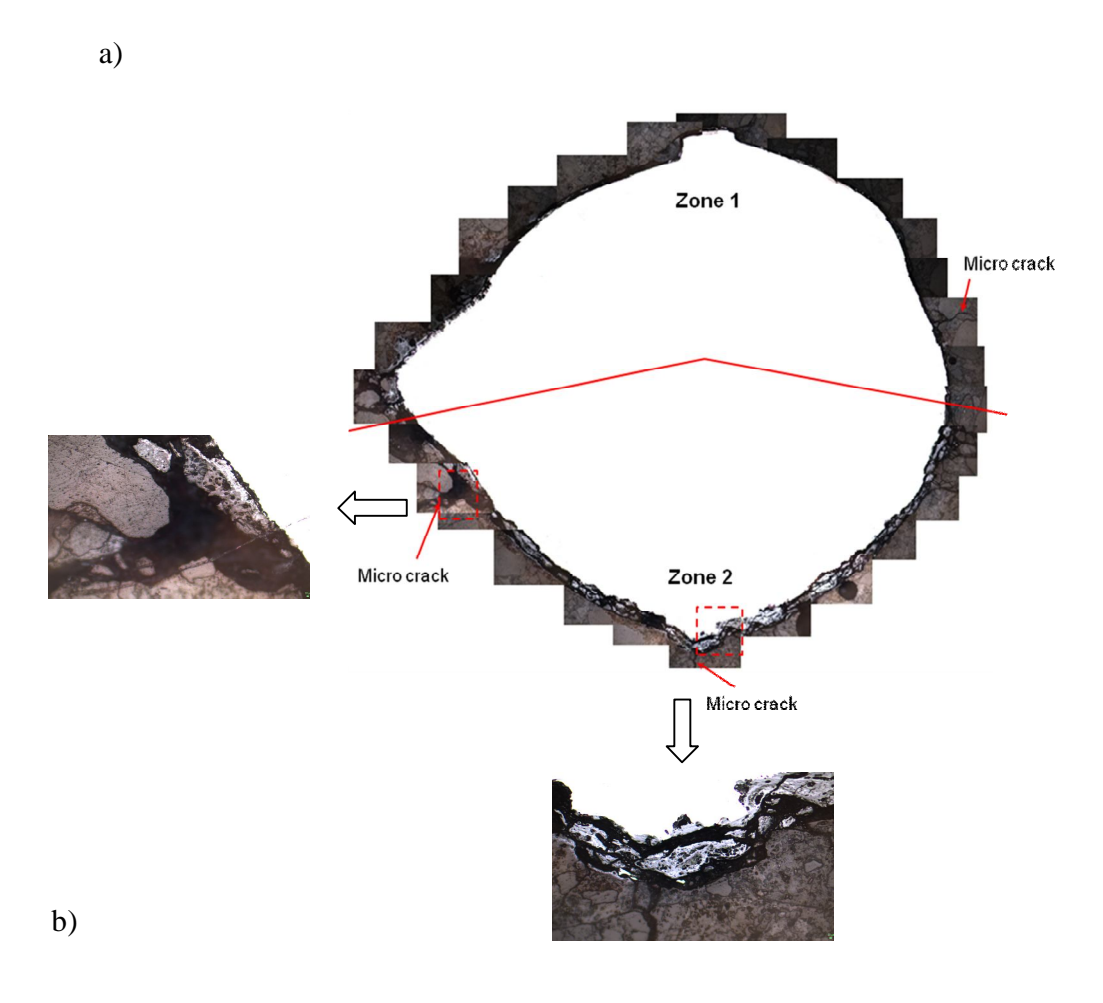


Fig.5. Section analysis by X-ray tomography of specimen N6

Specimen S5 prepared with mechanical pre-cracks but without corrosion cracks also exhibited many internal micro-cracks as seen in Fig. 7. The tiny internal cracks were distributed around the perimeter of the steel bar and had similar small openings of around $10 \, \mu m$. In this case, the thickness of the rust layer measured was quite uniform: i.e. the top-bar effect did not lead to differences in corrosion between the bottom and top parts of the steel

bar. The presence of cracks around the cross-section of the steel, induced by loading, is the most probable explanation for this. Interestingly, the corrosion layer thickness did not reach the maximum value at places where tiny cracks appeared. As a result, and similarly to previous specimens, there was no correlation between internal micro-cracks and rust layer thickness. However, such tiny internal cracks were quite close to the location where the corrosion layer was thickest.

Concerning the specimen S5, with both a mechanical pre-crack and a corrosion crack on the extrados, a cross-section of the rust layer and the crack pattern are shown in Fig. 8. Obviously, in comparison with specimens without visible corrosion cracks on the outer surface, (Fig.6), the degree of corrosion is much higher in this case.



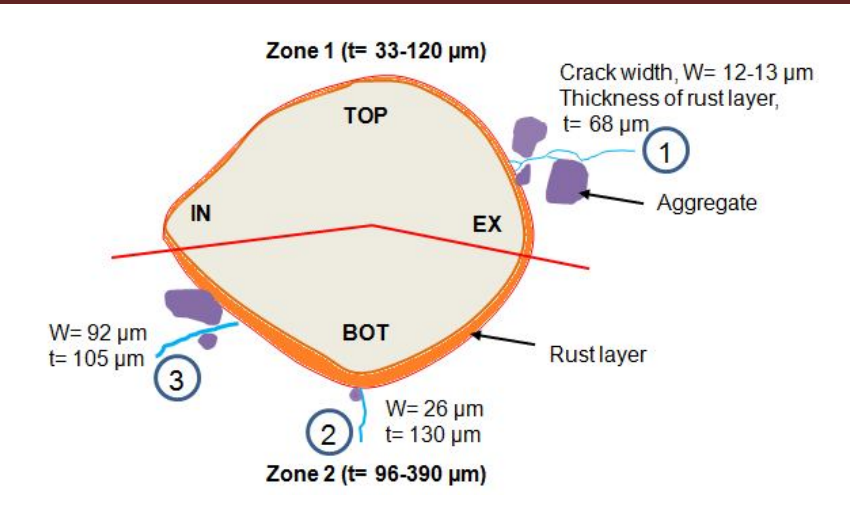
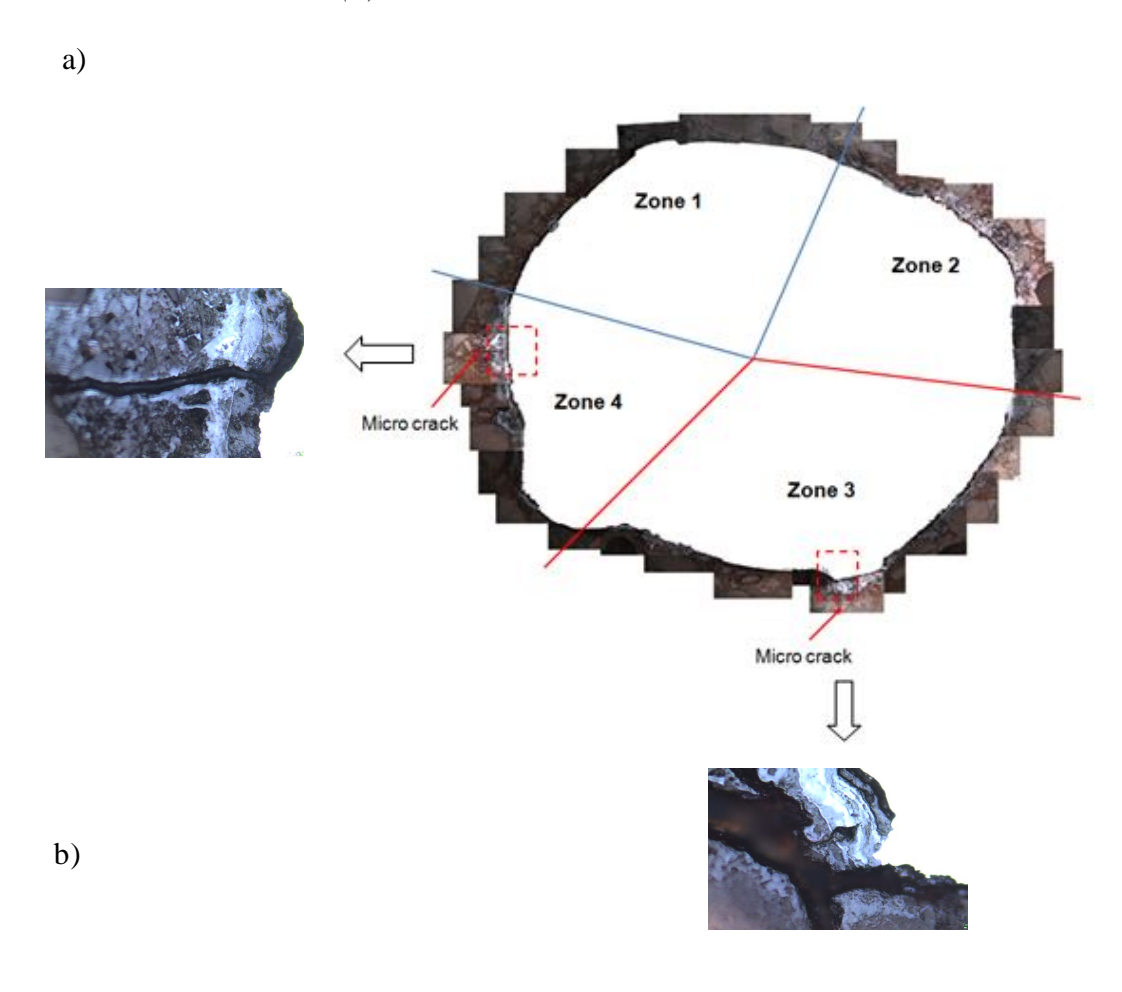


Fig.6. Optical microphotograph of specimen N5 with a mechanical crack (a) and its schematic cross section (b)



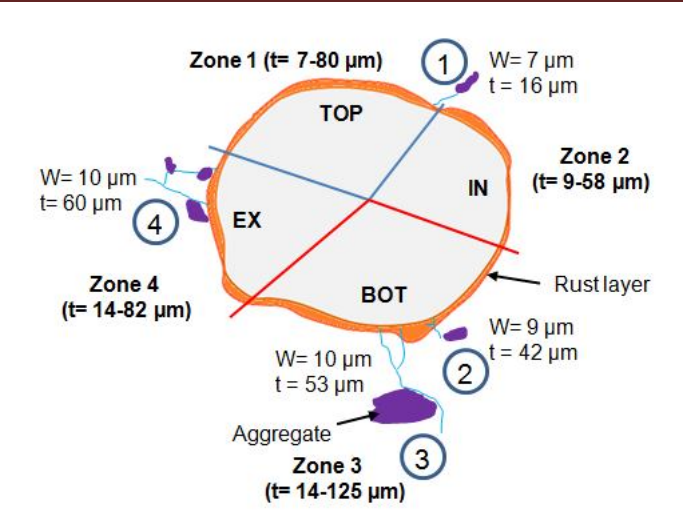
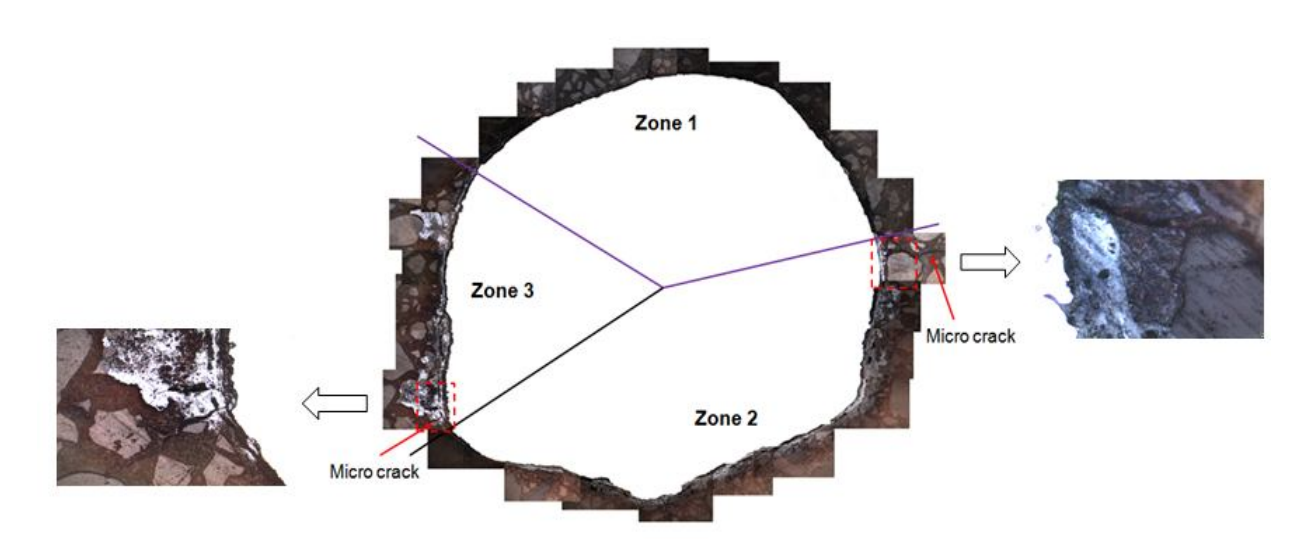


Fig.7. Optical microphotograph of specimen S5 with a mechanical crack (a) and its schematic cross section (b)

a)



b)

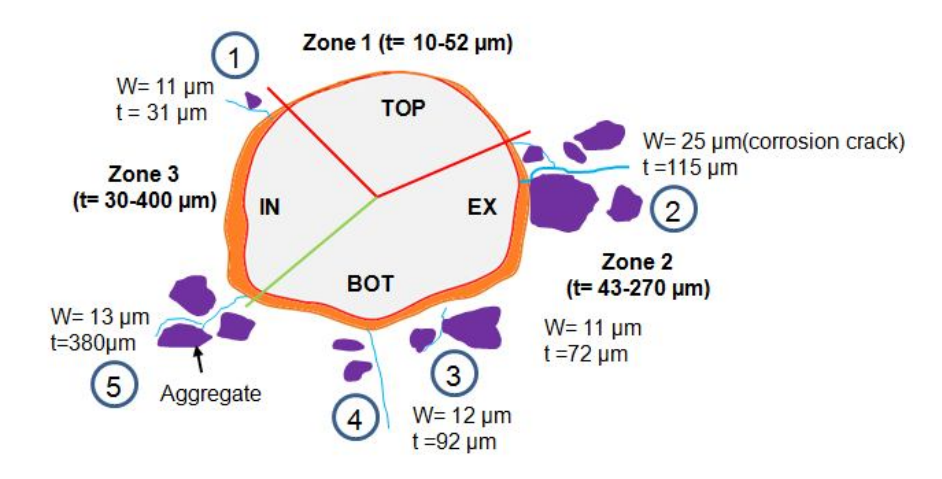


Fig.8. Optical microphotograph of specimen S5 with a mechanical crack and corrosion crack on extrados (a) and its schematic cross section (b)

The mechanical pre-cracks enabled the initiation of corrosion, which propagated and led to the appearance of corrosion cracks. The rust layer was then thicker in this specimen than in previous specimens where no visible corrosion appeared. Nevertheless, the top of the bar exhibited a relatively thin corrosion layer. Five internal micro-cracks were visible and one had propagated to the outer surface of the mortar (crack on the right - Fig. 8a or crack 2 - Fig. 8b).

Fig.9 displays the optical microphotograph and crack pattern of a slice of specimen N1A. For this slice, the average rust thickness is smaller than that of specimens N5 and S5. This is logical because the slice N1A is far away from the mechanical crack and there is no visible corrosion crack on the extrados. Internal micro-cracks due to the load and characterizing the interface damage between steel and mortar are also visible but less developed compared with previous specimens close to pre-cracks: the width of most micro-cracks is around 5 μ m. As in other specimens, the locations of internal cracks do not correspond to the locations where the rust is thickest.

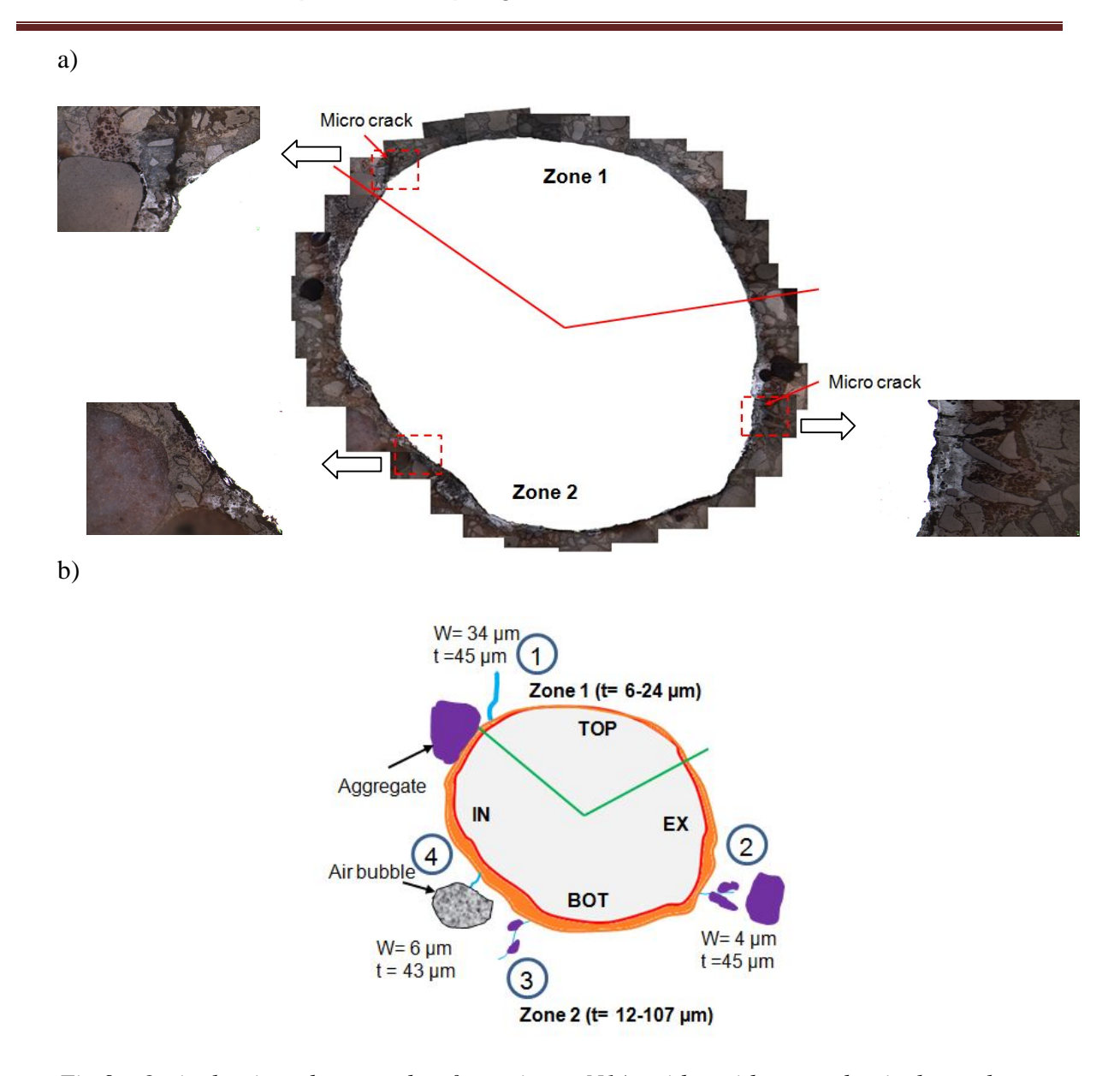


Fig.9. Optical microphotograph of specimen N1A with neither mechanical cracks nor corrosion cracks on the extrados (a) and its schematic cross section (b)

The rust distribution in cracks is also revealed in Figs. 6a, 7a, 8a, and 9a. It can be seen that the corrosion product induced by carbon dioxide is compact and has not filled up the internal cracks. This phenomenon differs from that found for corrosion products formed in a chloride environment, which are soluble and can move into the surrounding concrete and concrete cover [14, 15].

III.4.2. Cracks due to corrosion and rust layer thickness

Most results in the literature concern the relationship between the corrosion layer thickness and the appearance of the first corrosion crack visible on the outer surface of the concrete [16, 22], or the relation between the loss of cross-section and the width of corrosion cracks on the concrete surface [19, 21]. Very few corrosion cracks corresponding to these criteria were visible on the specimens tested. The experimental results show that there was propagation of internal cracks to the outer mortar surface only when the thickness of the rust layer was greater than 115 μ m.

To our knowledge, no expression has yet been proposed to link the width of visible corrosion cracks and rust layer thickness in carbon dioxide conditions. The reported studies consider the corrosion process under accelerated corrosion in a chloride environment or using impressed current or natural corrosion [16-20]. They predict the visible corrosion cracking on the external face of structures. The experimental results in the literature concern the loss of steel radius as a cause of cover cracking. For example, Andrade et al. [16] suggest that a steel radius loss of about 15-18 µm is needed to reach a surface crack width of 50 µm for $c/\phi \le 2$. While with $c/\phi > 2$, Alonso et al. [22] estimate that attack penetration of around 15-35 µm is necessary for the first visible crack to occur. They also state that surface crack widths of 0.3 mm appear for a loss of radius of about 100-200 µm. Concerning crack 2 of specimen S5, with $c/\phi = 2.62$ in Fig.8, this internal crack propagation into cover depth is shown in table 2. A local corrosion layer of 115 µm may induce a corrosion crack of 27 µm on the extrados. If the ratio of volume of corrosion layer to volume of steel consumed is assumed to vary between 2 and 4 [17, 23], the steel radius loss is about 28-57 µm, which is enough to generate the first crack [22]. However, results show that, in presence of pre-cracks due to mechanical loading, there are some internal micro-cracks at the steel-mortar interface, which may propagate due to the expansion of rust products. So it would be interesting to compare the minimal layer thickness needed to propagate an existing micro-crack with that needed to create a micro-crack. Moreover, the appearance of corrosion cracks depends on many parameters, such as c/\(\phi\), w/c, corrosion rate, steel-concrete interface, type of corrosion products, tensile strength of concrete, and fracture energy of concrete [22-24]. Thus, further

research is needed if the complex relationship between many factors is to be thoroughly understood.

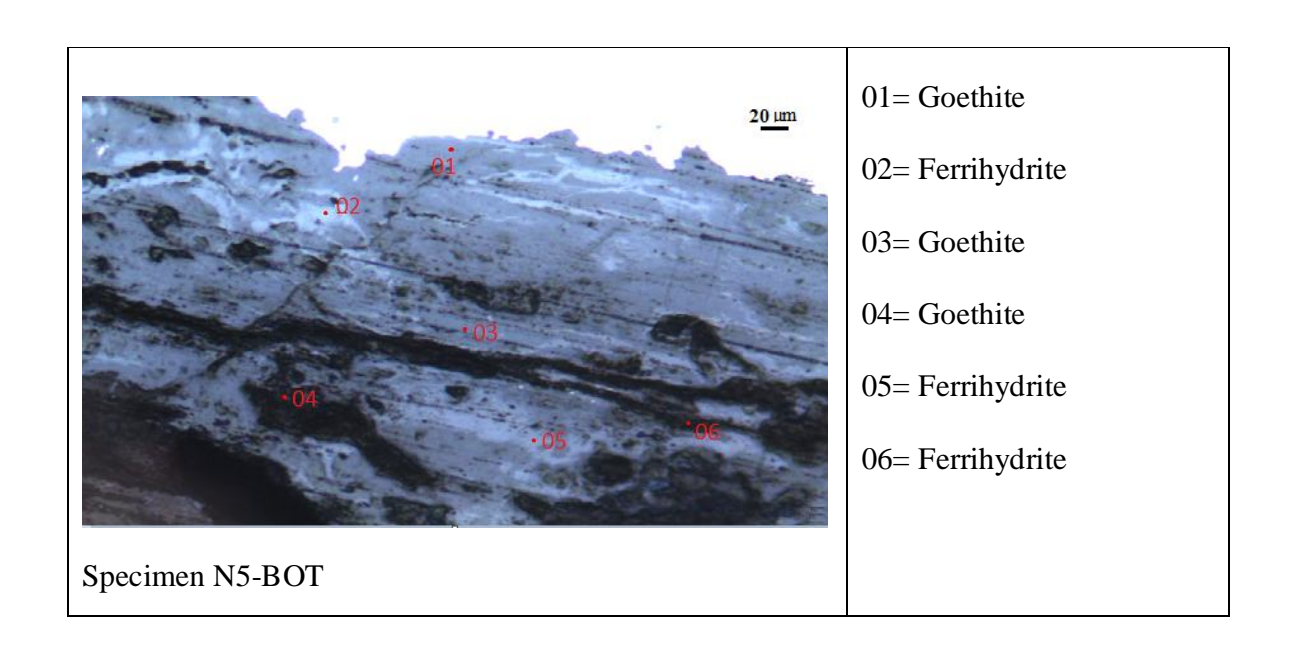
III.5. Nature of corrosion products

Because of the large number of spectra obtained from each specimen, only representative Raman spectra of each zone of each specimen are presented and analysed.

Table 3 gives a summary of the products detected at each location of the specimens. Two phases always present were ferrihydrite ($5\text{Fe}_2\text{O}_3.9\text{H}_2\text{O}$) and goethite ($\alpha\text{-Fe}_2\text{O}_3$). Other phases usually present in the steel corrosion products in this study were magnetite (Fe_3O_4) and hematite ($\alpha\text{-Fe}_2\text{O}_3$). The presence of ferrihydrite was not uniform along the rust layer that was not in contact with the steel substrate, while the distribution of goethite seemed fairly uniform and was in contact with the steel substrate (see Figs.10-12). This finding is in agreement with observations of L'Hostis et al. [26], and Chitty et al. [30]. Nevertheless, on some specimens, such as specimens N5-TOP (Fig.10) and N1A-TOP (Fig.13), no goethite was identified in the corrosion layer and magnetite was predominant in the corrosion products. It should be noted that these corrosion layer thicknesses only ranged from 10 to 35 µm, which means that the corrosion process was just initiated.

Table 3. Corrosion products identified in ring specimens

Specimen	Locations	Corrosion products
N5	TOP	Magnetite
	EX	Goethite, Ferrihydrite
	BOT	Goethite, Ferrihydrite
S5 with a mechanical crack	TOP	Goethite, Ferrihydrite, Magnetite, Hematite
	EX	Hematite, Goethite, Ferrihydrite, Magnetite
	ВОТ	Goethite, Ferrihydrite, Hematite
S5 with both mechanical crack and corrosion crack	TOP	Goethite
	EX	Ferrihydrite, Hematite, Goethite
N1A	TOP	Magnetite, Hematite
	EX	Goethite, Ferrihydrite
	ВОТ	Hematite, Goethite, Ferrihydrite, Magnetite, Lepidocrocite



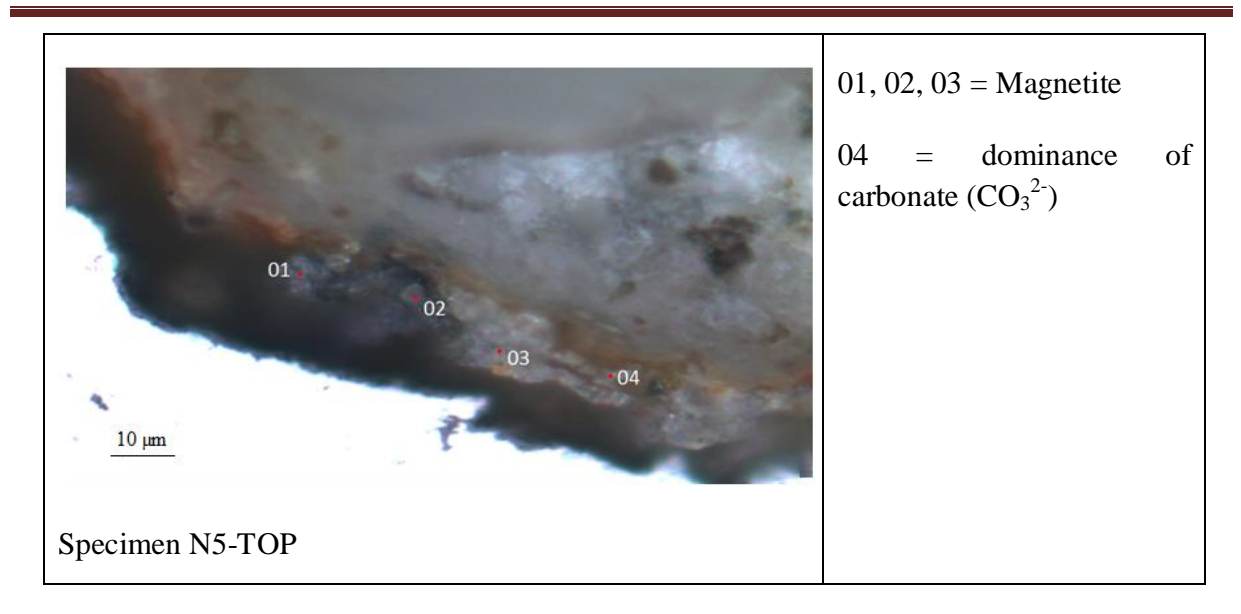
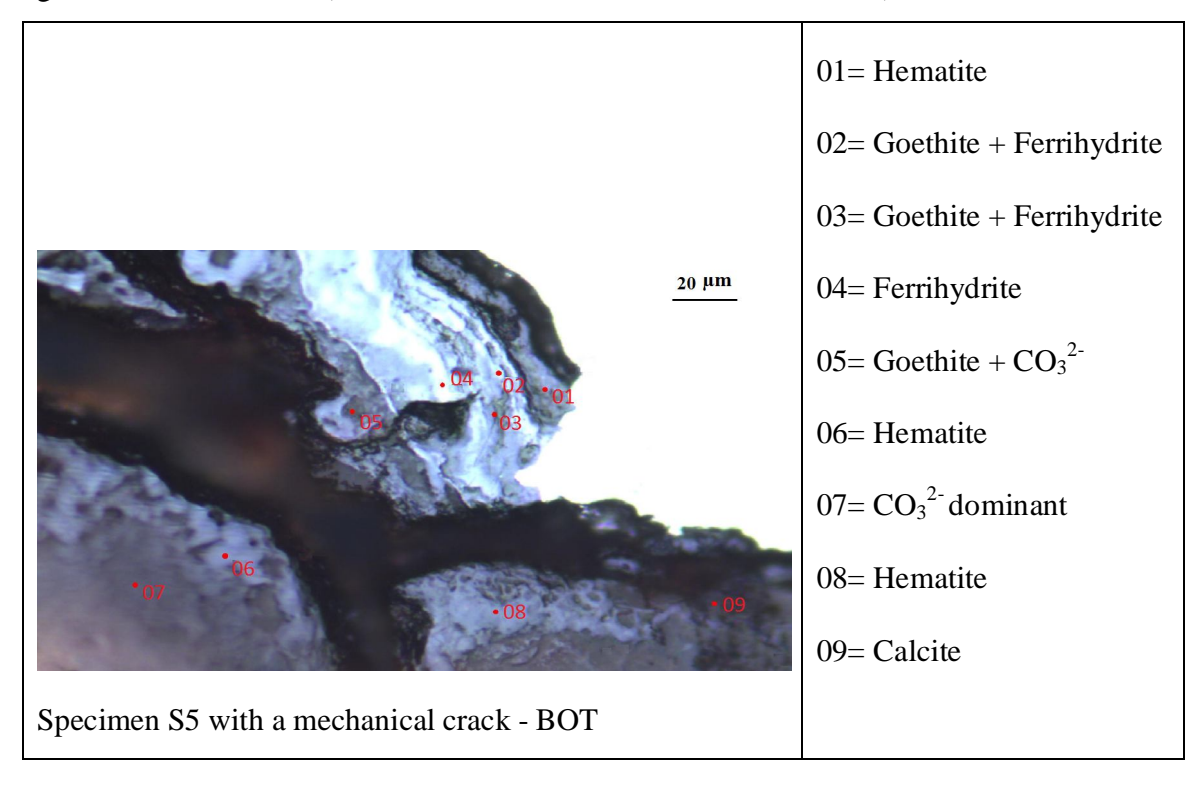


Fig.10. Typical corrosion layer observed on specimen N5 and nature of corrosion products identified.

During the initial corrosion process, due interaction among the phases, the disappearance of goethite is reasonable. (Demoulin et al. [25] and L'Hostis et al. [26]).



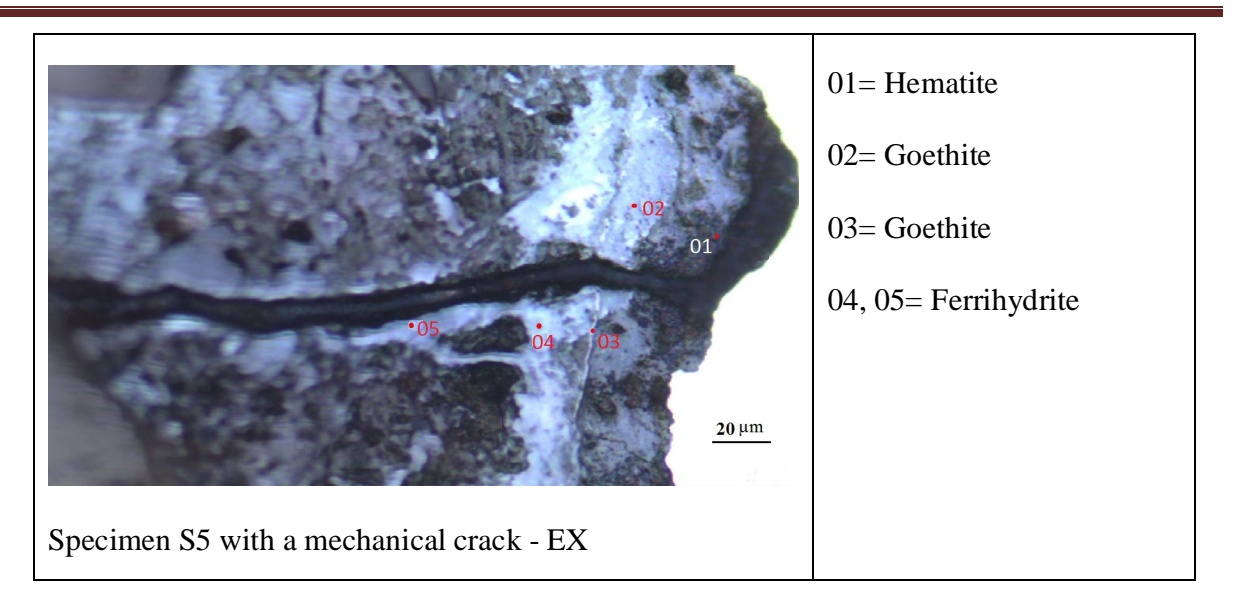
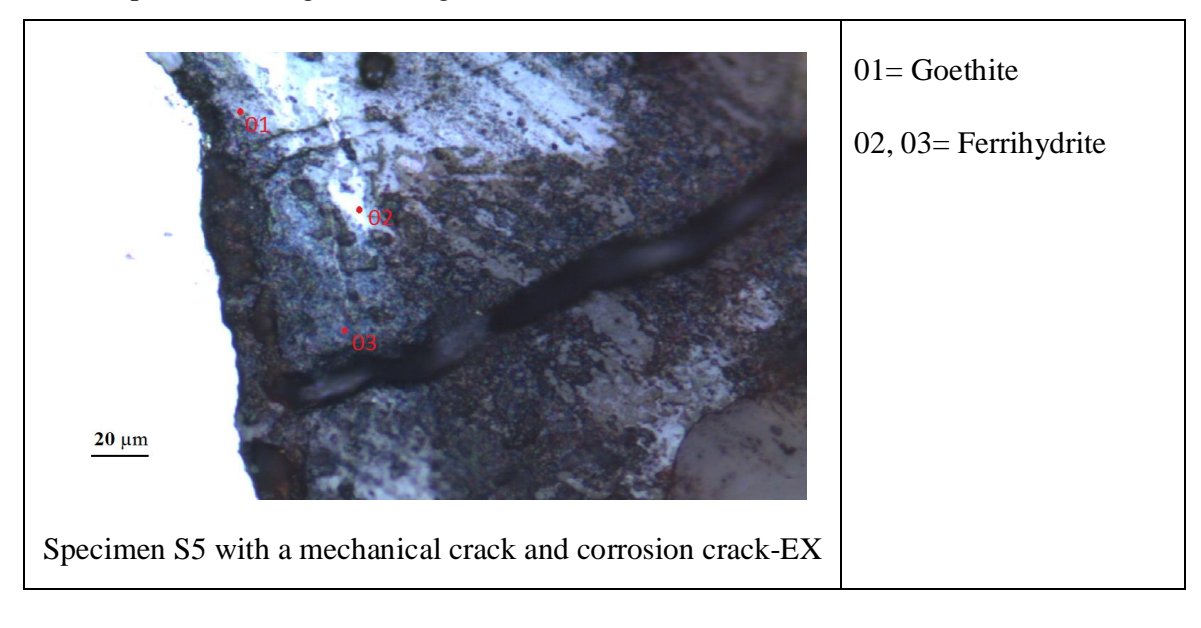


Fig.11. Typical corrosion layer observed on specimen S5 with a mechanical crack and nature of corrosion products identified.

In some specimens, carbonate ion (CO₃²-) was detected close to the surface of the mortar or midway between the metal substrate and the external corrosion layer. This implies the occurrence of transportation of ions from the rebar to the outer materials and conversely. This is illustrated by SEM and EDS analyses. Representative examples of spectra obtained from tested specimens are given in Fig. 14.



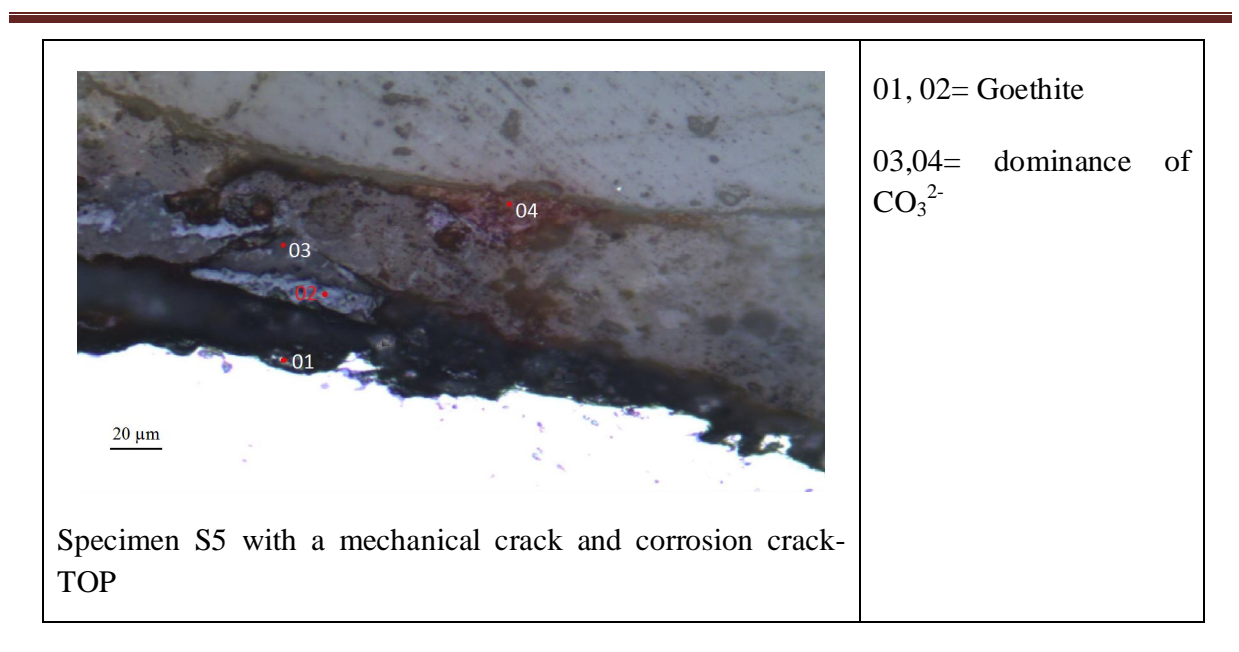
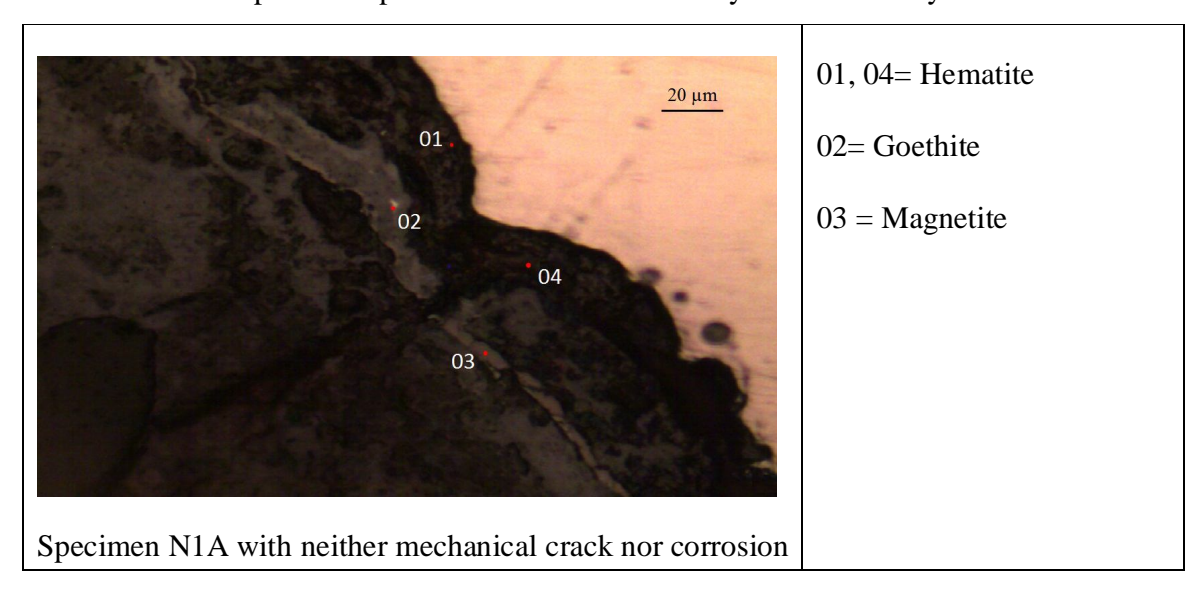


Fig.12. Typical corrosion layer observed on specimen S5 with a mechanical crack and corrosion crack, and nature of corrosion products identified

The phases were identified by comparing with data given by previous authors [31, 32]. Most of the spectra shown in Fig. 14 could be characterized exactly. However, the ferrihydrite phase was difficult to distinguish from feroxyhite (δ -FeOOH) by Raman spectroscopy because both of them present a common band in the 700 cm⁻¹ region. Thus, several spectra observed on the specimens proved to be mixes of ferrihydrite and feroxyhite.



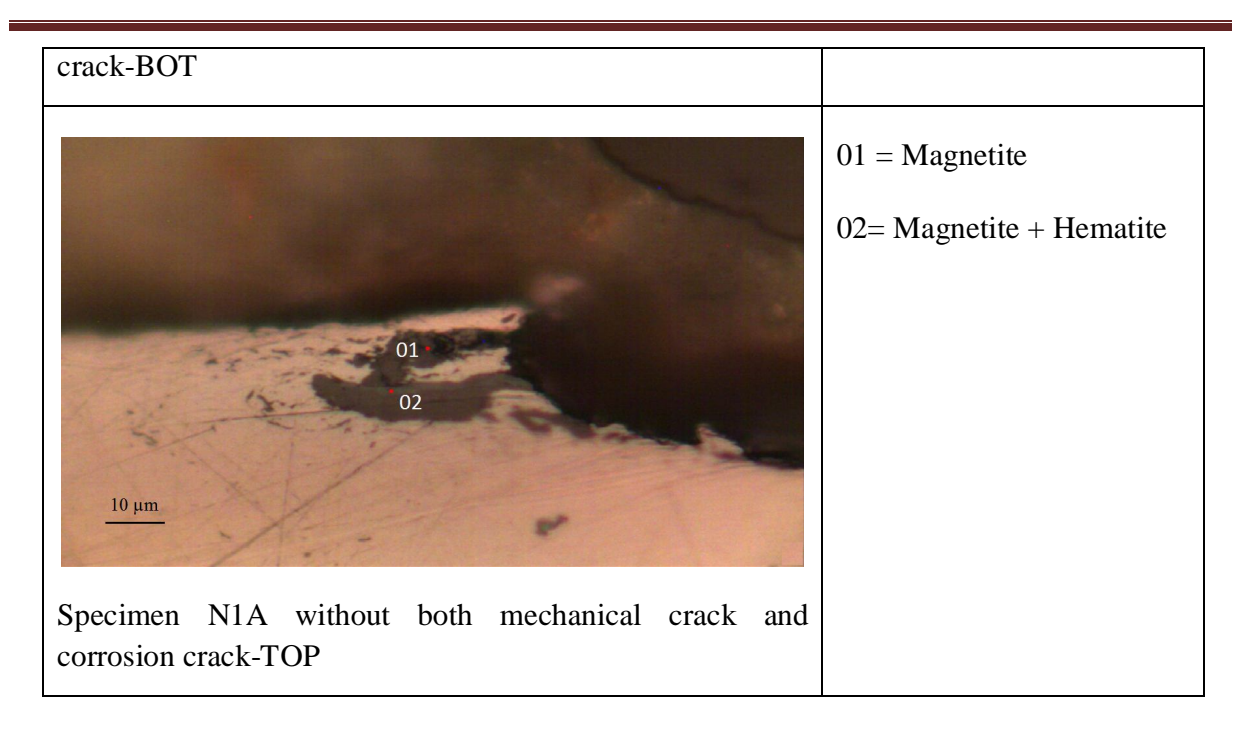
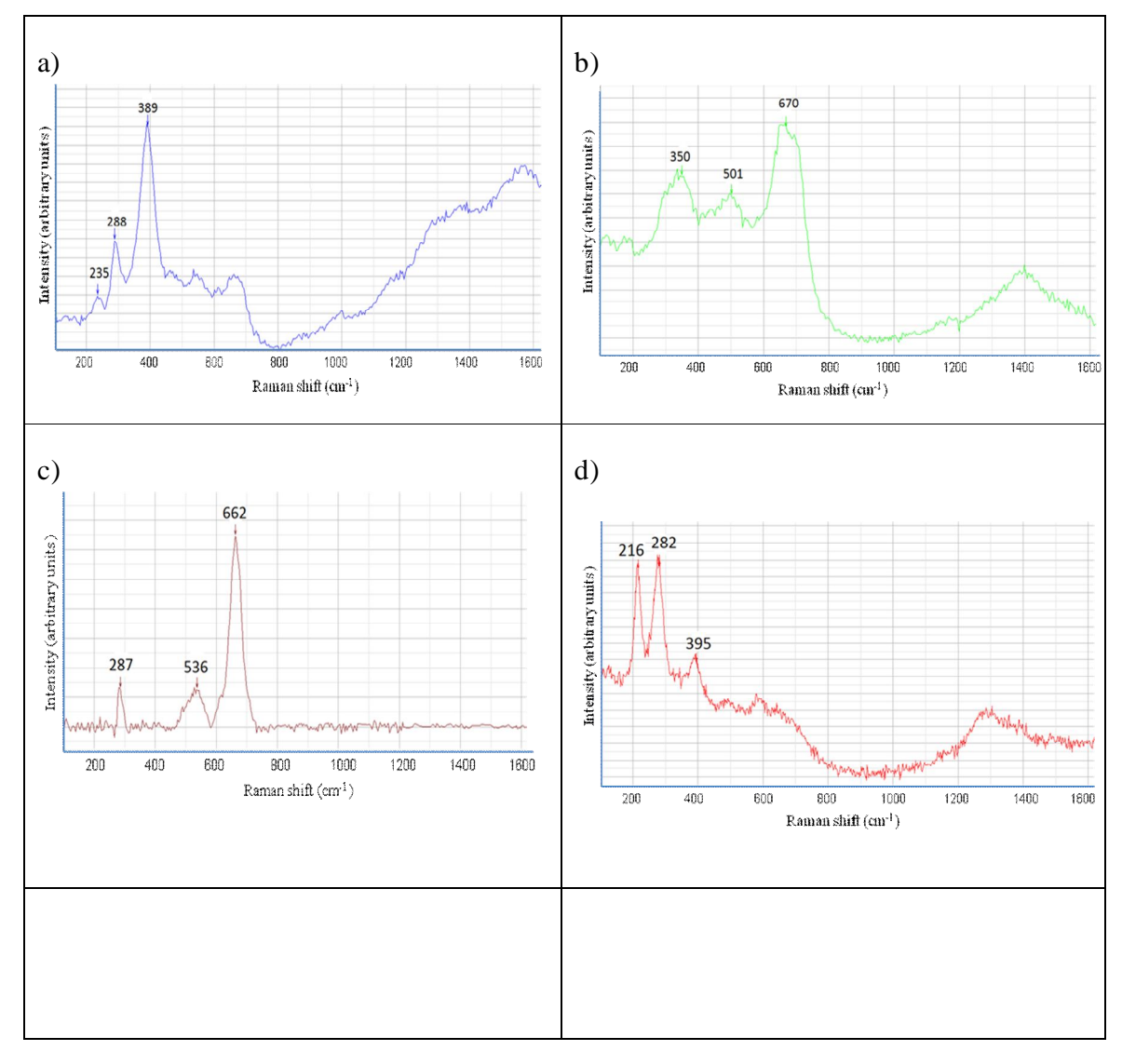


Fig.13.Typical corrosion layer observed on specimen N1A and nature of corrosion products identified

A possible scenario for the evolution of corrosion layers in mortar specimens is plotted in Fig.15. In observations on different specimens with average corrosion thickness of several tens of micrometres, part of the ferrihydrite phase could be seen in internal zones of the corrosion product while some was situated in the outermost layer as in Fig.15a. It could be expected that, because of the short time allowed for corrosion development (from 6 to 23 months), there was not enough time for poorly crystallized ferrihydrite phase to transform into crystallized goethite and hematite phases. An interesting observation was the presence of hematite at the rebar-corrosion product interface when corrosion was hundreds of micrometres thick (Fig.15b). Probably, some of the magnetite and ferrihydrite converted to hematite. In this case, there was no magnetite product detected in the rust layer but more ferrihydrite seemed to be identified in the external part of the rust. Part of the ferrihydrite phase found was intermingled with goethite. By comparison with Demoulin et al.'s study [25], where the corrosion pattern was observed on steel samples embedded in concrete extracted from two old buildings in France, it is clear that the distribution of ferrihydrite in

the current paper is very different. The goethite was predominantly found on cross sections of the rust layer. This is in accordance with observations by Demoulin et al. [25] and L'Hostis et al. [26]. This research once again indicates that the distribution and composition of corrosion products depend on the thickness of the rust layer. In other words, the corrosion rate greatly influences the multilayered structure of rust. The corrosion rate in turn depends on the location investigated on the rebar cross-section. The corrosion level is generally highest in the bottom part of the steel bar and is lowest in the top part of the steel bar (relative to the casting direction of mortar as discussed in Sec. *III.4.1*).



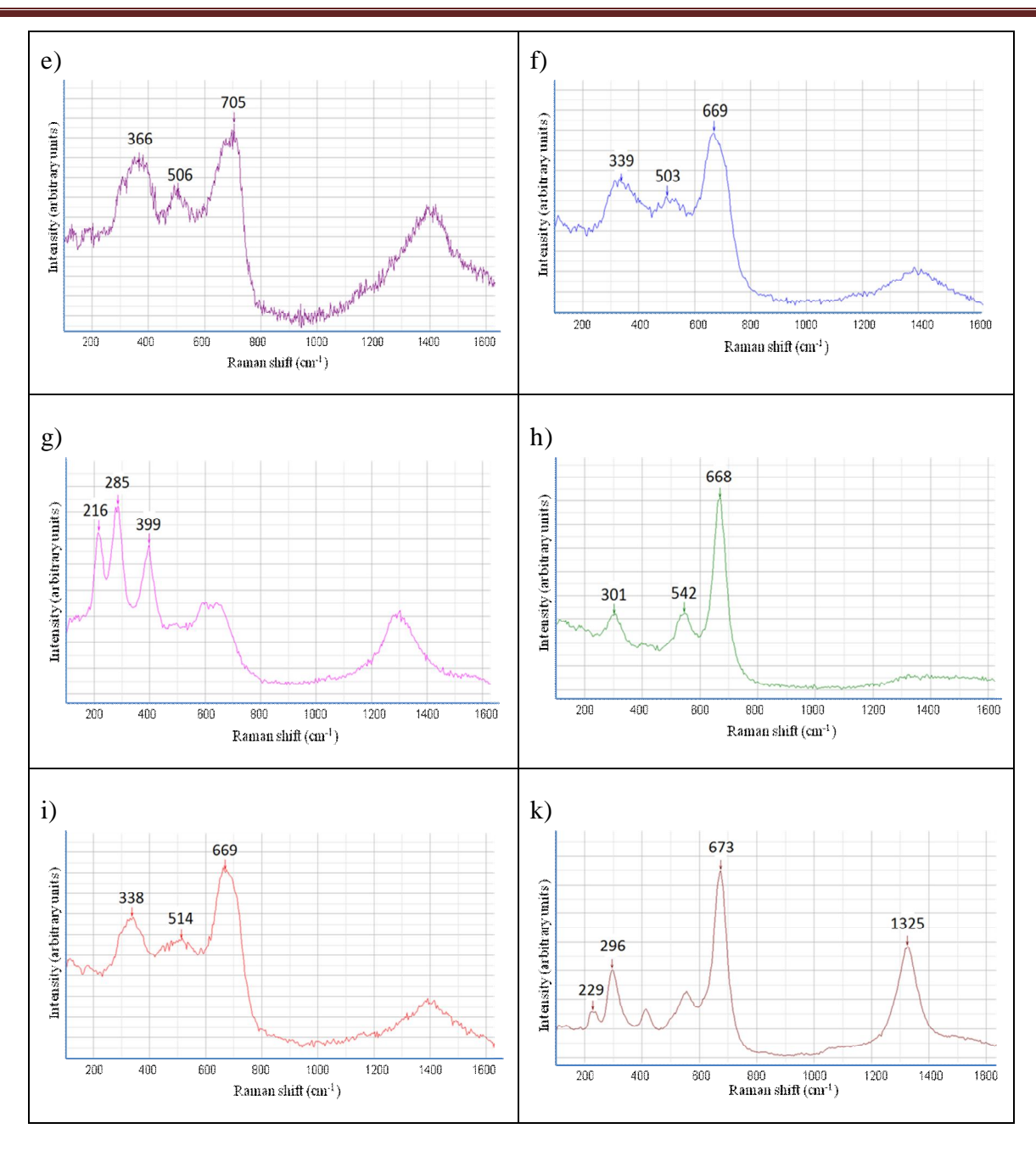


Fig.14. Representative Raman spectra of a) goethite, b) ferrihydrite obtained on specimen N5-BOT, c) magnetite obtained on specimen N5-TOP; d) hematite, e) ferrihydrite obtained on specimen S5-BOT with a mechanical crack; f) ferrihydrite, g) hematite obtained on specimen S5-EX with a mechanical crack and corrosion crack; h) magnetite, i) ferrihydrite

obtained on specimen N1A -BOT; k) mix of magnetite and hematite obtained on specimen N1A-TOP

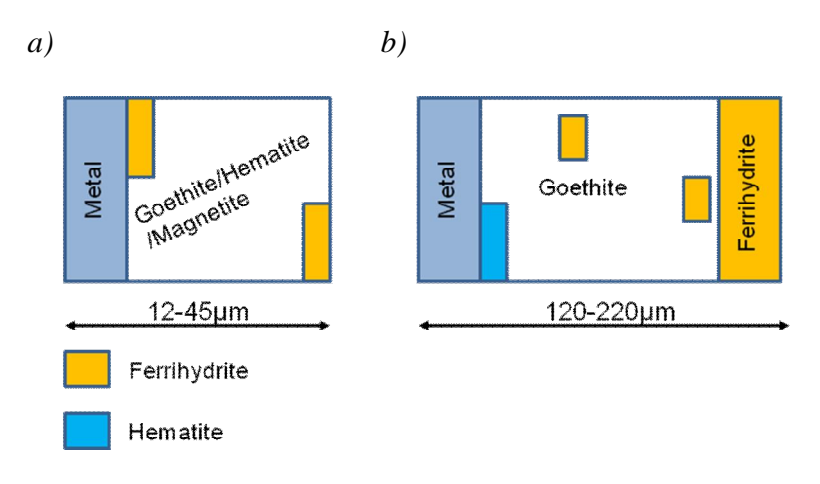


Fig.15.Evolution of the corrosion layer on the metal surface

Moreover, the results reveal a thicker corrosion layer found at the locations of pre-cracks or corrosion cracks or/and in their vicinities. These imply that the most active corrosion process occurred at the crack-steel bar intersection but the greatest activation could be close to the intersection between cracks and rebar. The possible reasons are, firstly, that pre-cracks connected and created a pathway for aggressive agents into the heart of the mortar, thus leading the corrosion progress to induce corrosion cracking. Secondly, due to the top-bar effect, voids were present under the steel bar so oxygen was available just after the drying cycles.

SEM analysis of a cross-section of rebars embedded in ring-shaped mortar specimens is presented in Fig.16-18. The points (site number) were arranged from the steel substrate, through the corrosion layer, to the cement matrix. These graphs show significantly reduced Fe contents while calcium contents increase greatly at points far away from the steel bar. Chitty et al. [30] stated that the zone where the average iron content decreases, which contains elements and phases coming from the Corrosion Product Layer (CPL), is Transformed Medium (TM). In addition, elements such as calcite and silicon also diffuse into TM from the cementitious matrix.

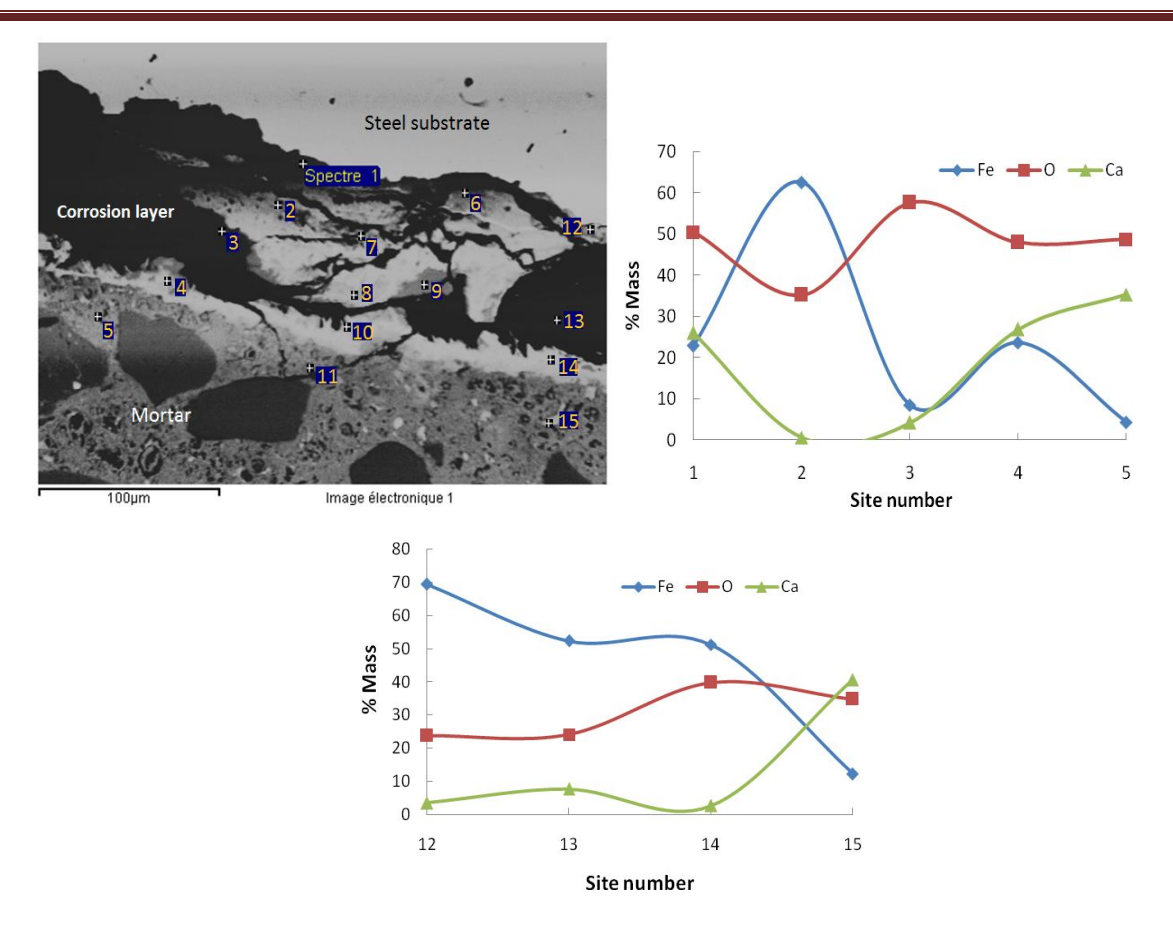
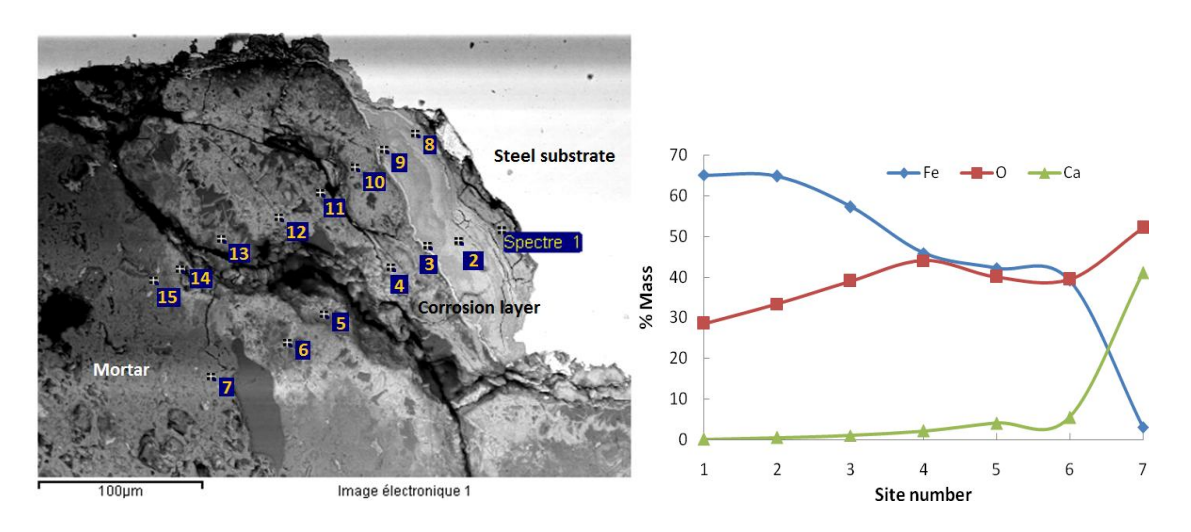


Fig.16. Distribution of Fe, Oxygen (O) and Calcium (Ca) along cross-section of specimen N5-BOT: site number $1 \div 5$ illustrates the large amount of calcium/calcite existing at the steel substrate- CPL interface



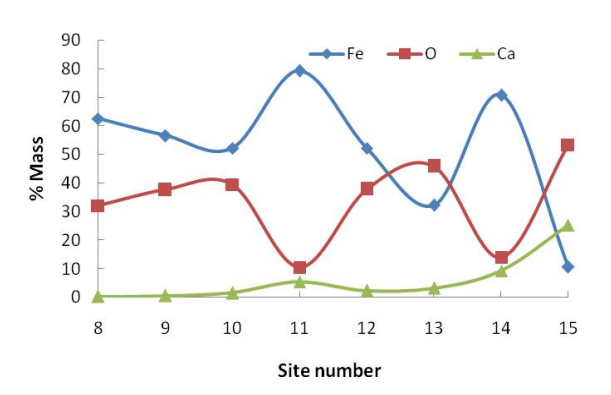


Fig.17. Distribution of iron (Fe), oxygen (O) and calcium (Ca) along cross-section of specimen S5-BOT with a mechanical crack

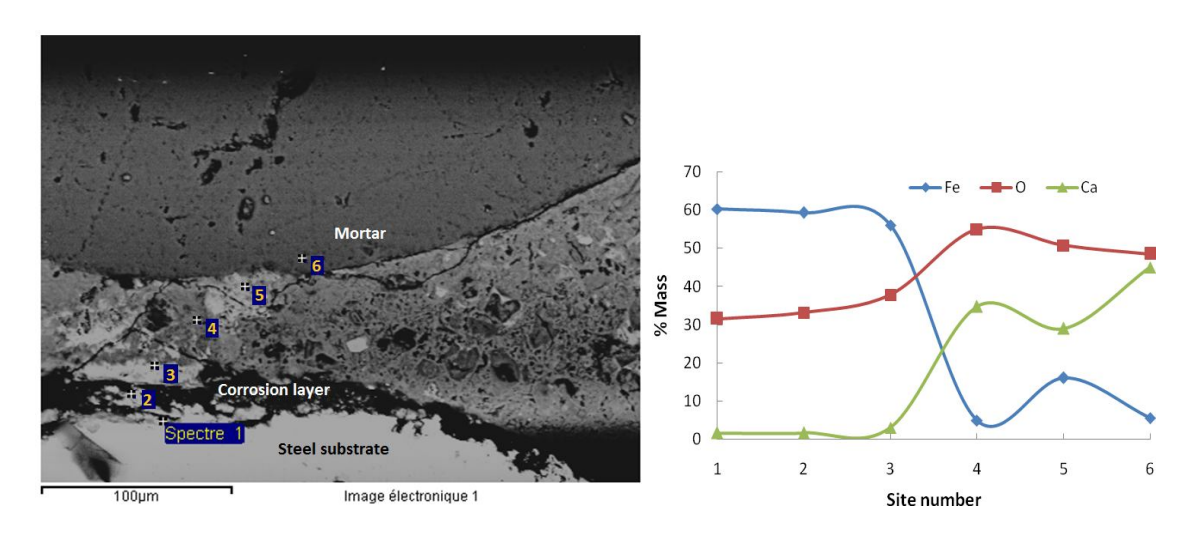


Fig.18. Distribution of iron (Fe), oxygen (O) and calcium (Ca) along cross-section of specimen S5-TOP with both mechanical crack and corrosion crack

With the increasing corrosion time along with the increased corrosion level, the TM layer gradually converts into the compact corrosion layer consisting of cement paste and corrosion products. Results by L'Hostis et al. [29] on steel samples embedded in chloride-containing cement pastes revealed that there was a TM layer about 40-50 µm thick located between the corrosion product layer and the cement paste. The present study also indicates that the rust products can move into the TM as the oxide phases are always present with around 35-45% in average mass at any site number. The oxides and iron are the main components of TM.

More interestingly, calcium/calcite from cementitious paste is able to move into the metal substrate-CPL interface as illustrated in Fig.16. This could be due to the absorption of iron oxides leading the substitution of anions in oxides [29].

IV. Conclusions

This paper studied the initiation and propagation of corrosion due to wetting-drying cycles in pre-cracked mortar specimens after carbonation of pre-crack walls and interface.

Results show that propagation of corrosion may be favoured by the cover controlled cracking induced by the load and corresponding to the internal damage to the mortar surrounding the steel bar reinforcement. This catalytic effect could be linked to the access of oxygen to the steel bar during drying cycles.

The appearance of corrosion cracks could be due to the development of internal micro-cracks formed during cover controlled cracking which propagate thanks to the pressure caused by the growth of rust products. This result is consistent with previous findings by François et al. [6], who showed that the first corrosion cracks appeared along the tensile bar in loaded RC specimens under climate accelerated corrosion in a chloride environment.

Rust was observed to develop all around the perimeter of the carbonated steel bar but the corrosion layer was thicker in the lower half surface of the reinforcement than in the upper half. The higher porosity and lower Ca(OH)₂ content at the bottom of the reinforcement [40] explained this heterogeneity in the rust layer thickness.

Results indicate that the distribution and composition of corrosion products depend on the thickness of the rust layer. As a result, the multilayered structure of rust is controlled by the corrosion level. SEM analysis also revealed that there was transportation of ions from the rebar to the outer material and the reverse. In particular, calcium/calcite could move from the cement matrix to the steel substrate.

References

- Peter Schießl and Michael Raupach, (1997), "Laboratory Studies and Calculations on the Influence of Crack Width on Chloride-Induced Corrosion of Steel in Concrete", ACI Materials Journal, V. 94, No. 1.
- 2. **R. Francois, J.C. Maso**, (1988), "Effect of damage in reinforced concrete on carbonation or chloride penetration", Cement and Concrete Research, Vol. 18, pp. 961-970.
- 3. **A.W. Beeby**, (1983), "Cracking, cover, and corrosion of reinforcement", Concrete international, pp. 35-40.
- 4. **C. Arya, F.K. Ofori-Darko**, (1996), "Influence of crack frequency on reinforcement corrosion in concrete", Cement and Concrete Research, Vol. 26, No. 3, pp. 345-353.
- 5. **Raoul François, Ginette Arliguie**, (1991), "Reinforced concrete: correlation between cracking and corrosion", ACI journal, SP 126-65, pp.1221-1238.
- 6. **R. François and G. Arliguie**, (1994), "Durability of Loaded Reinforced Concrete in Chloride Environment", ACI journal, SP 145-30, pp. 573-596.
- 7. **A. Castel, R. Francois, G. Arliguie**, (1999), "Effect of loading on carbonation penetration in reinforced concrete elements", Cement and Concrete Research 29, 561–565.
- 8. **S. Alahmad, A. Toumi, J. Verdier, R. Francois**, (2009), "Effect of crack opening on carbon dioxide penetration in cracked mortar samples", Materials and Structures 42: 559–566.
- 9. **Vu Hiep Dang, Raoul François, Valérie L'Hostis,** (2013), "Effects of cracks on both initiation and propagation of re-bar corrosion in pure carbon dioxide", EPJ Web of Conferences, Vol. 56, 06006.
- 10. **Tayfun A. Soylev, Raoul Francois,** (2006), "Effects of bar-placement conditions on steel-concrete bond", Materials and Structures (2006) 39:211–220.
- 11. Tarek Uddin Mohammed, Nobuaki Otsuki, Hidenori Hamada, and Toru Yamaji, (2002), "Chloride-Induced Corrosion of Steel Bars in Concrete with Presence of Gap at Steel-Concrete Interface", ACI Materials Journal/March-April 2002.

- 12. C.M. Aldea, S. P. Shah and A. Karr, (1999), "Permeability of cracked concrete", Materials and Structures/Materiaux et Constructions, Vol. 32, June 1999, pp 370-376.
- 13. **C.M. Aldea, S. P. Shah and A. Karr**, (1999), "Effect of cracking on water and chloride permeability of concrete", Journal of materials in Civil Engineering, 11(3), 181–187.
- 14. **Pease BJ, Michel A, Stang H,** (2012), "Quantifying movements of corrosion products in reinforced concrete using X-Ray attenuation measurements". In: Proceedings for 2nd International Conference on Microdurability, Amsterdam.
- 15. H.S. Wong, Y.X. Zhao, A.R. Karimi, N.R. Buenfeld, W.L. Jin, (2010), "On the penetration of corrosion products from reinforcing steel into concrete due to chloride-induced corrosion", Corrosion Science 52: 2469–2480.
- 16. **Andrade. C, Alonso. C, Molina. FJ,** (1993), "Cover cracking as a function of bar corrosion: part 1-experimental test", Mater Struct 26:453–464.
- 17. **Molina. FJ, Alonso. C, Andrade. C,** (1993), "Cover cracking as a function of bar corrosion: part 2-numeriacal model", Materials and Structures, 26, 532-548.
- 18. **T. Liu and R.W. Weyers**, (1998), "Modelling the dynamic corrosion process in chloride contaminated concrete structures", Cement and Concrete Research, Vol. 28, No. 3, pp. 365–379, 1998.
- 19. **T. Vidal, A. Castel, R. Francois,** (2004), "Analyzing crack width to predict corrosion in reinforced concrete", Cement and Concrete Research 34: 165 174.
- 20. Vu. K, Stewart. MG, Mullard. J, (2005), "Corrosion-induced cracking: experimental data and predictive models". ACI Struct J 102:719–726.
- 21. **Ruijin Zhang, Arnaud Castel, Raoul François**, (2010), "Concrete cover cracking with reinforcement corrosion of RC beam during chloride-induced corrosion process", Cement and Concrete Research 40: 415–425.
- 22. C. Alonso, C. Andrade, Rodriguez, J.M. Diez, (1998), "Factors controlling cracking of concrete affected by reinforcement corrosion", Materials and Structures/Materiaux et Constructions, Vol. 31, pp. 435-44.
- 23. **T. Liu and R.W. Weyers**, (1998), "Modeling the Time-to-Corrosion Cracking in Chloride Contaminated Reinforced Concrete Structures", ACI Materials Journal.

- 24. Anders Ole Stubbe Solgaard, Alexander Michel, Mette Geiker, Henrik Stan, (2013), "Concrete cover cracking due to uniform reinforcement corrosion", Materials and Structures DOI 10.1617/s11527-013-0016-6.
- 25. Amélie Demoulin, Charlotte Trigance, Delphine Neff, Eddy Foy, Philippe Dillmann, Valérie L'Hostis, (2010), "The evolution of the corrosion of iron in hydraulic binders analysed from 46-and 260-year-old buildings", Corrosion Science 52:3168–3179.
- 26. V. L'Hostis, D. Neff, L. Bellot-Gurlet and P. Dillmann, (2009), "Characterization of long-term corrosion of rebars embedded in concretes sampled on French historical buildings aged from 50 to 80 years", Materials and Corrosion, 60, No. 2.
- 27. D. Neff, J. Harnisch, M. Beck, V. L'Hostis, J. Goebbels and D. Meinel, (2011), "Morphology of corrosion products of steel in concrete under macro-cell and self-corrosion conditions", Materials and Corrosion, 62, No. 9.
- 28. V. L'Hostis, C. Emptaz, C. Paris, L. Bellot-gurlet, (2012), "Complete characterization of steel corrosion within reinforced concrete slabs in various environments", NUCPERF 2012, Cadarache-France.
- 29. V. L'Hostis, E. Amblard, W. Guillot, C. Paris and L. Bellot-Gurlet, (2012), "Characterization of the steel concrete interface submitted to chloride-induced-corrosion", Materials and Corrosion, 63, No. 9999.
- 30. Walter-John Chitty, Philippe Dillmann, Valerie L'Hostis, Caroline Lombard, (2005), "Long-term corrosion resistance of metallic reinforcements in concrete—a study of corrosion mechanisms based on archaeological artefacts", Corrosion Science 47: 1555–1581.
- 31. **Soumya Das, M. Jim Hendry**, (2011), "Application of Raman spectroscopy to identify iron minerals commonly found in mine wastes", Chemical Geology 290, 101–108.
- 32. **D.L.A.** de Faria, S.Venancio Silva and M.T. de Oliveira, (1997), "Raman microspectroscopy of some iron oxides and oxyhydroxides", Journal of Raman Spectroscopy, Vol. 28, 873-878.
- 33. **Y.M. Goto**, (1971), "Cracks formed in concrete around deformed tension bars", ACI Journal, Vol. 68, pp. 244-251.

- 34. **R. Gagné, R. François, P. Masse**, (2001), "Chloride penetration testing of cracked mortar samples". In: Banthia N, Sakai K, Gjory OE (2001) Concrete under severe conditions, vol.1. University of British Columbia, Vancouver, pp. 198–205.
- 35. **Adam Neville,** (2002), "Autogenous healing- a concrete miracle?", Concrete international 24(11), pp. 76-82.
- 36. **M.B. Otieno, M.G. Alexander, H.D. Beushausen**, (2010), "Corrosion in cracked and uncracked concrete-influence of crack width, concrete quality and crack reopening", Magazine of concrete research, 62, No.6, pp. 393-404.
- 37. **M. Ismail, A. Toumi, R. Francois, R. Gagne**, (2008), "Effect of crack opening on the local diffusion of chloride in cracked mortar samples", Cement and Concrete Research 38 (2008) 1106–1111.
- 38. **CEB-FIP Model Code,** Design code, 1992, Comite Euro-International du Beton and Federation International de precontainte, Thomas Telford, London.
- 39. **Scott AN and Alexander MG**, (2007), "The influence of binder type, cracking and cover on corrosion rates of steel in chloride-contaminated concrete", Magazine of Concrete Research 59(7): 495–505.
- 40. **A.T. Horne, I.G. Richardson, R.M.D. Brydson,** (2007), "Quantitative analysis of the microstructure of interfaces in steel reinforced concrete", Cement and Concrete Research 37, pp. 1613–1623.

General Conclusion

First objective of this thesis was to investigate the role of pre-cracks on the corrosion process in both chloride or carbon dioxide environment since this aspect is still in debate.

For this purpose, firstly, a new long term program is presented and first results are discussed. The experimental program is closed to the one built in 1984 by Raoul François but try to correct the side effects induced by the design of the loading device: i.e. coincidence of tensioned cracked surface with horizontal superior surface and top-bar defects induced during casting. The first results confirm the early initiation of corrosion at crack location but that the influence of cracks on the propagation of corrosion depends on both concrete cover and cracks location (i.e. upper or lower surface) versus chloride exposure. Secondly, annular shaped mortar samples with a circular steel reinforcement inside were casted and cracked using the "expansive core" developed by Gagné et al. 2001. After climate accelerated carbonation; these samples were exposed to wetting and drying cycles. It was found that whatever their width, mechanical crack paths and steel-mortar interface were carbonated. Then exposure to wetting-drying cycles lead to a development of corrosion all along the annular reinforcement but with a greater rust layer thickness at the bottom part of reinforcement due to a weaker quality of interface. Results show that the corrosion cracking induced by the development of rust layer arises from internal micro-cracks induced by the mechanical damage due to loading. This result is consistent with the development of corrosion cracks observed on the new set of beams exposed in saline environment.

The experimental programs in both chloride and carbon dioxide confirmed that the corrosion is always initiated in pre-cracked elements whatever crack width. This research work indicated even if a surface crack opening of 12µm, the corrosion initiation along the steel-mortar interface can occur. Therefore, a universal threshold crack width to prevent corrosion initiation can hardly be defined as the Eurocode or ACI recommendations. The interface damage seems to play a major role on the corrosion propagation. There is a scale effect between the beam and ring mortar samples. The exposure conditions i.e. cracked horizontal surface exposed directly to chloride played a principal role for corrosion development. However, the propagation of corrosion in pre-cracked concrete is delayed (induction phase)

in relation to cover concrete and exposure conditions. To better understanding the induction phase, it is necessary to carry out more study.

The second and third objective were to study the effect of corrosion on mechanical performance of RC beams in both shear and bending aspects and including the serviceability aspects, e.g. deflection and ductility. Flexural behavior of 26 and 28-year-old corroded beams was studied and compared with the one of 26 and 28 year-old control beam. It was found that the mechanical behavior of a corroded beam differs from its behavior before corrosion because of a change in the failure mode from concrete crushing to brittle failure of corroded rebar. The behavior in tension of corroded steel bar was carefully studied and despite the difficulty to measure the effective residual steel cross-section after pitting corrosion, it was found that true yield stress and true ultimate stress of steel are little affected by corrosion but on the contrary ultimate elongation of steel bar is strongly reduced by corrosion. These results justified the change in failure mode and confirm that the reduction in ultimate capacity is proportional to the loss of steel bar cross-section. The loss of beam ductility or ultimate deflection appears to be strongly correlated to the change in ductility of steel bar. A decrease in ductility of beam due to corrosion is much higher than the relative decrease in both yielding and ultimate load capacity. Thus, ductility factor should be the critical point for the safety and residual service life of corroded structures. New ductility factor for corroded beams failed by flexure was defined. A relationship between new ductility factor and corrosion level allow predicting the mode of failure of corroded slender beams. In order to study the shear performance of the corroded beams, both corroded beams and control beams were cut to extract a total of 6 small shear critical beams with different shear span to effective depth ratios. It was found that both corrosion of longitudinal tension reinforcement and corrosion of stirrups have a limited effect on the ultimate capacity of deep beams. These results can be explained by coupled behavior between arch action and beam action leading to change in load transfer mechanism and failure mode for corroded beam in comparison with control beams. In addition, the capacity of straight end anchorage of corroded reinforcement appears to be very much higher than expected despite the presence of corrosion cracks. Concrete confinement effect due to the end support reaction and the "natural" corrosion condition which do not lead to a homogeneous damage all around perimeter of re-bars may explain these surprising results.